Medical Radiology

Diagnostic Imaging

M.F. Reiser
H. Hricak
M. Knauth

Horst Urbach
Editor

MRI in Epilepsy

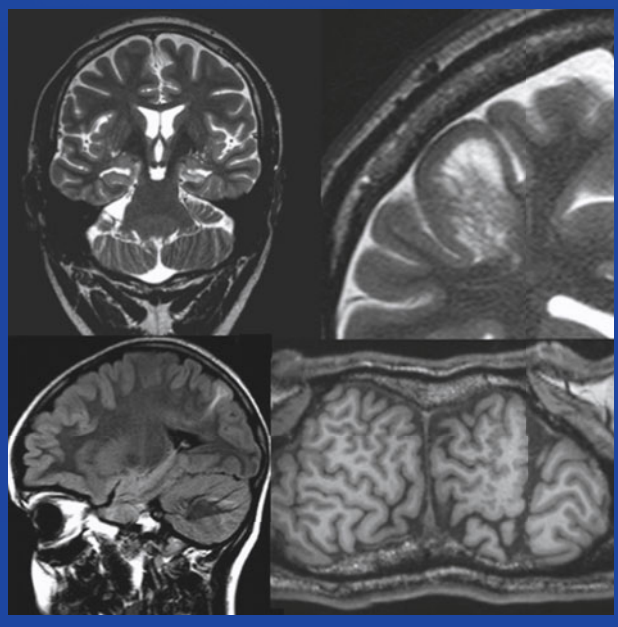

Springer

Medical Radiology

Diagnostic Imaging

For further volumes:
http://www.springer.com/series/4354

Horst Urbach
Editor

MRI in Epilepsy

Springer

Editor
Horst Urbach
Department of Neuroradiology
University Hospital Freiburg
Germany

ISSN 0942-5373
ISBN 978-3-642-25137-5 ISBN 978-3-642-25138-2 (eBook)
DOI 10.1007/978-3-642-25138-2
Springer Heidelberg New York Dordrecht London

Library of Congress Control Number: 2013932130

For Rita, Philipp, Vicky, and Oliver
And for my parents

Preface

Over the past 2 decades MRI has evolved into one of the most powerful tools for studying patients with neurological diseases. For epilepsy patients it is often the key entrance to a work-up which may end with epilepsy surgery and postsurgical seizure freedom. An epileptogenic lesion on MRI is the most important prognostic outcome parameter, but its proper identification is not as obvious. Sometimes lesions are misinterpreted, sometimes overlooked, and sometimes only identified after postprocessing of adequate imaging data. What is obvious for "specialists" in this field, may be different for those who rarely see these patients in their daily practice. What gets obvious when clinical examination, EEG and MRI are considered together, may remain obscured if these informations are not put together like the pieces of a puzzle. This book has been written in order to illustrate how single pieces (epileptogenic lesions) look like and how they could fit to the patient's seizures. Epilepsy may be a "1000 pieces puzzle" and you often see only what you know. However, what you have seen once before you may recognize again. In this sense, we have tried to illustrate each lesion with a typical imaging example.

Freiburg — Horst Urbach

Contents

MRI in Epilepsy

Epileptogenic lesions are often small and do not change during life. Moreover, several genetically determined epilepsy syndromes exist, which by definition are not caused by underlying structural lesions. Both cause a certain degree of uncertainty, whether an epileptogenic lesion is overlooked or is just not present.

This book provides radiologists and referring physicians with clinical and imaging informations essential to decide, when to initiate a MRI examination, how to decide if a MRI examination is sufficient to detect a lesion, and how to interpret imaging findings.

Contributors

Christian G. Bien Epilepsy Centre Bethel, Bielefeld, Germany

Sebastian Flacke Department of Radiology, Lahey Clinic, Burlington, MA, USA

Karolien Goffin Division of Nuclear Medicine, University Hospital Leuven and Katholieke Universiteit Leuven, Leuven, Belgium

Susanne Greschus Department of Radiology/Neuroradiology, University of Bonn, Bonn, Germany

Hans-Jürgen Huppertz Swiss Epilepsy Centre, Zurich, Switzerland

Timo Krings Department of Neuroradiology, University of Toronto, Toronto, ON, Canada

Jens Reimann Department of Neurology, University of Bonn, Bonn, Germany

Robert Sassen Department of Epileptology, University of Bonn, Bonn, Germany

H. Urbach Department of Neuroradiology, University Hospital Freiburg, Germany

Koen Van Laere Division of Nuclear Medicine, University Hospital Leuven and Katholieke Universiteit Leuven, Leuven, Belgium

Wim Van Paesschen Department of Neurology, University Hospital Leuven, Herestraat 49, 3000 Leuven, Belgium

Marec von Lehe Department of Neurosurgery, University of Bonn, Bonn, Germany

Jörg Wellmer Ruhr-Epileptology, Department of Neurology, University Hospital Knappschaftskrankenhaus Bochum, Germany

Friedrich G. Woermann MRI Unit, Mara Hospital, Bethel Epilepsy Center, 33617 Bielefeld, Germany

Part I

Epilepsy Patients and How to Examine Them

Epileptic Seizures and Epilepsy

Horst Urbach and Jörg Wellmer

Contents

Abstract

This chapter introduces the definitions of epileptic seizures, epilepsy, and drug-resistant epilepsy.

An epileptic seizure is defined as a transient occurrence of signs and/or symptoms due to abnormal excessive or synchronous neuronal activity in the brain (Fisher et al. 2005). Around 5% of persons suffer from one or more epileptic seizures during their lifetime. This number is derived from a nationwide surveillance system in Iceland, in which the mean annual incidence of the first unprovoked seizures was 56.8 per 100,000 person-years, including 23.5 per 100,000 person-years for single unprovoked seizures and 33.3 per 100,000 person-years for recurrent unprovoked seizures (Olafsson et al. 2005). The incidence is similar in males and females, and the age-specific incidence is highest in the first year of life (130 per 100,000 person-years) and in those 65 years old and older (130 per 100,000 person-years) (Olafsson et al. 2005).

Epilepsy is a disorder of the brain characterized by an enduring predisposition to generate epileptic seizures and by the neurobiologic, cognitive, psychological, and social consequences of this condition. The definition of epilepsy requires the occurrence of at least one epileptic seizure. However, in contrast to former classifications, one seizure permits the diagnosis of epilepsy if paraclinical EEG (e.g., 3 Hz spike-and-wave discharges) or MRI (e.g., hippocampal sclerosis) findings point to an increased epileptogenicity.

Epilepsy is considered as drug-resistant if seizures persist despite adequate medication with two, tolerated antiepileptic drugs (single drugs or in combination). A patient who has no seizures while taking antiepileptic drugs is considered seizure-free after an observation period of

H. Urbach (✉)
Department of Neuroradiology,
University Hospital Freiburg, Germany
e-mail: horst.urbach@uniklinik-freiburg.de

J. Wellmer
Ruhr-Epileptology, Department of Neurology,
University Hospital Knappschaftskrankenhaus
Bochum, Germany

H. Urbach (ed.), *MRI in Epilepsy*, Medical Radiology. Diagnostic Imaging,
DOI: 10.1007/174_2012_556, © Springer-Verlag Berlin Heidelberg 2013

1 year. This period can be longer if the patient had rare seizures before. In this situation, the observation period is 3 times the seizure interval the patient had before (rule of three) (Kwan et al. 2010). For example, if a patient had seizures with an interval of 6 months, the observation period is 18 months.

However, the core definition of drug resistance should be adapted to the particular clinical situation. It should rely on an individualized risk–benefit evaluation of continued antiepileptic drug medication versus epilepsy surgery. In the case of easily accessible epileptogenic lesions, low complication risks, and a high chance of freedom from seizures, epilepsy surgery may be offered after a second failed medical treatment (early relative drug resistance). If the risk of neurological deficits is high or the chance of freedom from seizures is low, relative drug resistance is assigned only after several more drug treatments (Wellmer et al. 2009).

References

Fisher RS, van Emde Boas W, Blume W, Elger C, Genton P, Lee P, Engel J Jr (2005) Epileptic seizures and epilepsy: definitions proposed by the International League Against Epilepsy (ILAE) and the International Bureau for Epilepsy (IBE). Epilepsia 46(4): 470–472. doi:10.1111/j.0013-9580.2005.66104.x

Kwan P, Arzimanoglou A, Berg AT, Brodie MJ, Allen Hauser W, Mathern G, Moshe SL, Perucca E, Wiebe S, French J (2010) Definition of drug resistant epilepsy: consensus proposal by the ad hoc task force of the ILAE commission on therapeutic strategies. Epilepsia 51(6):1069–1077. doi:10.1111/j.1528-1167.2009.02397.x

Olafsson E, Ludvigsson P, Gudmundsson G, Hesdorffer D, Kjartansson O, Hauser WA (2005) Incidence of unprovoked seizures and epilepsy in Iceland and assessment of the epilepsy syndrome classification: a prospective study. Lancet Neurol 4(10):627–634. doi:10.1016/S1474-4422(05)70172-1

Wellmer J, Weber B, Urbach H, Reul J, Fernandez G, Elger CE (2009) Cerebral lesions can impair fMRI-based language lateralization. Epilepsia 50(10):2213–2224. doi:10.1111/j.1528-1167.2009.02102.x

Classification of Epileptic Seizures

Horst Urbach and Jörg Wellmer

Contents

Abstract

Whether and how a patient should be studied with MRI depends on the type of the seizures and the epilepsy syndromes. Focal and generalized seizures and non-epileptic conditions mimicking epileptic seizures have to be considered.

As in earlier classifications in 1981 and 1989, the most recent proposal for the terminology of seizures and epilepsies of the International League Against Epilepsy (ILAE) (Berg et al. 2010) dichotomizes seizures into focal and generalized epileptic seizures. If there is insufficient evidence to characterize seizures as focal or generalized, they are referred to as unknown (Table 1). Some of the earlier-applied terms such as simple partial and complex partial are no longer proposed. Throughout this book we will refer to the 2010 proposal. However, since old terms are still abundantly used, for better understanding they will be given in parentheses.

Focal (old term: partial) seizures (Table 2) originate within networks *limited to one hemisphere*. They may be discretely localized or more widely distributed, and may originate in subcortical structures. For each seizure type, ictal onset is consistent from one seizure to another, with preferential propagation patterns that can involve the contralateral hemisphere. In some cases, however, there is more than one network, and more than one seizure type, but each individual seizure type has a consistent site of onset (Berg et al. 2010).

Generalized epileptic seizures originate at some point *within*, and rapidly engage, *bilaterally distributed networks*. Such bilateral networks can include cortical and subcortical structures, but do not necessarily include the entire cortex. Although individual seizure onsets can appear localized, the location and lateralization are not consistent from one seizure to another. Generalized seizures can be asymmetric (Berg et al. 2010).

According to their clinical appearance, focal seizures can be characterized according to one or more of the following features:

H. Urbach (✉)
Department of Neuroradiology,
University Hospital Freiburg, Germany
e-mail: horst.urbach@uniklinik-freiburg.de

J. Wellmer
Ruhr-Epileptology, Dept. of Neurosurgery,
University Hospital knappschaftskrankenhaus,
Bochum, Germany

H. Urbach (ed.), *MRI in Epilepsy*, Medical Radiology. Diagnostic Imaging,
DOI: 10.1007/174_2012_553, © Springer-Verlag Berlin Heidelberg 2013

Table 1 Outline of the International League Against Epilepsy (ILAE) classification of epileptic seizures. (From Berg et al. 2010, with permission)

Generalized seizures
Tonic–clonic (tonic contraction followed by clonus usually lasting 1–2 min)
Absence (altered consciousness and staring with minimal motor activity for a few seconds)
Typical
Atypical
With special features: myoclonic
With special features: eyelid myoclonia
Myoclonic (sudden, irregular muscle jerks of short duration; < 400 ms)
Myoclonic atonic
Myoclonic tonic
Clonic (repetitive short contractions of agonist and antagonist muscular groups at a rate of 0.2–5 Hz
Tonic (sustained contraction of muscles for at least 3 s)
Atonic
Focal seizures
Unknown
Epileptic spasms

Table 2 Outline of the ILAE classification of focal seizures (Adapted from Berg et al. 2010, with permission)

Without impaired consciousness
With objective motor and/or autonomic symptoms (simple partial seizures)
With only subjective sensory or psychic phenomena (aura)
With impaired consciousness (complex partial seizures)
With generalization to tonic, clonic, or tonic–clonic seizures (secondary generalized seizures)

aura (subjective sensory or psychic phenomena only: sensitive, gustatory, olfactory, visual, auditory, emotional, déjà vu), *motor* (including simple motor phenomena and automatisms), and *autonomic*. An impairment of awareness or responsiveness is described as dyscognitive (old term: complex partial seizure). Focal seizures may evolve to bilateral convulsive seizures (old term: seizures with secondary generalization).

Generalized seizures are subdivided into tonic–clonic, absence, myoclonic, tonic, clonic, and atonic seizures (Table 1).

Generalized tonic–clonic seizures, also referred to as grand mal seizures, are readily recognized by laypersons. They typically start with an initial fall and immediate loss of consciousness, followed by tonic contraction of the body musculature. Contraction of respiratory muscles leads to forced exhalation and vocalization in the form of a cry or moan. The eyes deviate upwards and pupils dilate. Incontinence can occur during the tonic phase or later when the sphincter relaxes. During the tonic phase, the patient may bite his or her tongue or cheek and respiration is disrupted, leading to cyanosis. The initial rigidity gradually evolves into generalized jerking, the clonic phase. Generalized flexor spasms alternate with relaxation, causing irregular respiration which is often associated with salivation and lack of swallowing. Most tonic–clonic seizures end within 2 min and are followed by a postictal phase which is characterized by diffuse hypotonia, slow deep respirations, und unresponsiveness. The subsequent recovery over minutes or hours is marked by sleepiness, variable headache, and musculoskeletal soreness upon wakening. Persistent back pain is suggestive of a vertebral compression fracture during the tonic phase.

Typical absence seizures present as brief staring spells with an immediate return to consciousness; they usually last a few seconds. These seizures usually have their onset in childhood. Atypical absence continues for longer than a few seconds, involves falling, or has more complex automatisms and can be difficult to distinguish from complex partial seizures.

Myoclonic seizures are myoclonic jerks that result from epileptic discharges in the brain. Myoclonic jerks are sudden, brief, shock-like contractions which may occur in several epilepsy syndromes but also in nonepileptic diseases. The term "progressive myoclonus epilepsy" refers to several progressive disorders in which either epileptiform or nonepileptiform myoclonus and progressive neurological dysfunctions are the prominent features.

Atonic seizures describe seizures with a sudden loss of postural tone, in which the patient drops or slumps to the ground. They are also referred to as drop attacks or astatic seizures and may result in head contusions and teeth violations.

Grand mal seizures can be primarily generalized seizures or can evolve from focal seizures (bilateral convulsive seizures, old term: secondarily generalized seizures). After a first seizure, differentiation usually requires observation of the seizure by a second person. A hint towards generalized, not focally generated seizures is the occurrence when waking up and during the first 2 h after waking up (wake-up seizures). On the other hand, if focal seizures show very rapid spread of activity over both hemispheres, bilateral convulsive seizures of focal onset may be mistaken as generalized seizures. This may especially occur when epileptogenic lesions are in prefrontal, occipital, or rather silent brain areas.

Status epilepticus applies to seizures that are prolonged or that recur at a frequency too rapid to permit proper recovery of consciousness or awareness between the seizures. A number of varieties can be distinguished:

1. Grand mal status. Tonic–clonic seizures occur at a frequency so rapid that the patient remains unresponsive between individual seizures. If the patient becomes responsive between seizures, it is referred to as grand mal series.
2. Focal (simple partial) status epilepticus including epilepsia partialis continua. Epilepsia partialis continua is defined as spontaneous regular or irregular clonic muscular twitching affecting a limited part of the body, sometimes aggravated by action or sensory stimuli, occurring for a minimum of 1 h, and recurring at intervals of no more than 10 s.
3. Nonconvulsive (complex partial) status epilepticus. This is an epileptic episode without distinct motor phenomena but with a fluctuating confusional state. The EEG may show focal fluctuating or frequently recurring discharges. The episode may last several days or weeks.
4. Absence status.
5. Electrical status epilepticus during slow-wave sleep.

Febrile seizures are seizures that occur in febrile children between the ages of 6 months and 5 years who do not have an intracranial infection, metabolic disturbance, or history of afebrile seizures. They are the most common type of convulsive events in infants and young children; the incidence is 2–5% until the age of 5 years. They occur most frequently between the 18th and 24th months of age (90% below 3 years of age, 50% within the second year of life).

Febrile seizures are subdivided into two categories: simple (80–90%) and complex (10–20%). Simple febrile seizures last for less than 15 min, are generalized (without a focal component), and occur once in a 24-h period, whereas complex febrile seizures are prolonged (more than 15 min), are focal, or occur more than once in 24 h. Simple febrile seizures are not associated with subsequent epilepsy or cognitive deficits, whereas complex febrile seizures are linked with the development of temporal lobe epilepsy and hippocampal sclerosis. Whether temporal lobe epilepsy is the consequence of complex febrile seizures or the child has complex febrile seizure because the hippocampus was previously damaged by a prenatal or perinatal insult or by genetic predisposition is a matter of debate. The current concept is to consider the association between complex febrile seizures and temporal lobe epilepsy resulting from complex interactions between several genetic and environmental factors.

Simple febrile seizures are not an indication for MRI, whereas complex febrile seizures are (King et al. 1998; Bernal and Altman 2003). In patients with temporal lobe epilepsy, 30% of patients with hippocampal sclerosis as compared with 6% of patients without hippocampal sclerosis had complex febrile seizures in childhood (Falconer et al. 1964).

Seizures are classified as focal or generalized on the basis of clinical and/or EEG findings.

The EEG (Fig. 1) records voltages from electrodes spaced across the scalp, and characterizes signatures of seizure disorders known as spikes, sharp waves, spike-and wave complexes, or ictal evolving rhythms. Just as there are several seizure types, there are several EEG patterns that mark epilepsy. The EEG recording can be interictal (between seizures), ictal (during a seizure), or postictal (within the few minutes after a seizure). A single EEG will be abnormal interictally in about 50% of people with epilepsy, but EEG sensitivity can rise to 80% with three or four recording sessions or with the use of special electrodes, sleep deprivation, flashing lights, or hyperventilation. Normal interictal EEG findings never rule out epilepsy, and it is reasonable to treat people who have a good likelihood of a seizure even if they have normal interictal EEG findings. EEG findings are usually abnormal during a seizure, but a small percentage of people will have false-negative EEG findings even during an ictal event, because of a deeply placed or very small seizure focus.

To standardize EEG recordings and reporting, the international 10–20 system has been developed. Four anatomical landmarks, the nasion, the inion, and the right and left tragus are used for positioning of the EEG electrodes. The distances between adjacent electrodes are either 10 or 20% of the fronto-occipital or right–left distances. Each site has a letter to identify the lobe and a number to identify the location of the hemisphere. “C” refers to the central region, and ”z” refers to an electrode placed in the midline. Even numbers (2, 4, 6, 8) refer to electrode positions on the right hemisphere and odd numbers (1, 3, 5, 7) refer to those on the left hemisphere.

The time needed to acquire a routine EEG is typically only 20–30 min and the EEG will therefore unlikely capture a seizure. Long-term video–EEG monitoring has a high likelihood of recording seizures and allows one to compare the patient’s behavior with EEG activity. For video–EEG monitoring, patients are admitted to a specially equipped hospital room with television cameras and digitally recorded multichannel electroencephalography.

Since not all symptoms caused by epileptic seizures are likewise recognized as such by nonepileptologists, some illustrative examples are given below. However, it must be acknowledged that nonepileptic seizure events may mimic epilepsy because of an overlap of symptoms. The most frequent nonepileptic seizures are psychogenic seizures and syncopes. An overview of nonepileptic events is given in Table 3.

The following are examples for epileptic and nonepilepetic seizures.

For about 3 years a 42-year-old patient has experienced repeated epigastric qualm, understood to be heartburn.

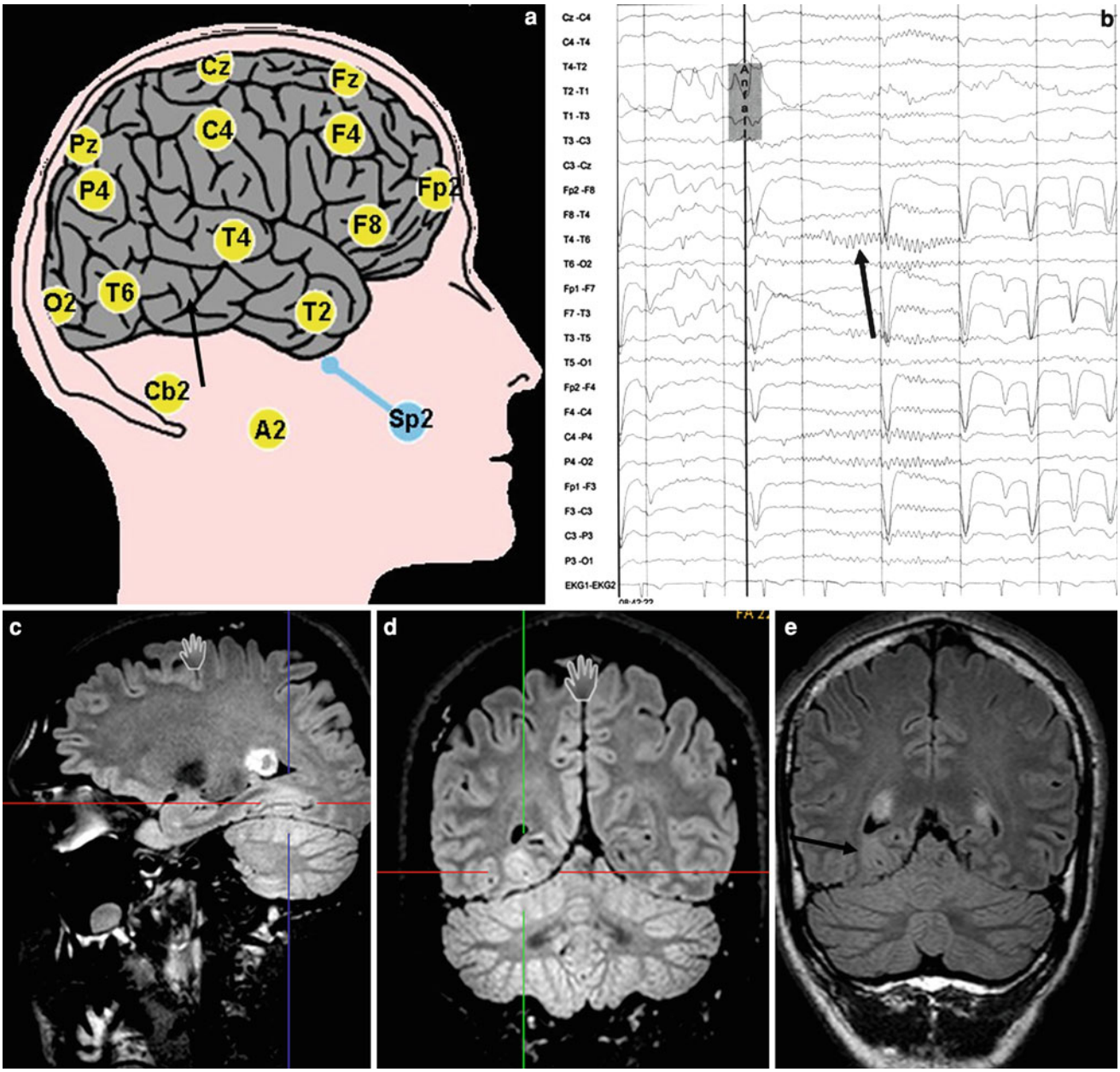

Fig. 1 EEG electrode positions of the international10/20 system (A): Right-sided electrodes have even, left-sided electrodes odd numbers. In an example of a 24 year old man with complex focal seizures since 18 years, the T4-T6 recording shows temporo-occipital ictal EEG activity (B) and helps to identify a small focal cortical dysplasia of the right lateral occipito-temporal gyrus (C, D: crosslines, E: arrow)

Gastroscopy findings were normal. The relatives reported that the patient is sometimes like a dreamer for about 30 s, does not respond appropriately when addressed, and shows smacking or swallowing. He sometimes says funny things not suitable for the situation. None of these events were recognized as epileptic. The patient now presents with a first tonic–clonic seizure. In fact, all reported symptoms are focal epileptic seizures of temporomesial origin. The classification is as follows: focal seizures with aura (epigastric) and motor symptoms (smacking or swallowing), impaired awareness, and now for the first time evolution from a focal to a bilateral convulsive seizure.

A 24-year-old woman was admitted to hospital after a first tonic–clonic seizure which occurred at 7.15 a.m., about 20 min after she rose from bed. The night before, she had a party and slept for only 3 h. She reported that she had never had seizures before. However, she confirmed that she has had impulsive myoclonic jerks in the early morning since the age of 14 years, but they were not recognized as epileptic. In fact, the patient suffers from generalized epilepsy

Table 3 Nonepileptic conditions that may mimic epileptic seizures

Type of disorder	Clinical description
Psychogenic seizures	Most common nonepileptic condition, urinary incontinence uncommon, possible psychiatric history, patients usually motionless or with agonistic-antagonistic movement patterns with closed eyes, which are forcefully kept closed
Syncope	Brief loss of consciousness, rapid return to normal, muscle jerking may occur at the end of syncope owing to hypoxia (convulsive syncope)
Transient ischemic attack	Sudden onset of neurological symptoms related to a vascular territory. Negative symptoms (aphasia, motor or sensory deficit) predominate
Hyperventilation	Deep and/or frequent breathing, perioral cyanosis, hand paresthesias, carpopedal spasms
Complex or classic migraine	Slow progression of neurological symptoms followed by headache, which may, however, be minimal or absent
Transient global amnesia	Sudden onset of isolated anterograde and retrograde amnesia for usually 2–8 h
Panic attack	Abrupt onset with intense feeling of fear, no loss of consciousness, autonomic features (tachycardia, nausea, sweating)
Sleep disorders (narcolepsy, cataplexy, periodic movements of sleep)	Narcolepsy: attacks of irrepressible sleep during daytime in patients with more or less continuous sleepiness Cataplexy: sudden loss of muscle tone, precipitated by laughter or excitement. No loss of consciousness Periodic movements of sleep—repeated rhythmic movements of the limbs
Vestibular disorders (benign positional vertigo, Meniere disease, labyrinthitis)	Dizziness, nystagmus, and vertigo predominate
Metabolic-toxic (endocrine, hypoglycemia, uremia, pheochromocytoma, thyroid dysfunction, carcinoid tumors, drug overdose or withdrawal)	Negative symptoms and vigilance disturbances predominate
Infectious (meningitis, encephalitis)	Fever, confusion, and vigilance disturbances predominate
Movement disorders, chorea and athetosis, tics and Tourette syndrome, focal dystonias, tremor, myoclonus	No loss of consciousness, involuntary movements predominate
In infants and children Sandifer syndrome Night terrors Breath-holding spells	Sandifer syndrome: sudden extension of the neck in an opistotonic position, often with twisting of the head. Hiatus hernia and/or gastroesophageal reflux Night terrors: age 18 months to 8 years. Arousal from deep sleep. Child starts screaming, sits up, and does not recognize its parents Breath-holding spells: age below 5 years. Harmless attacks provoked by fright, pain, anger, or frustration. The child initially cries, then holds its breath, becomes cyanotic and loses consciousness, and starts breathing again
Concussive convulsions	Rare non epileptic phenomenon within seconds after impact, typically in collision sports such as Football or Rugby. Initial period of tonic stiffening, followed by myoclonic jerks (up to 150 seconds), and rapid recovery of consciousness. No traumatic brain imaging abnormalities (McCrory et al. 1997)

with myoclonic and tonic–clonic seizures (juvenile myoclonic epilepsy).

A 35-year-old woman has suffered from sudden falls and consecutive bilateral jerking since the age of 15 years. The seizures last for up to 20 min. They are often refractory to benzodiazepines administered by paramedics. No clear provocation factor can be recognized. There are no further symptoms. The seizures are pharmacoresistant to five anticonvulsive drugs in different combinations. One seizure was observed in an epilepsy clinic. Here the jerking was recognized as fast agonistic–antagonistic movements of the arms and pedaling of the legs. Owing to the nonepileptic movement pattern, a diagnosis of psychogenic seizures could be made.

A 28-year-old man was admitted to hospital after an observed fall at a bus stop with consecutive clonic jerks for

about 10 s, then rapid reorientation. He had experienced similar events before, mostly from standing for a long time, but also one at a visit to a dentist. There were no further symptoms. In fact, the patient suffers from convulsive syncopes.

References

Berg AT, Berkovic SF, Brodie MJ, Buchhalter J, Cross JH, van Emde BW, Engel J, French J, Glauser TA, Mathern GW, Moshe SL, Nordli D, Plouin P, Scheffer IE (2010) Revised terminology and concepts for organization of seizures and epilepsies: Report of the ILAE commission on classification and terminology, 2005–2009. Epilepsia 51(4):676–685. doi:10.1111/j.1528-1167.2010.02522.x

Bernal B, Altman NR (2003) Evidence-based medicine: neuroimaging of seizures. Neuroimaging Clin N Am 13(2):211–224

Falconer MA, Serafetinides EA, Corsellis JA (1964) Etiology and pathogenesis of temporal lobe epilepsy. Arch Neurol 10: 233–248

King MA, Newton MR, Jackson GD, Fitt GJ, Mitchell LA, Silvapulle MJ, Berkovic SF (1998) Epileptology of the first-seizure presentation: a clinical, electroencephalographic, and magnetic resonance imaging study of 300 consecutive patients. Lancet 352(9133):1007–1011. doi:10.1016/S0140-6736(98)03543-0

McCrory PR, Bladin F, Berkovic SF (1997) Retrospective study of concussive convulsions in elite Australian rules and rugby league footballers: phenomenology, etiology, and outcome. BMJ 314(7075):171–174

Localization of Focal Seizures

Horst Urbach and Jörg Wellmer

Contents

Abstract

The semiology of a focal seizure without or prior to evolution to a bilateral convulsive (secondarily generalized) seizure may guide the radiologist to the location of the epileptogenic lesion. This information should be considered when planning and interpreting a MRI examination.

The radiologist's attention is directed to focal (partial) seizures, which are divided into focal seizures without impaired consciousness (old term: simple partial seizures), focal seizures with impaired consciousness (dyscognitive seizures; old term: complex partial seizures), and bilateral convulsive seizures (old term: seizures with secondary generalization). In focal seizures, the aura (defined as the initial part of a partial seizure that is remembered after the seizure has terminated) and/or the clinical symptoms (Table 1) often point to the region of the brain in which the seizures are generated (Urbach 2005):

- Focal motor or focal motor seizures with a march (Jacksonian seizure) → precentral gyrus. Focal motor seizures may be followed by a weakness of the involved muscle groups that lasts for up to several hours (Todd's paralysis).
- Versive seizures, which are tonic or clonic postural seizures with turning of the head and the eyes, and sometimes of the whole body to one side, usually away from the seizure focus. Sometimes, the patients exhibit a fencer's posture, extending one arm, looking down that arm, and flexing the opposite arm above the head. Quick ending of the seizure → motor cortex anterior to the precentral gyrus = supplementary motor area = Brodmann area 6, contralateral to the extended arm.
- Hypermotor activity mostly arising from sleep, with body turning along the horizontal axis, body rocking, crawling, crying, and grimacing with expression of fear, reacts appropriately immediately after the seizure, recalls items named during the seizure → anterior frontomesial, for example, anterior cingulate gyrus (Leung et al. 2008).

H. Urbach (✉)
Department of Neuroradiology, University Hospital Freiburg, Germany
e-mail: horst.urbach@uniklinik-freiburg.de

J. Wellmer
Ruhr-Epileptology, Department of Neurology, University Hospital Knappschaftskrankenhaus Bochum, Germany

H. Urbach (ed.), *MRI in Epilepsy*, Medical Radiology. Diagnostic Imaging,
DOI: 10.1007/174_2012_554, © Springer-Verlag Berlin Heidelberg 2013

Table 1 Symptoms of focal seizures

Anatomical description	Symptoms
Temporal lobe	
Mesial	Aura (epigastric, olfactory, gustatory, déjà vu, jamais vu) (80%) Oroalimentary automatisms (34%) Staring (40%) Arrest (20%) (Ipislateral) head turning (27%) Contralateral arm dystonia (38%) (Ipsilateral) nose wiping (rubbing of nose during or within 60 s of seizure termination) (50–85%)
Lateral	Aura (epigastric, olfactory, gustatory, déjà vu, jamais vu) (50%) Oroalimentary automatisms (45%) Staring (40%) Arrest (10%) (Ipislateral) head turning (20%) Contralateral arm dystonia (20%)
Frontal lobe	
Precentral gyrus	Simple partial motor seizures, tonic–clonic with or without Jacksonian march Partial myoclonus, predominantly distal Tonic postural motor seizures associated with clonic movements Partial unilateral clonic seizures Epilepsia partialis continua Reflex-triggered motor seizures
Premotor (supplementary motor area)	Bilateral asymmetric tonic and postural phenomena with adversion of the head and eyes (fencer's position), speech arrest
Mesial (cingulate gyrus, inferior bounder corpus callosum)	Ictal body turning along the horizontal axis (58%) Facial expression of anxiety and fear (40%) "Barking" (31%)
Frontal operuclum	Speech arrest, dysarthria, and/or vocalization in the dominant hemisphere, facial clonic jerks, tonic–clonic movements of arms and face, salivation, deglutition
Prefrontal dorsal	Forced thinking, eye-directed automatism, pseudocompulsive behavior, tonic deviation of eyes preceding head deviation (frontal eye field involvement)
Prefrontal ventral	
Frontolateral	Ictal body turning along the horizontal axis (6%), ictal body turning along an axis that produced sitting up (16%), restlessness (23%)
Fronto-orbital	Ictal body turning along an axis that produced sitting up (19%), restlessness (6%)
Parietal lobe	
Postcentral gyrus	Somatosensory seizures Lateralized ictal paresthesias, dysesthesias, or pain
Occipital lobe	Simple visual phenomena
Insula	Laryngeal discomfort, throacoabdominal constriction, or dyspnea followed by unpleasant paresthesias or focal motor manifestations Rapid seizure propagation induces a variety of visceral, motor, and somatosensory symptoms

Adapted from Elger CE. (2000), Leung et al. (2008), and Foldvary-Schaefer and Unnwongse (2011)

- Somatosensory perception as the earliest ictal symptom → postcentral gyrus.
- Visual symptoms of elementary or simple hallucinations, illusions, and visual loss → occipital lobe > anteromedial temporal or occipitotemporal lobe. Complex hallucinations (animals, people, scenes, etc.) and tunnel vision → anteromedial temporal or occipitotemporal, but not occipital lobe (Bien et al. 2000).

- Seizures with auditory symptoms → region of Heschl's gyrus. Although each hemisphere has bilateral innervation for auditory information, the contralateral ear is better represented in the auditory cortex. Sounds are therefore heard in the contralateral ear or bilaterally (Foldvary-Schaefer and Unnwongse 2011).
- Seizures with olfactory or gustatory symptoms → mesial temporal lobe.
- Vertiginous seizures (sensations of rotation or movement in all planes) → insular or temporoparietal cortex around the Sylvian fissure.
- Olfactory symptoms (unpleasant sensations, often associated with gustatory phenomena) → amygdala, olfactory bulb, insula, posterior orbitofrontal cortex (Foldvary-Schaefer and Unnwongse 2011).
- Autonomic symptoms within seizures are abdominal sensations, cephalic and thoracic sensations including pain, breathlessness, and altered breathing or heart rhythm, pallor or flushing, sweating, pupillary dilatation, vomiting, salivation, thirst, urinary incontinence, and genital sensations or orgasm. Abdominal or cephalic sensations are particularly common in mesial temporal lobe and insular epilepsy.
- Gelastic seizures (brief periods of laughter or grimacing with or without the feeling of cheerfulness)→ tuber cinereum, mesial temporal lobe.
- Epilepsia partialis continua (clonic or myoclonic seizures for hours or days, often also during sleep) → precentral gyrus.

Temporal lobe seizures and seizures from the precentral and postcentral gyri are easier to localize than seizures originating in other lobes. Frontal lobe seizures tend do generalize rapidly, postictal confusion is rather low, seizures are frequent and brief seizures, and most seizures occur during sleep. Most patients with parietal lobe seizures have no signs suggestive of involvement of the parietal lobe. Spread patterns are highly unpredictable, and only lateralized ictal paresthesias, dysesthesias, and pain are of localizing value.

Patients with occipital lobe seizures represent the smallest group referred to epilepsy surgery centers (less than 10% of patients). Occipital lobe seizures tend to spread rapidly to anterior areas. Multiple patterns of spread may be observed even in the same patient. Almost all patients with subjective symptoms describe visual phenomena such as hallucinations, illusions, amaurosis, and blurring of vision. Bright, colored, occasionally dark rings or spots and continuous or flashing simple geometric forms usually but not necessarily in the contralateral visual field are simple hallucinations pointing to involvement of the occipital and temporal lobes. In contrast, complex visual hallucinations such as animals, people, and scenes do not originate in the occipital lobe (Bien et al. 2000).

It should be kept in mind that seizure symptoms identified by interviewing patients or witnesses can be incomplete or the details may be sparse. Lateralizing hints may be remembered wrongly. The most objective way to sample clinical hints for the localization of the seizure onset is video–EEG recording of typical seizures. In practice this means that a MRI finding that was initially rated nonlesional is worth being reevaluated if new clinical information is available. The same is valid if in the later course of the diagnostic workup, localization information is acquired by PET, SPECT or MEG.

References

Bien CG, Benninger FO, Urbach H, Schramm J, Kurthen M, Elger CE (2000) Localizing value of epileptic visual auras. Brain 123(Pt 2): 244–253

Elger CE (2000) Semeiology of temporal lobe seizures: In: Oxbury JM, Polkey CE, DuchownyM (eds) Intractable focal epilepsy. pp 63–69

Foldvary-Schaefer N, Unnwongse K (2011) Localizing and lateralizing features of auras and seizures. Epilepsy Behav 20(2):160–166. doi:10.1016/j.yebeh.2010.08.034

Leung H, Schindler K, Clusmann H, Bien CG, Popel A, Schramm J, Kwan P, Wong LK, Elger CE (2008) Mesial frontal epilepsy and ictal body turning along the horizontal body axis. Arch Neurol 65(1):71–77. doi:10.1001/archneurol.2007.22

Urbach H (2005) Imaging of the epilepsies. Eur Radiol 15(3):494–500. doi:10.1007/s00330-004-2629-1

Epilepsy Syndromes

Horst Urbach, Robert Sassen, and Jörg Wellmer

Contents

Abstract

This chapter describes the ILAE classification of epilepsy syndromes and gives hints whether a MRI is likely normal or abnormal in a specific epilepsy syndrome.

In 1981 and 1989, the International League Against Epilepsy (ILAE) defined three groups of epilepsies:

1. Idiopathic epilepsies with a proven or presumed genetic cause
2. Symptomatic epilepsies with a proven structural cause
3. Cryptogenic epilepsies, in which a cause has not been found (yet)

In 2010, this classification was replaced by another three-tiered classification (Berg et al. 2010), in which (1) genetic, (2) structural and/or metabolic, and (3) unknown epilepsies are distinguished.

Both classifications represent a framework allowing for modifications in the future. In many epilepsy syndromes, genetic and environmental factors play a role. If one considers, e.g., a genetic defect (tuberous sclerosis complex) that causes structural lesions (cortical tubers and other lesions), the imperfectness of both classifications becomes obvious.

Some epilepsies with and without a known cause are distinctive disorders identifiable on the basis of a typical age of onset, specific EEG characteristics, seizure types, and often other features which, when taken together, permit a specific diagnosis. These epilepsies are denominated electroclinical syndromes (Berg et al. 2010). In addition to the electroclinical syndromes with strong developmental and genetic components, there are a number of entities that are not exactly electroclinical syndromes in the same sense but which represent clinically distinctive constellations on the basis of specific lesions or other causes. If a structural or metabolic cause is identified, the epilepsy syndrome is denominated on the basis of the structural or metabolic cause (Table 1). Some electroclinical syndromes are self-limiting at a specific age. Others cause an intermediate

H. Urbach (✉)
Department of Neuroradiology, University Hospital Freiburg, Germany
e-mail: horst.urbach@uniklinik-freiburg.de

R. Sassen
Department of Epileptology, University of Bonn, Bonn, Germany

J. Wellmer
Ruhr-Epileptology, Department of Neurology, University Hospital Knappschaftskrankenhaus Bochum, Germany

H. Urbach (ed.), *MRI in Epilepsy*, Medical Radiology. Diagnostic Imaging,
DOI: 10.1007/174_2012_555, © Springer-Verlag Berlin Heidelberg 2013

Table 1 Electroclinical syndromes and other epilepsies

Syndromes and epilepsies	Description	MRI
Electroclinical syndrome		
Neonatal period (up to 44 weeks' gestational age)		
Benign familial infantile epilepsy	Age: 1 week to 6 months Autosomal dominant: *KCNQ2* gene defect on chromosome band 20q13, *KCNQ3* gene defect on chromosome band 8q24 Unprovoked partial or generalized clonic seizures in the neonatal period or early infancy, benign course EEG: normal findings or focal abnormalities	MRI findings normal
Early myoclonic encephalopathy	Age: newborns Partial and myoclonic seizures within 10 days after birth EEG: burst suppression	Multiple different causes MRI dependent on cause
Ohtahara syndrome	Age: newborns Encephalopathic syndrome with tonic seizures within 10 days after birth EEG: burst suppression	Multiple different causes MRI dependent on cause
Infancy		
Epilepsy of infancy with migrating focal seizures	Age: within the first six months of life Encephalopathic syndrome with migrating, polymorphous seizures EEG: multifocal discharges	Initial MRI findings often normal Follow-up MRI may show brain atrophy. Hippocampal sclerosis has been described in around 15% of patients (Caraballo et al. 2011)
Infantile spasms (West syndrome)	Age: 3–8 months Encephalopathic syndrome with seizures consisting of sudden flexion, extension, or mixed extension–flexion of predominantly proximal and truncal muscles Duration of a few seconds. Series of up to 50 seizures Impaired consciousness during series EEG: hypsarrhythmia	MRI shows lesions in 61% of cases (Osborne et al. 2010)
Benign familial infantile epilepsy	Age: 3–9 months Focal seizures occurring in clusters, normal psychomotor development	MRI findings normal (Striano et al. 2007)
Severe myoclonic epilepsy of infancy (Dravet syndrome)	Age: around 6 months Encephalopathic syndrome with recurrent febrile hemiclonic, myoclonic, grand mal, and atypical absence seizures Poor prognosis and frequent death in childhood. Adults may show low intelligence, autism, and nocturnal grand mal seizures Mutations of the neuronal sodium channel type 1 subunit α gene (*SCN1A*) on chromosome band 2q24 (80%). The gene encodes a voltage-dependent sodium channel in the CNS, peripheral nerve system, and heart muscle EEG findings can be normal at onset, later multifocal abnormalities (spikes, spike- and-wave complexes, polyspikes, slow waves) occur (Guerrini et al. 2011) Myoclonic epilepsy in infancy may be considered a variant with a more benign course	Initial MRI findings often normal Follow-up MRI may show abnormalities in a minority of patients comprising cortical brain atrophy, hippocampal sclerosis (3–71%), gray matter–white matter demarcation loss, and other subtle cortical dysplasias (Siegler et al. 2005; Striano et al. 2007)
Myoclonic status in nonprogressive encephalopathies	Age: 1–5 years Several familial epilepsy syndromes with myoclonic features Chromosomal disorder (Angelman syndrome, 4p syndrome) in 50% of cases, family history of seizures in 20% of cases	MRI findings abnormal in 20% of cases

(continued)

Table 1 (continued)

Syndromes and epilepsies	Description	MRI
Childhood (1–12 years)		
Early-onset benign occipital epilepsy of childhood (Panayitopoulos syndrome)	Age: 1–14 years, mean 4.7 years Prolonged and nocturnal seizures Autonomic features (vomiting, pallor, sweating) followed by tonic eye deviation and impaired consciousness, may evolve to a hemiclonic or generalized seizure Excellent prognosis, treatment often unnecessary EEG: interictal runs of occipital sharp and slow wave complexes which attenuate on eye opening	MRI findings normal (Specchio et al. 2010)
Epilepsy with myoclonic atonic (previously astatic) seizures (Doose syndrome)	Age: 2–4 years Myoclonic jerks of arms, followed by astatic drops with loss of erect posture, jerking of facial muscles, with or without preserved consciousness Epileptic encephalopathy in some but not all children EEG: irregular spikes or polyspike-and wave complexes	MRI findings normal or abnormal
Benign epilepsy with centrotemporal spikes (rolandic epilepsy)	Age: 1–14 years, 75% starting between 7–10 years Male-to-female ratio 1.5 :1 Unilateral facial sensorimotor symptoms (30%), oropharyngolaryngeal symptoms (53%), speech arrest (40%), hypersalivation (30%) Progression to hemiconvulsions or grand mal seizures in around half of patients Brief seizures, lasting 1–3 min, mainly at sleep onset or just before awakening Centrotemporal spikes, mainly localized at the C3 and C4 electrodes, often bilateral, activated by drowsiness and slow (non-REM) sleep	MRI findings normal MRI not indicated (Gaillard et al. 2009)
Autosomal dominant nocturnal frontal lobe epilepsy	*CHRNA4* on chromosome band 20q13, *CHRNA2* on chromosome arm 8q, *CHRNB2* on chromosome band 1q21 Age: variable, onset usually in childhood or adolescence, persists throughout adult life 3 or more attacks lasting seconds to 3 min per night Clusters of brief nocturnal motor seizures with hyperkinetic or tonic manifestations EEG: ictal EEG findings often normal or obscured by movements, epileptiform discharges <10%	MRI findings normal
Late-onset benign occipital epilepsy of childhood (Gastaut type)	Age: 3–16 years, mean 8 years Frequent, brief, and diurnal seizures Initial visual hallucinations, simple partial seizures, postictal headache, rarely impaired consciousness Seizure remit within 2–5 years Increased familial risk of epilepsies (21–37%) and migraine (9–16%) EEG: interictal runs of occipital sharp and slow wave complexes which attenuate on eye opening	MRI findings normal
Idiopathic photosensitive occipital epilepsy	Age: 5–17 years Seizures induced by television and video games, diurnal, brief, visual hallucinations, tonic head and eye version EEG: occipital photoparoxysmal response at a wide range of flash frequencies	MRI findings normal
Epilepsy with myoclonic absence	Age: through childhood with a peak at 7 years Myoclonic absences with rhythmic jerking, mainly of the shoulders, arms, and legs. EEG: 3-Hz spikes and waves	MRI findings normal (Caraballo et al. 2011)

(continued)

Table 1 (continued)

Syndromes and epilepsies	Description	MRI
Lennox–Gastaut syndrome	Age: 1–7, mean 2 years Encephalopathic syndrome with multiple types of drug-resistant generalized seizures, drop attacks, mental retardation EEG: diffuse slow spikes and waves	Multiple different causes MRI dependent on cause
Epileptic encephalopathy with continuous spikes and waves during sleep	Age: 4–5 years Deterioration of neuropsychological and motor functions associated with or independent of the epileptic disorder EEG: continuous spikes and waves during slow sleep	MRI findings normal
Landau–Kleffner syndrome	Age: 3–8 Progressive loss of language functions after the age of 2 Waking EEG: burst of temporal or temporo-occipital spike and wave discharges. Continuous spike and wave discharges during slow sleep in 85% of cases	MRI findings normal
Childhood absence epilepsy	Age: 4–14 years Skin pallor, staring view for a few seconds, immediate return to consciousness Amnesia for episodes Rhythmic movements of arms, eyes, and head Duration: a few seconds Up to 100 seizures per day EEG: 3-Hz spikes and waves	MRI findings normal MRI not indicated (Gaillard et al. 2009)
Adolescence (12–18 years) and adulthood (> 18 years)		
Juvenile absence epilepsy	Age: 5–20 years Absence, generalized tonic–clonic (80%), and myoclonic (20%) seizures	MRI findings normal MRI not indicated (Gaillard et al. 2009)
Juvenile myoclonic epilepsy (Janz syndrome)	Age: 14–17 years Susceptibility locus on chromosome band 6q12-p11-12 (*EJM1*) or 15q14 (*EJM2*) Repetitive myoclonic jerks of shoulders and arms, preserved consciousness, duration 2–3 s EEG: polyspikes and waves	MRI findings normal MRI not indicated (Gaillard et al. 2009)
Epilepsy with generalized tonic–clonic seizures alone (wake-up grand mal epilepsy)	Age: 6–years to adulthood Generalized tonic–clonic seizures typically occurring after awakening EEG: generalized spikes and waves	MRI findings normal Cave: secondarily generalized tonic–clonic seizures
Progressive myoclonic epilepsies	Group of disorders with autosomal recessive or mitochondrial inheritance Myoclonic seizures, tonic–clonic seizures, and progressive neurological dysfunction	Multiple different causes MRI dependent on cause
Familial mesial temporal lobe epilepsy	Genetically heterogenous Age: onset in adolescence or adulthood Often prominent ictal déjà vu, dreamlike state, fear, and nausea, with simple partial and complex partial seizures and infrequent secondary generalization.	MRI findings normal (Crompton et al. 2010)
Familial lateral temporal lobe epilepsy	Idiopathic or autosomal dominant gene (*LGI1* on chromosome band 10q24, OMIM 600512) partial epilepsy with auditory features Age: onset 10–30 years Recurrent auditory aura usually followed by generalized seizures Low seizure frequency, good drug response	MRI findings normal (Michelucci et al. 2009)

(continued)

Table 1 (continued)

Syndromes and epilepsies	Description	MRI
Less specific age relationship		
Familial focal epilepsy with variable foci	Childhood to adulthood	MRI findings normal (Callenbach et al. 2003)
Reflex epilepsies, e.g., primary reading epilepsy	Primary reading epilepsy: age of onset adolescence, sensorimotor or motor speech aura occurring while reading, jaw jerks, and, if reading is continued, generalized seizure	MRI findings normal
Distinctive constellations		
Mesial temporal lobe epilepsy with hippocampal sclerosis		
Rasmussen encephalitis		
Hypothalamic hamartoma with gelastic seizures		
Hemiconvulsion–hemiplegia–epilepsy		
Epilepsy due to a structural–metabolic cause		
Malformations of cortical development (hemimegalencephaly, heterotopias, etc.)		
Neurocutaneous syndromes (tuberous sclerosis complex, Sturge–Weber syndrome, etc.)		
Tumor		
Infection		
Trauma		

Adapted from Berg et al. (2010) with permission

grade of impairment or a devastating and progressive disease process, which is called encephalopathic syndrome and is defined by the temporal relationship between the onset of epileptic seizures, ictal and interictal EEG activity, and the loss of cognitive and or motor/sensory functions (Berg et al. 2010).

It is recommended to use MRI in evaluating patients with new seizures or seizures not fully controlled by medication unless a traditional genetic (idiopathic) electroclinical syndrome is identified with confidence (Berg et al. 2010).

References

Berg AT, Berkovic SF, Brodie MJ, Buchhalter J, Cross JH, van Emde Boas W, Engel J, French J, Glauser TA, Mathern GW, Moshe SL, Nordli D, Plouin P, Scheffer IE (2010) Revised terminology and concepts for organization of seizures and epilepsies: report of the ILAE commission on classification and terminology, 2005–2009. Epilepsia 51(4):676–685. doi:10.1111/j.1528-1167.2010.02522.x

Callenbach PM, van den Maagdenberg AM, Hottenga JJ, van den Boogerd EH, de Coo RF, Lindhout D, Frants RR, Sandkuijl LA, Brouwer OF (2003) Familial partial epilepsy with variable foci in a dutch family: clinical characteristics and confirmation of linkage to chromosome 22q. Epilepsia 44(10):1298–1305

Caraballo RH, Darra F, Fontana E, Garcia R, Monese E, Dalla Bernardina B (2011) Absence seizures in the first 3 years of life: an electroclinical study of 46 cases. Epilepsia 52(2):393–400. doi:10.1111/j.1528-1167.2010.02926.x

Crompton DE, Scheffer IE, Taylor I, Cook MJ, McKelvie PA, Vears DF, Lawrence KM, McMahon JM, Grinton BE, McIntosh AM, Berkovic SF (2010) Familial mesial temporal lobe epilepsy: a benign epilepsy syndrome showing complex inheritance. Brain 133(11):3221–3231. doi:10.1093/brain/awq251

Gaillard WD, Chiron C, Cross JH, Harvey AS, Kuzniecky R, Hertz-Pannier L, Vezina LG (2009) Guidelines for imaging infants and children with recent-onset epilepsy. Epilepsia 50(9):2147–2153. doi:10.1111/j.1528-1167.2009.02075.x

Guerrini R, Striano P, Catarino C, Sisodiya SM (2011) Neuroimaging and neuropathology of Dravet syndrome. Epilepsia 52(Suppl 2): 30–34. doi:10.1111/j.1528-1167.2011.02998.x

Michelucci R, Pasini E, Nobile C (2009) Lateral temporal lobe epilepsies: clinical and genetic features. Epilepsia 50(Suppl 5):52–54. doi:10.1111/j.1528-1167.2009.02122.x

Osborne JP, Lux AL, Edwards SW, Hancock E, Johnson AL, Kennedy CR, Newton RW, Verity CM, O'Callaghan FJ (2010) The underlying etiology of infantile spasms (West syndrome): information from the United Kingdom Infantile Spasms Study (UKISS) on contemporary causes and their classification. Epilepsia 51(10):2168–2174. doi:10.1111/j.1528-1167.2010.02695.x

Siegler Z, Barsi P, Neuwirth M, Jerney J, Kassay M, Janszky J, Paraicz E, Hegyi M, Fogarasi A (2005) Hippocampal sclerosis in severe myoclonic epilepsy in infancy: a retrospective MRI study. Epilepsia 46(5):704–708. doi:10.1111/j.1528-1167.2005.41604.x

Specchio N, Trivisano M, Di Ciommo V, Cappelletti S, Masciarelli G, Volkov J, Fusco L, Vigevano F (2010) Panayiotopoulos syndrome: a clinical, EEG, and neuropsychological study of 93 consecutive patients. Epilepsia 51(10):2098–2107. doi:10.1111/j.1528-1167.2010.02639.x

Striano P, Mancardi MM, Biancheri R, Madia F, Gennaro E, Paravidino R, Beccaria F, Capovilla G, Dalla Bernardina B, Darra F, Elia M, Giordano L, Gobbi G, Granata T, Ragona F, Guerrini R, Marini C, Mei D, Longaretti F, Romeo A, Siri L, Specchio N, Vigevano F, Striano S, Tortora F, Rossi A, Minetti C, Dravet C, Gaggero R, Zara F (2007) Brain MRI findings in severe myoclonic epilepsy in infancy and genotype-phenotype correlations. Epilepsia 48(6):1092–1096. doi:10.1111/j.1528-1167.2007.01020.x

The Term "Epileptogenic Lesion" and How to Use it

Horst Urbach

Contents

Abstract

This chapter describes how to use the terms "epileptogenic lesion" and "typically epileptogenic lesion".

An *epileptogenic lesion* is defined as a radiographic lesion that causes seizures (Rosenow and Luders 2001). Although the radiologist does not know whether a radiographic lesion indeed causes epileptogenic seizures, some radiographic lesions are so typically associated with epileptic seizures that at least the term *typically epileptogenic lesion* is appropriate.

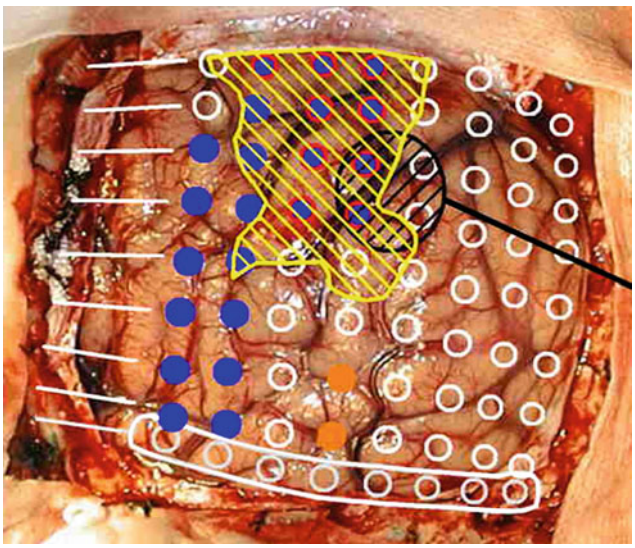

Fig. 1 Digital photogram of the brain surface before placement of a subdural 8 × 8 grid. A second photogram was taken after grid placement and digitally replaced by a schematic drawing detailing the results of electrical stimulations and ictal/ intraictal EEG activity. *Blue grid contacts* represent the eloquent zone, which is the motor cortex in this case. The *black area* represents the epileptogenic lesion, defined as the radiographic lesion that causes the seizures. The *yellow area* is the seizure onset zone, defined as the area from which the clinical seizures are generated. The seizure onset zone is often, but not necessarily, congruent with the epileptogenic zone, defined as the cortex area indispensable for the generation of seizures

H. Urbach (✉)
Department of Neuroradiology,
University Hospital Freiburg, Germany
e-mail: horst.urbach@uniklinik-freiburg.de

H. Urbach (ed.), *MRI in Epilepsy*, Medical Radiology. Diagnostic Imaging,
DOI: 10.1007/174_2012_557, © Springer-Verlag Berlin Heidelberg 2013

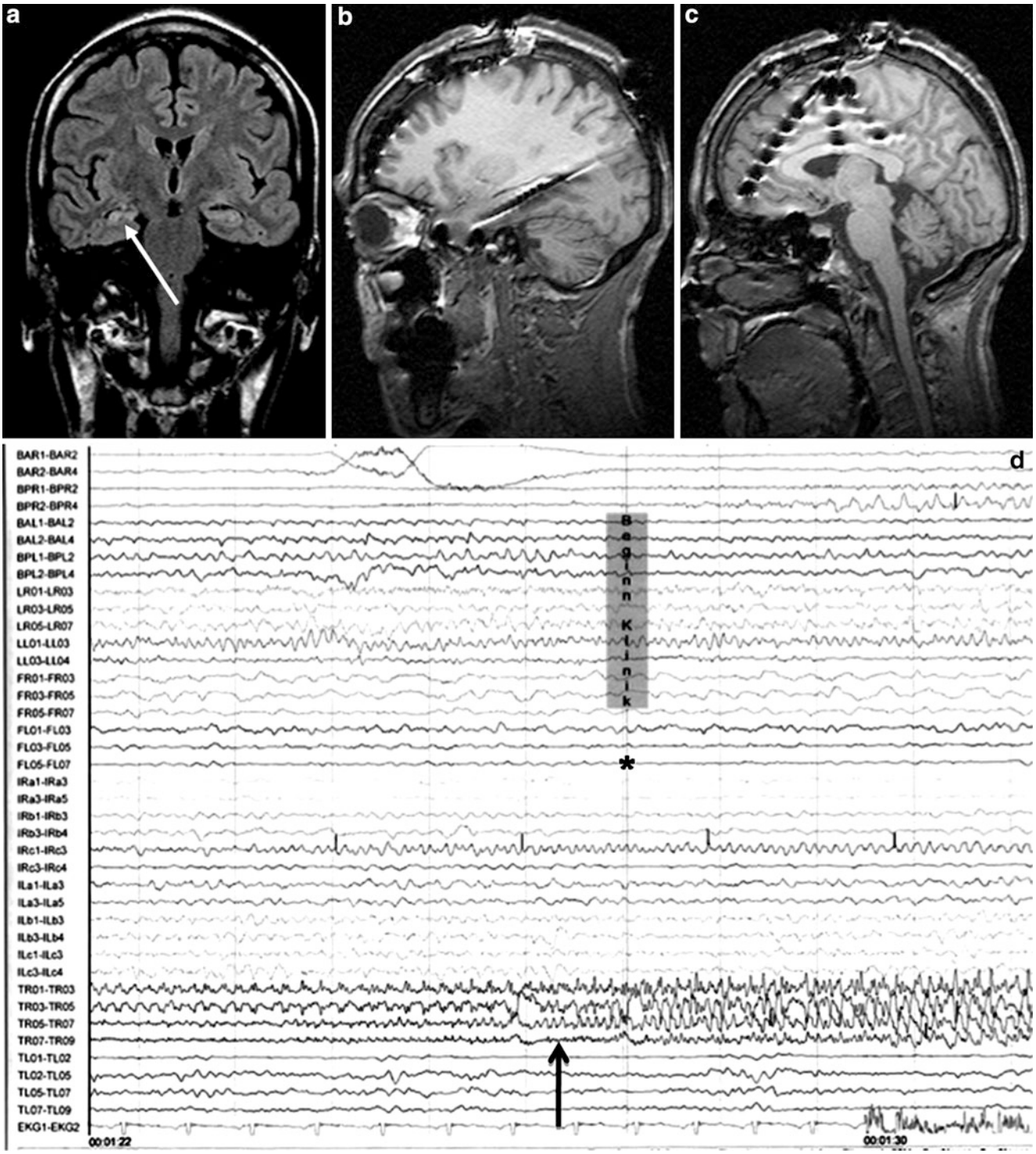

Fig. 2 Epileptogenic lesion and symptomatogenic zone. A 40-year-old woman suffered from complex focal seizures with a fearful face and body rocking. The symptoms thus pointed to the mesial frontal lobe as the origin. MRI shows right-sided hippocampal sclerosis (**a**, *arrow*). Simultaneous video and EEG recordings from interhemispheric (**c**) and convexity strip and intrahippocampal depth (**b**) electrodes show seizures starting in the right hippocampus (**d**, *arrow*). Clinical symptoms start around 1 s afterwards (**d**, *asterisk*)

To achieve freedom from seizures following epilepsy surgery, in some but not all cases not only the epileptogenic lesion itself but also some perilesional tissue must be removed. Conceptually, it is the *epileptogenic area* that has to be removed, which is defined as cortical area indispensable for the generation of seizures. Practically, it is the

seizure onset zone which it is intended to be removed, and this is defined as the brain area in which ictal EEG activity starts. The epileptogenic lesion usually shows at least some overlap with the seizure onset zone and is therefore a good indicator for its localization (Fig. 1).

Other frequently used terms are *irritative area*, defined as the brain area with interictal EEG activity, *eloquent cortex*, defined as the cortex area with important functions such as language, motor, and visual field functions, and *symptomatogenic area*, defined as the brain area in which epileptogenic activity leads to clinical symptoms. If epileptogenic activity spreads rapidly, the epileptogenic lesion and the symptomatogenic area can be far from each other (Fig. 2). Another term is the *functional deficit zone*, defined as the region of the cortex that in the interictal period is functionally abnormal, as indicated by neurological examination, neuropsychological testing, and functional imaging or nonepileptiform EEG or MEG abnormalities.

Reference

Rosenow F, Luders H (2001) Presurgical evaluation of epilepsy. Brain 124(9):1683–1700

What To Do After a First Seizure?

Horst Urbach

Contents

Abstract

This chapter describes the workup with MRI after a first seizure, which is highly dependent on the type of the seizure and the age at presentation.

A first seizure often refers to a bilateral convulsive seizure (old term: generalized tonic–clonic seizure) noticed as a frightening and traumatic event by the observers. However, around 17% of patients have had prior tonic–clonic seizures and 28% have had other epilepsy syndromes, including absence seizures, myoclonic seizures, aura phenomena, and other syndromes.

After the patient with a first seizure has been stabilized, one has to determine if the event was really a seizure, which is typically based on the history obtained from a reliable observer and a clinical examination looking for ictal sequelae such as open eyes, (lateral) tongue bite, enuresis, cyanosis, hypersalivation, and postictal sleepiness.

The differential diagnosis of a single seizure is broad (see Table 3 in "Classification of Epileptic Seizures"). It includes transient ischemic attacks, syncope, migraine, drug reaction or intoxication, mental disorders such as psychogenic seizures, and rarely movement disorders (Krumholz 1999; Beghi 2008).

The next step is to determine the cause of the seizure and to distinguish whether the seizure is acute symptomatic, provoked, or unprovoked. An acute symptomatic or situation-related seizure occurs in the presence of an acute disease with some immediately recognizable causes (e.g., meningitis, hypoglycemia, hyponatremia) often requiring prompt diagnosis and treatment (Wiebe et al. 2008).

H. Urbach (✉)
Department of Neuroradiology,
University Hospital Freiburg, Germany
e-mail: horst.urbach@uniklinik-freiburg.de

H. Urbach (ed.), *MRI in Epilepsy*, Medical Radiology. Diagnostic Imaging,
DOI: 10.1007/174_2012_558, © Springer-Verlag Berlin Heidelberg 2013

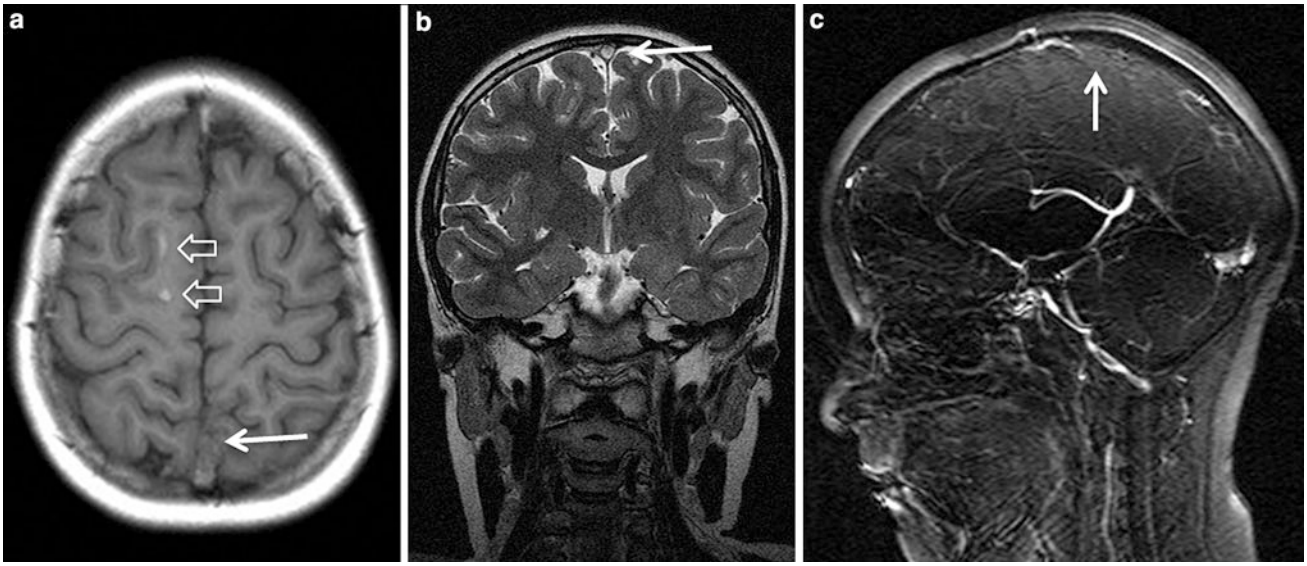

Fig. 1 An 8-year old girl presented with two focal motor seizures and postictal left arm paralysis. MRI shows superior sagittal sinus thrombosis (**a**–**c**, *arrows*) with two small hemorrhages at the gray matter–white matter junction in the right frontal lobe (**a**, *hollow arrows*)

A provoked seizure requires a seizure-provoking factors, e.g., sleep deviation. An unprovoked seizure does not require an immediate precipitating event and suggests the possibility of an underlying epilepsy syndrome, which is of genetic, structural–metabolic, or unknown cause (Herman 2004).

The risk of recurrence of unprovoked seizure within the first 2 years is around 40% (Berg and Shinnar 1991), and abnormalities on clinical examination or on electroencephalography (EEG) and focal seizures are predictive of further seizures. The EEG findings after a first unprovoked seizure are significantly abnormal in 29 cases (8–50%) of cases (Krumholz et al. 2007). MRI reveals significant abnormal findings in at least 10–15% of patients (King et al. 1998; Wiebe et al. 2008; Pohlmann-Eden and Newton 2008). Around 25% of patients with a first seizure have EEG-confirmed genetic epilepsies, and in these patients MRI—by definition—does not show a lesion. Note, however, that bilateral EEG discharges may have rapidly spread from a single, typically midline-near, often occipital epileptogenic lesion. In these rare cases, a focal (partial) epilepsy syndrome would be misclassified as generalized epilepsy syndrome (King et al. 1998).

How and when a patient with a first seizure should be "imaged" depends apart from the scanner availability on the suspected cause of the seizure.

In patients with acute symptomatic seizures, the underlying disease must be quickly recognized and adequately treated, and in these patients unenhanced CT to rule out an unexpected disease is sometimes sufficient. However, some clinical constellations, e.g., suspected sinus thrombosis, may require additional imaging such as CT angiography, MRI, and sometimes even catheter angiography (Fig. 1, 2). CSF examination is recommended in children (except for infants younger than 6 months of age) and adults only when cerebral infection is suspected or fever is present which cannot be explained by an extracranial origin (Hirtz et al. 2000; Beghi 2008).

In patients with unprovoked seizures and suspected genetic epilepsies derived from the clinical history, patient's age, and especially EEG findings, "routine" MRI is performed to exclude an unexpected underlying lesion. EEG is more helpful if it is performed within the first 24 h following a seizure (King et al. 1998). The diagnostic yield of additional sleep-deprived EEG is uncertain (King et al. 1998; Schreiner and Pohlmann-Eden 2003).

In patients with unprovoked, presumably focal seizures, an epilepsy-dedicated MRI protocol should be performed. In these patients, an initial CT scan to rule out an unexpected disease and a later high-resolution MRI scan when the patient is stable and able to tolerate an examination time of around 30 min should be performed.

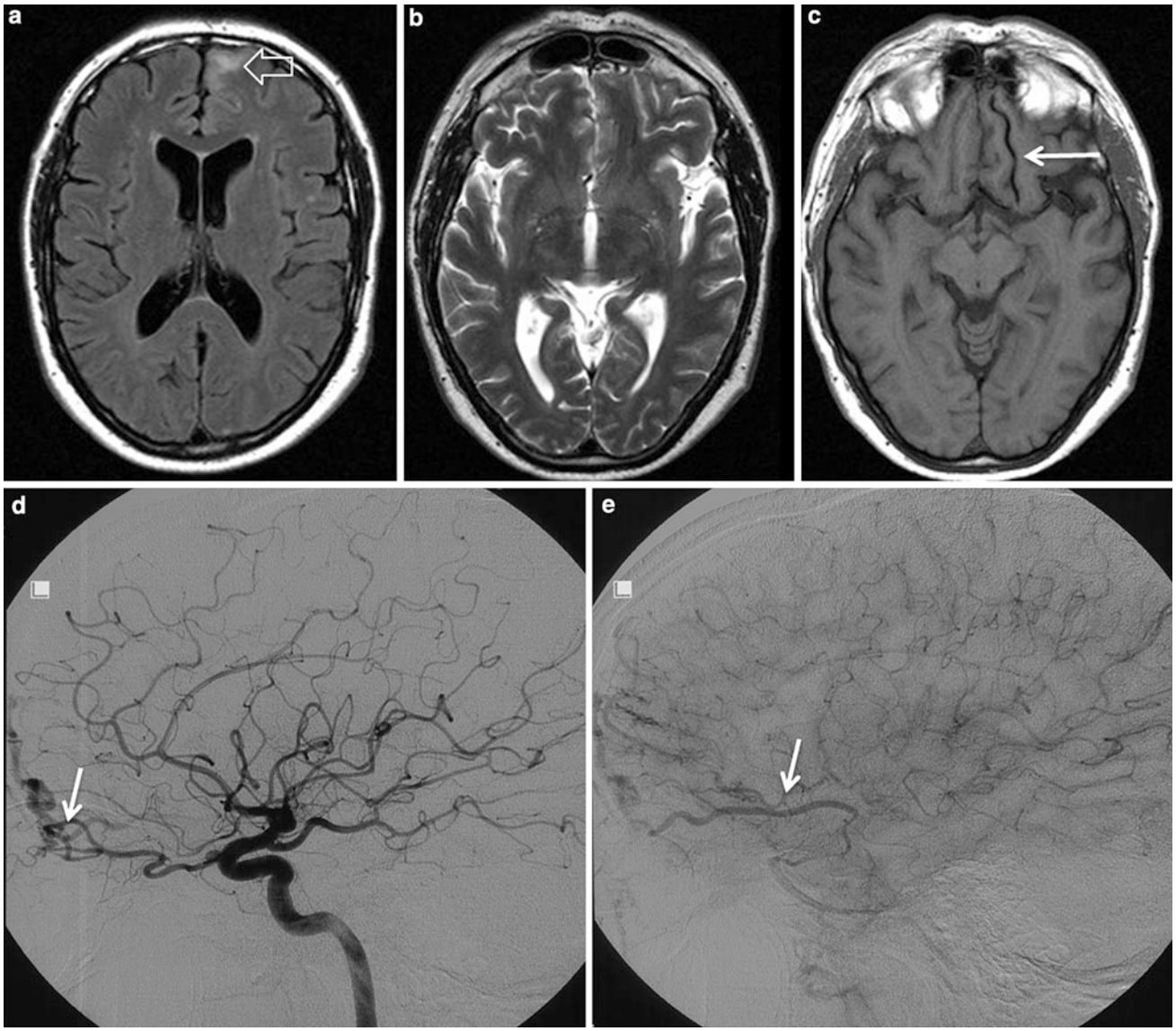

Fig. 2 Dural a. v. fistula. A 53-year-old man presented with two tonic–clonic seizures. MRI shows circumscribed edema in the left frontal lobe (**a**, *hollow arrow*) and an abnormal vessel running in the left sulcus rectus (**c**, *arrow*). The digital subtraction angiogram of the left internal carotid artery shows a frontobasal dural arteriovenous fistula fed via ethmoidal arteries (**d**, *arrow*) and confirms the abnormal vessel as a draining vein (**e**, *arrow*)

References

Beghi E (2008) Management of a first seizure. General conclusions and recommendations. Epilepsia 49(Suppl 1):58–61. doi:10.1111/j.1528-1167.2008.01452.x

Berg AT, Shinnar S (1991) The risk of seizure recurrence following a first unprovoked seizure: a quantitative review. Neurology 41(7): 965–972

Herman ST (2004) Single unprovoked seizures. Current treatment options in neurology 6(3):243–255

Hirtz D, Ashwal S, Berg A, Bettis D, Camfield C, Camfield P, Crumrine P, Elterman R, Schneider S, Shinnar S (2000) Practice parameter: evaluating a first nonfebrile seizure in children. Report of the Quality Standards Subcommittee of the American Academy of Neurology, the Child Neurology Society, and the American Epilepsy Society. Neurology 55(5):616–623

King MA, Newton MR, Jackson GD, Fitt GJ, Mitchell LA, Silvapulle MJ, Berkovic SF (1998) Epileptology of the first-seizure presentation: aclinical, electroencephalographic, and magnetic resonance imaging study of 300 consecutive patients. Lancet 352(9133):1007–1011. doi:10.1016/S0140-6736(98)03543-0

Krumholz A (1999) Nonepileptic seizures: diagnosis and management. Neurology 53(5 Suppl 2):S76–S83

Krumholz A, Wiebe S, Gronseth G, Shinnar S, Levisohn P, Ting T, Hopp J, Shafer P, Morris H, Seiden L, Barkley G, French J (2007) Practice parameter: evaluating an apparent unprovoked first seizure in adults (an evidence-based review). Report of the Quality Standards Subcommittee of the American

Academy of Neurology and the American Epilepsy Society. Neurology 69(21):1996–2007. doi:10.1212/01.wnl.0000285084.93652.43

Pohlmann-Eden B, Newton M (2008) First seizure: EEG and neuroimaging following an epileptic seizure. Epilepsia 49(Suppl 1):19–25. doi:10.1111/j.1528-1167.2008.01445.x

Schreiner A, Pohlmann-Eden B (2003) Value of the early electroencephalogram after a first unprovoked seizure. Clin Electroencephalogr 34(3):140–144

Wiebe S, Tellez-Zenteno JF, Shapiro M (2008) An evidence-based approach to the first seizure. Epilepsia 49(Suppl 1):50–57. doi:10.1111/j.1528-1167.2008.01451.x

How to Perform MRI

Horst Urbach

Contents

Abstract

This chapter provides Epilepsy-dedicated MRI protocols and useful informations regarding angulation, spatial resolution, and contrast to noise ratios.

1 Introduction

Patients with focal (partial) epilepsies in which an epileptogenic lesion has not been found (yet) should be studied using magnetic resonance (MR) scanners with a magnetic field strength B_0 of at least 1.5 Tesla. Theoretically and in clinical practice however, 3 Tesla scanners have advantages.

2 Theoretical Considerations

In accordance with the increasing number of parallel spins at higher field strengths, the MR signal is proportional to the magnetic field strength B_0 (signal-to-noise ratio proportional to B_0). The signal theoretically doubles from 1.5 to 3 Tesla; in reality, it increases by a factor of around 1.7–1.8. This signal gain can be utilized to increase the contrast-to-noise ratio and the spatial resolution or to decrease the acquisition time (Willinek and Kuhl 2006; Willinek and Schild 2008). One should always keep in mind that the MR signal decreases with the square of B_0 if the slice thickness is halved or the scan matrix is doubled.

High RF energy deposition is a theoretical limitation of 3 Tesla MRI. RF energy deposition scales with the square of B_0 and is monitored by measuring the specific absorption rate. The specific absorption rate must not exceed 4 W/kg over a 15-min period. For comparison, the RF energy deposition of most mobile phones is in the range 0.5–0.75 W/kg. High RF energy deposition can be compensated for with parallel data acquisition. Parallel data acquisition lowers the RF energy deposition by reducing the number of

H. Urbach (✉)
Department of Neuroradiology,
University Hospital Freiburg, Germany
e-mail: horst.urbach@uniklinik-freiburg.de

H. Urbach (ed.), *MRI in Epilepsy*, Medical Radiology. Diagnostic Imaging,
DOI: 10.1007/174_2012_559, © Springer-Verlag Berlin Heidelberg 2013

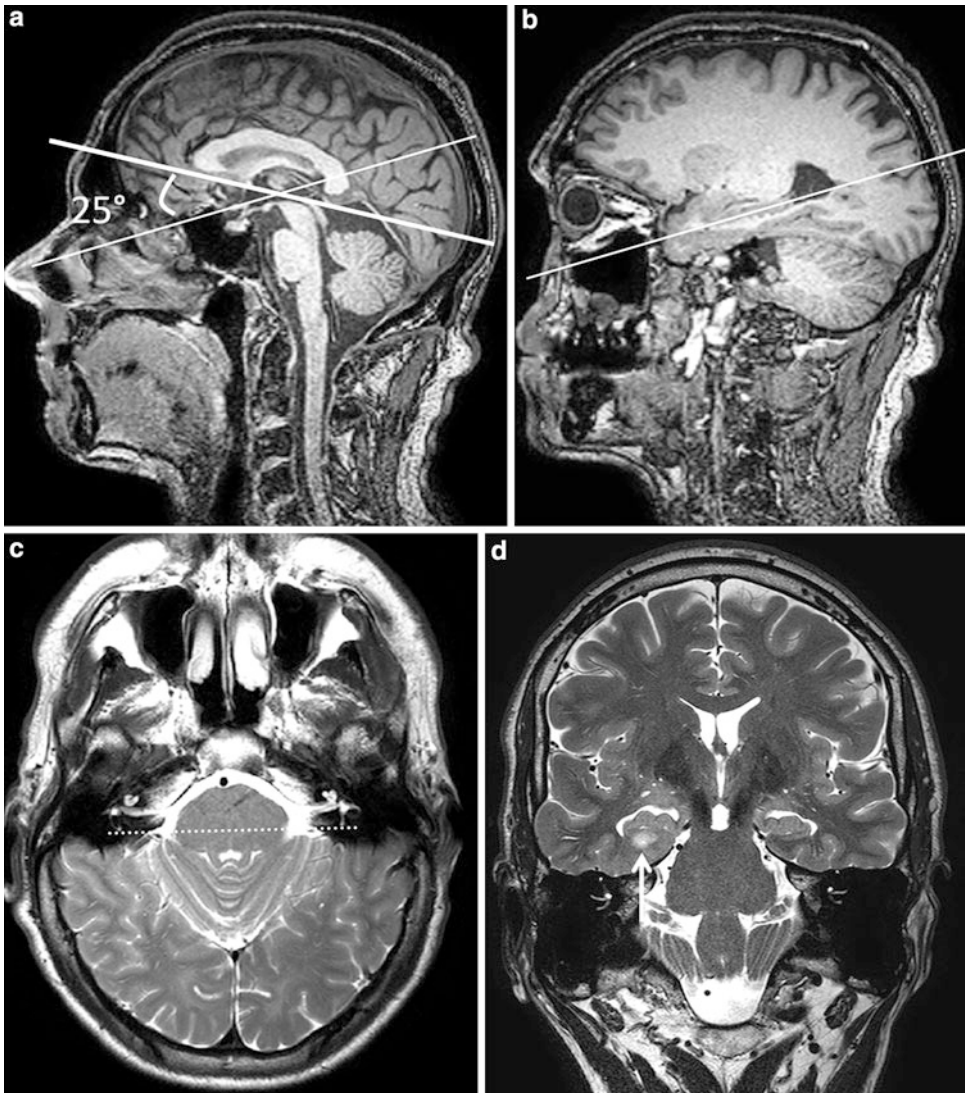

Fig. 1 The midsagittal image of a 3D T1-weighted gradient echo sequence (**a**) is chosen to align axial slices parallel to the commissura anterior–commissura posterior line. A parasagittal slice displaying the hippocampus is chosen to align slices parallel to the hippocampus (**b**). An axial T2-weighted sequence displaying the inner ear is acquired to avoid tilting in the coronal plane (**c**). In this example, the *dotted line* connects the posterior semicircular canals and shows no tilting in the coronal plane. Now, high-resolution coronal slices can be used for side comparisons. The 2-mm-thick coronal slice through the hippocampal heads (**d**) shows the semicircular canals in one plane. A small hyperintense lesion in the white matter of the parahippocampal gyrus just underneath the hippocampal head (*arrow*) was histologically a WHO grade I ganglioglioma

phase-encoding readouts (determined by the reduction factor R) for a given echo time, or it allows reduction of echo-train lengths, yielding a shorter, more effective echo time (Pruessmann et al. 1999; Bammer et al. 2001). This allows a substantial reduction in image distortion and improves image quality. In addition, the shorter echo time is more motion resistant and reduces blurring in the image.

The MR signal is proportional to the square root of R and the square root of the number of excitations. If R and the number of excitations are increased, the net signal and acquisition time are the same. However, the image can appear different when using parallel data acquisition, and although the images are noisier, specific structures of interest can be assessed better (see Fig. 1 in "MRI of Children").

The susceptibility ϖ is defined as the extent to which a material becomes magnetized when placed in a magnetic field. The susceptibility is proportional to the magnetic field strength B_0; therefore, all kinds of susceptibility artifacts are more pronounced in 3 T MRI. Important susceptibility-related artifacts are the signal loss around metallic implants such as intracranial electrodes and aneurysm clips and geometric distortions at interfaces between soft tissue and bone or air, especially at the skull base. Again, parallel-imaging techniques help to reduce these artifacts by reducing the echo-train length. Moreover, stronger susceptibility at 3 Tesla facilitates the detection of subtle hemosiderin-containing or calcified lesions, which can be overlooked with 1.5 Tesla scanners.

3 Clinical Practice

Three Tesla scanners generate 2–3-mm-thick slices with good contrast within an acceptable acquisition time per sequence. Epilepsy patients are often unable to remain quiet for sequences lasting longer than around 5 min. The spatial

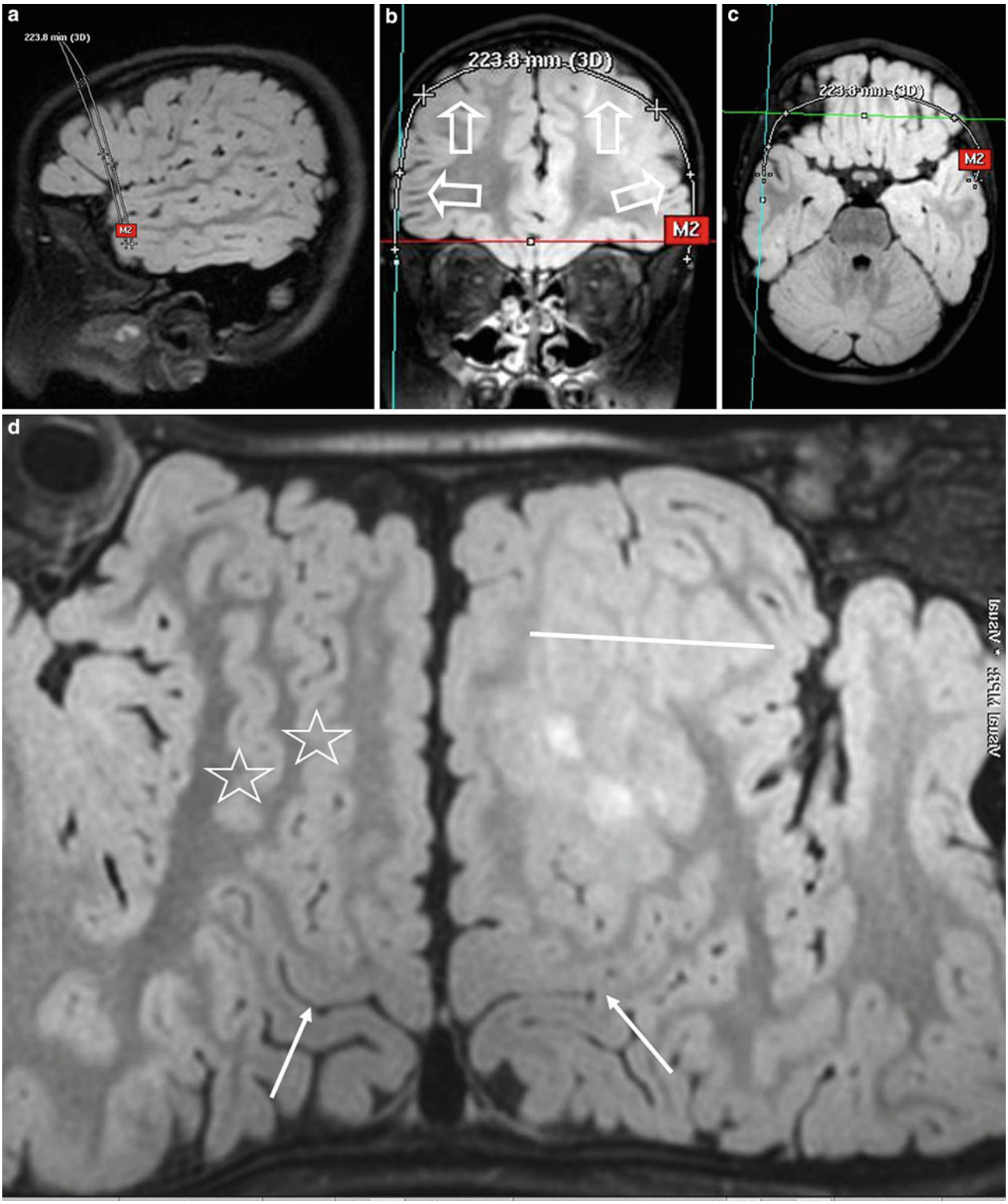

Fig. 2 Planar surface ("pancake") reformattion of a sagittal 3D fluid-attenuated inversion recovery fast spin echo sequence with isotropic voxel. A path is created along the brain surface on a coronal reformatted image (**b**, *hollow arrows*). The brain surface is unfolded along this path to facilitate anatomical orientation in the frontal lobes. On the unaffected right side, the superior and inferior frontal sulci are marked with *asterisks* (**d**). *Arrows* mark the hand knob of the central sulcus and the *line* marks the craniocaudal extension of a type IIB focal cortical dysplasia (**d**). The dysplasia reaches the precentral sulcus, but the precentral gyrus is not affected

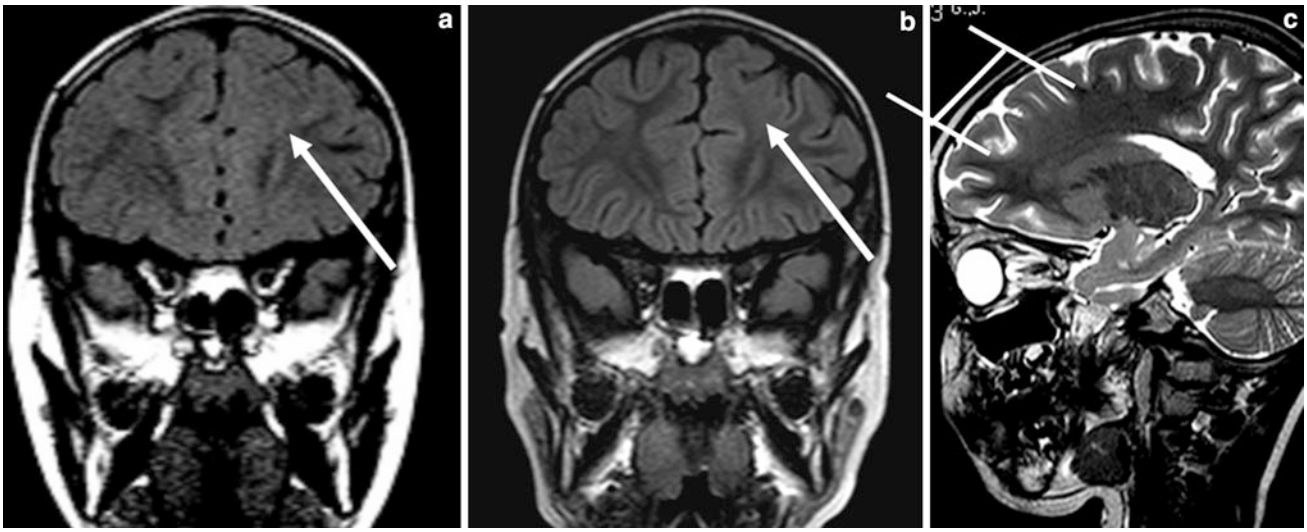

Fig. 3 Owing to a lower contrast-to-noise ratio, a faint gray white matter demarcation loss in the left frontal lobe is hardly visible at 1.5 T (**a** *arrow*) compared with 3 T (**b** *arrow*, **c** anterior–posterior extension)

resolution and signal-to-noise ratio are inversely correlated. If the acquisition time is prolonged, the likelihood of movement artifacts increases. A reasonable compromise must be found between image quality and acquisition time. If movement artifacts prohibit acquisition of images of sufficient quality, which is particularly common in children, MRI with general anesthesia is needed.

4 Requirements for MR Quality

4.1 Orientation

Coronal slices are almost always angulated perpendicular to the hippocampal long axis. To obtain this angulation, we start with a sagittal sequence, typically a 3D T1-weighted gradient echo sequence, and use a paramedian slice displaying the hippocampal long axis for planning. To avoid tilting in the coronal plane, coronal slices are also adjusted on an axial plane using symmetrical anatomical structures such as the semicircular canals or internal auditory canals as landmarks (Fig. 1).

Axial slices are angulated along the commissura anterior–commissura posterior line or along the long axis of the hippocampus ("temporal angulation"). Angulation is planned on a midsagittal slice for commissura anterior–commissura posterior angulation and on a sagittal slice through one hippocampus for temporal angulation. Temporal angulation on a midsagittal slice is obtained if slices are acquired along a line from the dorsal and lower border of the anterior skull base to the callosal splenium; this angulation is about 25° steeper than commissura anterior–commissura posterior angulation (Fig. 1).

Most patients with drug-resistant focal epilepsies and around one third of patients presenting with a first epileptic seizure have temporal lobe epilepsies, with hippocampal sclerosis being the most commonly operated on lesion (King et al. 1998). The hippocampus is best displayed on coronal slices angulated perpendicular to its long axis. Axial slices along the long axis display the hippocampus on one slice, whereas with the usual angulation along the commissura anterior–commissura posterior line hippocampal head, body, and tail are shown on three adjacent, 5-mm slices.

The recommendation to acquire sequences along or perpendicular to the hippocampal long axis ("temporal angulation") is somewhat because at the beginning of the MR era the vast majority of patients with structural epilepsies had temporal lobe lesions (ILAE recommendations from 1997 and 1998). In recent years, the percentage of patients with often subtle cortical dysplasias has steadily increased. Since cortical dysplasias in the dorsal frontal and parietal lobes can be missed on axial slices with temporal angulation, we recommend to acquire an axial fluid-attenuated inversion recovery (FLAIR) sequence with commissura anterior–commissura posterior angulation.

4.2 Spatial Resolution

Epileptogenic lesions are often small and do not change during life. One should bear in mind that lesions with sufficient contrast as compared with the surrounding tissue will be found if they measure double the pixel size. If the lesion is smaller, partial volume artifacts may obscure its detection.

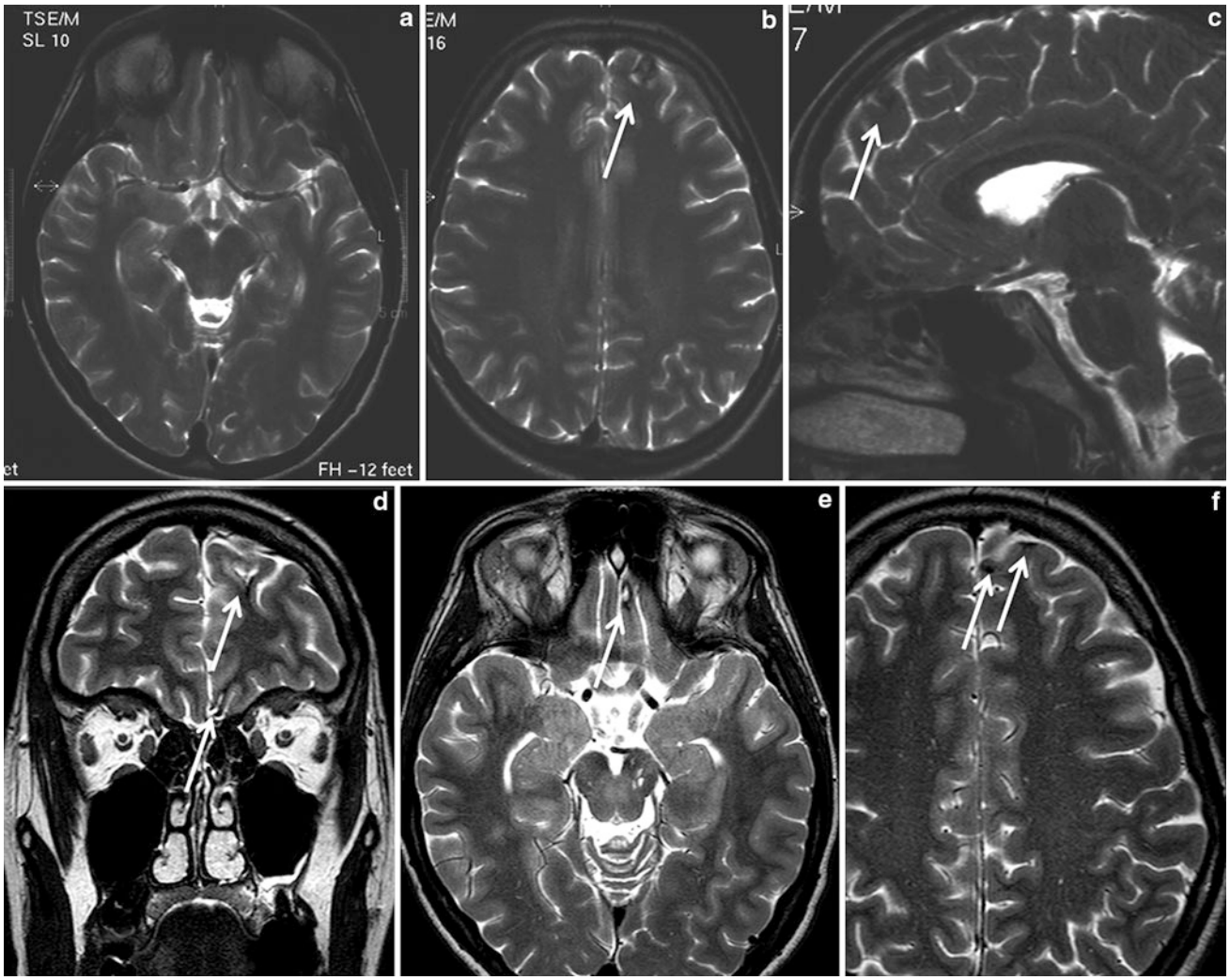

Fig. 4 On 1.5-T 5-mm-thick T2-weighted fast spin echo images a hypointense lesion (**b**, **c**, *arrow*) was interpreted as a cavernoma. High-resolution T2-weighted fast spin echo images at 3 T depict at least three hemosiderin-containing lesions (**d**, **e**, *arrows*) suggestive of old cortical contusions

We use a 3D T1-weighted gradient echo sequence since it produces 1-mm slices and 1-mm^3 voxel within a reasonable time. We acquire 2- or 3-mm-thick FLAIR slices, accepting that thinner slices reduce the signal-to-noise ratio in a way that contrast of smaller lesions becomes too low to outline them from the environment. If high-contrast FLAIR images with a slice thickness of 3 mm cannot be acquired through the whole brain, the clinically suspected region should be studied selectively (Urbach et al. 2004).

Recently, a 3D FLAIR fast spin echo sequence with isotropic 1-mm^3 voxel has been incorporated into our MRI protocol. This sequence depicts the whole brain with high spatial resolution and is—in addition—usable for multiplanar reformations and voxel-based analyses (Kassubek et al. 2002; Wilke et al. 2003; Wagner et al. 2011) (Fig. 2).

4.3 Contrast

The FLAIR sequence has by far the highest diagnostic yield owing to its superb contrast between gray matter and CSF. The gray matter FLAIR signal is different for different gray matter structures: the amygdala, hippocampus, cingulate gyrus, subcallosal area, and insula have higher signal intensity than the convexity cortices (Hirai et al. 2000). Epileptogenic lesions are usually gray matter lesions, and even larger lesions are overlooked on T2-weighted sequences. We acquire FLAIR sequences in axial, coronal, and sagittal orientations since the extension of subtle gray matter lesions into the subcortical matter is sometimes easier to detect on coronal or sagittal slices and vice versa. However, the aforementioned sagittal isotropic 3D FLAIR sequence with 1-mm^3 voxel may soon replace 2D sequences acquired in standard orientations, although reformatted 2-mm-thick axial or 3-mm-

Table 1 MRI "base" protocol

Sequence	3D T1-weighted FFE	FLAIR TSE	T2-weighted TSE	FLAIR TSE	T2-weighted TSE	FLAIR TSE	SWI
Orientation	Sagittal	Sagittal	Axial	Coronal	Coronal	Axial	Axial
FOV	256	240	230	230	240	256	220
RFOV	0.95	0.9	0.8	0.8	0.9	1	0.8
Matrix	256	256	512	256	512	256	256
Scan (%)	100	72.6	80	70.6	80	100	100
TI (ms)	833	2,850		2,850		2,850	
TR (ms)	8.2	12,000	3,272	12,000	5,765	12,000	16
TE (ms)	3.7	120	80	140	120	140	23
FA (°)	8	140	90	90	90	90	10
Turbo factor	193	36	15	36	25	32	
SENSE factor	1.3 (AP), 1.7 (RL)	No	No	No	3 (RL)	No	1.5 (RL)
Slice thickness	1	3.5	5	3	2	2	1
Interslice gap	0	0	1	0	0	0	0
No. of slices	140	40	24	40	40	60	200
No. of excitations	1	1	1	1	6	1	1
Acquisition voxel size (mm^3)	1 × 1 × 1	0.98 × 1.26 × 3.5	0.57 × 0.72 × 5	0.9 × 1.27 × 3	0.47 × 0.64 × 2	1 × 1 × 2	1 × 1 × 1
Recorded voxel size (mm^3)	1 × 1 × 1	0.49 × 0.49 × 3.5	0.45 × 0.45 × 5	0.45 × 0.45 × 3	0.23 × 0.23 × 2	1 × 1 × 2	0.43 × 0.43 × 0.5
Acquisition time	3 min 11 s	4 min 48 s	1 min 58 s	4 min	4 min 53 s	5 min 24 s	3 min 17 s

FFE fast field echo, *FLAIR* fluid-attenuated inversion recovery, *TSE* turbo spin echo, *FOV* field of view, *RFOV* rectangular field of view, *TI* inversion time, *TR* repetition time, *TE* echo time, *FA* flip angle, *SENSE* sensitivity encoding, *AP* anterior to posterior, *RL* right to left

thick coronal slices have a slightly lower contrast-to-noise ratio than the corresponding 2D slices.

High-resolution T2-weighted fast spin echo images have both high spatial resolution and a high contrast-to-noise ratio. They are particularly suited to assess white matter lesions. However, since CSF is also bright, hyperintense cortical lesions can be easily missed.

4.4 Contrast Medium Injection

The first goal of MRI in epilepsy patients is detection of an epileptogenic lesion. With careful MRI interpretation, lesions are visible without additional intravenous contrast medium injections. Contrast medium injections are usually needed to characterize a lesion but not to find it (Elster and Mirza 1991). We acquire contrast-enhanced T1-weighted spin echo sequences in epileptogenic lesions other than hippocampal slerosis in order to characterize the lesion.

5 MRI Interpretation

MRI interpretation comprises several steps addressing the following questions:

1. Is the contrast between gray matter, white matter, and CSF sufficient (Fig. 3)?
2. Is the spatial resolution and orientation appropriate to detect subtle epileptogenic lesions fitting to the semiology of the seizures (Fig. 4)?
3. Are anatomical structures displayed symmetrically and without imaging artifacts in order to detect subtle epileptogenic lesions by side comparisons (Fig. 1)?

6 MRI Protocols

Tables 1 and 2 include proposals for MRI protocols in epilepsy patients.

Table 2 Additional or alternative MRI sequences

Sequence	T1-weighted TSE	T2-weighted FFE	DWI	DTI	3D FLAIR
Orientation	Coronal	Axial	Axial	Axial	Sagittal
FOV	230	230	256	256	250
RFOV	0.8	0.8	1	1	100
Matrix	256	256	128	128	228
Scan (%)	79.9	79.9	97.8	98.4	100
TI (ms)					1,600
TR (ms)	550	601	3,151	11,374	4,800
TE (ms)	13	18	69	63	309
FA (°)	90	18	90	90	90
SENSE factor	No	No	3 (AP)	2.2 (AP)	2.5 (AP), 2 (RL)
Slice thickness	5	5	5	2	1.1
Interslice gap	1	1	1	0	0
No. of slices	24	24	24	60	327
No. of excitations	1	1	2	1	2
Acquisition voxel size (mm^3)	0.9 × 1.12 × 5	0.9 × 1.12 × 5	2 × 2.4 × 5	2 × 2.03 × 2	1.1 × 1.1 × 1.1
Recorded voxel size (mm^3)	0.45 × 0.45 × 5	0.45 × 0.45 × 5	1 × 1 × 5	2 × 2 × 2	0.43 × 0.43 × 0.55
Acquisition time	4 min 33 s	1 min 41 s	1 min 9 s	6 min 26 s	4 min 43 s

DWI diffusion-weighted imaging, *DTI* diffusion tensor imaging, *SWI* susceptibility-weighted imaging

Additional sequences are acquired on the basis of imaging findings or clinical hints.

If there is an epileptogenic lesion other than hippocampal sclerosis, nonenhanced and contrast-enhanced spin echo sequences are added. The goal is to specify a lesion, not to detect it (Urbach et al. 2002): Focal cortical dysplasias show contrast enhancement in exceptional cases only (Urbach et al. 2002). If a circumscribed cortical/subcortical lesion shows contrast enhancement, an epilepsy-associated tumor is more likely.

We recently added Susceptibility-weighted (SWI) sequences or —if not applicable —T2-weighted gradient echo (FFE) sequences to the MR base protocol due to their superb sensitivity to detect small hemosiderin deficits or calcifications (Saini et al. 2009)

The sagittal 3D gradient echo sequence producing isotropic 1-mm^3 voxel is reformatted in axial and coronal orientations. After a path along the brain surface has been defined on the coronal images, the planar curved surface (or "pancake") view is constructed by parallel shifting in an anterior and posterior direction. If the path in the direction of the surface gradients is collapsed, the whole brain is reformatted, and structures at any depth become visible. On these planar brain surface reformations both hemispheres are displayed in a mirror-like fashion, from the interhemispheric to the sylvian fissures. The central sulcus and neighboring gyri can be followed continuously (Hattingen et al. 2004). The planar brain surface view facilitates anatomical orientation and is helpful to determine the boundaries of epileptogenic lesions (Fig. 2).

Reversible splenium lesions on diffusion-weighted images occur in less than 1% of epilepsy patients. Rapid antiepileptic drug reduction or withdrawal in order to provoke epileptic seizures during presurgical workup has been identified as risk factor. If a faintly hyperintense, non-space-occupying splenium lesion is found on T2-weighted or FLAIR images, diffusion-weighed imaging showing reduced diffusion underscores the suspected diagnosis (Nelles et al. 2006) (see Fig. 7 in Other Epilepsy-Asspciated Diseases and Differential Diagnoses).

References

Bammer R, Keeling SL, Augustin M, Pruessmann KP, Wolf R, Stollberger R, Hartung HP, Fazekas F (2001) Improved diffusion-weighted single-shot echo-planar imaging (EPI) in stroke using sensitivity encoding (sense). Magn Reson Med 46(3):548–554

Elster AD, Mirza W (1991) MR imaging in chronic partial epilepsy: role of contrast enhancement. Am J Neuroradiol 12(1):165–170

Hattingen E, Hattingen J, Clusmann H, Meyer B, Koenig R, Urbach H (2004) Planar brain surface reformations for localization of cortical brain lesions. Zentralbl Neurochir 65(2):75–80. doi:10.1055/s-2004-816271

Hirai T, Korogi Y, Yoshizumi K, Shigematsu Y, Sugahara T, Takahashi M (2000) Limbic lobe of the human brain: evaluation

with turbo fluid-attenuated inversion-recovery MR imaging. Radiology 215(2):470–475

Kassubek J, Huppertz HJ, Spreer J, Schulze-Bonhage A (2002) Detection and localization of focal cortical dysplasia by voxel-based 3-D MRI analysis. Epilepsia 43(6):596–602

King MA, Newton MR, Jackson GD, Fitt GJ, Mitchell LA, Silvapulle MJ, Berkovic SF (1998) Epileptology of the first-seizure presentation: a clinical, electroencephalographic, and magnetic resonance imaging study of 300 consecutive patients. Lancet 352(9133): 1007–1011. doi:10.1016/S0140-6736(98)03543-0

Nelles M, Bien CG, Kurthen M, von Falkenhausen M, Urbach H (2006) Transient splenium lesions in presurgical epilepsy patients: incidence and pathogenesis. Neuroradiology 48(7):443–448. doi: 10.1007/s00234-006-0080-5

Pruessmann KP, Weiger M, Scheidegger MB, Boesiger P (1999) Sense: sensitivity encoding for fast MRI. Magn Reson Med 42(5):952–962

Saini J, Kesavadas C, Thomas B, Kapilamoorthy TR, Gupta AK, Radhakrishnan A, Radhakrishnan K (2009) Susceptibility weighted imaging in the diagnostic evaluation of patients with intractable epilepsy. Epilepsia 50(6):1462–1473

Urbach H, Hattingen J, von Oertzen J, Luyken C, Clusmann H, Kral T, Kurthen M, Schramm J, Blumcke I, Schild HH (2004) MR imaging in the presurgical workup of patients with drug-resistant epilepsy. Am J Neuroradiol 25(6):919–926

Urbach H, Scheffler B, Heinrichsmeier T, von Oertzen J, Kral T, Wellmer J, Schramm J, Wiestler OD, Blumcke I (2002) Focal cortical dysplasia of Taylor's balloon cell type: a clinicopathological entity with characteristic neuroimaging and histopathological features, and favorable postsurgical outcome. Epilepsia 43(1): 33–40

Wagner J, Weber B, Urbach H, Elger CE, Huppertz HJ (2011) Morphometric mri analysis improves detection of focal cortical dysplasia type II. Brain 134(Pt 10):2844–2854. doi:10.1093/brain/awr204

Wilke M, Kassubek J, Ziyeh S, Schulze-Bonhage A, Huppertz HJ (2003) Automated detection of gray matter malformations using optimized voxel-based morphometry: a systematic approach. Neuroimage 20(1):330–343

Willinek WA, Kuhl CK (2006) 3.0 T neuroimaging: technical considerations and clinical applications. Neuroimaging Clin N Am 16 (2):217–228. doi:10.1016/j.nic.2006.02.007

Willinek WA, Schild HH (2008) Clinical advantages of 3.0 T MRI over 1.5 T. Eur J Radiol 65(1):2–14. doi:10.1016/j.ejrad.2007.11.006

MRI of Children

Robert Sassen and Horst Urbach

Contents

Abstract

MRI in children with epilepsies is different for mainly two reasons: 1) Children are generally unable to lie still for MRI. In order to acquire high-resolution MR images general anaesthesia is the preferred sedation method. 2) Ongoing myelination during the first two or three years of life make MR interpretation difficult. In the first 6 months of life, high resolution T2-weighted images have the highest diagnostic potential. During the phase of signal reversal (between 6 and 18 months of age) it may be difficult to detect epileptogenic lesions. If a MRI scan is "negative" at this age, it should be repeated after the age of 2 or 3.

1 Clinical Presentation

The clinical context determines if and how MRI is performed:

1.1 Children with a First Seizure

When a child presents with a first seizure in life, one should have in mind that the risk of having a first seizure is highest in the first year of life and in patients older than 65 years (Olafsson et al. 2005). The most common seizure type in children is febrile seizures. Approximately one third of children in studies from emergency departments who are evaluated for a "first" seizure will be recognized as having an epilepsy syndrome (Gaillard et al. 2009). Up to one quarter of first seizures occur in the context of genetic (formerly idiopathic) generalized epilepsies, and another one fifth are genetic partial epilepsies, mainly benign rolandic and occipital epilepsies (King et al. 1998).

Imaging in children with a first seizure is performed to identify a lesion requiring urgent intervention (hydrocephalus, tumor, stroke, hemorrhage, sinus thrombosis, metabolic, etc.) (see Figs. 1, 2 in "What To Do After a First Seizure").

R. Sassen
Department of Epileptology,
University of Bonn, Bonn, Germany

H. Urbach (✉)
Department of Neuroradiology,
University Hospital Freiburg, Germany
e-mail: horst.urbach@uniklinik-freiburg.de

H. Urbach (ed.), *MRI in Epilepsy*, Medical Radiology. Diagnostic Imaging,
DOI: 10.1007/174_2012_560, © Springer-Verlag Berlin Heidelberg 2013

If the clinical history and the EEG, however, point to a genetic epilepsy syndrome and neurologic examination findings are normal, MRI is typically unrevealing. Genetic epilepsy syndromes without significant imaging abnormalities include rolandic epilepsy, childhood absence epilepsy, juvenile absence epilepsy, and juvenile myoclonic epilepsy (see Table 1 in "Epilepsy Syndromes") (Gaillard et al. 2009).

Febrile seizures occur with an incidence of 2–5% until the age of 5 years. They are defined as seizures occurring in febrile children between the ages of 6 months and 5 years who do not have an intracranial infection, metabolic disturbance, or a history of febrile seizures. They occur most frequently between the 18th and 24th months of age (90% below 3 years of age, 50% within the second year of life). Febrile seizures are subdivided into two categories: simple (80–90%) and complex (10–20%). Simple febrile seizures last for less than 15 min, are generalized (without a focal component), and occur once in a 24-h period, whereas complex febrile seizures are prolonged (mote than 15 min), are focal, or occur more than once in 24 h. Simple febrile seizures are not associated with subsequent epilepsy or cognitive deficits, whereas complex febrile seizures are linked with the development of temporal lobe epilepsy and hippocampal sclerosis. Whether temporal lobe epilepsy is the consequence of complex febrile seizures or the child has complex febrile seizure because the hippocampus was previously damaged by a prenatal or perinatal insult or by genetic predisposition is a matter of debate. The current concept is to consider the association between complex febrile seizures and temporal lobe epilepsy resulting from complex interactions between several genetic and environmental factors. Simple febrile seizures are not an indication for MRI, whereas complex febrile seizures are (King et al. 1998; Bernal and Altman 2003). In patients with temporal lobe epilepsy, 30% of patients with hippocampal sclerosis as compared with 6% of patients without hippocampal sclerosis had complex febrile seizures in childhood (Falconer et al. 1964).

1.2 Children with Epilepsy Syndromes

Children with epileptic encephalopathies (see Table 1 in "Epilepsy Syndromes") are studied with MRI to find an underlying structural lesion. For example, in infants with infantile spasms (West syndrome) tuberous sclerosis is a common finding. However, in around 40% of patients with this encephalopathic syndrome, no lesions are found (Osborne et al. 2010). Rarely, a circumscribed lesion may be found, enabling surgical resection and dramatically changing the child's prognosis (Fig. 1).

In children with seizure types, age at presentation, and EEG findings pointing to a genetic epilepsy syndrome of (see above), MRI is typically unrevealing. Because some nongenetic epilepsies may sometimes mimic these genetic epilepsy syndromes, MRI is recommended in these patients if they present with any atypical features such as abnormal neurologic or intellectual development, difficult-to-treat seizures, or unusual course. There is insufficient evidence to comment on the role of not imaging in other less common ''benign'' or generalized epilepsy syndromes which may be difficult to differentiate from symptomatic epilepsies [e.g., other idiopathic focal epilepsies (childhood epilepsy with occipital paroxysms), primary reading epilepsy, and idiopathic generalized epilepsies (benign neonatal convulsions, benign myoclonic epilepsies of infancy, and epilepsy with seizures precipitated by specific modes of activation)] (Caraballo et al. 1997a, b).

In children with focal, possibly drug-resistant epilepsy syndromes, the effort to generate high-quality magnetic resonance images is greatest. If these patients are uncooperative and unable to tolerate sequences lasting around 5 min, general anesthesia including sedation and intubation is needed. This effort is derived from the fact that focal cortical dysplasias which may be subtle are one of the most common causes of seizures in children with drug-resistant epilepsy, accounting for nearly 80% of all surgically treated cases in children under 3 years of age (Cepeda et al. 2006).

2 Preparation

Young children or those with learning difficulties are generally unable to lie still for neuroimaging. If general anesthesia is not available, orally administered chloral hydrate (50–100 mg/kg body weight, maximum 2 g) may serve as alternative (Cox et al. 2011; Schulte-Uentrop and Goepfert 2010). Finding the right chloral hydrate dose is difficult because children may refuse, spit out, or vomit the unpalatable syrup. If contrast-medium injection is needed, a "needle" has to be placed before administering chloral hydrate, otherwise the child will wake up, rendering contrast-enhanced MRI impossible. About 20% of the patients need oxygen to keep oxygen saturation above 92%. Snoring leads to vibration artifacts and the requirement of a special head and neck position in the scanner.

3 Imaging

Brain magnetic resonance images of children up to 3 years of age are different from those of adults mainly due to incomplete white matter myelination. After 3 years of age, the signal characteristics are similar to those in adult brains, but the heads are smaller. In children 8 years of age or older, the head size not longer increases appreciably with age.

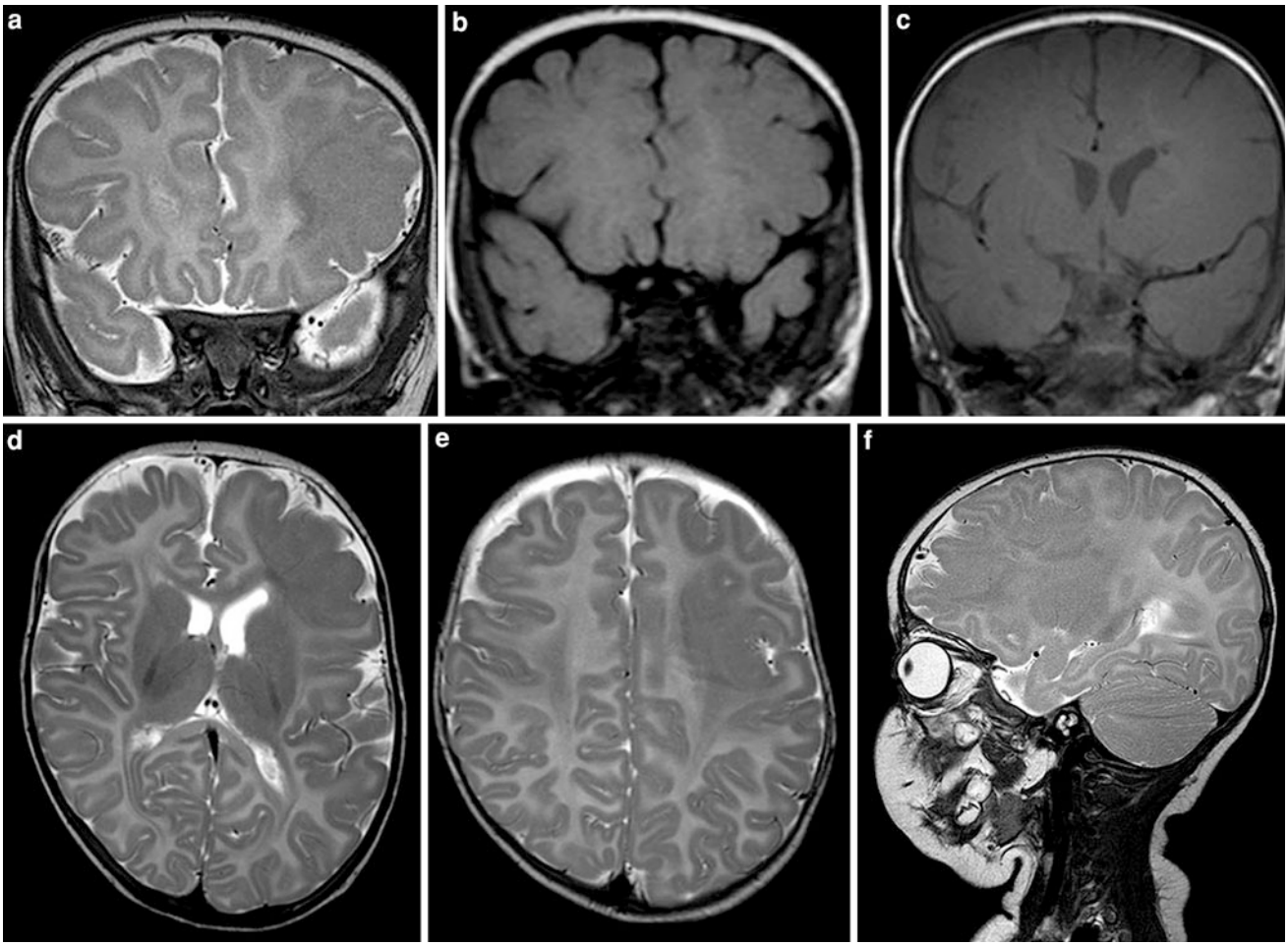

Fig. 1 Large left frontal focal cortical dysplasia type IIB in a 3-month-old girl with infantile spasms (West syndrome). The lesion is best visible on T2-weighted images (**a**, **d**–**f**), easily overlooked on fluid-attenuated inversion recovery (FLAIR) images (**b**), and not visible on T1-weighted images (**c**). Note the high (inversed) signal of the unmyelinated white matter on T2-weighted images. Contrast between gray matter and white matter on T1-weighted images is worse at 3 T as compared with 1.5 T as the T1 relaxation is around 30% shorter and the relaxation times of gray matter and white matter converge. White matter maturation leading to an increased signal on T1-weighted images starts in the deep white matter posteriorly and extends latest in the subcortical frontal and temporal lobe white matter (Barkovich. Pediatric Neuroimaging. Lippincott Williams and Wilkins, Philadelphia 2000)

Myelin is a lipid-rich membrane with low protein and water content. Myelin contains only 40% water, and the nonmyelin portion of white matter contains about 80% water (van der Knaap and Valk 1990, 2005, p 1-19). Myelination begins in the cranial nerves in the fifth fetal month. It proceeds from caudal to cephalad, from dorsal to ventral, and from central to peripheral. Functional systems that are used early in life (precentral and postcentral gyri, occipital cortex) myelinate before those using association fibers (posterior parietal, frontal, and temporal areas). Peripheral white matter myelinates last. Myelination starts at 9–12 months in the posterior parts, at 11–14 months in the frontal lobes, and thereafter in the temporal lobes. Increased white matter signal intensity in the anterior part of the temporal lobe, which accompanies hippocampal sclerosis in a significant percentage of patients, may therefore represent a maturation disorder and not an associated cortical dysplasia (Schijns et al. 2011).

On MRI, myelination is associated with shortening of the T1 and T2 relaxation times, reduced water diffusion, increased diffusion anisotropy, and increased magnetization transfer. Accordingly, the white matter signal changes from hypointense to hyperintense relative to gray matter on T1-weighted images and from hyperintense to hypointense relative to gray matter on T2-weighted images (Barkovich 2000; Barkovich et al. 1988) During the phase of signal reversal (between 6 and 18 months of age) it may be difficult to detect subtle epileptogenic lesions. It may be easier to detect, e.g., focal cortical dysplasias shortly after birth or at the age of 2 or 3 years, when signal differences between gray

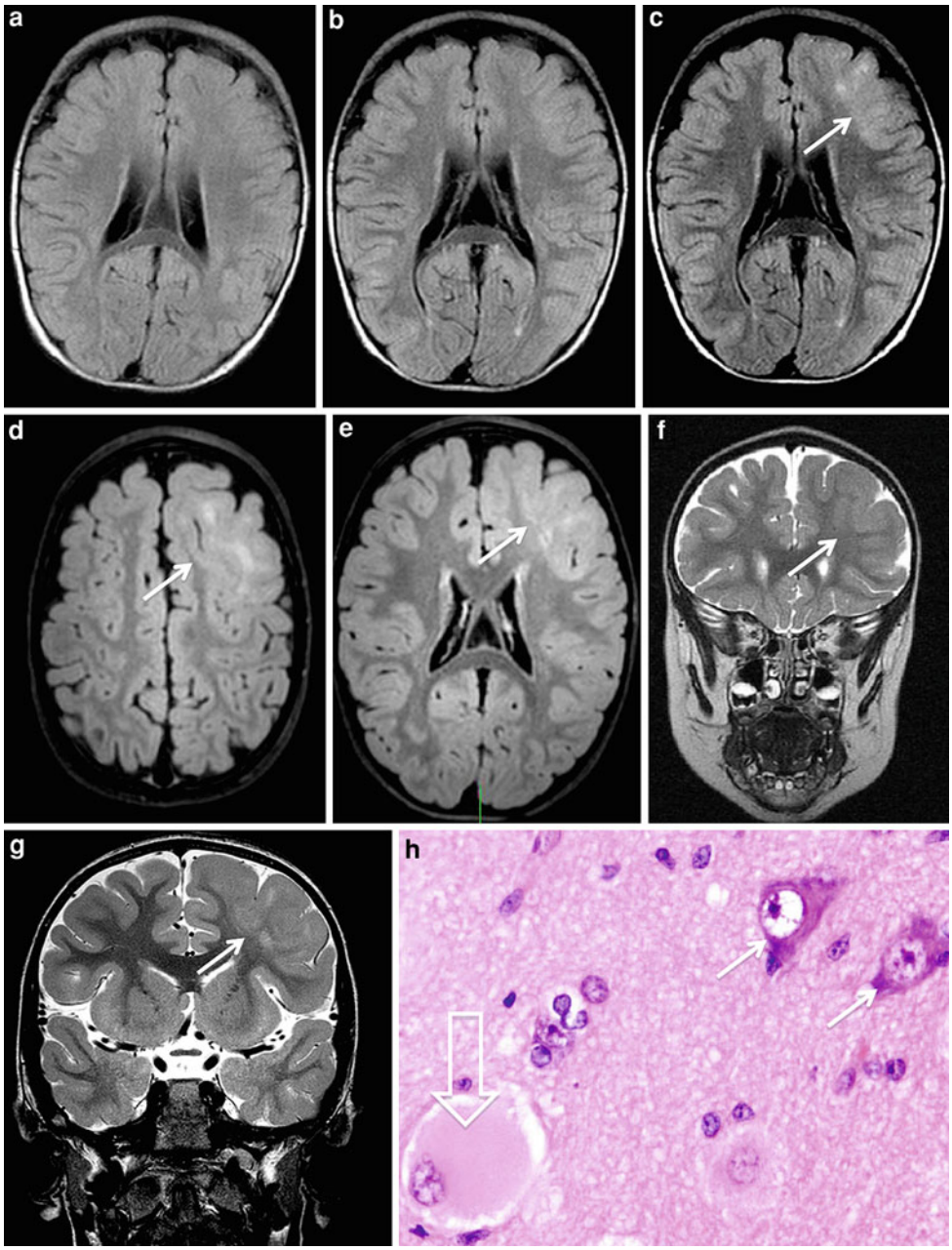

Fig. 2 Large left frontal focal cortical dysplasia type IIB in a boy with complex focal seizures. Axial FLAIR images were acquired at the age of 2 years (**a**), 2.5 years (**b**), 3.5 years (**c**), and 4 years (**d**–**f**; **e** shows a reformatted 1-mm-thick image from a sagittal 3D FLAIR data set with an orientation similar to that in **a**–**c**). FLAIR imaging is of little value in the first 3 years of life as the signal difference between cortex and white matter is low and the subcortical hyperintensity representing the balloon-cell-rich and hypomyelinated zone is not present yet. At these time points, T2-weighted images display the distorted cortical anatomy (**f**), which is better appreciated on high-field MRI owing to an increased signal-to-noise ratio and spatial resolution. Hematoxylin–eosin staining (×400) shows a balloon cell (*arrowhead*) with an eccentric nucleus and gigantic opaque/eosinophilic cytoplasm. Compare the size of the balloon cell and that of two neighboring neurons (*arrows*). (Courtesy of A. Becker, Department of Neuropathology, University of Bonn)

matter and white matter have evolved again (Eltze et al. 2005). If MRI is performed between 9 and 18 months of age and the findings are negative, another scan after 2 years of age should be performed (Vezina 2011).

Unmyelinated white matter is hyperintense on T2-weighted images. Increasing the repetition time (4,000–5,000 ms minimum) typically improves contrast. In addition, an increased echo time can help exploit minimal available contrast in infants. As the inherent signal-to-noise ratio of T2-weighted turbo spin echo images is high, these adjustments are made without adverse effects on overall image quality.

T1-weighted spin echo images in infants are noisy since infant brains have ample water but minimal myelin. At high field strengths, longer T1 relaxation time, converging T1 relaxation times of gray matter and white matter, and inherent magnetization transfer contrast effects further reduce contrast. By the age of 3 years, spin echo T1 contrast approximates that of adults. Three-dimensional T1-weighted gradient echo images are a good alternative to T1-weighted spin echo images in terms of spatial resolution, signal-to-noise ratio, and T1 contrast. However, contrast enhancement of lesions can be different and more prominent on spin echo images.

FLAIR sequences have a limited value in children up to 3 years due to their inherent T1 contrast and the lower signal to noise ratio of inversion recovery techniques (Fig. 2). In addition, the high heart rate of small children lead to more flow artifacts compared to adults.

Magnetization transfer imaging is a helpful alternative imaging modality in children older than 3 years. Magnetization transfer is based on the interaction between mobile free water protons and macromolecular bound protons. An off-resonance radiofrequency pulse saturates protons bound to macromolecules, mainly in the myelin sheaths. Owing to spin–spin interactions, the saturation effect is transferred to surrounding mobile free protons. This results in a signal decrease from the mobile protons and an overall suppression of signal from brain tissue. If a lesion has a low myelin fraction or contains abnormal myelin, signal suppression is lower than that in the healthy white matter. Thus, a lesion may appear as hyperintense on magnetization transfer images. Magnetization transfer images have been shown to be superior in the detection of white matter lesions in tuberous sclerosis complex (Pinto Gama et al. 2006; Woermann and Vollmar 2009), and similarly in some focal cortical dysplasias (Rugg-Gunn et al. 2003).

During the first 3 years of life, high-resolution T2-weighed fast spin echo images have the highest diagnostic yield to detect and to delineate epileptogenic lesions (Fig. 1). Afterwards, FLAIR sequences are the most important ones. If a 3D FLAIR sequence cannot be acquired, we recommend acquiring FLAIR sequences in axial, coronal, and sagittal orientations.

The first goal of MRI in epilepsy patients is the detection of an epileptogenic lesion. With careful MRI interpretation, lesions are visible without additional intravenous contrast medium injections. Contrast medium injections are usually needed to characterize a lesion but not to find it (Elster and Mirza 1991). Like in adults, we acquire contrast-enhanced T1-weighted spin echo sequences in epileptogenic lesions other than hippocampal sclerosis in order to characterize the lesion (Gaillard et al. 2009).

References

Barkovich AJ (2000) Concepts of myelin and myelination in neuroradiology. AJNR Am J Neuroradiol 21(6):1099–1109

Barkovich AJ, Kjos BO, Jackson DE Jr, Norman D (1988) Normal maturation of the neonatal and infant brain: MR imaging at 1.5 T. Radiology 166(1 Pt 1):173–180

Bernal B, Altman NR (2003) Evidence-based medicine: neuroimaging of seizures. Neuroimaging Clin N Am 13(2):211–224

Caraballo R, Cersosimo R, Galicchio S, Fejerman N (1997a) Benign infantile familial convulsions. Rev Neurol 25 (141):682–684

Caraballo RH, Cersosimo RO, Medina CS, Tenembaum S, Fejerman N (1997b) Idiopathic partial epilepsy with occipital paroxysms. Rev Neurol 25 (143):1052–1058

Cepeda C, Andre VM, Levine MS, Salamon N, Miyata H, Vinters HV, Mathern GW (2006) Epileptogenesis in pediatric cortical dysplasia: the dysmature cerebral developmental hypothesis. Epilepsy Behav 9(2):219–235. doi:10.1016/j.yebeh.2006.05.012

Cox RG, Levy R, Hamilton MG, Ewen A, Farran P, Neil SG (2011) Anesthesia can be safely provided for children in a high-field intraoperative magnetic resonance imaging environment. Paediatr Anaesth 21(4):454–458. doi:10.1111/j.1460-9592.2011.03528.x

Elster AD, Mirza W (1991) Mr imaging in chronic partial epilepsy: role of contrast enhancement. AJNR Am J Neuroradiol 12(1):165–170

Eltze CM, Chong WK, Bhate S, Harding B, Neville BG, Cross JH (2005) Taylor-type focal cortical dysplasia in infants: some MRI lesions almost disappear with maturation of myelination. Epilepsia 46(12):1988–1992. doi:10.1111/j.1528-1167.2005.00339.x

Falconer MA, Serafetinides EA, Corsellis JA (1964) Etiology and pathogenesis of temporal lobe epilepsy. Arch Neurol 10:233–248

Gaillard WD, Chiron C, Cross JH, Harvey AS, Kuzniecky R, Hertz-Pannier L, Vezina LG (2009) Guidelines for imaging infants and children with recent-onset epilepsy. Epilepsia 50(9):2147–2153. doi:10.1111/j.1528-1167.2009.02075.x

King MA, Newton MR, Jackson GD, Fitt GJ, Mitchell LA, Silvapulle MJ, Berkovic SF (1998) Epileptology of the first-seizure presentation: a clinical, electroencephalographic, and magnetic resonance imaging study of 300 consecutive patients. Lancet 352(9133):1007–1011. doi:10.1016/S0140-6736(98)03543-0

Olafsson E, Ludvigsson P, Gudmundsson G, Hesdorffer D, Kjartansson O, Hauser WA (2005) Incidence of unprovoked seizures and epilepsy in Iceland and assessment of the epilepsy syndrome classification: a prospective study. Lancet Neurol 4(10):627–634. doi:10.1016/S1474-4422(05)70172-1

Osborne JP, Lux AL, Edwards SW, Hancock E, Johnson AL, Kennedy CR, Newton RW, Verity CM, O'Callaghan FJ (2010) The underlying etiology of infantile spasms (West syndrome): information from the United Kingdom Infantile Spasms Study (UKISS) on contemporary causes and their classification. Epilepsia 51(10):2168–2174. doi:10.1111/j.1528-1167.2010.02695.x

Pinto Gama HP, da Rocha AJ, Braga FT, da Silva CJ, Maia AC Jr, de Campos Meirelles RG, Mendonca do RJI, Lederman HM (2006) Comparative analysis of MR sequences to detect structural brain lesions in tuberous sclerosis. Pediatr Radiol 36(2):119–125. doi:10.1007/s00247-005-0033-x

Rugg-Gunn FJ, Eriksson SH, Boulby PA, Symms MR, Barker GJ, Duncan JS (2003) Magnetization transfer imaging in focal epilepsy. Neurology 60(10):1638–1645

Schijns OE, Bien CG, Majores M, von Lehe M, Urbach H, Becker A, Schramm J, Elger CE, Clusmann H (2011) Presence of temporal gray-white matter abnormalities does not influence epilepsy surgery outcome in temporal lobe epilepsy with hippocampal sclerosis. Neurosurgery 68 (1):98–106; discussion 107. doi:10.1227/NEU.0b013e3181fc60ff

Schulte-Uentrop L, Goepfert MS (2010) Anaesthesia or sedation for MRI in children. Curr Opin Anaesthesiol 23(4):513–517. doi:10.1097/ACO.0b013e32833bb524

van der Knaap M, Valk J (1990) MR imaging of the various stages of normal myelination during the first year of life. Neuroradiology 31(6):459–470

van der Knaap M, Valk J (2005) Magnetic resonance of myelination and myelin disorders. Springer Berlin Heidelberg, New York, pp 1–19

Vezina LG (2011) MRI-negative epilepsy: protocols to optimize lesion detection. Epilepsia 52(Suppl 4):25–27. doi:10.1111/j.1528-1167.2011.03147.x

Woermann FG, Vollmar C (2009) Clinical MRI in children and adults with focal epilepsy: a critical review. Epilepsy Behav 15(1):40–49. doi:10.1016/j.yebeh.2009.02.032

Functional MRI

Jörg Wellmer

Contents

Abstract

Functional magnetic resonance imaging (fMRI) is an abundantly applied tool for the preoperative localization and/or lateralization of brain functions. It is noninvasive and therefore apparently without risk for patients. However, the particular risk of fMRI lies in several methodological limitations which can give rise to misinterpretations. These can result in fatal surgical decisions, for example, the resection of undetected functional cortex or the unnecessary sparing of tissue which has to be removed to achieve freedom from seizures. This chapter explains the methodological aspects of fMRI with special focus on its limitations, but also gives recommendations for safe clinical application of fMRI.

1 Introduction

Epilepsy surgery aims at achieving freedom from seizures by resecting the *epileptogenic zone* without causing unexpected neurological sequelae. A particular challenge is that in epilepsy patients the functional anatomy of sensorimotor, language, and memory systems shows interindividual variability (Helmstaedter et al. 1997; Staudt 2010). The reasons for intrahemispheric or interhemispheric shift of functions can be interictal or ictal epileptic discharges or morphological lesions (Staudt 2010; Janszky et al. 2003; Weber et al. 2006).

Traditionally, inactivating methods such as the Wada test (Baxendale 2009) or electrical stimulation mapping (ESM) (Berger et al. 1989; Hamberger 2007) are applied to identify the individual functional anatomy. These methods produce a transient functional lesion and indicate whether surgery in the inactivated area would cause a persisting functional deficit. Both methods carry some risk of morbidity although for the Wada test large studies have shown a risk of permanent morbidity of only around 0.5% (Loddenkemper et al. 2008; Haag et al. 2008). Also, extraoperative electrical stimulation has an acceptable risk–benefit ratio (Wellmer et al. 2012).

J. Wellmer (✉)
Ruhr-Epileptology, Department of Neurology,
University Hospital Knappschaftskrankenhaus
Bochum, Germany
e-mail: joerg.wellmer@kk-bochum.de

H. Urbach (ed.), *MRI in Epilepsy*, Medical Radiology. Diagnostic Imaging,
DOI: 10.1007/174_2012_563,

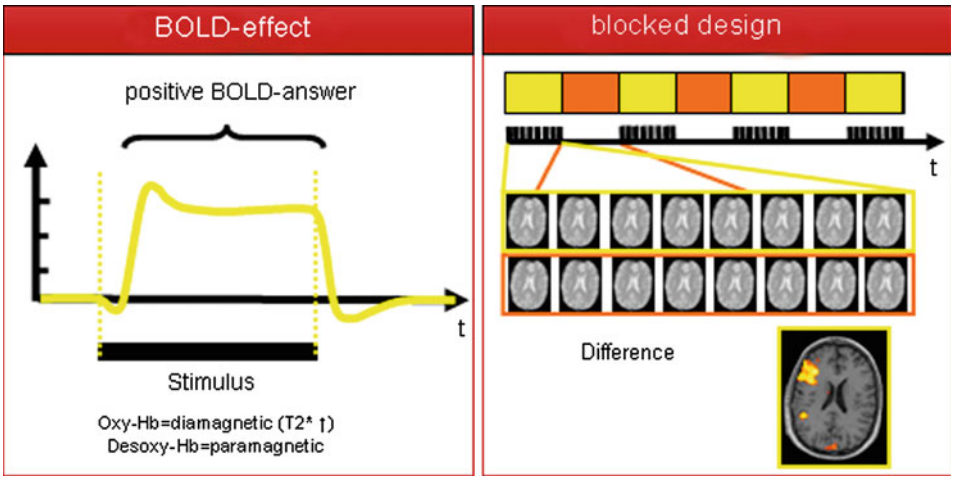

Fig. 1 Principle of fMRI, blocked design. Panel A: blood oxygenation level dependent (BOLD) effect: following a defined stimulus the oxygen-need is increased in areas associated with stimulus processing. This causes a regional transient decrease of oxy-Hb (1), but due to the neurovascular response the regional supply with oxy-Hb increases, exceeding the oxygen-consumption (2). After the stimulus processing ends (3) excess perfusion stops and the oxy-Hb level returns to baseline. Panel B: Oxy-Hb is more diamagnetic than desoxy-Hb. The regional oxy-Hb hyperperfusion leads to subtle magnetic changes which can be identified in serial T2* weighted images. By statistical comparison of MRI-scans acquired during the active and the control condition, stimulus-associated T2*-changes can be identified and visualized, for example overlaid to a morphological MRI scan of the patient. Alternative to the blocked design shown here event-related protocols can be applied. However, they are statistically less robust in clinical routine

However, several alternative methods have been developed which allow noninvasive lateralization and localization of cerebral functions. The most abundantly distributed is functional MRI (fMRI). As most noninvasive methods, fMRI is an activation method (Desmond and Annabel Chen 2002). Patients are instructed to perform specific tasks following a strict protocol, and via a surrogate parameter (spatial distribution of activation-related cerebral perfusion changes) the intracerebral localization of the tested function is determined (Fig. 1). In fact, many studies have described congruence between fMRI and the Wada test (Binder et al. 1996) or ESM (FitzGerald et al. 1997; Yetkin et al. 1997), in particular for language lateralization and localization. Yet, fMRI has several methodological limitations which can affect its validity. These limitations have to be known to physicians who apply or request fMRI in a presurgical setting. Therefore, this chapter addresses the methodological aspects and shortcomings of fMRI before finally giving recommendations regarding its safe clinical application. For reasons of clarity, this chapter concentrates on fMRI for sensorimotor, language, and memory functions.

1.1 Methodology of fMRI

For fMRI the patient is positioned in a standard MRI scanner. Following a predefined time schedule, the patient has to perform simple motor to complex cognitive tasks alternating with control conditions. Instructions are given to the patient either auditorily (through headphones) or visually (via a mirror or goggles). For fMRI of the sensory system, tactile stimuli are applied to the patient.

In response to the execution of the task, neuronal activity and oxygen consumption are elevated in areas associated with this task (e.g., finger-tapping results in increased neuronal activity in the hand motor cortex). The oxygen consumption results in a transient increase in deoxyhemoglobin (desoxy-Hb), but neurovascular coupling leads to an immediate regional surplus of oxyhemoglobin (oxy-Hb). The relative oxy-Hb surplus persists until shortly after termination of the task, then the oxy-Hb/desoxy-Hb ratio drops back to the baseline. Since oxy-Hb is more diamagnetic than desoxy-Hb, regional oxy-Hb hyperperfusion leads to subtle magnetic changes which can be identified in serial T2*-weighted images (for review, see Logothetis 2002). By statistical parametric mapping (http://www.fil.ion.ucl.ac.uk/spm/) or other techniques, one can statistically evaluate subsequent series of images acquired during the active condition and the control condition. Areas that show changes in magnetic signal temporally associated with the protocol-defined course of the active and the control condition are identified and visualized.

1.2 Shortcomings of fMRI

Although the principle of fMRI is simple and logical, there are a number of limitations to this technique which call for care when interpreting activation patterns. Six exemplary limitations are as follows.

1. *Thresholds for activated versus nonactivated voxels*. Whether brain areas (more precisely, voxels) are considered activated or not depends on a threshold definition. The magnitude of T2*-signal changes between the active and the resting condition is usually expressed as p or z scores. To prevent unspecific activation from blurring task-related activation, only activation increases above a defined threshold are regarded as clinically significant. However, there is no standard threshold which is valid for different tasks, patients, or even repeated experiments in the same individual (Loring et al. 2002; Jansen et al. 2006). In consequence, the size of cortex attributed to a given task varies as a function of an arbitrarily chosen activation threshold. In language fMRI, the choice of activation threshold even can determine whether a predominance of left or right hemispheric activation is seen (Ruff et al. 2008). Both false-negative and false-positive activations have to be avoided (Desmond and Annabel Chen 2002; Loring et al. 2002). There have been attempts to adjust the threshold to the activation level of an individual examination. Fernandez et al. (2001) suggest determining the z-score threshold as follows: 50% of the median z score of those 5% of voxels which show the maximum activation changes. Another possibility to overcome threshold dependency is the use of a bootstrap algorithm which takes different thresholds into account and also allows one to detect statistical outliers (Wilke and Schmithorst 2006). Still, the selection of the threshold remains to some extent arbitrary, making the result of an fMRI examination dependent on subjective assumptions (Jansen et al. 2006).
2. *Choice of regions of interest*. Language and memory tasks more than sensorimotor tasks result in complex activation patterns; however, not all activated voxels necessarily correlate with the target parameter (e.g., activated visual cortex in the case of a visually presented language task). Predefined regions of interest (ROIs) can help to focus evaluation on the target parameter and to exclude unspecific activation from the determination of lateralization indices (LIs) (Rutten et al. 2002; Spreer et al. 2002; Loring et al. 2002). In fact, LIs are higher when determination of left and right hemispheric activation is restricted to ROIs compared with whole hemispheric evaluations (Rutten et al. 2002). However, protocol-specific ROIs are often created by random effects analysis of examinations in healthy controls. Problems arise when in epilepsy patients language areas moved out of the ROIs because of plasticity. Then, the LI determined is too low and the result may be incorrectly interpreted as bilateral language representation.
3. *Choice of activation protocols*. In sensorimotor protocols, the selection of activation tasks is rather simple: repetitive movements or tactile stimulation against rest. In language and memory fMRI, simple activation tasks often cannot display the anatomy of the whole functional system (Price 2000; Swanson et al. 2007; Bonelli et al. 2010). Relying on a task which depicts only one subaspect of the functional system may result in wrong lateralization, for example, in the case of crossed expressive and receptive language dominance (Kurthen et al. 1994) or crowding of mnestic functions (Helmstaedter et al. 2004). Language tasks relying on a semantic decision making, however, can activate several language subsystems (Swanson et al. 2007). In more complex language and memory protocols, evaluation of more than the ROI can help to identify the underlying anatomy (Wellmer et al. 2008; Bonelli et al. 2010). Applying a task battery can increase the sensitivity for atypical language organization. However, each task should be evaluated separately for hints at atypical representation. Combined task analysis (Ramsey et al. 2001) may produce robust statistical results, but areas activated just in one of several tasks may be missed.

   Not only the active condition of a protocol has an influence on the result of an examination. The final fMRI activation pattern usually results from a subtraction of the control from the active condition. In the case of language and memory fMRI, continued or self-initiated semantic or linguistic processing cannot be excluded when the control condition is passive (blank screen or crosshair) (Binder et al. 1999; Swanson et al. 2007). This, however, would result in a contrast *language* minus *language*. So, even a strong language lateralization can be missed. The same applies for memory tasks. Ideally, language and memory fMRI protocols follow the principle of a "tight comparison" (Donaldson and Buckner 2001) and use attention demanding nonlinguistic or nonmemory control conditions with continuous performance control.
4. *Choice of LI for lateralized or bilateral language or memory functions*. When for clinical purposes language or memory activation patterns are to be trichotomized into unilateral left, bilateral, or unilateral right, quotients of left and right activation can be calculated and threshold values defined. Again, there are no generally accepted thresholds. Studies comparing language fMRI with the Wada test commonly apply very liberal thresholds for unilateral language dominance. They often range between $\pm$ 0.1 and 0.265 (Liegeois et al. 2004; Adcock et al. 2003). Low LI thresholds are problematic for two reasons. Firstly, they lead to the overdiagnosis of unilaterality of language. Patients with bilateral language organization according to a Wada test but some lateralization in fMRI (e.g., above an LI of 0.2) will be misdiagnosed as unilateral dominant. In a semantic

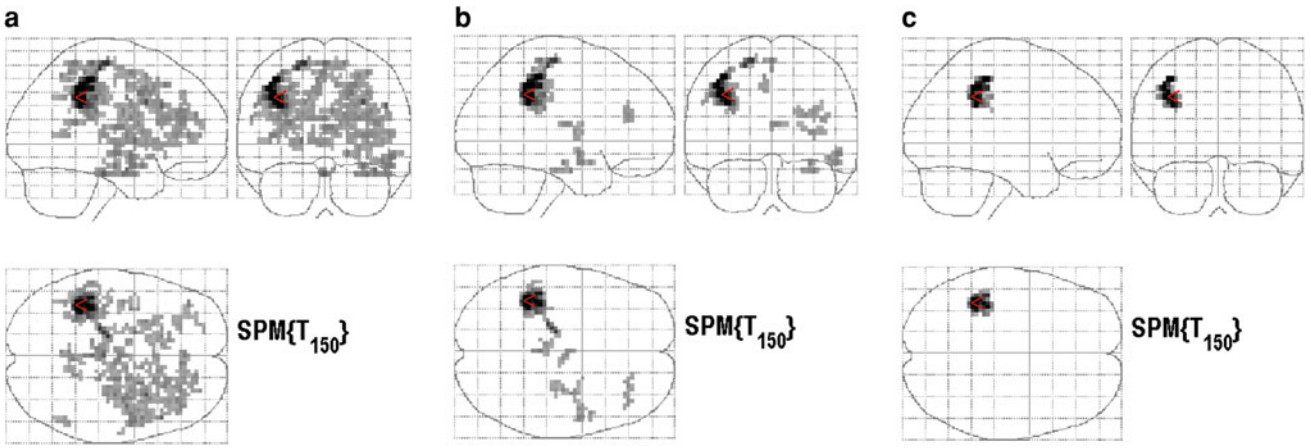

Fig. 2 Finger tapping paradigm (*right hand*). The extent of activation depends on the chosen statistical threshold for activated vs. non-activated voxels. A: T=1.29; B: T=1.66; C: T=2.61. At even higher thresholds, the activation disappears. The choice of threshold is arbitrary. Surgeons should not define margins of functions based on fMRI-activations

comparison task (word pairs vs. letter string pairs) we found that only an LI of 0.85 for the least lateralized of three ROIs allowed diagnosis of unilateral language dominance in accordance with the Wada test (Wellmer et al. 2008). Below an LI of 0.85 for the least lateralized ROI, fMRI was not able to discriminate between unilateral and bilateral language dominance.

Secondly, application of low LI thresholds leads to an overestimation of concordance rates between fMRI and the Wada test. In the study of Sabbah et al. (2003) for an LI threshold of 0.2, the concordance between fMRI and the Wada test was 95%. However, for LI thresholds of 0.4, 0.6, and 0.8, the concordance rates would have been 80, 35, and 15%, respectively. Therefore, it must be hypothesized that a number of studies comparing fMRI and the Wada test gave too optimistic concordance rates.

5. *No discrimination of function-essential and function-associated cortex*. In contrast to inactivation methods which test for the functional reserve capacity of noninactivated cortex, fMRI indicates in which brain areas metabolic changes occur temporally associated with a particular task. This does not mean that the activated part of the brain is essential for the correct execution of the task and that its removal during epilepsy surgery has to be prevented (Desmond and Annabel Chen 2002).
6. *Questionable validity of fMRI near lesions*. A key indication for fMRI is to validate if the relevant functions overlap or are close to cerebral lesions. However, this assumes that fMRI is not affected by the lesion itself. A comparison of patients without lesions and with lesions with potential to interfere with the blood-oxygen-level-dependent (BOLD) effect (e.g., by altered vasoreactivity or susceptibility artifacts due to hemosiderin deposits) or large defects affecting automated MRI normalization showed that the validity of fMRI activation patterns close to lesions cannot be taken for granted (Wellmer et al. 2009). However, further examinations have to follow. Until innocuousness is proven, uncritical interpretation of fMRI activation patterns close to lesions should be avoided.

1.3 Safe Clinical Application of fMRI for Different Indications

The methodological shortcomings affect different fMRI applications to a variable extent.

The most relevant problem for sensorimotor fMRI is shortcoming 1. By changing the statistical threshold for activated versus nonactivated voxels, one can generate any result from no activation (high threshold) to abundant bilateral activation (low threshold) (Fig. 2); therefore, fMRI is by no means able to exactly define the limits of functional cerebral structures. Never should a neurosurgeon perform a resection on the basis of an activation pattern which is based on an arbitrarily chosen threshold. Shortcoming 6 raises concerns regarding the validity of fMRI near lesions. However, further studies addressing the effect of lesions on fMRI are required. Sensorimotor fMRI should only be applied for orientation. A robust fMRI activation can be a strong indicator for the localization of a function, but for precise localization of essential functions ESM should be applied.

Language fMRI is prone to all the shortcomings listed. A way to apply language fMRI safely is to maximize its specificity for unilateral language dominance and to embed it into an algorithm with the Wada test and ESM. As summarized in Table 1, the threshold for activated voxels should be adjusted to the individual activation level or other sophisticated threshold determinations should be applied.

Table 1 Effects of subjective presettings on the result of fMRI-based language lateralization and localization, related to the six discussed pitfalls. If a clinical decision shall be made on fMRI, its specificity must be maximized (small α). If fMRI fails to deliver an unequivocal result, inactivation techniques such as the Wadatest and ESM school be applied according to an indication-specific algorithms (Fig. 3)

	Type I error	Type II error	Clinical requirement
Activation threshold	Low	High	α small
ROI	Large	Small	α small
LI threshold	Low	High	α small
Protocol design	Loose comparison	Tight comparison	α small
Control task	Passive	Active	α small
Effect of lesions	Ignore	Regard	α small

ROI region of interest, *LI* lateralization index

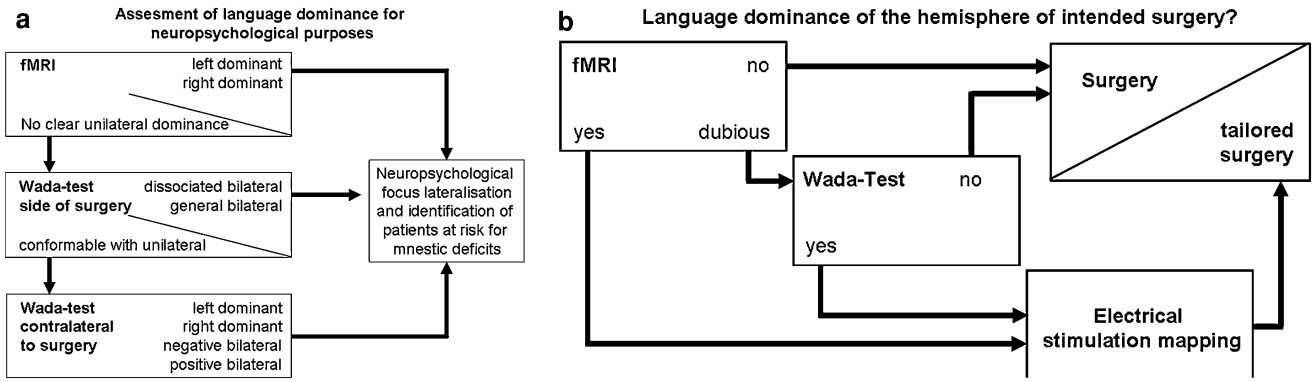

Fig. 3 **a** Algorithm for the application of fMRI and Wada-test when language dominance assessment is performed to allow the interpretation of neuropsychological results. The key question is whether a patient is unilateral left or right dominant for language (Helmstaedter et al. 2004). If fMRI is performed according to the methodological requirements and shows protocol specific clear unilateral language dominance, this result is reliable and no further examination is required. If the result of fMRI is ambiguous, a unilateral Wada Test on the hemisphere of intended surgery should be performed. If this already proves bilateral language distribution, no futher Wada-test is required, the result is atypical language dominance. If the first Wada is still conformable with unilateral language dominance, the contralateral Wada has to be performed. Now, a definite language lateralization score can be computed. For the principle of uni- and bilateral Wada-performance see: (Wellmer et al. 2005). **b** Algorithm for the application of fMRI, Wada-test and electrical stimulation mapping (ESM) for language localization. Key issue is to exclude relevant language cortex in the area of intended surgery. If fMRI is performed according to the methodological requirements and shows unilateral language dominance contralateral to the intended surgery, nor further language localization is necessary. If the fMRI result is ambiguous, a unilateral Wada test ipsilateral to the intended surgery is performed. Does this exclude language in the hemisphere of intended surgery (by undisturbed language function), again the algorithm ends. In case that fMRI or Wada indicate language in the surgical hemisphere, ESM should be performed to map the extent of language cortex in comparison to the seizure onset area. For the principle of ESM for language mapping see: (Wellmer et al. 2009)

Protocol-specific ROIs should be applied. The LI threshold for unilateral language dominance should be high, ideally protocol-specific and validated with Wada-tested patients. The protocol applied should be designed as a tight comparison where the language–control contrast reliably shows only language functions. It should stimulate receptive and expressive language functions. Application of a task battery can increase the sensitivity for atypical dominance as long as the tasks are evaluated separately. The control condition should prevent self-initiated linguistic processing, and active and control conditions should underlie continuous performance control to recognize malcompliance during either condition. Finally, if lesions with potential to interfere with the BOLD effect lie in or close to an ROI, the validity of fMRI (in particular in the case of the absence of activation) should be scrutinized. If fMRI is applied according to the specified requirements and shows clear unilateral dominance, its result can be utilized in the presurgical workup. If fMRI fails to meet the protocol-specific criteria for unilateral language dominance, its result should be disregarded. Then a Wada test and/or ESM should be performed. Algorithms describing the application of fMRI, the Wada test, and ESM for language lateralization and localization are given in Fig. 3.

Memory fMRI is the most challenging of the three applications discussed here. Again, all methodological limitations described have to be taken into account. The most complicated aspect of memory fMRI is the definition of an activation protocol. In memory fMRI not only the choice of verbal and nonverbal material is of relevance for quantifying dominant

or nondominant temporal or frontal lobe function and the contralateral reserve capacity. Further issues are whether to explore the encoding or retrieval of material, the assessed quality of recalling (e.g., to remember vs. to know), and if subjects use encoding strategies depending on materials presented (e.g., verbalization of figural material). For a review of these issues, see Golby et al. 2001). Another problem of memory fMRI is that the most relevant area of interest consists of the temporomesial structures. This results in problems because of susceptibility artifacts and geometric distortions close to pneumatized paranasal sinuses.

Several attempts have been made to predict the effects of surgery on memory in individual subjects. In the most elaborate study so far, Bonelli et al. (2010) concluded that memory fMRI alone is not sufficient for prediction of post-operative memory loss. Positive predictive values for post-operative verbal or visual memory changes are around 30% because of a relatively large number of false positives. Only when the covariates language lateralization assessed with language fMRI and preoperative memory scores according to neuropsychological tests are taken into account, acceptable positive predictive values (70 and 100%, respectively) can achieved (Bonelli et al. 2010). Because memory fMRI is still a subject of intensive research, it is not yet robust enough for routine clinical application by nonspecialists.

Acknowledgments I thank S. Bonelli, MD, PhD, for critically reviewing the manuscript.

References

Adcock JE, Wise RG, Oxbury JM, Oxbury SM, Matthews PM (2003) Quantitative fMRI assessment of the differences in lateralization of language-related brain activation in patients with temporal lobe epilepsy. Neuroimage 18(2):423–438

Baxendale S (2009) The Wada test. Curr Opin Neurol 22(2):185–189.

Berger MS, Kincaid J, Ojemann GA, Lettich E (1989) Brain mapping techniques to maximize resection, safety, and seizure control in children with brain tumors. Neurosurgery 25(5):786–792

Binder JR, Swanson SJ, Hammeke TA, Morris GL, Mueller WM, Fischer M, Benbadis S, Frost JA, Rao SM, Haughton VM (1996) Determination of language dominance using functional MRI: a comparison with the Wada test. Neurology 46(4):978–984

Binder JR, Frost JA, Hammeke TA, Bellgowan PS, Rao SM, Cox RW (1999) Conceptual processing during the conscious resting state. A functional MRI study. J Cogn Neurosci 11(1):80–95

Bonelli SB, Powell RH, Yogarajah M, Samson RS, Symms MR, Thompson PJ, Koepp MJ, Duncan JS (2010) Imaging memory in temporal lobe epilepsy: predicting the effects of temporal lobe resection. Brain 133(Pt 4):1186–1199

Desmond JE, Annabel Chen SH (2002) Ethical issues in the clinical application of fMRI: factors affecting the validity and interpretation of activations. Brain Cogn 50(3):482–497

Donaldson DI, Buckner RL (2001) Effective paradigm design. In: Mathews PM, Jezzard P, Evans AC (Eds.) Functional magnetic resonance imaging of the brain: methods for neuroscience. Oxford University Press, Oxford 177–95

Fernandez G, de Greiff A, von Oertzen J, Reuber M, Lun S, Klaver P, Ruhlmann J, Reul J, Elger CE (2001) Language mapping in less than 15 min: real-time functional MRI during routine clinical investigation. Neuroimage 14(3):585–594

FitzGerald DB, Cosgrove GR, Ronner S, Jiang H, Buchbinder BR, Belliveau JW, Rosen BR, Benson RR (1997) Location of language in the cortex: a comparison between functional MR imaging and electrocortical stimulation. AJNR Am J Neuroradiol 18(8): 1529–1539

Golby AJ, Poldrack RA, Brewer JB, Spencer D, Desmond JE, Aron AP, Gabrieli JD (2001) Material-specific lateralization in the medial temporal lobe and prefrontal cortex during memory encoding. Brain 124(Pt 9):1841–1854

Haag A, Knake S, Hamer HM, Boesebeck F, Freitag H, Schulz R, Baum P, Helmstaedter C, Wellmer J, Urbach H, Hopp P, Mayer T, Hufnagel A, Jokeit H, Lerche H, Uttner I, Meencke HJ, Meierkord H, Pauli E, Runge U, Saar J, Trinka E, Benke T, Vulliemoz S, Wiegand G, Stephani U, Wieser HG, Rating D, Werhahn K, Noachtar S, Schulze-Bonhage A, Wagner K, Alpherts WC, Boas WE, Rosenow F (2008) The Wada test in Austrian, Dutch, German, and Swiss epilepsy centers from 2000 to 2005: a review of 1421 procedures. Epilepsy Behav 13(1):83–89

Hamberger MJ (2007) Cortical language mapping in epilepsy: a critical review. Neuropsychol Rev 17(4):477–489

Helmstaedter C, Kurthen M, Linke DB, Elger CE (1997) Patterns of language dominance in focal left and right hemisphere epilepsies: relation to MRI findings, EEG, sex, and age at onset of epilepsy. Brain Cogn 33(2):135–150

Helmstaedter C, Brosch T, Kurthen M, Elger CE (2004) The impact of sex and language dominance on material-specific memory before and after left temporal lobe surgery. Brain 127(Pt 7):1518–1525

Jansen A, Menke R, Sommer J, Forster AF, Bruchmann S, Hempleman J, Weber B, Knecht S (2006) The assessment of hemispheric lateralization in functional MRI—robustness and reproducibility. Neuroimage 33(1):204–217

Janszky J, Jokeit H, Heinemann D, Schulz R, Woermann FG, Ebner A (2003) Epileptic activity influences the speech organization in medial temporal lobe epilepsy. Brain 126(Pt 9):2043–2051

Kurthen M, Helmstaedter C, Linke DB, Hufnagel A, Elger CE, Schramm J (1994) Quantitative and qualitative evaluation of patterns of cerebral language dominance. An amobarbital study. Brain Lang 46(4):536–564

Liegeois F, Connelly A, Cross JH, Boyd SG, Gadian DG, Vargha-Khadem F, Baldeweg T (2004) Language reorganization in children with early-onset lesions of the left hemisphere: an fMRI study. Brain 127(Pt 6):1229–1236

Loddenkemper T, Morris HH, Moddel G (2008) Complications during the Wada test. Epilepsy Behav 13(3):551–553

Logothetis NK (2002) The neural basis of the blood-oxygen-level-dependent functional magnetic resonance imaging signal. Philos Trans R Soc Lond Ser B Biol Sci 357(1424):1003–1037

Loring DW, Meador KJ, Allison JD, Pillai JJ, Lavin T, Lee GP, Balan A, Dave V (2002) Now you see it, now you don't: statistical and methodological considerations in fMRI. Epilepsy Behav 3(6):539–547

Price CJ (2000) The anatomy of language: contributions from functional neuroimaging. J Anat 197(Pt 3):335–359

Ramsey NF, Sommer IE, Rutten GJ, Kahn RS (2001) Combined analysis of language tasks in fMRI improves assessment of hemispheric dominance for language functions in individual subjects. Neuroimage 13(4):719–733

Ruff IM, Petrovich Brennan NM, Peck KK, Hou BL, Tabar V, Brennan CW, Holodny AI (2008) Assessment of the language laterality index in patients with brain tumor using functional MR imaging: effects of thresholding, task selection, and prior surgery. AJNR Am J Neuroradiol 29(3):528–535

Rutten GJ, Ramsey NF, van Rijen PC, van Veelen CW (2002) Reproducibility of fMRI-determined language lateralization in individual subjects. Brain Lang 80(3):421–437

Sabbah P, Chassoux F, Leveque C, Landre E, Baudoin-Chial S, Devaux B, Mann M, Godon-Hardy S, Nioche C, Ait-Ameur A, Sarrazin JL, Chodkiewicz JP, Cordoliani YS (2003) Functional MR imaging in assessment of language dominance in epileptic patients. Neuroimage 18(2):460–467

Spreer J, Arnold S, Quiske A, Wohlfarth R, Ziyeh S, Altenmuller D, Herpers M, Kassubek J, Klisch J, Steinhoff BJ, Honegger J, Schulze-Bonhage A, Schumacher M (2002) Determination of hemisphere dominance for language: comparison of frontal and temporal fMRI activation with intracarotid amytal testing. Neuroradiology 44(6):467–474

Staudt M (2010) Reorganization after pre- and perinatal brain lesions. J Anat 217(4):469–474

Swanson SJ, Sabsevitz DS, Hammeke TA, Binder JR (2007) Functional magnetic resonance imaging of language in epilepsy. Neuropsychol Rev 17(4):491–504

Weber B, Wellmer J, Reuber M, Mormann F, Weis S, Urbach H, Ruhlmann J, Elger CE, Fernandez G (2006) Left hippocampal pathology is associated with atypical language lateralization in patients with focal epilepsy. Brain 129(Pt 2):346–351

Wellmer J, Fernández G, Linke DB, Urbach H, Elger CE, Kurthen M (2005) Unilateral intracarotid amobarbital procedure for language lateralization. Epilepsia 46:1764–1772

Wellmer J, Weber B, Urbach H, Reul J, Fernandez G, Elger CE (2009) Cerebral lesions can impair fMRI-based language lateralization. Epilepsia 50(10):2213–2224

Wellmer J, von der Groeben F, Klarmann U, Weber C, Elger CE, Urbach H, Clusmann H, von Lehe M. (2012) Risk-benefit ratio of chronic invasive presurgical evaluation of epilepsy patients using subdural and intracerebral electrodes. Epilepsia 2012 Aug 53(8):1322−1332. doi:10.1111/j.1528-1167.2012.03545.x

Wellmer J, Weber B, Weis S, Klaver P, Urbach H, Reul J, Fernandez G, Elger CE (2008) Strongly lateralized activation in language fMRI of atypical dominant patients—implications for presurgical work-up. Epilepsy Res 80:67–76

Wilke M, Schmithorst VJ (2006) A combined bootstrap/histogram analysis approach for computing a lateralization index from neuroimaging data. Neuroimage 33(2):522–530

Yetkin FZ, Mueller WM, Morris GL, McAuliffe TL, Ulmer JL, Cox RW, Daniels DL, Haughton VM (1997) Functional MR activation correlated with intraoperative cortical mapping. AJNR Am J Neuroradiol 18(7):1311–1315

The Wada Test

Horst Urbach and Jörg Wellmer

Contents

Abstract

The Wada test or intracarotid amobarbital procedure (IAP) consists of the short inactivation of one brain hemisphere due to the injection of amobarbital or another short-acting anesthetic into the supplying internal carotid artery (ICA). During the subsequent inactivation period, neurological functions such as language and memory can be tested to assess the respective functional reserve capacity of the contralateral hemisphere. Less frequent indications for a Wada test are the assessment of motor function and the identification of secondary bilateral synchrony in EEG. With the advent of high-resolution structural MRI assuring the morphological integrity of the contralateral temporal lobe or hemisphere and functional MRI (fMRI) the number of Wada tests within the presurgical work up of epilepsy patients has decreased. However, it is still method of choice in epilepsy patients with suspected atypical or bilateral language representations according to fMRI, in patients with lesions interfering with the BOLD effect (e.g., cavernomas), and in children or intellectually challenged patients, in which fMRI cannot be used.

1 Introduction

The neurologist Juhn Wada (Wada 1949, translation in Wada 1997) reported the effects of unilateral intracarotid injections of amobarbital on language in an article published in Japanese in 1949. While at the Montreal Neurologic Institute in the 1950s, Wada introduced his technique in the presurgical evaluation of epilepsy patients to determine language lateralization before surgery (Wada and Rasmussen 1960). Within a few years, it became evident that this technique could also be used to assess memory capacity in patients who were candidates for temporal lobectomy or amygdalohippocampectomy. In this pre-imaging era, further indications were the lateralization of the seizure focus and the prediction of

H. Urbach (✉)
Department of Neuroradiology,
University Hospital Freiburg, Germany
e-mail: horst.urbach@uniklinik-freiburg.de

J. Wellmer
Ruhr-Epileptology, Department of Neurology,
University Hospital Knappschaftskrankenhaus,
Bochum, Germany

H. Urbach (ed.), *MRI in Epilepsy*, Medical Radiology. Diagnostic Imaging,
DOI: 10.1007/174_2012_619, © Springer-Verlag Berlin Heidelberg 2013

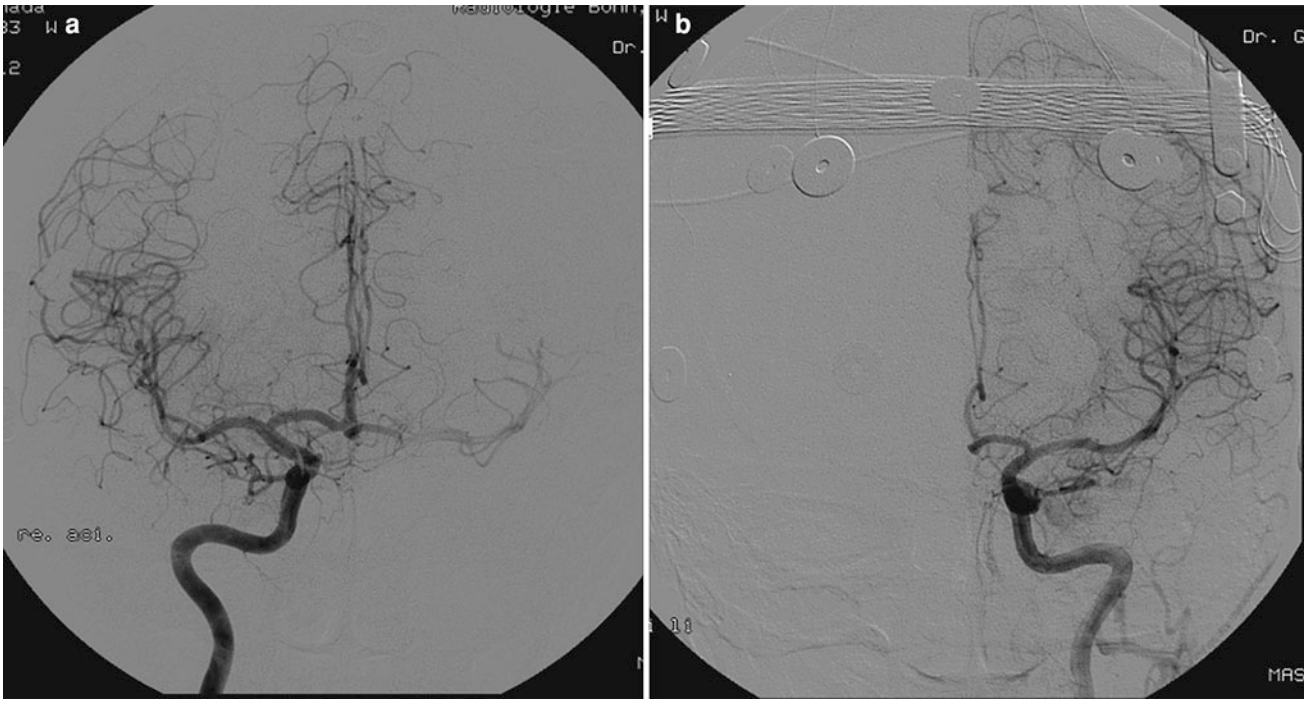

Fig. 1 IAP in a 28 year old woman with right-sided frontal lobe epilepsy and bilateral fMRI language representation. Bilateral ICA angiograms before a left-sided IAP show a more prominent right- than left-sided A1 segment of the anterior cerebral artery (ACA). With manual high pressure contrast injection into the right ICA, retrograde ACA and MCA opacification is obtained. However, with gentle and slow amoabarbital injections, each hemisphere is likely anaesthetized via the ipsilateral ICA

postoperative outcome (Spencer et al. 2000; Lee et al. 2003; Baxendale et al. 2008, Baxendale 2009). For more selective memory testing and in order to avoid confounding effects of hemispheric language inactivation, selective Wada tests with amobarbital injections into the posterior cerebral artery (PCA), the anterior choroidal artery (AchoA) or the middle cerebral artery or its branches have been developed (Jack et al. 1988, 1989; Wieser et al. 1997; Urbach et al. 2001, 2002). However, as an invasive procedure with an inherent risk of permanent neurological deficits, Wada tests are performed on selected patients only occasionally (Haag et al. 2008; Wagner et al. 2012).

2 Angiographic Work-Up

2.1 IAP

A 5F sheath is placed in the femoral artery ipsilateral to the intended intracarotid injection side. A 5F vertebral catheter is navigated into both common carotid arteries and digital subtraction angiograms are obtained before the catheter is advanced into the ICA on the injection side. The reason for bilateral anterior circulation angiograms is to rule out prominent anastomotic channels from the ICA to the vertebrobasilar system and to assess the angiographic supply to the hemispheres (Fig. 1). For example, if both anterior cerebral arteries are fed via one ICA, amobarbital injection in this ICA often leads to an "mutistic" patient for the test period.

Before amobarbital is injected via the placed catheter, the epileptological team starts the continuous EEG recording and may present initial memory material for later recall. In the Bonn protocol, the patient is then asked to elevate both arms and to count backwards from 100. While counting backwards, a 2 ml dose containing 200 mg amobarbital in a 10 % solution is manually injected with a rate of approximately 1 ml/s (Kurthen et al. 1994; Wellmer et al. 2005). For alternative anesthetics, see below.

During the injection period, the contralateral arm will fall and be gently caught captured by a third person. If the arm is hemiplegic and the EEG shows an ipsilateral slowing, hemispheric inactivation is likely and the catheter withdrawn, while the neurologist proceeds with the test.

2.2 Selective Wada Test

A 6F guiding catheter is introduced through a 6F sheath and placed in the ICA the dominant vertebral artery. A 0.010 microcatheter is navigated under fluoroscopic and "roadmapping" control in the P2-segment of the PCA (Figs. 2, 3), the origin of the AChoA, or the middle cerebral artery (Fig. 4).

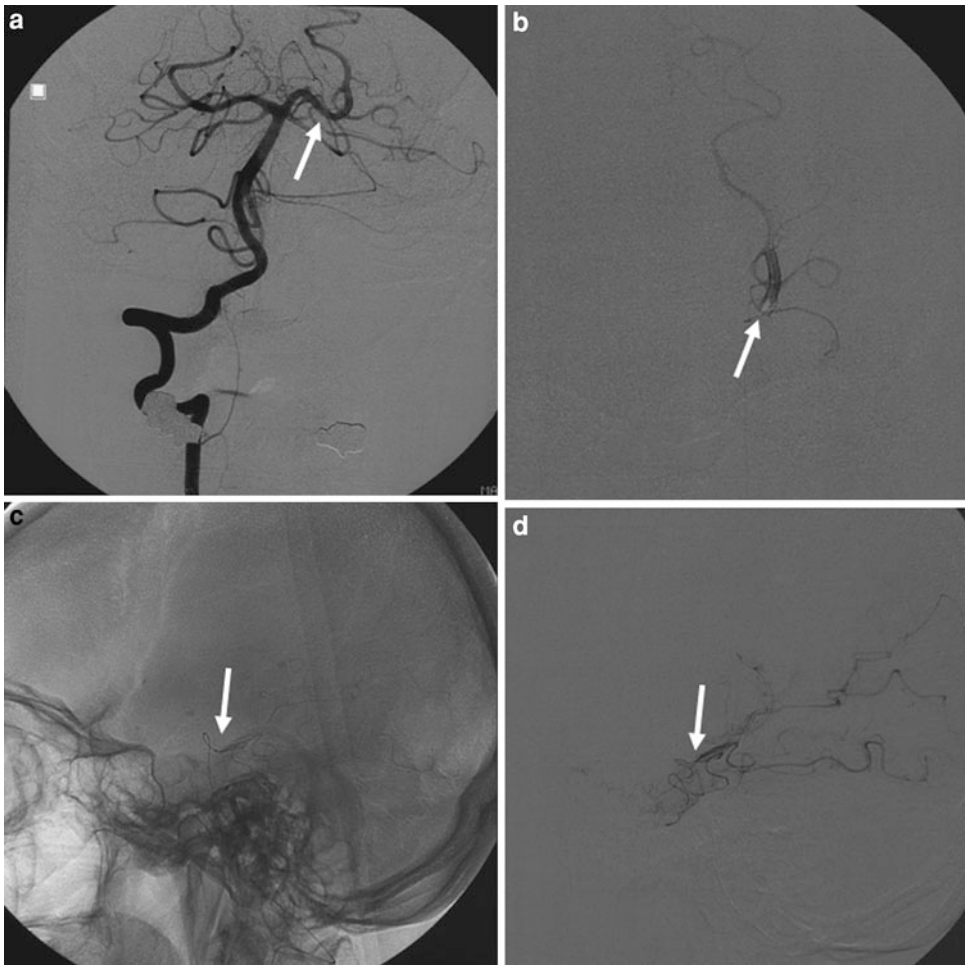

Fig. 2 Selective PCA Wada test in a 53 year old woman with left-sided hippocampal sclerosis. **a** 6 French guiding catheter was placed in the dominant vertebral artery (**a**). The microcatheter was placed in the P2-segment of the left PCA (**b**–**d**: arrow pointing to the microcatheter tip) and 80 mg amobarbital in a 1 % solution were injected together with 99mTc-HMPAO. During the test the patient showed homonymous hemianopia to the right side, no hemiparesis or aphasia. She was unable to recall or remember previously presented verbal items suggesting verbal memory capacity of the left hippocampus

Depending on the brain area that is intended to be anesthetized distal M1 segment or superior or inferior MCA trunk placements may be sufficient. Blood flow is proven by gentle contrast injections and catheter wedge positions have to be avoided. A 4–8 ml dose containing 40–80 mg amobarbital in a 1 % solution is manually injected with a rate of approximately 0.5 ml/s.

The amobarbital distribution within a brain hemisphere can be visualized if amobarbital is simultaneously injected with ^{99m}Tc-hexamethyl-propylene amine oxime (^{99m}Tc-HMPAO). Within about 2 h following the injection, the HMPAO distribution can be depicted with single photon emission tomography (SPECT) co-registered to MRI (Coubes et al. 1995; Von Oertzen et al. 2000; Brechtelsbauer et al. 1998). IAPs is mostly performed without SPECT-control.

3 Complications Related to the Wada-Test

In the largest multi-center survey, 15 complications were reported out of 1,421 Wada tests (1.09 %). Four of them were likely of thromboembolic origin; one occurred following a PCA Wada test. Permanent morbidity rate was 0.36 % (Haag et al. 2008). Loddenkemper et al. 2008 reported a similar permanent morbidity rate (0.3 % out of 1,225 procedures). The rather low complication rate in both series may be due to the fact that Wada tests are mostly performed in relatively younger patients without pre-existing vascular pathology as compared to patients who receive cerebral angiography for cerebrovascular events.

4 Neuropsychological Work-Up

It is beyond the scope of this volume to describe the neuropsychological work-up in detail; moreover IAP protocols vary among several institutions (Kurthen et al. 1994; Woremann et al. (2003) Wellmer et al. 2005; Haag et al. 2008). Most centers apply a formalized test protocol for assessing expressive and receptive language functions as well as verbal and figural memory (Haag et al. 2008). The results of language and memory tests are usually given in categories such as unilateral left or right language dominance or various degrees or qualities of mixed dominance (Kurthen et al. 1994). The interpretation of test results with

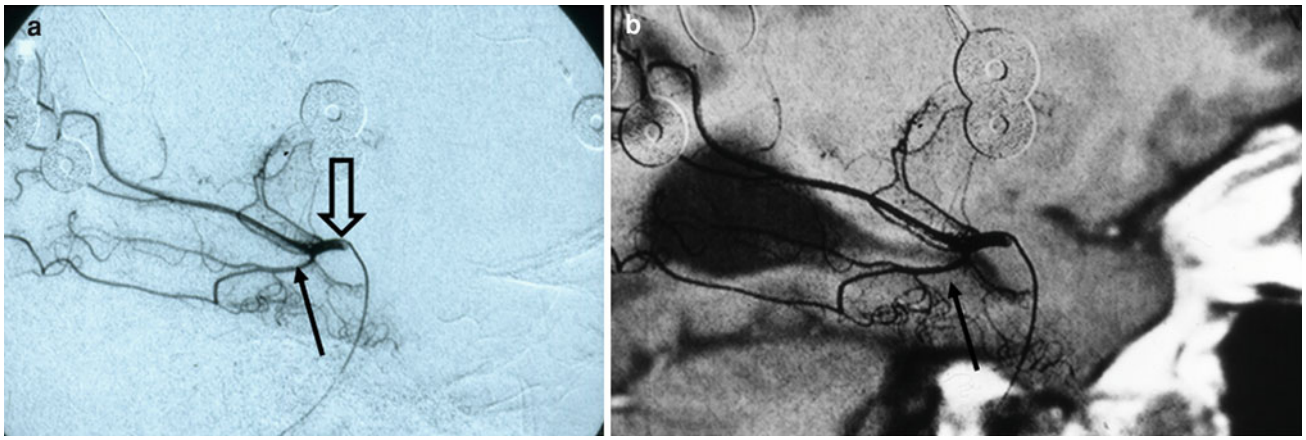

Fig. 3 Lateral angiogram via a microcatheter with its tip placed in the PCA (**a**) and angiogram superimposed on a sagittael T1-weighted image through the mesial temporal lobe (**b**) show a prominent inferior temporal artery supplying most of the mesial temporal lobe

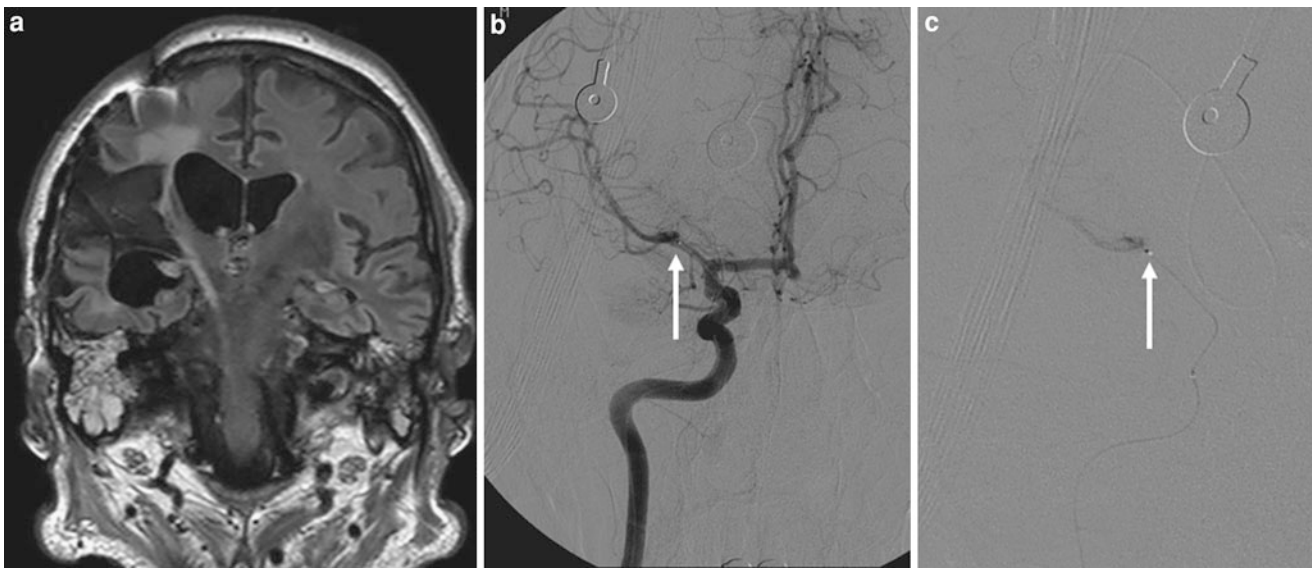

Fig. 4 Right-sided middle cerebral artery (MCA) Wada test in a 45 year old man with a right-sided posttraumatic tissue defect and status epilepticus since three months. In order to test the hypothesis that bilateral spike and wave EEG complexes originated in the right and propagated to the left hemisphere a right-sided IAP was scheduled. Right-sided ICA angiogram showed a thin right MCA and prominent A1 segment of the right-sided anterior cerebral artery (ACA) feeding both ACAs (**a**). With intracarotid amobarbital injection amobarbital distribution to the left-sided ACA territory is likely. It was decided to place a microcatheter in the distal M1 segment of the right MCA (**b**, **c**: *arrow*) and to inject 100 mg amobarbital in a 1% solution. With amobarbital injection into the MCA bilteral EEG spike and wave complexes right-sided EEG complexes disappeared, left-sided did not

regard to risk of postsurgical language or memory deficits may require additional biographical information on the patient such as age at seizure onset (Helmstaedter 2004).

Independent of the applied protocol it is essential to monitor the duration of action of the anesthetic during the test, either by EEG (presence of ipsilateral slowing) or clinically (grip strength or arm paresis). In case of ceasing action of the anesthetic the neuropsychological test must be stopped in order to prevent false negative or false positive results. A repeated injection of the anesthetic is possible, but the second dose must be chosen depending on the half-life time to prevent the accumulation of the anesthetic.

The same accounts for Wada tests subsequently testing both hemispheres. Between two high dose amobarbital tests one night of recovery is recommended. Short acting drugs without the risk of accumulation may be injected in both hemispheres with only a short break in between.

5 Drugs

5.1 Amobarbital

Amobarbital was considered the ideal drug for the Wada test for a long time, owing to its brief action, low toxicity, and the its great success substance. In the Bonn Epilepsy Surgery program, initially 200 mg sodium amobarbital was injected into the left and the right ICA on two separate days (Kral et al. 2002; Kurthen et al. 1994; Urbach et al. 1999). This procedure was chosen since successive injections of high doses of amobarbital can lead to significant drowsiness that cannot be fully avoided by bridging the time between two injections in one day. A dose lower than 200 mg reduces confidence in the inactivation of the injected hemisphere (Wellmer et al. 2005). However, a bilateral Wada test is not required in all indications. If the Wada-test is performed on the side of the intended surgery, in most instances a unilateral Wada-test is sufficient to predict whether the patient is at risk for post-operative language disturbance or not (Wellmer et al. 2005). This makes the application of high-dose amobarbital Wada tests practicable.

Since amobarbital is difficult to obtain in several countries, alternative drugs have been evaluated in the meantime. In our opinion, none of the alternatives can yet recommended as being equally safe and effective.

5.2 Methohexital

Methohexital, which had initially been investigated by Buchtel and colleagues, is a short-lasting drug, so that two successive injections are needed for each hemisphere (Buchtel et al. 2002). In a series of patients between 2005 and 2007, we manually injected a 3 ml dose containing 3 mg Brevimytal in a 0.1 % solution with a rate of approximately 1 ml/s. If the Brevimytal effect was expected to disappear (estimated clinically or after an interval of 90 s), another 2 mg were injected. When the test for one side was finished, the catheter was navigated into the contralateral ICA, and the procedure repeated. Yet, methohexital has siginificant disadvantages. In our experience, the duration of action of the first dose of 3 mg of methohexital varies considerably among patients. According to EEG, in 13 % of 54 procedures the action of amobarbital ended before 90 s had gone by. This signifies a likely gap of action before the second injection. In other patients, a single 3 mg injection produced ipsilateral EEG slowing for up to 260 s. In these cases, the second injection (after 90 s) leads to prolonged drowsiness that prevents further testing (unpublished observations). The rapid decrease of action of methohexital, however, makes a careful clinical testing of persistent action parallel to the neuropsychological assessment difficult. Another drawback is that methohexital may decrease seizure thresholds and trigger seizures (Loddenkemper et al. 2008). We stopped using methohexital and returned to amobarbital.

5.3 Etomidate

Etomidate is a nonbarbiturate hyponotic drug with no analgesic properties, with a rapid onset, and short duration of action. Jones-Gotman and colleagues reported bolus administration of 2 mg (0.03–0.04 mg/kg) and subsequent infusion of 0.003–0.004 mg/kg/minute can more likely assure a guaranteed period of hemianesthesia, averaging over 4 min in their study of 30 injections. Reported side effects in the Montreal study included a shivering-like tremor in the contralateral arm in about half of the injections, and either evidence of contralateral EEG slowing following most injections, or an increase in interictal spike activity in the hemisphere ipsilateral to injection (Jones-Gotman et al. 2005). Another concern is that etomidate may cause adrenal insufficiency, particularly in critically ill patients (Grote and Meador 2005).

5.4 Propofol

Propofol seems to work like amobarbital (Takayama et al. 2004), but the risk of adverse advent is higher. In the study by Mikuni and colleagues, about one-third of patients had an adverse event following propofol injection, with 12 % of all patients having increased muscle tone with twitching and rhythmic movements or tonic posturing. Patients older than 55, and a total injection dose greater than 20 mg, were predictors of more significant adverse events, which in turn carry a risk of incompletion or inaccuracy of the Wada test (Mikuni et al. 2005). Previous studies have also shown risks associated with propofol injection, including pain upon injection and anaphylaxis (Grote and Meador 2005).

References

Baxendale S (2009) The Wada test. Curr Opin Neurol 22(2):185–189

Baxendale S, Thomson PJ, Duncan JS (2008) Evidence-based practice: a reevaluation of the intracarotid amobarbital procedure (Wada test). Arch Neurol 65:841–845

Brechtelsbauer D, Klemm E, Urbach H, Koehler W, Solymosi L (1998) Amobarbitalverteilung im intrakarotidalen Wadatest: korrelation von Angiogramm und hochauflösendem SPECT. Klin Neuroradiol 8:182–185

Buchtel HA, Passaro EA, Selwa EM, Deveikis J, Gomez-Hassan D (2002) Sodium methohexital (Brevital) as an anaesthetic in the Wada test. Epilepsia 43:1056–1061

Coubes P, Baldy-Moulinier M, Zanca M et al (1995) Monitoring sodium methohexital distribution with (99mTc)HMPAO single photon emission computed tomography during Wada test. Epilepsia 36:1041–1049

Grote CL, Meador K (2005) Has amobarbital expired? considering the future of the Wada. Neurology 65:1692–1693

Haag A, Knake S, Hamer HM, Boesebeck F, Freitag H, Schulz R, Baum P, Helmstaedter C, Wellmer J, Urbach H, Hopp P, Mayer T, Hufnagel A, Jokeit H, Lerche H, Uttner I, Meencke HJ, Meierkord H, Pauli E, Runge U, Saar J, Trinka E, Benke T, Vulliemoz S, Wiegand G, Stephani U, Wieser HG, Rating D, Werhahn K, Noachtar S, Schulze-Bonhage A, Wagner K, Alpherts WC, Boas WE (2008) Arbeitsgemeinschaft für prächirurgische epilepsiediagnostik und operative epilepsietherapie e.V. The Wada test in Austrian, Dutch, German, and Swiss epilepsy centers from 2000 to 2005: a review of 1421 procedures. Epilepsy Behav 13(1):83–89

Helmstaedter C (2004) Neuropsychological aspects of epilepsy surgery. Epilepsy Behav 5:S45–S55

Jack CR, Nichols DA, Sharbrough et al (1988) Selective posterior cerebral artery amytal test for evaluating memory function before surgery for temporal lobe seizures. Radiology 168:787–793

Jack CR, Nichols DA, Sharbrough et al (1989) Selective posterior cerebral artery injection of amytal: new method of preoperative memory testing. Mayo Clin Proc 64:965–975

Jones-Gotman M, Sziklas V, Djordjevic J et al (2005) Etomidate speech and memory test (eSAM): a new drug and improved intracarotid procedure. Neurology 65:1723–1729

Kral T, Clusmann H, Urbach H, Schramm J, Elger CE, Kurthen M, Grunwald T (2002) Prächiurgische abklärung bei der epilepsiechirurgie (bonner algorithmus). Zentralbl Neurochir 63:106–110

Kurthen M, Helmstaedter C, Linke DB, Hufnagel A, Elger CE, Schramm J (1994) Quantitative and qualitative assessment of patterns of cerebral language dominance: an amobarbital study. Brain Lang 46:534–564

Lee GP, Park YD, Westerveld M, Hempel A, Blackburn LB, Loring DW (2003) Wada memory performance predicts seizure outcome after epilepsy surgery in children. Epilepsia 44:936–943

Loddenkemper T, Moddel G, Schuele SU et al (2007) Seizures during intracarotid metohexital and amobarbital testing. Epilepsy Behav 10:49–54

Loddenkemper T, Morris HH, Möddel G (2008) Complications during the Wada test. Epilepsy Behav 13:551–553

Mikuni N, Takayama M, Satow T et al (2005) Evaluation of adverse effects in intracarotid propofol injection for Wada test. Neurology 65:1813–1816

Spencer DC, Morrell MJ, Risinger MW (2000) The role of the intracarotid amobarbital procedure in evealuation of patients for epilepsy surgery. Epilepsia 41:320–325

Takayama M et al (2004) Intracarotid propofol test for speech and memory dominance in man. Neurology 63:510–515

Urbach H, Kurthen M, Klemm E, Grunwald T, Van Roost D, Linke DB, Biersack HJ, Schramm J, Elger CE (1999) Amobarbital effects on the posterior hippocampus during the intracarotid amobarbital test. Neurology 52:1596–1602

Urbach H, Klemm E, Linke DB, Behrends K, Biersack HJ, Schramm J, Schild HH (2001) Posterior cerebral artery Wada test: amobarbital distribution and functional deficits. Neuroradiology 43:290–294

Urbach H, von Oertzen J, Klemm E, Koenig R, Kurthen M, Schramm J, Elger CE (2002) Selective middle cerebral artery Wada tests as a part of presurgical evaluation in patients with drug-resistant epilepsies. Epilepsia 43:1217–1223

Von Oerzten J, Klemm E, Urbach H, Kurthen M, de Greiff A, Linke DB, Biersack HJ, Elger CE (2000) SATSCOM- Selective amobarbital test intraarterial SPECT coregistered to MRI: description of a method assessing selective perfusion. Neuroimage 12:617–622

Wada J (1949) A new method for determination of the side of cerebral speech dominance: a preliminary report on the intracarotid injection of sodium Amytal in man. Igaku to Seibutsugaku 14:221–222

Wada J (1997) Clinical experimental observations of carotid artery injections of sodium Amytal. Brain Cogn 33:11–13

Wada J, Rasmussen T (1960) Intracarotid injections of sodium Amytal for the lateralization of cerebral speech dominance: experimental and clinical observations. J Neurosurg 17:266–282

Wagner K, Hader C, Metternich B, Buschmann F, Schwarzwald R, Schulze-Bonhage A (2012) Who needs a Wada test? Present clinical indications for amobarbital procedures. J Neurol Neurosurg Psychiatry 83(5):503–509

Wellmer J, Fernandez G, Linke DB, Urbach H, Elger CE, Kurthen M (2005) Unilateral intracarotid amobarbital procedure (IAP) for language lateralization. Epilepsia 46:1764–1772

Wieser HG, Mueller S, Schiess R et al (1997) The anterior and posterior selective temporal lobe amobarbital tests: angiographic, clinical, electroencephalographic, PET, SPECT findings, and memory performance. Brain Cogn 33:71–97

Woermann FG, Jokeit H, Luerding R, Freitag H, Schulz R, Guertler S, Okujava M, Wolf P, Tuxhorn I, Ebner A (2003) Language lateralization by Wada test and fMRI in 100 patients with epilepsy. Neurology 61:699–701

Magnetic Resonance Spectroscopy in Chronic Epilepsy

Friedrich G. Woermann

Contents

Abstract

The cornerstone of lesion detection in chronic epilepsy is structural imaging, mainly magnetic resonance imaging. Metabolic information from magnetic resonance spectroscopy (MRS) might serve as an additional or as a surrogate marker for the epileptogenic lesion. MRS might also help to differentiate similarly appearing lesions from one another; it might detect contralateral/remote dysfunction. However, the clinical role of MRS is unclear, albeit another non-invasive diagnostic tool.

Magnetic resonance spectroscopy (MRS) measures the concentrations of metabolites in the brain noninvasively. In epilepsy, MRS aims to aid the identification of the epileptogenic lesion. Ultimately it aims to predict the postoperative outcome after surgical removal of these lesions. MRS results in epilepsy show similar abnormalities (loss of neuronal markers) associated with different pathological entities in different anatomical locations (Table 1). It is believed that MRS might give insights into the mechanisms of seizure generation (McLean et al. 2008).

1 Methodological Considerations

Physical principles underlying MRS are the same as for MRI, which means that most clinical scanners can be used for MRS. In epilepsy, proton-MRS studies are most common. The ^{1}H nucleus (a single proton) is abundant. MRS exploits minor differences in resonance frequency of ^{1}H depending on the metabolite to which protons are bound. MRS of certain brain metabolites needs techniques to exclude the strong signals arising from water and macromolecules (lipids and proteins, which both contain large numbers of protons) in order to study the smaller signals from more interesting metabolites (amino acids, sugars, etc.). Techniques to suppress the water peak and to reduce

F. G. Woermann (✉)
MRI Unit, Mara Hospital, Bethel Epilepsy Center,
33617 Bielefeld, Germany
e-mail: friedrich.woermann@mara.de

H. Urbach (ed.), *MRI in Epilepsy*, Medical Radiology. Diagnostic Imaging,
DOI: 10.1007/174_2012_761, © Springer-Verlag Berlin Heidelberg 2013

Table1 Textbook knowledge* on MRS in surgically remediable lesions in chronic epilepsy: low NAA and moderatly increased Cho are frequent findings.

Pathology	MRS finding*
Hippocampal sclerosis/mesial temporal sclerosis (MTS)	↓ NAA in hippocampus, temporal lobe; NAA/Cho < 0.8 suggests MTS; if scan patient within 24 hours of seizure, lactate/lipid peaks reported
Benign tumours	↑ Cho, ↓ NAA (vs. malignant tumours: ↑–↑↑↑ Cho, ↑ lactate/lipid)
Ganglioglioma	↑ Cho, ↓ NAA
Diffuse astrocytoma, low grade	↑–↑↑ Cho, ↓ NAA typical but not specific; relatively high Ins/Cr (compared to anaplastic astrocytoma)
DNT	Nonspecific (↑ Cho, ↓ NAA), but lactate present in some
Focal cortical dysplasia	↓ NAA, (↑ Cho); but ↓ NAA less pronounced compared to low grade astrocytomas
Other malformations of cortical development	Heterotopia: NAA and Cho are variable; Pachygyria-Polymicrogyria: ↓ NAA
Tuberous sclerosis	↓ NAA/Cr, ↑ Ins/Cr; lactate in seizure onset?
Cavernoma	(-)
Porencephaly	Absence of normal brain metabolites
Scars due to chronic cerebral infarction	↓ NAA
Posttraumatic scars	↓ NAA
Rasmussen encephalitis	↓ NAA, ↓ Cho; ↑ Ins, ↑ glutamine/glutamate
Hemiconvulsion-Hemiplegia-Epilepsy-Syndrome (following a febrile status epilepticus)	Within 24 hours of status: lactate and lipids; later: ↓ NAA
Arteriovenous Malformation	(-)
Hemimegalencephaly (a hemispheric malformation of cortical development)	Progressive ↓ NAA, ↑ Cho, ↑ Cr, ↑ Ins
Sturge Weber Syndrome	↓ NAA, ↑ Cho
Neurocysticercosis	↓ NAA, ↓ Cr; ↑ Cho, ↑ lactate, ↑ alanine

*extracted and modified from: Osborn A (Ed). Diagnostic Imaging—Brain. Amirsys, Salt Lake City, 2004
NAA N-Acetyl-aspartate; Cho choline, Cr creatine, Ins myo-inositol, ↓ decrease, ↑ increase, (-) no information available

or spatially exclude unwanted macromolecule signals are inherent parts of the examination. Spatial exclusion (also known as outer volume suppression) is needed because of intense lipid signals arising from the scalp. Disturbances from fat, but also inhomogeneities near the base of the skull, can make MRS a tedious technique in epilepsy as epileptogenic lesions are often mesiotemporal or cortical.

In vivo MRS measures only metabolites present at concentrations of about 1 mM or higher. The metabolites studied are shown in Fig. 1. At long echo times (TE ≥ 135 ms), a large signal is present from N-acetyl aspartate (NAA), a neuronal marker, or better, a marker of neuronal function. Other peaks stem from creatine plus phosphocreatine (Cr) supposedly representing the energy level and cellular density; choline-containing compounds (Cho) represent membrane turnover. At shorter echo times (e.g., 30 ms, as shown in Fig. 1), additional interesting peaks can be detected from myo-inositol (Ins; representing gliosis) and glutamate and glutamine (Glx; excitatory amino acids), but sophisticated modeling is necessary to distinguish the latter from the overlapping peaks, and baseline irregularities remain a major source of error at shorter echo times.

In single-voxel spectroscopy (SV-MRS), slice-selective excitation in three orthogonal planes excites a cuboid volume at their intersection (Fig. 1). The other common localization tool uses phase encoding, as in imaging. This is known as spectroscopic imaging (MRSI), sometimes called chemical shift imaging (CSI), and produces a slice with a grid of multiple voxels (Fig. 2).

Since the areas under the curves of metabolite signals are directly proportional to their concentrations in the tissue, spectra can be looked at qualitatively, or metabolite concentrations can be estimated quantitatively. Most commonly, the ratio of one peak to another is reported, such as NAA/Cr or NAA/(Cr + Cho). This has the advantage that any temporal, spatial, or intersubject differences in machine performance cancel out. Ratios can vary both in different tissues of the brain and in disease.

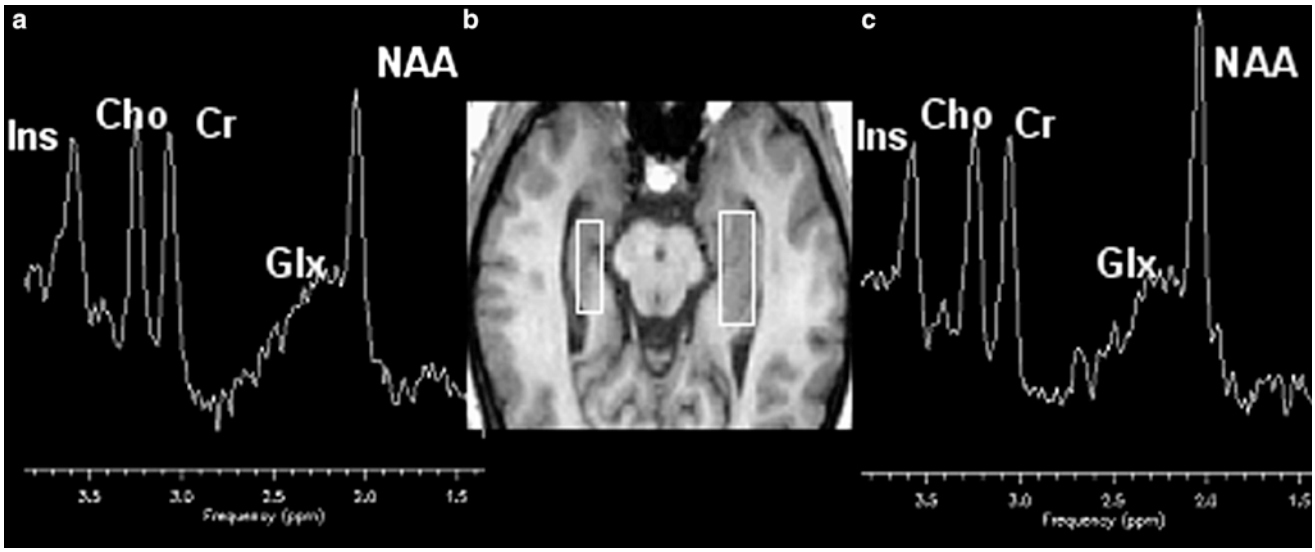

Fig. 1 Single-voxel short-TE MRS in a patient with right-sided hippocampal sclerosis. NAA on the affected side (**a**) is lower than on the contralateral side (**c**). The size of the voxel is tailored to atrophy of right-sided hippocampus to reduce the diluting influence of nearby CSF (**b**). Modified from Woermann et al. (1999b)

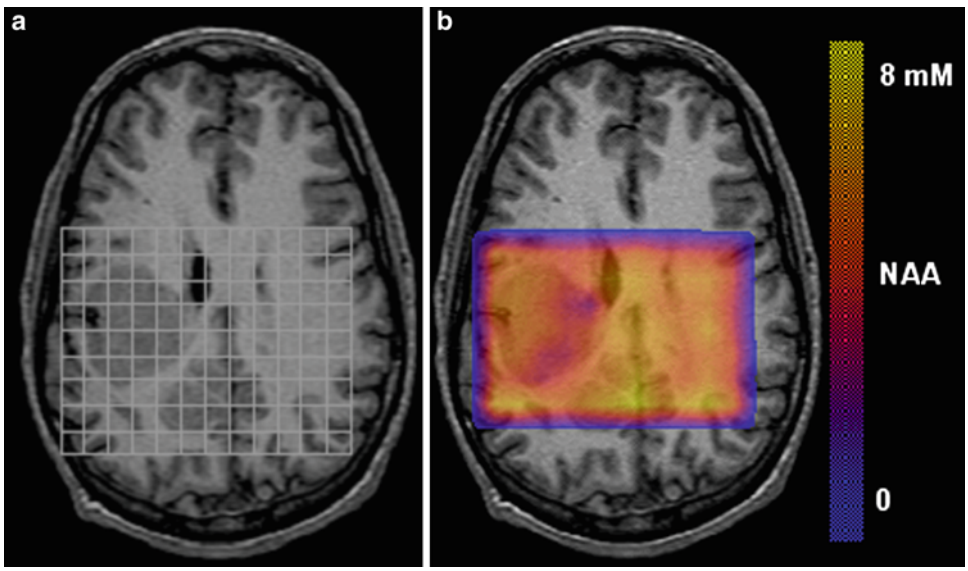

Fig. 2 Epilepsy patient with large heterotopia in a pericentral region on the right side. MR spectroscopic imaging produced a slice of multiple voxels (**a**). NAA can be quantified and concentration can be displayed as a color map (**b**). This map illustrates that NAA concentration varies within the large malformation of cortical development. Modified from Woermann et al. (2001)

2 MRS: Diagnostic Accuracy in Epilepsy

In the evaluation of patients with epilepsy, the potential value of ^{1}H-MRS (or -MRSI) depends on the method's ability to detect localized metabolic changes not only in clear-cut cases with visible lesions, but also in patients with normal MRI ("MRI-negative"). Ultimately, the clinical value of ^{1}H-MRS in this patient group is based on studies correlating presurgical measurements with postsurgical seizure and neuropsychological outcome.

Recently, diagnostic accuracies of different neuroimaging techniques in epilepsy were thoroughly reviewed (Whiting et al. 2006; Burch et al. 2012). MRS studies in epilepsy were included in case they allowed the computation of test-quality data correlating MRS results and post-surgical outcome or other gold standards in individual patients (Cross et al. 1996; Cendes et al. 1997; Knowlton et al. 1997; Achten et al. 1998; Kuzniecky et al. 1998; Li et al. 2000; Antel et al. 2002; Lee et al. 2005). These reviews resulted in very careful statements ("There was a trend for localisation of abnormalities to be associated with

a beneficial outcome"), but mainly stated, "Due to the limitations of the included studies, the results of this review do little to inform clinical practice."

3 MRS in Temporal Lobe Epilepsy and Hippocampal Sclerosis

In hippocampal sclerosis there are neuronal loss and gliosis. Typical MRS changes in the epileptogenic hippocampus are a reduction of NAA and sometimes an elevation of Cr and Cho (or corresponding changes to ratios like NAA/Cr, NAA/Cr + Cho, or Cr/NAA) relative to normal control subjects (Fig. 1). The contralateral hippocampus may be normal or may show a lesser degree of abnormality.

A recent meta-analysis (Willmann et al. 2006) aimed to assess the additional preoperative value of ^{1}H-MRS and correlated individual MRS data and seizure outcome. Unilateral MRS changes were reported to have a predictive value of 82 % for good postsurgical outcome, that is, predicting postsurgical freedom or marked improvement of seizures. TLE patients with unilateral MRS abnormality had a markedly better chance of becoming seizure free compared to patients with bilateral abnormalities.

The predictive value of bilateral MRS abnormalities (for unfavorable outcome) is less clear. Bilateral temporal MRS abnormalities have been observed to a varying degree in different studies in 0–70 % of patients (Cendes et al. 2002). Further reducing specificity, a postoperative metabolic normalization on the nonoperated side was observed (Kuzniecky et al. 2001). It led to the view that not only does a decrease in NAA represent neuronal loss in HS, but also that NAA might be a putative reversible, thus functional, marker in the contralateral hippocampus.

Some TLE patients with an apparently normal MRI ("MRI-negative") were the subject of feasibility studies or part of studies correlating typical MRS changes (low NAA ratios ipsilateral to the seizure onset with a relatively low degree of contralateral abnormality) with good postsurgical outcome. It is still unclear whether MRS is a valuable tool in this patient group (McLean et al. 2008).

Extrahippocampal or extratemporal abnormalities in patients with mesiotemporal/hippocampal sclerosis are called *dual pathology*. Dual pathology is rarely identified in a hypothesis-driven way, allowing the targeted placement of regions of interest. ^{1}H-MRS/MRSI could only contribute to the detection of these changes when single voxels or single MRSI slices were placed outside the hippocampus and/or outside the temporal lobe or by the use of multislice ^{1}H-MRSI (Mueller et al. 2002). When multislice ^{1}H-MRSI was used in combination with tissue segmentation, significantly lower NAA in ipsi- and contralateral frontal gray and nonfrontal white matter compared with controls was found although not correlated to outcome.

Although ^{1}H-MRS/MRSI has been advocated as part of a cluster or a sequence of clinical tests prior to epilepsy surgery in TLE, its contribution to the overall validity of the cluster or sequence remains to be determined. Influential epilepsy surgery programs with early enthusiasm for ^{1}H-MRS/MRSI ("NAA/Cho is an excellent marker for localizing the epileptogenic zone in TLE"; Ng et al. 1994) abandoned this noninvasive but tedious method as part of their presurgical evaluation of patients with TLE (McLean et al. 2008).

4 MRS in Extratemporal Neocortical Epilepsy

Studies correlating presurgical ^{1}H-MRS/MRSI data with postsurgical seizure outcome in patients with extratemporal neocortical epilepsy seem to be scarce especially when looking for studies allowing the estimation of test-quality data (Lee et al. 2005). Following the temporal lobes, the second-most frequent site of epileptogenic lesions is the frontal lobes. In the relatively large frontal lobes, the use of a restricted region-of-interest approach (single voxel or single slice) is expected to reduce the sensitivity of ^{1}H-MRS/MRSI for the localization or lateralization of extratemporal lesions (McLean et al. 2008).

5 MRS in Neocortical Epilepsies Due to Malformations of Cortical Development

Some proton MRS studies have been performed in patients with malformations of cortical development (MCD; Woermann et al. 2001). A decrease in NAA was the most frequent finding in individual MCD and in group comparisons. Measurements of individual metabolites were abnormal in some malformations and normal in others, suggesting metabolic heterogeneity. Even within a single MCD, metabolically normal regions were interspersed with metabolically abnormal regions (Fig. 2).

Whether MR spectroscopy can contribute to the distinction between low-grade gliomas and focal MCD (especially focal cortical dysplasia) remains unclear. Promising results from group comparisons (less NAA in tumors compared to MCD) await replication and prospective translation to clinical practice in individual patients (Vuori et al. 2004).

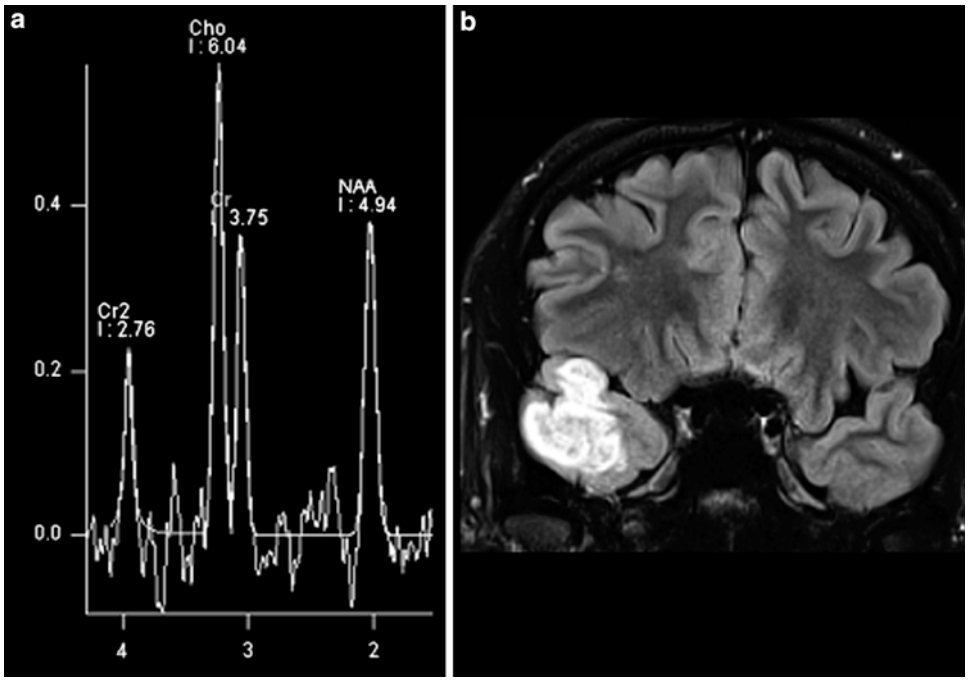

Fig. 3 MRS **a** with increase in choline **b** in a low grade tumor in the right temporal lobe

Prototypically in epilepsy patients with tuberous sclerosis, the presence of multiple bilateral lesions can make it difficult to identify a single lesion responsible for intractable epileptic seizures. Using MRS, a lactate peak was detected in the regions corresponding to an epileptic focus in some patients (Yapici et al. 2005).

In contrast to the numerous ^{1}H-MRS of TLE, there are only a few reports in other types of localization-related epilepsies. These studies suggest that the potential of correct seizure focus lateralization is less than in TLE.

6 MRS in Tumors

There is a wealth of literature on the use of MR spectroscopy in neurooncology [for a systematic review, see Hollingworth et al. (2006)]. Malignant tumors may be characterized by a relatively large increase in choline, a loss of NAA, and sometimes the detection of lactate or lipids. A ratio of Cho/NAA larger than 2 has been associated with brain malignancy, but it remains unclear whether this is more accurate than results from MRI with contrast enhancement (or whether this is more accurate than MR perfusion). The incremental benefit of MRS in the differentiation of low- from high-grade brain tumors is unclear.

In MRS of low-grade tumors, an increase of choline might be visible (Fig. 3).

7 MRS in Metabolic Disease and Epilepsy

In the neuronal ceroid lipofuscinoses (NCL), probably the most common progressive metabolic encephalopathies of childhood associated with seizures, MRS is said help to distinguish different subtypes. Infantile NCL was characterized by a complete loss of NAA, a marked reduction of Cr and Cho, and an elevation of myo-inositol and lactate in both gray and white matter. Reduced NAA and elevated lactate were also detected in gray and white matter of late infantile NCL. In contrast to the infantile forms, juvenile NCL exhibited normal metabolic profiles (McLean et al. 2008). It is questionable whether these differences are more important for diagnosis than the age of onset.

Lactate is usually not seen in spectra of normal adult brain. Lactate has been detected in patients with mitochondrial encephalopathies, but as with all other means used to diagnose rare disorders, MR spectroscopy does not depict elevated lactate in all cases.

8 MRS in Juvenile Myoclonic Epilepsy

Juvenile myoclonic epilepsy is a frequent electroclinical epilepsy syndrome. It is considered to be a generalized epilepsy that is treated medically and not surgically. A long-

existing, strong belief was that there are no changes in neuroimaging in these patients. Recent results from voxel-based morphometry implicating mesiofrontal cortical areas (Woermann et al. 1999a) were developed into a network hypothesis on the etiology of juvenile myoclonic epilepsy. This hypothesis has also been supported by MRS data showing NAA/Cr decreases in mesiofrontal and pericentral as well as thalamic areas (Lin et al. 2009).

9 Conclusion

MRS detects relevant metabolite changes in patients with hippocampal sclerosis and in patients with brain tumors. The impact of these findings on clinical decision making is unclear. Most epilepsy surgery programs do not use MRS in their sequence of presurgical tests. One important neuroradiological question, however, remains: Can proton MR spectroscopy differentiate between focal cortical dysplasia and low-grade tumors? Still another aim is to increase the sensitivity of different MR techniques in epilepsy so that epileptogenic lesions can be identified and treated surgically whenever possible.

References

Achten E, Santens P, Boon P et al (1998) Single-voxel proton MR spectroscopy and positron emission tomography for lateralization of refractory temporal lobe epilepsy. Am J Neuroradiol 19:1–8

Antel SB, Li LM, Cendes F et al (2002) Predicting surgical outcome in temporal lobe epilepsy patients using MRI and MRSI. Neurology 58:1505–1512

Burch J, Hinde S, Palmer S et al (2012) The clinical effectiveness and costeffectiveness of technologies used to visualise the seizure focus in people with refractory epilepsy being considered for surgery: a systematic review and decision-analytical model. Health Technol Assess 16(34):1–164

Cendes F, Caramanos Z, Andermann F et al (1997) Proton MR spectroscopic imaging and MRI volumetry in the lateralization of temporal lobe epilepsy: a series of 100 patients. Ann Neurol 42:737–746

Cendes F, Knowlton RC, Novotny E et al (2002) Magnetic resonance spectroscopy in epilepsy: clinical issues. Epilepsia 43 (Suppl. 1):32–39

Cross JH, Connelly A, Jackson GD et al (1996) Proton magnetic resonance spectroscopy in children with temporal lobe epilepsy. Ann Neurol 39:107–113

Hollingworth W, Medina LS, Lenkinski RE et al (2006) A systematic literature review of magnetic resonance spectroscopy for the characterization of brain tumors. Am J Neuroradiol 27:1404–1411

Knowlton RC, Laxer KD, Ende G et al (1997) Presurgical multimodality neuroimaging in electroencephalographic lateralized temporal lobe epilepsy. Ann Neurol 42:829–837

Kuzniecky R, Hugg JW, Hetherington H et al (1998) Relative utility of 1H spectroscopic imaging and hippocampal volumetry in the lateralization of mesial temporal lobe epilepsy. Neurology 51:66–71

Kuzniecky R, Palmer C, Hugg J et al (2001) Magnetic resonance spectroscopic imaging in temporal lobe epilepsy: neuronal dysfunction or cell loss? Arch Neurol 58:2048–2053

Lee SK, Kim DW, Kim KK et al (2005) Effect of seizure on hippocampus in mesial temporal lobe epilepsy and neocortical epilepsy: an MRS study. Neuroradiology 47:916–923

Li LM, Cendes F, Antel SB et al (2000) Prognostic value of proton magnetic resonance spectroscopic imaging for surgical outcome in patients with intractable temporal lobe epilepsy and bilateral hippocampal atrophy. Ann Neurol 47:195–200

Lin K, Carrete H Jr, Lin J et al (2009) Magnetic resonance spectroscopy reveals an epileptic network in juvenile myoclonic epilepsy. Epilepsia 50:1191–1200

McLean MA, Koepp M, Woermann FG (2008) Magnetic resonance spectroscopy in patients with epilepsy. In: Lüders H (ed) Textbook of epilepsy Surgery. Informa Healthcare, London

Mueller SG, Suhy J, Laxer KD et al (2002) Reduced extrahippocampal NAA in mesial temporal lobe epilepsy. Epilepsia 43:1210–1216

Ng TC, Comair YG, Xue M et al (1994) Temporal lobe epilepsy: presurgical localization with proton chemical shift imaging. Radiology 193:465–472

Vuori K, Kankaanranta L, Hakkinen AM et al (2004) Low-grade gliomas and focal cortical developmental malformations: differentiation with proton MR spectroscopy. Radiology 230:703–708

Whiting P, Gupta R, Burch J et al (2006) A systematic review of the effectiveness and cost-effectiveness of neuroimaging assessments used to visualise the seizure focus in people with refractory epilepsy being considered for surgery. Health Technol Assess 10(4):1–164

Willmann O, Wennberg R, May T et al (2006) The role of 1H magnetic resonance spectroscopy in pre-operative evaluation for epilepsy surgery. A meta-analysis. Epilepsy Res 71:149–158

Woermann FG, Free SL, Koepp MJ et al (1999a) Abnormal cerebral structure in juvenile myoclonic epilepsy demonstrated with voxel-based analysis of MRI. Brain 122:2101–2108

Woermann FG, McLean MA, Bartlett PA et al (1999b) Short echo time single-voxel 1H magnetic resonance spectroscopy in magnetic resonance imaging-negative temporal lobe epilepsy: different biochemical profile compared with hippocampal sclerosis. Ann Neurol 45:369–376

Woermann FG, McLean MA, Bartlett PA et al (2001) Quantitative short echo time proton magnetic resonance spectroscopic imaging study of malformations of cortical development causing epilepsy. Brain 124:427–436

Yapici Z, Dincer A, Eraksoy M (2005) Proton spectroscopic findings in children with epilepsy owing to tuberous sclerosis complex. J Child Neurol 20:517–522

SPECT and PET

Wim Van Paesschen, Karolien Goffin and Koen Van Laere

Contents

Abstract

Ictal perfusion single photon emission computed tomography and positron emission tomography of brain metabolism are functional nuclear imaging modalities that are useful in the presurgical evaluation of patients with refractory focal epilepsy, and provide information on the ictal onset zone, seizure propagation pathways, and functional deficit zones. Combined with electrophysiological and coregistered MRI data, these techniques allow a noninvasive presurgical evaluation in a growing number of patients with refractory focal epilepsy, and are particularly useful in patients with normal MRI findings, focal dysplastic lesions, dual pathology and discordant seizure symptoms, and electrophysiology and morphological data. In addition, these techniques may provide crucial information in the planning of invasive electroencephalography studies.

1 Introduction

Single photon emission computed tomography (SPECT) and positron emission tomography (PET) are functional nuclear imaging modalities. SPECT allows the study of cerebral perfusion during the ictal and interictal states (Kapucu et al. 2009), and PET allows the study of cerebral metabolic and neurochemical processes. In the epilepsy clinic, 2-[^{18}F]fluoro-2-deoxy-D-glucose PET (FDG-PET) is commonly used to assess interictal and rarely ictal cerebral metabolism.

Functional nuclear imaging is most useful in the presurgical evaluation of patients with refractory focal epilepsy, and can delineate the ictal onset, seizure propagation, and functional deficit zones (Rosenow and Lüders 2001). "Functional" means that the imaging results are critically dependent on the timing of tracer injection, i.e., ictal, postictal, or interictal, and the seizure type (Van Paesschen et al. 2007a; Goffin et al. 2008). For ictal

W. Van Paesschen (✉)
Department of Neurology, University Hospital Leuven, Herestraat 49, 3000 Leuven, Belgium
e-mail: wim.vanpaesschen@uzleuven.be

K. Goffin · K. Van Laere
Division of Nuclear Medicine, University Hospital Leuven and Katholieke Universiteit Leuven, Leuven, Belgium

H. Urbach (ed.), *MRI in Epilepsy*, Medical Radiology. Diagnostic Imaging,
DOI: 10.1007/174_2012_561, © Springer-Verlag Berlin Heidelberg 2013

SPECT interpretation, it is, therefore, important to be aware of the seizure types, the timing of the injection, ictal symptoms, and electroencephalography (EEG) data. Both FDG-PET and ictal SPECT can predict seizure-free outcome after epilepsy surgery (Knowlton et al. 2008). Ictal SPECT is probably the most sensitive imaging modality to delineate the ictal onset zone in extratemporal lobe epilepsy (Knowlton et al. 2008; Kim et al. 2009).

2 Ictal Onset Zone, Propagation Pathways, and Functional Deficit Zone

Focal seizures start in the ictal onset zone, and can propagate through the brain (Rosenow and Lüders 2001). The functional deficit zone is the part of the cortex with an abnormal function between seizures, due to morphological or functional factors, or both. Understanding these concepts is crucial for proper interpretation of functional nuclear images.

2.1 Ictal SPECT

In the absence of seizure propagation, the largest hyperperfusion cluster with the highest z score represents the ictal onset zone. This pattern is usually observed with early ictal injections during simple or complex focal seizures, or in brain regions where ictal propagation is slow, and allows a reliable localization of the ictal onset zone on blinded assessment without prior knowledge of other data from the presurgical evaluation (Dupont et al. 2006).

Often, ictal SPECT shows propagated ictal activity, which is due to the slow time resolution of ictal SPECT with respect to seizure propagation. The transit time of a perfusion tracer from an arm vein to cerebral arteries is around 30 s. In addition, there is often a delay between seizure onset and injection of the perfusion tracer. Further, only around 60% of the perfusion tracer is extracted by nerve cells on the first pass (the other 40% is extracted later), contributing to the slow time resolution of ictal SPECT. Propagation patterns can be seen in all focal epilepsies, but most often in frontal lobe epilepsy (Dupont et al. 2006). Ictal SPECT injections during secondary generalized seizures show more areas of propagation than during focal seizures without generalization (Varghese et al. 2009). In the case of propagation, ictal hyperperfusion can be observed outside the ictal onset zone. The propagated activity may be represented by the largest hyperperfusion cluster with the highest z score, and is usually connected with the hyperperfusion cluster of the ictal onset zone though a small trail of hyperperfusion, which we have called an "hourglass pattern" (Dupont et al. 2006). Propagation may be towards another lobe, ipsilateral, or contralateral. A reliable blinded assessment of subtraction ictal SPECT coregistered with MRI (SISCOM) data without knowledge of the other data from the presurgical evaluation is often not possible.

2.2 2-[^{18}F]Fluoro-2-deoxy-D-glucose PET

Hypometabolism on FDG-PET usually encompasses the ictal onset zone, but tends to be larger. There is evidence to suggest that both the ictal onset zone and seizure propagation pathways become hypometabolic interictally, representing the functional deficit zone (Rosenow and Lüders 2001; Van Paesschen et al. 2007a). The pattern of hypometabolism reflects the seizure types prior to PET scanning (Savic et al. 1997). The difference between the ictal onset zone and the functional deficit zone is most clearly demonstrated in the rare event of ictal FDG-PET scanning (Van Paesschen et al. 2007b). In these cases, the ictal onset zone is hypermetabolic and the functional deficit zone is hypometabolic (Fig. 1).

3 Coregistration of SPECT and PET with MRI

The most common epileptic lesions causing refractory focal epilepsy include hippocampal sclerosis, malformations of cortical development, tumor, vascular malformations, and infarct/contusion (Li et al. 1995). Subtraction ictal SPECT is routinely coregistered with MRI (SISCOM) because it improves the clinical usefulness in localizing the ictal onset zone and is predictive of seizure outcome (O'Brien et al. 1998, 2000). FDG-PET/MRI coregistration improves the detection of small dysplastic lesions (Chassoux et al. 2010; Goffin et al. 2010; Salamon et al. 2008).

4 Functional Nuclear Imaging in the Presurgical Evaluation of Refractory Focal Epilepsy

4.1 Mesial Temporal Lobe Epilepsy with Hippocampal Sclerosis

4.1.1 Ictal SPECT

Ictal SPECT during a complex focal seizure in mesial temporal lobe epilepsy with hippocampal sclerosis usually shows early ipsilateral neocortical temporal lobe hyperperfusion, frontal lobe hypoperfusion (ipsilateral more than contralateral), contralateral cerebellar hypoperfusion, and later parietal lobe hypoperfusion (Van Paesschen et al.

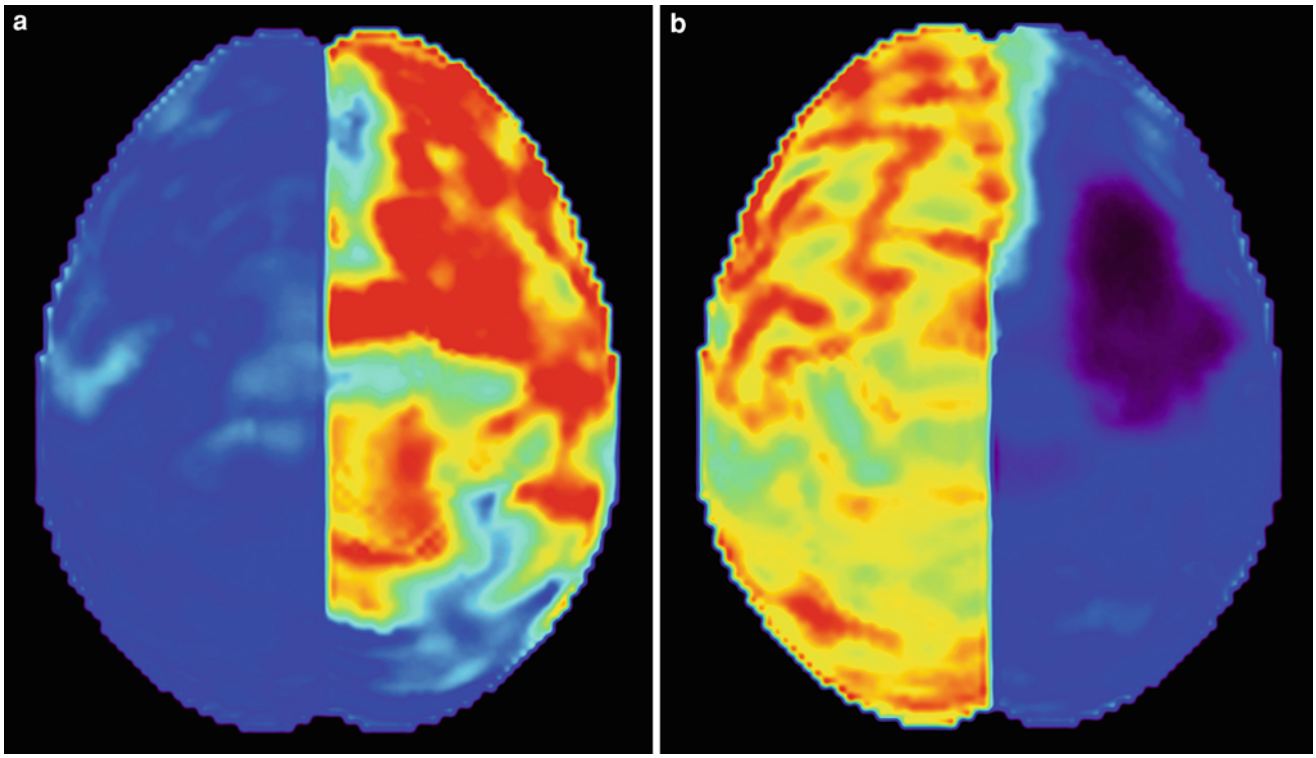

Fig. 1 2-[^{18}F]Fluoro-2-deoxy-D-glucose positron emission tomography (PET) in Rasmussen encephalitis. **a** Three-dimensional stereotactic surface projection analysis of ictal PET. The patient was a 26-year-old woman with Rasmussen encephalitis affecting the *right* cerebral hemisphere, with left-sided focal motor status epilepticus. Ictal PET was performed because electroencephalography did not allow lateralization, and showed hypermetabolism in the right hemisphere, consistent with status epilepticus. The left hemisphere was severely hypometabolic. **b** Stereotactic surface projection analysis of interictal PET images 1 year after a right functional hemispherotomy, which rendered her seizure-free. The *right* hemisphere became hypometabolic. The structurally normal *left* hemisphere became normometabolic, which was accompanied by important cognitive improvements, consistent with a recovery of the functional deficit zone

2003; Blumenfeld et al. 2004) (Fig. 2). Ictal SPECT during simple focal seizures in mesial temporal lobe epilepsy with hippocampal sclerosis can show a small hyperperfusion cluster confined to the temporal lobe, or may reveal no hyperperfusion in around 40% of cases (Van Paesschen et al. 2000; Van Paesschen and Ictal 2004), probably because the hyperperfusion is below the spatial resolution of ictal SPECT, which is around 7 mm. Seizure propagation towards the ipsilateral basal ganglia together with hypoperfusion of associative brain regions correlates with contralateral dystonic posturing of the arm (Kim et al. 2007; Chassagnon et al. 2009). Seizures can propagate to the contralateral temporal lobe, and when the ictal SPECT injection is given after seizure propagation, SISCOM may show hyperperfusion in the contralateral temporal lobe (Cho et al. 2010). Early ictal SPECT injection can obviate this problem of seizure propagation (Van Paesschen et al. 2000). Different propagation patterns in mesial temporal lobe epilepsy with hippocampal sclerosis are not of prognostic significance with respect to seizure outcome after epilepsy surgery (Kim et al. 2007).

4.1.2 2-[^{18}F]Fluoro-2-deoxy-D-glucose PET

Interictal FDG-PET findings in mesial temporal lobe epilepsy with hippocampal sclerosis have been well described. Hypometabolism is present in the ipsilateral temporal lobe in around 95% of cases, but also in regions outside the ictal onset zone, including the contralateral temporal lobe in up to 40% of cases, the ipsilateral thalamus in around 65% of cases, ipsilateral basal ganglia in 45% of cases, the ipsilateral insula in 50% of cases, the ipsilateral basal frontal lobe in around 30% of cases, and the ipsilateral parietal lobe in up to 30% of cases (Henry et al. 1990, 1993) (Fig. 2). In mesial temporal lobe epilepsy with hippocampal sclerosis, the extent and severity of hypometabolism is not related to surgical outcome (Lee et al. 2002). Interictal ipsilateral frontal lobe hypometabolism in mesial temporal lobe epilepsy with hippocampal sclerosis tends to coincide with ictal SPECT hypoperfusion, which could represent surround inhibition (Nelissen et al. 2006). Frontal lobe hypometabolism in mesial temporal lobe epilepsy with hippocampal sclerosis could explain frontal lobe cognitive deficits (Takaya et al. 2006; Jokeit et al. 1997).

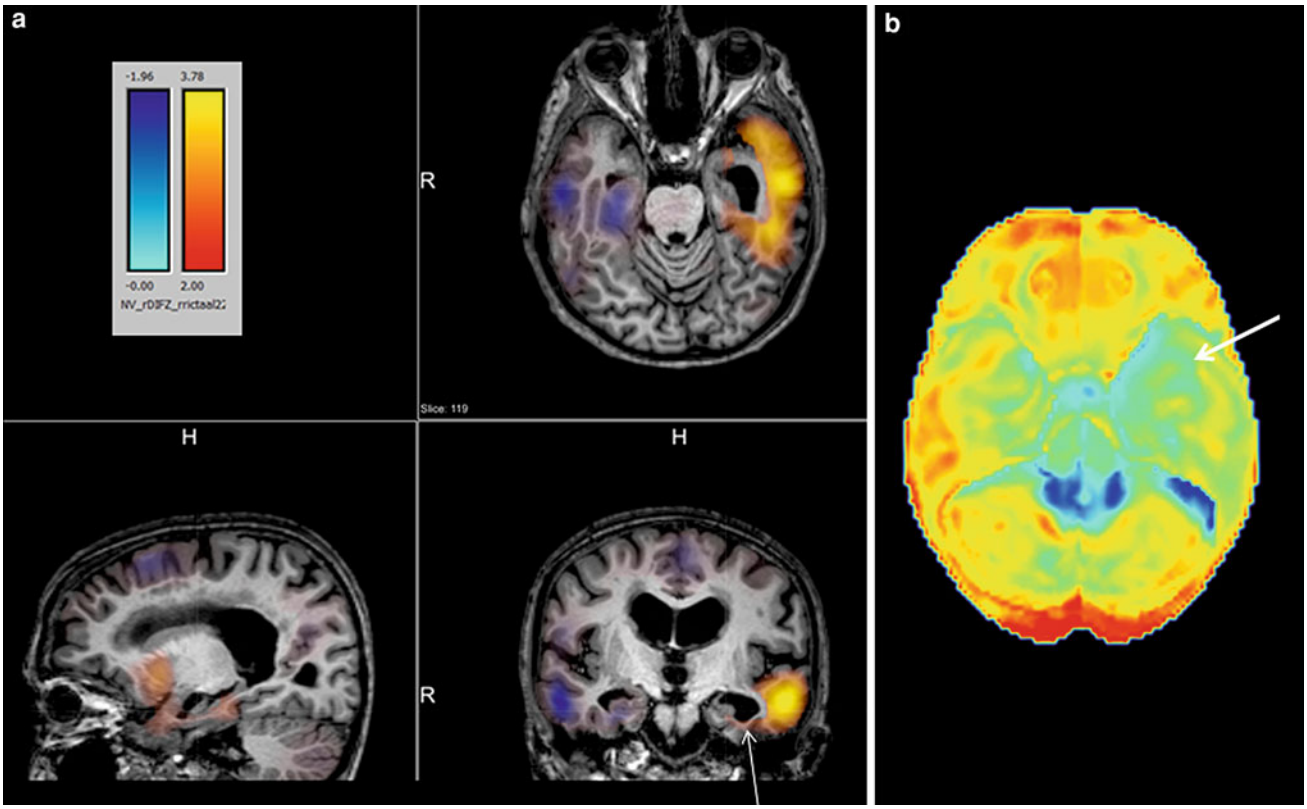

Fig. 2 Ictal single photon emission computed tomography (SPECT) and FDG-PET in mesial temporal lobe epilepsy with hippocampal sclerosis. The patient was a 55-year-old woman with mesial temporal lobe epilepsy associated with left hippocampal sclerosis. **a** Subtraction ictal SPECT coregistered with MRI (SISCOM) of a complex focal seizure which lasted 73 s, with initiation of ictal SPECT tracer injection 38 s after seizure onset. The largest hyperperfusion cluster (*yellow–red*) with the highest *z* score was in the left superior and middle temporal gyrus, and was connected with a small trail of hyperperfusion (*white arrow*) coming from the left hippocampal sclerosis, i.e., the largest hyperperfusion cluster probably represented propagated seizure activity. Areas of hypoperfusion (*blue*) visible on this image were the contralateral temporal lobe and frontal lobe at the midline. **b** Three-dimensional stereotactic surface projection analysis of FDG-PET images showed left temporal lobe hypometabolism (*white arrow*)

4.2 Malformations of Cortical Development

Malformations of cortical development represent a spectrum of congenital structural abnormalities of cerebral cortical development, which are a major cause of refractory focal epilepsy (Barkovich et al. 2005; Palmini et al. 2004). Malformations due to abnormal proliferation (Barkovic class I), including cortical hamartomas, cortical dysplasia with balloon cells, dysembryoplastic neuroepithelial tumors, gangliogliomas, and gangliocytomas, have a better outcome than malformation due to abnormal proliferation (Barkovic class II) and malformations due to abnormal cortical organization (Barkovic class III) (Chang et al. 2011). Focal cortical dysplasia, characterized by abnormal neuroglial proliferation, is the most frequent malformation of cortical development in patients referred for presurgical evaluation (Lüders and Schuele 2006). Focal cortical dysplasia can be classified into three types (Blümcke et al. 2011). Complete resection of electrocorticographic and structural abnormalities appears to be most predictive of long-term seizure outcome (Chang et al. 2011). Functional nuclear imaging is a useful technique in the presurgical evaluation of refractory focal epilepsy due to malformations of cortical development.

4.2.1 Ictal SPECT

Malformations of cortical development are intrinsic epileptogenic lesions, since the ictal onset zone is within the dysplastic cortex. Dysplastic cortex may not always be visible on MRI and, therefore, the ictal onset zone may be at the border of an MRI-visible dysplastic lesion (Blümcke et al. 2011; Marusic et al. 2002). Ictal SPECT is particularly useful to delineate the ictal onset zone in focal dysplastic lesions, even when these are not visible on MRI (Van Paesschen et al. 2007a; Dupont et al. 2006; Kim et al. 2011). O'Brien et al. (2004) reported that a model combining SISCOM concordance with the surgical resection site and the extent of MRI lesion resection was predictive of postoperative seizure

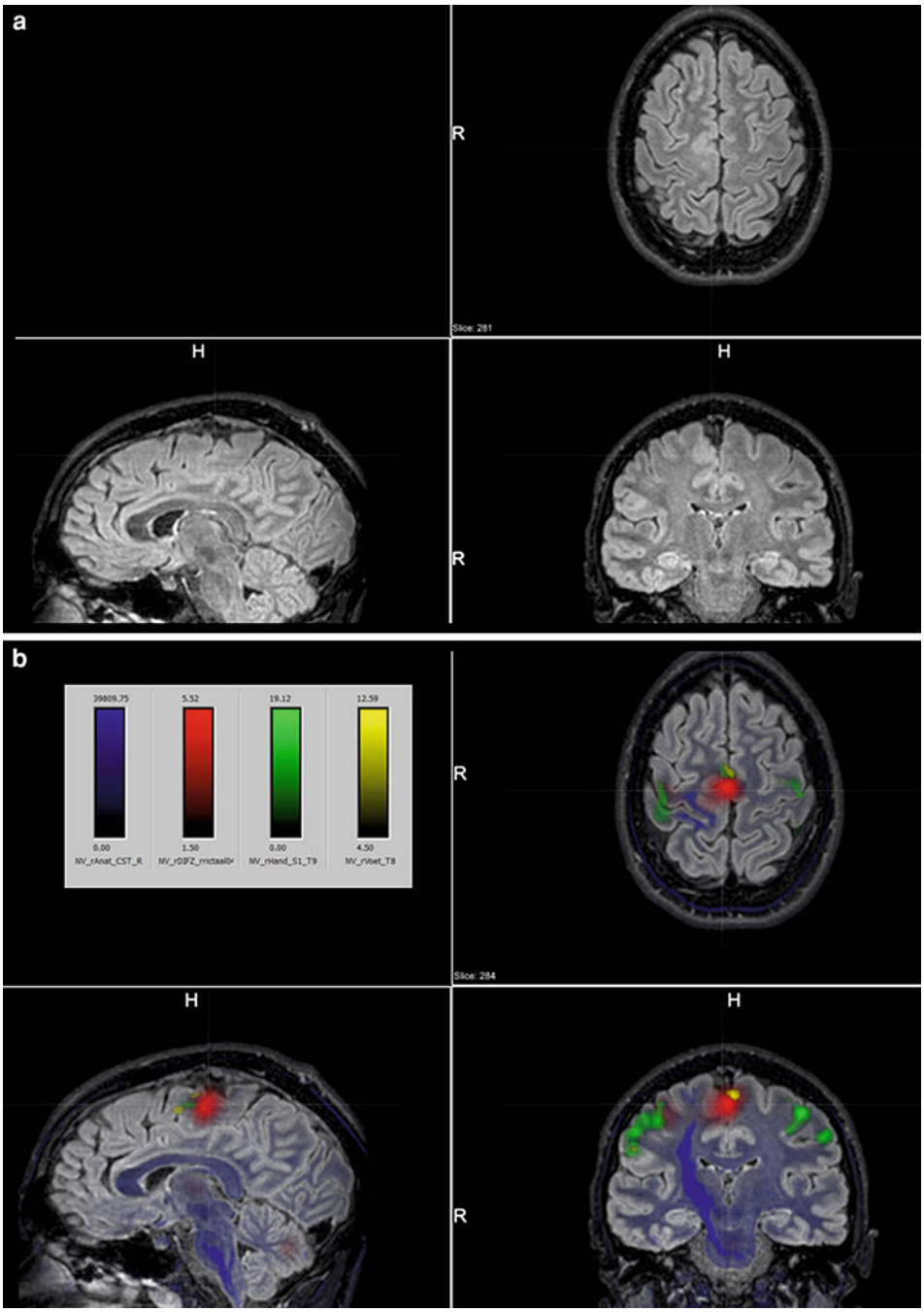

Fig. 3 Multimodality imaging in the presurgical evaluation of refractory focal epilepsy. The patient was a 14-year-old boy with refractory frontal lobe epilepsy with focal motor seizures in his left limbs. **a** Fluid-attenuated inversion recovery (FLAIR) showed a focal cortical dysplasia that was visible as an area of slightly hyperintense and thickened cortex, located on the medial border of the right superior frontal gyrus (*white cross*). **b** Multimodal imaging including magnetization-prepared rapid gradient echo, subtracted ictal SPECT (*red*), and motor functional MRI of the foot (*yellow*), hand (*green*), and corticospinal tract (*blue*), coregistered with FLAIR (**a**). The SISCOM hyperperfusion cluster overlapped with the focal cortical dysplasia, which provided an excellent delineation of the epileptogenic zone, i.e., the region that the neurosurgeon has to remove to render the patient seizure-free. However, motor functional MRI of the foot confirmed that the epileptic lesion was within eloquent cortex. Surgery has not been offered

outcome. In refractory focal epilepsy due to a single MRI-visible focal dysplastic lesion, we found that overlap between the SISCOM hyperperfusion cluster and the MRI-visible focal dysplastic lesion in a noninvasive presurgical evaluation with concordant data may suffice to proceed to epilepsy surgery aimed at removing the MRI-visible focal dysplastic lesion and the part of the hyperperfusion cluster within and immediately surrounding the focal dysplastic lesion (Dupont et al. 2006) (Fig. 3).

4.2.2 2-[^{18}F]Fluoro-2-deoxy-D-glucose PET

Focal cortical dysplasia shows a focal or regional area of hypometabolism on FDG-PET in around 65–80% of cases (Chassoux et al. 2010; Goffin et al. 2010; Salamon et al. 2008; Kim et al. 2011). FDG-PET/MRI coregistration and partial volume correction improves detection of cortical dysplasia (Chassoux et al. 2010; Goffin et al. 2010; Salamon et al. 2008). FDG-PET is especially useful to detect the milder Palmini type I lesions, which may not be visible on

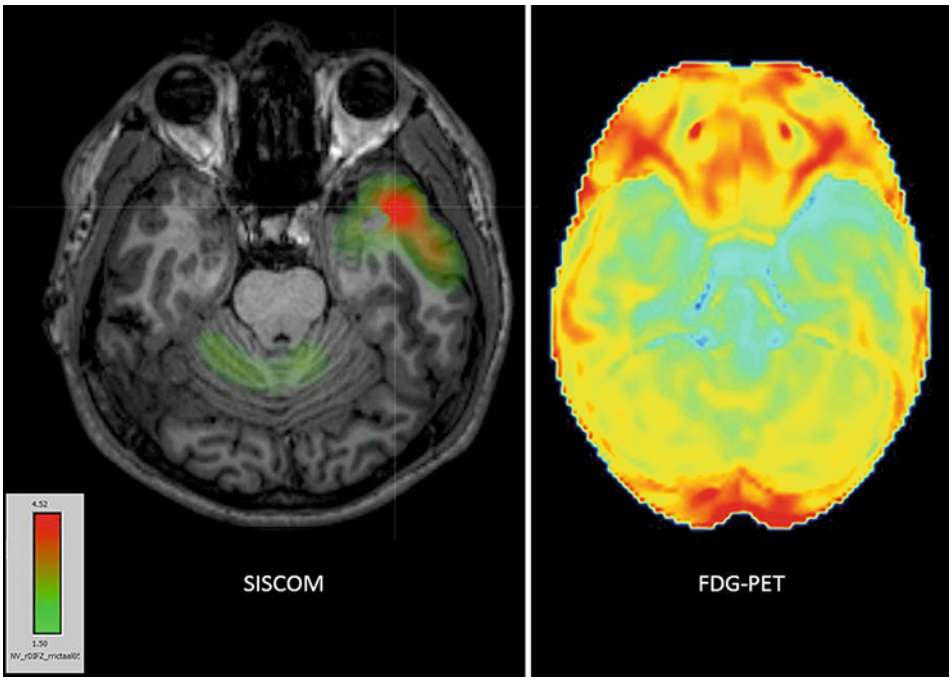

Fig. 4 MRI-negative, SPECT/PET-positive temporal lobe epilepsy. The patient was a 27-year-old man with a 5-year history of refractory MRI-negative temporal lobe epilepsy. SISCOM showed a left anterotemporal hyperperfusion cluster. FDG-PET showed left temporal hypometabolism. He underwent a left anterotemporal lobectomy, including the amygdala and with sparing of the hippocampus. He has remained seizure-free for more than 1 year. Pathology demonstrated focal cortical dysplasia type I

MRI (Kim et al. 2009; Salamon et al. 2008) (Fig. 4). FDG-PET hypometabolism is often present outside the location of the focal dysplastic lesion, consistent with the observation that the functional deficit zone tends to be larger than the epileptogenic zone (Goffin et al. 2010). It remains, therefore, important to interpret FDG-PET in the context of a full presurgical evaluation.

4.3 Dual Pathology

Dual pathology, i.e., two or more epileptic lesions, is detected on MRI in around 5–20% of patients referred for presurgical evaluation (Li et al. 1999). Often, one of the two lesions is hippocampal sclerosis. Malformations of cortical development and porencephalic cysts are more frequently associated with hippocampal sclerosis than other epileptic lesions, such as low-grade gliomas and vascular malformations (Blümcke et al. 2011; Cendes et al. 1995). Focal cortical dysplasia type III occurs in combination with hippocampal sclerosis, epilepsy-associated tumors, vascular malformations, and epileptogenic lesions acquired in early life (i.e., traumatic injury, ischemic injury, or encephalitis) (Blümcke et al. 2011).

4.3.1 Ictal SPECT

In patients with dual pathology including hippocampal sclerosis, removal of the two lesions may be the best surgical approach (Li et al. 1999). However, patients with mesial temporal lobe epilepsy and hippocampal sclerosis and an extratemporal porencephalic cyst can be rendered seizure-free after temporal lobectomy (Burneo et al. 2003). In our experience, ictal SPECT can be highly accurate to pinpoint hippocampal sclerosis as the ictal onset zone in patients with dual pathology (Fig. 5). Valenti et al. (2002) reported ictal SPECT hyperperfusion within dysembryoplastic neuroepithelial tumors, extending into areas of dysplastic tissue that were not visible on MRI.

4.3.2 2-[^{18}F]Fluoro-2-deoxy-D-glucose PET

Diehl et al. (2003) reported FDG-PET in patients with hippocampal sclerosis with and without associated microscopic cortical dysplasia. In hippocampal sclerosis with concurrent temporal neocortical microscopic cortical dysplasia, the most prominent hypometabolism was in the temporal neocortex. In isolated hippocampal sclerosis without cortical dysplasia, the most pronounced hypometabolism was in the mesial temporal lobe. Patients with tuberous sclerosis complex tend to have multiple tubers. Removal of the epileptic tubers may render these patients seizure-free. FDG-PET is useful in the non-invasive presurgical evaluation of these patients. Some of the tubers in the epileptogenic zone may display the largest volume of hypometabolism relative to the actual tuber volume (Salamon et al. 2008; Wu et al. 2010).

4.4 MRI-Negative Refractory Focal Epilepsy

Around 25% of patients with refractory focal epilepsy have no epileptic lesion on MRI (Li et al. 1995; Duncan 2010). As a group, around 40% of patients with MRI-negative

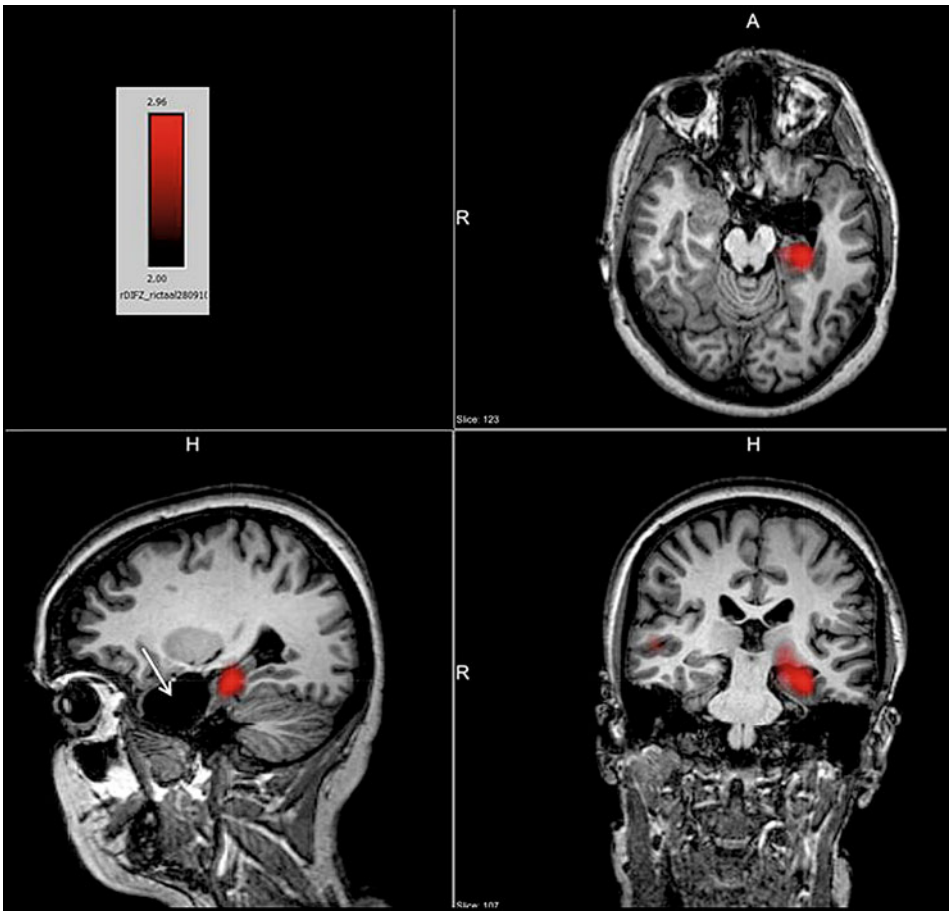

Fig. 5 SISCOM in dual pathology. The patient was a 36-year-old woman who had developed epilepsy at the age of 7 years. She underwent a neurosurgical operation with removal of a pilocytic astrocytoma. She remained seizure-free without antiepileptic medication until the age of 23 years. She then had recurrent seizures and developed a refractory left temporal lobe epilepsy. SISCOM showed a very focal cluster of hyperperfusion (*red*) in the hippocampus just posterior of the resection site (*white arrow*). This region was resected, rendering her seizure-free. Pathology showed hippocampal sclerosis

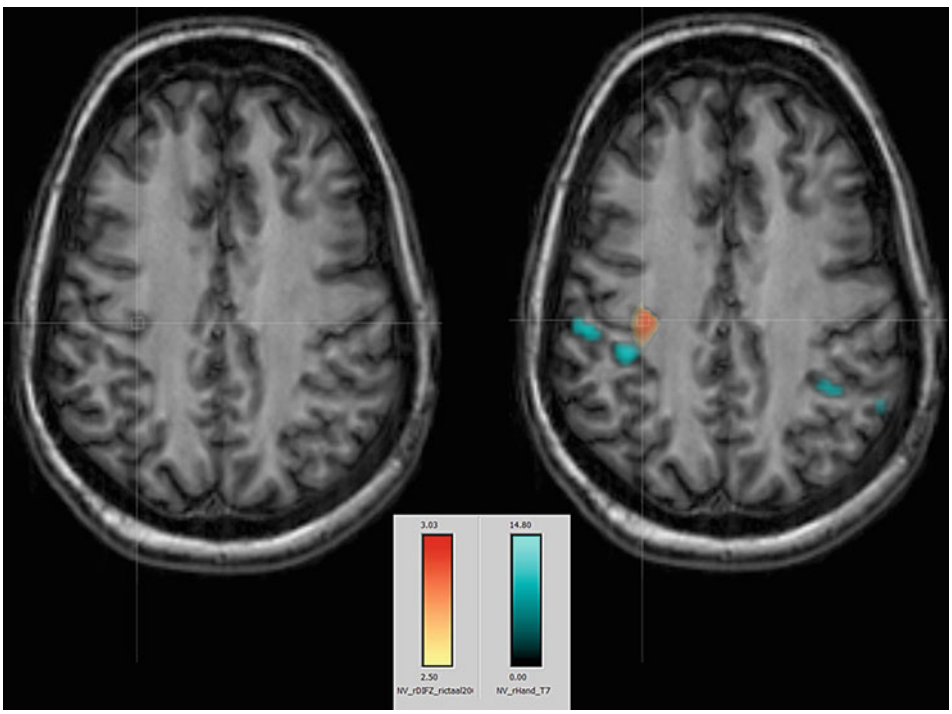

Fig. 6 Detection of a small focal cortical dysplasia guided by ictal SPECT on an MRI scan that was initially read as showing normal findings. The patient was a 32-year-old woman with a refractory right frontal lobe epilepsy. Her MRI scan of the brain was initially read as showing normal findings. Ictal SPECT was performed during a motor seizure that lasted 21 s, with initiation of the ictal SPECT tracer injection 3 s after seizure onset. SISCOM showed a hyperperfusion cluster (*red–yellow* area) in the right frontal lobe near primary motor cortex (motor functional MRI: *blue* areas). Reanalysis of the MRI scan showed a bottom-of-sulcus cortical dysplasia at the place of the SISCOM hyperperfusion cluster

focal epilepsy are rendered seizure-free after epilepsy surgery, and have a worse prognosis compared with patients with refractory focal epilepsy and an epileptic lesion on MRI (Lee et al. 2005).

4.4.1 Ictal SPECT

In MRI-negative refractory focal epilepsy, reevaluation of the MRI, guided by the ictal SPECT, reveals small focal dysplastic lesions in around 15% of cases (Van Paesschen et al. 2007a; Van Paesschen and Ictal 2004) (Fig. 6). SISCOM can be used to guide placement of intracranial electrodes (Ahnlide et al. 2007). SISCOM may alter and extend the strategy for electrode placement in invasive recording. Favorable surgical outcome has been observed when intracranial EEG was concordant with SISCOM hyperperfusion. SISCOM localization, therefore, is an independent method with an impact in patients with refractory partial epilepsy scheduled for intracranial EEG studies. In comparison with MRI, FDG-PET, magnetoencephalography, and scalp EEG, ictal SPECT is probably the most sensitive technique to localize the ictal onset zone in extratemporal lobe epilepsy, and to predict a seizure-free outcome after epilepsy surgery (Knowlton et al. 2008; Kim et al. 2009).

4.4.2 2-[^{18}F]Fluoro-2-deoxy-D-glucose PET

FDG-PET may be useful in MRI-negative temporal lobe epilepsy. Good surgical results have been reported in patients with MRI-negative refractory temporal lobe epilepsy and unilateral temporal hypometabolism (Fig. 4). MRI-negative, PET-positive temporal lobe epilepsy may represent a surgically remediable syndrome distinct from mesial temporal lobe epilepsy, with focal hypometabolism involving primarily lateral neocortical rather than mesial temporal structures (Lee et al. 2005; Carne et al. 2004). FDG-PET is most useful in patients with temporal lobe epilepsy when MRI findings are normal or when MRI does not show unilateral temporal lobe abnormalities, and when ictal EEG results are not concordant with MRI findings or seizure symptoms (Uijl et al. 2007).

5 Conclusion

Ictal SPECT and FDG-PET are functional nuclear imaging modalities which may provide additional information in the noninvasive presurgical evaluation of patients with refractory focal epilepsy when MRI shows a malformation of cortical development (Dupont et al. 2006), dual pathology, or MRI-negative cases, or when the data from the presurgical evaluation are discordant. Both may facilitate the detection of a subtle focal dysplastic lesion when the MRI findings were initially reported as normal, and may allow epilepsy surgery after a noninvasive presurgical evaluation. Ictal SPECT may guide placement of electrodes and grids for invasive EEG studies. Ictal SPECT and FDG-PET can be integrated in a multimodal image, including MRI, tractography, EEG–functional MRI and magnetoencephalography, allowing accurate surgical planning. Both FDG-PET and ictal SPECT can predict seizure-free outcome after epilepsy surgery (Knowlton et al. 2008).

References

Ahnlide JA, Rosen I, Linden-Mickelsson TP, Kallen K (2007) Does SISCOM contribute to favorable seizure outcome after epilepsy surgery? Epilepsia 48:579–588

Barkovich AJ, Kuzniecky RI, Jackson GD, Guerrini R, Dobyns WB (2005) A developmental and genetic classification for malformations of cortical development. Neurology 27(65):1873–1887

Blümcke I, Thom M, Aronica E et al (2011) The clinicopathologic spectrum of focal cortical dysplasias: a consensus classification proposed by an ad hoc task force of the ILAE Diagnostic Methods Commission. Epilepsia 52:158–174

Blumenfeld H, McNally KA, Vanderhill SD et al (2004) Positive and negative network correlations in temporal lobe epilepsy. Cereb Cortex 14:892–902

Burneo JG, Faught E, Knowlton RC et al (2003) Temporal lobectomy in congenital porencephaly associated with hippocampal sclerosis. Arch Neurol 60:830–834

Carne RP, O'Brien TJ, Kilpatrick CJ et al (2004) MRI-negative PET-positive temporal lobe epilepsy: a distinct surgically remediable syndrome. Brain 127:2276–2285

Cendes F, Cook MJ, Watson C et al (1995) Frequency and characteristics of dual pathology in patients with lesional epilepsy. Neurology 45:2058–2064

Chang EF, Wang DD, Barkovich AJ et al (2011) Predictors of seizure freedom after surgery for malformations of cortical development. Ann Neurol 70:151–162

Chassagnon S, Namer IJ, Armspach JP et al (2009) SPM analysis of ictal-interictal SPECT in mesial temporal lobe epilepsy: relationships between ictal semiology and perfusion changes. Epilepsy Res 85:252–260

Chassoux F, Rodrigo S, Semah F et al (2010) FDG-PET improves surgical outcome in negative MRI Taylor-type focal cortical dysplasias. Neurology 14(75):2168–2175

Cho JW, Hong SB, Lee JH et al (2010) Contralateral hyperperfusion and ipsilateral hypoperfusion by ictal SPECT in patients with mesial temporal lobe epilepsy. Epilepsy Res 88:247–254

Diehl B, LaPresto E, Najm I et al (2003) Neocortical temporal FDG-PET hypometabolism correlates with temporal lobe atrophy in hippocampal sclerosis associated with microscopic cortical dysplasia. Epilepsia 44:559–564

Duncan JS (2010) Imaging in the surgical treatment of epilepsy. Nat Rev Neurol 6:537–550

Dupont P, Van Paesschen W, Palmini A et al (2006) Ictal perfusion patterns associated with single MRI-visible focal dysplastic lesions: implications for the noninvasive delineation of the epileptogenic zone. Epilepsia 47:1550–1557

Goffin K, Dedeurwaerdere S, Van Laere KJ, Van Paesschen W (2008) Neuronuclear assessment of patients with epilepsy. Semin Nucl Med 38:227–239

Goffin K, Van Paesschen W, Dupont P et al (2010) Anatomy-based reconstruction of FDG-PET images with implicit partial volume correction improves detection of hypometabolic regions in patients

with epilepsy due to focal cortical dysplasia diagnosed on MRI. Eur J Nucl Med Mol Imaging 37:1148–1155
Henry TR, Mazziotta JC, Engel J Jr et al (1990) Quantifying interictal metabolic activity in human temporal lobe epilepsy. J Cereb Blood Flow Metab 10:748–757
Henry TR, Mazziotta JC, Engel J Jr (1993) Interictal metabolic anatomy of mesial temporal lobe epilepsy. Arch Neurol 50:582–589
Jokeit H, Seitz RJ, Markowitsch HJ, Neumann N, Witte OW, Ebner A (1997) Prefrontal asymmetric interictal glucose hypometabolism and cognitive impairment in patients with temporal lobe epilepsy. Brain 120(Pt 12):2283–2294
Kapucu OL, Nobili F, Varrone A et al (2009) EANM procedure guideline for brain perfusion SPECT using 99mTc-labelled radiopharmaceuticals, version 2. Eur J Nucl Med Mol Imaging 36:2093–2102
Kim JH, Im KC, Kim JS et al (2007) Ictal hyperperfusion patterns in relation to ictal scalp EEG patterns in patients with unilateral hippocampal sclerosis: a SPECT study. Epilepsia 48:270–277
Kim JT, Bai SJ, Choi KO et al (2009) Comparison of various imaging modalities in localization of epileptogenic lesion using epilepsy surgery outcome in pediatric patients. Seizure 18:504–510
Kim YH, Kang HC, Kim DS et al (2011) Neuroimaging in identifying focal cortical dysplasia and prognostic factors in pediatric and adolescent epilepsy surgery. Epilepsia 52:722–727
Knowlton RC, Elgavish RA, Bartolucci A et al (2008) Functional imaging: II. Prediction of epilepsy surgery outcome. Ann Neurol 64:35–41
Lee SK, Lee DS, Yeo JS et al (2002) FDG-PET images quantified by probabilistic atlas of brain and surgical prognosis of temporal lobe epilepsy. Epilepsia 43:1032–1038
Lee SK, Lee SY, Kim KK, Hong KS, Lee DS, Chung CK (2005) Surgical outcome and prognostic factors of cryptogenic neocortical epilepsy. Ann Neurol 58:525–532
Li LM, Fish DR, Sisodiya SM, Shorvon SD, Alsanjari N, Stevens JM (1995) High resolution magnetic resonance imaging in adults with partial or secondary generalised epilepsy attending a tertiary referral unit. J Neurol Neurosurg Psychiatry 59:384–387
Li LM, Cendes F, Andermann F et al (1999) Surgical outcome in patients with epilepsy and dual pathology. Brain 122(Pt 5):799–805
Lüders H, Schuele SU (2006) Epilepsy surgery in patients with malformations of cortical development. Curr Opin Neurol 19:169–174
Marusic P, Najm IM, Ying Z et al (2002) Focal cortical dysplasias in eloquent cortex: functional characteristics and correlation with MRI and histopathologic changes. Epilepsia 43:27–32
Nelissen N, Van Paesschen W, Baete K et al (2006) Correlations of interictal FDG-PET metabolism and ictal SPECT perfusion changes in human temporal lobe epilepsy with hippocampal sclerosis. Neuroimage 15(32):684–695
O'Brien TJ, So EL, Mullan BP et al (1998) Subtraction ictal SPECT co-registered to MRI improves clinical usefulness of SPECT in localizing the surgical seizure focus. Neurology 50:445–454
O'Brien TJ, So EL, Mullan BP et al (2000) Subtraction peri-ictal SPECT is predictive of extratemporal epilepsy surgery outcome. Neurology 12(55):1668–1677
O'Brien TJ, So EL, Cascino GD et al (2004) Subtraction SPECT coregistered to MRI in focal malformations of cortical development: localization of the epileptogenic zone in epilepsy surgery candidates. Epilepsia 45:367–376
Palmini A, Najm I, Avanzini G et al (2004) Terminology and classification of the cortical dysplasias. Neurology 23(62):S2–S8
Rosenow F, Lüders H (2001) Presurgical evaluation of epilepsy. Brain 124:1683–1700
Salamon N, Kung J, Shaw SJ et al (2008) FDG-PET/MRI coregistration improves detection of cortical dysplasia in patients with epilepsy. Neurology 11(71):1594–1601
Savic I, Altshuler L, Baxter L, Engel J Jr (1997) Pattern of interictal hypometabolism in PET scans with fludeoxyglucose F 18 reflects prior seizure types in patients with mesial temporal lobe seizures. Arch Neurol 54:129–136
Takaya S, Hanakawa T, Hashikawa K et al (2006) Prefrontal hypofunction in patients with intractable mesial temporal lobe epilepsy. Neurology 14(67):1674–1676
Uijl SG, Leijten FS, Arends JB, Parra J, van Huffelen AC, Moons KG (2007) The added value of [18F]-fluoro-D-deoxyglucose positron emission tomography in screening for temporal lobe epilepsy surgery. Epilepsia 48:2121–2129
Valenti MP, Froelich S, Armspach JP et al (2002) Contribution of SISCOM imaging in the presurgical evaluation of temporal lobe epilepsy related to dysembryoplastic neuroepithelial tumors. Epilepsia 43:270–276
Van Paesschen W (2004) Ictal SPECT. Epilepsia 45(Suppl 4): 35–40
Van Paesschen W, Dupont P, Van Heerden B et al (2000) Self-injection ictal SPECT during partial seizures. Neurology 23(54): 1994–1997
Van Paesschen W, Dupont P, Van Driel G, Van Billoen H, Maes A (2003) SPECT perfusion changes during complex partial seizures in patients with hippocampal sclerosis. Brain 126:1103–1111
Van Paesschen W, Dupont P, Sunaert S, Goffin K, Van Laere KJ (2007a) The use of SPECT and PET in routine clinical practice in epilepsy. Curr Opin Neurol 20:194–202
Van Paesschen W, Porke K, Fannes K et al (2007b) Cognitive deficits during status epilepticus and time course of recovery: a case report. Epilepsia 48:1979–1983
Varghese GI, Purcaro MJ, Motelow JE et al (2009) Clinical use of ictal SPECT in secondarily generalized tonic-clonic seizures. Brain 132:2102–2113
Wu JY, Salamon N, Kirsch HE et al (2010) Noninvasive testing, early surgery, and seizure freedom in tuberous sclerosis complex. Neurology 2(74):392–398

Morphometric MRI Analysis

Hans-Jürgen Huppertz

Contents

Abstract

Morphometric MRI analysis may facilitate the detection and visualization of focal cortical dysplasia and other potentially epileptogenic cortical malformations by highlighting structural alterations such as abnormal gyration, blurring of the gray-white matter junction, and abnormal thickness of the cortical ribbon. In this chapter, a voxel-based implementation of this kind of MRI postprocessing using algorithms of the SPM5 software is presented. The description of methods is accompanied by illustrative examples which show how this approach may aid in the detection of subtle cortical dysplasia, polymicrogyria and gray matter heterotopia, in the delineation of the extent of lesions, and in the differentiation between different types of lesions. Thereby, it increases the diagnostic yield of MRI and appears to be a useful additional tool in the diagnostics and especially presurgical evaluation of epilepsy patients.

1 Introduction

Focal cortical dysplasia (FCD) is a highly epileptogenic cortical malformation resulting from abnormal proliferation of neurons during the first trimester and/or from abnormal cortical organization during the third trimester of pregnancy (Barkovich and Kuzniecky 1996; Hagemann et al. 2000; Redecker et al. 2000; Barkovich et al. 2001; Hildebrandt et al. 2005). The spectrum of histopathological changes ranges from abnormal cortical lamination to extensive malformations with atypical cell types affecting the whole cortex and subcortical white matter (Gomez-Anson et al. 2000). In the past 15 years, owing to improved MRI capabilities, these lesions have been increasingly recognized as an underlying cause of formerly cryptogenic epilepsy and now account for up to 25% of patients with focal epilepsy in presurgical epilepsy centers (Kuzniecky et al. 1993; Fauser et al. 2004; Lerner et al. 2009). More than 70% of these epilepsies are resistant to pharmacological treatment (Semah et al. 1998),

H.-J. Huppertz (✉)
Swiss Epilepsy Centre, Zurich, Switzerland
e-mail: hans-juergen.huppertz@swissepi.ch

H. Urbach (ed.), *MRI in Epilepsy*, Medical Radiology. Diagnostic Imaging,
DOI: 10.1007/174_2012_564,

and epilepsy surgery seems to be the best available treatment option. However, before surgery it is necessary to localize the lesion and to delineate its extent. Detection on MRI is crucial since both the probability of undergoing surgical therapy and the postoperative outcome are significantly better in MRI-positive patients (Berg et al. 2003; Bien et al. 2009). Typical MRI features of FCD include abnormal gyral contours, thickening of the cortex, abnormal differentiation of the gray matter−white matter boundary, and sometimes signal hyperintensity in T2- and fluid-attenuated inversion recovery (FLAIR)-weighted images (Kuzniecky et al. 1995; Raymond et al. 1995; Chan et al. 1998; Gomez-Anson et al. 2000; Urbach et al. 2002). In subtle cases, however, diagnosis is time-consuming and difficult, and although MRI techniques have markedly improved over the last years, conventional MRI can be unrevealing (Tassi et al. 2002; Widdess-Walsh et al. 2006; Krsek et al. 2008). Therefore, attempts have been made to facilitate lesion detection by modern image postprocessing strategies such as curvilinear reformatting of 3D MRI data (Bastos et al. 1999), quantifying the regional distribution of gray matter and white matter by voxel-based morphometry or autoblock analysis (Sisodiya et al. 1995a, b; Woermann et al. 1999; Merschhemke et al. 2003; Bonilha et al. 2006; Bruggemann et al. 2007), measuring the thickness of the cerebral cortex (Fischl and Dale 2000), texture analysis (Bernasconi et al. 2001; Antel et al. 2002, 2003), and quantitative intensity analysis (Rugg-Gunn et al. 2005; Salmenpera et al. 2007; Focke et al. 2008). In addition, there have been promising approaches for automated lesion detection, for example, by searching for maximum deviations from a normal database (Kassubek et al. 2002; Wilke et al. 2003), by using a Bayesian classifier (Antel et al. 2003), by thresholding *z*-score maps (Colliot et al. 2006), by applying classifiers based on neural networks (Besson et al. 2008b), and by statistical parametric mapping, either applied to structural data in the framework of voxel-based morphometry or combined with signal intensity analysis. An overview of the different approaches can be found in the review by Bernasconi et al. (2011).

The following presentation concentrates on a method for morphometric MRI analysis which is based on algorithms in the freely available software program for statistical parametric mapping SPM (SPM5, Wellcome Department of Imaging Neuroscience Group, London, UK; http://www.fil.ion.ucl.ac.uk/spm) and compares individual brain anatomy with a normal database. The whole processing is performed by a fully automated MATLAB® script called Morphometric Analysis Program (MAP) which is in clinical use in about a dozen epilepsy centers in Europe and the USA. From a high-resolution T1-weighted 3D MRI data set, three new feature maps (called "extension image," "junction image," and "thickness image") are derived which characterize three different potential features of FCD: the abnormal extension of gray matter into white matter (i.e., abnormal deep sulci), the blurring of the gray matter−white matter junction, and the abnormal thickness of the cortical ribbon. By highlighting suspicious cortical regions, the MAP results can guide a second look at the MRI data and thereby increase the sensitivity of MRI evaluation (Huppertz et al. 2005; Wellmer et al. 2010; Wagner et al. 2011).

2 Methods

The MRI postprocessing presented here uses standard procedures available within SPM5 (e.g., normalization, segmentation) and additional simple computations and filters (e.g., calculation of a difference image, conversion to a binary image, masking, smoothing). Starting with a T1-weighted MRI volume data set of usually 1-mm^3 voxel resolution and preferably high contrast between gray matter and white matter, the calculation of the morphometric maps comprises the following steps (see also Fig. 1; the numbers within the figure correspond to these processing steps).

2.1 Preprocessing

Normalization and intensity correction (step 1) and simultaneous *segmentation* (step 2). SPM5 includes a probabilistic framework (called "unified segmentation") whereby image registration, tissue classification, and bias correction are integrated within the same generative model (Ashburner and Friston 2005). By use of this framework, the 3D MRI data set of each patient is normalized to the standard brain of the Montreal Neurological Institute (MNI) included in the SPM5 distribution, segmented into different brain compartments, i.e., gray matter, white matter, and cerebrospinal fluid, and is simultaneously corrected for small intensity inhomogeneities (using default SPM5 parameters).

2.2 Computation of the Junction Image

Filtering and conversion to a binary image (step 3). The means and standard deviations of the voxel intensities in the gray matter and white matter compartments are used to determine individual upper and lower intensity thresholds for filtering and conversion of the normalized and intensity-corrected image to a binary image. The thresholds are given by the functions

$$T_{\text{Lower Threshold}} = \text{Mean GM} + 1/2\ \text{SD GM} \quad \text{and}$$
$$T_{\text{Upper Threshold}} = \text{Mean WM} - 1/2\ \text{SD WM}$$

where "mean" and SD are the mean and standard deviation of the voxel intensities in the respective tissue class, and GM and WM are gray matter and white matter, respectively. Each voxel with a gray value between these thresholds is set to 1 in

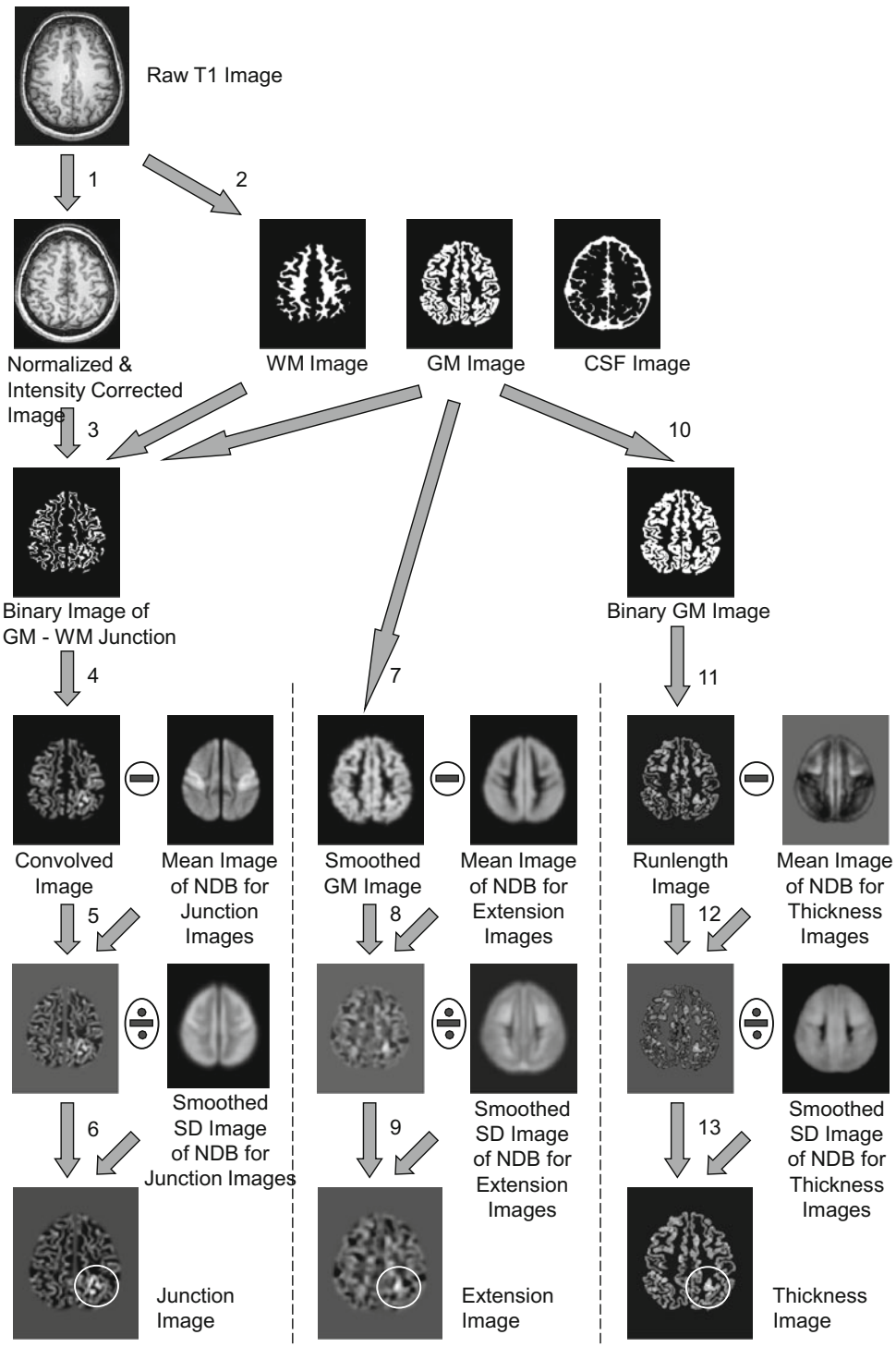

Fig. 1 Overview of the image processing steps required for calculating the morphometric images. Preprocessing: *1* normalization and intensity correction and *2* simultaneous segmentation. Computation of the junction image: *3* filtering and conversion to a binary image containing voxels of the gray matter–white matter interface, *4* convolution, *5* comparison with a normal database, and *6* calculation of the *z*-score image. Computation of the extension image: *7* smoothing, *8* comparison with a normal database, and *9* calculation of the *z*-score image. Computation of the thickness image: *10* conversion to a binary gray matter image, *11* estimation of cortical thickness, *12* comparison with a normal database, and *9* calculation of the *z*-score image. See the text for details

the resulting binary image, and the other voxels are set to zero. Furthermore, brain regions outside the cerebral cortex such as basal ganglia, brainstem, and cerebellum are masked out by a predefined mask.

Convolution (step 4). The binary image is smoothed by performing a 3D convolution with a convolution kernel of 5^3 1's. In the resulting "convolved image" brain regions where voxels of value 1 are clustered appear bright.

Comparison with a normal database (step 5). To compensate for the variability of the gray matter–white matter transition zone in different brain regions, the convolved patient image is compared with a normal database. Preferably, the normal database consists of T1-weighted images of healthy controls measured using the same magnetic resonance (MR) scanner with the same MR protocol as for the patient investigated. The data sets forming the normal database are processed in the same way as described

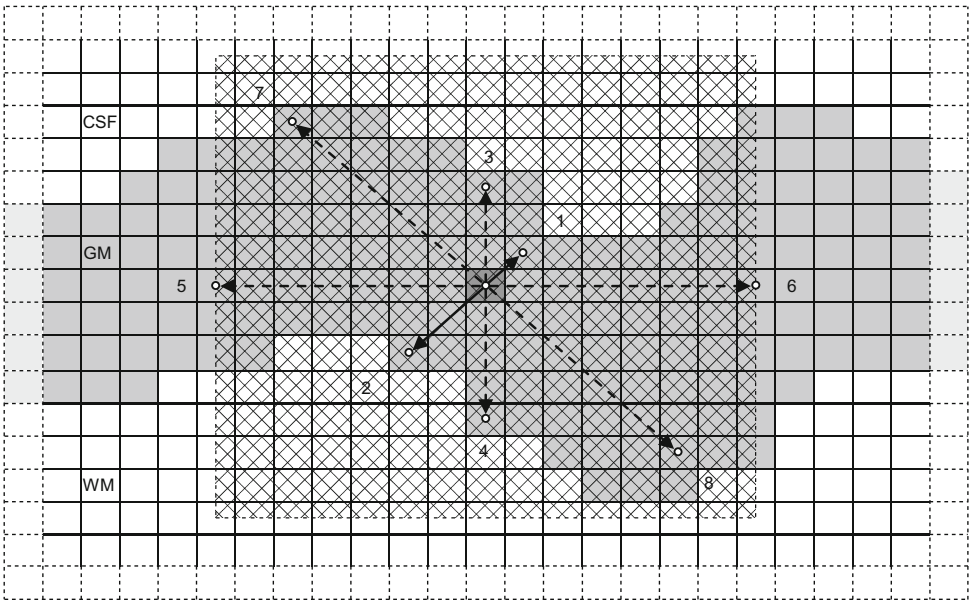

Fig. 2 Two-dimensional illustration of the approach used for estimating cortical thickness. For each voxel within the gray matter compartment, run-length vectors are determined in different directions to either the nearest boundary voxel of the gray matter compartment or the boundary of a predefined search space (represented by the *checkered area*) around the starting voxel. In this example, opposing run-length vectors 1 and 2 represent the shortest connection between gray matter–white matter and gray matter–CSF interfaces passing through the starting voxel. The Euclidean lengths of both vectors are summed and the value obtained is inserted at the starting voxel in the resulting "run-length image"

in steps 1–4 and are then averaged. The resulting mean image is subtracted voxel by voxel from the convolved patient image.

Calculation of the z-score image (step 6). The convolved images of the controls are also used to calculate a "standard deviation image" providing standard deviations of the normal database for all voxels. In the last step, the difference image from step 5 is divided by this standard deviation image of the normal database to get the final "junction image" with *z*-score-normalized data. To avoid outlier values at the border of the standard brain where only a few subjects contribute to the normal database and its standard deviation, the standard deviation image is previously smoothed by using a fixed Gaussian kernel of 6-mm full width at half maximum (FWHM).

Bright regions in the junction image primarily correspond to cortical areas with a less defined border between gray matter and white matter and a broader transition zone as compared with the normal database. However, other brain areas (e.g., subcortical structures) may be highlighted as well if their signal intensities fall within the range between normal gray matter and white matter as defined in step 3 and differ from the normal database in this respect.

2.3 Computation of the Extension Image

Smoothing (step 7). The gray matter image resulting from segmentation is smoothed by a Gaussian kernel of 6-mm FWHM (i.e., about the size of the lesions to be detected). In the smoothed gray matter image, each voxel encodes the average concentration of gray matter from around the voxel (defined by the form of the smoothing kernel) at the corresponding position in the original structural MR image.

Comparison with a normal database (step 8). As in step 5, the mean smoothed gray mater image of the normal database is subtracted voxel by voxel from the smoothed gray matter image of the patient investigated.

Calculation of the z-score image (step 9).The difference image from step 8 is divided by the standard deviation image of the normal database to obtain *z*-score-normalized data for the final "extension image." In this image, those brain areas appear bright where gray matter extends abnormally into the white matter as compared with the normal database.

2.4 Computation of the Thickness Image

Conversion to a binary image (step 10). The gray matter image from segmentation is converted to a binary image using the ImCalc tool of SPM5 with a cutoff of 0.5.

Estimation of cortical thickness (step 11). Similar to the method described by Bernasconi et al. (2001), for each voxel within the gray matter compartment, run-length vectors are determined in 26 spatial directions from the starting voxel to the nearest boundary voxel of the gray matter compartment. To reduce the processing time, the search space is limited to a cube of 15^3 voxels centred at the starting voxel. Thus, all run-length vectors are clipped at a maximum length of seven voxel units. For each pair of opposing run-length

vectors, the Euclidean lengths of both vectors are summed. The minimum of the resulting 13 distance measurements is determined and this value is inserted at the starting voxel in the resulting "run-length image." The approach is illustrated in Fig. 2 for the 2D situation, but actually a 3D implementation is used. The minimum length of all vector pairs passing through the starting voxel approximates the shortest connection between the gray matter–white matter and the gray matter–CSF interfaces. Compared with mean or median values, it is less prone to outliers in long gyri, e.g., the cingulate gyrus (Antel et al. 2002). In comparison with more sophisticated model-based methods with deformable surfaces (Fischl and Dale 2000; Besson et al. 2008a; Thesen et al. 2011), a data-driven approach as described above without the need to model the cortical surfaces requires significantly less processing time (Scott et al. 2009).

Comparison with a normal database (step 12). To compensate for the variability of cortical thickness in different brain regions, the mean run-length image of the normal database is subtracted from the run-length image of the patient investigated. In the mean image of the normal database all voxels with value zero after averaging (i.e., where none of the healthy controls have gray matter) are set to a median thickness value (determined from the nonzero voxels). In this way, any abnormality of cortical thickness can also be assessed in regions where no subject from the normal database has shown gray matter tissue so far. Otherwise, unusually deep sulci would differ very much from the normal database even if the cortical thickness were normal at this location. This would lead to undesired overlap with the FCD characteristic highlighted already by the extension image.

Calculation of the z-score image (step 13). The difference image from step 12 is divided by the standard deviation image of the normal database to obtain *z*-score-normalized data for the final "thickness image." Again, the standard deviation image is previously smoothed by a Gaussian kernel of 6-mm FWHM to avoid outlier values at the border of the standard brain. In the thickness image, bright areas highlight regions of abnormally thick cortex.

3 Examples

The following examples illustrate the use of morphometric MRI analysis in clinical practice and especially in the presurgical evaluation of epilepsy patients.

3.1 Focal Cortical Dysplasia

The three morphometric maps highlight different aspects and typical features of FCD and thereby complement each other. Whereas the extension and thickness images often only point to the most abnormal part of the dysplastic lesion, the junction image is more apt to show the extent of the dysplasia, even within cortex band which is not abnormally thick or located abnormally deep (Fig. 3a). When the lesion is already known and detection is not an issue, morphometric MRI analysis can still be useful for delineation of the extent of the lesion, especially with help of the junction image.

Morphometric analysis is most helpful when all morphometric maps highlight typical FCD features in the same location (Fig. 3b). However, not every FCD shows all signs of a dysplastic lesion. The presence of these signs depends on the histopathological subtype (Krsek et al. 2008). Frequently, only one of the morphometric maps points to an abnormality and the other maps are inconspicuous. In this situation, the junction image exhibits both the highest sensitivity and the highest specificity of the three morphometric maps, perhaps because blurring of the gray matter−white matter junction is found to a large extent in all FCD subtypes. Even in FCD type I according to Palmini and Luders (2002) it is present in most cases, whereas signs such as increased cortical thickness or abnormal gyral/sulcal patterns are seen in less than 10% and 17% of cases, respectively (Krsek et al. 2008). Figure 3c demonstrates such an example where only the junction image led to detection of the lesion. In this 11-year-old boy with gelastic and hypermotor seizures, the epilepsy had remained cryptogenic in spite of four MRI investigations with three different 3-T scanners between 2005 and 2008. The junction image finally highlighted subtle blurring of the gray matter−white matter junction in the right frontal lobe and guided the placement of subdural electrodes. Invasive electroencephalography (EEG) recording proved seizure onset in this region, and after resection FCD type IIb was confirmed histologically (Kröll-Seger et al. 2011). Nevertheless, as shown in Fig. 4a there are also cases where only the extension or the thickness image alone shows an abnormality and leads to detection of FCD (Altenmüller and Huppertz 2006).

It is noteworthy that in the example in Fig. 3c the junction image was calculated with *interpolated* voxel resolution of 0.5 mm^3. This option is a spin-off from processing of high-resolution 7-T MRI data (Speck et al. 2009) and has proven to be useful also for MRI data acquired with normal voxel resolution of 1 mm^3 when detailed delineation of the lesion is needed, however at the expense of significantly increased processing time and disk space.

Morphometric MRI analysis can also help to uncover the reasons for unsuccessful epilepsy surgery. Figure 4b shows the example of an 8-year-old girl who had been operated on abroad for an FCD in the right frontal lobe, however with no effect on seizure frequency. An MRI scan performed 5 years after surgery only showed the resection zone and

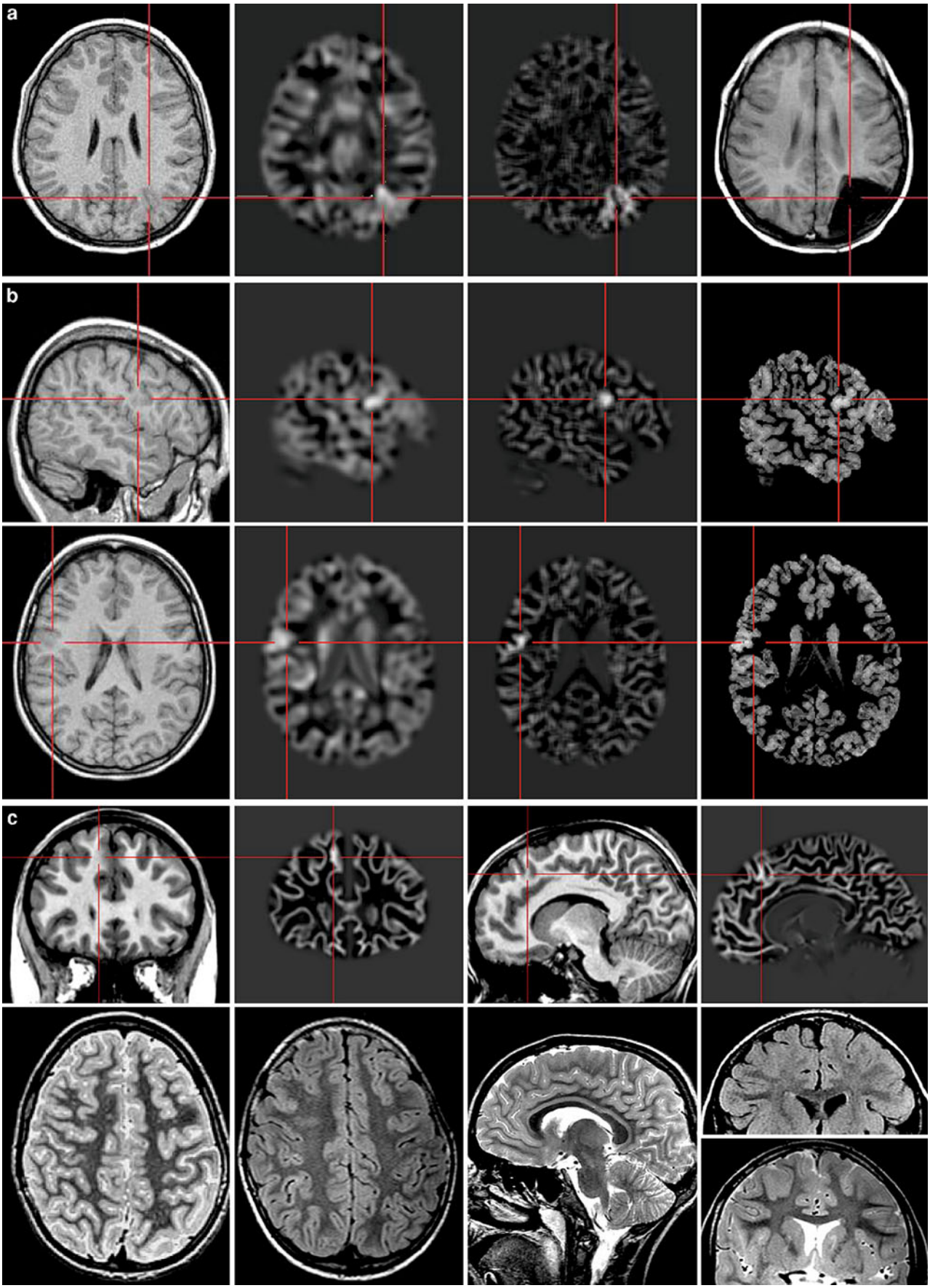
a
b
c

◀ **Fig. 3** Morphometric MRI analysis in focal cortical dysplasia. **a** T1-weighted image, extension image, junction image, and postoperative image in a patient with focal cortical dysplasia (FCD) type IIb. Whereas the extension image only highlights the "tip of the iceberg," the junction image demonstrates the extent of the lesion, fitting well the final resection zone. **b** T1-weighted, extension, junction, and thickness images in FCD IIb: the morphometric maps show all the signs of a dysplastic lesion, i.e., the abnormal gyration, the blurring of the gray−white matter junction, and the abnormal thickness of the cortical ribbon. **c** Coronal and sagittal T1-weighted and junction images (*upper row*) and corresponding T2- and fluid-attenuated inversion recovery (FLAIR)-weighted images (*lower row*) in a patient with gelastic and hypermotor seizures of unknown cause in spite of four MRI investigations with three different 3-T scanners. Only the junction image led to detection of the lesion. Even retrospectively, the dysplasia is hardly recognizable in the conventional magnetic resonance images

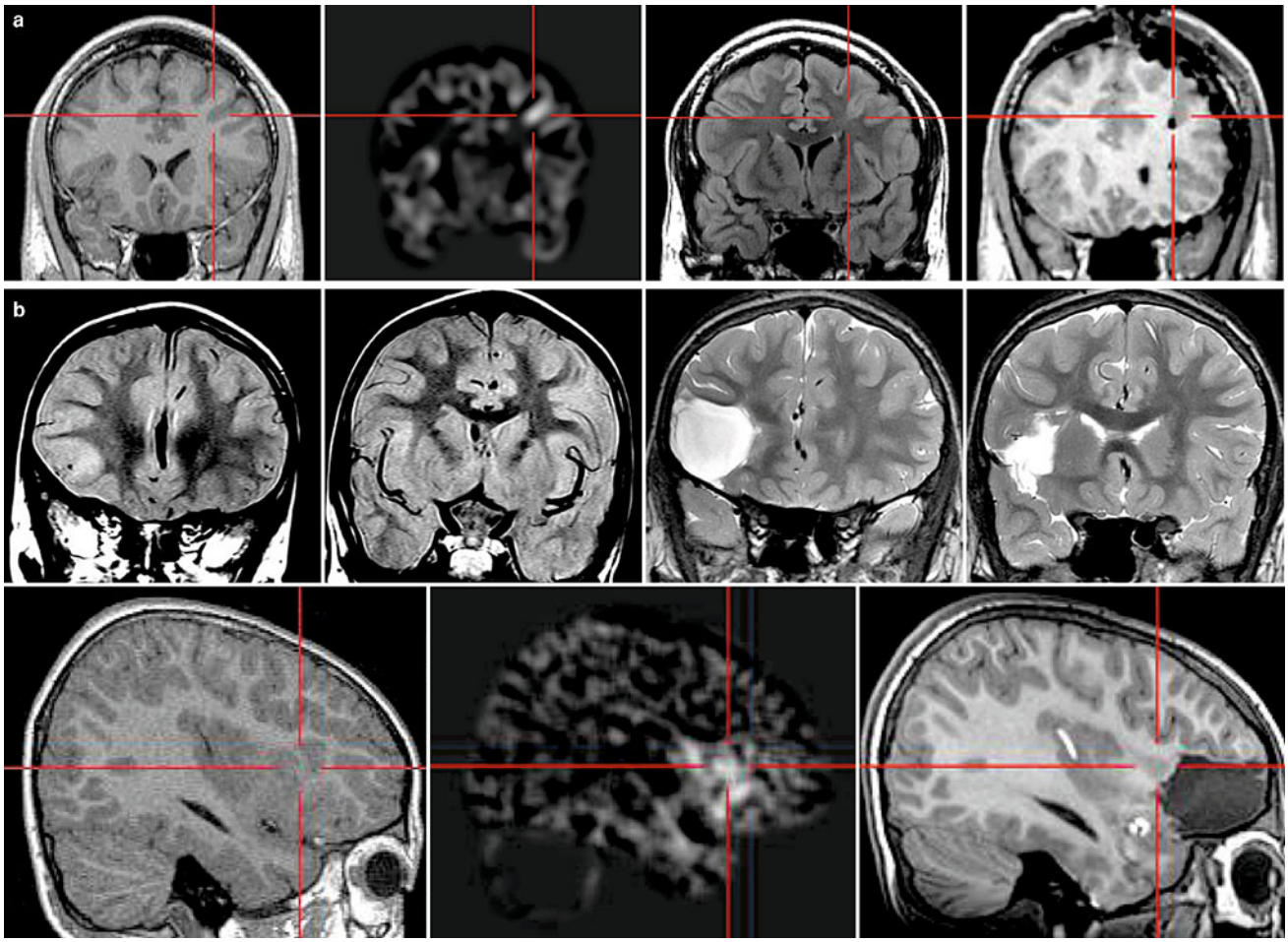

Fig. 4 Further examples of morphometric analysis in FCD. **a** T1- and FLAIR-weighted images, extension image, and T1-weighted image after electrode implantation in a patient with epigastric auras and hypermotor seizures. The epilepsy was previously cryptogenic in spite of 1.5- and 3-T MRI. The extension image led to detection of the lesion by highlighting an abnormally deep sulcus in the left frontal lobe and guided the placement of a depth electrode in this suspicious sulcus, which after resection turned out to harbor FCD type IIb. The very subtle transmantle sign in the FLAIR image was recognized only retrospectively. **b** Preoperative FLAIR and postoperative T2 images in an 8-year-old girl with FCD in the right frontal lobe (*upper row*). The comparison of preoperative T1 and junction images with the coregistered postoperative T1 image (*lower row*) reveals residual dysplastic tissue posterior to the resection zone

postoperative gliosis but no signs of residual dysplasia. Only morphometric analysis based on a preoperative MRI scan revealed in comparison with the coregistered postoperative MRI scan that dysplastic tissue has remained in the right anterior insula just behind the resection zone. This finding provides the opportunity for a second and hopefully final resection (Kröll and Huppertz 2008).

Apart from detection of lesions and delineation of the extent for final resection, the results of morphometric MRI analysis can also guide the implantation of subdural or depth electrodes for invasive EEG recording and mapping (Fig. 4a). For this purpose, the morphometric maps which have been normalized to the SPM5 standard brain during preprocessing can be transferred back to native space by inverse normalization and are then ready to be imported into an intraoperative neuronavigation system (Wellmer et al. 2010). This is especially helpful when the lesion is not recognizable in the conventional MR sequences.

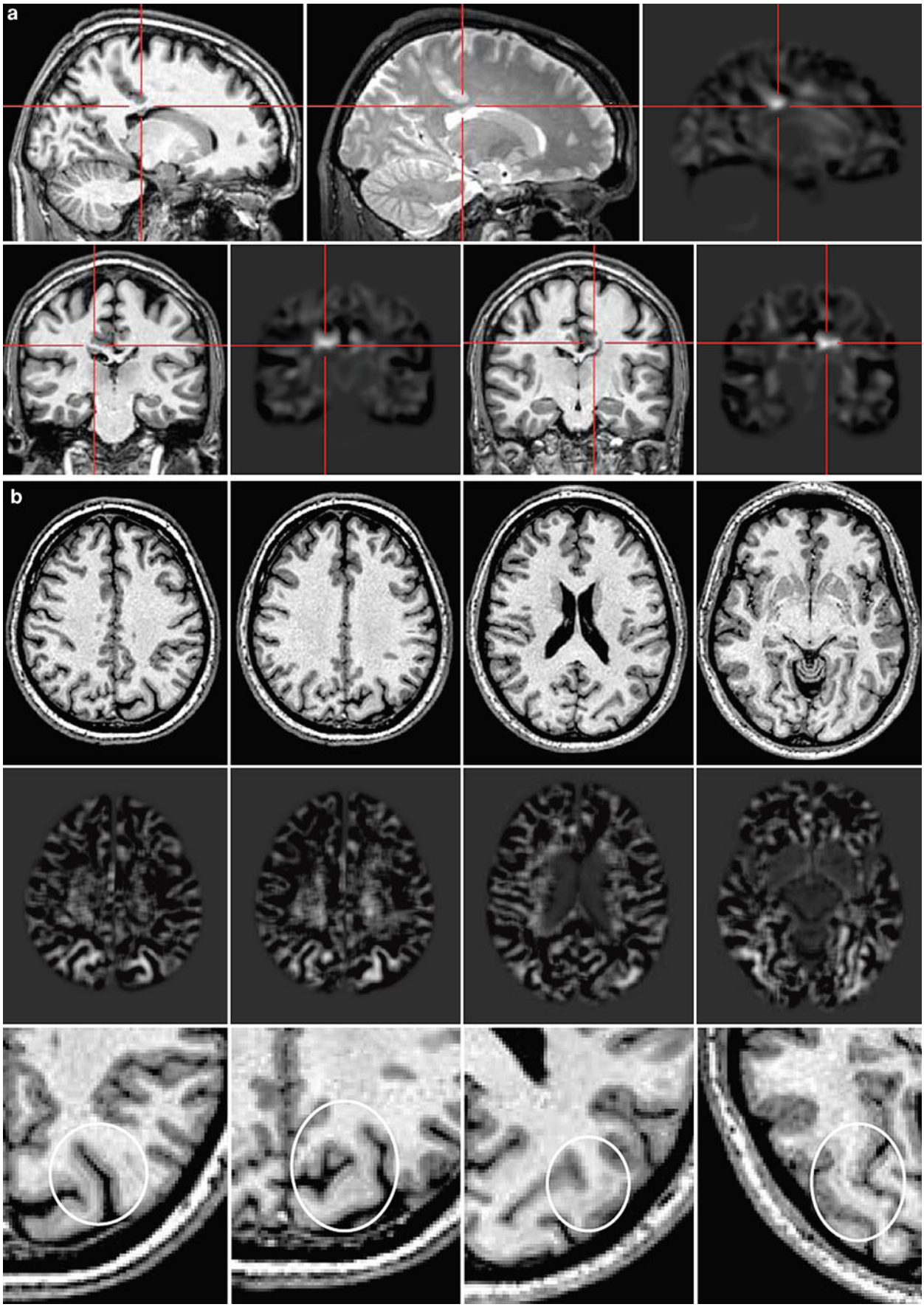
a
b

◀ **Fig. 5** Morphometric MRI analysis in gray matter heterotopia. **a** Sagittal T1- and T2-weighted images with the extension image (*upper row*), and coronal T1 and extension images (*lower row*) in a patient with bilateral periventricular nodular heterotopia. The heterotopia was overlooked in two 1.5- and 3-T MRI investigations and was only detected with the help of the extension image. **b** Axial T1 images (*upper row*), corresponding junction images (*middle row*), and enlarged T1 images (*lower row*) in a patient with very subtle subcortical band heterotopia not recognized in two previous MRI investigations. The junction image was not only crucial in establishing the diagnosis but also helped to assess the extent of these malformations and to verify the bilateral distribution

3.2 Gray Matter Heterotopia

Although morphometric MRI analysis is primarily meant to support detection and visualization of FCD, the method may also facilitate the recognition of other malformations of cortical development. Figure 5a shows the example of a 30-year-old man with rare generalized tonic–clonic seizures with intervals of 1–2 years without any focal symptoms. The findings of two MRI investigations at 1.5 and 3 T were regarded as normal. Only the extension image calculated from the last MRI scan revealed two subtle nodules of gray matter in the roofs of the lateral ventricles, representing bilateral periventricular nodular heterotopia. It is noteworthy that morphometric analysis in this case helped not only to detect the heterotopia but also highlighted the overlying cortex, which seems to extend abnormally deep into the white matter (Fig. 5a).

A clear-cut double cortex syndrome with a broad band of subcortical heterotopic gray metter throughout the brain is hardly missed in the MRI investigation. But there are also very subtle forms of subcortical band heterotopia (SBH). Figure 5b shows images of a 42-year-old man suffering from seizures with metamorphopsia in the lower-left visual field. Ictal EEG demonstrated a nonlateralizing seizure pattern over the biposterior regions and interictal EEG multiregional spike-and-wave complexes over the posterior temporal regions. The findings of two MRI investigations, performed when the man was 22 and 42 years old, were considered normal. The junction image derived from the second MRI investigation (3 T) highlighted subcortical thin and discontinuous band-like structures confined to the parietal and occipital lobes of both hemispheres. After reevaluation of the MRI investigations in these regions, a partial double cortex syndrome with very subtle SBH in posterior brain regions was diagnosed, thus explaining very well the ictal visual symptoms and EEG findings. In a subsequent survey of 378 epilepsy patients in three different epilepsy centers, morphometric analysis detected five cases of SBH which had been overlooked previously. This indicates that a considerable number of patients with SBH remain unrecognized by conventional MRI (Huppertz et al. 2008).

Furthermore, subtle forms of SBH such as in Fig. 5b can only be recognized in thin-sliced T1 images, preferably with 1-mm^3 voxel resolution in each direction. Reconstructions with thicker slices of 3–5 mm are not sufficient to detect these lesions. On the other hand, a thorough inspection of high-resolution T1 volume data sets of 150–180 slices requires special attention, patience, and time. The additional use of morphometric analysis can help to save time by directing the attention to these subtle malformations.

3.3 Polymicrogyria

Polymicrogyria is usually easy to detect on MRI, especially with bilateral presentation or when associated with schizencephaly. But there also subtle circumscribed and unilateral forms which might go unrecognized, particularly when thin-sliced T1 images either have not been acquired or—for time-saving reasons—are discarded in exchange for reconstructed images of greater slice thickness. Figure 6 shows such an example of a polymicrogyria which had been overlooked in a previous MRI investigation and had been misinterpreted as FCD in a recent 3-T MRI investigation. However, morphometric analysis can not only aid in detecting the lesion (as in this example) but may also help to differentiate between FCD and polymicrogyria. In contrast to FCD, a polymicrogyria lesion is predominantly highlighted by the extension and thickness images, whereas the junction image (not shown here) displays no or only scarce hints for a blurring of the gray−white matter junction.

4 Diagnostic Yield

The diagnostic yield of morphometric MRI analysis was analyzed prospectively in 2006 at the Swiss Epilepsy Centre. Morphometric MRI analysis was applied for all patients who had an MRI scan in that year and for whom a digital T1-weighted volume data set was available. These constituted 215 out of a total of 363 epilepsy patients who had an MRI scan in 2006. Thirty patients had malformations of cortical development (FCD, $n = 20$; heterotopia, $n = 4$; others, $n = 6$). Morphometric MRI analysis was performed in 26 of these patients (four dropouts owing to severe movement artifacts or missing digital MRI data). All malformations were identified in the morphometric maps. However, in 16 of these patients, these malformations had been overlooked in previous MRI investigations, and in nine of these 16 patients even in the MRI investigations in 2006, which were the basis for postprocessing. In an additional seven patients, the epileptogenic lesions were misinterpreted concerning their cause and/or their extension. Overall, this corresponds to a diagnostic

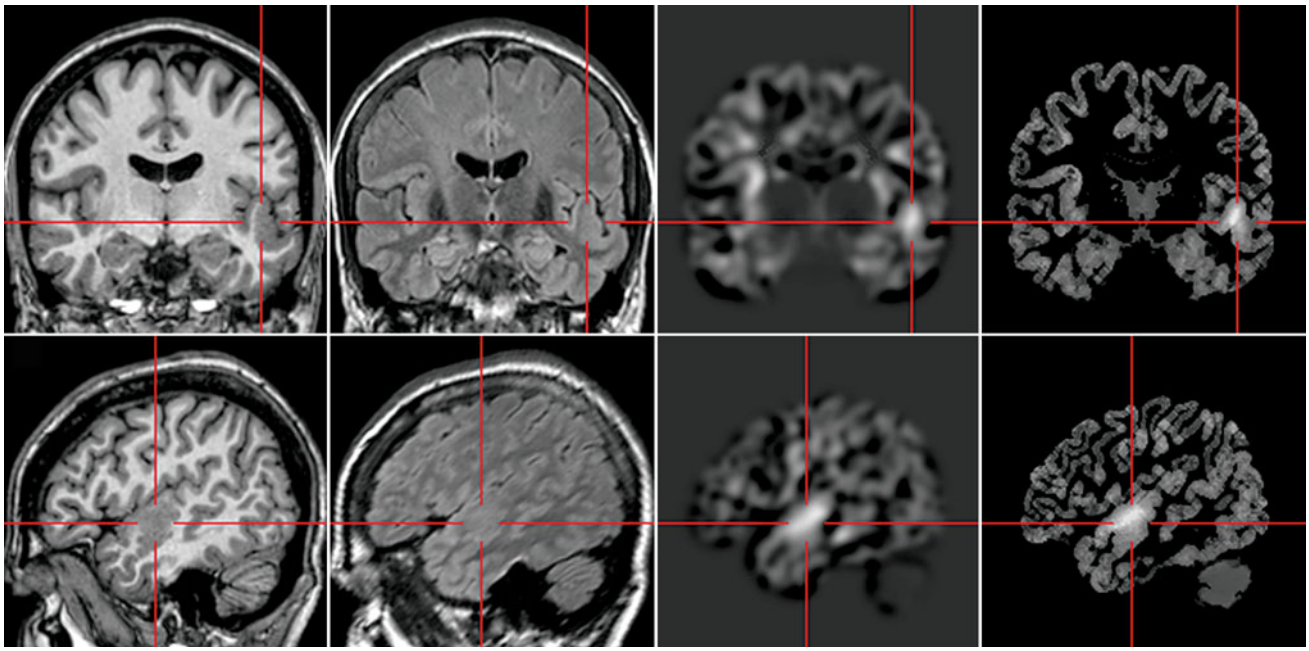

Fig. 6 Morphometric MRI analysis in polymicrogyria. Coronal (*upper row*) and sagittal (*lower row*) T1, FLAIR, extension, and thickness images, with the two morphometric maps highlighting an area of abnormal gyration and thick-appearing cortex in the left lateral temporal lobe which upon closer examination apparently consists of multiple small gyri

yield of about 7–8%, i.e., in this portion of patients, morphometric analysis provided additional valuable information.

A larger study has recently finished in the Department of Epileptology at the University of Bonn, Germany. In this study, the potential diagnostic value of morphometric analysis was compared with that of conventional visual analysis in 91 patients with histologically proven FCD operated on at this center between 2000 and 2010 (17 patients with FCD type IIa, 74 patients with FCD type IIb). All preoperative MRI scans were evaluated independently (1) by an experienced neuroradiologist on the basis of conventional visual analysis and (2) by a neurologist using morphometric analysis. Both evaluators had the same clinical information but were blinded to the results of each other. The FCD detection rate using morphometric analysis was superior to that of conventional visual analysis in the FCD type IIa subgroup (82% vs. 65%), whereas no difference was found in the FCD type IIb subgroup (92% vs. 91%). However, the combination of conventional visual analysis and morphometric analysis provided complementary information and detected 89 out of all 91 FCDs (98%). It was significantly superior to conventional visual analysis alone in both subgroups, resulting in a higher diagnostic sensitivity (94% vs. 65%, $P = 0.031$ for FCD type IIa; 99% vs. 91%, $P = 0.016$ for FCD type IIb) (Wagner et al. 2011).

5 Limitations

The morphometric analysis only highlights *structural* abnormalities. It does not account for signal hyperintensities on FLAIR and/or T2 images, which are often associated with FCD. Therefore, the method does not help to detect FCDs that have no structural abnormalities and that are only characterized by cortical and/or subcortical hyperintensities. As a consequence, morphometric analysis cannot replace an experienced neuroradiologist and cannot obviate the need to read other MR sequences apart from T1 images. The post-processing should be rather regarded as a supportive method increasing the diagnostic sensitivity for certain lesions.

Furthermore, the interpretation of the morphometric maps requires some experience. At the current stage, the method does not detect the lesion automatically. The morphometric maps direct the attention of the investigator to suspicious regions and can increase the conspicuity of a lesion. A visual confirmation by taking into account the conventional MR images is still necessary. Furthermore, the morphometric maps may highlight regions that have no pathological correlate in the conventional MR sequences, for example, regions of delayed white matter myelination in children or venous anomalies. Owing to ongoing myelination or reversed

T1 contrasts, segmentation may also fail in patients below the age of 2 years (Wagner et al. 2011).

6 Conclusion

The morphometric maps described in this chapter characterize different features of FCD and other cortical malformations and thereby complement each other. Their voxel-based technique allows a comprehensive 3D analysis of volumetric MRI data which may reveal abnormalities that are not visible when the data are viewed as 2D images only and which is less prone to misinterpretation due to partial volume effects. In addition, the method includes an inherent comparison with a normal database to compensate for physiological variations of sulcal morphology, cortical thickness, and the thickness of the gray−white matter transition zone in different brain regions. In contrast, visual analysis of conventional MR images requires that the investigator knows and keeps in mind normal variations of morphology. Furthermore, the calculation of the feature maps is completely automated and observer-independent. The method employs standard procedures of the SPM5 program and additional simple computations which can be easily implemented in a MATLAB® script. Except for the commercial MATLAB® platform required for SPM5, the method is thus based on freely available software. However, the key steps of this method (i.e., normalization, segmentation, filtering) could also be realized in other image processing environments which are freeware, e.g., the FMRIB Software Library (FSL; http://www.fmrib.ox.ac.uk/fsl) or AFNI (http://afni.nimh.nih.gov/afni), thus removing the need for a MATLAB® license (Huppertz et al. 2008). Finally, it is economic that the method does not require the acquisition of special MR sequences but is based on ordinary T1-weighted volume data sets which are already part of recommended MR protocols for epilepsy patients. In conclusion, the method of morphometric MRI analysis appears to be a helpful additional tool in the diagnostics and especially presurgical evaluation of epilepsy patients.

References

Altenmüller DM, Huppertz HJ (2006) Kombinierter Einsatz von morphometrischer MRT-analyse und gezielter invasiver EEG-Diagnostik bei fokaler kortikaler Dysplasie. Epileptologie 3:117–125

Antel SB, Bernasconi A, Bernasconi N, Collins DL, Kearney RE, Shinghal R, Arnold DL (2002) Computational models of MRI characteristics of focal cortical dysplasia improve lesion detection. Neuroimage 17:1755–1760

Antel SB, Collins DL, Bernasconi N, Andermann F, Shinghal R, Kearney RE, Arnold DL, Bernasconi A (2003) Automated detection of focal cortical dysplasia lesions using computational models of their MRI characteristics and texture analysis. Neuroimage 19:1748–1759

Ashburner J, Friston KJ (2005) Unified segmentation. Neuroimage 26:839–851

Barkovich AJ, Kuzniecky RI (1996) Neuroimaging of focal malformations of cortical development. J Clin Neurophysiol 13:481–494

Barkovich AJ, Kuzniecky RI, Dobyns WB (2001) Radiologic classification of malformations of cortical development. Curr Opin Neurol 14:145–149

Bastos AC, Comeau RM, Andermann F, Melanson D, Cendes F, Dubeau F, Fontaine S, Tampieri D, Olivier A (1999) Diagnosis of subtle focal dysplastic lesions: curvilinear reformatting from three-dimensional magnetic resonance imaging. Ann Neurol 46:88–94

Berg AT, Vickrey BG, Langfitt JT, Sperling MR, Walczak TS, Shinnar S, Bazil CW, Pacia SV, Spencer SS (2003) The multicenter study of epilepsy surgery: recruitment and selection for surgery. Epilepsia 44:1425–1433

Bernasconi A, Antel SB, Collins DL, Bernasconi N, Olivier A, Dubeau F, Pike GB, Andermann F, Arnold DL (2001) Texture analysis and morphological processing of magnetic resonance imaging assist detection of focal cortical dysplasia in extra-temporal partial epilepsy. Ann Neurol 49:770–775

Bernasconi A, Bernasconi N, Bernhardt BC, Schrader D (2011) Advances in MRI for 'cryptogenic' epilepsies. Nat Rev Neurol 7:99–108

Besson P, Bernasconi N, Colliot O, Evans A, Bernasconi A (2008a) Surface-based texture and morphological analysis detects subtle cortical dysplasia. Med Image Comput Comput Assist Interv 11:645–652

Besson P, Bernasconi N, Colliot O, Evans A, Bernasconi A (2008b) Surface-based texture and morphological analysis detects subtle cortical dysplasia. Med Image Comput Comput Assist Interv11: 645–652

Bien CG, Szinay M, Wagner J, Clusmann H, Becker AJ, Urbach H (2009) Characteristics and surgical outcomes of patients with refractory magnetic resonance imaging-negative epilepsies. Arch Neurol 66:1491–1499

Bonilha L, Montenegro MA, Rorden C, Castellano G, Guerreiro MM, Cendes F, Li LM (2006) Voxel-based morphometry reveals excess gray matter concentration in patients with focal cortical dysplasia. Epilepsia 47:908–915

Bruggemann JM, Wilke M, Som SS, Bye AM, Bleasel A, Lawson JA (2007) Voxel-based morphometry in the detection of dysplasia and neoplasia in childhood epilepsy: combined grey/white matter analysis augments detection. Epilepsy Res 77:93–101

Chan S, Chin SS, Nordli DR, Goodman RR, DeLaPaz RL, Pedley TA (1998) Prospective magnetic resonance imaging identification of focal cortical dysplasia, including the non-balloon cell subtype. Ann Neurol 44:749–757

Colliot O, Bernasconi N, Khalili N, Antel SB, Naessens V, Bernasconi A (2006) Individual voxel-based analysis of gray matter in focal cortical dysplasia. Neuroimage 29:162–171

Fauser S, Schulze-Bonhage A, Honegger J, Carmona H, Huppertz HJ, Pantazis G, Rona S, Bast T, Strobl K, Steinhoff BJ, Korinthenberg R, Rating D, Volk B, Zentner J (2004) Focal cortical dysplasias: surgical outcome in 67 patients in relation to histological subtypes and dual pathology. Brain 127:2406–2418

Fischl B, Dale AM (2000) Measuring the thickness of the human cerebral cortex from magnetic resonance images. Proc Natl Acad Sci USA 97:11050–11055

Focke NK, Symms MR, Burdett JL, Duncan JS (2008) Voxel-based analysis of whole brain FLAIR at 3 T detects focal cortical dysplasia. Epilepsia 49:786–793

Gomez-Anson B, Thom M, Moran N, Stevens J, Scaravilli F (2000) Imaging and radiological-pathological correlation in histologically proven cases of focal cortical dysplasia and other glial and neuronoglial malformative lesions in adults. Neuroradiology 42:157–167

Hagemann G, Redecker C, Witte OW (2000) Cortical dysgenesis: current classification, MRI diagnosis, and clinical review. Nervenarzt 71: 616–628

Hildebrandt M, Pieper T, Winkler P, Kolodziejczyk D, Holthausen H, Blümcke I (2005) Neuropathological spectrum of cortical dysplasia in children with severe focal epilepsies. Acta Neuropathol (Berl) 110:1–11

Huppertz HJ, Grimm C, Fauser S, Kassubek J, Mader I, Hochmuth A, Spreer J, Schulze-Bonhage A (2005) Enhanced visualization of blurred gray−white matter junctions in focal cortical dysplasia by voxel-based 3D MRI analysis. Epilepsy Res 67:35–50

Huppertz HJ, Wellmer J, Staack AM, Altenmuller DM, Urbach H, Kroll J (2008) Voxel-based 3D MRI analysis helps to detect subtle forms of subcortical band heterotopia. Epilepsia 49:772–785

Kassubek J, Huppertz HJ, Spreer J, Schulze-Bonhage A (2002) Detection and localization of focal cortical dysplasia by voxel-based 3-D MRI analysis. Epilepsia 43:596–602

Kröll J, Huppertz HJ (2008) Nachweis von postoperativ verbliebenem dysplastischen Kortex mittels morphometrischer MRI-Analyse. Schweiz Z Psychiatr Neurol 2:17–20

Kröll-Seger J, Grunwald T, Mothersill IW, Bernays R, Krämer G, Huppertz HJ (2011) Lachen ohne Heiterkeit—Morphometrische MRT-analyse in der prächirurgischen Abklärung einer MRT-negativen kindlichen Epilepsie mit gelastischen Anfällen. Epileptologie 28(2):78–83

Krsek P, Maton B, Korman B, Pacheco-Jacome E, Jayakar P, Dunoyer C, Rey G, Morrison G, Ragheb J, Vinters HV, Resnick T, Duchowny M (2008) Different features of histopathological subtypes of pediatric focal cortical dysplasia. Ann Neurol 63:758–769

Kuzniecky R, Murro A, King D, Morawetz R, Smith J, Powers R, Yaghmai F, Faught E, Gallagher B, Snead OC (1993) Magnetic resonance imaging in childhood intractable partial epilepsies: pathologic correlations. Neurology 43:681–687

Kuzniecky R, Morawetz R, Faught E, Black L (1995) Frontal and central lobe focal dysplasia: clinical, EEG and imaging features. Dev Med Child Neurol 37:159–166

Lerner JT, Salamon N, Hauptman JS, Velasco TR, Hemb M, Wu JY, Sankar R, Donald SW, Engel J Jr, Fried I, Cepeda C, Andre VM, Levine MS, Miyata H, Yong WH, Vinters HV, Mathern GW (2009) Assessment and surgical outcomes for mild type I and severe type II cortical dysplasia: a critical review and the UCLA experience. Epilepsia 50:1310–1335

Merschhemke M, Mitchell TN, Free SL, Hammers A, Kinton L, Siddiqui A, Stevens J, Kendall B, Meencke HJ, Duncan JS (2003) Quantitative MRI detects abnormalities in relatives of patients with epilepsy and malformations of cortical development. Neuroimage 18:642–649

Palmini A, Luders HO (2002) Classification issues in malformations caused by abnormalities of cortical development. Neurosurg Clin N Am 13:1–16

Raymond AA, Fish DR, Sisodiya SM, Alsanjari N, Stevens JM, Shorvon SD (1995) Abnormalities of gyration, heterotopias, tuberous sclerosis, focal cortical dysplasia, microdysgenesis, dysembryoplastic neuroepithelial tumour and dysgenesis of the archicortex in epilepsy. Clinical, EEG and neuroimaging features in 100 adult patients. Brain 118(Pt 3):629–660

Redecker C, Hagemann G, Gressens P, Evrard P, Witte OW (2000) Cortical dysgenesis. Current views on pathogenesis and pathophysiology. Nervenarzt 71:238–248

Rugg-Gunn FJ, Boulby PA, Symms MR, Barker GJ, Duncan JS (2005) Whole-brain T2 mapping demonstrates occult abnormalities in focal epilepsy. Neurology 64:318–325

Salmenpera TM, Symms MR, Rugg-Gunn FJ, Boulby PA, Free SL, Barker GJ, Yousry TA, Duncan JS (2007) Evaluation of quantitative magnetic resonance imaging contrasts in MRI-negative refractory focal epilepsy. Epilepsia 48:229–237

Scott ML, Bromiley PA, Thacker NA, Hutchinson CE, Jackson A (2009) A fast, model-independent method for cerebral cortical thickness estimation using MRI. Med Image Anal 13:269–285

Semah F, Picot MC, Adam C, Broglin D, Arzimanoglou A, Bazin B, Cavalcanti D, Baulac M (1998) Is the underlying cause of epilepsy a major prognostic factor for recurrence? Neurology 51:1256–1262

Sisodiya SM, Free SL, Fish DR, Shorvon SD (1995a) Increasing the yield from volumetric MRI in patients with epilepsy. Magn Reson Imaging 13:1147–1152

Sisodiya SM, Free SL, Stevens JM, Fish DR, Shorvon SD (1995b) Widespread cerebral structural changes in patients with cortical dysgenesis and epilepsy. Brain 118:1039–1050

Speck O, Tempelmann C, Matzen J, Huppertz HJ (2009) Morphometric MRI analysis based on high resolution 3D imaging at 7 tesla highlights focal cortical dysplasia in epilepsy. Proc Intl Soc Mag Reson Med 17:971

Tassi L, Colombo N, Garbelli R, Francione S, Lo RG, Mai R, Cardinale F, Cossu M, Ferrario A, Galli C, Bramerio M, Citterio A, Spreafico R (2002) Focal cortical dysplasia: neuropathological subtypes, EEG, neuroimaging and surgical outcome. Brain 125:1719–1732

Thesen T, Quinn BT, Carlson C, Devinsky O, DuBois J, McDonald CR, French J, Leventer R, Felsovalyi O, Wang X, Halgren E, Kuzniecky R (2011) Detection of epileptogenic cortical malformations with surface-based MRI morphometry. PLoS One 6:e16430

Urbach H, Scheffler B, Heinrichsmeier T, von Oertzen J, Kral T, Wellmer J, Schramm J, Wiestler OD, Blümcke I (2002) Focal cortical dysplasia of Taylor's balloon cell type: a clinicopathological entity with characteristic neuroimaging and histopathological features, and favorable postsurgical outcome. Epilepsia 43:33–40

Wagner J, Weber B, Urbach H, Elger CE, Huppertz HJ (2011) Morphometric MRI analysis improves detection of focal cortical dysplasia type II. Brain 13:2844–2854

Wellmer J, Parpaley Y, von Lehe M, Huppertz HJ (2010) Integrating MRI post-processing results into neuronavigation for electrode implantation and resection of subtle focal cortical dysplasia in previously cryptogenic epilepsy. Neurosurgery 66:187–194

Widdess-Walsh P, Diehl B, Najm I (2006) Neuroimaging of focal cortical dysplasia. J Neuroimaging 16:185–196

Wilke M, Kassubek J, Ziyeh S, Schulze-Bonhage A, Huppertz HJ (2003) Automated detection of gray matter malformations using optimized voxel-based morphometry: a systematic approach. Neuroimage 20:330–343

Woermann FG, Free SL, Koepp MJ, Ashburner J, Duncan JS (1999) Voxel-by-voxel comparison of automatically segmented cerebral gray matter—a rater-independent comparison of structural MRI in patients with epilepsy. Neuroimage 10:373–384

Metallic Implants

Horst Urbach and Sebastian Flacke

Contents

Abstract

Patients with vagus nerve, deep brain stimulators or depth and subdural electrodes have to be examined according to the manufacturer guidelines, which in general require the use of transmit/receive head coils limiting the RF deposition to the brain.

Vagus nerve stimulators (VNS), deep brain stimulators (DBS), and depth and/or subdural strip or grid electrodes are medical devices which may interfere with MRI examinations in epilepsy patients.

VNS use mild electrical pulses to stimulate the vagus nerve, which in turn transmits them to the brain. They consist of a small pulse generator and thin flexible stimulation wires with a pair of spiral platinum electrodes at the end. The pulse generator is typically placed within the left side of the patient's chest wall and the platinum electrodes are wrapped around the vagus nerve on the left side of the patient's neck (George et al. 2000). The rationale behind stimulating the left vagus nerve is that it has fewer cardiac fibers supplying the sinuatrial node (Kotagal 2011).

DBS use mild chronic electrical stimulation of certain brain structures, e.g., the anterior nucleus or the centromedian nucleus of the thalamus. An implanted pulse generator containg a battery and programmable hardware is typically (Kotagal 2011, Zrinzo et al. 2011) placed within the patient's chest wall, and an extension cable is tunneled underneath the skin and is connected to the stimulation electrodes, with the extracranial portion coiled underneath the scalp and the intracranial portion stereotactically placed via drilled burr holes (Kotagal 2011).

Subdural strip and grid electrodes and depth electrodes record epileptic EEG activity or are stimulated to localize brain functions.

The following theoretical concerns arise if patients with these devices are studied with MRI:

H. Urbach (✉)
Department of Neuroradiology,
University Hospital Freiburg, Germany
e-mail: horst.urbach@uniklinik-freiburg.de

S. Flacke
Department of Radiology, Lahey Clinic, Burlington, MA, USA

H. Urbach (ed.), *MRI in Epilepsy*, Medical Radiology. Diagnostic Imaging,
DOI: 10.1007/174_2012_562, © Springer-Verlag Berlin Heidelberg 2013

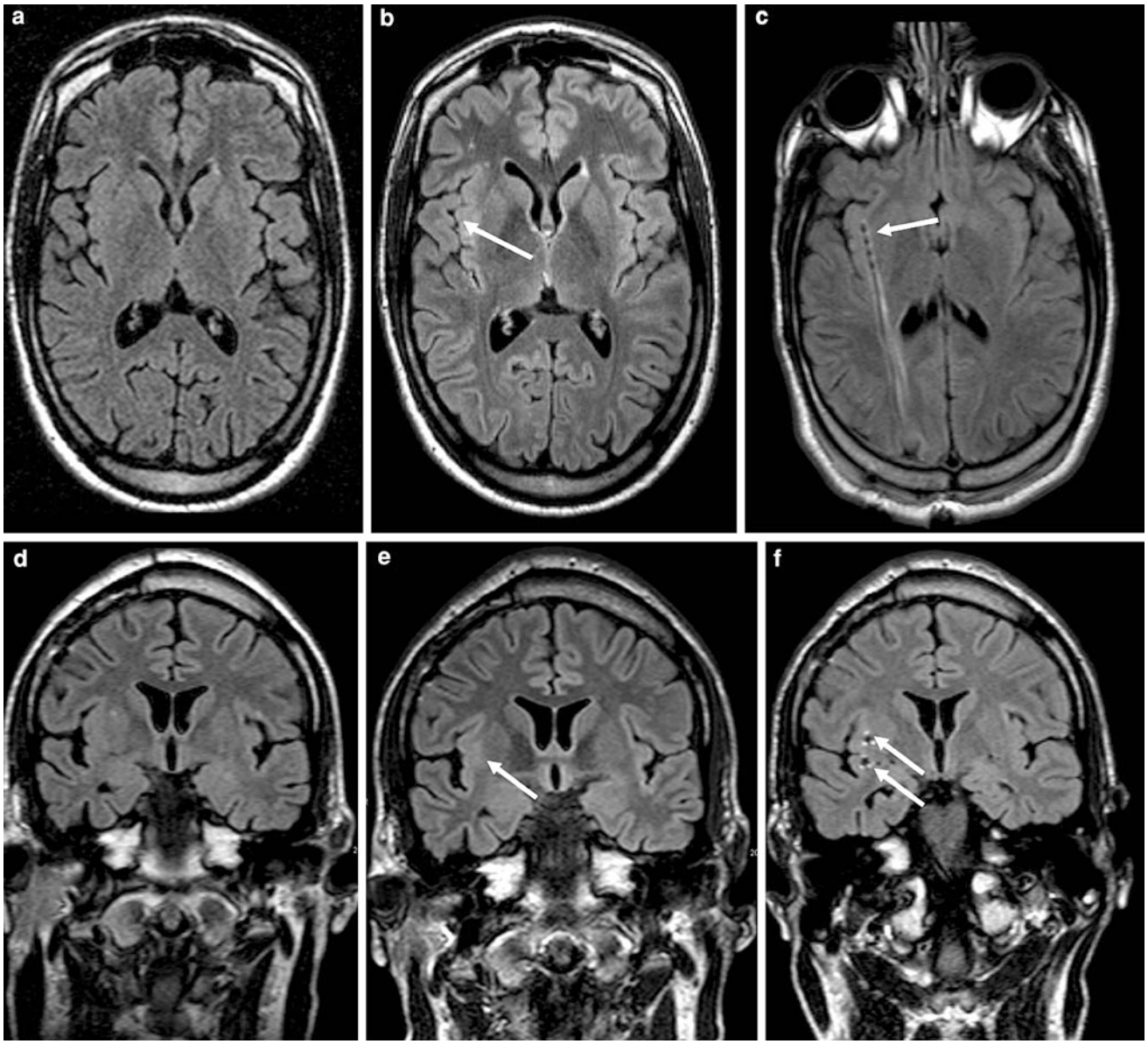

Fig. 1 After uneventful presurgical evaluation including right frontal subdural grid implantation, a 24-year-old man with drug-resistant temporal lobe seizures received a vagus nerve stimulator. With the vagus nerve stimulator (VNS) turned off, he was again studied in a 1.5-T MRI scanner. A transmit/receive head coil was used, and pulse sequences with reduced high-frequency energy deposition (specific absorption rate less than 0.1 W/kg for 15 min) were acquired. This examination again failed to show a lesion (**a**, **d**). In the next step, the VNS was explanted, the VNS leads were cut as short as reasonably possible, and the patient was studied with the epilepsy-dedicated 3-T MRI protocol. Axial and coronal fluid-attenuated inversion recovery sequences were suggestive of a small insular dysplasia (**b**, **e**, *arrow*). Epileptic EEG activity was recorded with stereotactically placed depth electrodes, whose positions were depicted with 1.5-T MRI under VNS conditions (**c**, **f**, *arrows*). Finally, the patient was operated on and a type IIB focal cortical dysplasia was histologically proven

1. Device displacement by force and torque induced during patient positioing in themagmetic field B_0.
2. Heating effects on material components, especially leads. These heating effects are produced by radiofrequency (RF) pulses which induce eddy currents in the leads, with possible thermal injury at the lead–tissue interfaces.
3. Unintended neurostimulation mainly produced by the low-frequency gradient fields. The induced currents are proportional to the rate of change of the gradient pulses with time (dB/dt), the effective loop area created by the VNS or DBS lead system, and the location of the lead system with respect to the gradient coils of the MRI system.

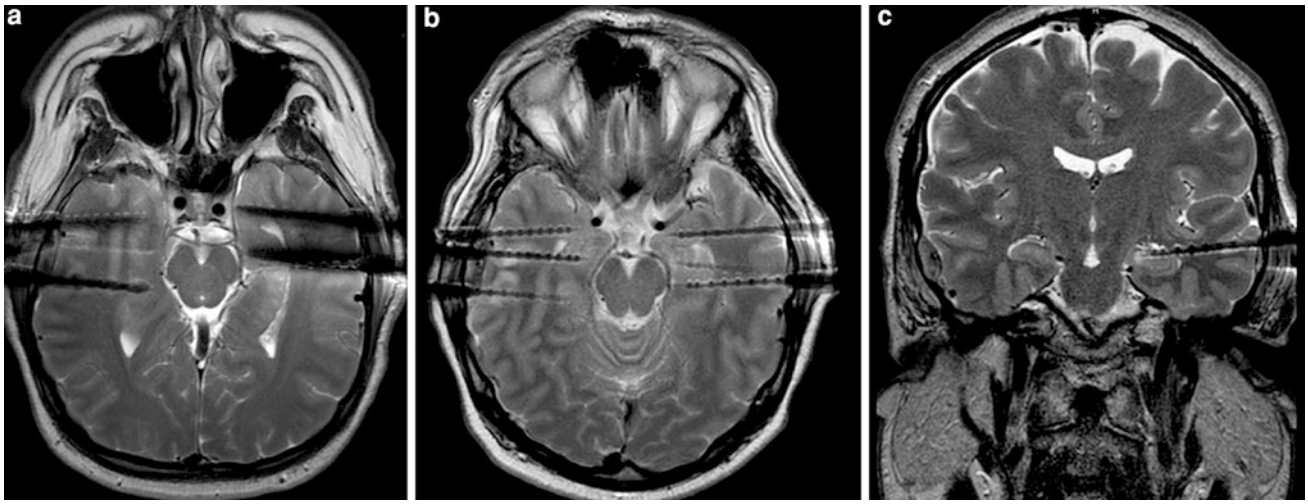

Fig. 2 Reduced susceptibility artifacts of depth electrodes at 1.5 T (**b**, **c**) compared with 3 T (**a**)

4. Electromagnetic compatibility.
5. Acoustic noise.
6. Interaction among devices
7. Safe functioning of the device.
8. Safe operation of the MRI system.

The greatest concern is thermal injury from RF pulses. Heating may occur around the VNS or DBS or along the subdural or depth electrodes, but is more likely to occur at the noninsulated ends of the electrodes. Experimental investigations of cardiac pacemakers showed a higher temperature increase in patients with abandoned leads than in patients with leads attached to the pacemaker (Langman et al. 2011). Thus, patients with abandoned or broken leads around the vagus nerve after explanting a VNS could show a higher temperature increase than patients with an implanted VNS. Heating is considered harmful as it could result in tissue damage in the brain parenchyma or the vagus nerve and/or surrounding structures in the carotid sheath.

A measure to assess the amount of energy deposited by a radiofrequency field in a certain mass of tissue is the specific absorption rate. The units for SAR are therefore given in watts per kilogram [W/kg]. The SAR produced during an MRI study is a complex function of various variables. SAR is proportional to the square of the field strength, the square of the RF flip angle, the duty cycle which is influenced by the repetition time, the type of transmit coil and the volume, electrical conductivity and anatomical configuration of the tissue contained within the transmit coil. This relationship already implies that stronger magnets and larger RF flip-angles applied in a short time interval will result in higher energy deposition (Shellock 2008). Unfortunately, the SAR is calculated differently by different MRI system manufacturers and even varies for different systems with identical field strength produced by the same manufacturer. For example, the SAR is higher in a long-bore system than in a short-bore system. The SAR can be averaged over the whole body or the head only, and the averaged whole-body SAR should not exceed 4 W/kg in any MRI examination. For a given MRI system, a higher SAR leads to greater heating.

Other concerns with respect to VNS or DBS are inadvertent device reset erasing historical information stored in the device or inadvertent magnet mode activation from the magnetic fields.

In 2005, ASTM International introduced the criteria MRI-safe, MRI-conditional and MRI-unsafe (ASTM International 2005). With respect to these criteria, the devices mentioned above are defined as MRI-conditional, i.e., MRI is considered safe under specified conditions of use. Interestingly, neither the FDA nor the International Electrotechnical Commission has specified these conditions for the different metallic implants, but instead has left this task to the manufacturers (Gupte et al. 2011). The manufacturers provide this information within their manuals and MRI healthcare professionals are advised to contact the respective manufacturer to obtain the latest safety information. Provisional information and guidance to the respective manufacturer's websites can be obtained via the website http://www.mrisaftey.com.

In general, MRI examinations with implanted VNS or DBS or subdural grid or strip electrodes or depth electrodes should be performed as follows: magnetic field strength of 1.5 T or less; head SAR of less than 0.1 W/kg; $dB/dt < 20$ T/s; output current of the implanted pulse generator set to 0 mA; testing and reprogramming of the devices after scanning (Benbadis et al. 2001; Roebling et al. 2009; Shellock et al. 2006; Shellock 2002; Kainz 2007; Gupte et al. 2011).

In clinical practice, the following situations may occur:

1. Searching for an epileptogenic lesion in a patient with an implanted VNS. This condition is considered MRI-conditional (Gorny et al. 2010). In 2011, the manufacturer Cyberonics (Houston, TX, USA) received FDA approval for 3-T scanning for models 100, 102, and 103 under specified conditions of use.
2. Searching for an epileptogenic lesion after explantation of a VNS with abandoned or broken leads around the vagus nerve in the neck. The manufacturer Cyberonics warns against performing MRI in patients with abandoned or broken leads, acknowledging that this situation has not been characterized nor has safety been demonstrated. Clinical experience under off-label-use conditions, however, is that patients can benefit from 3-T MRI using a transmit/receive head coil and reducing the SAR (Fig. 1)
3. Localization of depth or subdural electrodes. MRI at 3 T under the conditions specified above is allowed for some electrodes. Since susceptibility artifacts are stronger at 3 T (susceptibility $\varpi \approx B_0$), 1.5-T MRI under the conditions specified above is preferred (Fig. 2).

References

ASTM International (2005) F2503–05. Standard practice for marking medical devices and other items for safety in the magnetic resonance environment. ASTM International, West Conshohocken

Benbadis SR, Nyhenhuis J, Tatum WO 4th, Murtagh FR, Gieron M, Vale FL (2001) MRI of the brain is safe in patients implanted with the vagus nerve stimulator. Seizure 10(7):512–515

George MS, Sackeim HA, Rush AJ, Marangell LB, Nahas Z, Husain MM, Lisanby S, Burt T, Goldman J, Ballenger JC (2000) Vagus nerve stimulation: a new tool for brain research and therapy. Biol Psychiatry 47(4):287–295

Gorny KR, Bernstein MA, Watson RE Jr (2010) 3 tesla MRI of patients with a vagus nerve stimulator: initial experience using a T/R head coil under controlled conditions. J Magn Reson Imaging 31(2):475–481

Gupte AA, Shrivastava D, Spaniol MA, Abosch A (2011) MRI-related heating near deep brain stimulation electrodes: more data are needed. Stereotact Funct Neurosurg 89(3):131–140

Kainz W (2007) Response to Shellock et al. Vagus nerve stimulation therapy system: in vitro evaluation of magnetic resonance imaging-related heating and function at 1.5 and 3 tesla. Neuromodulation 10(1):76–77

Kotagal P (2011) Neurostimulation: vagus nerve stimulation and beyond. Semin Pediatr Neurol 18(3):186–194

Langman DA, Goldberg IB, Finn JP, Ennis DB (2011) Pacemaker lead tip heating in abandoned and pacemaker-attached leads at 1.5 tesla MRI. J Magn Reson Imaging 33(2):426–431

Roebling R, Huch K, Kassubek J, Lerche H, Weber Y (2009) Cervical spinal MRI in a patient with a vagus nerve stimulator (VNS). Epilepsy Res 84(2–3):273–275

Shellock FG (2002) Magnetic resonance safety update. J Magn Reson Imaging 16:485–496

Shellock FG (2008) Reference manual for magnetic resonance safety, implants, and devices. Biomedical Research Group, Los Angeles

Shellock FG, Begnaud J, Inman DM (2006) Vagus nerve stimulation therapy system: in vitro evaluation of magnetic resonance imaging-related heating and function at 1.5 and 3 tesla. Neuromodulation 9(3):204–213

Zrinzo L, Yoshida F, Hariz MI, Thornton J, Foltynie T, Yousry TA, Limousin P (2011) Clinical safety of brain magnetic resonance imaging with implanted deep brain stimulation hardware: large case series and review of the literature. World Neurosurg 76(1–2):164–172

Part II

Epileptogenic Lesions

Hippocampal Sclerosis

Horst Urbach

Contents

Abstract

Hippocampal sclerosis is by far the most common cause of temporal lobe epilepsy. The familiar reader detects it on MRI in more than 95% of cases but should be aware of typical "pitfalls", namely bilateral hippocampal sclerosis, "dual pathology" and insufficient image Quality.

1 Terminology

Hippocampal sclerosis, Ammon's horn sclerosis and mesial temporal sclerosis are used synonymously.

2 Epidemiology

First histopathological description by the German psychiatrist W. Sommer in 1880. By far the most common cause of temporal lobe epilepsy (TLE) and found in 50–65% of patients undergoing resective surgery.

3 Pathogenesis

Half of the patients undergoing surgery have experienced a precipitating injury before the age of 4 years (complex fever seizures, 70%; birth trauma, meningitis, head injury, 30% Blümcke et al. 2002). Mean age at the onset of complex partial seizures is between 9 and 11 years, and mean age at the time of epilepsy surgery around the age of 30 (Blümcke et al. 2002). The long latency between a possible initial precipitating injury, the onset of epileptic seizures, and epilepsy surgery renders assessment of the pathogenesis of hippocampal sclerosis difficult.

Current concept is a genetically determined susceptibility and a precipitating injury induce temporo-mesial seizures and hippocampal sclerosis. A substantial argument is the fact, that 1/3 of non-affected individuals in families

H. Urbach (✉)
Department of Neuroradiology,
University Hospital Freiburg, Germany
e-mail: horst.urbach@uniklinik-freiburg.de

H. Urbach (ed.), *MRI in Epilepsy*, Medical Radiology. Diagnostic Imaging,
DOI: 10.1007/174_2011_524, © Springer-Verlag Berlin Heidelberg 2013

Table 1 Neuropathological grading of hippocampal sclerosis [adapted from Wyler et al. (1992)]

Grade	Classfication	Neuropathological description	MRI
Wyler I	Mild mesial temporal damage	Gliosis with slight (<10%) or no hippocampal neuronal dropout involving sectors CA1, CA3, and/or CA4	Not visible
Wyler II	Moderate mesial temporal damage	Gliosis with moderate (10–50%) neuronal dropout of CA1, CA3, and/or CA4. If Involvement limited to CA3 and 4 = end folium sclerosis	Loss of internal structure on high resolution T2-weighted images
Wyler III	"Classical" ammon's horn sclerosis	Gliosis with >50% neuronal dropout of CA1, CA3, and CA4, but sparing CA2	Atrophy and increased T2/FLAIR signal
Wyler IV	"Total" ammon's horn sclerosis	Gliosis with >50% neuronal dropout of all sectors	Atrophy and increased T2/FLAIR signal visible

Table 2 Neuropathological grading of hippocampal sclerosis [adapted from Blümcke et al. (2007)]

Grade	Description	Frequency (%)	MRI
Blümcke MTS 1a	Severe neuronal loss in CA1, moderate neuronal loss in other subfields	23	Atrophy and increased T2/FLAIR signal
Blümcke MTS 1b	Extensive neuronal loss in all subfields	68	Atrophy and increased T2/FLAIR signal
Blümcke MTS 2	Severe neuronal loss restricted to CA1	7	?
Blümcke MTS 3	Severe neuronal loss restricted to hilar region = end folium sclerosis	5	Loss of internal structure on high resolution T2-weighted images

with familial TLE show hippocampal sclerosis on MRI (Kobayashi et al. 2002).

If patients develop temporal lobe seizures or subacute memory deficits after the age of 20, one has to think of limbic encephalitis, which is mediated via antibodies and found in up to 30% of patients in this age group (Soeder et al. 2009).

4 Clinical Presentation

A typical mesial temporal lobe seizure starts with an epigastric aura (definition of aura = initial part of a partial seizure, that is remembered after the seizure has terminated). The aura is followed by objective phenomena like staring, restlessness, oroalimentary automatism, and (ipsilateral) head deviation, which last from around 30 seconds to several minutes. In the postictal phase, gradual reorientation occurs which may be accompanied by dysphasia and other sympoms.

5 Pathology

Hippocampal sclerosis is characterized by neuronal loss and gliosis, most prominent in the CA1 field of the hippocampus, followed by the hilus, CA3 field, and dentate granule layer, while the CA2 field is relatively spared. These alterations are accompanied by a dispersion of the dentate granuale layer with ectopic neurons being found in the molecular layer.

Extent of hippocampal sclerosis is graded according to Wyler et al. (Table 1) or more recently according to Blümcke et al. (Table 2) (Wyler et al. 1992; Blümcke et al. 2007). Note that more than 90% of patients, who undergo selective amygdalohippocampectomy with MRI suspected hippocampal sclerosis have Wyler grade III and IV hippocampal sclerosis. Both are easily recognized on perfectly angulated high resolution T2- and FLAIR images due to their atrophy and increased signal intensity. In contrast, only a minority of patients (3–5%) has atypical variants either confined to the CA1 field or CA4 field (= end folium sclerosis). These atypical variants do not show significant atrophy and may be only detected due to a loss of the internal hippocampal structure (Fig. 1). However, if a hippocampus is normal on MRI an unrevealing histology is more likely.

6 Imaging

MRI correlate of hippocampal slerosis are atrophy and increased signal intensity, which are best visualized on coronal FLAIR and T2-weighted fast spin echo images angulated perpendicularly to the hippocampal long axis. Increased signal intensity T2-signal abnormalities appears to correlate with gliosis and may not be directly related to the degree of neuronal loss (Briellman et al. 2002). On FLAIR sequences, contrast to noise ratio (C/N) is higher

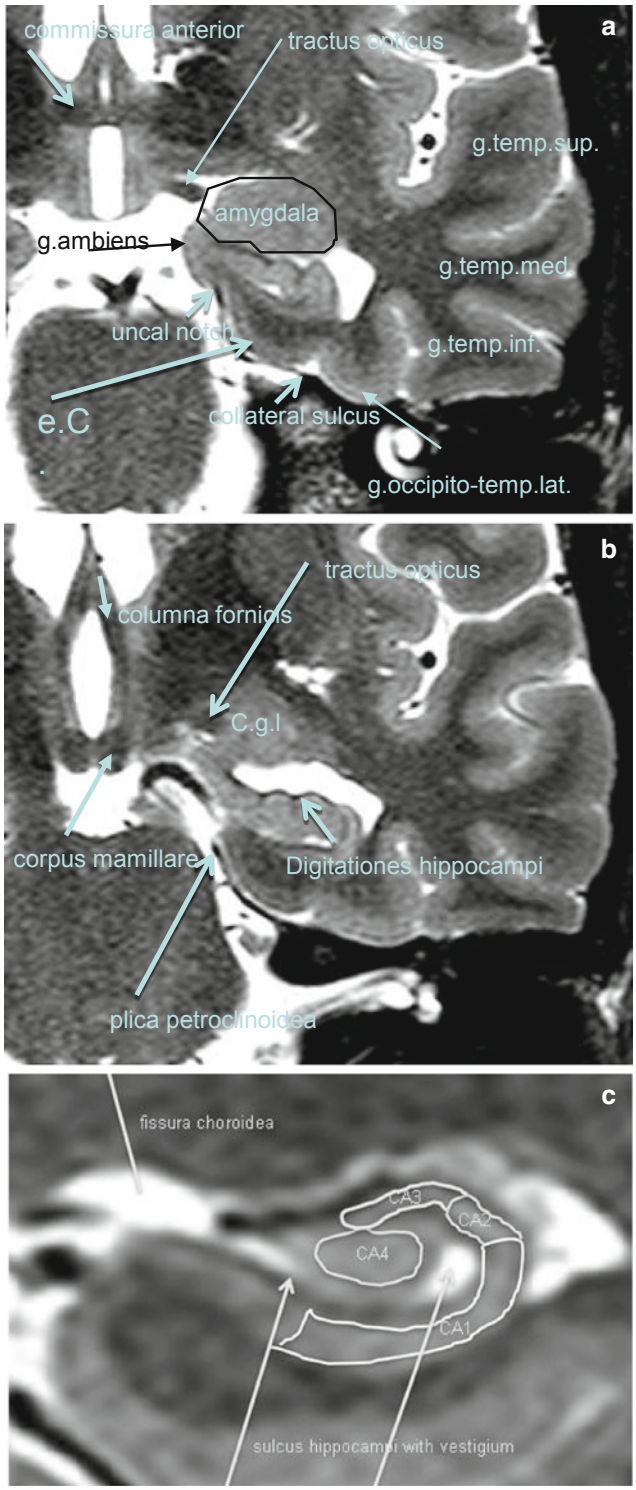

Fig. 1 Temporomesial MR anatomy on coronal 2 mm thick T2-weighted images. **a** shows a slice at the level of the amygdala, **b** at the level of the hippocampal head, and **c** at a level of the hippocampal body. Note that slices are displayed with different magnifications depending on the structures of interest

than on T2-weighted sequences, however, one has to be aware that normal limbic structures already have a higher FLAIR signal than the remaining cortex (Hirai et al. 2000). T2-weighted sequences display the hippocampal substructures in more detail and are complementarily used to diagnose hippocampal sclerosis. In order to assess atrophy and signal intensity, side comparisons are helpful. An accurate angulation avoiding tilting in the coronal plane is fundamental (Fig. 2). However, 10–20% of patients have bilateral hippocampal sclerosis (Margerison et al. 1966, Malter et al. in press), which can be overlooked when side comparison is the only criterion and no "engramm" of a normally sized hippocampus exists. T2 volumetry or T2 relaxometry can be helpful in these cases.

Hippocampal sclerosis is usually diagnosed on coronal slices through the hippocampal head, which displays the highest relative volume of hippocampal tissue on a slice. The neuropathological diagnosis relies on slices through the hippocampal body allowing to assess the single CA subfields (Fig. 3).

More subtle hippocampal sclerosis signs are a loss of the internal structure and loss of hippocampal head digitations (Oppenheim et al. 1998; Howe et al. 2011), which are both best appreciated on high resolution T2-weighted images (Fig. 4). Dilatation of the temporal horn is common, but occurs also in healthy persons as variant and even contralateral to the sclerotic hippocampus as falsely lateralizing finding (Wieser and ILAE Commission on Neurosurgery of Epilepsy 2004).

Hippocampal sclerosis with atrophy but without increased signal intensity has been described in 5% of patients. However, it is likely due to poor image quality not suited to visualize increased signal intensity.

Hippocampal sclerosis as incidental finding is extremly rare. There may be signal increase in healthy patients, however, signal increase and atrophy together almost never occur (Labate et al. 2010; Menzler et al. 2010).

MRI scans of older patients, however, often show some degree of atrophy including loss of digitations of the hippocampal head and increased signal intensity (on FLAIR) images. The histopathological substrate typically remains unclear, it may be related to normal ageing or Alzheimer's disease or so-called pure hippocampal sclerosis which occurs in around 10% of individuals older than 85 years and which is often misdiagnosed as Alzheimer's disease (Dickson et al. 1994; Ala et al. 2000; Nelson et al. 2011).

Secondary findings: Apart from hippocampal sclerosis the following structures of the limbic system can be atrophic: amygdala, entorhinal cortex, ipsilateral mamillary body, ipsilateral fornix, posterior thalamus (with increased signal), cingulate gyrus, contralateral cerebellum (Chan et al. 1997; Urbach et al. 2005) There is more often a temporal lobe or even hemispheric atrophy with atrophy pronounced in the anterior temporal lobe. The anterior temporal lobe shows reduced white matter volume and white matter signal is increased as compared to the opposite side or remaining white matter. Findings may be subtle and obscured or falsely highlighted by B1 field inhomogeneities

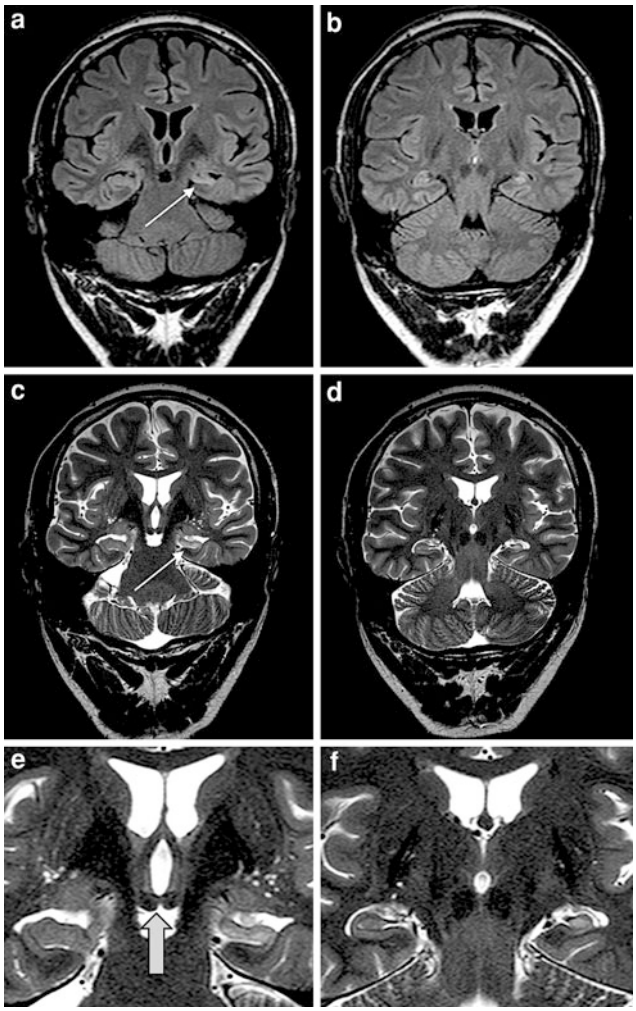

Fig. 2 Left-sided hippocampal sclerosis (**a**, **b**: coronal 3 mm thick FLAIR, **c**–**e**: coronal 2 mm thick T2-weighted fast spin echo images) indicated by increased signal intensity and atrophy of the left hippocampus. These findings are best appreciated on slices through the hippocampal head (**a**, **c**, **e**: *arrow*) since they contain the highest amount of hippocampal tissue per slice. In contrast, neuropathological diagnosis is based on slices through the hippocampal body (**b**, **d**, **f**), which allow a better anatomical orientation with respect to the CA subfiels. In order to allow side comparisons tilting in the coronal plane must be avoided. Exact angulation is proven by displaying small pairy structures (e.g. columnae fornicis (**e**: *hollow arrow*); semicircular canals) on one slice.

and narrow "windowing". There is usually an a.p. gradient with a higher white matter signal in the temporal pole that gradually diminishs and is already absent if slices through the amygdala or hippocampal head are inspected. Since white matter has a higher signal, contrast to gray matter is reduced and the term "gray white matter demarcation loss" has been designated to describe this condition.

The histopathological substrate of "gray white matter demarcation loss" is not clear. Some describe a higher amount of ectopic neurons within the white matter, however, a higher amount of white matter neurons in the anterior temporal lobe is also physiologic. Some consider "gray white matter demarcation loss" as mild maformation of cortical development (Palmini et al. 2004; Blümcke et al. 2011), others as focal cortical dysplasias (FCD) type I (Fauser et Schulze-Bonhage 2006), and others as maturation disorder, in which the process of cerebral myelination is disturbed due to an early precipitating injury (Mitchell et al. 2003; Schijns et al. 2011). Recent work investigating the pathological substrate of gray-white matter demarcation loss with 7 Tesla MRI revealed dishomogeneous myelin staining of the white matter, reduction in the number of axons and presence of axonal degeneration (Garbelli et al. 2012). A hint for a maturation disorder are early precipitating injuries and early seizure onset (often before the age of two) of patients with a "gray white matter demarcation loss" as compared to those who do not have these changes (Mitchell et al. 2003; Schijns et al. 2011). (Figs. 5, 6).

In around 10% of patients hippocampal sclerosis is associated with another extrahippocampal epileptogenic lesion (Fig. 7). This is called *dual pathology* and associated with a poorer prognosis regarding postsurgical seizure outcome. Most common dual lesions are cortical dysplasias and gliotic lesions acquired in early childhood. Note that in the initial description 30% of patients had dual lesions (Levesque 1991). This high number is explained by the fact that 10% of patients in this series had gliomas and temporal lobe seizures. They underwent hippocamopectomy and showed only mild hippocampal cell loss on histopathology. Some authors consider "gray white matter demarcation loss" of the anterior temporal pole as type I dysplasia and thus a dual lesion (Fauser et Schulze-Bonhage 2006). In order to have a strict definition of dual pathology, the ILAE proposed the following definition: *Dual Pathology* refers only to patients with hippocampal sclerosis, who have a second principal lesion affecting the brain (which may be located also outside the ipsilateral temporal lobe), that is, tumor, vascular malformation, glial scar, limbic/Rasmussen encephalitis, or MCD (including FCD Type IIa/IIb). Ipsilateral temporopolar atrophy with increased T2 signal changes on MRI is not included as its histopathologic correlate has yet to be specified. Histopathologically confirmed architectural abnormalities in the temporal lobe associated with hippocampal sclerosis should not be diagnosed as FCD Type I or ''Dual Pathology'' but FCD Type IIIa (Blümcke et al. 2011).

PET: positron emission tomography (PET) has become part of the presurgical evaluation in many epilepsy centers. The central finding is that the temporal lobe is hypometabolic for uptake of glucose on the side of the seizure focus during the interictal period. The region of hypometabolism can be both medial and lateral, and commonly exceeds the size of tissue that needs to be removed for cure of seizures.

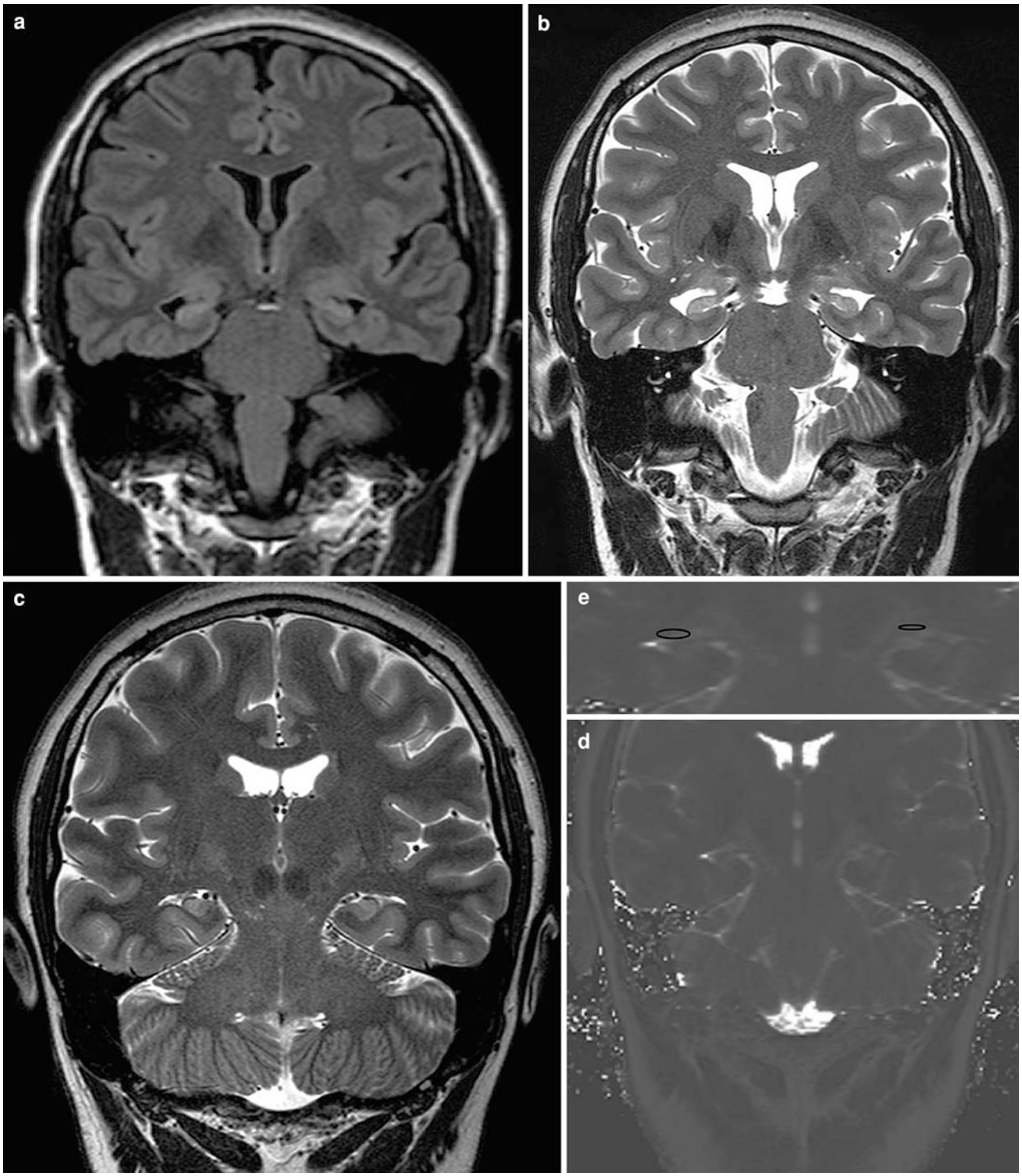

Fig. 3 Bilateral hippocampal sclerosis indicated by bilateral atrophy and increased signal intensity on FLAIR (**a**) and T2-weighted (**b**, **c**) fast spin echo images through the hippocampal heads (**a**, **b**) and bodies (**c**). If one has no engramm of a normal hipppocampus, T2 relaxometry (**d**) is helpful which revealed T2 relaxation times (**e**: ROI placements) with a mean of 132 ms in both hippocampi

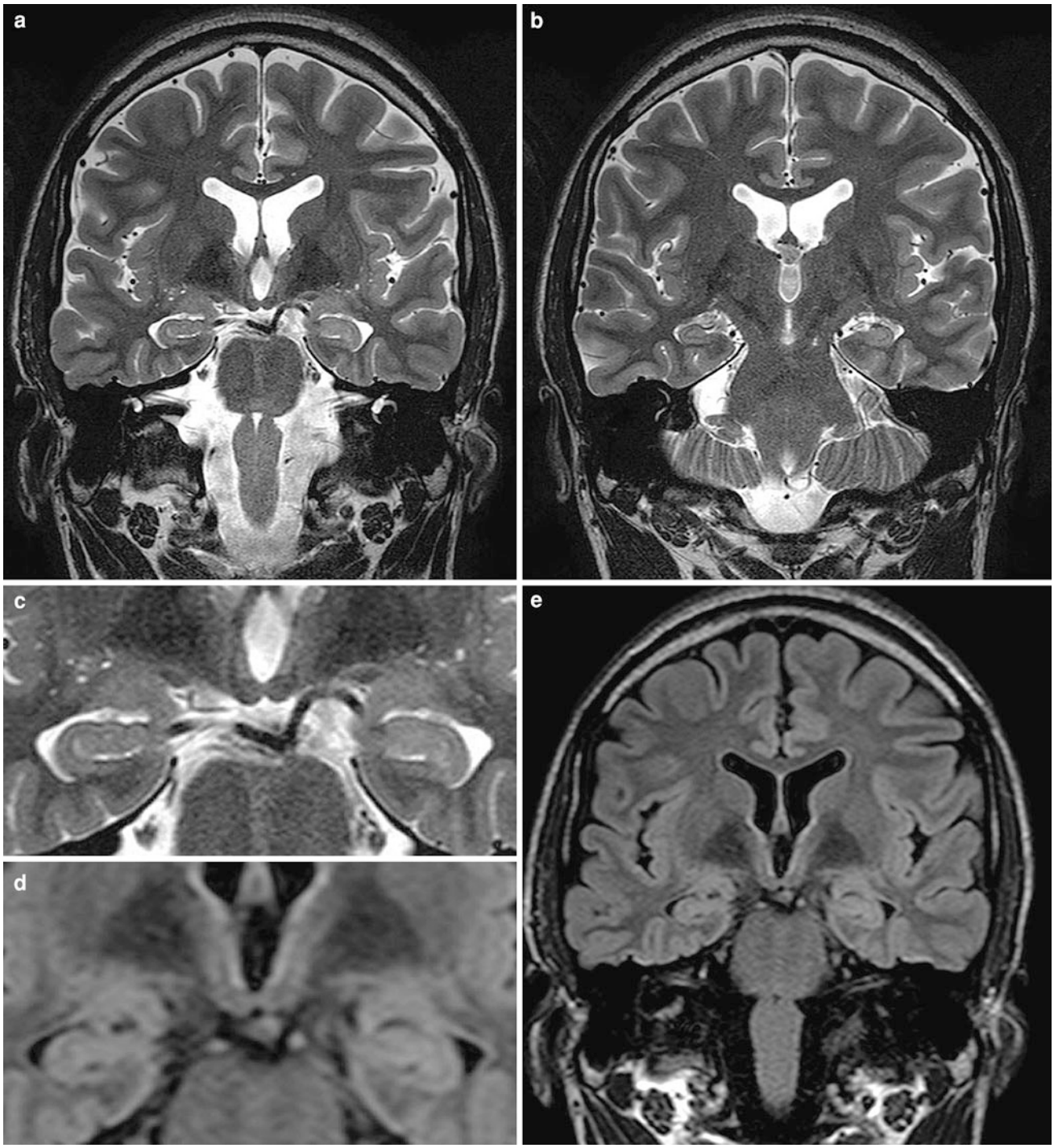

Fig. 4 A 21 year old man with complex partial seizures since the age of 18 underwent left-side selective amgydalohippocampectomy. On MRI, the left hippocampus is of normal size (**a**–**c**: 2 mm thick T2-weighted fast spin echo images, **d**, **e**: 3 mm thick FLAIR fast spin echo images). If there is an abnormality at all, hippocampal head substructures (digitationes hippocampi, CA fields) are better to delineate on the *right* (**c**) than on the *left* side

7 Treatment

Selective amygdalohippocampectomy (removal of amygdala, hippocampus and part of the parahippocampal gyrus) and anterior temporal lobectomy (additional removal of the anterior 4.5 cm on the left and 5.5 cm on the right side) are the most appropriate treatments and lead to seizure freeness (Engel-class I) in 75% of patients. Another 12% benefit with a distinct reduction of seizure frequency (Engel class II). With antiepileptic drugs only 8% of patients get seizure free (Engel et al. 1993; Wiebe et al. 2001). Note that

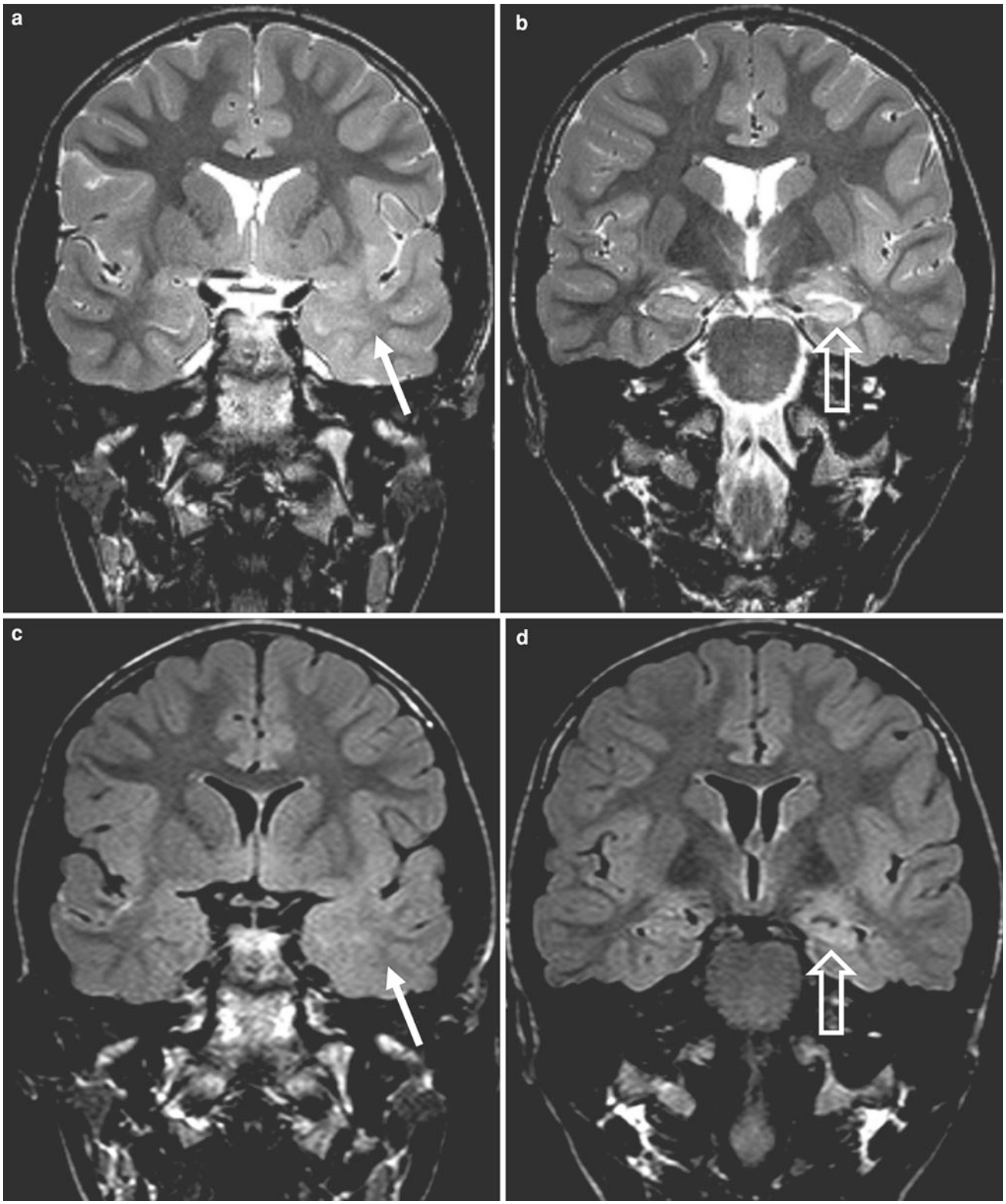

Fig. 5 Left-sided hippocampal sclerosis (**b**, **d**: *hollow arrow*) and "gray white matter demarcation loss" of the anterior temporal lobe (**a**, **c**: *arrow*) in a 32 year old man with varicella zoster virus infection as infant and complex partial seizures since this time

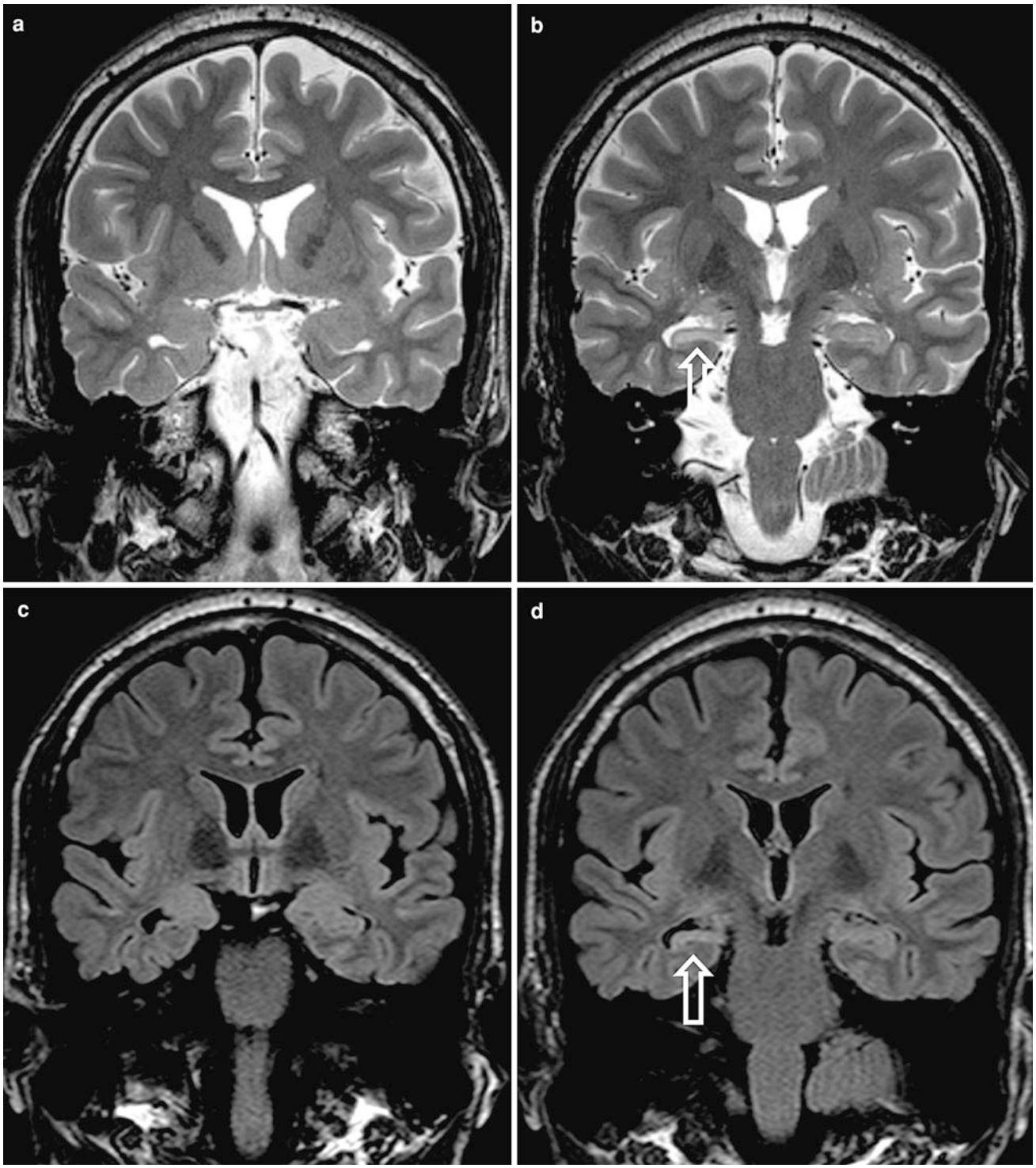

Fig. 6 Right-sided hippocampal sclerosis (**b**, **d**: *hollow arrow*) with slight atrophy of the anterior tempopral lobe but without "gray white matter demarcation loss"(**a**, **c**) in a 30 year old man without precipitating injury and complex partial seizures since the age of 5

seizure freeness is even reached, if only the anterior parts of the hippocampus and adjacent structures are removed.

Bilateral hippocampal sclerosis (20% of patients) was for a long time considered a knock-out-criterion for epilepsy surgery, since memory capacity of the non-resected hippocampus and chance for seizure freedom were considered low. However, individual patients can be operated successfully: If intrahippocampal depth electrodes show seizure origin in one hippocampus and event-related potentials sufficient memory capacity of the contralateral

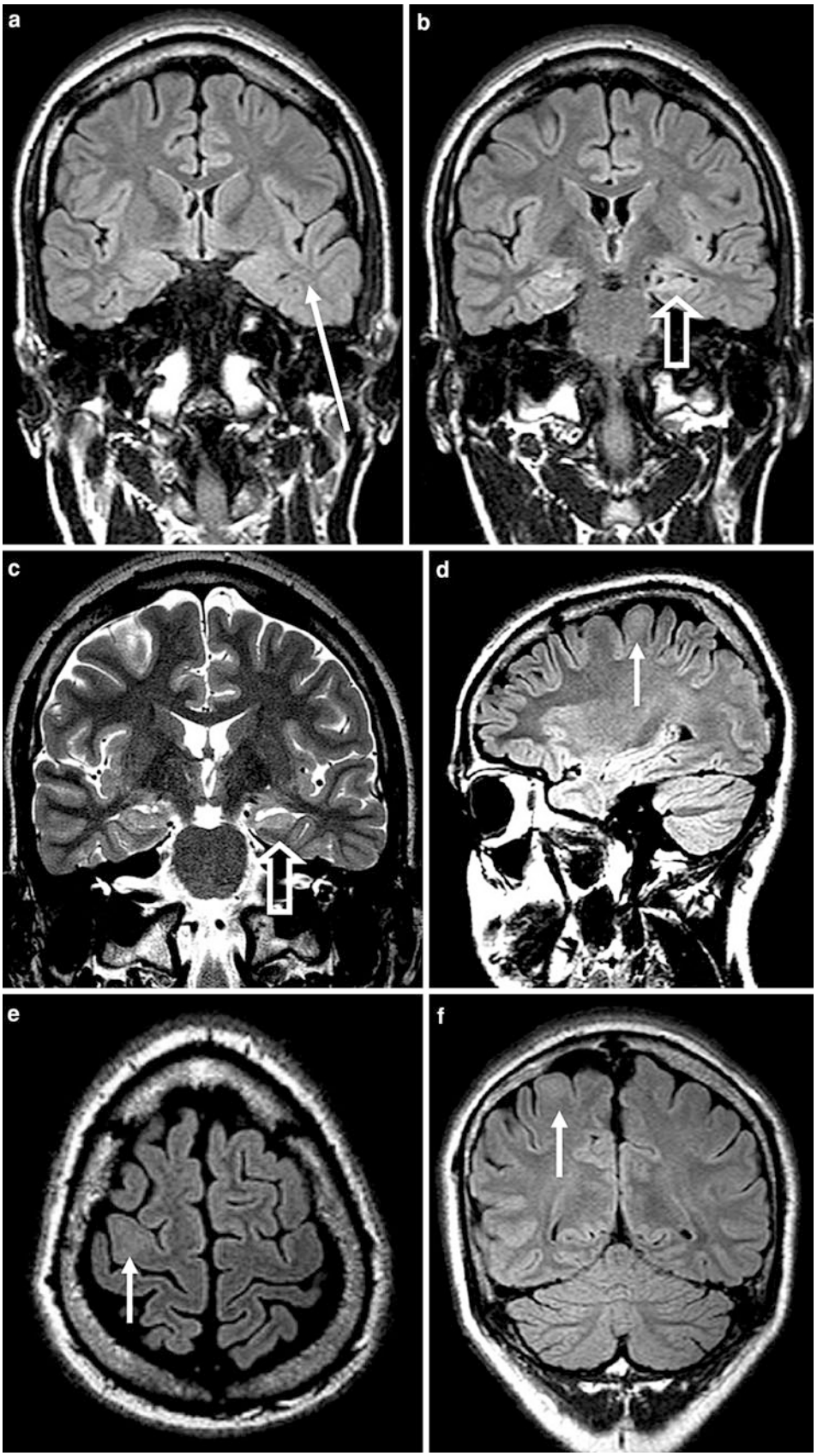

Fig. 7 16 year old male with complex focal seizures and left sided hippocampal sclerosis (**b**, **c**: *hollow arrow*l) and "gray white matter demarcation loss" of the anterior temporal lobe (**a**: *arrow*) as well as a dysplasia in the right precentral gyrus (**d–f**: *arrow*). The "gray white matter demarcation loss" is rather a maturation disorder of the anterior temporal lobe which myelinates latest. It is often seen in patients who have a precipitating injury and start to have temporal lobe seizures within the first two years of life. The dysplasia in the right precentral gyrus is a "dual pathology" strictu sensu

hippocampus, selective amygdalohippocampetcomy leads to seizure freedom without significant memory impairment in the more than 70% of patients.

References

Ala TA, Beh GO, Frey WH 2nd (2000) Pure hippocampal sclerosis: a rare cause of dementia mimicking Alzheimer's disease. Neurology 54:843–848

Briellman RS, Kalnins RM, Berkovic SF, Jackson GD (2002) Hippocampal pathology in refractory temporal lobe epilepsy: T2-weighted signal change reflect dentate gliosis. Neurology 58: 265–271

Blümcke I, Thom M, Wiestler OD (2002) Ammon's horn sclerosis: a maldevelopmental disorder associated with temporal lobe epilepsy. Brain Pathol 12:199–211

Blümcke I, Pauli E, Clusmann H, Schramm J, Becker A, Elger C, Merschhemke M, Meencke HJ, Lehmann T, von Deimling A, Scheiwe C, Zentner J, Volk B, Romstöck J, Stefan H, Hildebrandt M (2007) A new clinico-pathological classification system for mesial temporal sclerosis. Acta Neuropathol 113(3): 235–244

Blümcke I, Thom M, Aronica E, Armstrong DD, Vinters HV, Palmini A, Jacques TS, Avanzini G, Barkovich AJ, Battaglia G, Becker A, Cepeda C, Cendes F, Colombo N, Crino P, Cross JH, Delalande O, Dubeau F, Duncan J, Guerrini R, Kahane P, Mathern G, Najm I, Ozkara C, Raybaud C, Represa A, Roper SN, Salamon N, Schulze-Bonhage A, Tassi L, Vezzani A, Spreafico R (2011) The clinicopathologic spectrum of focal cortical dysplasias: a consensus classification proposed by an ad hoc Task Force of the ILAE Diagnostic Methods Commission. Epilepsia 52:158–174

Chan S, Erickson J, Yoon S (1997) Limbic system abnormalities associated with mesial temporal sclerosis: a model of chronic cerebral changes due to seizures. RadioGraphics 17:1095–1110

Dickson DW, Davies P, Bevona C, et al (1994) Hippocampal sclerosis: a common pathological feature of dementia in very old (> or = 80 years of age) humans. Acta Neuropathol (Berl) 88:212–221

Engel J Jr, Van Ness PC, Rasmussen TB, Ojemann LM (1993) Outcome with respect to epileptic seizures. In: Engel J Jr (ed) Surgical treatment of the epilepsies. Raven Press, New York, pp 609–621

Fauser S, Huppertz HJ, Bast T, Strobl K, Pantazis G, Altenmueller DM, Feil B, Rona S, Kurth C, Rating D, Korinthenberg R, Steinhoff BJ, Volk B, Schulze-Bonhage A (2006) Clinical characteristics in focal cortical dysplasia: a retrospective evaluation in a series of 120 patients. Brain 129:1907–1916

Garbelli R, Milesi G, Medici V, Villani F, Didato G, Deleo F, D'Incerti L, Morbin M, Mazzoleni G, Giovagnoli AR, Parente A, Zucca I, Mastropietro A, Spreafico R (2012) Blurring in patients with temporal lobe epilepsy: clinical, high-field imaging and ultra structural study. Brain 135(Pt 8):2337–2349

Hirai T, Korogi Y, Yoshizumi Y, Shigematsu Y, Sugahara T, Takahashi M (2000) Limbic lobe of the human brain: evaluation with turbo fluid-attenuated inversion-recovery MR imaging. Radiology 215:470–475

Howe KL, Dimitri D, Heyn C, Kiehl TR, Mikulis D, Valiante T. Histologically confirmed hippocampal structural features revealed by 3T MR imaging: potential to increase diagnostic specificity of mesial temporal sclerosis. AJNR Am J Neuroradiol 2010 Jun 10

Kobayashi E, Li LM, Lopes-Cendes I, Cendes F (2002) Magnetic resonance imaging evidence of hippocampal sclerosis in asymptomatic, first-degree relatives of patients with familial mesial temporal lobe epilepsy. Arch Neurol 59(12):1891–1894

Labate A, Gambardella A, Aguglia U, Condino F, Ventura P, Lanza P, Quattrone A (2010) Temporal lobe abnormalities on brain MRI in healthy volunteers a prospective case-control study. Neurology 74:1

Levesque MF, Naksato N, Vinters HV et al (1991) Surgical treatment of limbic encephalitis associated with extrahippocampal lesions: the problem of dual pathology. J Neurosurg 75:364–370

Malter MP, Tschampa HJ, Helmstaedter C, Urbach H, von Lehe M, Becker A, Clusmann H, Elger CE, Bien CG (2011) Seizure and memory outcome after epilepsy surgery in patients with bilateral ammon's horn sclerosis. Ann Neurol (in press)

Margerison JH, Corsellis JAN (1966) Epilepsy and the temporal lobes: a clinical, electroencephalographic and neuropathological study of the brain in epilepsy, with particular reference to the temporal lobes. Brain 89:499–530

Menzler K, Iwinska-Zelder J, Shiratori K, Jaeger RK, Oertel WH, Hamer HM, Rosenow F, Knake S (2010) Evaluation of MRI criteria (1.5 T) for the diagnosis of hippocampal sclerosis in healthy subjects. Epilepsy Res 89:349–354

Mitchell LA, Harvey AS, Coleman LT, Mandelstam SA, Jackson GD (2003) Anterior temporal changes on MR images of children with hippocampal sclerosis: an effect of seizures on the immature brain? Am J Neuroradiol 24:1670–1677

Nelson PT, Schmitt FA, Lin Y, Abner EL, Jicha GA, Patel E, Thomason PC, Neltner JH, Smith CD, Santacruz KS, Sonnen JA, Poon LW, Gearing M, Green RC, Woodard JL, Van Eldik LJ, Kryscio RJ (2011) Hippocampal sclerosis in advanced age: clinical and pathological features. Brain 134(Pt 5):1506–1518

Oppenheim C, Dormont D, Biondi A et al (1998) Loss of digitations of the hippocampal head on high-resolution fast spin-echo MR: a sign of mesial temporal sclerosis. AJNR Am J Neuroradiol 19:457–463

Palmini A, Najm I, Avanzini G, Babb T, Guerrini R, Foldvary-Schaefer N, Jackson G, Lüders HO, Prayson R, Spreafico R, Vinters HV (2004) Terminology and classification of the cortical dysplasias. Neurology 62(6 Suppl 3):S2-8. Review

Schijns OE, Bien CG, Majores M, von Lehe M, Urbach H, Becker AJ, Schramm J, Elger CE, Clusmann H (2011) Temporal gray-white-matter abnormalities are not part of the epileptogenic zone in temporal lobe epilepsy with hippocampal sclerosis. Neurosurgery 68:98–106

Soeder BM, Gleissner U, Urbach H, Clusmann H, Vincent A, Bien CG (2009) Causes, presentation and outcome of lesional adult-onset mediotemporal lobe epilepsy. J Neurol Neurosurg Psychiatry 80: 894–899

Urbach H, Siebenhaar G, Koenig R, von Oertzen J, Scorzin J, Kurthen M, Schild HH (2005) Limbic system abnormalities associated with Ammon's horn sclerosis do not alter seizure outcome after amygdalohippocampectomy. Epilepsia 46(4):549–555

Wiebe S, Blume WT, Girvin JP, Eliasziw M (2001) A randomized, controlled trial of surgery for temporal lobe epilepsy. New Engl J Med 38:154–163

Wieser HG, ILAE Commission on Neurosurgery of Epilepsy (2004) ILAE commission report: mesial temporal lobe epilepsy with hippocampal sclerosis. Epilepsia 45:695–714

Wyler AR, Dohan FC, Schweitzer JB, Berry AD (1992) A grading system for mesial temporal pathology (hippocampal sclerosis) from anterior temporal lobectomy. J Epilepsy 5:220–225

Limbic Encephalitis

Horst Urbach and Christian G. Bien

Contents

Abstract

Limbic encephalitis refers to an autoimmune-mediated encephalitis with preferential involvement of temporomesial structures. Amygdala and hippocampus may be initially asymmetrically swollen and bilateral hippocampal sclerosis occurs in its further course. At least one third of patients > 20 years of age with the typical clinical syndrome and temporomesial MRI changes suffer from limbic encephalitis.

1 Definition

Limbic encephalitis is a cliniconeuropathological/radiological syndrome, initially described by Brierley et al. (1960) and Corsellis et al. (1968), respectively. The clinical characteristics are subacutely (over days to 12 weeks) evolving memory deficits, temporal lobe seizures, confusion, and other psychiatric symptoms. Neuropathological characteristics are infiltrates consisting of T lymphocytes and microglia activation.

2 Pathogenesis and Classification

The clinicopathological/radiological diagnosis of limbic encephalitis needs refining because it is not a uniform entity. The key to a refined categorization of limbic encephalitis cases is antineuronal antibodies found in serum and CSF of affected patients. So, the usual diagnostic workflow is as follows. The identification of typical clinical symptoms and the MRI features of mediotemporal encephalitis antibody triggers antibody diagnostics (plus a tumor search). The results of these additional diagnostic efforts finally enable a working diagnosis to be made and a prognosis to be given as described in the following.

H. Urbach (✉)
Department of Neuroradiology,
University Hospital Freiburg, Germany
e-mail: horst.urbach@uniklinik-freiburg.de

C. G. Bien
Epilepsy Centre Bethel, Bielefeld, Germany

H. Urbach (ed.), *MRI in Epilepsy*, Medical Radiology. Diagnostic Imaging,
DOI: 10.1007/174_2012_572, © Springer-Verlag Berlin Heidelberg 2013

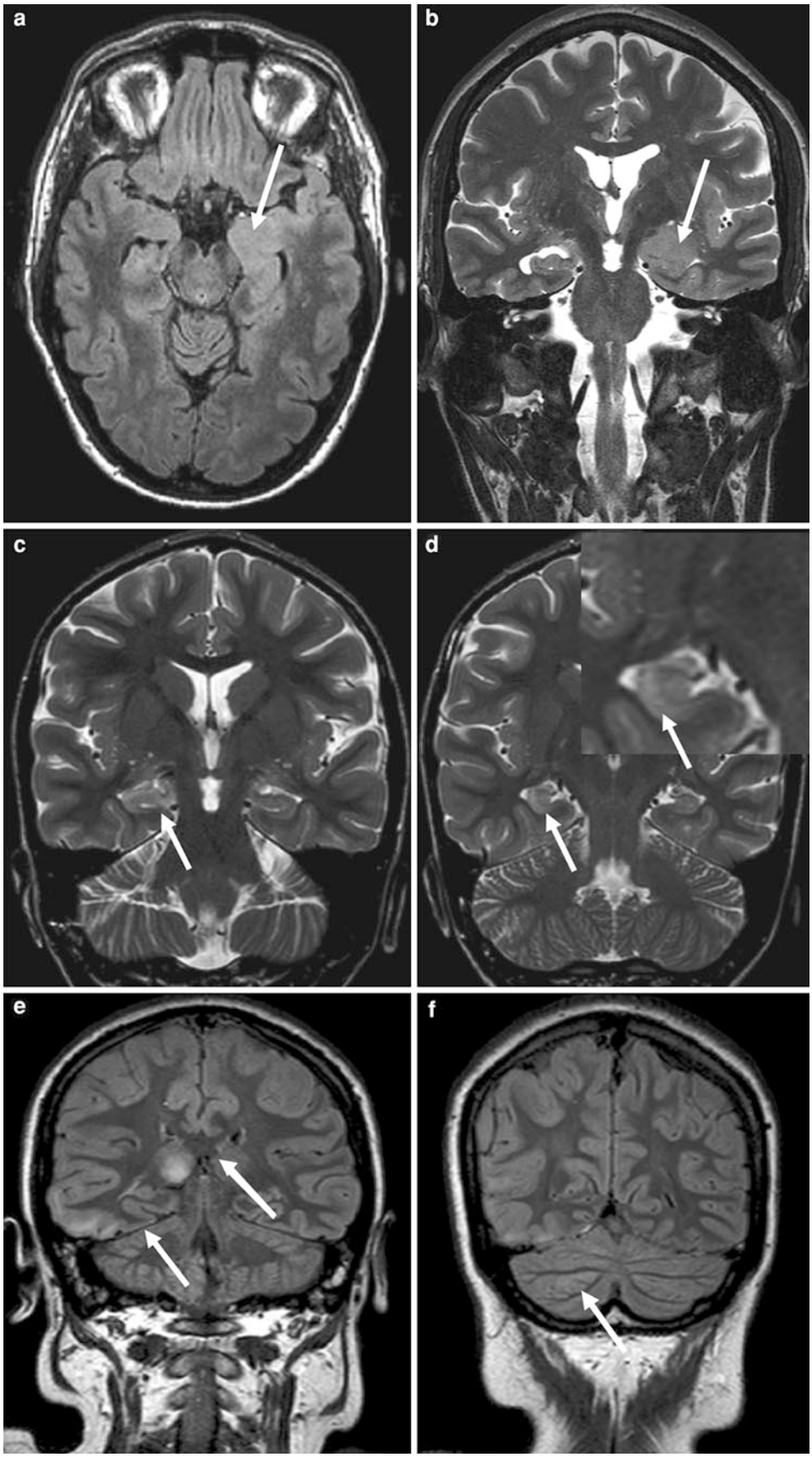

Fig. 1 Three female patients with *N*-methyl-D-asparate receptor antibody associated limbic encephalitis and different MRI findings. **a**, **b** A 7-year-old girl with volume increase of uncus and amygdala on the left (*arrow*). **c**, **d** A 43-year-old woman with signal increase of the CA1 segment of the right hippocampus (*arrow*). **e**, **f** A 25-year-old woman with signal increase of the right pulvinar thalami, the right temporobasal cortex, and the right cerebellar folia (*arrows*). Signal increase of the pulvinar thalami is likely due to frequent seizures

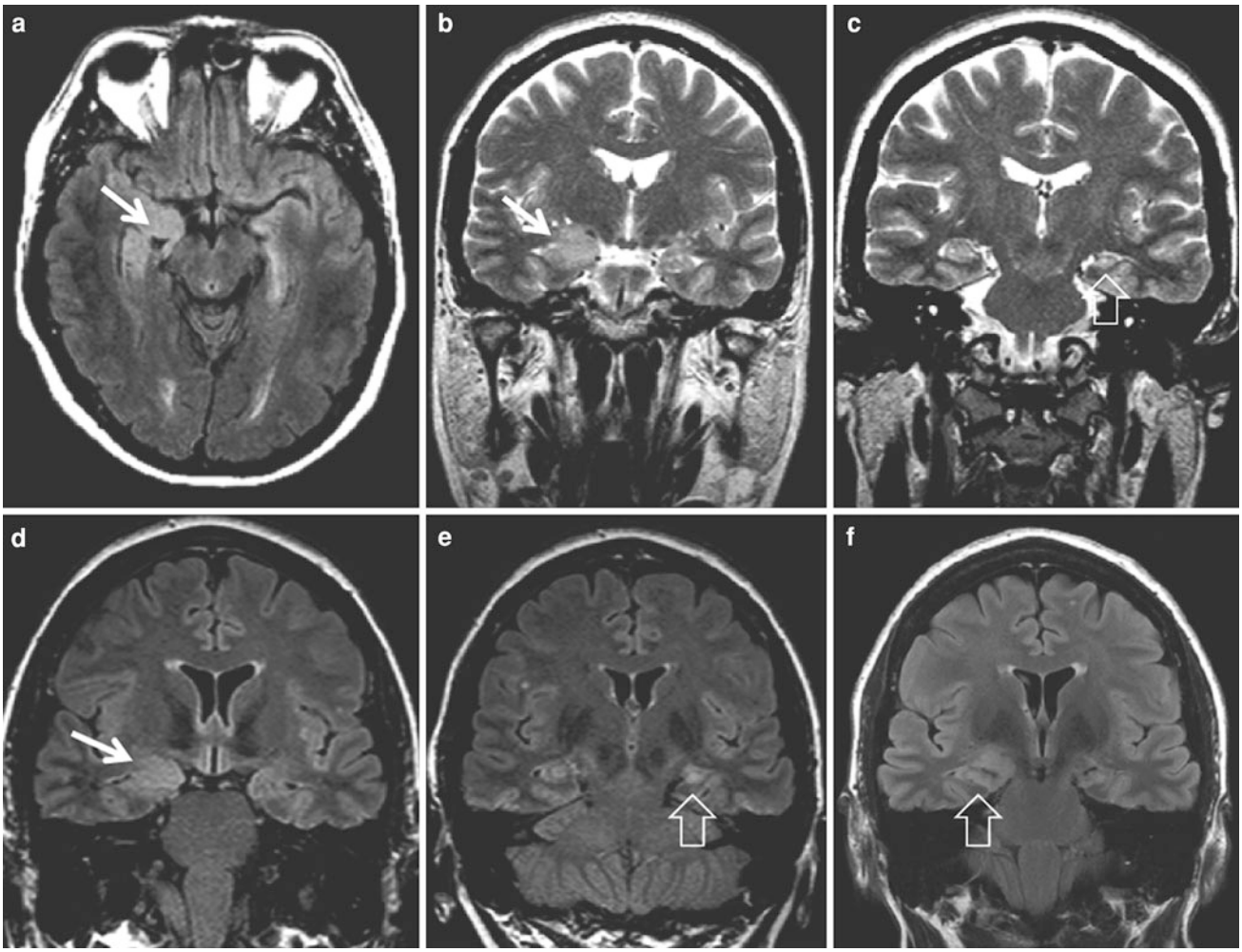

Fig. 2 Limbic encephalitis associated with voltage-gated potassium channel (VKKC) antibodies in a 53-year-old woman. Whereas the right hippocampal head and amygdala are hyperintense and swollen (**a**, **b**, **d**, *arrow*), the left side of the hippocampus is already sclerotic (**c**, **e**, *hollow arrow*). Follow-up MRI after 1 year shows the beginning atrophy also on the right side (f)

2.1 Antibodies

1. Antibodies against intracellular antigens:
   - Onconeural antibodies (Hu, CV2, Ma2, amphiphysin) (Gultekin et al. 2000; Graus et al. 2004)
   - Antibodies against the enzyme glutamic acid decarboxylase (GAD) (Malter et al. 2010).
2. Antibodies against antigens on the surface of neurons:
   - Proteins associated with voltage-gated potassium channels [VGKC; the VGKC complex comprising the antigenic targets leucine-rich glioma inactivated protein 1, contactin-2 associated protein (CASPR2) and other, still undefined targets) (Vincent et al. 2004; Irani et al. 2010; Lai et al. 2010; Lancaster et al. 2011)
   - *N*-Methyl-D-asparate receptor (NMDAR). Most patients with NMDAR antibodies have a severe diffuse encephalopathy termed anti-NMDAR encephalitis, not a limbic syndrome, which has been described in one case (Dalmau et al. 2007, 2008; Novillo-López et al. 2008)
   - γ-Aminobutyic acid receptor type B ($GABA_BR$) (Lancaster et al. 2010)
   - α-Amino-3-hydroxy-5-methyl-4-isoxazolpropionic acid receptor (AMPAR) (Lai et al. 2009).

The antibody specificity predicts the likelihood of having a neoplasm as the origin of the neurological disease, i.e., a paraneoplastic syndrome. It is more than 90% in the case of onconeural antibodies, and 50% or greater in patients with antibodies against NMDAR (usually ovarian teratomas in young females), against the $GABA_BR$, or against AMPAR (in the latter two, small-cell lung cancer is frequent). Patients with VGKC-complex antibodies seem to have tumors almost exclusively if the antibodies react with CASPR2; thymomas are neoplasms found most often (Vincent and Irani 2010).

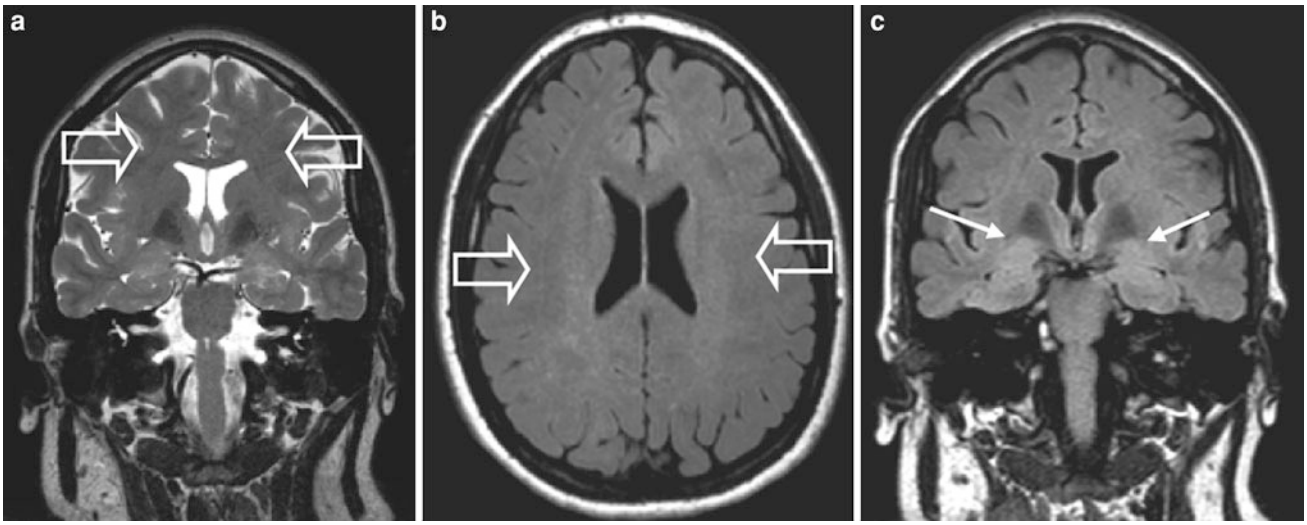

Fig. 3 Limbic encephalitis associated with VGKC antibodies in a 69-year-old man. Both amygdalae and hippocampal heads are somewhat prominent and hyperintense (**c**, *arrow*). In addition, reduced gray white matter contrast due to an increased signal of the supratentorial white matter (**a**, **b**, *hollow arrows*) is obvious. This MRI pattern is found in around 15% of patients with limbic encephalitis associated with VGKC antibodies

Forty percent of patients with limbic encephalitis and a related tumor may be antibody-negative, so antibody negativity excludes neither a tumor nor the possibility of a limbic encephalitis. Antibody-negative patients without tumors therefore are a special challenge because diagnostic and therapeutic decisions need to be made without the chance to refer to published experience (relevant limbic encephalitis series have—understandably—only been published in cohorts with definite antibody reactivities).

Apart from their tumor-predictive value, antibodies predict the treatment response to immunotherapies in non-paraneoplastic patients (who account for most of all limbic encephalitis cases). In general, the outcome of patients with antibodies against surface antigens is more favorable than that of patients with antibodies against intracellular antigens.

With increasing data on the presentation and the course of antibody-defined patients with limbic encephalitis, subtle peculiarities even regarding the MRI appearance of the mediotemporal changes may emerge. However, at this point, every patient with the clinicoradiological features of limbic encephalitis should undergo complete antibody testing for the reactivities listed above.

3 Clinical Presentation

The neurological syndrome as described above is the key element of the syndrome limbic encephalitis; however, the limbic encephalitis subtypes may show some clinical pecuilarities.

Patients with limbic encephalitis associated with VGKC antibodies typically improve with cortisone therapy (Soeder et al. 2005).

Patients with limbic encephalitis associated with antibodies against GAD are mostly woman with temporal lobe seizures and psychiatric abnormalities (Malter et al. 2010). Patients may show oligoclonal bands in CSF and do not respond well to cortisone therapy. Patients with GAD65 antibodies may suffer from type 1 diabetes mellitus, epilepsy with grand mal seizures, stiff person syndrome, and/or ataxia.

Patients with NMDAR antibodies (Fig. 1) have a severe diffuse encephalopathy termed anti-NMDAR encephalitis rather than a limbic syndrome. It typically occurs in young women (male-to-female ratio 1:9) who show dyskinesias, reduced consciousness, hypoventilation, cardiac conduction abnormalities, psychiatric abnormalities (agitation, confusion, depression, hallucinations, pathologic laughing), and neurologic deficits (aphasia, visual disturbances, hemiparesis and others). Around half of the patients have tumors, typically ovarian teratomas. Three of four patients improve under therapy, and one of four patients survives with severe deficits or dies.

4 Imaging

Limbic encephalitis typically starts as an acute disease with unilateral or bilateral swollen temporomesial structures that are hyperintense on fluid-attenuated inversion recovery (FLAIR) and T2-weighted sequences (Urbach

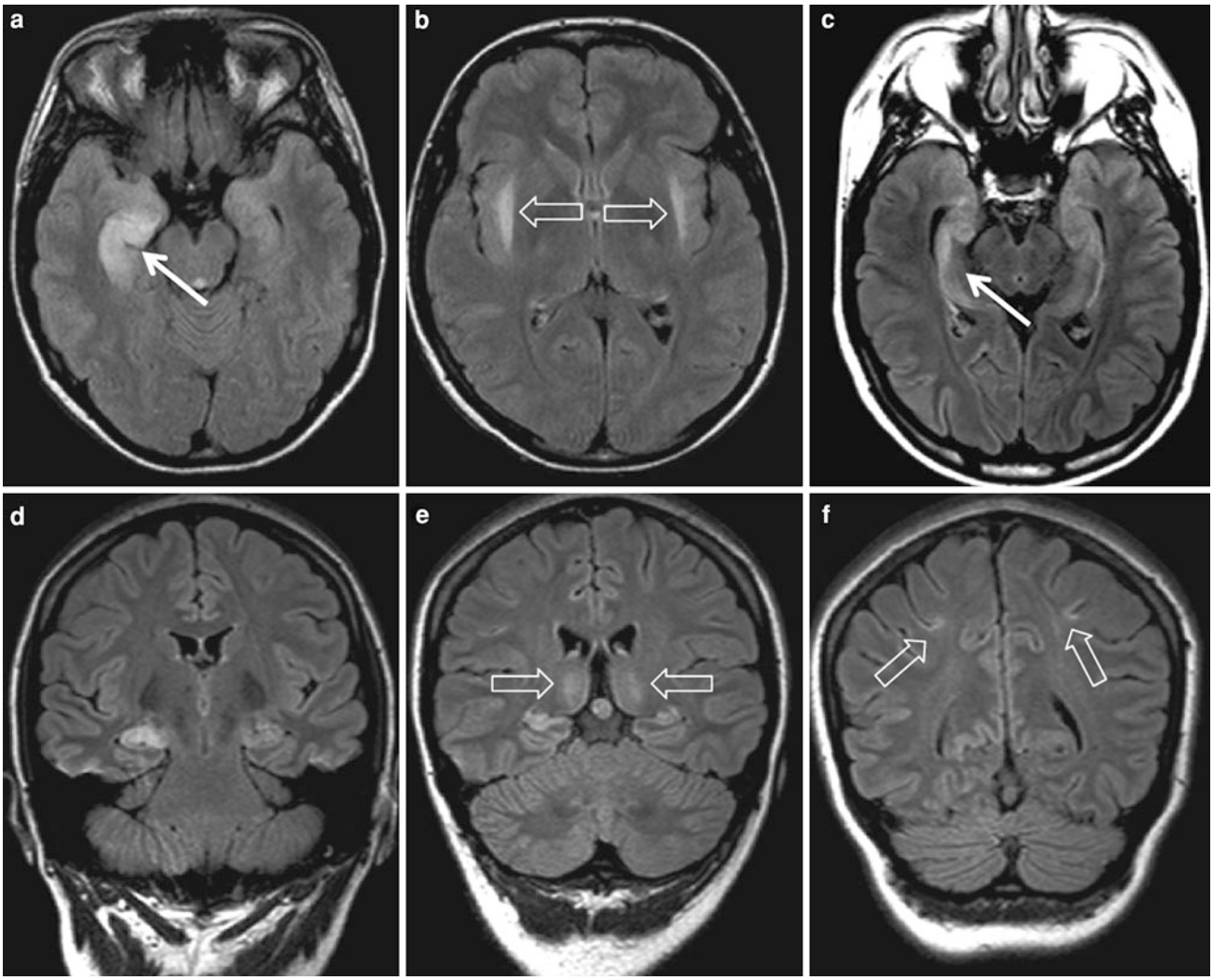

Fig. 4 Two female patients with limbic encephalitis associated with GAD antibodies. Notice the typical course with initial hippocampal swelling (**a**, *arrow*) evolving into hippocampal sclerosis (**c**, *arrow*). Extratemporal, often symmetric signal abnormalities like in these examples in the external capsule (**b**, *hollow arrows*), the thalami (**e**, *hollow arrows*), or the depth of the parietal sulci (**f**, *hollow arrows*) are common in this limbic encephalitis subtype

et al. 2006b). In many patients, the amygdalae are particularly swollen and hyperintense. When only one side is swollen, the contralateral amygdala and hippocampus may be normal or even atrophic (Fig. 2). Swelling and hyperintensity may persist over months to years, but in most cases hyperintensity persists and progressive temporomesial atrophy develops. Although inconstant, significant atrophy is visible approximately 1 year after onset of disease. It is unclear whether swelling and hyperintensity are related to the disease itself or are simply the result of frequent (subclinical) temporal lobe seizures (Urbach et al. 2006a).

Around one third of patients with clinical features of limbic encephalitis and specific antibodies has normal findings on MRI scans (Gultekin et al. 2000; Irani et al. 2010; Lancaster et al. 2010). Thus, temporomesial signal abnormalities and volume changes are not a necessary condition for the diagnosis of limbic encephalitis.

With respect to the limbic encephalitis subtypes, around 15% of patients with VGKC antibodies show increased signal intensity of the supratentorial white matter (Fig. 3). In paraneoplastic limbic encephalitis and in limbic encephalitis associated with GAD antibodies, extratemporal abnormalities are frequent often than in other subtypes (Fig. 4).

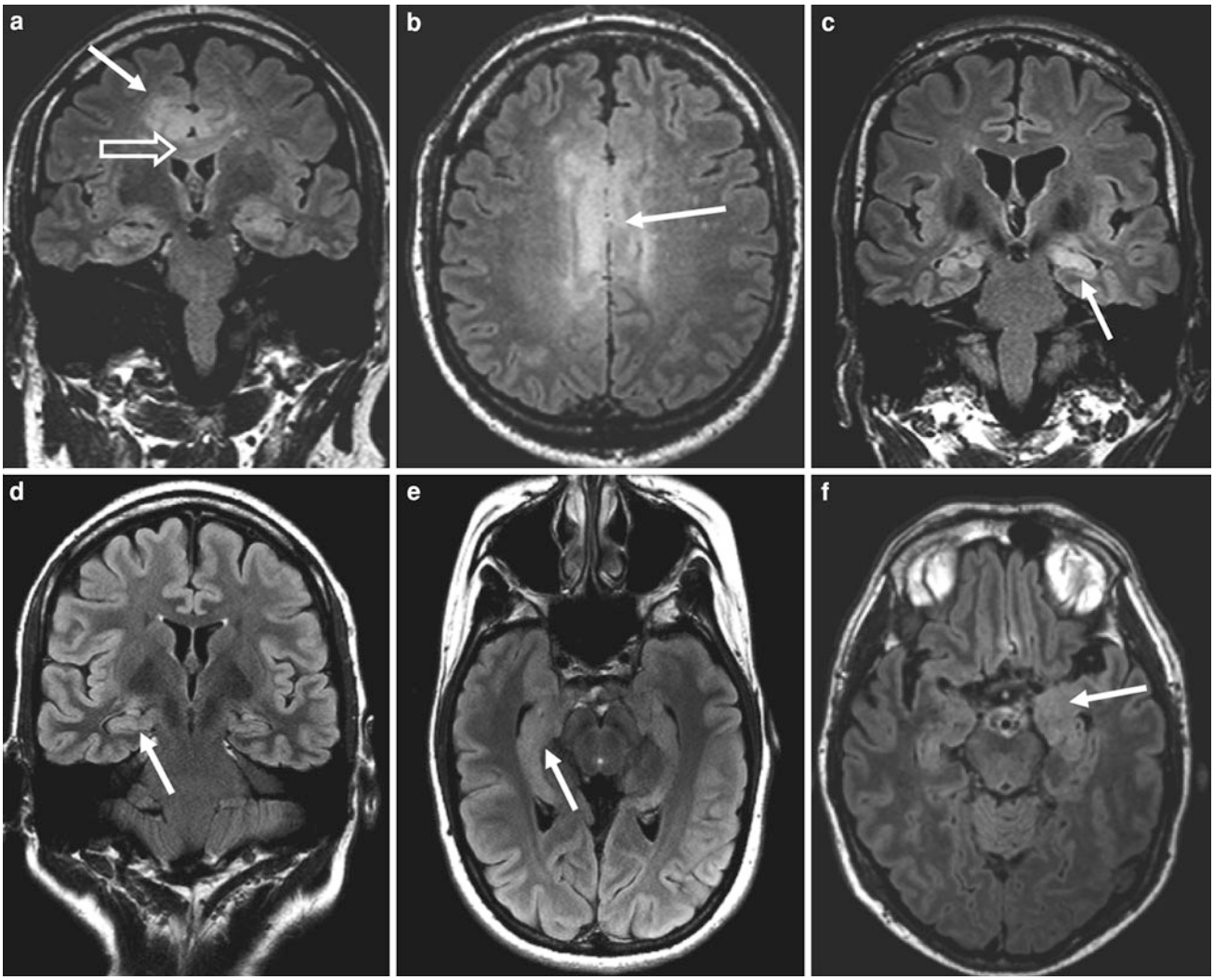

Fig. 5 Imaging differential diagnoses of limbic encephalitis: some astrocytomas tend to infiltrate within the limbic system. Cingulate gyrus (**a**, **b**, *arrow*) and corpus callosum (**a**, *hollow arrow*) infiltration favor a glioma. Bilateral, somewhat asymmetric amygdala lesions can be associated with neurofibromatosis type 1 (**c**, *arrow*). Systemic lupus erythematosus may mimic limbic encephalitis not only clinically. MRI may show subtle volume and signal changes that are often detectable only by side comparisons (**d**, **e**, *arrow*). If the amygdala and hippocampus are enlarged in older patients presenting with temporal lobe seizures, memory deficits, and/ or depression, limbic encephalitis can often not be proven, and histology is unrevealing. These lesions (**f**, *arrow*) are considered unclear

Differential diagnoses include diffusely infiltrating astrocytoma, "unclear" amygdala lesions, status epilepticus, infectious encephalitis including herpes simplex encephalitis type 1, and—in immunocompromised patients—human herpes virus 6 encephalitis (Bower et al. 2003; Baskin and Hedlund 2007; Soeder et al. 2009), lymphomatous infiltration, steroid-responsive encephalopathy associated with autoimmune thyroiditis, amygdala lesions associated with neurofibromatosis type 1 (Gill et al. 2006), limbic encephalitis associated with systemic lupus erythematosus (Stübgen 1998; Kano et al. 2009), Rasmussen encephalitis, and other diagnoses.

Diffusely infiltrating astrocytomas usually involve the limbic system in a more widespread, often multifocal fashion (Fig. 5).

"Unclear" amygdala lesions refer to a unilaterally enlarged amygdala with homogenously increased signal on FLAIR and T2 MRI sequences. Compared with limbic encephalitis patients, the patients are older at epilepsy onset (mean age more than 50 years), and histopathology is typically unrevealing (Fig. 5) (Bower et al. 2003; Soeder et al. 2009). Steroid-responsive encephalopathy associated with autoimmune thyroiditis (SREAT) is a neurologic complication of autoimmune thyroiditis which is, however,

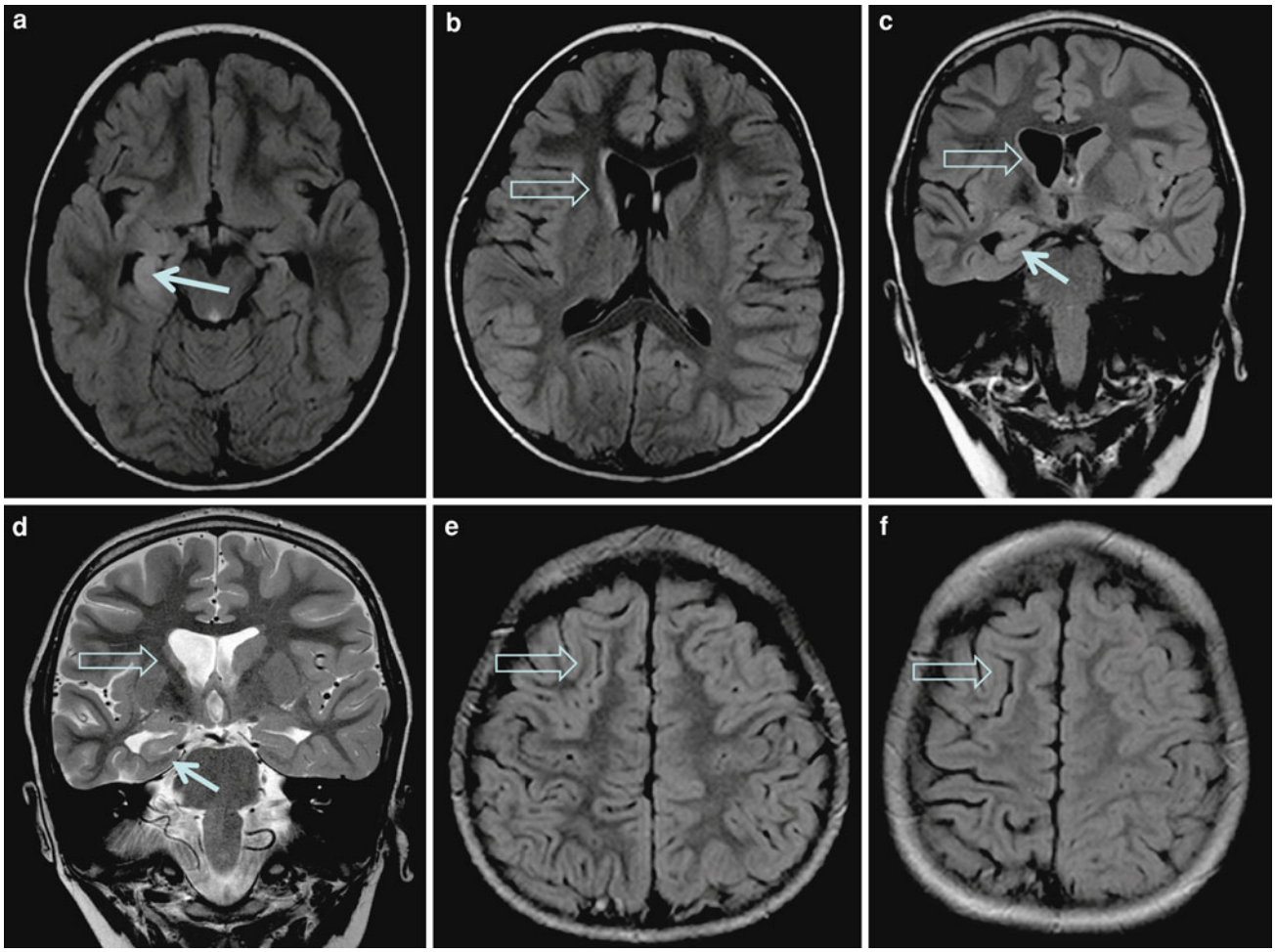

Fig. 6 Rasmussen encephalitis mimicking limbic encephalitis. A 6-year-old boy presented with frequent simple partial seizures with oroalimentary automatisms pinpointing the mesial temporal lobe. MRI showed right-sided hippocampal swelling and T2/ fluid-attenuated inversion recovery hyperintensity (**a**, **c**, **d**, *arrow*). At this time, the right caudate head is already atrophic and discretely hyperintense (**b**–**d**, *hollow arrow*). The patient underwent amygdalohippocampectomy, and histology revealed inflammation with cytotoxic T lymphocytes and glial fibrillary acidic protein (GFAP)-positive astrocytes. Two year later, the patient developed epilepsia partialis continua with continuous jerking of the left arm. Follow-up MRI after 2 years revealed right-sided hemiatrophy (**f**, *hollow arrow*) which was not obvious before (**e**, *hollow arrow*)

independent of the thyroid status. Patients present with encephalopathy, seizures (66%), myoclonus (38%), psychiatric (36%), and stroke-like symptoms (27%) (Chong et al. 2003; Castillo et al. 2006). The key elements are elevated anti-thyroid (microsomal and/or thyroperoxidase) antibodies and a response to corticosteroid therapy (Castillo et al. 2006). Imaging abnormalities have been reported in 25–50% of cases and consisted mostly of focal or diffuse non-enhancing white matter abnormalities, which normalized or regressed on corticosteroid therapy. A patient with dural enhancement has also been reported (Mahad et al. 2005; Castillo et al. 2006). However, there is no characteristic MRI and whether formerly called Hashimoto encephalopathy truly exists is still a matter of debate (Chong et al. 2003).

In 80% of children and an unknown proportion of older patients with neurofibromatosis type 1, coronal FLAIR and T2-weighted fast spin echo images show both hippocampi with higher volume and signal intensity than in healthy controls. There may be some asymmetry and involvement of the amygdala and parahippocampal gyrus as well (Gill et al. 2006).

Systemic lupus erythematosus may mimic limbic encephalitis clinically, and in some cases MRI shows a subtle volume and signal intensity increase of the amygdala and hippocampus, which may only be detectable by side comparisons (Stübgen 1998) (Fig. 5).

Around 50% of Ramussen encephalitis cases have temporomesial signal changes. Ramussen encephalitis is typically a unihemispheric disease clinically characterized by intractable focal seizures, namely, epilepsia partialis continua, and progressive deterioration of functions within the affected hemisphere. If Rasmussen encephalitis rarely starts with temporomesial seizures, caudate head and cerebral atrophy may guide the MRI reader to the correct diagnosis (Fig. 6).

References

Baskin HJ, Hedlund G (2007) Neuroimaging of herpesvirus infections in children. Pediatr Radiol 37:949–963

Bower SP, Vogrin SJ, Morris K et al (2003) Amygdala volumetry in "imaging-negative" temporal lobe epilepsy. J Neurol Neurosurg Psychiatry 74:1245–1249

Brierley JB, Corsellis JA, Hierons R, Nevin S (1960) Subacute encephalitis of later adult life, mainly affecting the limbic areas. Brain 83:357–368

Castillo P, Woodruff B, Caselli R, Vernino S, Lucchinetti C, Swanson J, Noseworthy J, Aksamit A, Carter J, Sirven J, Hunder G, Fatourechi V, Mokri B, Drubach D, Pittock S, Lennon V, Boeve B (2006) Steroid-responsive encephalopathy associated with autoimmune thyroiditis. Arch Neurol 63:197

Chong JY, Rowland LP, Utiger RD (2003) Hashimoto encephalopathy: syndrome or myth? Arch Neurol 60(2):164–171

Corsellis JA, Goldberg GJ, Norton AR (1968) "Limbic encephalitis" and its association with carcinoma. Brain 91:481

Dalmau J, Tüzün E, Wu HY, Masjuan J, Rossi JE, Voloschin A, Baehring JM, Shimazaki H, Koide R, King D, Mason W, Sansing LH, Dichter MA, Rosenfeld MR, Lynch DR (2007) Paraneoplastic anti-N-methyl-D-aspartate receptor encephalitis associated with ovarian teratoma. Ann Neurol 61:25–36

Dalmau J, Gleichman AJ, Hughes EG, Rossi JE, Peng X, Lai M, Dessain SK, Rosenfeld MR, Balice-Gordon R, Lynch DR (2008) Anti-NMDA-receptor encephalitis: case series and analysis of the effects of antibodies. Lancet Neurol 7(12): 1091–1098

Gill DS et al (2006) Age-related findings on MRI in neurofibromatosis type 1. Pediatr Radiol 36:1048–1056

Graus F, Delattre JY, Antoine JC, Dalmau J, Giometto B, Grisold W et al (2004) Recommended diagnostic criteria for paraneoplastic neurological syndromes. J Neurol Neurosurg Psychiatry 75: 1135–1140

Gultekin SH, Rosenfeld MR, Voltz R, Eichen J, Posner JB, Dalmau J (2000) Paraneoplastic limbic encephalitis: neurological symptoms, immunological findings and tumour association in 50 patients. Brain 123:1481–1494

Irani SR, Alexander S, Waters P, Kleopa KA, Pettingill P, Zuliani L et al (2010) Antibodies to Kv1 potassium channel-complex proteins leucine-rich, glioma inactivated 1 protein and contactin-associated protein-2 in limbic encephalitis morvan's syndrome and acquired neuromyotonia. Brain 133:2734–2748

Kano O, Arasaki K, Ikeda K, Aoyagi J, Shiraishi H, Motomura M, Iwasaki Y (2009) Limbic encephalitis associated with systemic lupus erythematosus. Lupus 18(14):1316–1319

Lancaster E, Lai M, Peng X, Hughes E, Constantinescu R, Raizer J et al (2010) Antibodies to the GABA(B) receptor in limbic encephalitis with seizures: case series and characterisation of the antigen. Lancet Neurol 9:67–76

Lancaster E, Huijbers MG, Bar V, Boronat A, Wong A, Martinez-Hernandez E et al (2011) Investigations of caspr2, an autoantigen of encephalitis and neuromyotonia. Ann Neurol 69:303–311

Lai M, Hughes EG, Peng X, Zhou L, Gleichman AJ, Shu H et al (2009) AMPA receptor antibodies in limbic encephalitis alter synaptic receptor location. Ann Neurol 65:424–434

Lai M, Huijbers MG, Lancaster E, Graus F, Bataller L, Balice-Gordon R et al (2010) Investigation of LGI1 as the antigen in limbic encephalitis previously attributed to potassium channels: a case series. Lancet Neurol 9:776–785

Mahad DJ, Staugaitis S, Ruggieri P, Parisi J, Kleinschmidt-Demasters BK, Lassmann H, Ransohoff RM (2005) Steroid-responsive encephalopathy associated with autoimmune thyroiditis and primary CNS demyelination. J Neurol Sci 228(1):3–5

Malter M et al (2010) Antibodies to glutamic acid decarboxylase define a form of limbic encephalitis. Ann Neurol 67:470–478

Novillo-López ME, Rossi JE, Dalmau J, Masjuan J (2008) Treatment-responsive subacute limbic encephalitis and NMDA receptor antibodies in a man. Neurology 70:728–729

Soeder BM, Urbach H, Elger CE, Bien CG, Beyenburg S (2005) VGKC antibodies associated with limbic encephalitis. Nervenarzt 76(6):760–762

Soeder BM, Gleissner U, Urbach H, Clusmann H, Elger CE, Vincent A et al (2009) Causes, presentation and outcome of lesional adult-onset mediotemporal lobe epilepsy. J Neurol Neurosurg Psychiatry 80:888–893

Stübgen JP (1998) Nervous system lupus mimics limbic encephalitis. Lupus 7(8):557–560

Urbach H, Sassen R, Soeder BM, Flacke S, Becker A, Bien CG (2006a) Serial MRI in patients with acquired hippocampal sclerosis. Clin Neuroradiol 16:47–52

Urbach H, Soeder BM, Jeub M, Klockgether T, Meyer B, Bien CG (2006b) Serial MRI of limbic encephalitis. Neuroradiology 48:380–386

Vincent A, Irani SR (2010) Caspr2 antibodies in patients with thymomas. J Thorac Oncol 5:S277–S280

Vincent A, Buckley C, Schott JM, Baker I, Dewar BK, Detert N et al (2004) Potassium channel antibody-associated encephalopathy: a potentially immunotherapy-responsive form of limbic encephalitis. Brain 127:701–712

Epilepsy Associated Tumors and Tumor-Like Lesions

Horst Urbach

Contents

H. Urbach (✉)
Department of Neuroradiology, University Hospital Freiburg, Germany
e-mail: horst.urbach@uniklinik-freiburg.de

Abstract

Glioneuronal rather than glial tumors are found in around 20% of patients with drug-resistant focal epilepsies. Gangliogliomas, dysembryoplastic neuroepithelial tumours (DNTs), angiocentric gliomas, pilocytic astrocytomas, and pleomorphic xanthoastrocytomas (PXAs) show characteristic imaging profiles clearly different from diffusely infiltrating gliomas. Epidermoids and dermoids are considered tumor like lesions with likewise specific imaging findings.

1 Introduction

In around 20% of patients with long-term drug-resistant epilepsy intra-axial brain tumours are found (Luyken et al. 2003; Urbach et al. 2004; Bien et al. 2013). Clinically, two different groups exist in this cohort. The first contains typical epilepsy-associated tumours such as gangliogliomas, dysembryoplastic neuroepithelial tumours (DNTs), angiocentric gliomas, pleomorphic astrocytomas (pXAs), and supratentorial pilocytic astrozytomas, WHO grade I, with an usually benign behaviour. The second group consists of diffuse astrocytomas, WHO grade II, oligodendrogliomas, WHO grade II, with a five year-survival rate of 50–65%, and a few anaplastic cases, classified as WHO grade III, with a median survival time of 2–3 years. Histopathologically, glioneuronal and glial tumours can be distinguished. Among the glioneuronal tumours, gangliogliomas and DNTs are well characterized on MRI. Another tumor with a characteristic MR imaging pattern designed as angiocentric

H. Urbach (ed.), *MRI in Epilepsy*, Medical Radiology. Diagnostic Imaging,
DOI: 10.1007/174_2011_525, © Springer-Verlag Berlin Heidelberg 2013

glioma has recently been added to the WHO classification of brain tumors (Louis et al. 2007). Due to the uncertain histogenesis it is grouped in the category "other neuroepithelial tumors".

Since some tumor-like lesions like epidermoid or dermoid may cause drug-resistant seizures, they are also illustrated in this chapter.

2 Ganglioglioma

2.1 Epidemiology

Usually benign intraaxial tumors first described by Perkins in (1926). Most common long-term epilepsy associated tumor.

2.2 Clinical Presentation

Drug-resistant epilepsy with usually focal seizures. Temporo-mesial gangliogliomas likely induce complex focal, gangliogliomas in other locations simple focal seizures. Secondary generalization occurs in around 30% of cases.

Extratemporal location, male gender, age at surgery <40 years, a history without epilepsy, incomplete tumor resection, and histopathological presence of a gemistocytic cell component have been identified as poor prognostic outcome parameters (Rumana et al. 1999; Majores et al. 2008). Tumorvolume of gangliogliomas in early childhood (<10 years) is significantly larger than that of gangiogliomas encountered in adults, especially the cystic part (Provenzale et al. 2000).

2.3 Pathology

Tumor composed of dysplastic neurons and neoplastic glial cells. Both cell populations may show heterogeneity, with the morphological spectrum ranging from a predominantly neuronal phenotype to a predominant glial population. The immunohistochemical profile (e.g., expression of the stem cell epitope CD34) usually allows a specific diagnosis (Blümcke et al. 1999, 2002).

85% of gangliogliomas correspond to WHO grade I, around 10% to WHO grade II and 5% to WHO grade III tumours, respectively (Blümcke et al. 2002; Luyken et al. 2004; Majores et al. 2008). Note that with the 2007 WHO classification only WHO grade I and III gangliogliomas are distinguished (Louis et al. 2007). Overall recurrence rate is around 7%, but distinctly higher for grade II (33%) and grade III (60%) tumors. If there is tumor recurrence, nearly half of the tumors are glioblastomas (Majores et al. 2008).

2.4 Imaging

Location in the cortex or in the cortex and subcortical white matter. Spatial preponderance for the parahippocampal and lateral temporo-occipital gyri. Classical imaging feature is the combination of intracortical cyst(s), a circumscribed area of cortical (and subcortical) signal increase on FLAIR and T2-weighted images and a contrast enhancing nodule (Figs. 1, 2).

Calcifications occur in 1/3 of cases (Zentner et al. 1994).

If contrast enhancement is absent (≈70% of cases), gangliogliomas may be difficult to distinguish from cortical dysplasias. Especially, in these cases intracortical cysts are highly diagnostic.

Gangliogliomas typically have no perifocal oedema. If oedema is present, malignant degeneration (from the glial component) to a WHO grade II or III ganglioglioma or anaplastic glial tumours including PXA with anaplastic features should be suspected.

3 Dysembryoplastic Neuroepithelial Tumor

3.1 Epidemiology

Second most common epilepsy associated tumor, which was first described by Daumas-Duport in (1988). DNT is mistaken for oligodendroglioma rather than diffuse astrocytoma in 15% of cases (Campos et al. 2009).

3.2 Clinical Presentation

Drug-resistant epilepsy with usually focal seizures, which may secondarily generalize. Temporo-mesial DNTs likely induce complex focal, DNTs in other locations simple focal seizures.

3.3 Pathology

WHO grade I-tumor. Location: temporal (66%), frontal (20%), parietal > occipital lobe.

Histopathological hallmark is the so-called glioneuronal element, which contains oligodendrocyte-like cells attached to bundles of axons and neurons floating in a myxoid interstitial fluid (Daumas-Duport et al. 2000). If only the glioneuronal element is present, it is referred to as simple

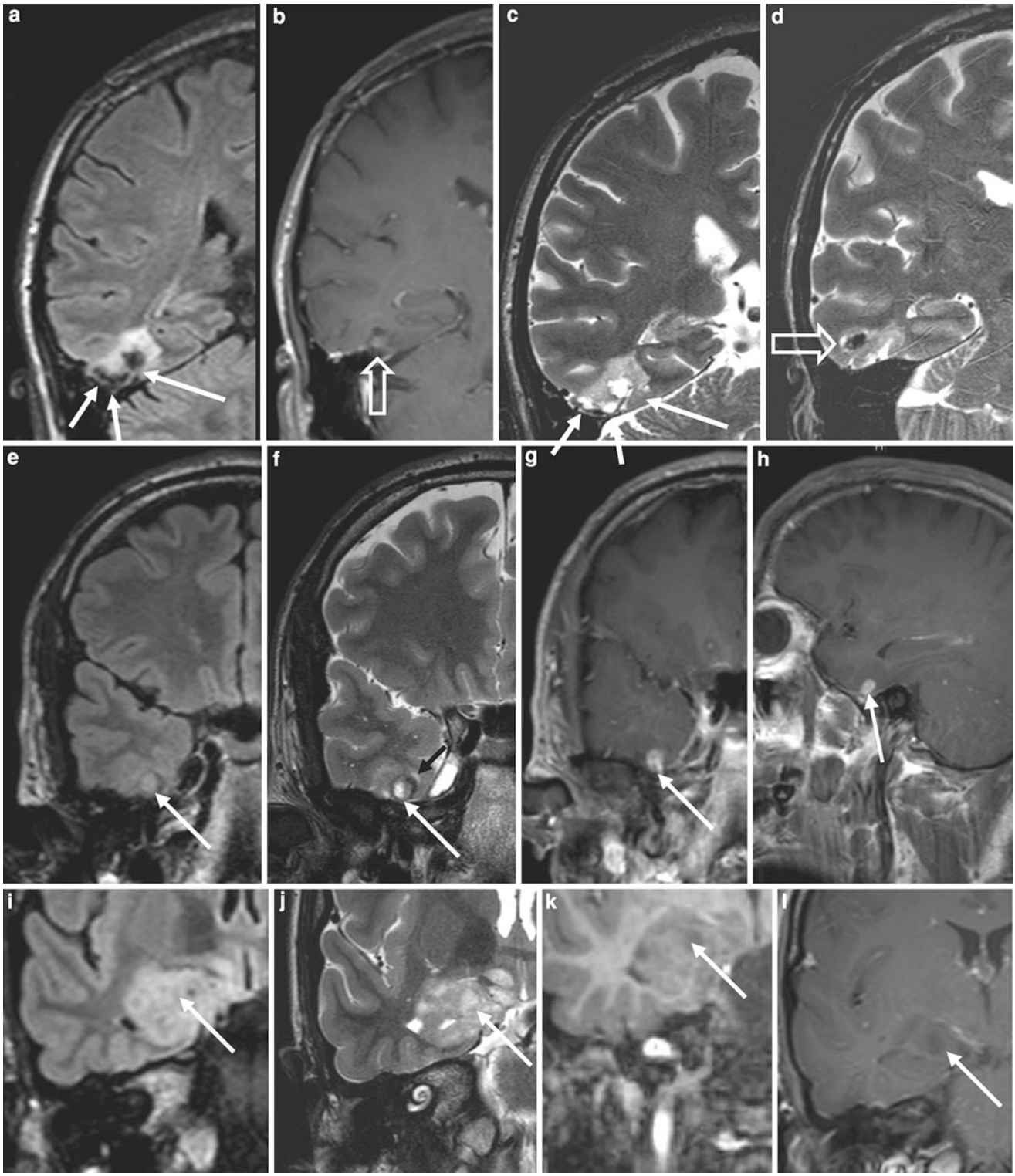

Fig. 1 Imaging examples of three temporal lobe gangliogliomas WHO grade I: the *upper row* shows a ganglioglioma with all characteristic imaging features: A cortical and subcortical tumor with intracortical cysts (**a**, **c**: *arrows*), contrast enhancing (**b**: *hollow arrow*), and calcified tumor portions (**d**: *hollow arrow*), and increased white matter signal intensity (**b**: *arrow*). In the mid row, a small cortical tumor with a lateral solid (**e**: *arrow*), contrast enhancing (**f**–**h**: *arrow*) and a medial hypointense tumor portion (**f**: *black arrow*), which was not calcified on CT, is also highly suggestive of a ganglioglioma. In the lower row (**i**–**l**), a tumor of the right amygdala shows cystic components, and no contrast enhancement. It could be considered as a DNT, albeit the tumor cysts are not as regular as in a DNT

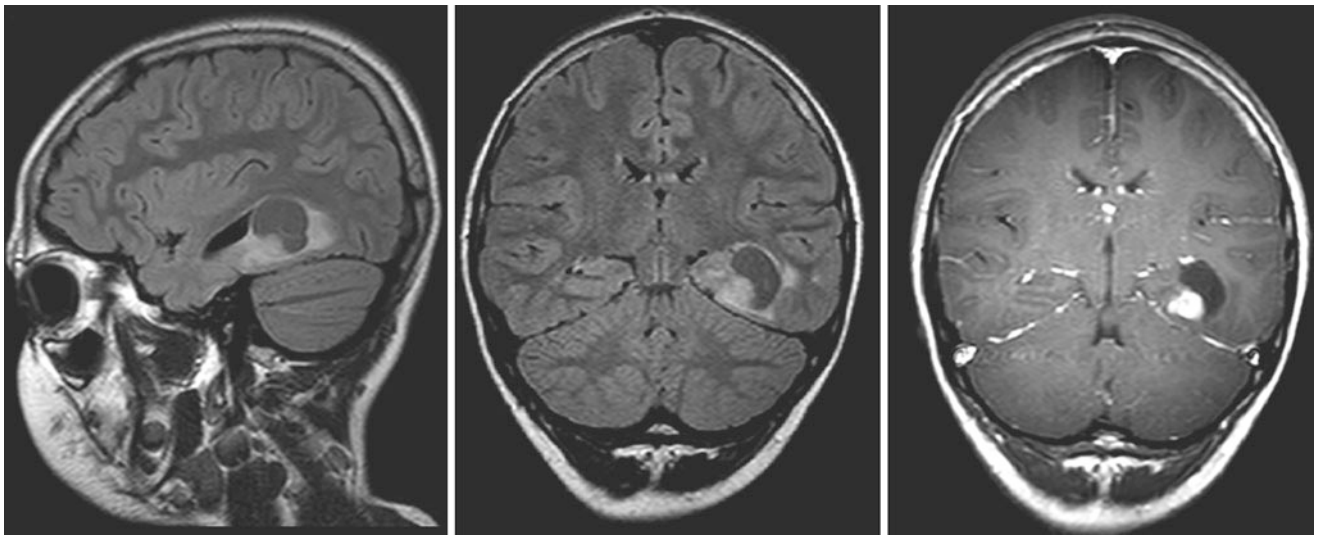

Fig. 2 Ganglioglioma WHO grade I of the left occipito-temporal gyrus. The tumor has a cystic and a contrast enhancing tumor portion and is indistinguishable from a pilocytic atsrocytoma. However, in a patient with drug-resistant epilepsy like in this 9 year old girl with complex focal seizures since the age of 7 a ganglioglioma is more likely

variant. Complex DNT variants additionally may contain glial nodules resembling astrocytomas, oligodendrogliomas or oligoastrocytomas, foci of cortical dysplasia, calcification and hemorrhages.

Tumor growth or recurrence is extremly rare, it may occur in the complex variant group also characterized by an earlier seizure onset, and more extratemporal locations, characterized by the so called glioneuronal element.

It is rather the oligodendrocyte-like cells of the glioneuronal element than adjacent glial nodules as part of the complex DNT variant that cause misclassification of DNTs (Fig. 4) (Campos et al. 2009).

3.4 Imaging

MRI hallmark are multilobulated cysts, rarely only one large cyst is present. The cysts represent the glioneuronal element and are located in the cortex or in the cortex and subcortical white matter, sometimes single smaller cysts are located in the vicinity of the tumor, from which they are clearly separated (Fig. 3). The multilobulated cysts are either oriented in a ball-like fashion or perpendicular to the cortical surface; they are hypointense on T1-weighted and strongly hyperintense on T2-weighted images. On FLAIR images, they have a mixed signal intensity, most of the "lobuli within the cyst" are hypointense. On DWI, DNTs are hypointense.

Parts of the glioneuronal element may show nodular, ring-like or heterogenous contrast enhancement (25%). Contrast enhancement may vary on follow-up examinations in that way, that sharply marginated contrast-enhancing nodules occur while others have disappeared (Fig. 3) (Campos et al. 2009).

Next to the multicystic tumor portion solid, nearly T1w-isointense and FLAIR/T2 less hyperintense tumor portions can be found in 90% of patients. Larger solid tumor portions are in favour of a complex DNT variant.

Calcifications are found in 10% of complex DNTs, mostly within the deeper located tumor portions, usually in the vicinity of the contrast enhancing regions and—if rarely present—always in the vicinity of hemorrhage (Fig. 4) (Campos et al. 2009).

4 Angiocentric Glioma

Synonym: Angiocentric Neuroepithelial Tumor (ANET)

4.1 Epidemiology

Epilepsy associated tumor with histological similarities to astrocytoma and ependymoma. The tumor was initially described by Lellouch-Tubiana et al. 2005 and Wang et al. (2005) and added as clinico-pathological entity to the 2007 WHO classification of CNS tumors (Louis et al. 2007). Less than 20 cases have been described so far, but older cases may have been misclassified as (cortical) ependymoma or astrocytoma.

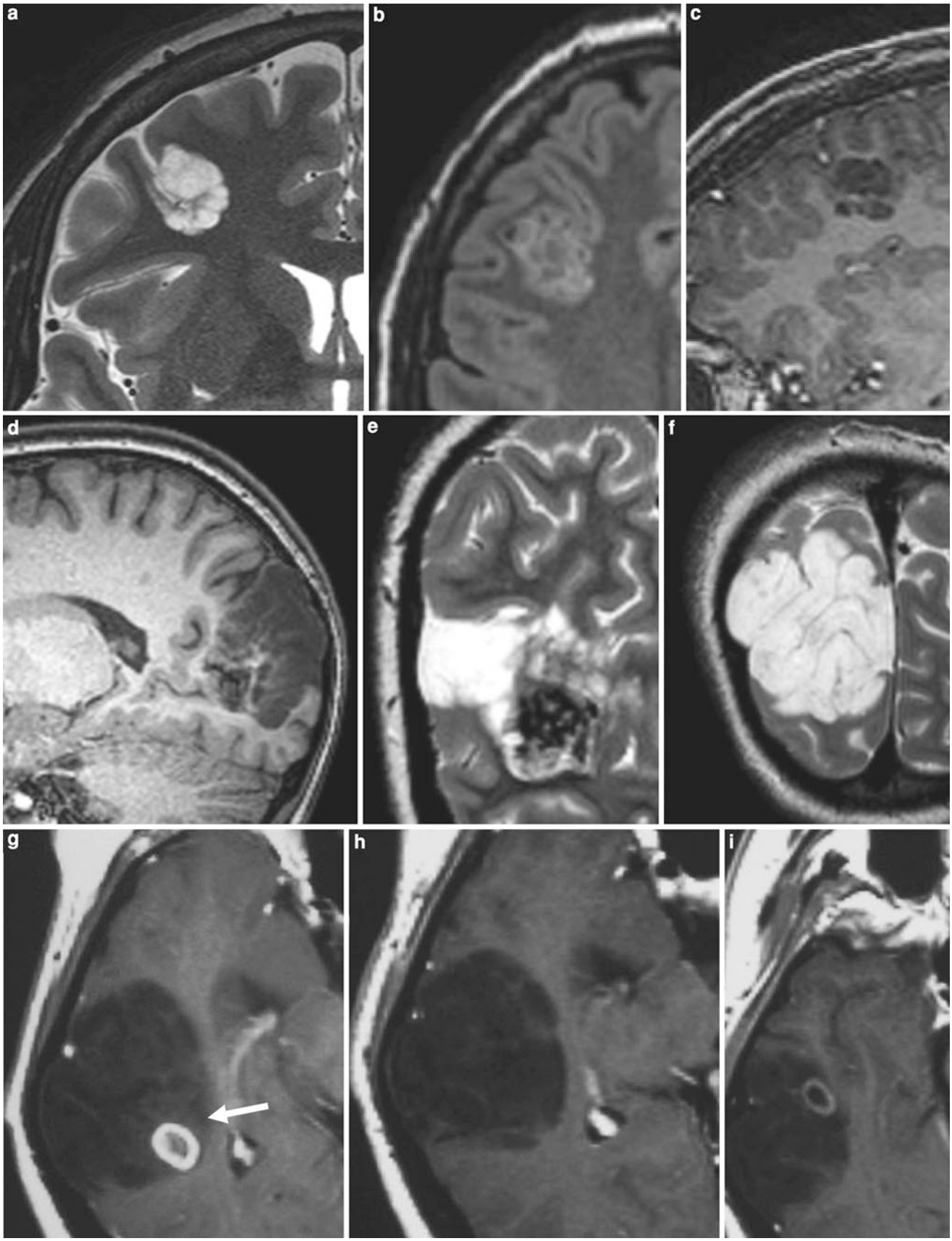

Fig. 3 **a–c** *Small right* frontal DNT, consisting only of the glioneuronal element (*simple variant*). In contrast, the complex DNT variant in case **d–e** shows a deep-seated calcified portion. The interval between **g** and **h–i** is 3 years: A ring-like contrast enhancing lesion in the posterior tumor portion has disappeared (*arrow*), in another location a new ring-enhancing lesion has occurred

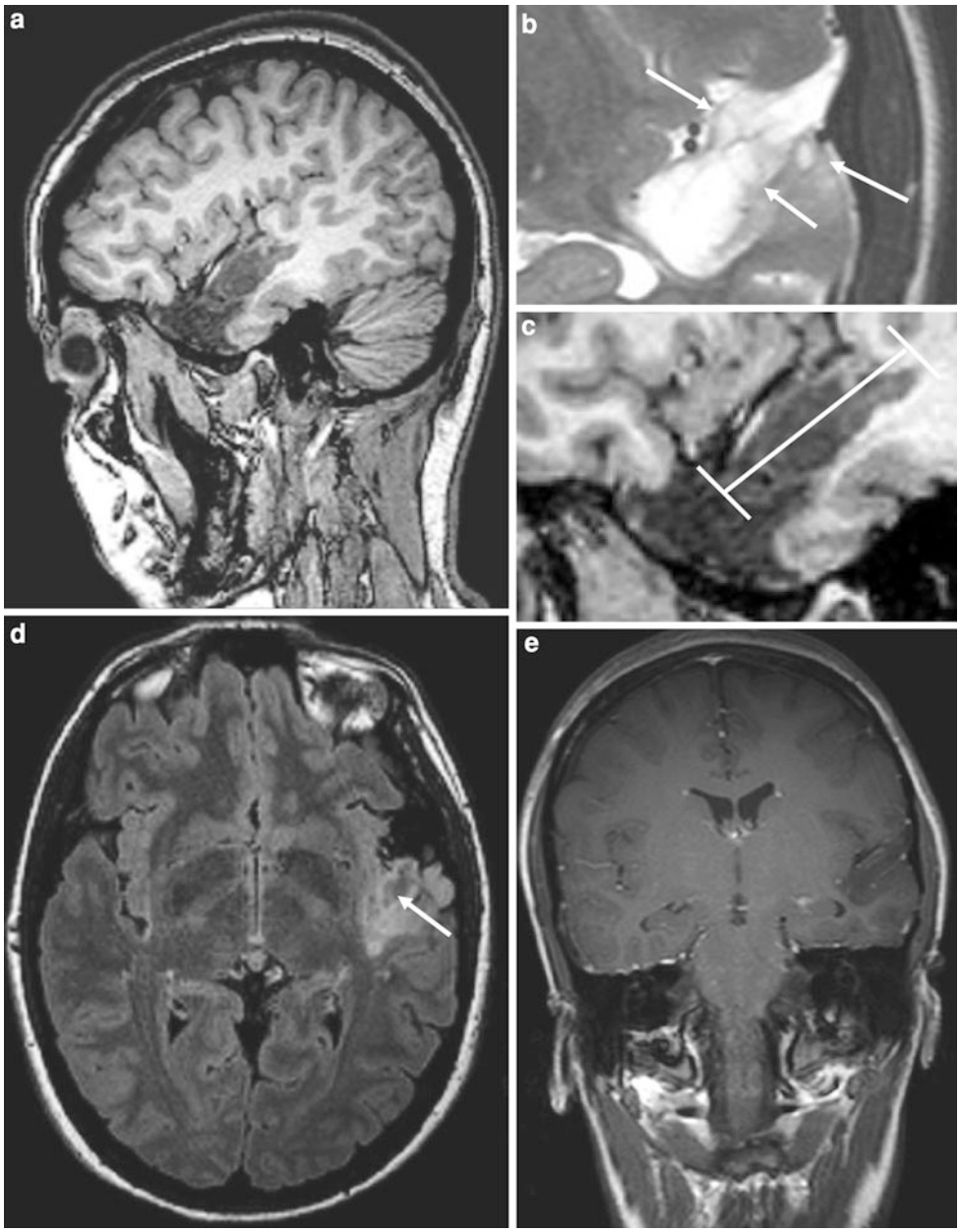

Fig. 4 MRI after surgery of an "oligodendroglioma" in 1991. Posteriorly to the surgical defect, there is a 28 x 12 mm cystic lesion with slightly higher signal intensity than CSF on T1-weighted images (**a**, **c**, **e**). Diagnostic hallmark are tiny cysts within the DNT, which are best appreciated on high-resolution T2-weighted images (**b**: *arrows*). Larger cysts are hypointense on FLAIR-images (**d**: *arrow*)

4.2 Clinical Presentation

Children and young adults with focal seizures, ♂ = ♀.

4.3 Pathology

Radial arrangement of GFAP-positive, fusiform and bipolare astrocytic cells around blood vessels. Variable infiltrative pattern.

4.4 Imaging

Cortical and subcortical tumor with a stalk-like extension towards the lateral ventricle. Predilection for the posterior (parietal and occipital) brain segments. A ribbon-like hyperintensity within the cortex on unenhanced T1-weighted spin echo images is considered pathognomonic. No calcifications. No contrast enhancement (Lellouch-Tubiana et al. 2005; Wang et al. 2005; Majores et al. 2007; Shakur et al. 2009) (Fig. 5).

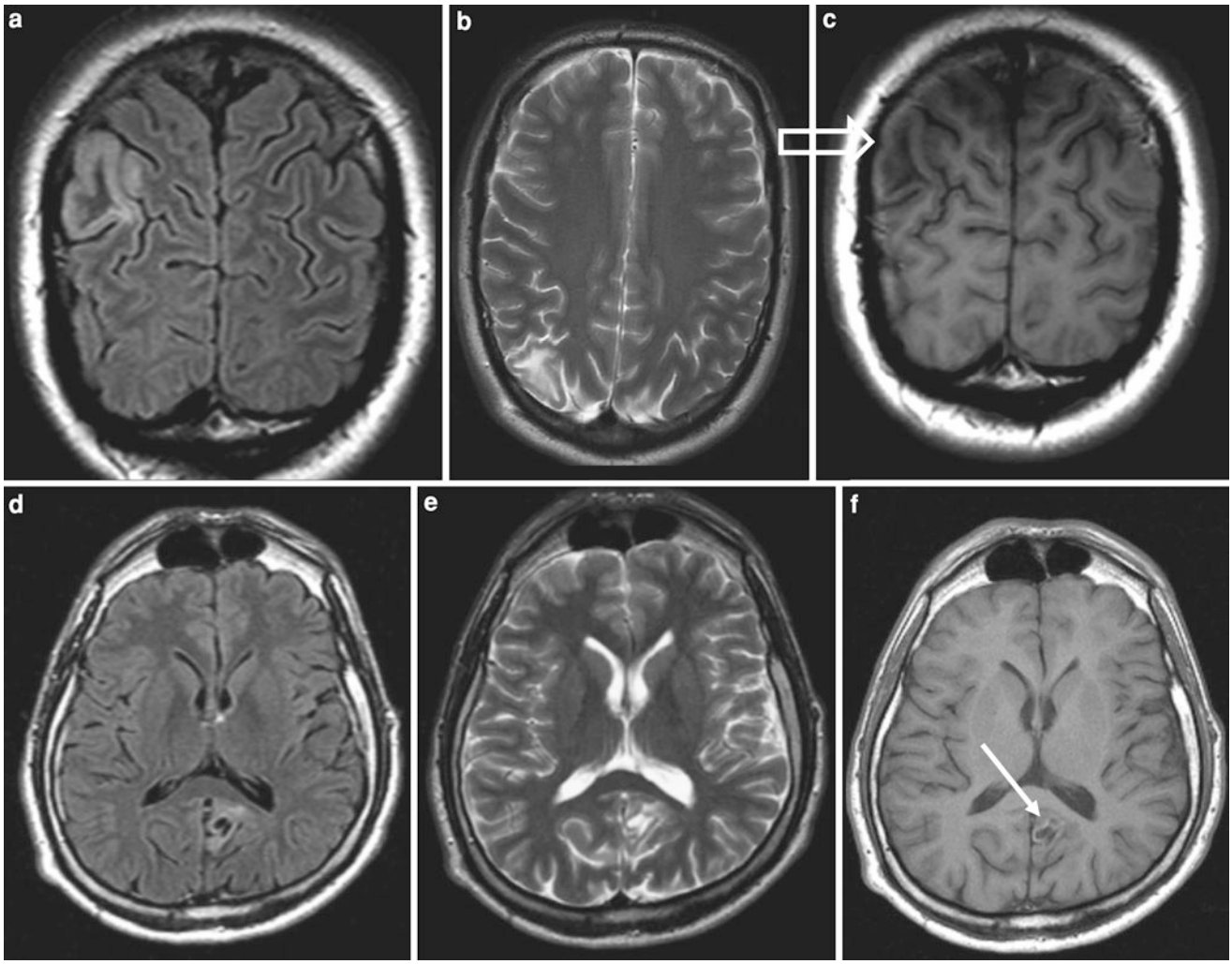

Fig. 5 Two angiocentric gliomas (or ANETs) (**a–c**, **d–f**). These tumors are characterized by a rather posterior location, a lack of space-occuyping effect and distinct signal intensity differences between cortical and subcortical tissue. A ribbon-like cortical hyperintensity on unenhanced T1-weighted images is considered pathognomonic (**f**: *arrow*). However, as demonstrated in the upper example (**a–c**), it may be absent or difficult to detect (**c**: *hollow arrow*)

5 Pilocytic Astrocytoma

5.1 Epidemiology

Pilocytic astrocytomas are a rather rare cause of drug-resistant epilepsy, but the most common brain tumor in infants. More than 75% manifest in children and adolescents, with a peak incidence between 8 and 13 years. Pilocytic astrocytomas of the cerebral hemispheres manifest at an older age than those of the more common location of the cerebellum, optic nerve and chiasm, and brainstem. Among those, the mesial temporal lobe is a classical location.

5.2 Clinical Presentation

Children and young adults with focal seizures without and with secondary generalization, ♂ = ♀. Some patients present with signs of high intracranial pressure due to a space occuypying effect of large pilocytic astrocytoma.

5.3 Pathology

Circumscribed astrocytic tumor with a biphasic pattern in which highly fibrillated pilocytic areas containing compact bipolar cells with Rosenthal fibers are interminged with loose-structured, microcystic tumor tissue and a mucinous

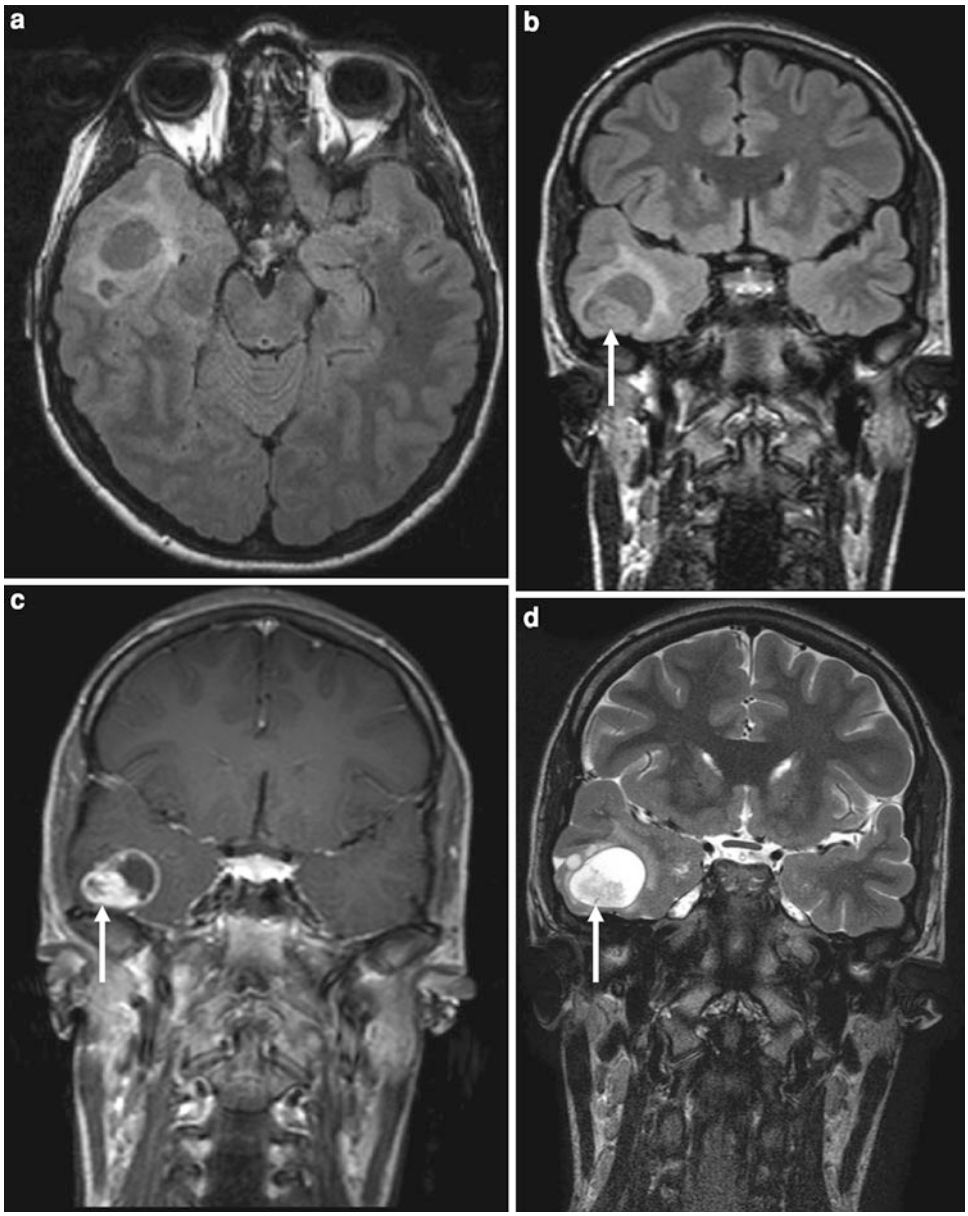

Fig. 6 Pilocytic astrocytoma WHO grade I: 17 year old woman with a single tonic-clonic seizure. MRI shows a three 3 cm large tumor with a large cyst, a solid, contrast enhancing tumor portion at the border of the cyst (**a**–**d**: *arrow*) and a perifocal oedema. The size of the cyst, a single seizure, and perifocal oedema are in favor against a ganglioglioma and for a pilocytic astrocytoma. However, the superficial contrast enhancement fits to a pleomorphic xanthoastrocytoma (PXA)

background. The tumor stroma is highly vascular with glomeruloid features and has a low MIB-1 index of around 1%. An admixture of ganglion cells is occasionally observed. However, if located in the mesial tempral lobe, a ganglioglioma is more likely since the glial component of a ganglioglioma can be pilocytic in appearance.

5.4 Imaging

Pilocytic astrocytomas appear as cystic, round to oval lesions with a larger cystic and a smaller contrast enhancing tumor portion (Fig. 6). Cysts walls occasionally enhance. Pilocytic astrocytomas may spread through subarachnoid space in rare cases (although there a still WHO grade I tumors) (Fig. 7).

They may be difficult to distinguish from gangliogliomas, however, pilocytic astrocytomas tend to be larger than gangliogliomas, especially with respect to the cystic portion.

6 Pleomorphic Xanthoastrocytoma

6.1 Epidemiology

Rare, Epilepsy-associated astrocytic tumours with superficial location in the cerebral hemispheres and involvement of the meninges.

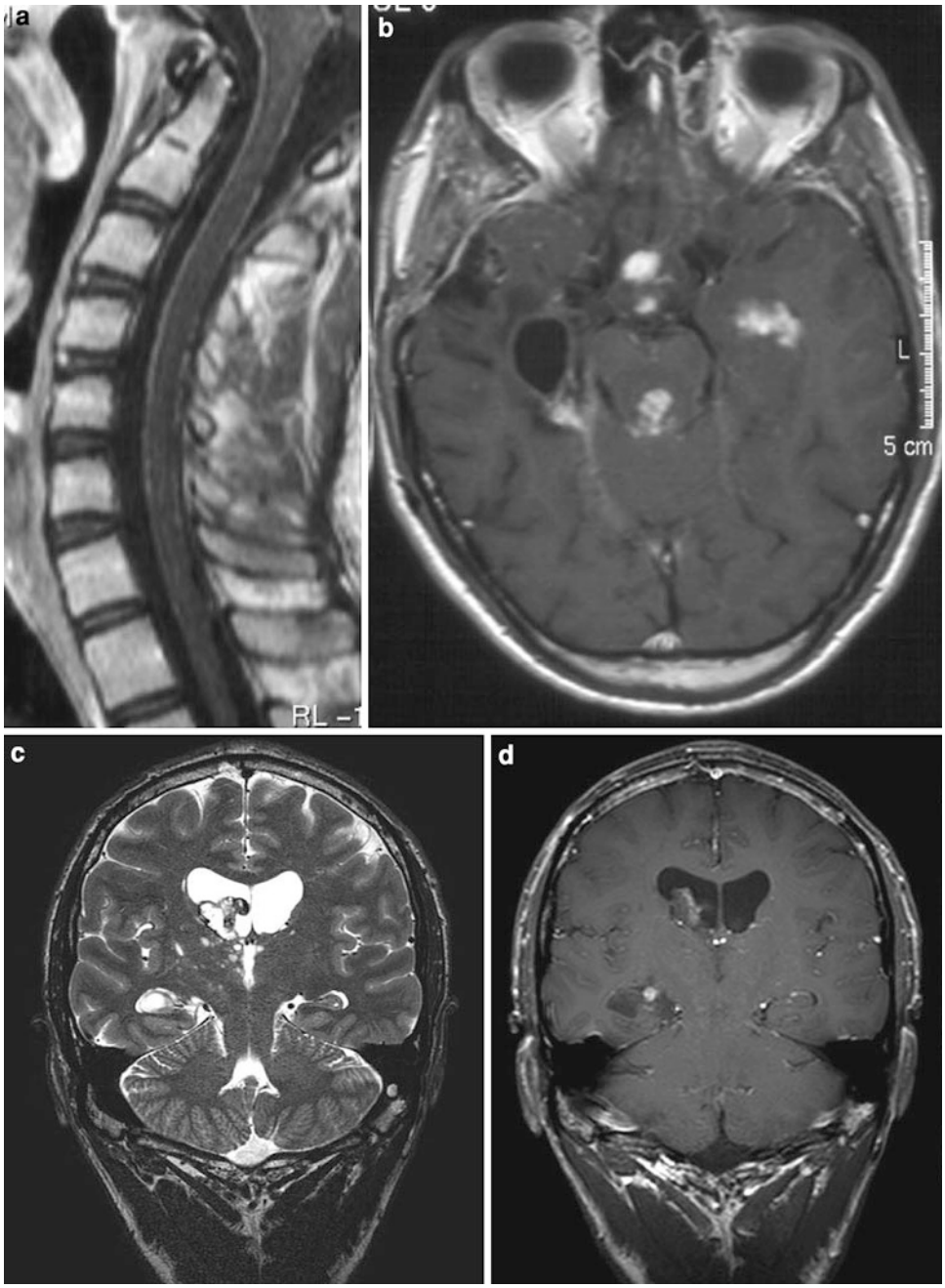

Fig. 7 Pilocytic astrocytoma WHO grade I with leptomeningeal spread in a 15 year old (**a**, **b**) and a 38 olde man (**c**, **d**) with temporal lobe seizures

6.2 Clinical Presentation

Typically children and young adults with focal seizures without and with secondary generalization, ♂ = ♀. 2/3 of patients are younger than 20 years, however, PXAs also occur in adults.

6.3 Pathology

Tumor with solid and cystic portions with multinucleated and lipidized giant cells and a reticulin-positive stroma. In most cases WHO grade II tumor. For tumors with significant mitotic activity (5 or more mitoses per 10 high power fields) the term PXA with anaplastic features is used. A significant portion of PXAs dedifferentiates to glioblastomas.

It has been postulated that PXAs originate from subpial astrocytes. However, the demonstration of synaptophysin and neurofilament protein in some PXAs suggests neuronal differentiation and a more complex histogenesis.

6.4 Imaging

A meningo-cerebral contrast enhancement on T1-weighted spin echo images reflecting the extensive involvement of the subarachnoid space is characteristic (Fig. 8). Some

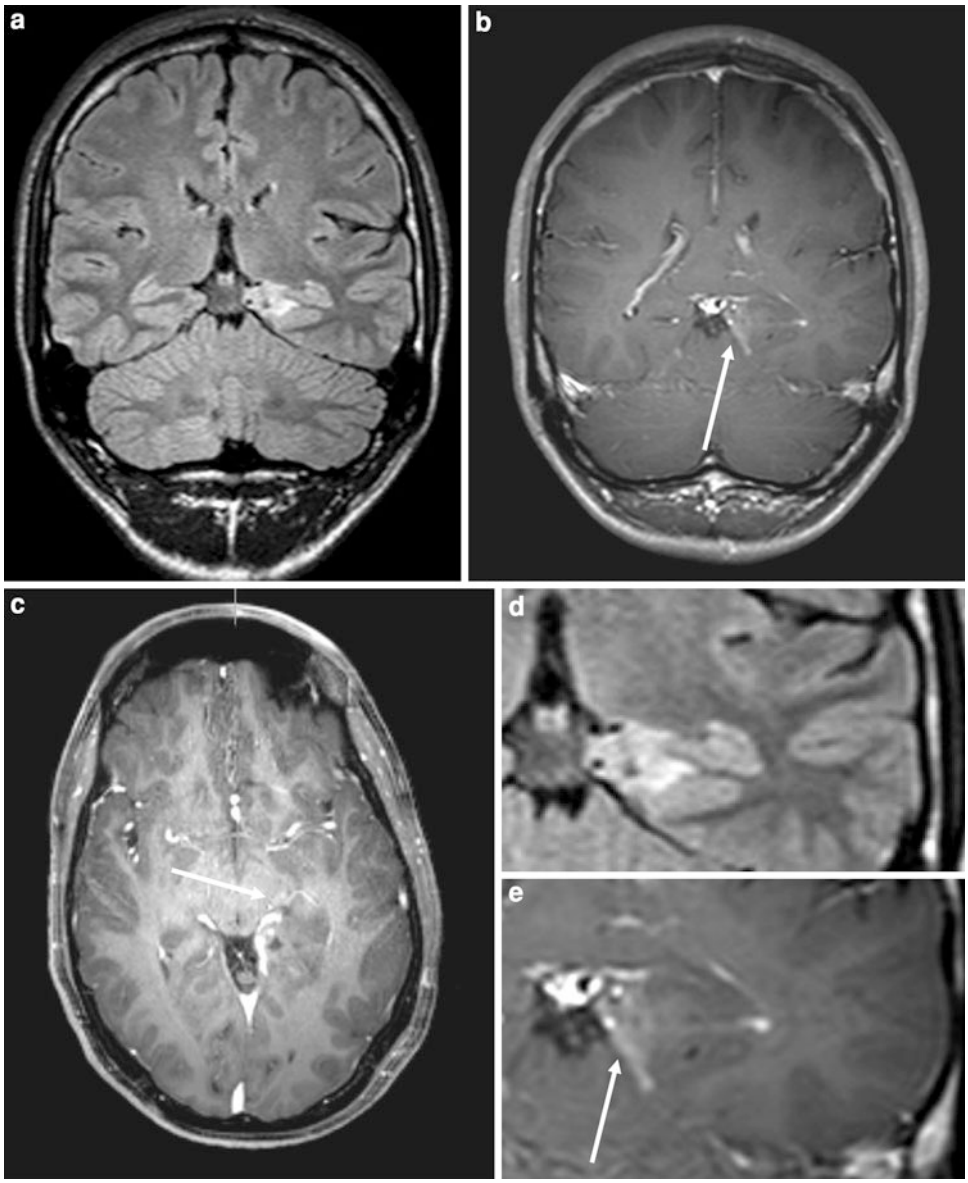

Fig. 8 Small pleomorphic xanthosatrocytoma WHO grade II of the posterior part of the left parahippocampal gyrus. The cortical/subcortical lesion is hyperintense on FLAIR sequences (**a**, **d**) and shows superficial contrast enhancement on T1-weighted sequences (**b**, **c**, **e**). Although it is not possible to fully distinguish it from a ganglioglioma, superficial so called meningo-cerebral contrast enhancement (**b**, **c**, **e**: *arrow*) is suggestive for a pleomorphic xanthosatrocytoma

tumors have white matter edema on T2-weighted and FLAIR images. Calcifications and a space-occupying effect are possible.

7 Diffuse Gliomas

7.1 Epidemiology

Diffusely infiltrating, glial brain tumors cause epileptic seizures in 20–45% of patients. Typically, WHO grade II astrocytomas, WHO grade III (anaplastic) astrocytomas, WHO grade II oligodendrogliomas, WHO grade III (anaplastic) oligodendrogliomas, and glioblastomas multiforme are distinguished. Tumor containing astrocytic and oligodendroglial elements are refered to as oligoastrocytomas.

It has been hypothesized that so-called low grade or WHO II gliomas associated with epileptic seizures carry a better prognosis with respect to the recurrence free interval and overall survival time. However, many of these tumors are located in the temporal lobe and are likely detected at a comparable earlier point of time: While the mean age of presentation of low grade astrocytomas is 39 years of age (Okamato et al. 2004), it is under 30 in patients with drug-resistant epilepsies (Luyken et al. 2003). And, at least in the Bonn series, a significant proportion of tumors was—by means of MRI and later confirmed with CD34 immunohistochemistry-gangliogliomas and DNTs (Luyken et al. 2003).

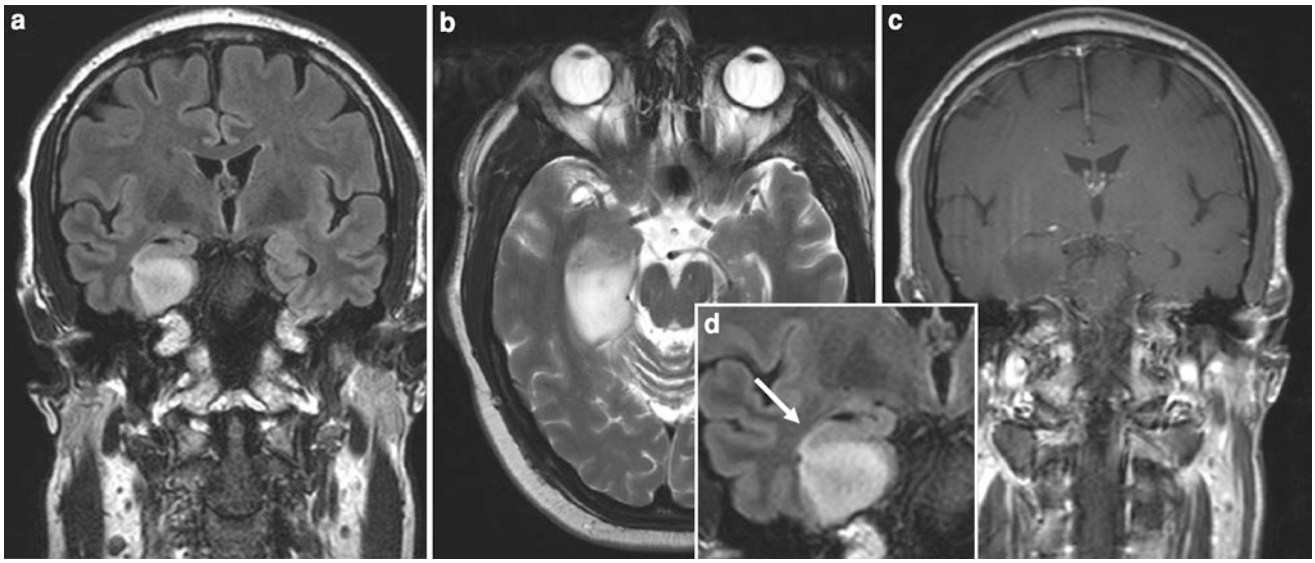

Fig. 9 WHO grade II astrocytoma in a 42 year old male with complex-focal seizures since seven years. The right parahippocampal gyrus is enlarged and shows a relatively homogenous signal increase (**a**, **b**, **c**). Contrast enhancement is absent (**c**) and FLAIR images show the tumor infiltrating the hippocampus (**a**, **d**: *arrow*)

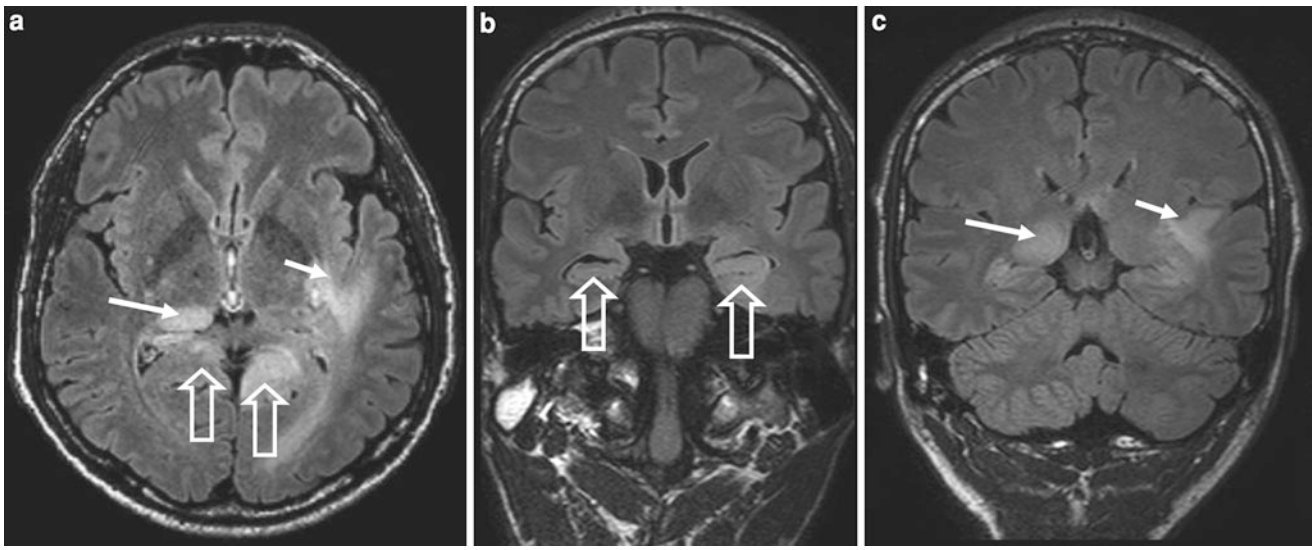

Fig. 10 "Multifocal" WHO grade II astrocytoma in a 52 year old woman with complex focal and secondarily generalized tonic-clonic seizures. There is a tendency of some astrocytomas to "grow" within the limbic system with a frequent involvement of the posterior thalamus (**a**, **c** *white arrows*) and the insula (**a**, **c**: *short white arrows*). Note left-prominent infiltration of both hippocampi (**b**: *hollow arrows*) and of the isthmus of the cingulate gyrus (**a**: *hollow arrows*)

7.2 Pathogenesis

The underlying pathophysiology of seizures secondary to brain tumors is poorly understood. A variety of hypotheses have been proposed, including altered neuronal regulation and connections, deranged vascular permeability, abnormal BBB, and impaired glial cell function. The tumor itself may be the seizure focus, or the tumor may cause secondary perilesional tissue alterations such as growth, inflammation, edema, or necrosis, thereby triggering seizure activity.

Oligodendrogliomas are more prone to cause epileptic seizures than astrocytomas, which is likely due to the typically broad-based cortical involvement (Fig. 11).

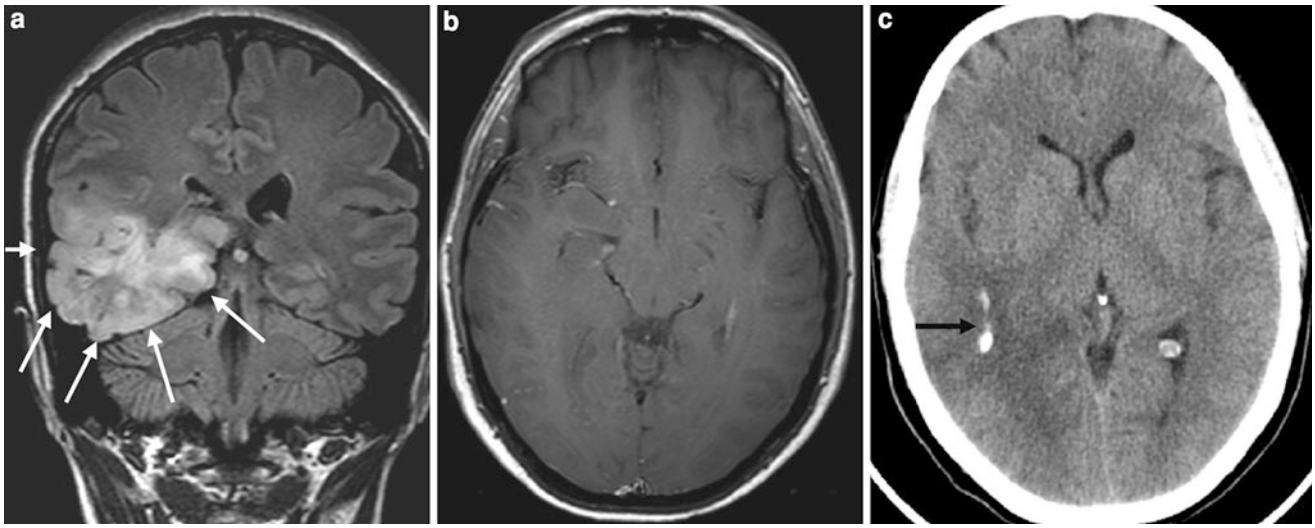

Fig. 11 Oligodendoglioma WHO grade III in a 43 year old woman with three complex focal seizures. The tumor is somewhat inhomogenous (**a**) and shows no contrast enhancement (**b**). The broad cortical infiltration (**a**: *arrows*) and clumpy calcifications—as highlighted with CT (**c**: *arrow*)—suggest the diagnosis oligodendroglioma or oligoastrocytoma

A significant number of diffusely infiltrating astrocytomas grows within or is "multifocal" in the limbic system, it may be defined as gliomatosis cerebri (Fig. 10).

7.3 Clinical Presentation

Epileptic seizures due to brain tumors typically manifest as focal seizures with secondary generalization and are commonly refractory to antiepileptic drug treatment. Compared to diffuse gliomas without epileptic seizures patients are younger and gliomas are more often located in the temporal lobe.

7.4 Imaging

Diffusely infiltrating astrocytomas are characterized by a hyperintense space occuyping white matter lesion on FLAIR and T2-weighted images (Fig. 9). Although the lesion may appear well demarcated on MRI, tumor cells are found beyond the abnormal signal intensity. Tumor inhomogeneity and contrast enhancement are considered to indicate dedifferentiation or malignant progression to a WHO grade III (anaplastic) astrocytoma.

Oligodendrogliomas typically involve the cortex and the subcortical white matter. They are more inhomogenous as compared to astrocytomas; inhomogeneity is caused by typically clumped calcifications, cystic changes and blood products. Additional unenhanced CT is often helpful to illustrate calcifications (Fig. 11).

8 Epidermoid

8.1 Epidemiology

Developmental lesion without dermal appendages. 10–15% of epidermoids are found in a parasellar, middle cranial fossa location, where they tend to cause temporal lobe seizures.

8.2 Clinical Presentation

Despite their congenital nature, they occur at any age with a peak age around 40, ♂ = ♀.

8.3 Pathology

Epidermoids are generally well-demarcated encapsulated lesion with a mother-of-pearl sheen. The outer surface is smooth, nodular or lobulated. Within the subarachnoid space they tend to creep into clefts and fissures and to engulf blood vessels and nervs.

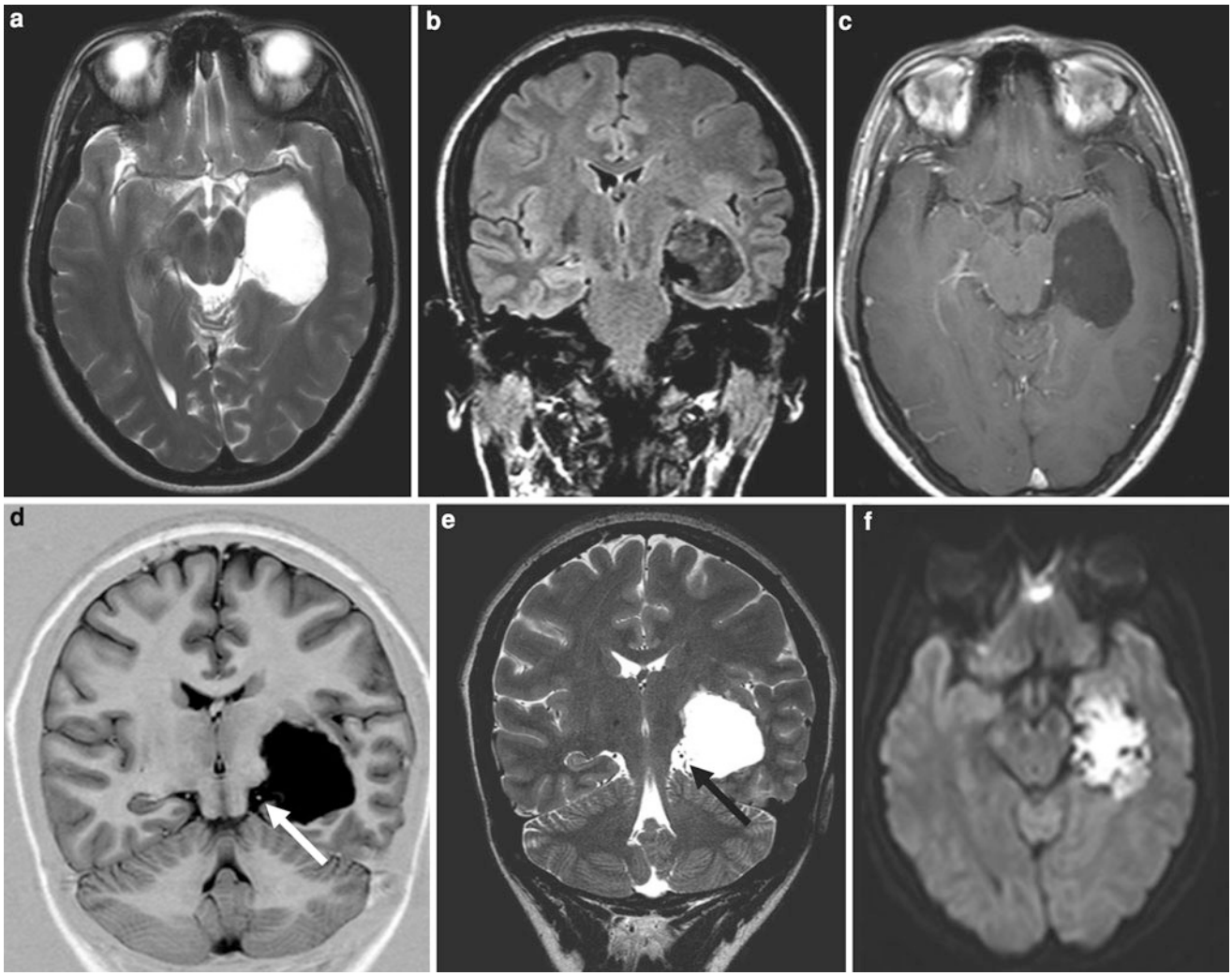

Fig. 12 Epidermoid of a 26 year old patient with temporal lobe seizures. The lesion is nearly isointense to CSF on T2-weighted (**a**), FLAIR (**b**), and T1-weighted sequences (**c**), but is distinctly hyperintense on DWI (**f**). The extraaxial location of the epidermoid is derived from the widening of the choroidal fissurre (**d**, **e**: *arrow*)

8.4 Imaging

Extraaxial space-occupying off-midline lesion expanding the subarachnoid space. Signal intensity is close to CSF in all sequences except DWI, in which epidermoids are distinctly hyperintense. High resolution MRI enables to visualize the cauliflower-like structure within the subarachnoid space (Fig. 12).

9 Dermoid

9.1 Epidemiology

Developmental lesions which are distinctly rarer than epidermoids.

9.2 Clinical Presentation

♂ > ♀. Headaches and seizures (20% of cases) are common symptoms.

9.3 Imaging

The diagnostic clue is to elaborate the fat component of the typically well delinated cystic lesions as indicated by T1-hyperintensity, CT hypodensity, signal loss on fat-suppressed sequences and chemical shift artifacts. Calcifications are found in 20% of cases. Small dermoid droplets in CSF indicated rupture of dermoid cysts and should be carefully searched for (Fig. 13).

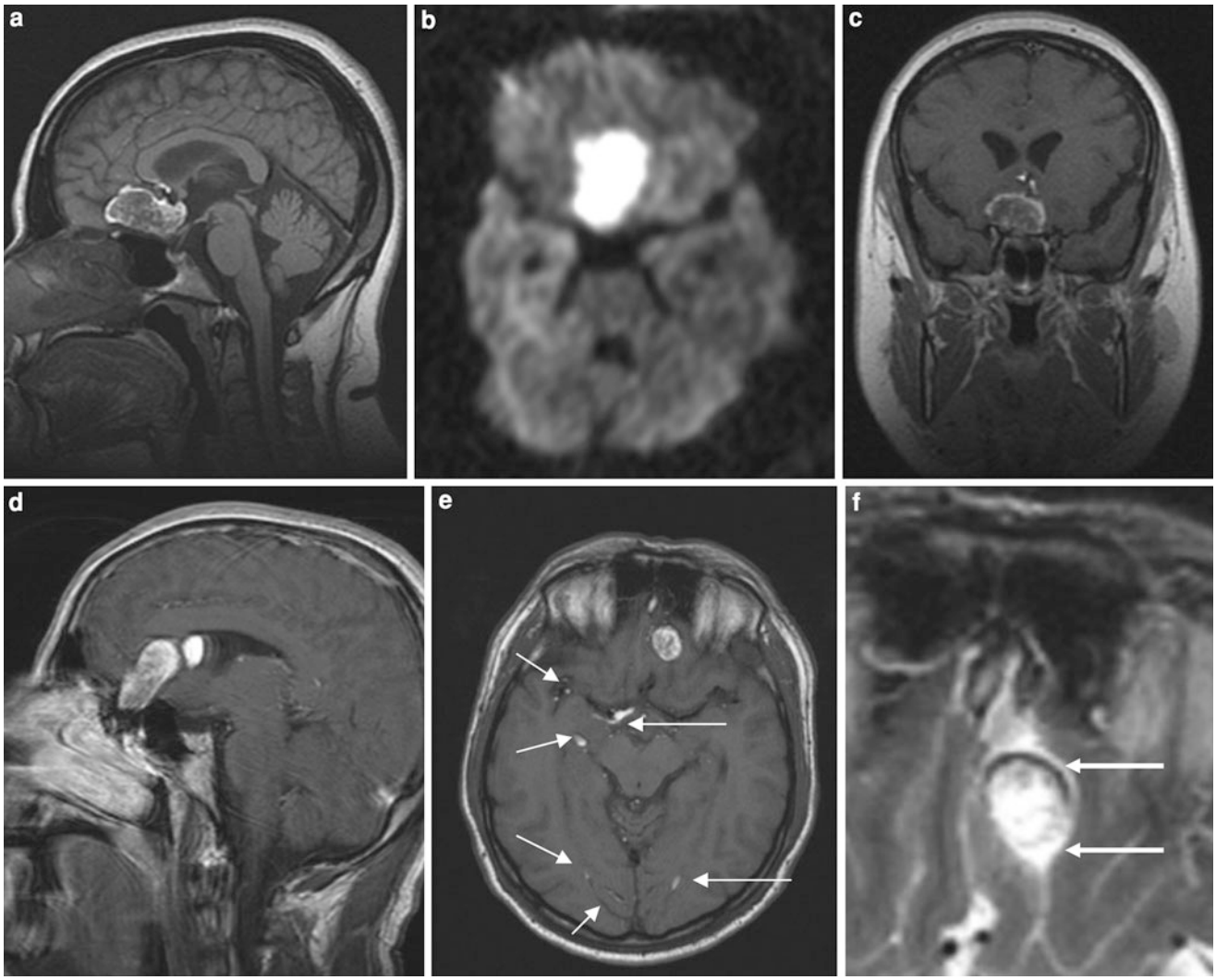

Fig. 13 A 30 year old woman (**a–c**) and a 36 year old man (**d–f**) suffered from drug-resistant seizured difficult to localize. MRI showed frontobasal "midline" dermoids, which are hyperintense on T1-weighted (**a**, **c**, **d**, **e**), T2-weighted (**f**) and Diffusion-weighted images (**b**). Note dermoid droplets in the subarachnoid space (**e**: *arrows*) and chemical shift artefact (**f**). The chemical shift artetfact is caused by different resonance frequencies of hydrogene nuclei bound to fat and water molecules.The dermoid contains fat-bound hydrogen nuclei and is displaced in the frequency-encoding direction with a low signal band anteriorly and a high-signal band posteriorly (**f**: *arrows*)

References

Bien CG, Raabe AL, Schramm J, Becker AJ, Urbach H, Elger CE (2013) Trends in presurgical evaluation and surgical treatment of epilepsy at one centre from 1988 to 2009. J Neurol Neurosurg Psychiatry, Jan 84(1):54–61. doi:10.1136/jnnp-2011-301763

Blümcke I, Wiestler OD (2002) Gangliogliomas: an intriguing tumor entity associated with focal epilepsies. J Neuropathol Exp Neurol 61:575–584

Blümcke I, Giencke K, Wardelmann E et al (1999) The CD34 epitope is expressed in neoplastic and malformative lesions associated with chronic, focal epilepsies. Acta Neuropathol 97:481–490

Campos AR, Clusmann H, von Lehe M, Niehusmann P, Becker AJ, Schramm J, Urbach H (2009) Simple and complex dysembryoplastic neuroepithelial tumors (DNT): clinical profile MRI and histopathology. Neuroradiology 51:433–443

Daumas-Duport C, Scheithauer BW, Chodkiewicz JP, Laws ER Jr, Vedrenne C (1988) Dysembryoplastic neuroepithelial tumor: a surgically curable tumor of young patients with intractable partial seizures. Report of 39 cases. Neurosurgery 23:545–556

Daumas-Duport C, Pietsch T, Lantos PL (2000) Dysembryoplastic neuroepithelial tumour. In: Kleihues P, Cavenee K(eds) Pathology and genetic of tumours of the nervous system. IARC press, Lyon

Lellouch-Tubiana A, Boddaert N, Bourgeois M, Fohlen M, Jouvet A, Delalande O, Seidenwurm D, Brunelle F, Saint-Rose C (2005) Angiocentric neuroepithelial tumor (ANET): a new Epilepsy-related clinicopathological entity with distinctive MRI. Brain Pathol 15:281–286

Louis DN, Ohgaki H, Wiestler OD, Cavenee WK, Burger PC, Jouvet A, Scheithauer BW, Kleihues P (2007) The 2007 WHO classification of tumours of the central nervous system. Acta Neuropathol 114:97–109

Luyken C, Blümcke I, Fimmers R, Urbach H, Wiestler OD, Schramm J (2003) The spectrum of long-term epilepsy associated

tumors: long-term seizure and tumor outcome and neurosurgical aspects. Epilepsia 44:822–830

Luyken C, Blümcke I, Fimmers R, Urbach H, Wiestler OD, Schramm J (2004) Supratentorial gangliogliomas. Histopathological grading and tumor recurrence in 184 patients with a median follow-up of eight years. Cancer 101:146–155

Majores M, Niehusmann P, von Lehe M, Blümcke I, Urbach H (2007) Angiocentric neuroepithelial tumour mimicking Ammon's horn sclerosis. Clin Neuropathol 26:311–316

Majores M, von Lehe M, Fassunke J, Schramm J, Becker AJ, Simon M (2008) Tumor recurrence and malignant progression of gangliogliomas. Cancer 113:3355–3363

Okamoto Y, Di Patre PL, Burkhard C, Horstmann S, Jourde B, Fahey M, Schüler D, Probst-Hensch NM, Yasargil MG, Yonekawa Y, Lütolf UM, Kleihues P, Ohgaki H (2004) Population-based study on incidence, survival rates, and genetic alterations of low-grade diffuse astrocytomas and oligodendrogliomas. Acta Neuropathol 108(1):49–56

Perkins OC (1926) Gangliogliomas. Arch Pathol Lab Med 2:11–17

Provenzale JM, Ali U, Barboriak DP, Kallmes DF, Delong DM, McLendon RE (2000) Comparison of patient age with MR imaging features of gangliogliomas. Am J Roentgenol 174:859–862

Rumana CS, Valadka AB, Contant CF (1999) Prognostic factors in supratentorial ganglioglioma. Acta Neurochir (Wien) 141:63–69

Shakur SF, McGirt MJ, Johnson MW, Burger PC, Ahn E, Carson BS, Jallo GI (2009) Angiocentric glioma: a case series. J Neurosurg Pediatr 3:197–202

Wang M, Tijan T, Rojiani AM, Bodhireddy SR, Prayson RA, Iacuone JJ, Alles AJ, Donahue DJ, Hessler RB, Kim JH, Haas M, Rosenblum MK, Burger PC (2005) Monomorphous angiocentric glioma: a distinctive epileptogenic neoplasm with features of infiltrating astrocytoma and ependymoma. J Neuropathol Exp Neurol 64:875–881

Zentner J, Wolf HK, Ostertun B, Hufnagel A, Campos MG, Solymosi L, Schramm J (1994) Gangliogliomas: clinical, radiological and histopathological findings in 51 patients. J Neurol Neurosurg Psychiatry 57:1497–1502

Malformations of Cortical Development

Horst Urbach and Susanne Greschus

Contents

Abstract

Malformations of cortical development are arranged in different ways. Recently, the ILAE published a consensus classification incorporating pathological, imaging, and genetic findings (Blümcke et al. 2011). Some lesions

H. Urbach (✉)
Department of Neuroradiology,
University Hospital Freiburg, Germany
e-mail: horst.urbach@uniklinik-freiburg.de

S. Greschus
Deptartment of Radiology/Neuroradiology,
University of Bonn, Bonn, Germany

H. Urbach (ed.), *MRI in Epilepsy*, Medical Radiology. Diagnostic Imaging,
DOI: 10.1007/174_2012_749, © Springer-Verlag Berlin Heidelberg 2013

(namely FCD 2B) from this classification are clearly visible on MRI and pathologically classified with a high concordance between different pathologists. If they are fully resected, seizure freedom rate is > 80 %. Other lesions (namely FCD 1) are more difficult to detect or "unvisible" even with voxel-based MRI analyses and harbored with a high interrater-variability between different pathologists. Chance of postsurgical seizure freedom is distinctly < 50 %. A patient will likely benefit from surgery if a distinct MRI lesion is found underlining the importance of high-quality MRI acquisition and interpretation.

Definition. Cortical development can be disturbed at different time points and due to different causes. Resulting lesions are summarized under the umbrella term *malformations of cortical development* (*MCD*). The term *cortical dysplasia* refers to a MCD subtype, where the abnormality is strictly or largely intracortical (Palmini et al. 2004). Depending on whether MCD are arranged from a genetic and imaging (Table 1) or a histopathological (Table 2) perspective, different classifications result.

Development of the Cerebral Cortex: The exact mechanisms of cortical development are still being elucidated; a simplified description is as follows. Between week 4 and 6 of gestation neurons deriving from the epithelium of the neural tube start to proliferate in the medial and caudal ganglionic eminences, and the dorsal (pallial) ventricular zone (Barkovich et al. 2012). After their final mitotic division they dislocate from other elements in the ventricular zone and migrate tangentially (from the medial ganglionic eminences) or radially (from the dorsal ventricular zone), the latter along radial glial fibers with close apposition to their membrane surfaces. Migration in the human brain begins around the sixth gestational week and tapers down by midgestation. Full radial glial fibers span the distance from the ventricular zone to the later cortical plate as shown by glial fiber acid protein (GFAP) staining at week 12 of gestation (Friede 1989). After the migration of cortical neurons has been completed, radial glial scaffolding disappears as some of these glial cells degenerate, and others re-enter the mitotic cycle and transform into astrocytes (Rakic 1988).

Initially, at week 6–8 of gestation, a three-layered structure with a ventricular zone, an intermediate zone, and a marginal zone is visible. At week 10–11 of gestation a transient structure, the preplate, splits into an inner portion designated as the subplate, and an outer portion, the cortical plate. The subplate eventually disappears by term birth. The cortical plate transforms into the cortex in this way, that—with the exception of layer I—later migrating neurons bypass previously migrated neurons and settle in peripheral cortical layers (inside–outside pattern). Finally, a six-layered cortex is created with the outer layer I representing the molecular layer, and inner cortex layers II–VI developing from the former preplate.

1 Microcephalies

1.1 Definition

A head is microcephalic when the occipital-frontal circumference is <2 standard deviations than the mean for age and gender. If it is <3 standard deviations, it may be called extreme microcephaly (Ashwal et al. 2009). Microcephaly is often associated with a simplified gyral pattern and a reduced depth of the sulci. The cortex can be of normal thickness or thicker than normal. If the gyral pattern is simplified and the cortex is thicker than normal, microcephaly may be referred to as microlissencephaly (Barkovich et al. 1996, 1998; Dobyns and Barkovich 1999; Ashwal et al. 2009; Adachi et al. 2011) (Fig. 1).

1.2 Epidemiology

The incidence of microcephaly is around 1 % and of extreme microcephaly around 0.1 % in the general population (Ashwal et al. 2009).

1.3 Pathogenesis

Microcephalies and microlissencephalies can be isolated or part of a syndrome. Syndromic microcephalies comprise among others trisomy 21, 13, 18, Angelman syndrome, Rett syndrome, MEHMO syndrome, Mowat–Wison syndrome, 4p deletion (Wolf–Hirschhorn), 5p deletion (cri-du-chat), 7q11.23 deletion (Williams), 22q11 deletion (velocardiofacial), Cornelia de Lange, Smith–Lemli–Opitz, and Seckel syndrome (Ashwal et al. 2009) (Figs. 2, 3, 4).

Microcephalies can be divided into primary and secondary forms. Primary microcephalies have a known or presumed genetic cause resulting in a reduced neuronal and glial cell proliferation or an increased apoptosis (Shen et al. 2010). The Online Mendelian Inheritance in Man (OMIM) database lists more than 500 genetic syndromes associated with microcephalies (http://www.ncbi.nlm.nih.gov/omim), some of the more common primary microcephalies are mentioned here: autosomal-recessive microcephalies in patients with a normal or slightly short status and only mild developmental delay comprise mutations of the *MCPH1* gene (Jackson 2002), of the *ASPM* gene on chromosome 1q31 (Bond et al. 2002, 2003), of the *CDK5RAP2* gene on chromosome 9q34

Table 1 Imaging and genetic classification according to Barkovich [modified from Barkovich et al. (2012), with permission]

Disturbance of neuronal and glial proliferation or apoptosis	
1. Congenital microcephaly (premigrational proliferation ↓/apoptosis ↑)	(a) Microcephaly with severe intrauterine growth deficiency and short stature (b) Microcephaly with variable short stature (severe intrauterine growth deficiency to mildly short), moderate to severe (c) Microcephaly with mildly short stature or normal growth, mild to moderate developmental delay, normal to thin cortex, with or without simplified gyral pattern, with or without callosal hypogenesis, and with or without periventricular nodular heterotopia (d) Microcephaly with mildly short stature or normal growth, severe developmental delay, variable cortical development with simplified gyral pattern or cortical dysgenesis, and with or without callosal hypogenesis (e) Microcephaly with variable anomalies and less well characterized syndromes (with or without simplified gyral pattern, with or without callosal hypogenesis, and with or without cerebellar hypoplasia) (f) Microcephaly with severe developmental delay and evidence of degeneration, with or without simplified gyral pattern, with or without enlarged extra-axial spaces, with or without callosal hypogenesis, and with or without atypical cortical dysgenesis (g) Microcephaly with lissencephaly (cortex thick or relatively thick, smooth gray–white matter border) (h) Microcephaly with brain volume loss and enlarged ventricles (hydrocephalus ex vacuo or hydranencephaly), with or without cortical dysgenesis, and with or without callosal hypogenesis
2. Megalencephaly	(a) Megalencephaly with normal cortex (or presumed normal cortex) (b) Megalencephaly with periventricular nodular heterotopia (c) Megalencephaly with polymicrogyria and other cortical dysgenesis
3. Malformations due to abnormal cell proliferation	(a) Cortical hamartomas of tuberous sclerosis complex (TSC) (b) Focal cortical dysplasia (FCD) with balloon cells (c) Hemimegalencephaly
Disturbance of neuronal migration	
1. Malformations with neuroependymal abnormalities: Periventricular heterotopia	(a) Anterior predominant and diffuse periventricular nodular heterotopia (b) Posterior predominant (temporal-trigonal or infrasylvian) periventricular nodular heterotopia (c) Periventricular heterotopia, not nodular (uni- or bilateral)
2. Malformations due to generalized abnormal transmantle migration (radial and nonradial)	(a) Anterior predominant or diffuse classic (four-layered) lissencephaly and subcortical band heterotopia (b) Posterior predominant or diffuse classic (four-layered) and two-layered (without cell sparse zone) lissencephaly and subcortical band heterotopia (c) X-linked lissencephaly (three-layered, without cell sparse zone) with callosal agenesis, ambiguous genitalia (d) Reelin-type lissencephaly (inverted cortical lamination, without cell sparse zone) (e) Variant lissencephaly
3. Malformations presumably due to localized abnormal late radial or tangential transmantle migration	(a) Subcortical heterotopia (clinically defined with unknown cause) (b) Sublobar dysplasia (clinically defined with unknown cause)
4. Malformations due to abnormal terminal migration and defects in pial limiting membrane	(a) Dystroglycan-laminin complex abnormalities with cobblestone malformation complex, with or without congenital muscular dystrophy (Walker–Warburg syndrome, muscle–eye–brain disease, Fukuyama congenital muscular dystrophy, congenital muscular dystrophy with cerebellar hypoplasia) (b) Cobblestone malformations in congenital disorders of glycolysation (c) Cobblestone malformations with no known glycolysation defect (d) Other syndromes with cortical dysgenesis and marginal glioneuronal heterotopia, but with normal cell types

(continued)

Table 1 (continued)

Disturbance of neuronal and glial proliferation or apoptosis	
Disturbance of cortical organization	
1. Malformations with polymicrogyria or cortical malformations resembling polymicrogyria	(a) Polymicrogyria with transmantle clefts (schizencephaly) or calcification (b) Polymicrogyria without transmantle clefts or calcification, classified by location (c) Syndromes with polymicrogyria
2. Cortical dysgenesis secondary to inborn errors of metabolism	(a) Mitochondrial and pyruvate metabolic disorders (b) Peroxisomal disorders
3. Focal cortical dysplasia (FCD) without dysmorphic neurons, due to late developmental disturbances	
4. Postmigrational developmental microcephaly (birth occipito-frontal diameter (OFD)—3 SD or lower, later OFD-4 SD, no evidence of brain injury)	

Classification considers normal cortical development as separated into three overlapping steps and distinguishes malformations caused by disturbed neuronal/glial proliferation and apoptosis (Step 1), neuronal migration (Step 2), and cortical organization (Step 3). The classification scheme has been continuously updated, incorporating new genetic findings, and is considered to be a framework but not a finalized classification (Barkovich et al. 1996, 2001, 2005, 2012)

Table 2 Neuropathologic classification according to Palmini and Lüders and Blümcke et al. [adapted from Palmini and Lüders (2002), Palmini et al. (2004), and Blümcke et al. (2011)]

Palmini type	Blümcke type	Neuropathological description	MRI
Mild malformations of cortical development type 1 = ectopic neurons in or adjacent to cortical layer 1		Molecular layer neurons Persistent subpial granular layer Marginal glioneuronal heterotopia	Normal
Mild malformations of cortical development type 2 = neuronal heterotopia outside layer 1		Small aggregates of heterotopic white matter neurons Dysgenesis of the hippocampal formation	Normal or Gray–white matter demarcation loss
FCD type 1A, 1B = cytoarchitectural abnormalities without dysmorphic neurons or balloon cells	FCD type 1a FCD type 1b FCD type 1c	A: dyslamination only B: dyslamination and hypertrophic or immature neurons a: microcolumnar (vertical) dyslamination b: radial dyslamination c: vertical and radial dyslamination	Normal (1/3 of cases) or Gray–white matter demarcation loss
FCD type 2A, 2B = cytoarchitectural abnormalities with dysmorphic neurons or balloon cells	FCD type 2A, 2B = cytoarchitectural abnormalities with dysmorphic neurons or balloon cells	A: dysmorphic neurons B: dysmorphic neurons and balloon cells	A: cortical thickening, abnormal depth of sulcus B: cortical thickening, abnormal depth of sulcus, subcortical funnel-shaped hyperintensity

Classification considers histopathological cell types and cortical lamination. It distinguishes normal neurons in an abnormal location and distribution; hypertrophic, immature, and dysplastic neurons; as well as balloon cells. Recent ILAE classification introduces a Focal cortical dysplasia (FCD) type III, in which mild and FCD type I malformations are associated with hippocampal sclerosis (FCD IIIa), tumors (FCD IIIb), vascular malformations (FCD IIIc), or other principal lesions acquired during early life (FCD IIId)

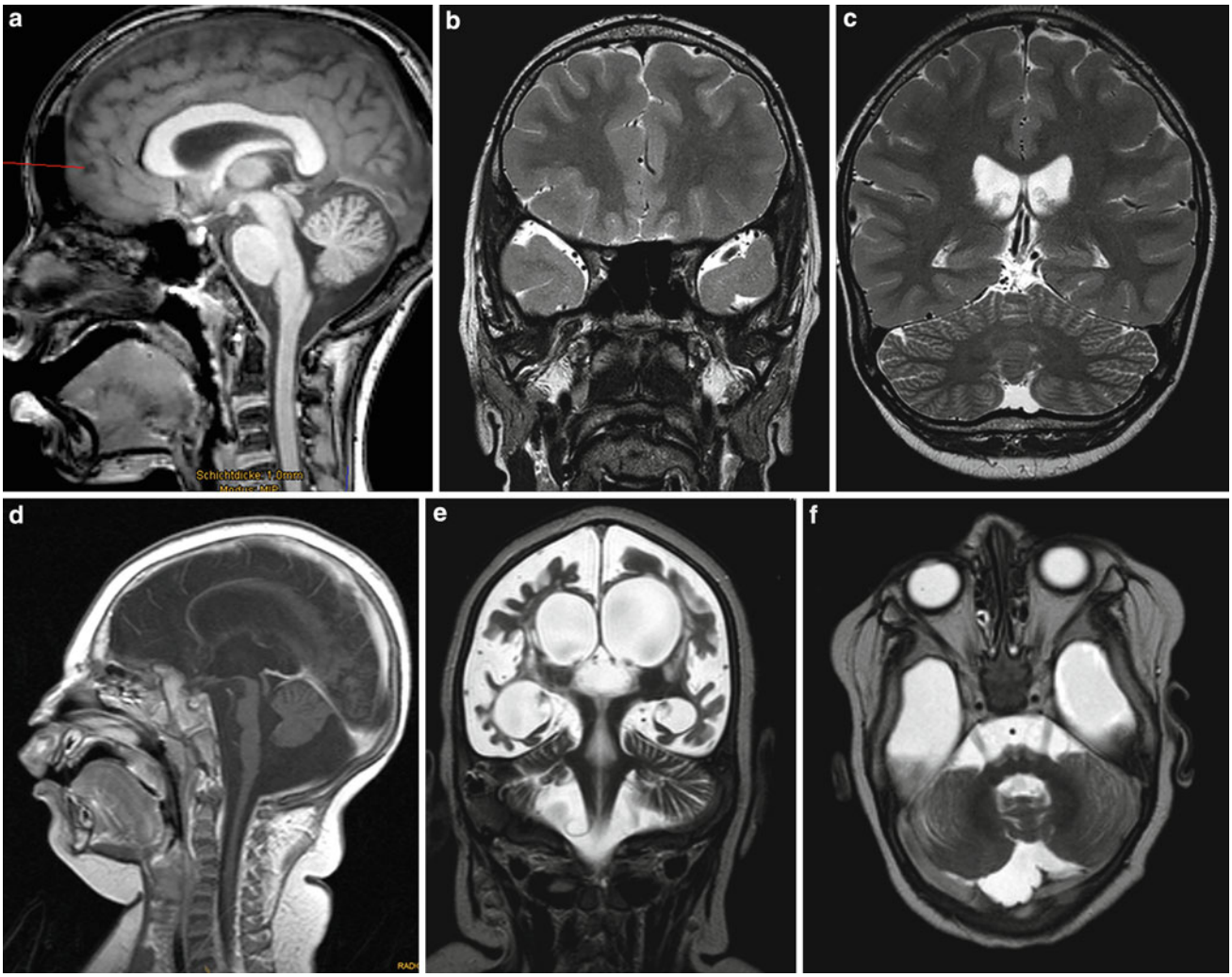

Fig. 1 Moderate microcephaly in a 11 year old boy with psychomotor developmental delay (**a–c**) and extreme microcephaly in a 16 months year old girl with hypotonia at birth, abnormal neonatal reflexes, and myoclonic seizures starting in the first days of life (**d–f**). In the *upper row*, the head is too small, the brain has too little gyri, and the depth of the sulci is lower than normal. In the *lower row*, the head is far too small, the subarachnoid space is extremely widened, the cortex is thin, the depth of the sulci is distinctly lower than normal, and the brain stem and to a lesser degree the cerebellum are hypoplastic

(Bond et al. 2002, 2003; Pattison et al. 2000) and of the *CENPJ* gene on chromosome 13q12.2 (Bond et al. 2005). Autosomal-recessive microcephalies in severely impaired patients include Amish lethal microcephaly with a *SLC25A19* mutation on chromosome 17q25.3 and 2-ketoglutaric aciduria (Rosenberg et al. 2002) and microcephaly with periventricular heterotopia and an *ARGEF2* mutation on chromosome 20q13.13 (Sheen et al. 2004).

Secondary microcephalies have a nongenetic cause and result from ante- and postnatal injuries affecting the fetus or infant's normal brain growth. Typical nongenetic causes are maternal TORCH and HIV infections, hypoxic-ischemic encephalopathies, fetal alcohol syndrome, maternal radiation or toxin exposure, metabolic disorders, and nonaccidental brain injuries.

1.4 Clinical Presentation

Microcephalic newborns typically have severe neurological deficits and seizures. However, the clinical phenotype is variable and ranges from mild to severe developmental delay.

In children with secondary microcephalies, the head can have a normal size at birth, but subsequently fails to grow whereas the face continues to develop, producing a child with a small head and a receding forehead. Development of motor functions and speech is delayed. Hyperactivity, mental retardation, and epileptic seizures are common. Motor ability varies, ranging from clumsiness in some to spastic quadriplegia in others.

The overall prevalence of epileptic seizures in microcephalic patients is around 40 %. Seizures are often refractory

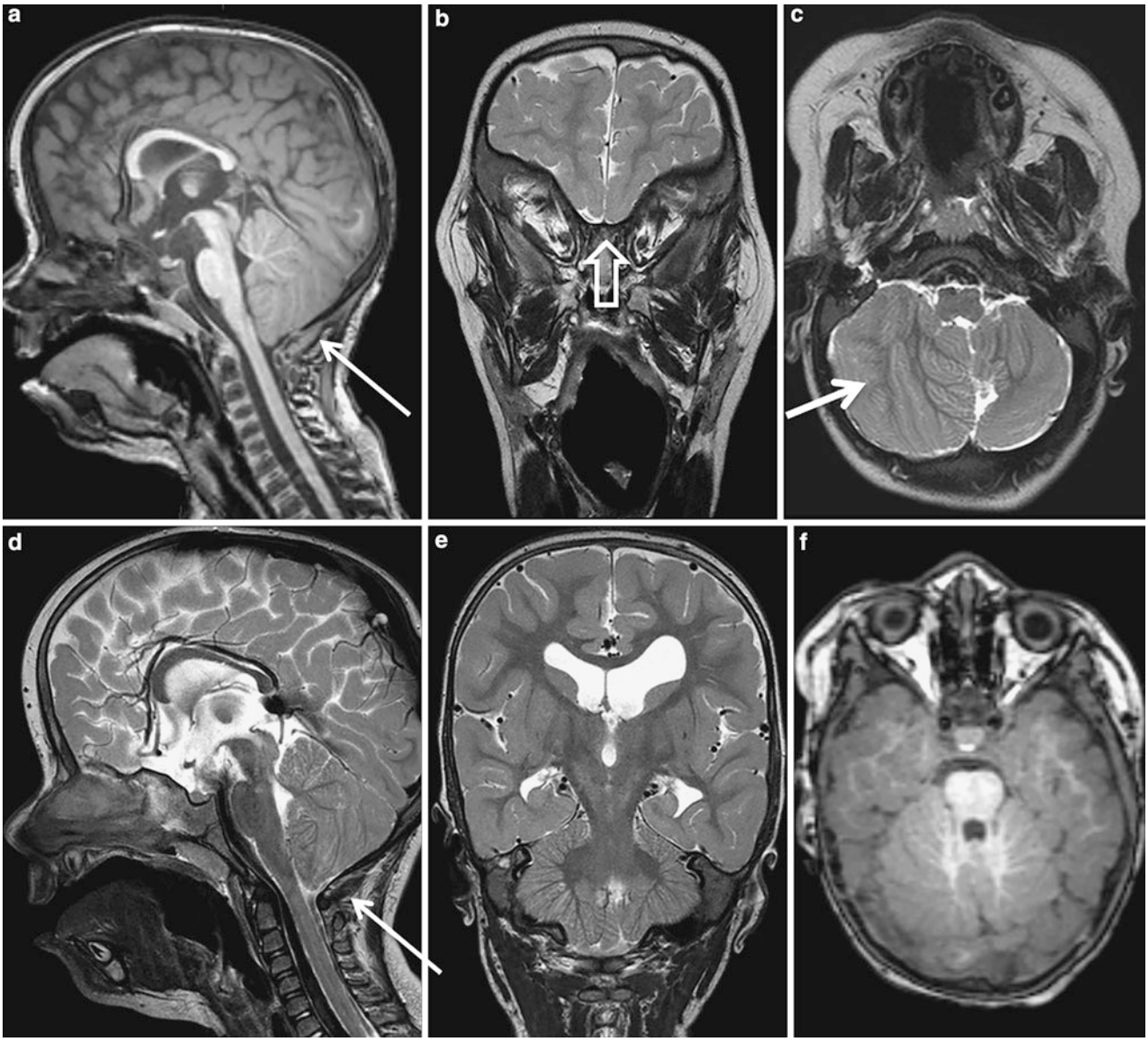

Fig. 2 Patau syndrome (trisomy 13) in a 18 months old boy with generalized tonic-clonic seizures. The boy shows moderate microcephaly, the cortex is of normal thickness and the sulci are of normal depth. Note the disproportionate size of the posterior fossa (**a**, **c**–**d**: *arrow*, **e**–**f**), cerebellar dysplasia (**c**: *thick arrow*), hypogenetic corpus callosum, small ocular globes, malrotated hipoocampi, (**e**), and olfactory bulb hypoplasia (**b**: *hollow arrow*)

to medical treatment and more common in secondary than in primary forms (Ashwal et al. 2009).

1.5 Imaging

A microcephalic head may be missed if the child is not inspected and the technician adapts the field of view to the child's head size. However, considering the cranio–facial ratio and the ratios between hindbrain and forebrain on a midsagittal T1-weighted image should guide the MRI reader to the correct diagnosis. The cranio–facial ratio relates the size of the intracranial structures to the size of the face. The ratio is normally large at birth and slowly diminishes with increasing age. It is typically small in microcephalic patients. Hindbrain and forebrain structures can be proportional to each other, however, in many cases cerebellum and brain stem are disproportionally large (Adachi et al. 2011).

The size of the forebrain correlates with (1) the gryal pattern: severe microcephalic brains typically have an extremely simplified gyral pattern (Adachi et al. 2011). It also correlates with (2) the white matter volume, and (3) associated callosal anomalies. In most patients, the corpus callosum is hypoplastic (thin, but all parts are formed); in

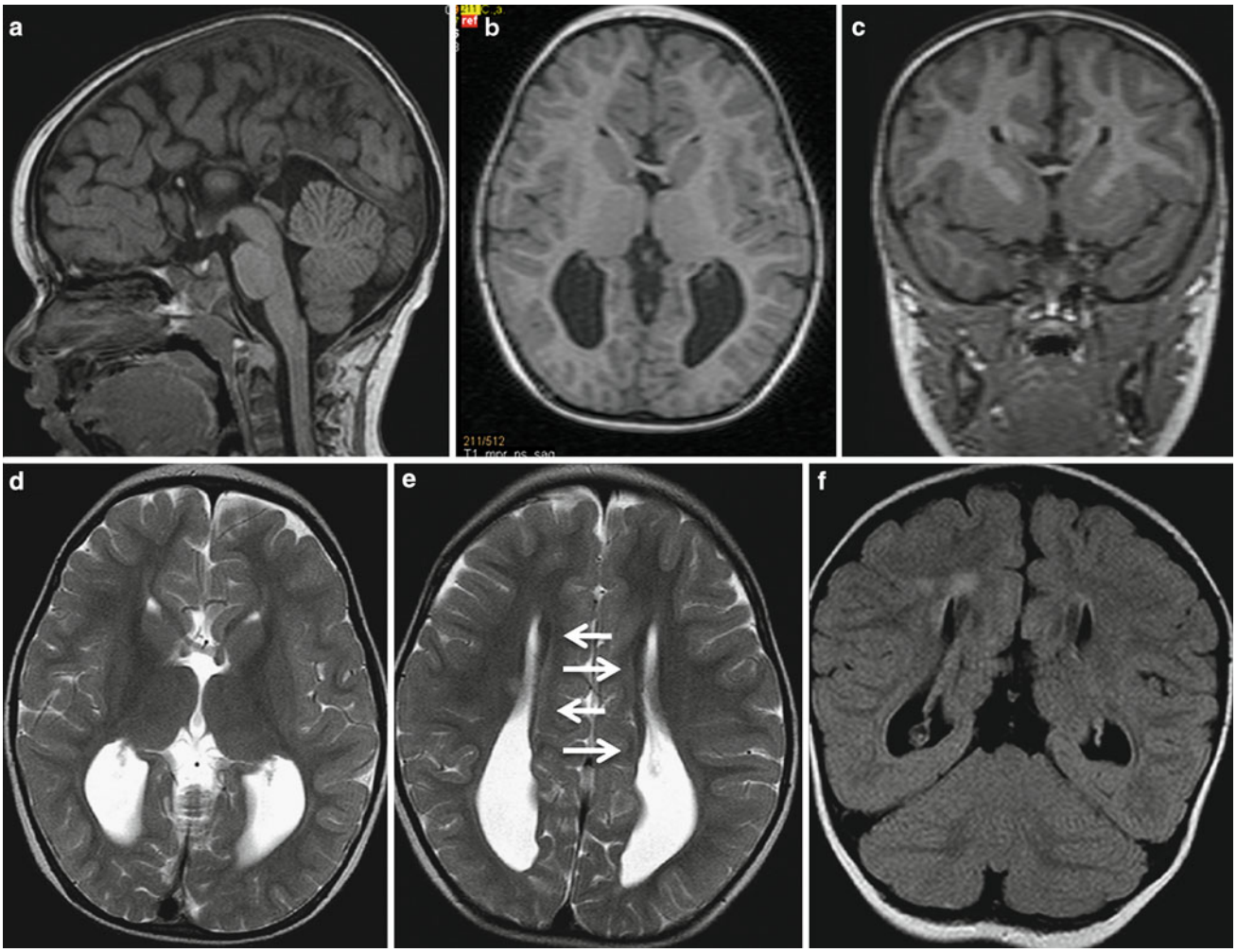

Fig. 3 A 2 year old girl presented with seizures since the age of 2 months. Mowat-Wilson syndrome, a complex developmental disorder with microcephaly, mental retardation, distinct facial features, and with or without Hirschsprung disease was genetically proven. Microcephaly can be suspected considering the ratio between posterior fossa and supratentorial structures (**a**). However, complete corpus callosum agenesis is the most striking MRI finding (**a**–**f**). See the lateral callosal bundles of Probst as hypointense stripes on T2-weighted images running parallel to the interhemispheric fissure and indenting the medial walls of the lateral ventricles (**e**: *arrows*)

some patients it is hypo- or agenetic. Heterotopia may be present or absent (Fig. 4).

2 Lissencephaly Type 1, Subcortical Band Heterotopia

2.1 Definition

Lissencephaly means smooth brain ($\lambda\iota\sigma\sigma o\varsigma$ = smooth); affected brains may be without convolutions (agyria) or with broad and shallow convolutions (pachygyria). Lissencephalies have been traditionally divided into two distinct forms: type 1 (also known as classic) lissencephalies and type 2 (also known as cobblestone) lissencephalies, the latter caused by defective protein glycolisation. Recent genetic and pathologic findings have questioned this two-tiered classification and suggest at least four different lissencephaly types (Barkovich et al. 2012; Forman et al. 2005).

2.2 Pathogenesis and Pathology

Type I lissencephaly is a neuronal migration disorder with at least six causative genes (*LIS1, DCX, RELN, ARX, TUBA1A*, *VLDLR*) and one modifier gene (*YWHAE*) identified (Dobyns 2010). Moreover, intrauterine infections (particularly CMV) and toxins may cause type I lissencephaly.

Recently, four distinct histopathological subtypes have been described (Forman et al. 2005):

1. Four-layered cortex consisting of an outermost molecular layer (layer 1), a band of pyramidal neurons (layer 2),

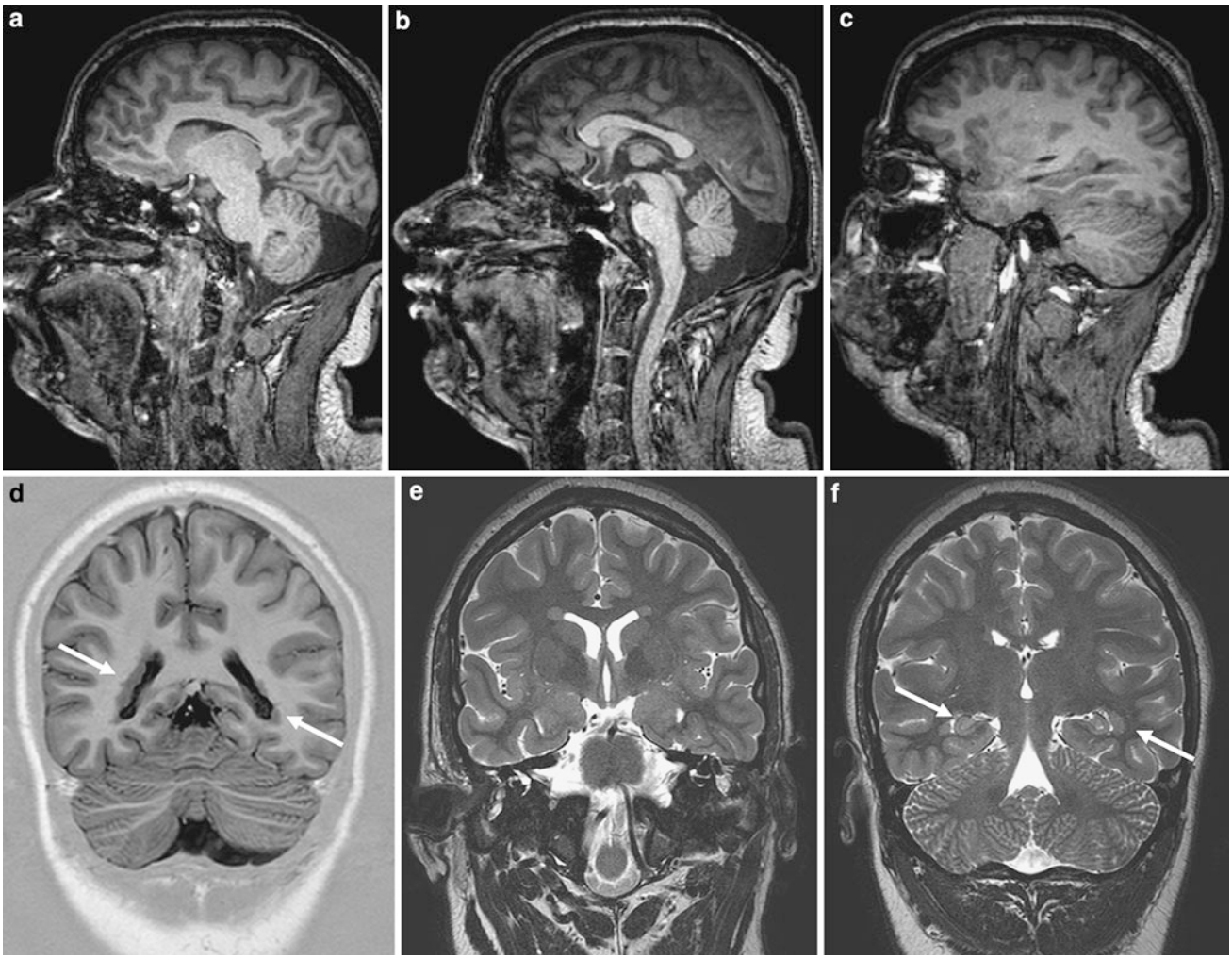

Fig. 4 A 20 year old boy with microcephaly, micrognathy, and short status suggestive of a Seckel syndrome suffered from complex focal and generalized seizures since the age of 10. Note that microcephaly is best visible on sagittal images considering the relative sizes of the face and the brain (**a**–**c**). This boy also showed bilateral periventricular nodular heterotopia (**d**–**f**: *arrows*)

a sparsely cellular myelinated layer (layer 3), and a broad band of disorganized neurons (layer 4)
2. Four-layered cortex similar to that in 1, but with a transition from the lissencephalic cortex to multiple nodules of subcortical heterotopia
3. Three-layered cortex without a hypomyelinated cell sparse zone
4. Two-layered cortex (Forman et al. 2005).

These histopathological subytpes also differ from each other by the type and severity of posterior fossa abnormalities (Forman et al. 2005; Jissendi-Tchofo et al. 2009) (Table 3).

2.3 Clinical Presentation

Children with type 1 lissencephalies typically present with neurological deficits in the first weeks or months consisting of poor feeding, hypotonia, and abnormal arching behavior or opisthotonus (Dobyns 2010). Nearly all have onset of seizures during the first year of life, often consisting of infantile spasms, Lennox–Gastaut syndrome, and others. Apart from epilepsy, major medical problems result from feeding problems including gastroesophageal reflux and recurrent aspiration and pneumonia (Dobyns 2010).

Isolated lissencephaly (ILS) occurs in patients with mutations of the *LIS1, DCX,* or *TUBA1A* genes. Onset of epilepsy is usually between 3 and 12 months, but may be later. Mortality exceeds 50 % by 10 years and few children live longer than 20 years (Dobyns 2010).

Children with Miller–Dieker syndrome (chromosome 17p13(.3) deletions affecting *LIS1* and several adjacent genes), most types of LIS with cerebellar hypoplasia (LCH), or X-linked lissencephaly with abnormal genitalia (XLAG) have an even more severe course and higher mortality rate (Ross et al. 2001).

Table 3 Involved genes, type 1 lissencephaly subtypes, characteristic MRI and neuropathological features

Gene mutation	Lissencephaly type 1 subtype	MRI	Neuropathology
LIS1	Isolated lissencephaly (ILIS)	Agyria/pachygyria in parietal and occipital > frontal lobes Cell sparse zone between a thin outer layer cortex and a thick inner layer of gray matter	Four-layered cortex, predominantly posterior, normal three-layered cerebellar cortex, normal to small pons
17p13.3 deletions → *LIS1* + other genes	Miller–Dieker syndrome (severe lissencephaly + facial features)	s.a.	s.a.
Xq22.3-q23 → *DCX*	– in ♂: ILIS – in ♀: SBH	Frontal > parietal and occipital lobes Cell sparse zone between a thin outer layer cortex and a thick inner layer of gray matter	Four-layered cortex, predominantly anterior, transition from the lissencephalic cortex to multiple nodules of subcortical heterotopia, normal three-layered cerebellar cortex, normal to small pons
TUBA1A	– ILIS – Lissencephaly with cerebellar hypoplasia ± corpus callosum agenesis (LCH ± CCA) – LIS-CCA	ILIS: Parietal and occipital > frontal lobes LCH ± CCA: posterior frontal, parietal, and occipital > anterior frontal lobes LIS-CCA: posterior frontal lobes	No horizontal or radial organization
RELN, VLDLR	lissencephaly with cerebellar hyoplasia (LCH) mild frontal	Mild frontal accentuation Decreased hippocampal rotation No cell sparse zone	Dysorganized cortex (cortex layers 1-6-5-4-3-2)
ARX	X-linked lissencephaly with abnormal genitalia (XLAG)	Posterior agyria, CCA Small dysplastic basal ganglia	Three-layered cortex, small pons
No known genetic defect			Two-layered cortex Brainstem and cerebellar abnormalities (disorganization, white matter heterotopia, hypoplasia)

CCA corpus callosum agenesis

Lissencephaly occurs in males with mutations of the X-linked gene Doublecortin (*DCX*) whereas hemizygous females with the same mutations exhibit subcortical band heterotopia (SBH) with a rather normal cortical surface and an additional subcortical gray matter band. Although males with *DCX* mutations are usually severely disabled, females with SBH show variable intellectual abnormalities and epileptic seizures correlating with the thickness of the subcortical band. However, less severe (mosaic or missense) mutations of the *LIS1* or the *DCX* gene can cause SBH even in males (Sicca et al. 2003; Tampieri et al. 1993; Pilz et al. 1998, 1999).

In around 50 % of mostly female patients who have drug-resistant seizures, some intellectual impairment, and different grades of pachygyria on MRI, the underlying genetic defect is never clarified (Fig. 6).

2.4 Imaging

On MRI, the brain surface appears smooth with areas of absent (agyria) and abnormally wide gyri (pachygyria). The cortex is abnormally thick (Fig. 5). Common associated malformations include rounded hippocampi, enlarged posterior portions of the lateral ventricles, flat anterior portion of the corpus callosum, and very variable hypoplasia of the cerebellum, especially the midline vermis (Dobyns 2010).

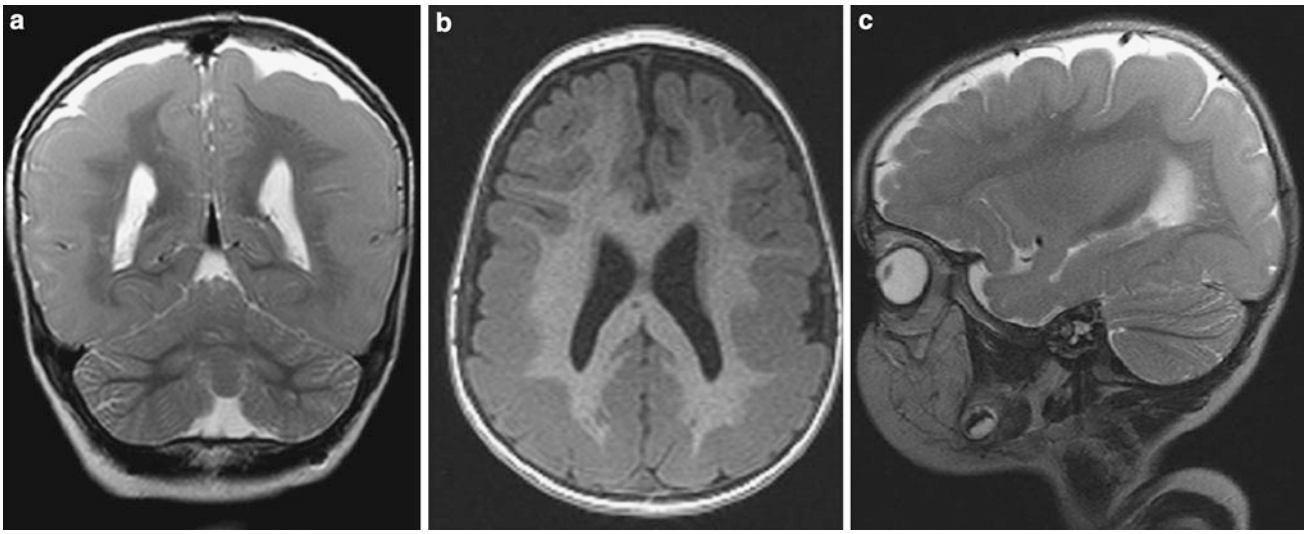

Fig. 5 Type I lissencephaly with "posterior" accentuation suggesting a *LIS1* gene mutation. This 17 months year old girl showed global developmental delay and suffered from generalized seizures since the age of 8 months

In SBH, the brain surface appears superficially normal, except that the sulci between gyri are shallow, and the cortex is normal and not thick (Barkovich et al. 1994; Dobyns et al. 1996). Just beneath the cortex, often separated from it by just a few millimeters of white matter, lies a smooth band of neurons that never reached the true cortex. This band has a variable thickness and thin bands are easily overlooked but highlighted by voxel-based morphometric analysis (Fig. 7) (Huppertz et al. 2008).

The spectrum of LIS and SBH varies from complete or nearly complete absence of cerebral convolutions or agyria (grades 1 and 2) to abnormally wide convolutions or pachygyria (grade 4) to normal convolutions separated by shallow sulci overlying SBH (grade 6). Intermediate grades consist of mixed agyria–pachygyria (grade 3) and mixed pachygyria–SBH (grade 5) (Dobyns 2010).

Paucity of cerebral gyri often shows a gradient, which is useful in determining the most likely genetic cause. If lissencephaly and SBH are pronounced in the anterior frontal lobes, a *DCX* mutation should be considered. More severe changes in the parietal and occipital lobes point to *LIS1* or *TUB1A* mutations. Lissencephaly with cerebellar hypoplasia point to *RELN* and *VLDLR* mutations, if pronounced in the frontal lobes, and to *TUB1A* mutations, if pronounced in the posterior frontal lobes, perisylvian, or parietal and occipital lobes, repectively. Lissencephaly with corpus callosum agenesis point to *ARX* mutations if agyria or pachygyria is pronounced in the temporal and posterior brain regions.

Most lissencephalies have a genetic cause, however, periventricular and subcortical calcifications suggest an infectious (particularly CMV) cause (Figs. 5-7).

3 Cobblestone Lissencephaly, Congenital Muscular Dystrophies

3.1 Definition

Congenital muscular dystrophy syndromes or so-called dystroglycanopathies represent a heterogeneous group of congenital diseases affecting the muscles and frequently the brain and eyes, which are characterized by defective protein glycolization. Protein glycolization is a complex mechanism, in which sugars (glycans) are attached to proteins modulating their stability, conformity, and function (Barkovich et al. 2005). For example, in the developing brain radial glial cells have end feet attached to the pial basement membrane, and defective basement membrane formation results in cobblestone lissencephaly with neurons migrating too far (e.g., neurons destinated for cortex layers II and III migrate and populate the marginal zone) (Clement et al. 2008).

The clinical spectrum comprises severe [Walker–Warburg syndrome (WWS), Fukuyama congenital muscular dystrophy, muscle–eye–brain disease] and milder forms with or without brain involvement (congenital muscular dystrophy CMD, merosin-deficient congenital muscular dystrophy, merosin-positive congenital muscular dystrophy C1C, merosin-positive congenital muscular dystrophy C1D, limb girdle muscular dystrophies LGMD2I, LGMD2K, LGMD2L, LGMD2M). Several mutations in genes encoding for proteins of the dystrophin glycoprotein complex have been found (protein-O-mannosyl transferase 1 *POMT1*, OMIM 607423; protein-O-mannosyl transferase 2 *POMT2,* OMIM 607439; protein-O-mannose 1,2-*N*-acetylglucosaminyltransferase1

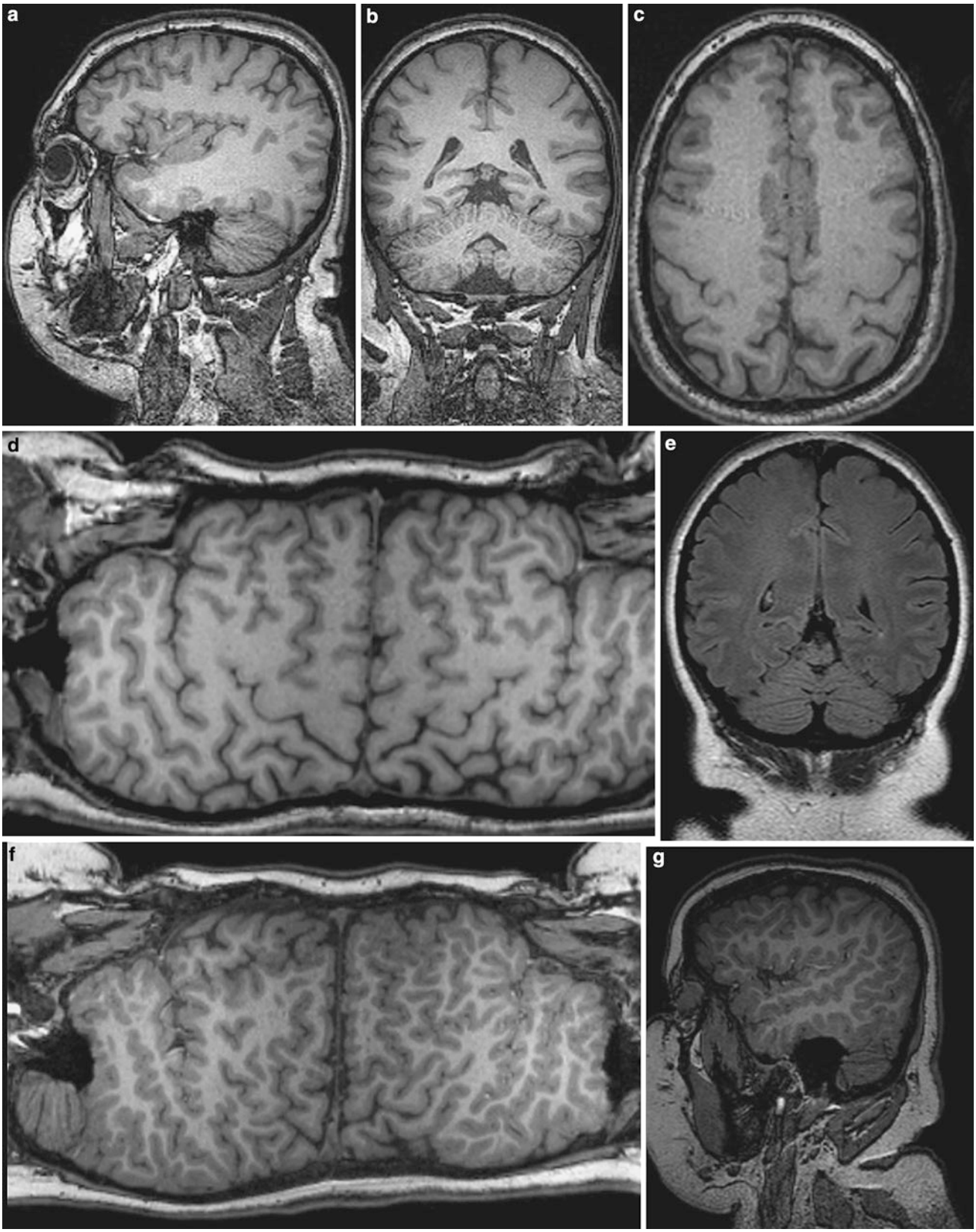

Fig. 6 Pachygyria in a 30 year old woman with epileptic seizures since the age of 7. Note the rather broad and shallow convolutions on sagittal (**a**), coronal (**b**), and axial (**c**) 1 mm thick reformations, on a planar surface view (**d**), and—more difficult to see—on a coronal 3 mm thick FLAIR slice (**e**). In this example, paucity of gyri becomes more obvious if the images are compared to those of a healthy person (**f**, **g**)

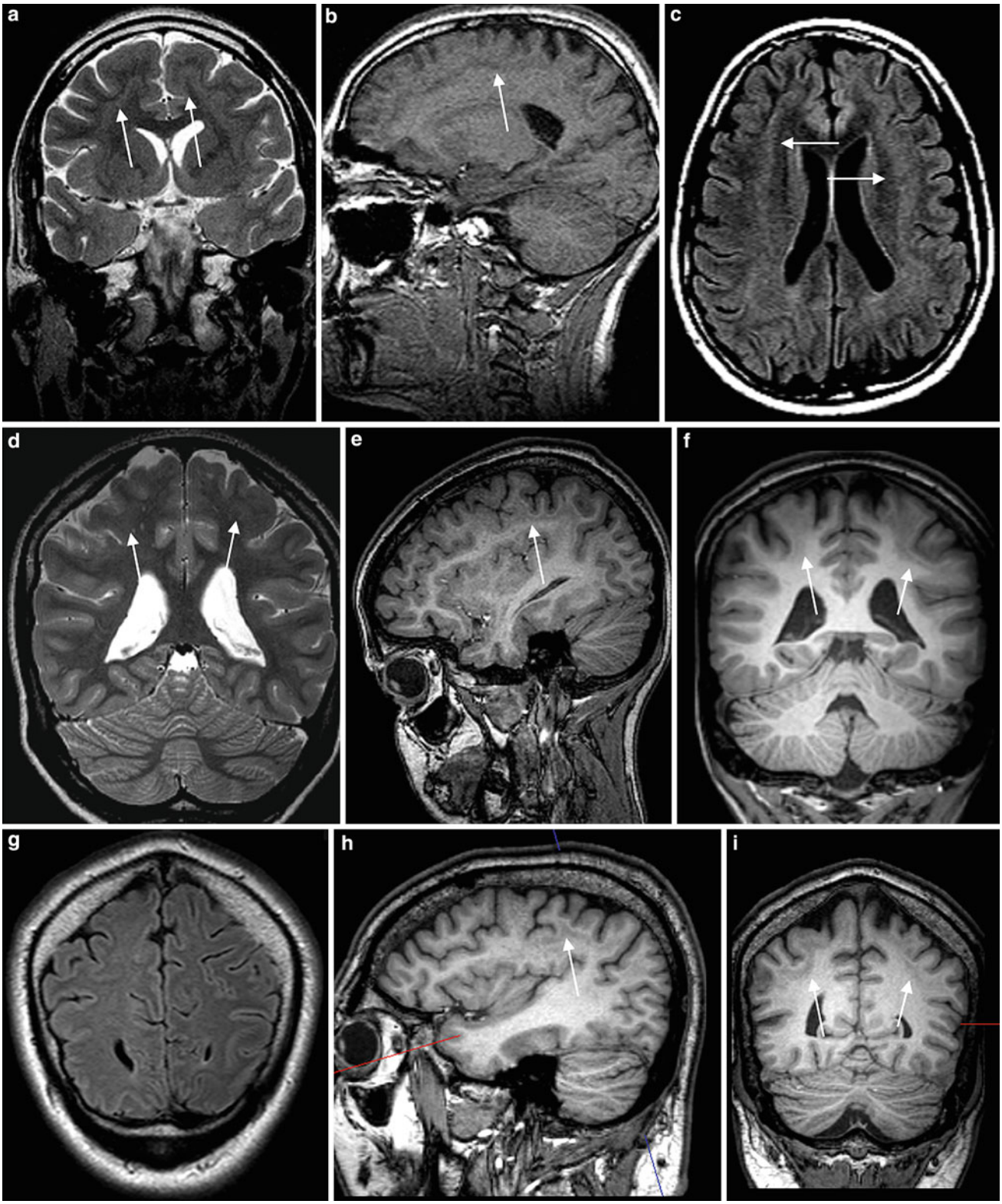

Fig. 7 Subcortical band heterotopia in a 21 year old woman (**a**–**c**), in a 13 year old girl (**d**–**f**), and a 31 year old man (**g**–**i**). Note the different thickness of the subcortical bands (*arrows*). In the lower example, subtle stripes in the parietal lobes are only visible on 1 mm thick T1-weighted gradient echo images (**h**, **i**)

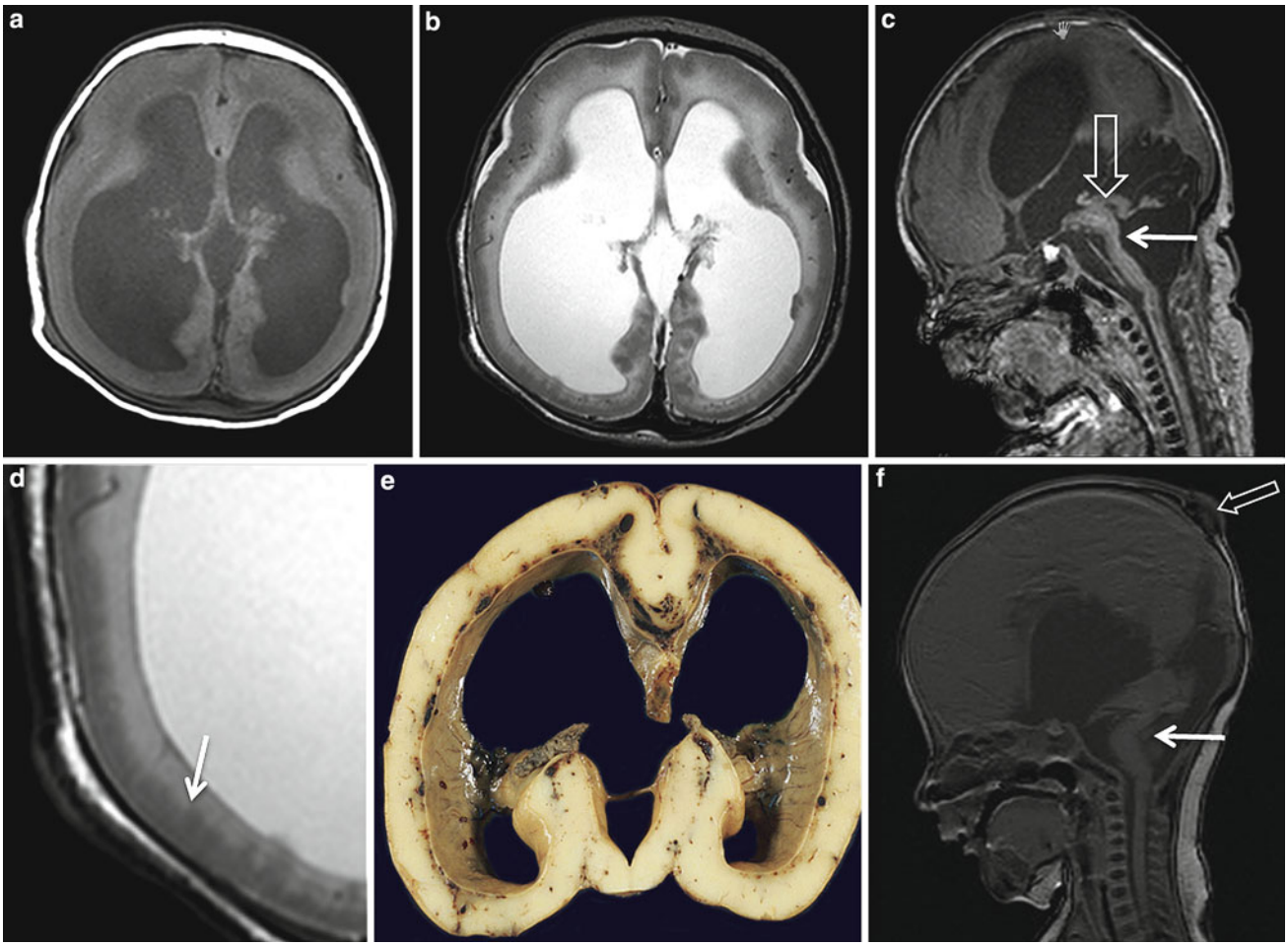

Fig. 8 Cobblestone (type II) lissencephaly in a male new born of consanguine parents with Walker-Warburg syndrome due to *POMT1* mutation (**a**–**d**) and a female with unknown gene defect who died within 36 hours after spontaneous delivery (**e**, **f**). The brain pallium is thin and the surface smooth. A bumpy surface due to overmigrating neurons, which do not stop at the pial basement membrane cannot be resolved macroscopically, (**d**, **e**), however the gray–white matter interface appears bumpy (**d**: *arrow*). Note other characteristic features like Z-form of the hypoplastic brain stem (**c**, **f**), fused inferior and superior colliculi (**c**: *hollow arrow*), parietal meningocele (**f**: *hollow arrow*), vermian dysgenesis, hyperintense white matter, and hydrocephalus

POMGnT1, OMIM 606822; *Fukutin*, OMIM 607440; *Fukutin*-related protein *FKRP*, OMIM 606596; *LARGE*, OMIM 603590). MRI may show different grades of brain involvement, but it is not suited to differentiate between different clinical and genetic diseases.

3.2 Walker–Warburg Syndrome

3.2.1 Epidemiology

This is the most severe congenital muscular dystrophy syndrome. Symptoms and signs are already present at birth, children often die within the first 12 months and rarely live longer than 5 years.

3.2.2 Pathogenesis

Autosomal-recessive inheritance and mutations of the *POMT1* gene on chromsosome 9q34.1 encoding for the enzyme O-methyltransferase 1 of the dystrophin glycoprotein complex are found in 20 % of cases.

3.2.3 Clinical Presentation

This includes profound muscular hypotonia at birth ("floppy newborn"), epileptic seizures, and anterior (cataracts, shallow anterior chamber, microcornea, microphthalmia, lens defects) and posterior eye anomalies (retinal detachment or dysplasia, hypoplasia or atrophy of the optic nerve and macula and coloboma). Glaucoma or buphthalmos may be present, as well as small genitalia in boys, and occasionally cleft lip and palate.

3.2.4 Imaging

Distinct hydrocephalus is shown. The brain surface is smooth; it is either agyric or contains only some broad and shallow gyri. The brain parenchyma consists of a thin band of bumpy gray and hypomyelinated and thus hyperintense white matter. The bumpy surface is explained with the fact that migrating neurons do not stop at the pial basement membrane but migrate too far (cobblestone or type II lissencephaly). Brain segments may also show polymicrogyria. The corpus callosum is thin and extended, inferior and superior colliculi are fused, and the brainstem is hypoplastic with a kinking between the pons and mesencephalon (Z-form). The posterior fossa is small with a vermis dygenesis resembling a Dandy–Walker variant; in some cases there is a posterior meningo- or encephalocele (Fig. 8).

4 Focal Cortical Dysplasias

4.1 Definition

Focal cortical dysplasias are largely or purely intracortical malformations, which are histopathologically divided into two types (Palmini and Lüders 2002; Palmini et al. 2004): FCDs type 1 are so called cytoarchitectural abnormalities without (type 1A according to Palmini) or with giant or immature neurons (type 1B according to Palmini), but without dysmorphic neurons or balloon cells. FCDs type 2 contain dysmorphic neurons (type 2A) or dysmorphic neurons and balloon cells (type 2B).

Recently, Blümcke and the ILAE Diagnostic Methods Commission refined the histopathological classification of FCD type 1 (Blümcke et al. 2011). They now distinguish FCD type 1a with an altered vertical orientation of cortical neurons, FCD type 1b with an altered horizontal orientation, and FCD type 1c with a combination of both features. The border with the subcortical white matter is usually less sharply demarcated due to an increased number of neurons. In addition, cellular abnormalities including immature neurons with a small diameter, hypertrophic pyramidal neurons outside layer 5 or normal neurons with disoriented dendrites can be encountered (Blümcke et al. 2011).

From a histopathological perspective, balloon cells as the histopathological hallmark of FCD type 2B are easily to identify, whereas the discrimination between normal, immature, giant, and dysmorphic neurons as well as assessment of the cortical layering is more difficult. Balloon cells are large round cells with a diameter of 20–90 μm. They have an eccentric nucleus and a pale and eosinophilic cytoplasm in H&E stains (Fig. 2 in "Metallic Implants"). Balloon cells are preferentially located in deeper cortical layers and the subcortical white matter, and reflected with additional hypomyelination as subcortical funnel-shaped FLAIR hyperintensity on MRI (Urbach et al. 2002). It is important to note that balloon cells are pluripotent brain cells with characteristics of both neuronal and glial lineage. They likely fail to differentiate into a specific cell type within the first trimester. Lesions containing balloon cells (FCD type 2B, hemimegalencephaly, tuberous sclerosis complex) are therefore considered as lesions due to disturbed neuronal/glial proliferation and apoptosis.

Dysmorphic neurons are distinguished by giant or hypertrophic neurons due to their abnormal orientation. Giant or hypertrophic neurons have significantly larger cross-sectional areas than immature neurons, which are round or oval cells with a diameter of 10–12 μm and a thin rim of cytoplasm (Cepeda et al. 2003).

In addition to FCDs, Palmini and coworkers described the category of mild MCD (mMCD) previously referred to as microdysgenesis or architectural dysplasias (Palmini and Lüders 2002; Palmini et al. 2004). mMCD type 1 include ectopic neurons placed in or adjacent to cortex layer 1, and mMCD type 2 ectopic neurons outside layer 1. However, ectopic neurons with variable morphology can be present in normal white matter, particularly in the temporal lobe.

The critical issues are whether and which types of mMCD and FCD are reliably distinguished on neuropathological specimens and which types can be identified on MRI. There is some evidence that FCD type 2B and to a lesser degree FCD type 2A are concordantly identified by neuropathologists whereas interobserver agreement is low for FCD type 1 and mMCD (Chamberlain et al. 2009). FCD type 2B are readily identified on MRI due to their funnel-shaped FLAIR hyperintensity, however, smaller lesions in the depth of a sulcus can be easily overlooked (Wagner et al. 2011a, b). FCD type 2A are more difficult to detect because the only abnormality may be an altered cortical thickness (Wagner et al. 2011a, b). mMCD and FCD type 1 are either MRI normal (around 1/3 of cases) (Tassi et al. 2010) or may show a reduced brain volume and/or an increased white matter signal approaching the gray matter signal on FLAIR and T2-weighted sequences. This pattern may be described as gray–white matter demarcation loss (Schijns et al. 2011). The pathological substrate of gray–white matter demarcation loss may be the increased number of subcortical white matter neurons or—as recently suggested—dishomogeneous staining of the white matter, reduction in the number of axons and axonal degeneration (Garbelli et al. 2012) is likely the increased number of subcortical white matter neurons. If gray–white matter demarcation loss is absent on MRI or if only cortical dyslamination is present on neuropathological specimens, FCD type 1 are likely missed on MRI.

5 Mild Cortical Malformations and Focal Cortical Dysplasias Type 1

5.1 Definition

This encompasses developmental or acquired malformation of cortical development affecting neocortical lamination.

5.2 Epidemiology

The incidence is unknown inasmuch as MRI negative lesions may be missed and the relative frequencies depend on the age groups and vary among large epilepsy surgery centers (Fauser et al. 2006; Krsek et al. 2008, 2009a; Lerner et al. 2009; Tassi et al. 2010; Hildebrandt et al. 2005; Chamberlain et al. 2009).

5.3 Pathogenesis and Pathology

FCD type 1A according to Blümcke and the ILAE commission is characterized by abundant microcolumnar organization. A microcolumn is defined by more than eight neurons aligned in a vertical direction provided the section is cut perpendicular to the pial surface, a 4-μm thin paraffin embedded section and NeuN immunohistochemistry are used, and aligned neurons have a small diameter and cell size of $<250\ \mu m^2$ (Hildebrandt et al. 2005). However, microcolumns can be also seen at lower frequency and with fewer neurons in nonepileptic brain samples, as well as in the vicinity of other epileptogenic lesions.

FCD type 1B according to Blümcke and the ILAE commission is characterized by an abnormal tangential cortical lamination. No cortical layers (with the exception of layer 1) may be recognized or blurred demarcation between cortical layers exists.

FCD type 1C comprises lesions with abnormal radial and tangential cortical lamination.

In FCD type 1, the border towards white matter is usually less sharply demarcated due to increased numbers of heterotopic neurons. Cellular abnormalities can be encountered in this variant, and include immature small diameter neurons or hypertrophic pyramidal neurons outside layer 5 (Blümcke et al. 2011).

5.4 Imaging

FCD type 1 can be detected on MRI if the affected brain region has a smaller volume and/or if an increased density of subcortical white matter neurons causes a higher white matter signal and impedes the demarcation of gray and white matter (gray–white matter demarcation loss). One-third of FCD type I are considered MRI negative (Tassi et al. 2010) which is reasonable if cortical dyslamination is the only histopathological substrate.

6 Focal Cortical Dysplasia Type 2A

6.1 Definition

Malformation of cortical development with dysmorphic neurons but without balloon cells. It is considered that malformation occurs during the cortical organization stage (Barkovich et al. 2005).

6.2 Epidemiology

In most but not all larger epilepsy surgery programs, FCD type 2A are distinctly less frequent than FCD type 2B (Fauser et al. 2006; Krsek et al. 2008; Lerner et al. 2009; Wagner et al. 2011a, b; Chang et al. 2011).

6.3 Pathogenesis and Pathology

FCD type 2A are characterized by a disturbed cortical architecture with dysmorphic neurons but without balloon cells. Because balloon cells accumulate within the subcortical, distinctly FLAIR hyperintense lesion parts and it is not necessary to resect these lesion parts to achieve seizure freeness following surgery (Wagner et al. 2011a, b), FCD type 2B lesions can be misclassified as FCD type 2A lesions.

6.4 Clinical Presentation

Drug-resistant epilepsy with focal (complex focal > simple focal) without or with secondarily generalized seizures.

6.5 Imaging

FCD type 2A are characterized by an altered cortical relief and thickness. The border to the subcortical white matter is sometimes blurred. The distinct, often funnel-shaped or ribbonlike FLAIR hyperintensity as the imaging hallmark of FCD type 2B is lacking, therefore lesions are overlooked on MRI but highlighted by voxel-based morphometry. In the Bonn epilepsy surgery program, detection rates for visual and voxel-based morphometry were 65 and 82 % for FCD type 2A as compared to 91 and 92 % for FCD type 2B, respectively (Wagner et al. 2011a, b) (Fig. 9).

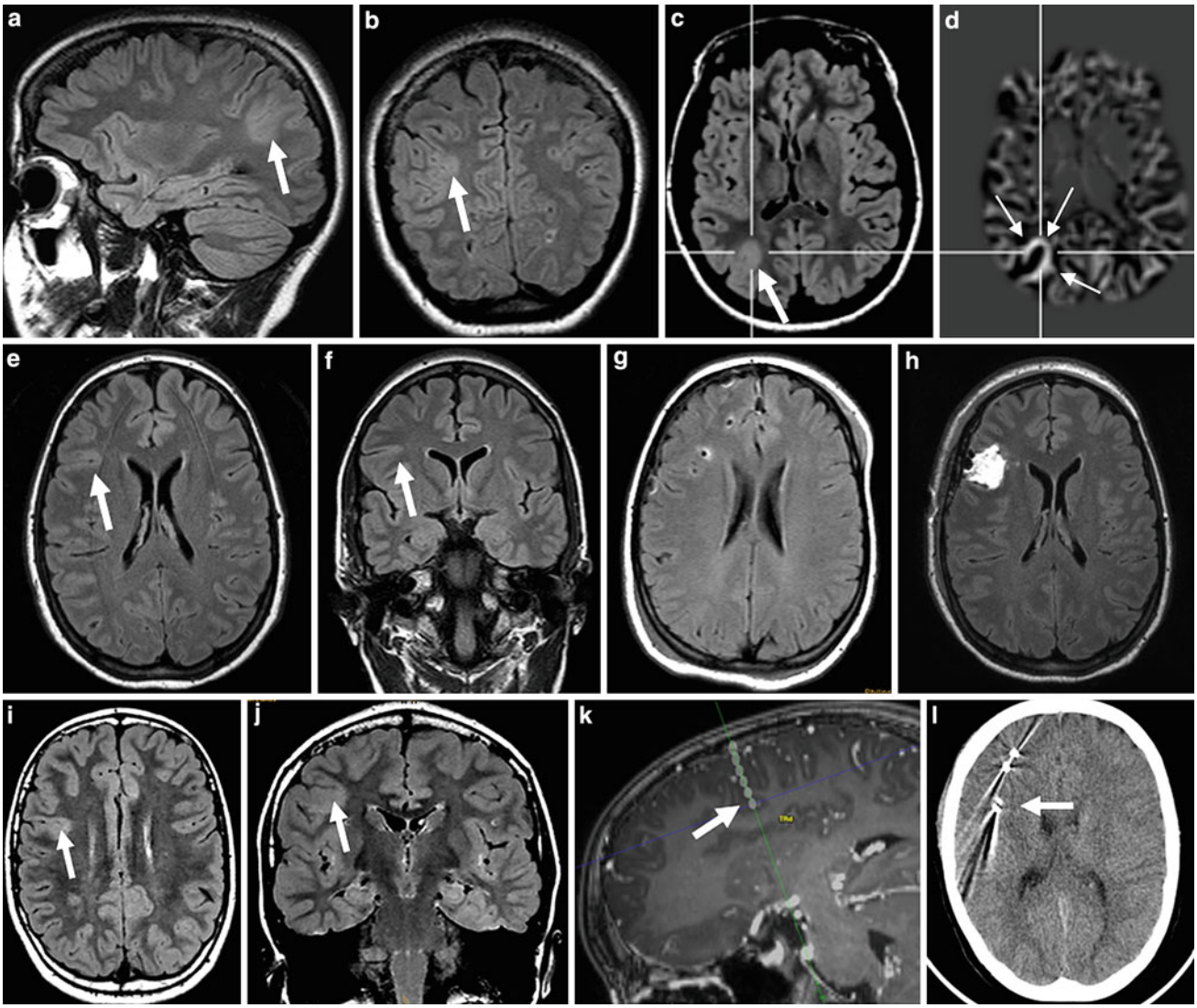

Fig. 9 FCD 2A are characterized by an altered cortical architecture with focal cortical thickening, but without significant signal changes. On visual analysis, they are more often overlooked as compared to FCD 2B. Proof of epileptogenicity by depth electrodes is typically needed. **a–d** a FCD 2A detected on visual analysis (**a–c**: *arrow*) and proven by Voxel-based morphometry, in which the junction map (**d**) shows the focal cortical thickening highlighting, what is subcortical white matter in healthy patients (**d**: *arrows*). **e–h** a FCD II a suspected on FLAIR sequences (**a**, **b**: *arrow*), unproven by Voxel-based morphometry, which epileptogenicity was proven by depth electrodes (**c**: *arrows*) and postsurgical seizure freeness (**h**). **i–l** a FCD II a overlooked on visual analysis (**i**, **j**: *arrows*), detected by Voxel-based morphometry, which epileptogenicity was proven by depth electrodes (**k**, **l**) and postsurgical seizure freeness

7 Focal Cortical Dysplasia Type 2B

Synonym(s): FCD with balloon cells, Taylor type dysplasia, and transmantle dysplasia.

7.1 Definition

FCD 2B is the malformation of cortical development affecting the stage of neuronal and gial proliferation and apoptosis.

7.2 Epidemiology

In 1971, Taylor et al. described ten patients with FCDs; seven of them had balloon cells within their histological specimens. Taylor described these cells as "malformed cells of uncertain origin with large, sometimes multiple, nuclei surrounded by an excess of opalescent, pseudopodic cytoplasm. These grotesque forms were concentrated in the deeper layers of the disorganized cortex and in the underlying white matter" (Taylor et al. 1971).

FCD 2B is the most common resected cortical dysplasia. Numbers in epilepsy surgery centers range from 18 to 80 %

in part depending on whether mild malformations are counted as FCDs.

7.3 Pathogenesis and Pathology

Two-thirds of patients have polymorphisms or loss of heterozygosity of the *TSC1* gene on the short arm of chromosome 9 (9q34). The *TSC1* gene encodes for the protein hamartin, and one polymorphism is located on exon 17, which is the region of the hamartin protein interacting with the protein tuberin as a product of the *TSC2* gene. Hamartin and tuberin together have a tumor-suppressor function on maturating neurons, and the same hamartin polymorphism is also found in tuberous sclerosis patients (Becker et al. 2002).

Histopathological specimens show an altered cortical architecture with dysmorphic neurons, giant neurons, and balloon cells. Balloon cells accumulate within the subcortical, distinctly FLAIR hyperintense lesion parts.

7.4 Clinical Presentation

Drug-resistant epilepsy with focal (complex focal > simple focal) without or with secondarily generalized seizures.

Following surgery, >80 % of patients are seizure-free. The major reason for persistent seizures after surgery is incomplete resection of the cortical part of the FCD (Krsek et al. 2009b). Resection of the funnel-shaped subcortical part is not necessary to achieve freedom from seizures (Wagner et al. 2011a).

7.5 Imaging

MRI hallmark is a distinct funnel-shaped FLAIR hyperintensity tapering towards the lateral ventricle, which has been called the transmantle sign and which is found in 90 % of cases (Taylor et al. 1971; Barkovich et al. 1997; Urbach et al. 2002; Widdess-Walsh et al. 2005). In some instances, the FLAIR hyperintensity can be followed towards the lateral ventricle; in other instances it appears as a penlike line along the inner cortical surface.

The dysplastic cortex is isointense on T1-weighted images. FCD 2B are therefore only visible on T1-weighted images if the cortex is markedly thickened or if they are distinct adjacent to white matter changes. The dysplastic cortex is isointense (1/3) or slightly hyperintense (2/3) on T2-weighted, and slightly hyperintense on FLAIR fast spin echo sequences.

FCDs 2B are typically single neocortical lesions; the most common location is—likely due to the lobe size—the frontal lobe. If there is more than one dysplasia, one should consider tuberous sclerosis and carefully look for subependymal giant cell astrocytoma and subependymal nodules. FCDs with balloon cells on surgical specimens are identical or similar to cortical tubers of tuberous sclerosis and may indeed represent a forme fruste or phenotypic variation of tuberous sclerosis.

FCDs 2B are of different sizes. Small lesions are either restricted to the cortex at the bottom of a sulcus (bottom of sulcus dysplasia) or at the crown of a gyrus (Barkovich et al. 2005; Besson et al. 2008). If they are located at the bottom of a sulcus, the sulcus itself is often somewhat deeper and widened (Besson et al. 2008) (Figs. 10, 11). The bottom of sulcus dysplasia can be easily overlooked, especially on axial FLAIR images. Due to their spatial orientation, coronal and sagittal FLAIR sequences, isotropic 3D FLAIR sequences, and/or voxel-based analyses may be needed (Wagner et al. 2011a, b).

With increasing size, two or more adjacent gyri are affected. If a large amount of tissue of a lobe or an entire hemisphere is involved, separation from focal megalencephaly may be impossible (Fig. 12). Moreover, the cortical aspect of these lesions cannot be completely resected and the chance of seizure freedom declines to less than 50 % (Wagner et al. 2011a).

Calcification within the subcortical lesion parts may occur in larger lesions; contrast enhancement is typically absent.

8 Hemimegalencephaly

8.1 Epidemiology

Severe malformation of cortical development due to a disturbance in the neuronal and glial proliferation stage (Table 1). The first description was by Sims in 1835 after reviewing 253 autopsies (Sims 1835). Three types are distinguished (Flores-Sarnat 2002):

1. Isolated form without systemic involvement.
2. Syndromic form which may occur as hemihypertrophy of part or all of the ipsilateral body. It has been described in patients with organoid (formerly: epidermal) nevus syndrome (→ Neurocutaneous Diseases (Phakomatoses) 7 g), Proteus syndrome (→ Neurocutaneous Diseases (Phakomatoses) 7 g), neurofibromatosis type 1 (Neurocutaneous Diseases (Phakomatoses) 4 c), hypomelanosis of Ito (→ Neurocutaneous Diseases (Phakomatoses) 6 f), Klippel–Trenaunay–Weber syndrome, and tuberous sclerosis (→ Neurocutaneous Diseases (Phakomatoses) 1 a) (Barkovich and Chuang 1990; Broumandi et al. 2004; Wolpert et al. 1994).
3. Total hemimegalencephaly with enlargement of the ipsilateral half of the brainstem and cerebellum.

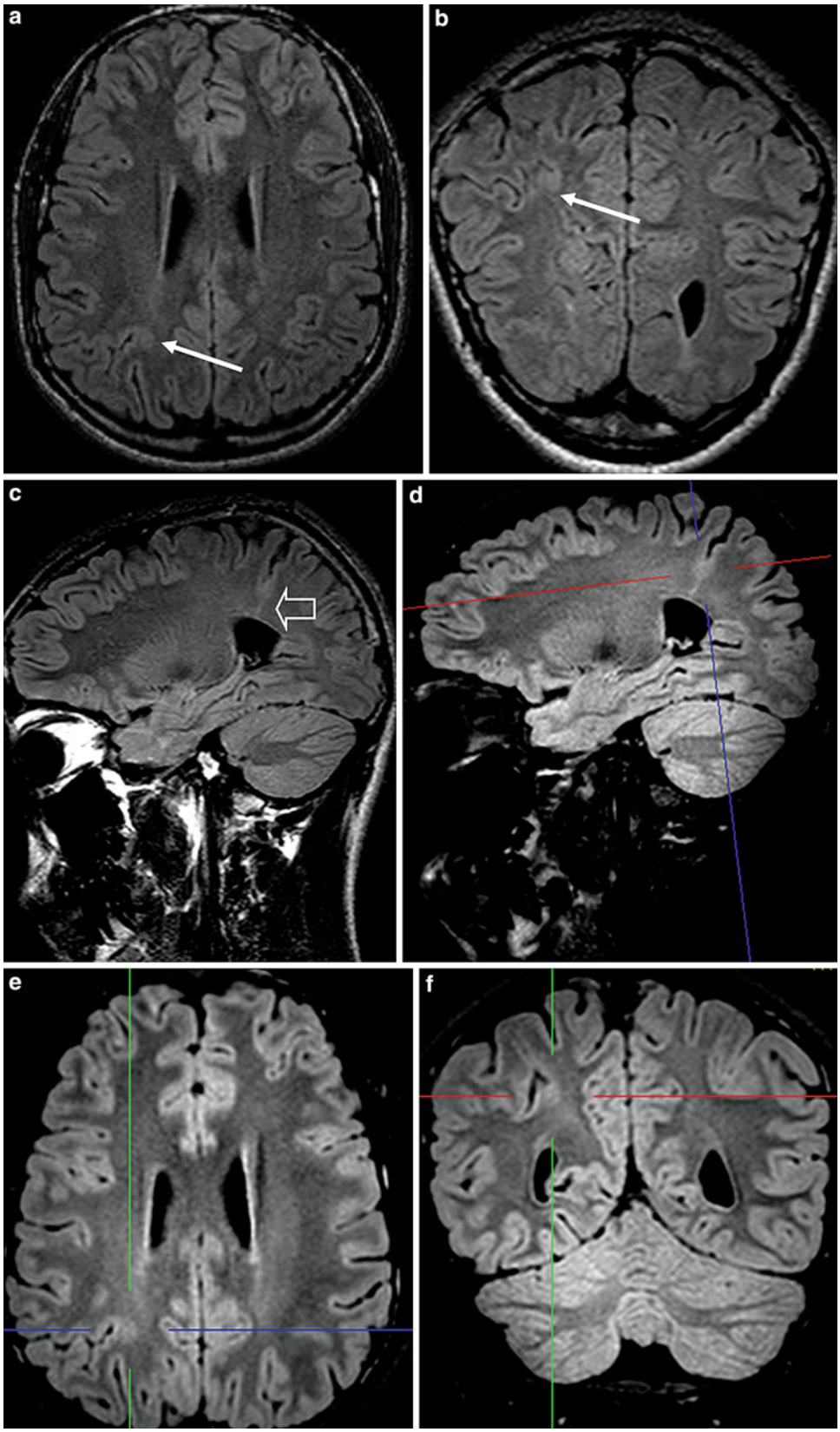

Fig. 10 FCD 2B in the depth of a sulcus (bottom of sulcus-dysplasia): a circumscribed thickening of the cortex in the depth of the right intraparietal sulcus is difficult to detect on axial (**a**) and coronal (**b**) FLAIR images (*arrow*). Sagittal FLAIR-MRI shows thickening of the cortex and funnel-shaped hyperintensity tapering to the wall of the lateral ventricle (**c**: *hollow arrow*). Acquisition of a 3D-FLAIR-sequence (**d**) with isotropic voxel enables reformation in three orthogonal planes (**e**, **f**)

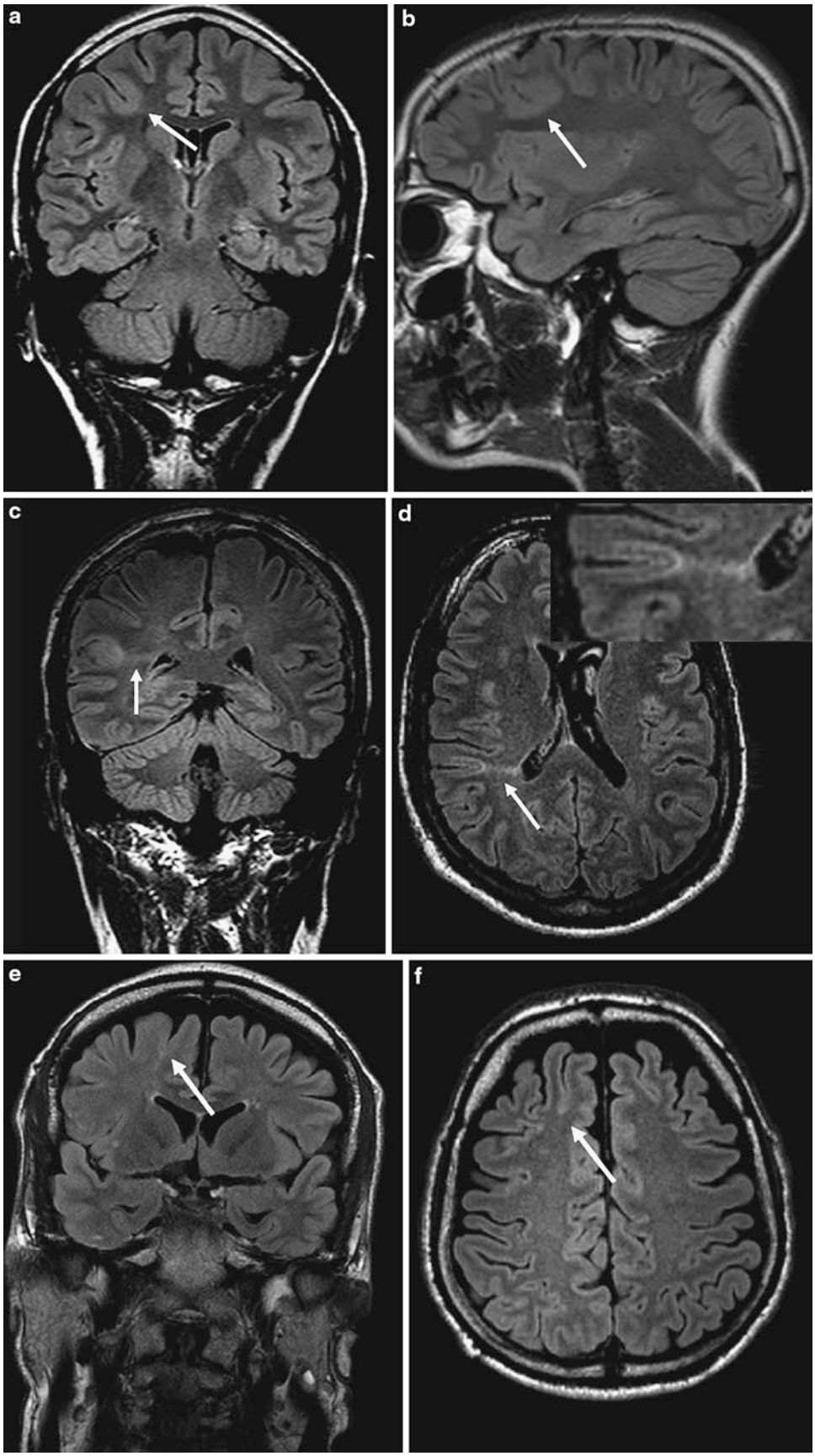

Fig. 11 Examples of small FCDs 2B (bottom of sulcus dysplasias). In the *upper row*, a circumscribed cortex thickening around a somewhat deeper sulcus exists (*arrow*) (**a**, **b**), the middle row shows a champagner glass-like hyperintensity to the lateral ventricle (transmantle sign) (*arrow*) (**c**, **d**), the *lower row*, a point-like hyperintensity in the depth of a somewhat deeper additional sulcus (*arrow*) (**e**, **f**)

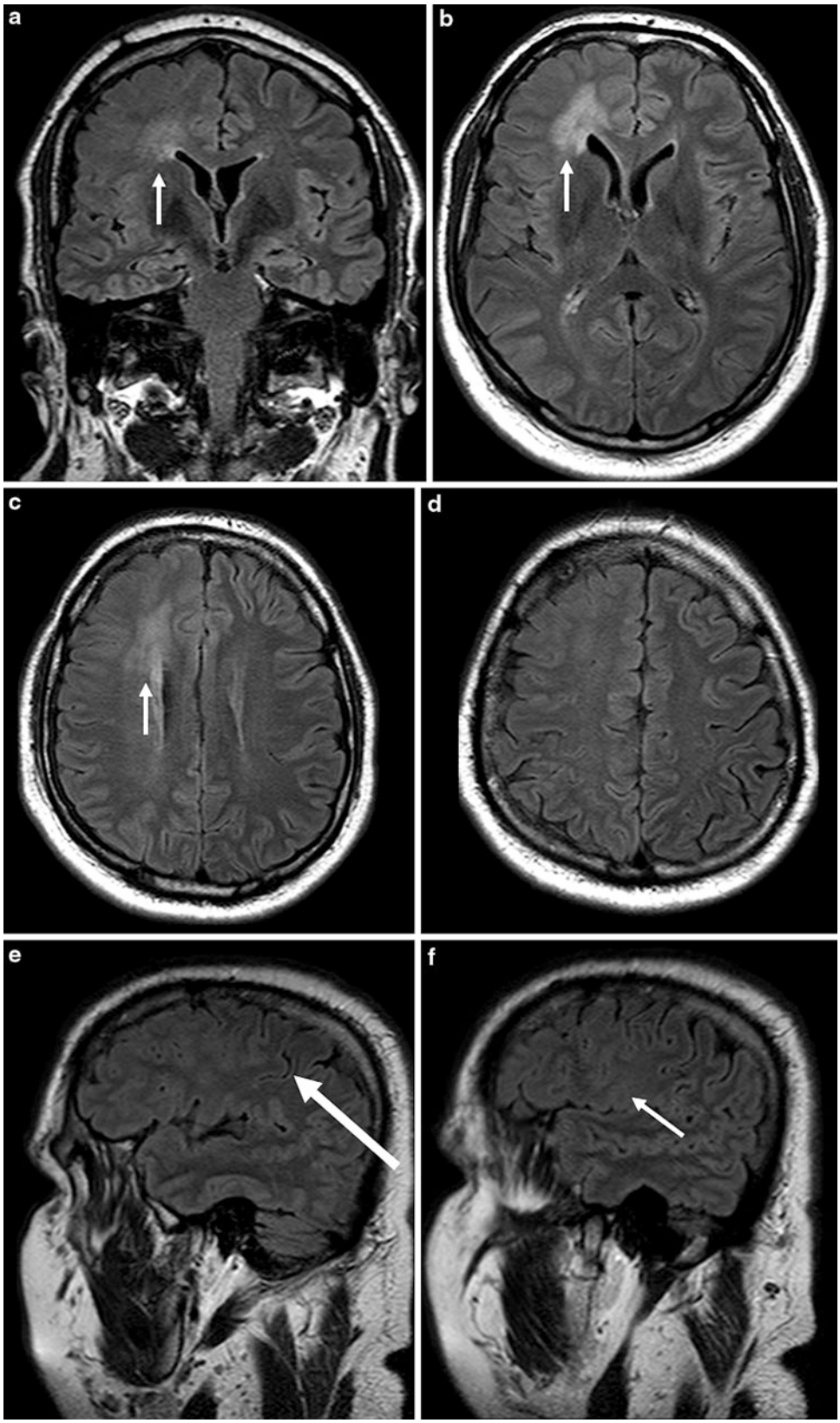

Fig. 12 Large FCD IIB of the right frontal lobe. Diagnostic clue is the distinct subcortical hyperintensity (**a**-**c**: *arrow*, **d**–**f**) and when related to the size of the lesion the nearly lacking space occupying effect. The lesion involves the basal part of the precentral gyrus (**e**: *arrow*: "handknob") and could therefore not be fully resected. Following incomplete resection the patient did not become seizure free

8.2 Pathogenesis and Pathology

Hemimegalencephaly means an hamartomatous overgrowth of an entire or parts of a hemisphere. The affected hemisphere is larger and has a higher weight than normal. Gyral pattern is abnormal and may include areas of agyria, pachygyria, and polymicrogyria. Microscopically, a horizontal layering of the cortex is lacking and the underlying white matter is not really demarcated. Neurons are larger and less densely packed, and the number of glial cells is increased.

Similar to FCD 2B and hamartomas of tuberous sclerosis, tissue contains balloon cells with immunoreactivity for both glial (glial fibrillary acid protein GFAP, S-100β) and neuronal proteins (microtubule-associated protein 2 MAP2, neuronal nuclear antigen, chromogranin A, neurofilament protein) (Flores-Sarnat et al. 2003).

8.3 Clinical Presentation

Drug-resistant epilepsy with frequent seizures often propagating to the contralateral hemisphere. Due to the severity of the seizures, functional hemispherectomy is the treatment of choice. The aim of this treatment is to interrupt seizure propagation to the contralateral hemisphere. ♂ = ♀.

8.4 Imaging

The abnormal hemisphere is larger than the contralateral one, and the midline is pushed to the contralateral side (Figs. 13, 14). The lateral ventricle is enlarged; straightening of the ipsilateral frontal horn is considered characteristic (Barkovich and Chuang 1990).

The cortex appears thickened and enlarged, the gyri are usually broad and flat and the sulci shallow. The Sylvian fissure is short and thickened and the posterior end is open.

Gray and white matter are difficult to delineate from each other. White matter volume is increased and the white matter signal on T2-weighted images is clearly abnormal. In neonates, the white matter signal on T2-weighted images is low as opposed to normal neonates, in which the white matter signal is higher than that of gray matter. A low white matter signal in the fetus and the neonate is explained with advanced myelination at this age (Yagishita et al. 1998) (Figs. 13, 14, 15). In older children with hemimegalencephalies, the white matter signal becomes higher than normal reflecting lack of myelin (Adamsbaum et al. 1998).

If only parts of the hemisphere show enlargement and dysplastic features, the disease may be called focal megalencephaly or large FCD 2B (Figs. 12, 15). In these instances, the subcortical white matter often shows a hyperintense FLAIR signal likely reflecting the balloon-cell rich part of the lesion. The critical part in the interpretation of the MRI is the exclusion of a contralateral lesion.

9 Heterotopia

9.1 Definition

Heterotopias are conglomerate masses of gray matter in an abnormal location. They can be uni- or bilateral, of a nodular, ribbonlike, chainlike, ball-like, or curvilinear configuration and located attached to the ventricle wall, within the white matter, or attached to the cortex (Barkovich 2000). Microscopically, there are neurons and glial tissue without consistent arrangement; rudimentary layering may be present.

From an imaging point of view, it is helpful to distinguish subependymal (periventricular), subcortical, and band heterotopias (Barkovich 2000). Note that band heterotopias are genetically linked and grouped together with type 1 lissencephalies.

9.2 Epidemiology

Heterotopias are quite common MCD.

9.3 Pathogenesis

Heterotopias typically result from impaired migration of neurons from the germinal matrix in the wall of the lateral ventricle to the cortex. These "macroscopic" heterotopias must be separated from "microscopic" heterotopias in mMCD including ectopic neurons within the white matter, marginal zone, and subpial heterotopias (Palmini and Lüders 2002; Barkovich and Kuzniecky 2000). Epileptic seizures may be generated within the heterotopic neurons or in the overlying cortex conceptually missing these neurons or containing displaced neurons (Kirschstein et al. 2003). Heterotopias may be isolated findings or part of genetically defined syndromes (e.g., trisomy 18, trisomy 21, Cornelia de Lange syndrome).

9.4 Clinical Presentation

1. Bilateral periventricular (subependymal) nodular heterotopias (BPNH): This common disorder with BPNH is associated with mutations of the filamin 1-gene (*FLN1*, *FLNA*) on the short arm of the X-chromosome (Xq28) (OMIM 309550) (Fox et al. 1998). *FLNA* encodes an actin-cross-linking phosphoprotein that enables the attachment of

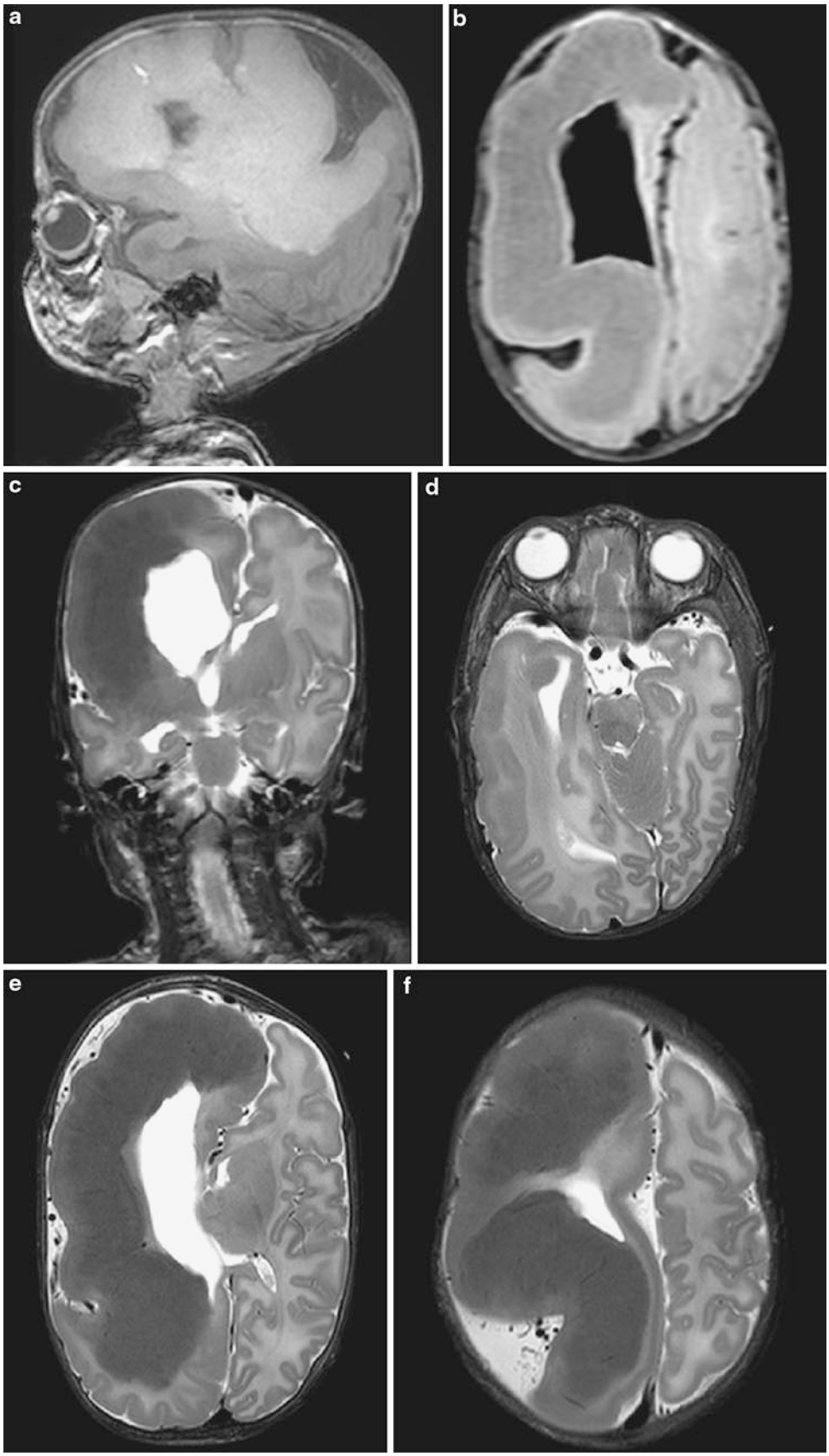

Fig. 13 Right-sided hemimegalencephaly in a 10 months old boy with enlargement of the right hemisphere including the lateral ventricle, displacement of the mildline to the left side, nearly agyric cortex, poor demarcation of gray and white matter, and T1-weighted hyperintense/T2-weighted hypointense white matter signal suggesting "advanced" myelination (**a**–**f**)

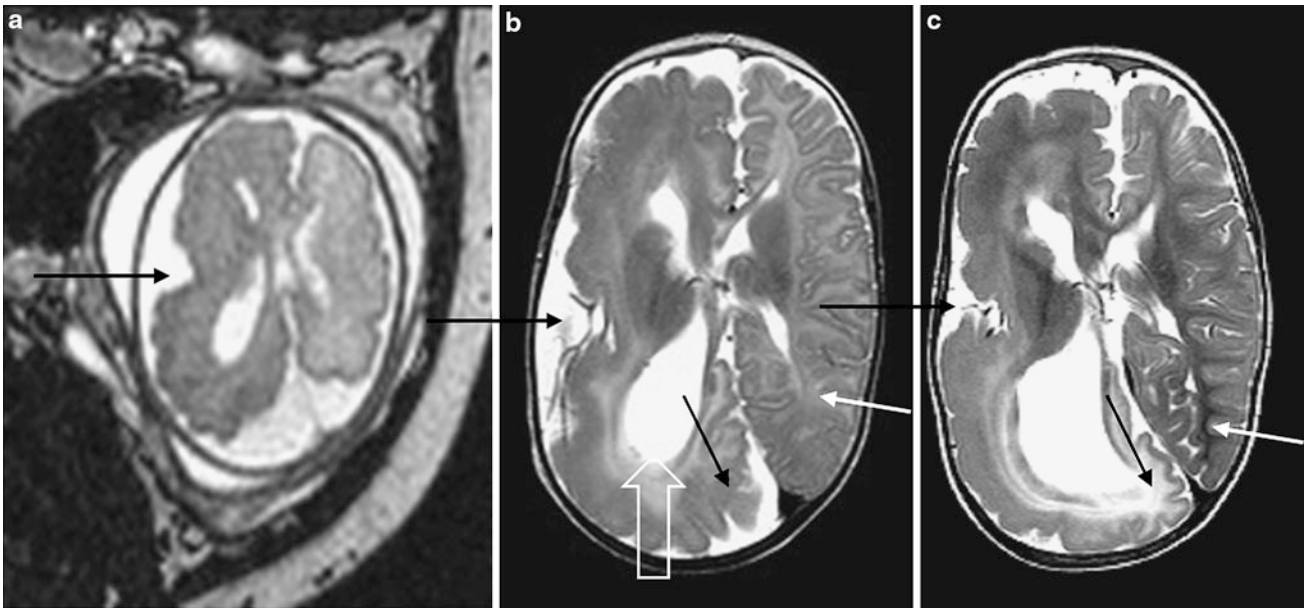

Fig. 14 Right-sided hemimegalencephaly in a female at the 35th gestational week (**a**), at the age of 7 months (**b**), and at the age of 12 months (**c**). Enlargement of the right hemisphere and the lateral ventricle (**b**: *hollow arrow*) and an "open" end of a rudimentary Sylvian fissure (**a**–**c**: *black arrows*) are typical findings. The hypointense white matter signal is already visible in utero (**a**). Normal myelination turning a hyperintense into a hypointense white matter signal only takes place in the left hemisphere (**b**, **c**: *white arrow*)

neurons to radial glial cells. Neurons that are not attached to radial glial fibers cannot migrate towards the cortex. Hints for X-chromosomal inheritance are prior abortions because boys with one X-chromosome often die embryonically. Alive males have a higher incidence of neurodevelopmental and other disabilities including cerebellar hypoplasia and syndactyly, short gut syndrome, congenital nephrosis, frontonasal dysplasia, coagulopathies, patent ductus arteriosus, and others (Dobyns et al. 1997; Palm et al. 1986; Guerrini and Dobyns 1998; Fox et al. 1998). Female patients may show normal intelligence or slight or moderate mental retardation; 80 % are affected by variable epilepsy syndromes with seizures usually starting in the second decade of life (Barkovich and Kuzniecky 2000).

Other BPNH types are frequently associated with microcephaly and include mutations of the *MCPH1* gene on chromosome 8p23 encoding for microcephalin (Jackson 2002), mutations of the *ASPM* gene on chromosome 1q31 (Bond et al. 2002), and mutations of the *ARFGEF2* gene on chromosome 20q13.3 (Sheen et al. 2004). Another BNPH type is associated with mutations on chromosome 5, yet the gene defect is unknown (Sheen et al. 2003).

2. Subcortical heterotopias: These are less common than subependymal heterotopias. They can be uni- or bilateral, and size, extent, and location of the lesion(s) are fairly correlated with the patient's symptoms. Associated brain anomalies are common (callosal agenesis/hypoplasia, 70 % of cases; ipsilateral basal ganglia dysmorphy).

3. Laminar or band heterotopia: Laminar heterotopia is more common than previously thought (Huppertz et al. 2008). Broad bands of heterotopic gray matter which are often associated with distinct mental retardation and drug-resistant epilepsy syndromes are easily recognized. Thin strips of heterotopic gray matter, however, are often associated with only mild mental retardations and are easily missed.

9.5 Imaging

Heterotopias typically have a signal isointense to gray matter in all MRI sequences. However, in rare cases nodular heterotopias may be calcified, likely reflecting degenerative changes (Urbach et al. 2003).

Nodular heterotopias are typically attached to the lateral ventricle walls and often bulge into its cavity. Typical locations are the corners of the lateral ventricles or the ventrolateral circumferences of the temporal horns (Fig. 16).

Subcortical heterotopias can be found in any location and with different sizes. They consist either of multiple nodules, have a curvilinear configuration with the appearance of an enfolded cortex, or a mixture of both with the nodular configuration closer to the ventricle and the curvilinear configuration peripherally (Barkovich 2000) (Fig. 17).

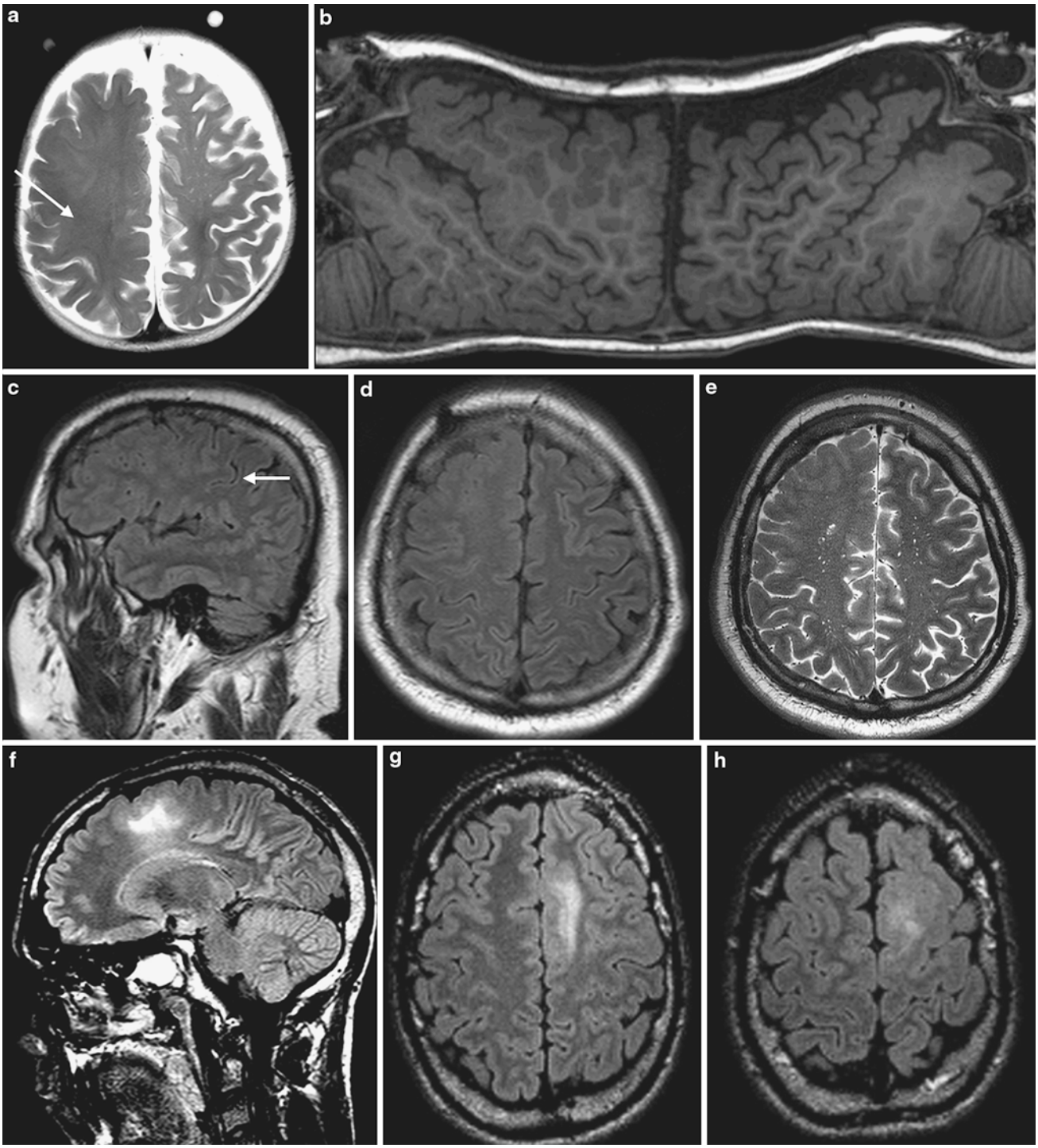

Fig. 15 Three examples of large dysplastic lesions containing balloon cells. **a**–**b** from a 1 year old girl show enlargement of the right hemisphere sparing its posterior parts. For side comparison, see planar surface view of both hemispheres (**b**). Hypointense white matter signal (**a**: *arrow*) suggests "advanced" myelination. **c**–**e** from a 36 year old male and **f**–**h** from a 29 year old male can be classified as large FCD IIB or as focal megalencephaly (**c**: *arrow* marks central sulcus)

Laminar heterotopias consist of bands of heterotopic matter beneath the cortex. If these bands are thin, high-resolution images, specially reformatted T1-weighted gradient echo images in coronal orientation are needed to detect them (Fig. 6).

Since heteropias can occur alone or with other malformations (polymicrogyria, pachygyria, callosal agenesis, microcephaly, et al.), it is sometimes difficult to clearly separate heterotopias and, for example, polymicrogyria.

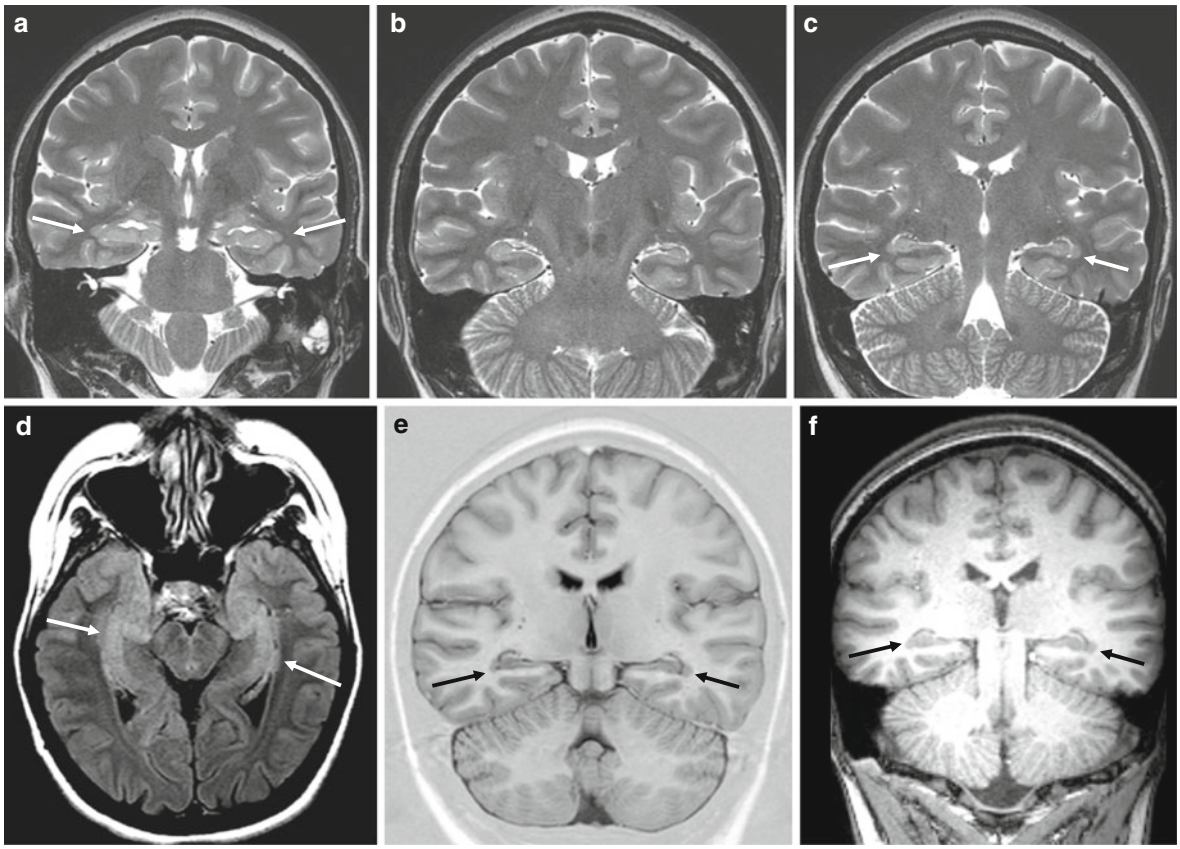

Fig. 16 Bilateral nodular periventricular heterotopias with relatively small nodules along the inferior horns of the lateral ventricles (**a**, **c**–**f**: *arrows*). The 31 year old woman suffered from temporal lobe seizures since 3 years and did not take antiepileptic drugs so far

10 Polymicrogyria and Schizencephaly

10.1 Epidemiology

Rather frequent malformation of cortical development, which is considered to be caused in the late stage of neuronal migration or in the stage of cortical organization. The result is a derangement of the normal six-layered lamination of the cortex associated with derangement of sulci and fusion of the molecular layer across sulci. ♂: ♀ = 3:2 (Leventer et al. 2010).

10.2 Pathogenesis

The etiology is heterogeneous comprising intrauterine ischemia, intrauterine infections (particularly cytomegalovirus, toxoplasmosis, varicella zoster, syphillis), and several genetic (Xq21.33-q23 → *SRPX2*, 2q21.3 → *RAB3GAP1*, 3q21.3-p21.2 → *EOMES*, 6p25 → *TUBB2B*, 1q22.1 → *KIAA1279*, 11q13 → *PAX6*, 21q22.3 → *COLI18A1*, 22q11.2 → multiple genes, Xq28, 16q12.2-21 → *GPR56* (Barkovich 2010) and metabolic diseases.

Symmetric polymicrogyrias are suggestive of genetic causes, however, an unilateral familiar syndrome has been described (Jansen and Andermann 2005; Chang et al. 2006). Common symmetric polymicrogyrias are bilateral perisylvian polymicrogyria (Kuzniecky syndrome) due to mutations on three gene loci on the X chromosome (Xq21.33-q23, 22q12, Xq28), bilateral fronto-parietal (autosomal-recessive, 16q12.2-21 → *GPR56*), and bilateral parasagittal parieto-occipital polymicrogyria (Kuzniecky et al. 1993). In bilateral fronto-parietal polymicrogyria due to *GPR56* mutations, the gene product is important for the attachment of radial glial cells to the pial limiting membrane. If this attachment fails, neurons migrate too far and a cobblestone pattern results. Associated anomalies are a small pons and a small dysplastic cerebellum. With the pathophysiological mechanism of neurons migrating too far, this syndrome belongs rather to malformations due to abnormal terminal migration and defects in pial limiting membrane (see Table 1) (Barkovich et al. 2012).

Polymicrogyria is often associated with other malformative lesions such as corpus callosum agnenesis or hypogenesis, cerebellar hypoplasia, periventricular nodular heterotopia, and subcortical heterotopia.

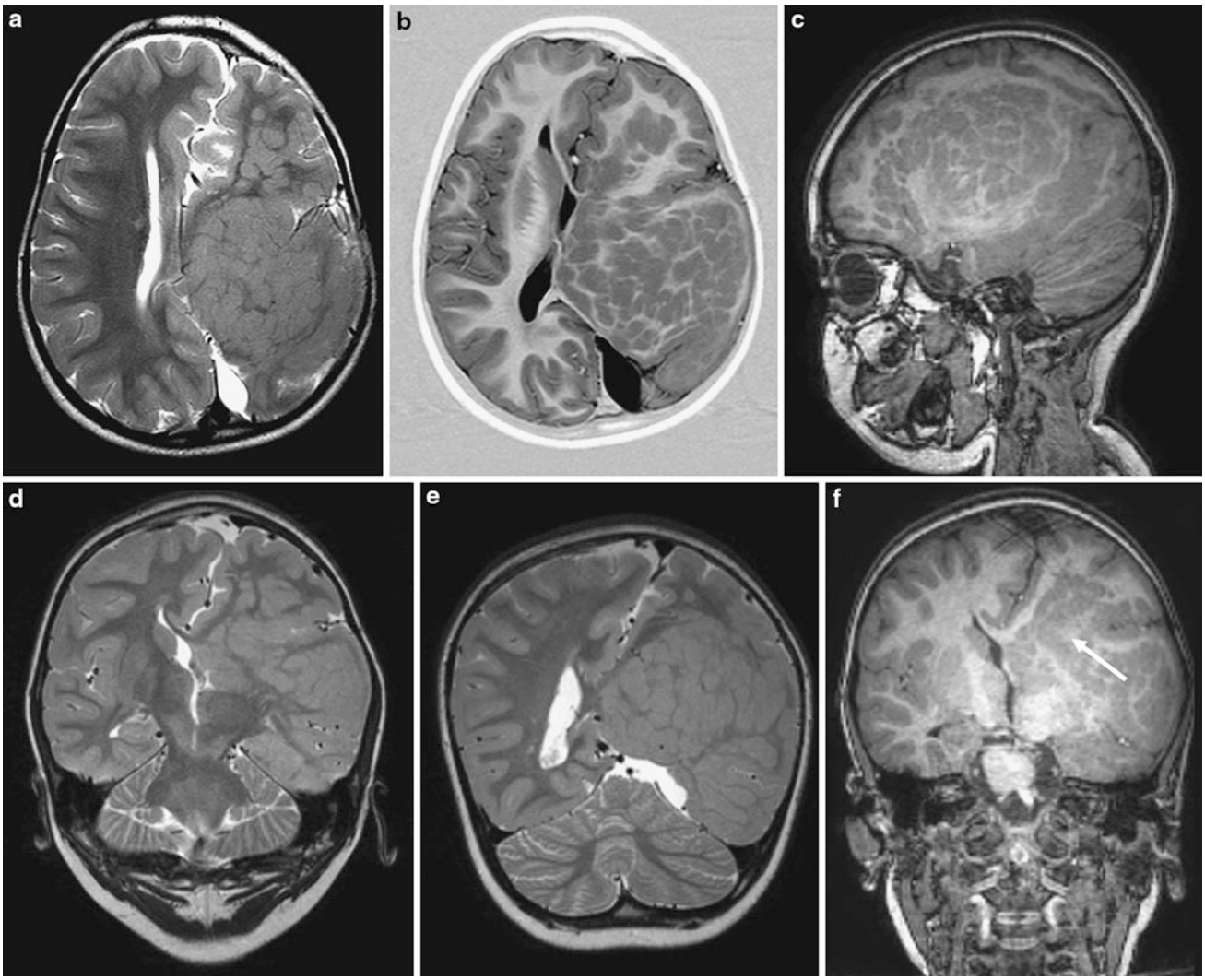

Fig. 17 Large subcortical heterotopia with a curvilinear pattern in a 3.5 year old boy with a right-sided spastic hemiparesis and daily drug-resistant atonic seizures. The heteropia is isointense to gray matter in all sequences and resembles enfolded polymicrogyriform cortex. Note the abnormal sulcation and the fact that the affected hemisphere is small as compared to the opposite hemisphere (**a**–**f**)

Schizencephaly is always associated with polymicrogyria; it means cleft brain and is characterized by a communication between ventricle and subarachnoid space. Cortical lips are either attached (closed lips) or separated by CSF (open lips) (Barkovich 2002).

10.3 Clinical Presentation

Broad spectrum of ranging from intellectual impairment to hemiparesis, tetraparesis, and drug-resistant epilepsy. Seizures are present in 80 % of cases and may be of many clinical types (Leventer et al. 2010). Severity of clinical presentation and age at presentation are related to the extent of cortical involvement and associated abnormalities. In severe cases, pseudobulbar paralysis (oropharyngeal dysfunction, dysarthria), epilepsy, mental retardation, and congenital arthrogyposis may result.

Another syndrome complex is polymicrogyria associated with megalencephaly, postaxial syndactyly, cutis marmorata, distinct facial features including frontal bossing, a low nasal bridge, large eyes, and midfacial vascular malformations. Affected children have epileptic seizures and delayed or a lack of motor and intellectual development. Apart from mostly perisylvian polymicrogyria, MRI shows (progressive) hydrocephalus, a thick corpus callosum, and caudal tonsillar displacement. These megalencephalies associated with polymicrogyria were formerly denominated as megalencephaly–polymicrogyria–polydactyly–hydrocephalus, macrocephaly–capillary malformation, and macrocephaly–cutis marmorata telangiectata congenita syndromes, respectively (Garavelli et al. 2007; Gripp et al. 2009; Barkovich et al. 2012). Polymicrogyria may be among others a part of the following diseases (Barkovich 2010; Hermier et al. 2010; Barkovich et al.

Aicardi syndrome (→ 18 h)	OMIM 304050
Delleman syndrome (oculo-cerebral-cutaneous syndrome)	OMIM 164180
DiGeorge (22q11.2 deletions) syndrome	OMIM 188400
Warburg micro syndrome	OMIM 600118
D-bifunctional protein deficiency syndrome	OMIM 261515
Joubert syndrome and related disorders including Meckel–Gruber syndrome, Arima (cerebro-oculo-renal) syndrome	OMIM 608629, …
Adams–Oliver syndrome	OMIM 100300
Hereditary hemorrhagic telangiectasia (Rendu–Osler disease)	OMIM 187300, 600376
Apert syndrome (Acrocephalosyndactyly)	OMIM 101200

2012; Hevner 2005; Dixon-Salazar et al. 2004; Giordano et al. 2009).

10.4 Pathology

Unlayered and four-layered polymicrogyria are distinguished. In unlayered polymicrogyria, there is a thin undulating ribbon consisting of a molecular layer and a neuronal layer without lamination. The molecular layer is fused across the sulci, and the brain surface may appear coarse or delicate.

Four-layered polymicrogyria is less common; it consists of a molecular layer and two layers of neurons separated by an intermediate layer of few neurons and myelinated fibers.

10.5 Imaging

Affected patients can be microcephalic (50 %), normo-, or macrocephalic.

Polymicrogyria can be focal, multifocal, or diffuse, unilateral, bilateral-asymmetrical, and bilateral symmetrical. The most common location is around the posterior portions of the Sylvian fissure (60–70 % of cases), which typically takes a steeper course. This region should be carefully inspected on sagittal 3D-T1-weighted gradient echo images (Fig. 19) According to the severity on the MRI, four grades are distinguished: grade 1, with perisylvian polymicrogyria extending to the frontal or occipital pole; grade 2, with polymicrogyria extending beyond the perisylvian region, but not to either pole; grade 3, with polymicrogyria of the perisylvian region only; and grade 4, with polymicrogyria restricted to the posterior perisylvian region (Jansen and Andermann 2005).

The cortical surface shows either multiple small gyri or it appears thick and bumpy or paradoxically smooth because the outer cortical layer (molecular layer) fuses over the microsulci. The overlying subarachnoid space is focally widened and may contain enlarged flow void structures representing anomalous venous drainage (around 50 % of cases; Fig. 18) (Hayashi et al. 2002).

Significant signal changes of the cortex are lacking, however, the degree of myelination of subcortical or intracortical fibers alters the appearance: in unmyelinated regions, the inner surface of the polymicrogyric cortex looks thin (2–3 mm); in myelinated regions it looks thicker (5–8 mm) and relatively smooth (Takanashi and Barkovich 2003) (Figs. 19, 20).

11 Aicardi Syndrome

11.1 Epidemiology

Rare, X-chromosomal-inherited disease in girls. Boys with one X-chromosome are not viable. The initial description was by the French neurologist Dr. Aicardi and coworkers in 1965 (Aicardi et al. 1965).

11.2 Pathogenesis and Pathology

Probably de novo mutation on the short arm of the X-chromosome.

Pathological core features are callosal agenesis, interhemispheric cysts, and ocular abnormalities (microphthalmia, chorioretinal lacunae, colobomas).

Other abnormalities may be found in the hemispheres (subependymal and subcortical heterotopias, polymicrogyria), in the posterior fossa (cerebellar hypoplasia, arachnoid cysts), in the vascular system (A. cerebri anterior azygos), in the ventricles (choroidal plexus cysts and papillomas), and in the spine and bony system (fusion of vertebral bodies, hemivertebra, fused ribs, scoliosis, spina bifida, hand and finger anomalies).

11.3 Clinical Presentation

Callosal agenesis and interhemispheric cysts are usually detected by ultrasound in utero. Newborns are typically blind and suffer from infantile spasms. A significant number of girls, however, seem to develop normally until around the age of 3 months, when they begin to have infantile spasms. Ocular examination reveals zones of depigmentation of the pigmented epithelium characterized as chorioretinal lacunae (Hoyt et al. 1978). Only 40 % of girls get older than 15 years of age.

11.4 Imaging

In a blind female newborn with epileptic seizures look for callosal agenesis, interhemispheric cyst(s), and cortical

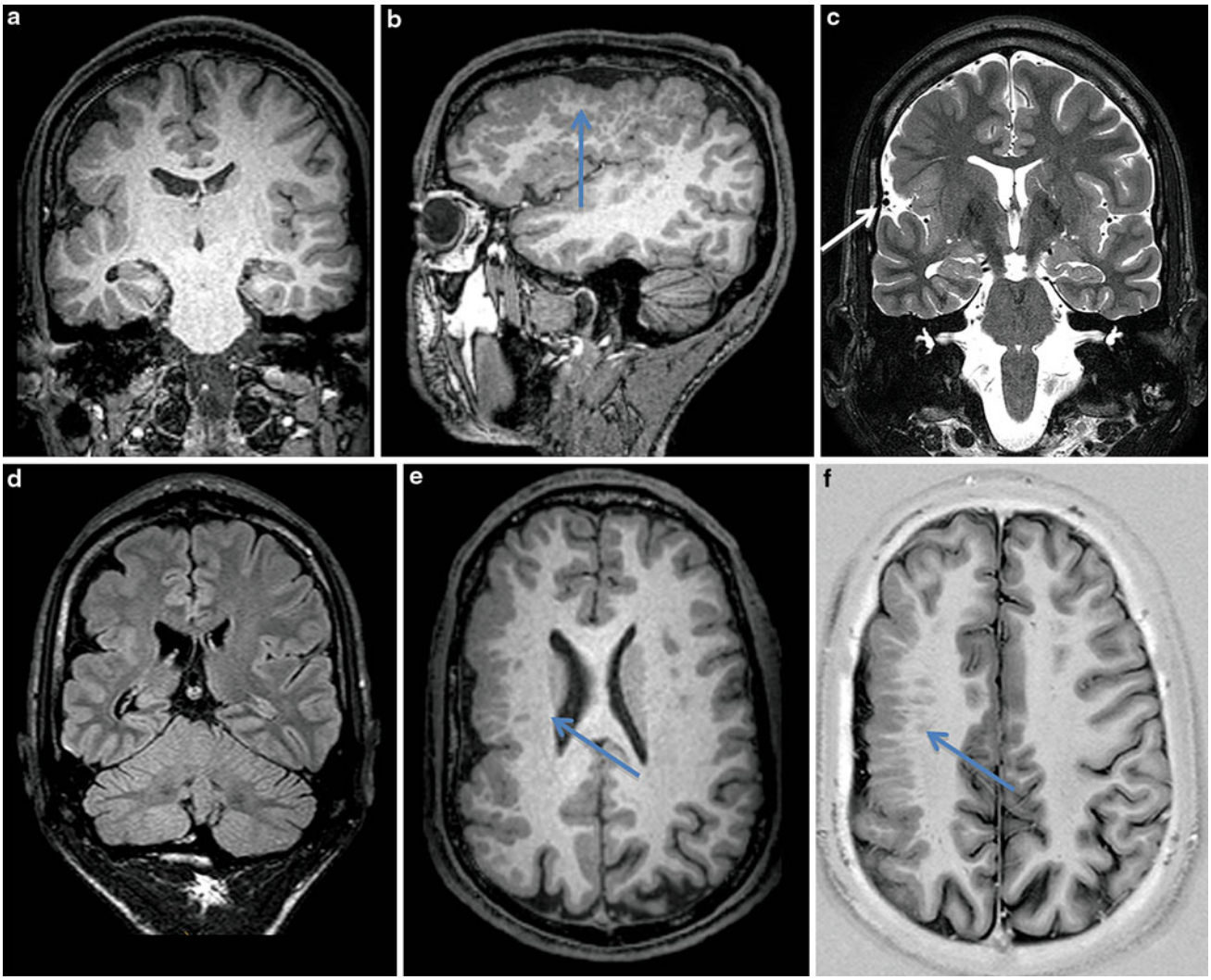

Fig. 18 Right-sided polymicrogyria in a 26 year old man with atonic and complex focal seizures with secondary generalization. Note the enlarged subarachnoid space (**a**–**f**) with enlarged flow void structures (**c**: *arrow*) and a steeper course of the Sylvian fissure (**b**). The brain surface appears rather smooth due to a fusion of the outer cortical layer (molecular layer) above the sulci and only the inner cortical boundary reveals multiple small gyri (**e**, **f**: *arrow*)

dysplasias (heterotopias, polymicrogyria) (Figs. 21, 22). Since myelination is yet incomplete or delayed, cortical dysplasias can be easily overlooked.

12 Tuber Cinereum and Hypothalamic Hamartomas

12.1 Epidemiology

This is rare congenital gray matter "heterotopia" of the tuber cinereum and hypothalamus in children with precocious puberty at a very young age and/or gelastic seizures.

12.2 Clinical Presentation

Precocious puberty (75 % of patients) occurs in young children, for example, a 3-year-old boy shows the sexual development of a 16-year-old boy. 1/3 of patients with precocious puberty has tuber cinereum hamartomas.

Gelastic seizures occur in 50 % of patients. Apart from gelastic seizures complex-focal and secondary generalized tonic–clonic seizures mimicking temporal lobe seizures may occur. In addition, patients show mental and behavioral abnormalities.

Consider Pallister–Hall syndrome (7p13, GLI3 frame-shift-mutations) in children with tuber cinereum hamartoma,

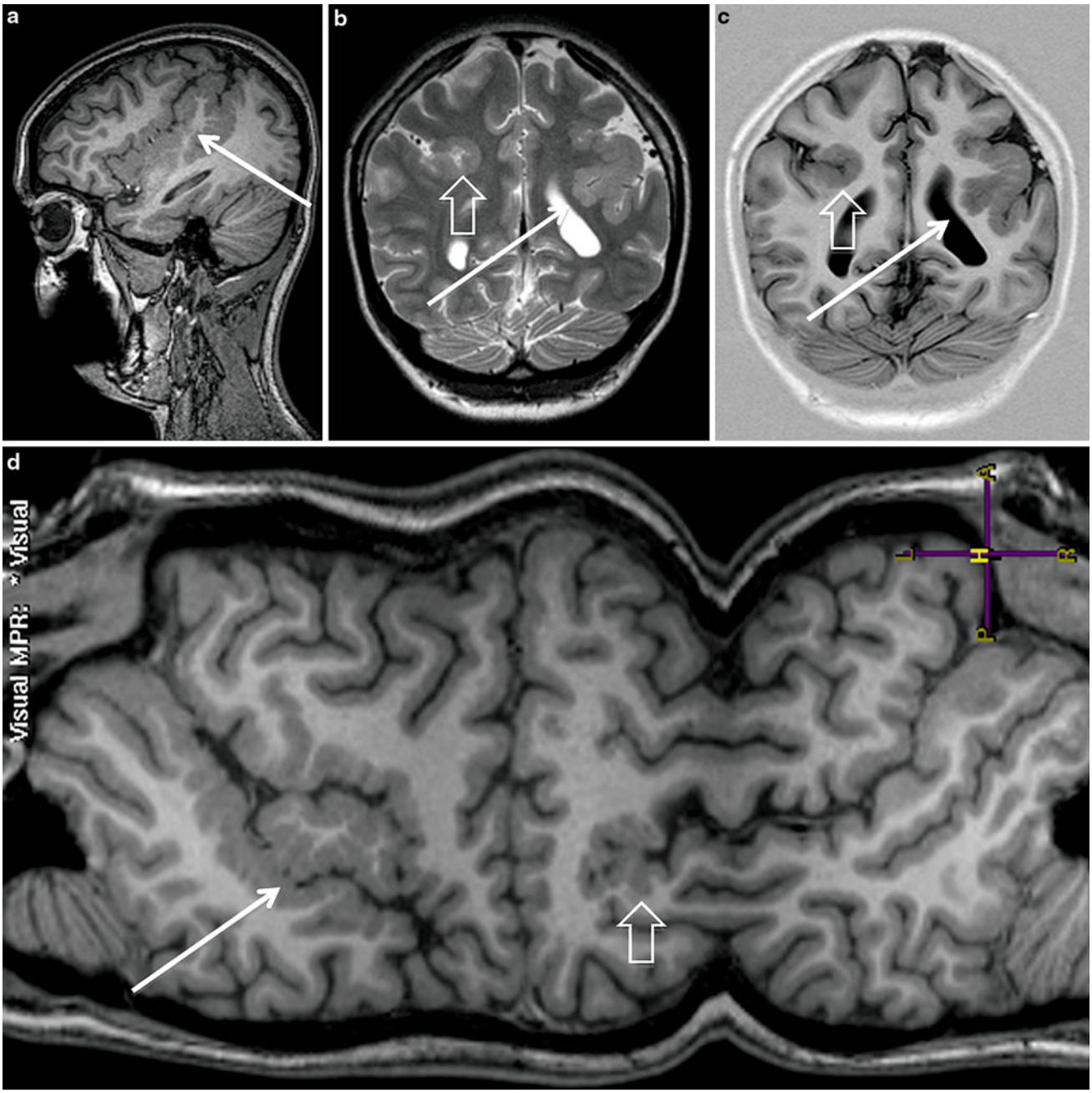

Fig. 19 Bilateral perisylvian polymicrogryia in a 16 year old girl with sleep-related complex focal seizures. Sagittal T1-weighted gradient echo image (**a**) shows a steeper course of the Sylvian fissure and the left side (*arrow*) more severely affected than the right side. In order to recognize a bilateral distribution, it is important to inspect the posterior border of the Sylvian fissure (**b–d**: *hollow arrow*)

hand (ossa metacarpalia, syndactyly, polydactyly), and other malformations (epiglottis, larynx, heart, kidneys, anus).

12.3 Pathology

The tuber cinereum is a gray matter protuberance within the dorsal wall of the infundibulum. Hypothalamic or tuber cinereum hamartomas are congenital malformations with neurons similar to hypothalamic neurons, myelinated and unmyelinated axons, and variable amounts of fibrillary gliosis. They may express several hormones (especially GnRH) associated with premature activation of hypothalamic–pituitary–gonadal axis secretion.

12.4 Imaging

Round, sessile, or pedunculated mass lesion dorsal to the infundibular stalk, involving the mammillary region of the

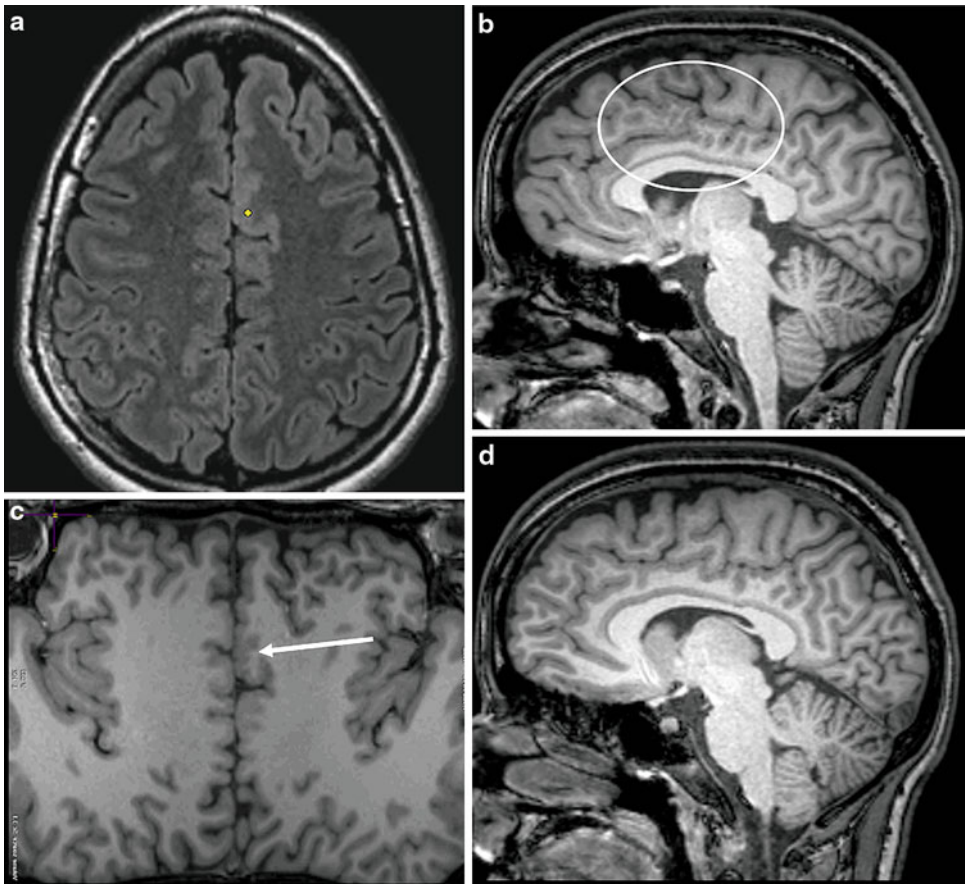

Fig. 20 Focal polymicrogyria of the left cingulate gyrus in a 21 year old woman with focal frontomesial seizures since the age of 1. The microgyri are not visible on a 5 mm thick axial FLAIR image (**a**: point). In contrast, a 1 mm thick sagittal T1-weighted gradient echo image shows microgyri (**b**, **d**: unaffected right side). A planar surface view allows to compare both cingulate gyri and displays the focal polymicrogyria more clearly (**c**: *arrow*)

hypothalamus, with attachment to one or both mammillary bodies is seen. The size is a few millimeters up to several centimeters, which does not increase on follow-up MRI. In larger hamartomas, the intrahypothalamic component lies in the wall of the third ventricle between the postcommissural fornix anteriorly, the mammillothalamic tract posteriorly, and the mammillary body inferiorly.

The signal intensity is close to gray matter: slightly hypointense or isointense on T1-weighted, slightly hyperintense on T2-weighted images, and hyperintense on FLAIR sequences. Note that small lesions can be missed on FLAIR sequences due to CSF flow artifacts. There is no contrast enhancement. Cystic portions and calcifications are rare; if present other lesions (e.g., craniopharyngioma) should be considered.

Hypothalamic hamartomas associated with epilepsy have a sessile attachment to the hypothalamus and displace normal hypothalamic structures, whereas those associated with precocious puberty alone are rather pedunculated (Valdueza et al. 1994; Freeman et al. 2004; Frazier et al. 2009).

Some patients also have temporal arachnoid cysts and (more common) unilateral or bilateral anterior temporal gray–white matter demarcation loss. For those with unilateral abnormality it is ipsilateral to the side of predominant hypothalamic hamartoma attachment. It may reflect ictal involvement of the temporal lobe during postnatal brain development and suggests anterior temporal gray–white matter demarcation loss as a maturation disorder of the temporal pole.

13 Anomalies of the Ventral Prosencephalon Development

13.1 Holoprosencephalies

13.1.1 Epidemiology

Holoprosencephaly was initially described by Yakovlev (1959). It means a median holosphere instead of two hemispheres (Yakovlev 1959). It is a brain malformation in which the cleavage of the telencephalic vesicle into two hemispheres and the separation of the eye fields are disturbed. This cleavage normally takes place around week 6 of gestation. Associated craniofacial abnormalities range from cyclopia to mild microcephaly with a single central incisor (Roessler and Muenke 1999; Moog et al. 2001). Holoprosencephaly is a continuous disease spectrum ranging from severe (alobar) to mild (lobar) forms. The prevalence is 1:16,000 live births, however, many fetuses

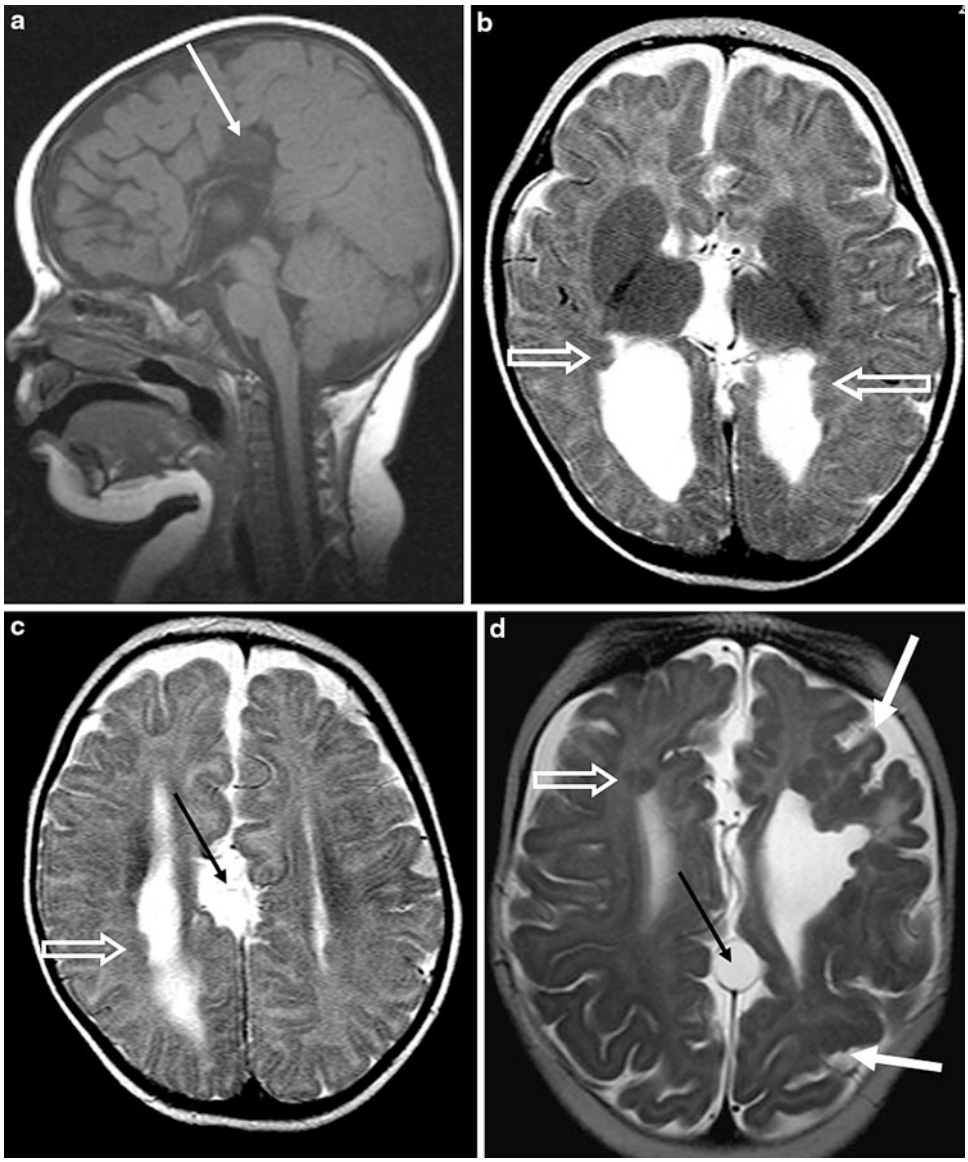

Fig. 21 Aicardi syndrome: **a–c** 7 month old girl with callosal agenesis, interhemispheric cyst (**a**, **c**: *arrow*) and subependymal heterotopias, which are difficult to delineate due to incomplete myelination (*hollow arrows*). **d** With higher field strength and signal to noise ratio—as in this example of a 5 month old girl—heterotopias are better detectable (*hollow arrow*). Also note polymicrogyria (*white arrows*) and interhemsipheric cyst (*black arrow*)

(approximately 1:250) die spontaneously or by induced abortion (Roach et al. 1975; Matsunaga and Shiota 1977; Moog et al. 2001).

13.1.2 Pathogenesis

The etiology of holoprosencephaly is heterogeneous including genetic (at least 12 genetic loci = HPE 1–12) and environmental (e.g., maternal diabetes, teratogenes) factors (Moog et al. 2001).

13.1.3 Clinical Presentation

Holoprosencephaly patients present with a wide range of manifestations: severely affected children with alobar holoprosencephaly are usually diagnosed by fetal ultrasound, have distinct facial abnormalities, are either not viable or survive with neonatal seizures, infantile spasms, apnea, rigidity, and temperature imbalances. Less severely affected patients suffer from different grades of mental retardation, spasticity, chorea-athetosis, and endocrine and visual disturbances. Nearly half of these patients have some kind of seizures, which, however, are drug-resistant in only a minority of patients (Lewis et al. 2002).

Associated syndromes are Smith–Lemli–Opitz syndrome (autosomal-recessive disorder of cholesterol biosynthesis with cleft palate, genital malformations, polydactyly, and holoprosencephaly), Genoa syndrome (cleft soft palate, holoprosencephaly, craniosynostosis, Dandy–Walker malformation, bilateral microphthalmia, scoliosis, aortal coarctation), and CHARGE syndrome (coloboma, heart anomaly, retardation, genital and ear anomalies) (Tortori-Donati 2005).

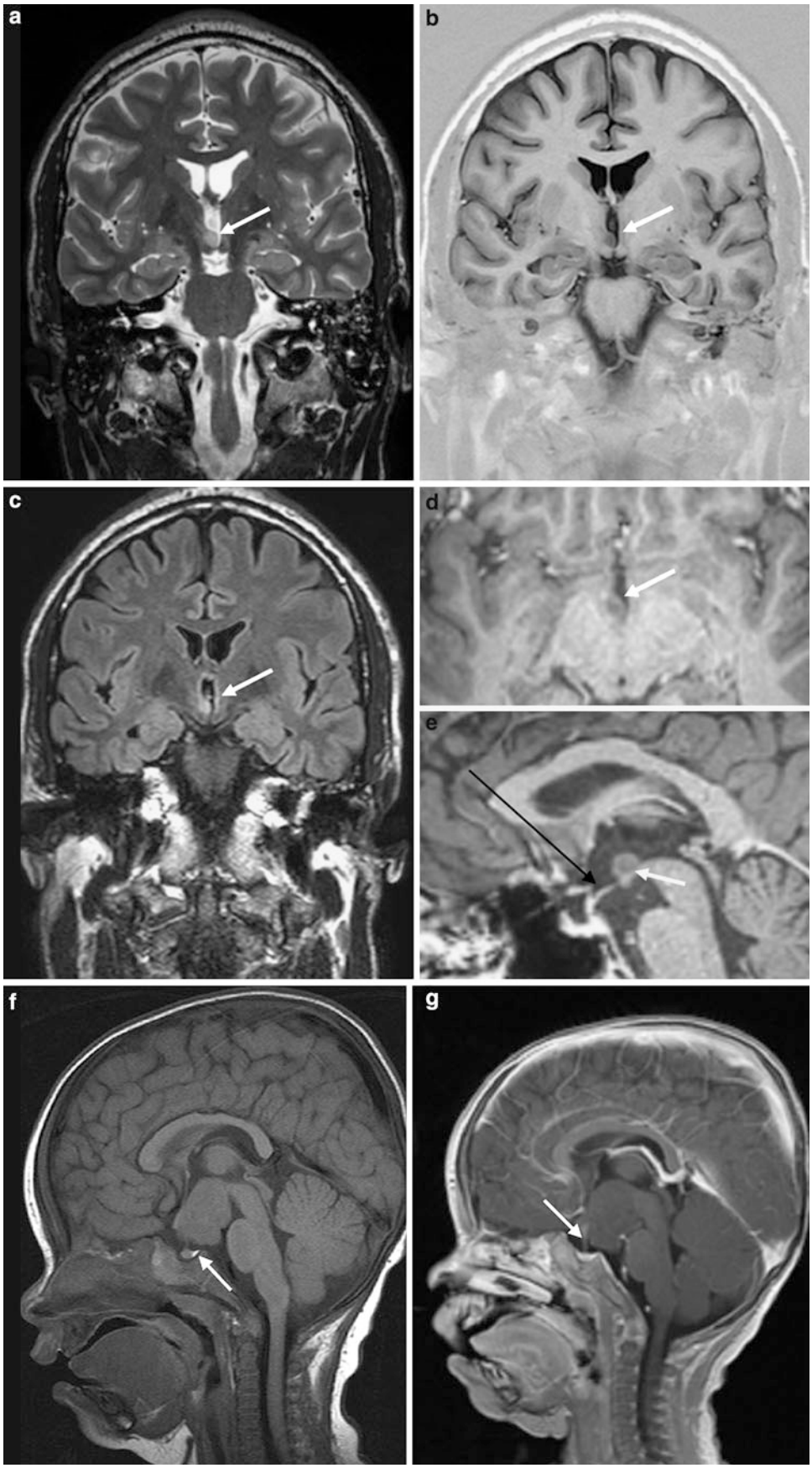

Fig. 22 Tuber cinereum hamartomas: **a–f** a 4 mm large sessile hamartoma in a 46 year old man with gelastic seizures. The hamartoma indents the dorsal wall of the third ventricle (**e**: *black arrow* pointing to the infundibular recess) and is medial and above the right mamillary body (**a–e**: *white arrow*). It is isointense to gray matter on T2-weighted (**a**), Inversion Recovery (**b**), and T1-weighted gradient echo (**d**, **e**), but hyperintense on FLAIR sequences (**c**). **f–g** a 3 cm hamartoma in a 1 year old girl with gelastic seizures and visual disturbances. The center of the hamartoma is dorsal and above the pituitary gland (**f**: *arrow* points to the hyperintense signal of the neurohypophysis) and the infundibular stalk (**g**: *arrow*)

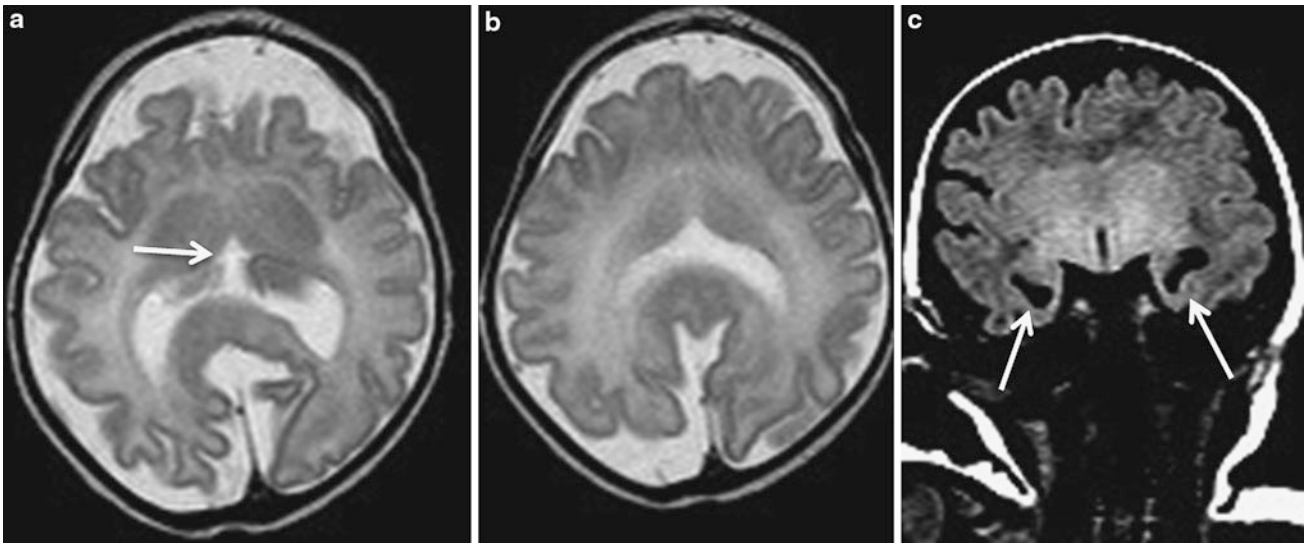

Fig. 23 Semilobar holoprosencephaly in a 4 days old girl. The frontal portions of the brain hemispheres are non-cleaved. A partially cleaved "holoventricle" with rudimentary temporal horns (**c**: *arrow*), a rudimentary third ventricle (**a**: *arrow*) and partially separated thalami are visible

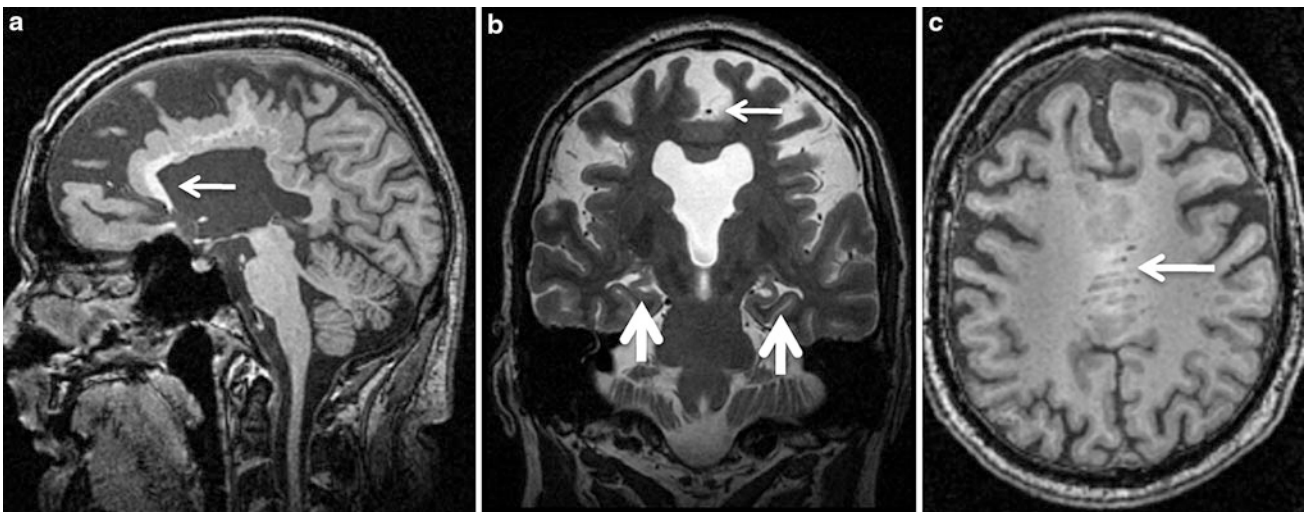

Fig. 24 Middle interhemispheric variant of holoprosencephaly in a 45 year old man. The anterior portion of the corpus callosum including the genu is thin but present (**a**: *arrow*). The hemispheres are non-cleaved only within their central segments, while an anterior interhemispheric fissure was built (**c**: *arrow*). Note the absent septum pellucidum, a box-like shape of the anterior horns of the lateral ventricles, vertically oriented hippocampi (**b**: *thick arrows*) and an azygos anterior cerebral artery (**b**: *arrow*)

13.1.4 Imaging

Four types are distinguished (DeMyer et al. 1964; Barkovich and Quint 1993):

1. Alobar holoprosencephaly
2. Semilobar holoprosencephaly
3. Lobar holoprosencephaly
4. Middle interhemispheric variant of holoprosencephaly, syntelencephaly.

Alobar, semilobar, and lobar holoprosencephaly represent a continuous disease spectrum, in which anterior structures and those located towards the midline are more or less noncleaved. Alobar holoprosencephaly is characterized by a large holoventricle continuous with a large dorsal cyst. Midline structures (superior sagittal sinus, septum pellucidum, corpus callosum, third ventricle, pituitary gland, olfactory bulbs) are lacking (Simon et al. 2001).

In semilobar holoprosencephaly, there is some degree of cleavage of the posterior brain structures (Fig. 23). A so-called pseudosplenium, which is in fact an enlarged hippocampal commissure and not a true splenium, is present and the degree of anterior extension is considered as a marker of the severity of holoprosencephaly (Oba and Barkovich 1995).

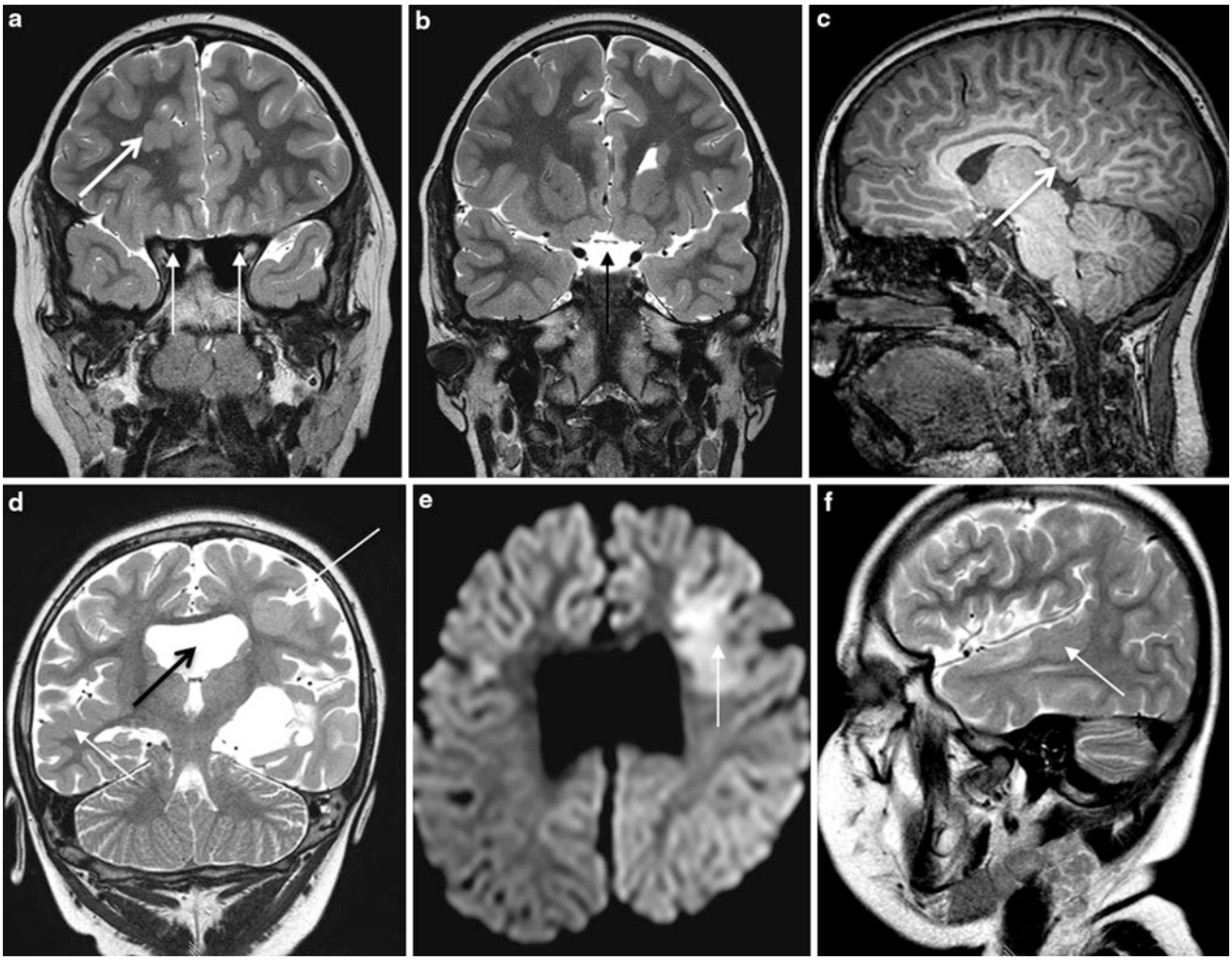

Fig. 25 Septooptic dysplasia plus in a 9 year old boy (**a**–**c**) and a 3 year old girl (**d**–**e**). The 9 year old boy has hypoplastic optic nerves (**a**: *thin arrows*) and optic chiasm (**b**: *arrow*), heterotopic gray matter nodules (**a**: *thick arrow*), and agenesis of the corpus callosum splenium (**c**: *arrow*). The 3 year old girl shows absent septum pellucidum (**a**: *black arrow*) and gray matter masses in both hemispheres (**a**, **c**, **f**: *white arrows*). Cytotoxic edema on DWI (**b**: *arrows*) with ADC normalization on follow-up-MRI 10 days later (not shown) suggests transient ictal activity of the left frontal lesion

Lobar holoprosencephaly is the mildest form; patients may be normal or only mildly retarded. An absent septum pellucidum with a boxlike shape of the lateral ventricles on coronal slices may be the only sign of lobar holoprosencephaly and is distinguished from septo-optic dysplasia by normal optic nerves and chiasm. However, even in these circumstances the hippocampi are typically malrotated showing a vertical orientation.

The middle interhemispheric variant is characterized by noncleavage of the frontodorsal and parietal brain regions whereas the rostrobasal forebrain has cleaved and an anterior interhemispheric fissure and in some cases even a septum pellucidum are present (Fig. 24) (Robin et al. 1996). Patients with the middle interhemispheric variant may be severely retarded but have no facial abnormalities (Tortori-Donati 2005).

13.2 Septo-Optic Dysplasia (De Morsier Syndrome)

13.2.1 Epidemiology

Rather brain malformation (1 in 50,000 live births) with absent septum pellucidum, optic nerve and chiasm hypoplasia, and pituitary dysfunction. The term septo-optic dysplasia was introduced by De Morsier (1956), who described 36 patients with absent septum pellucidum, nine of whom had optic nerve hypoplasia (De Morsier 1956).

13.2.2 Pathogenesis

Septo-optic dysplasia is a disorder of midline prosencephalic development (and thus can be considered as a mild holoprosencephaly variant) occurring in the latter half of the second through the third month of gestation (Miller et al.

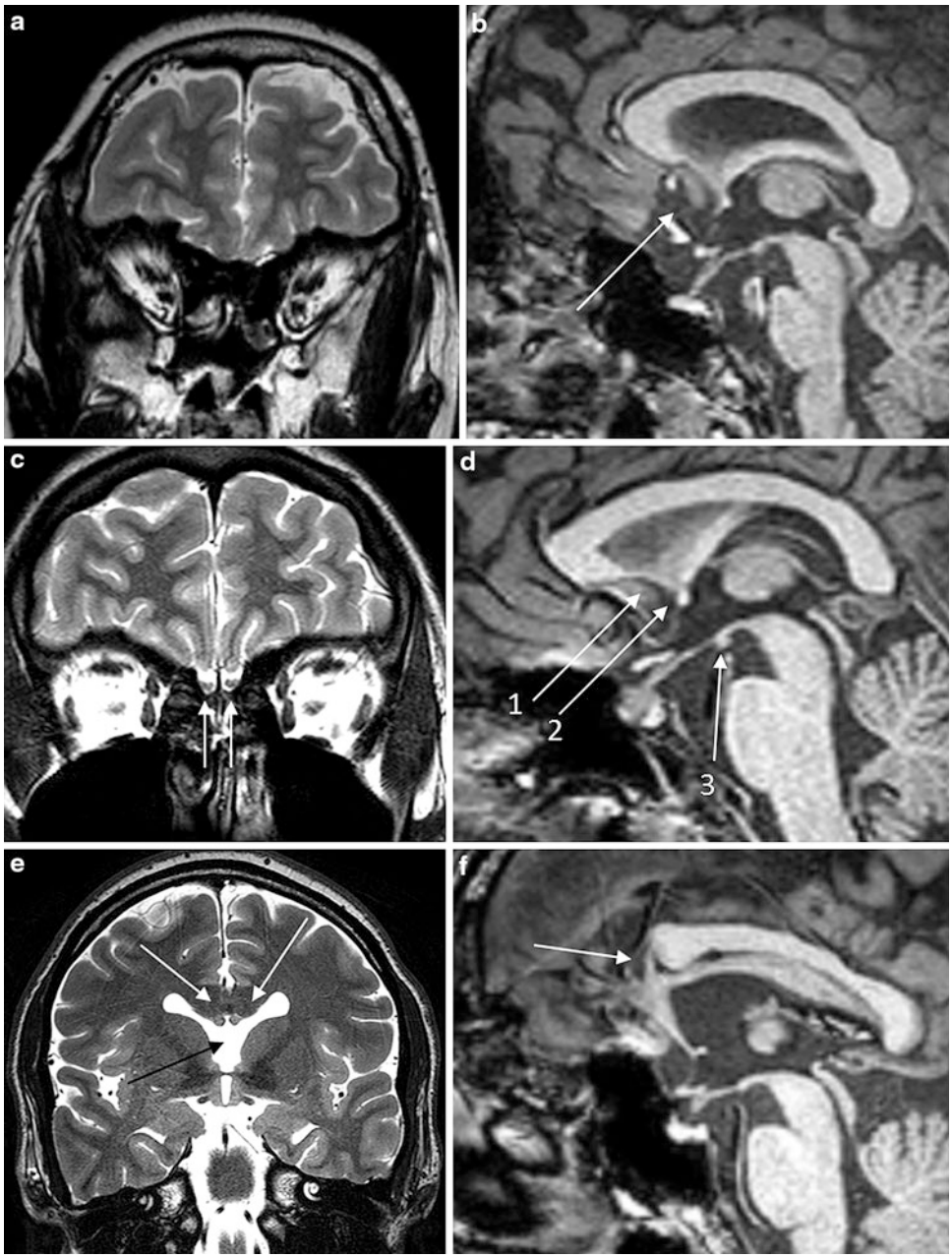

Fig. 26 Kallmann syndrome (**a**, **b**) in a 25 year old woman with olfactory bulb a/hypoplasia (**a**) and hypoplasia of the subcallosal area and pituitary gland (**b**: *arrow*). Shapiro syndrome (**e**, **f**) in a 38 year old man with anterior callosal agenesis (**f**), absent septum pellucidum (**e**: *black arrow*) and elevated fornices (**e**, **f**: *white arrows*). Normal MRI (**c**, **d**) for comparison with olfactory bulbs best visible on coronal T2-weighted images (**c**) and rostrum corporis callosi (**d**:1), anterior commissure (**d**:2), mamillary body (**d**:3)

2000). At this time, the optic nerves, germinal matrix, and septum pellucidum are forming (Barkovich et al. 1989). Although most cases are sporadic, autosomal dominant and recessive forms with mutations in the homeobox *HESX1* gene located on chromosome 3p21.21–3p21.2 have been described. Intrauterine infections (particularly cytomegalovirus infection), vascular events, antiepileptic drugs, maternal alcohol, and maternal diabetes are considered as other etiological factors.

Septo-optic dysplasia associated with MCD (septo-optic dysplasia plus) is considered a genetic disorder affecting multiple stages of cortical development (Miller et al. 2000; Camino and Arjona 2003). The most common associated malformation is schizencephaly/polymicrogyria, and this condition has been coined as septo-optic dysplasia–schizencephaly syndrome (Barkovich et al. 2005).

13.2.3 Clinical Presentation

Children may present with visual impairment (uni- or bilateral blindness, nystagmus), short status, hypothalamic–pituitary dysfunction (60 % of patients), and developmental delay (Barkovich et al. 1989). If they have associated MCD, focal seizures with and without secondary generalization are common (Fig. 25).

13.2.4 Imaging

The syndrome is defined by absence or partial absence of the septum pellucidum and optic nerve hypoplasia. Pituitary hyoplasia with or without ectopic hyperintensity of the posterior lobe is present in 2/3 of cases.

Associated brain abnormalities include schizencephaly/polymicrogyria (1/3–1/2 of patients), as well as other MCD including heterotopias (Barkovich et al. 1989; Camino and Arjona 2003), callosal dysgenesis, ocular abnormalities (coloboma, anophthalmia, microphthalmia), and olfactory bulb hypoplasia.

13.3 Kallmann Syndrome

13.3.1 Epidemiology and Pathogenesis

This rare (prevalence 1 to 1:10,000 in men and 1:50,000 in women) congenital malformation was initially described by Kallmann et al. (1944). Olfactory cells that normally express LHRH fail to migrate from the medial olfactory placode into the forebrain. In addition, projections from the lateral olfactory placode to the forebrain are insufficient to induce olfactory bulb formation (Truwit et al. 1993). Inheritance is X-linked (mutations of the *KAL1* gene on Xp22.3), autosomal recessive, or autosomal dominant.

13.3.2 Clinical Presentation

Hyposmia or anosmia, hypogonadism due to hypothalamic insufficiency, involuntary movements of a body segment in reply to voluntary movements of the similar contralateral segment (mirror movements) and renal abnormalities (e.g., unilateral agenesis) in X-linked Kallmann syndrome. ♂ > ♀

13.3.3 Imaging

Kallmann syndrome appears as olfactory bulb, tract, and sulcus a-/hypoplasia, and small adenohypophysis due to insufficient hypothalamic stimulation, posterior pituitary lobe is normal (Knorr et al. 1993) (Fig. 26).

13.4 Shapiro Syndrome

13.4.1 Epidemiology and Pathogenesis

This very rare syndrome initially described by Shapiro in 1969 is characterized by the triad of spontaneous hypothermia, hyperhidrosis, and corpus callosum a/hypogenesis (Shapiro et al. 1969).

13.4.2 Clinical Presentation

Recurrent episodes of diffuse hyperhidrosis and hypothermia usually last several hours and are likely caused by hypothalamic dysfunction (Tambasco et al. 2005; Dundar et al. 2008).

13.4.3 Imaging

Anterior callosal a/hypogenesis (Fig. 26). A single case with normal corpus callosum and increased perfusion of the thalamus, basal ganglia, and inferior frontal areas indicating ictal activity has been described (Dundar et al. 2008).

References

Adachi Y, Poduri A, Kawaguch A, Yoon G, Salih MA, Yamashita F, Walsh CA, Barkovich AJ (2011) Congenital microcephaly with a simplified gyral pattern: associated findings and their significance. AJNR Am J Neuroradiol 32(6):1123–1129

Adamsbaum C, Robain O, Cohen PA, Delalande O, Fohlen M, Kalifa G (1998) Focal cortical dysplasia and hemimegalencephaly: histological and neuroimaging correlations. Pediatr Radiol 28(8):583–590

Aicardi J, Lefebvre J, Leriqu-Koechlin A (1965) A new syndrome: spasm in flexion, callosal agenesis, ocular abnormalities. Electroencephalogr Clin Neurophysiol 19:609–610

Ashwal S, Michelson D, Plawner L (2009) Quality Standards Subcommittee of the American Academy of Neurology and the Practice Committee of the Child Neurology Society. Practice parameter: evaluation of the child with microcephaly (an evidence-based review): report of the Quality Standards Subcommittee of the American Academy of Neurology and the Practice Committee of the Child Neurology Society. Neurology 73(11):887–897

Barkovich AJ, Fram EK, Norman D (1989) Septo-optic dysplasia. MR Imaging. Radiology 171:189–192

Barkovich AJ, Chuang SH (1990) Unilateral megalencephaly: correlation of MR imaging and pathologic characteristics. AJNR Am J Neuroradiol 11:523–531

Barkovich AJ, Quint DJ (1993) Middle interhemispheric fusion: an unusual variant of holoprosencephaly. AJNR Am J Neuroradiol 14(2):431–440

Barkovich AJ, Guerrini R, Battaglia G, Kalifa G, N'Guyen T, Parmeggiani A, Santucci M, Giovanardi-Rossi P, Granata T, D'Incerti L (1994) Band heterotopia: correlation of outcome with magnetic resonance imaging parameters. Ann Neurol 36:609–617

Barkovich AJ, Kuzniecky RI, Dobyns WB, Jackson GD, Becker LE, Evrard P (1996) A classification scheme for malformations of cortical development. Neuropediatrics 27:59–63

Barkovich AJ, Kuzniecky RI, Bollen AW, Grant PE (1997) Focal transmantle dysplasia: a specific malformation of cortical development. Neurology 49(4):1148–1152

Barkovich AJ, Ferriero DM, Barr RM, Gressens P, Dobyns WB, Truwit CL, Evrard P (1998) Microlissencephaly: a heterogeneous malformation of cortical development. Neuropediatrics 29:113–119

Barkovich AJ (2000) Morphologic characteristics of subcortical heterotopia: MR imaging study. AJNR Am J Neuroradiol 21:290–295

Barkovich AJ, Kuzniecky RI (2000) Gray matter heterotopia. Neurology 55:1603–1608

Barkovich AJ, Kuzniecky RI, Jackson GD, Guerrini R, Dobyns WB (2001) Classification system for malformations of cortical development: update 2001. Neurology 57:2168–2178

Barkovich AJ (2002) Morphological features and associated anomalies of schizencephaly in the clinical population: detailed analysis of MR images. Neuroradiology 44:647–655

Barkovich AJ, Kuzniecky RI, Jackson GD, Guerrini R, Dobyns WB (2005) A developmental and genetic classification for malformations of cortical development. Neurology 65:1873–1887

Barkovich AJ (2010) Current concepts of polymicrogyria. Neuroradiology 52:479–487

Barkovich AJ, Guerrini R, Kuzniecky RI, Jackson GD, Dobyns WB (2012) A developmental and genetic classification for malformations of cortical development: update 2012. Brain 135:1348–1369

Becker AJ, Urbach H, Scheffler B, Baden T, Normann S, Lahl L, Pannek H, Tuxhorn I, Elger CE, Schramm J, Wiestler OD, Blümcke I (2002) Focal cortical dysplasia of Taylor's balloon cell type: mutational analysis of the TSC1 gene indicates a pathogenic relationship to tuberous sclerosis. Ann Neurol 52:29–37

Besson P, Andermann F, Dubeau F, Bernasconi A (2008) Small focal cortical dysplasia lesions are located at the bottom of a deep sulcus. Brain 131:3246–3255

Blümcke I, Thom M, Aronica E, Armstrong DD, Vinters HV, Palmini A, Jacques TS, Avanzini G, Barkovich AJ, Battaglia G, Becker A, Cepeda C, Cendes F, Colombo N, Crino P, Cross JH, Delalande O, Dubeau F, Duncan J, Guerrini R, Kahane P, Mathern G, Najm I, Ozkara C, Raybaud C, Represa A, Roper SN, Salamon N, Schulze-Bonhage A, Tassi L, Vezzani A, Spreafico R (2011) The clinicopathologic spectrum of focal cortical dysplasias: a consensus classification proposed by an ad hoc Task Force of the ILAE Diagnostic Methods Commission. Epilepsia 52:158–174

Bond J, Roberts E, Mochida GH, Hampshire DJ, Scott S, Askham JM, Springell K, Mahadevan M, Crow YJ, Markham AF, Walsh CA, Woods CG (2002) ASPM is a major determinant of cerebral cortical size. Nat Genet 32:316–320

Bond J, Scott S, Hampshire DJ, Springell K, Corry P, Abramowicz MJ, Mochida GH, Hennekam RC, Maher ER, Fryns JP, Alswaid A, Jafri H, Rashid Y, Mubaidin A, Walsh CA, Roberts E, Woods CG (2003) Protein-truncating mutations in ASPM cause variable reduction in brain size. Am J Hum Genet 73:1170–1177

Bond J, Roberts E, Springell K, Lizarraga SB, Scott S, Higgins J, Hampshire DJ, Morrison EE, Leal GF, Silva EO, Costa SM, Baralle D, Raponi M, Karbani G, Rashid Y, Jafri H, Bennett C, Corry P, Walsh CA, Woods CG (2005) A centrosomal mechanism involving CDK5RAP2 and CENPJ controls brain size. Nat Genet 37:353–355

Broumandi DD, Hayward UM, Benzian JM, Gonzalez I, Nelson MD (2004) Best cases from the AFIP: hemimegalencephaly. Radiographics 24(3):843–848

Camino R, Arjona A (2003) Septo-optic dysplasia plus. Lancet Neurol 2:436

Cepeda C, Hurst RS, Flores-Hernández J, Hernández-Echeagaray E, Klapstein GJ, Boylan MK, Calvert CR, Jocoy EL, Nguyen OK, André VM, Vinters HV, Ariano MA, Levine MS, Mathern GW (2003) Morphological and electrophysiological characterization of abnormal cell types in pediatric cortical dysplasia. J Neurosci Res 72(4):472–486

Chamberlain WA, Cohen ML, Gyure KA, Kleinschmidt-DeMasters BK, Perry A, Powell SZ, Qian J, Staugaitis SM, Prayson RA (2009) Interobserver and intraobserver reproducibility in focal cortical dysplasia (malformations of cortical development). Epilepsia 50:2593–2598

Chang BS, Aspe KA, Caraballo A, Cross JH, Mclellan A, Jacobson RD, Valente KD, Barkovich AJ, Walsh CA (2006) A familiar syndrome of unilateral polymicrogyria affecting the right hemisphere. Neurology 66:133–135

Chang EF, Wang DD, Barkovich AJ, Tihan T, Auguste KI, Sullivan JE, Garcia PA, Barbaro NM (2011) Predictors of seizure freedom after surgery for malformations of cortical development. Ann Neurol 70(1):151–162

Clement E, Mercuri E, Godfrey C, Smith J, Robb S, Kinali M, Straub V, Bushby K, Manzur A, Talim B, Cowan F, Quinlivan R, Klein A, Longman C, McWilliam R, Topaloglu H, Mein R, Abbs S, North K, Barkovich AJ, Rutherford M, Muntoni F (2008) Brain involvement in muscular dystrophies with defective dystroglycan glycosylation. Ann Neurol 64(5):573–582

de Morsier G (1956) Etudes sum les dysraphies cranio-encephaliques. III. Agenesie du septum lucidum avec malformation du tractus optique: Ia dysplasie septo-optique. Schweiz Arch Neurol Psychiatr 77:267–292

DeMyer W, Zeman W, Palmer GG (1964) The face predicts the brain. Diagnostic significance of median facial anomalies for holoprosencephaly (arhinencephaly). Pediatrics 34:256–263

Dixon-Salazar T, Silhavy JL, Marsh SE, Louie CM, Scott LC, Gururaj A, Al-Gazali L, Al-Tawari AA, Kayserili H, Sztriha L, Gleeson JG (2004) Mutations in the AHI1 gene encoding jouberin cause Joubert syndrome with cortical polymicrogyria. Am J Hum Genet 75:979–987

Dobyns WB (2010) The clinical patterns and molecular genetics of lissencephaly and subcortical band heterotopia. Epilepsia 51(Suppl. 1):5–9

Dobyns WB, Barkovich AJ (1999) Microcephaly with simplified gyral pattern (oligogyric microcephaly) and microlissencephaly. Neuropediatrics 30:105–106

Dobyns WB, Andermann E, Andermann F, Czapansky-Beilman D, Dubeau F, Dulac O, Guerrini R, Hirsch B, Ledbetter DH, Lee NS, Motte J, Pinard JM, Radtke RA, Ross ME, Tampieri D, Walsh CA, Truwit CL (1996) X-linked malformations of neuronal migration. Neurology 47(2):331–339

Dobyns WB, Guerrini R, Czapansky-Beilman DK, Pierpont ME, Breningstall G, Yock DH Jr, Bonanni P, Truwit CL (1997) Bilateral periventricular nodular heterotopia with mental retardation and syndactyly in boys: a new X-linked mental retardation syndrome. Neurology 49(4):1042–1047

Dundar NO, Boz A, Duman O, Aydin F, Haspolat S (2008) Spontaneous periodic hypothermia and hyperhidrosis. Pediatr Neurol 39:438–440

Fauser S, Huppertz HJ, Bast T, Strobl K, Pantazis G, Altenmueller DM, Feil B, Rona S, Kurth C, Rating D, Korinthenberg R, Steinhoff BJ, Volk B, Schulze-Bonhage A (2006) Clinical characteristics in focal cortical dysplasia: a retrospective evaluation in a series of 120 patients. Brain 129:1907–1916

Flores-Sarnat L (2002) Hemimegalencephaly. I. Genetic, clinical, and imaging aspects. J Child Neurol 17:373–384

Flores-Sarnat L, Sarnat HB, Dávila-Gutiérrez G, Alvarez A (2003) Hemimegalencephaly: part 2. Neuropathology suggests a disorder of cellular lineage. J Child Neurol 18(11):776–785

Forman MS, Squier W, Dobyns WB, Golden JA (2005) Genotypically defined lissencephalies show distinct pathologies. J Neuropathol Exp Neurol 64(10):847–857

Fox JW, Lamperti ED, Ekşioğlu YZ, Hong SE, Feng Y, Graham DA, Scheffer IE, Dobyns WB, Hirsch BA, Radtke RA, Berkovic SF, Huttenlocher PR, Walsh CA (1998) Mutations in filamin 1 prevent migration of cerebral cortical neurons in human periventricular heterotopia. Neuron 21(6):1315–1325

Frazier JL, Goodwin CR, Ahn ES, Jallo GI (2009) A review on the management of epilepsy associated with hypothalamic hamartomas. Childs Nerv Syst 25:423–432

Freeman JL, Coleman LT, Wellard RM, Kean MJ, Rosenfeld JV, Jackson GD, Berkovic SF, Harvey AS (2004) MR imaging and

spectroscopic study of epileptogenic hypothalamic hamartomas: analysis of 72 cases. AJNR Am J Neuroradiol 25:450–462
Friede R (1989) Developmental neuropathology, 2nd edn. Springer, Berlin
Garavelli L, Guareschi E, Errico S, Simoni A, Bergonzini P, Zollino M, Gurrieri F, Mancini GM, Schot R, Van Der Spek PJ, Frigieri G, Zonari P, Albertini E, Giustina ED, Amarri S, Banchini G, Dobyns WB, Neri G (2007) Megalencephaly and perisylvian polymicrogyria with postaxial polydactyly and hydrocephalus [MPPH]: report of a new case. Neuropediatrics 38:200–203
Garbelli R, Milesi G, Medici V, Villani F, Didato G, Deleo F, D'Incerti L, Morbin M, Mazzoleni G, Giovagnoli AR, Parente A, Zucca I, Mastropietro A, Spreafico R (2012) Blurring in patients with temporal lobe epilepsy: clinical, high-field imaging and ultrastructural study. Brain, Aug 135(Pt 8):2337–2349
Giordano L, Vignoli A, Pinelli L, Brancati F, Accorsi P, Faravelli F, Gasparotti R, Granata T, Giaccone G, Inverardi F, Frassoni C, Dallapiccola B, Valente EM, Spreafico R (2009) Joubert syndrome with bilateral polymicrogyria: clinical and neuropathological findings in two brothers. Am J Med Genet A 149A:1511–1515
Gripp KW, Hopkins E, Vinkler C, Lev D, Malinger G, Lerman-Sagie T, Dobyns WB (2009) Significant overlap and possible identity of macrocephaly capillary malformation and megalencephaly polymicrogyria-polydactyly hydrocephalus syndromes. Am J Med Genet A 149A:868–876
Guerrini R, Dobyns WB (1998) Bilateral periventricular nodular heterotopia with mental retardation and frontonasal malformation. Neurology 51(2):499–503
Hayashi N, Tsutsumi Y, Barkovich AJ (2002) Polymicrogyria without porencephaly/schizencephaly. MRI analysis of the spectrum and the prevalence of macroscopic findings in the clinical population. Neuroradiology 44(8):647–655
Hermier M, Montavont A, Dupuis-Girod S, Cho TH, Honnorat J, Plauchu H (2010) Polymicrogyria: an underrecognized cause of epilepsy in in patients with hereditary hemorrhagic telangiectasia (Rendu-Osler disease). Epilepsia 51(Suppl 4):1–189
Hevner RF (2005) The cerebral cortex malformation in thanatophoric dysplasia: neuropathology and pathogenesis. Acta Neuropathol 110(3):208–221
Hildebrandt M, Pieper T, Winkler P, Kolodziejczyk D, Holthausen H, Blümcke I (2005) Neuropathological spectrum of cortical dysplasia in children with severe focal epilepsies. Acta Neuropathol 110(1):1–11
Hoyt CS, Billson F, Ouvrier R, Wise G (1978) Ocular features of Aicardi's syndrome. Arch Ophthalmol 96:291–295
Huppertz HJ, Wellmer J, Staack AM, Altenmüller DM, Urbach H, Kröll J (2008) Voxel-based 3-D MRI analysis helps to detect subtle forms of subcortical band heterotopia. Epilepsia 49(5):772–785
Jackson AP (2002) Identification of microcephalin, a protein implicated in determining the size of the human brain. Am J Hum Genet 71(1):136–142
Jansen A, Andermann E (2005) Genetics of the polymicrogyria syndromes. J Med Genet 42(5):369–378
Jissendi-Tchofo P, Kara S, Barkovich AJ (2009) Midbrain–hindbrain involvement in lissencephalies. Neurology 72(5):410–418
Kallmann FT, Schoenfeld WA, Barrera SE (1944) The genetics aspects of primary eunuchoidism. Am J Mental Deficits 48:203–208
Kirschstein T, Fernandez G, Grunwald T, Pezer N, Urbach H, Blümcke I, Van Roost D, Lehnertz K, Elger CE (2003) Heterotopias, cortical dysplasias and glioneural tumors participate in cognitive processing in patients with temporal lobe epilepsy. Neurosci Lett 338:237–241
Knorr JR, Ragland RL, Brown RS, Gelber N (1993) Kallmann syndrome: MR findings. AJNR Am J Neuroradiol. 14(4):845–851
Krsek P, Maton B, Korman B, Pacheco-Jacome E, Jayakar P, Dunoyer C, Rey G, Morrison G, Ragheb J, Vinters HV, Resnick T, Duchowny M (2008) Different features of histopathological subtypes of pediatric focal cortical dysplasia. Ann Neurol 63(6):758–769
Krsek P, Pieper T, Karlmeier A, Hildebrandt M, Kolodziejczyk D, Winkler P, Pauli E, Blümcke I, Holthausen H (2009a) Different presurgical characteristics and seizure outcomes in children with focal cortical dysplasia type I or II. Epilepsia 50(1):125–137
Krsek P, Maton B, Jayakar P, Dean P, Korman B, Rey G, Dunoyer C, Pacheco-Jacome E, Morrison G, Ragheb J, Vinters HV, Resnick T, Duchowny M (2009b) Incomplete resection of focal cortical dysplasia is the main predictor of poor postsurgical outcome. Neurology 72(3):217–223
Kuzniecky R, Andermann F, Guerrini R (1993) Congenital bilateral perisylvian syndrome: study of 31 patients. The congenital bilateral perisylvian syndrome multicenter collaborative study. Lancet 341:608–612
Lerner JT, Salamon N, Hauptman JS, Velasco TR, Hemb M, Wu JY, Sankar R, Donald Shields W, Engel J Jr, Fried I, Cepeda C, Andre VM, Levine MS, Miyata H, Yong WH, Vinters HV, Mathern GW (2009) Assessment of surgical outcomes for mild type I and severe type II cortical dysplasia: a critical review and the UCLA experience. Epilepsia 50:1310–1335
Leventer RJ, Jansen A, Pilz DT, Stoodley N, Marini C, Dubeau F, Malone J, Mitchell LA, Mandelstam S, Scheffer IE, Berkovic SF, Andermann F, Andermann E, Guerrini R, Dobyns WB (2010) Clinical and imaging heterogeneity of polymicrogyria: a study of 328 patients. Brain 133:1415–1427
Lewis AJ, Simon EM, Barkovich AJ, Clegg NJ, Delgado MR, Levey E, Hahn JS (2002) Middle interhemispheric variant of holoprosencephaly: a distinct cliniconeuroradiologic subtype. Neurology 59(12):1860–1865.
Matsunaga E, Shiota K (1977) Holoprosencephaly in human embryos: epidemiologic studies of 150 cases. Teratology 16:261–272
Miller SP, Shevell MI, Patenaude Y, Poulin C, O'Gorman AM (2000) Septo-optic dysplasia plus: a spectrum of malformations of cortical development. Neurology 54:1701–1703
Moog U, De Die-Smulders CE, Schrander-Stumpel CT, Engelen JJ, Hamers AJ, Frints S, Fryns JP (2001) Holoprosencephaly: the Maastricht experience. Genet Couns 12(3):287–298
Oba H, Barkovich AJ (1995) Holoprosencephaly: an analysis of callosal formation and its relation to development of the interhemispheric fissure. AJNR Am J Neuroradiol 16:453–460
Palm L, Hägerstrand I, Kristoffersson U, Blennow G, Brun A, Jörgensen C (1986) Nephrosis and disturbances of neuronal migration in male siblings–a new hereditary disorder? Arch Dis Child 61(6):545–548
Palmini A, Lüders H (2002) Classification issues in malformations caused by abnormalities of cortical development. Neurosurg Clin N Am 13:1–16
Palmini A, Najm I, Avanzini G, Babb T, Guerrini R, Foldvary-Schaefer N, Jackson G, Lüders HO, Prayson R, Spreafico R, Vinters HV (2004) Terminology and classification of the cortical dysplasias. Neurology 62(6 Suppl 3):S2–S8. Review
Pattison L, Crow YJ, Deeble VJ, Jackson AP, Jafri H, Rashid Y, Roberts E, Woods CG (2000) A fifth locus for primary autosomal recessive microcephaly maps to chromosome 1q31. Am J Hum Genet 67:1578–1580
Pilz DT, Matsumoto N, Minnerath S, Mills P, Gleeson JG, Allen KM, Walsh CA, Barkovich AJ, Dobyns WB, Ledbetter DH, Ross ME (1998) LISI and XLIS (DCX) mutations cause most classical lissencephaly, but different patterns of malformation. Hum Mol Genet 7:2029–2037
Pilz DT, Kuc J, Matsumoto N, Bodurtha J, Bernadi B, Tassinari CA, Dobyns WB, Ledbetter DH (1999) Subcortical band heterotopia in

rare affected males can be caused by missense mutations in DCX (XLIS) or LIS1. Hum Mol Genet 8(9):1757–1760
Rakic P (1988) Defects of neuronal migration and the pathogenesis of cortical malformation. Prog Brain Res 73:15–37
Roach E, Demyer W, Conneally PM, Palmer C, Merritt AD (1975) Holoprosencephaly: birth data, benetic and demographic analyses of 30 families. Birth Defects Orig Artic Ser 11(2):294–313
Robin NH, Ko LM, Heeger S, Muise KL, Judge N, Bangert BA (1996) Syntelencephaly in an infant of a diabetic mother. Am J Med Genet 66:433–437
Roessler E, Muenke M (1999) The molecular genetics of holoprosencephaly: a model of brain development for the next century. Child's Nerv Syst 15:646–651
Rosenberg MJ, Agarwala R, Bouffard G, Davis J, Fiermonte G, Hilliard MS, Koch T, Kalikin LM, Makalowska I, Morton DH, Petty EM, Weber JL, Palmieri F, Kelley RI, Schäffer AA, Biesecker LG (2002) Mutant deoxynucleotide carrier is associated with congenital microcephaly. Nat Genet 32(1):175–179
Ross ME, Swanson K, Dobyns WB (2001) Lissencephaly with cerebellar hypoplasia (LCH): a heterogeneous group of cortical malformations. Neuropediatrics 32:256–263
Schijns OE, Bien CG, Majores M, von Lehe M, Urbach H, Becker A, Schramm J, Elger CE, Clusmann H (2011) Presence of temporal gray–white matter abnormalities does not influence epilepsy surgery outcome in temporal lobe epilepsy with hippocampal sclerosis. Neurosurgery 68(1):98–106
Shapiro WR, Williams GH, Plum F (1969) Spontaneous recurrent hypothermia accompanying agenesis of the corpus callosum. Brain 92:423–436
Sheen VL, Wheless JW, Bodell A, Braverman E, Cotter PD, Rauen KA, Glenn O, Weisiger K, Packman S, Walsh CA, Sherr EH (2003) Periventricular heterotopia associated with chromosome 5p anomalies. Neurology 60(6):1033–1036
Sheen VL, Ganesh VS, Topcu M, Sebire G, Bodell A, Hill RS, Grant PE, Shugart YY, Imitola J, Khoury SJ, Guerrini R, Walsh CA (2004) Mutations in ARFGEF2 implicate vesicle trafficking in neural progenitor proliferation and migration in the human cerebral cortex. Nat Genet 36(1):69–76
Shen J, Gilmore EC, Marshall CA, Haddadin M, Reynolds JJ, Eyaid W, Bodell A, Barry B, Gleason D, Allen K, Ganesh VS, Chang BS, Grix A, Hill RS, Topcu M, Caldecott KW, Barkovich AJ, Walsh CA (2010) Mutations in PNKP cause microcephaly, seizures and defects in DNA repair. Nat Genet 42(3):245–249
Sicca F, Kelemen A, Genton P, Das S, Mei D, Moro F, Dobyns WB, Guerrini R (2003) Mosaic mutations of the LISI gene cause subcortical band heterotopia. Neurology 61(8):1042–1046
Simon EM, Hevner RF, Pinter J, Clegg NJ, Delgado M, Kinsman SL, Hahn JS, Barkovich AJ (2001) The dorsal cyst in holoprosencephaly and the role of the thalamus in its formation. Neuroradiology 43:787–791
Sims J (1835) On hypertrophy and atrophy of the brain. Med Quir Trans 19:315–380
Takanashi J, Barkovich AJ (2003) The changing MR imaging appearance of polymicrogyria: a consequence of myelination. AJNR Am J Neuroradiol 24(5):788–793
Tambasco N, Corea F, Bocola V (2005) Subtotal corpus callosum agenesis with recurrent hyperhidrosis-hypothermia (Shapiro syndrome). Neurology 65:124
Tampieri D, Walsh CA, Truwit CL (1993) X-linked malformations of neuronal migration. Neurology 47:331–339
Tassi L, Garbelli R, Colombo N, Bramerio M, Lo Russo G, Deleo F, Milesi G, Spreafico R (2010) Type I focal cortical dysplasia: surgical outcome is related to histopathology. Epileptic Disord 3:181–191
Taylor DC, Falconer MA, Bruton CJ, Corsellis JA (1971) Focal dysplasia of the cerebral cortex in epilepsy. J Neurol Neurosurg Psychiatry 34(4):369–387
Tortori-Donati P (2005) Pediatric neuroradiology brain. Springer, Berlin
Truwit CL, Barkovich AJ, Grumbach MM, Martini JJ (1993) MR imaging of Kallmann syndrome, a genetic disorder of neuronal migration affecting the olfactory and genital systems. AJNR Am J Neuroradiol 14(4):827–838
Urbach H, Scheffler B, Heinrichsmeier T, von Oertzen J, Kral T, Wellmer J, Schramm J, Wiestler OD, Blümcke I (2002) Focal cortical dysplasia of Taylor's balloon cell type: a clinicopathological entity with characteristic neuroimaging and histopathological features, and favorable postsurgical outcome. Epilepsia 43:33–40
Urbach H, Blümcke I, Becker A, Solymosi L (2003) Störungen der kortikalen Entwicklung: Bildgebung und Klassifizierung. Klin Neuroradiol 13:163–172
Valdueza JM, Cristante L, Dammann O, Bentele K, Vortmeyer A, Saeger W, Padberg B, Freitag J, Herrmann HD (1994) Hypothalamic hamartomas: with special reference to gelastic epilepsy and surgery. Neurosurgery 34:949–958
Wagner J, Wellmer J, Urbach H, Niehusmann P, von Lehe M, Elger CE (2011a) Focal cortical dysplasia type IIb: completeness of cortical, not subcortical resection is necessary for seizure freedom. Epilepsia 52:1418–1424
Wagner J, Weber B, Urbach H, Elger CE, Huppertz HJ (2011b) Morphometric MRI analysis improves detection of focal cortical dysplasia type II. Brain 134(Pt 10):2844–2854
Widdess-Walsh P, Kellinghaus C, Jeha L, Kotagal P, Prayson R, Bingaman W, Najm IM (2005) Electro-clinical and imaging characteristics of focal cortical dysplasia: correlation with pathological subtypes. Epilepsy Res 67:25–33
Wolpert SM, Cohen A, Libenson MH (1994) Hemimegalencephaly: a longitudinal MR study. AJNR Am J Neuroradiol 15:1479–1482
Yagishita A, Arai N, Tamagawa K, Oda M (1998) Hemimegalencephaly: signal changes suggesting abnormal myelination on MRI. Neuroradiology 40(11):734–738
Yakovlev PI (1959) Pathoarchitectonic studies of cerebral malformations. III. Arhinencephalies (holoprosencephalies). J Neuropathol Exp Neurol 18:22–55

Neurocutaneous Diseases (Phakomatoses)

Horst Urbach

Contents

Abstract

This chapter describes phakomatoses associated with epilepsy, namely, tuberous sclerosis complex, Sturge–Weber syndrome, neurofibromatosis type 1, meningioangiomatosis, hypomelanosis of Ito, epidermal nevus syndrome and variants, incontinentia pigmenti, lipoproteinosis, and linear scleroderma, which is also known as en coup de sabre syndrome.

1 Introduction

Phakomatosis is an umbrella term for several diseases with hamartomas/hamartomatous tumors in the brain and the skin. The term is derived from the Greek word *φακός*, meaning "lens" or "spot." Relevant phakomatoses with respect to epilepsy comprise tuberous sclerosis complex (TSC), Sturge–Weber syndrome, neurofibromatosis type 1, meningioangiomatosis, hypomelanosis of Ito, and epidermal nevus syndrome and variants. Others, like incontinentia pigmenti, lipoproteinosis, and linear scleroderma (en coup de sabre syndrome), are rare conditions, yet is their pathogenesis fully understood. Seizures in neurofibromatosis type 2 patients are rather rare and likely secondary to leptomeningeal tumors (meningioma, meningioangiomatosis).

2 Tuberous Sclerosis Complex

Synonym: M. Bourneville–Pringle

Epidemiology: The second-most common phakomatosis after NF1, characterized by multiple hamartomas in different organs. The prevalence is 1:30,000, and the birth incidence 1:6,000 (Osborne et al. 1991). The incidence of forme fruste forms is likely higher.

Pathogenesis: Autosomal-dominant disease with variable expressivity and low penetrance. High percentage of de novo mutations. Two genes have been identified: The *TSC1*

H. Urbach (✉)
Department of Neuroradiology,
University Hospital Freiburg, Germany
e-mail: horst.urbach@uniklinik-freiburg.de

H. Urbach (ed.), *MRI in Epilepsy*, Medical Radiology. Diagnostic Imaging,
DOI: 10.1007/174_2012_780,

Table 1 Tuberous sclerosis complex (TSC): diagnostic criteria and modalities

	Frequency, clinical characteristics, and imaging modality of choice
Major features	
Facial angiofibroma or forehead plaque	Rare before age of 4, often "butterfly" distribution
Nontraumatic ungual or periungual fibroma	20–35 % of postpubertal patients
Three or more hypomelanotic macules	Present at birth, demonstrated by Wood's light
Shagreen patch (connective tissue nevus)	20–35 % of postpubertal patients
Multiple retinal nodular hamartomas	
Cortical tubers	Indistinguishable from FCDs IIB
Subependymal nodules	50 % calcify, T2-weighted gradient echo and SWI sequences, CT
Subependymal giant cell astrocytoma	Around 20 % of TSC patients, peak incidence in second decade, grow with different velocities in region of foramen of Monroe. Contrast-enhanced T1-weighted MRI with follow-up is mandatory
Cardiac rhabdomyoma, single or multiple	Cardiac ultrasound
Lymphangiomyomatosis[a]	Chest computed tomography
Renal angiomyolipoma[a]	Ultrasound
Minor features	
Multiple, randomly distributed pits in dental enamel	Inspection
Hamartomatous rectal polyps	Histologic confirmation is suggested
Bone cysts	Radiographic proof is sufficient
Cerebral white matter radiation lines	MRI proof is sufficient
Gingiva fibromas	Inspection
Nonrenal hamartomas	Histologic confirmation is suggested
Retinal achromic patch	Fundoscopy
"Confetti" skin lesions	Inspection
Multiple renal cysts	Histologic confirmation is suggested

[a] When both lymphangiomyomatosis and renal angiomyolipoma are present, other TSC features are needed to establish a definite diagnosis
Adapted from Roach et al. (1998)

gene on chromosome 9q34 encodes for a protein called tuberin, while the *TSC2* gene on chromosome 16p13 encodes for a protein called hamartin. Both genes act together as tumor suppressor genes. *TSC2* mutations are more common than *TSC1* mutations, and both somatic and germline mosaicisms have been described.

Clinical presentation: Up to 90 % of patients have drug-resistant seizures, which often start as infantile spasms in the first months of life. In addition, mental retardation, behavioral problems, and learning difficulties are common (Table 1).

Imaging: Cranial MRI may show the classical triad of cortical tubers indistinguishable from FCDs IIB, subependymal calcified nodules, and subependymal giant cell astrocytoma. Subependymal giant cell astrocytoma may develop with different velocities most often in the region of the Foramen of Monro. Contrast-enhanced T1-weighted MRI with follow-up studies is therefore mandatory. Recent studies indicate that subependymal giant cell astrocytomas shrink under a drug therapy with everolimus (Krueger et al. 2010) (Fig. 1).

3 Sturge–Weber Syndrome

Synonym: Encephalotrigeminal angiomatosis

Epidemiology: Rare (1:50,000), sporadic, congenital, noninherited, but sometimes familial neurocutaneous disease; m = f. Initial description by William Allen Sturge in 1879.

Pathogenesis: Faulty "involution" of fetal cortical veins with the creation of a pial angiomatosis characterized by numerous small and tortuous dark purple venules. Due to progressive venous occlusion and chronic venous ischemia, brain atrophy and "tram-track" calcifications in the cortex underlying the angioma and in the subcortical white matter result.

Clinical presentation: Port-wine nevus in the territory of cranial nerves V1 and V2 is present at birth. Fifty percent of patients have additional trunk and limb port-wine nevi and mucous membrane angiomatosis. The port-wine nevus almost always lies above the palpebral fissure involving the upper eyelid and the frontal region. Lesions close to the midline are commonly associated with anteriorly located

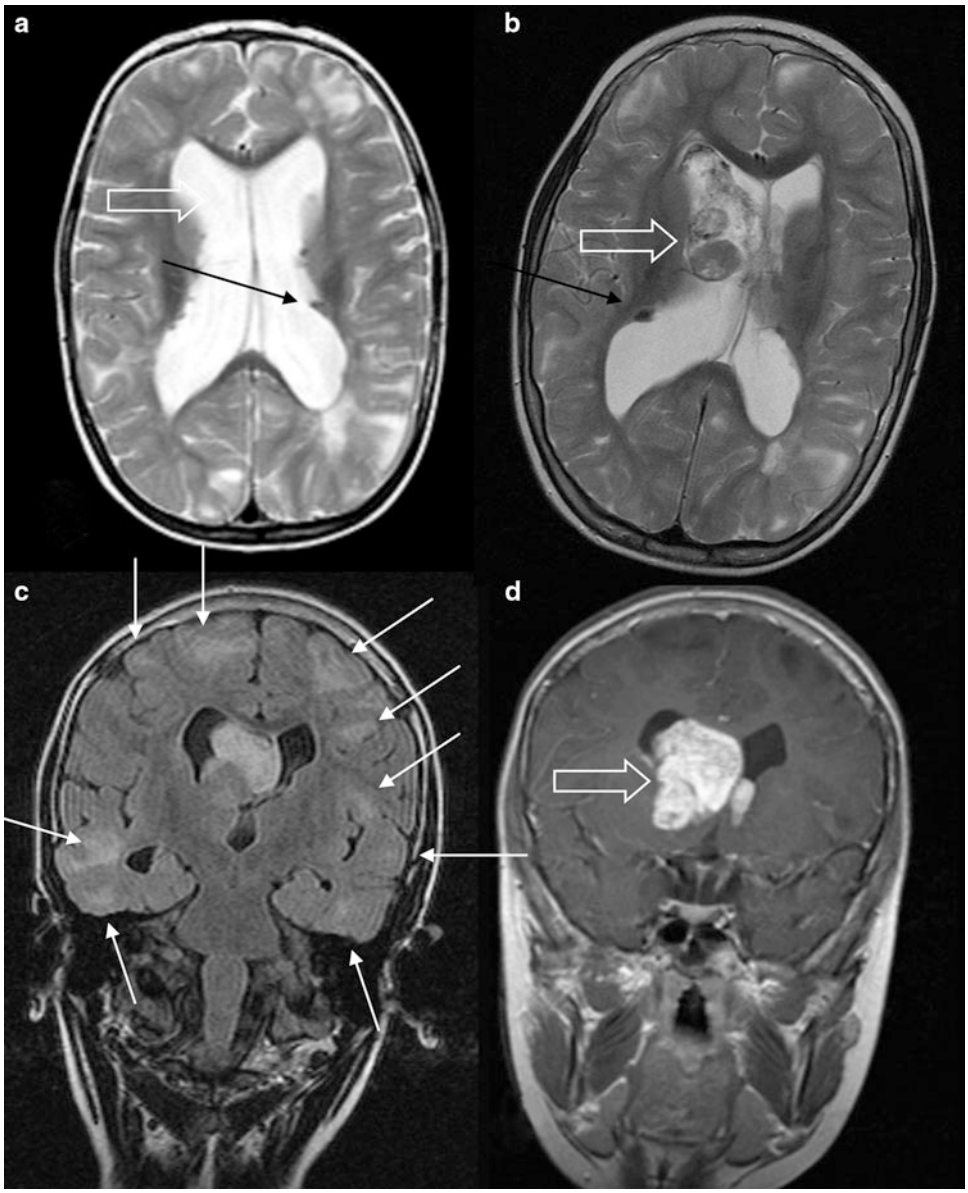

Fig. 1 Tuberous sclerosis complex with multiple cortical tubers (**c**: *white arrows*), subependymal nodules (**a**, **b**: *black arrows*), and a subependymal giant cell astrocytoma (**b**, **d**: *hollow arrow*). Six years before, the subependymal giant cell astrocytoma did not exist (**a**: *hollow arrow*). Cortical tubers are histopathologically and on MRI similar to FCD IIB. Subependymal nodules calcify in around 50 % of cases and are therefore T2-hypointense. The subependymal giant cell astrocytoma is typically adjacent to the Foramen of Monro and the frontal horn of the lateral ventricle

pial angiomatosis, off-midline lesions with the more frequent parietooccipital angiomas (Enjolras et al. 1985).

Choroidal angioma (70 %) may cause congenital glaucoma and buphthalmos. Retinal telangiectatic vessels, scleral angioma, iris heterochromia.

Epileptic seizures (90 %) usually start in the first year of life: infantile spasms, tonic–clonic, myoclonic seizures.

Hemiparesis, hemianopia (66 %).

Migraine episodes starting with a mean age of 8 years.

Hypothyroidism.

Imaging: Unilateral > bilateral brain atrophy developing during the first years of life. Pial angiomatosis: present at birth, unilateral (80 %), bilateral (20 %). Occipital > parietal > frontal, temporal lobes > diencephalon > cerebellar involvement (Fig. 2).

"Tram-track" calcifications: can be present at birth, but usually develop during the first years of life.

Enlarged ipsilateral choroid plexus subjacent to pial angiomatosis.

In the early stage, increased white matter volume and T2-weighted signal due to accelerated myelin maturation. In late stages, atrophy, gliosis, and compensatory thick dipole and hyperpneumatized sinuses.

Orbital enhancement (>50 %) due to choroidal angioma, periorbital soft tissues, bony orbit, and frontal lobes.

Sometimes polymicrogyria and heterotopias (Fig. 3).

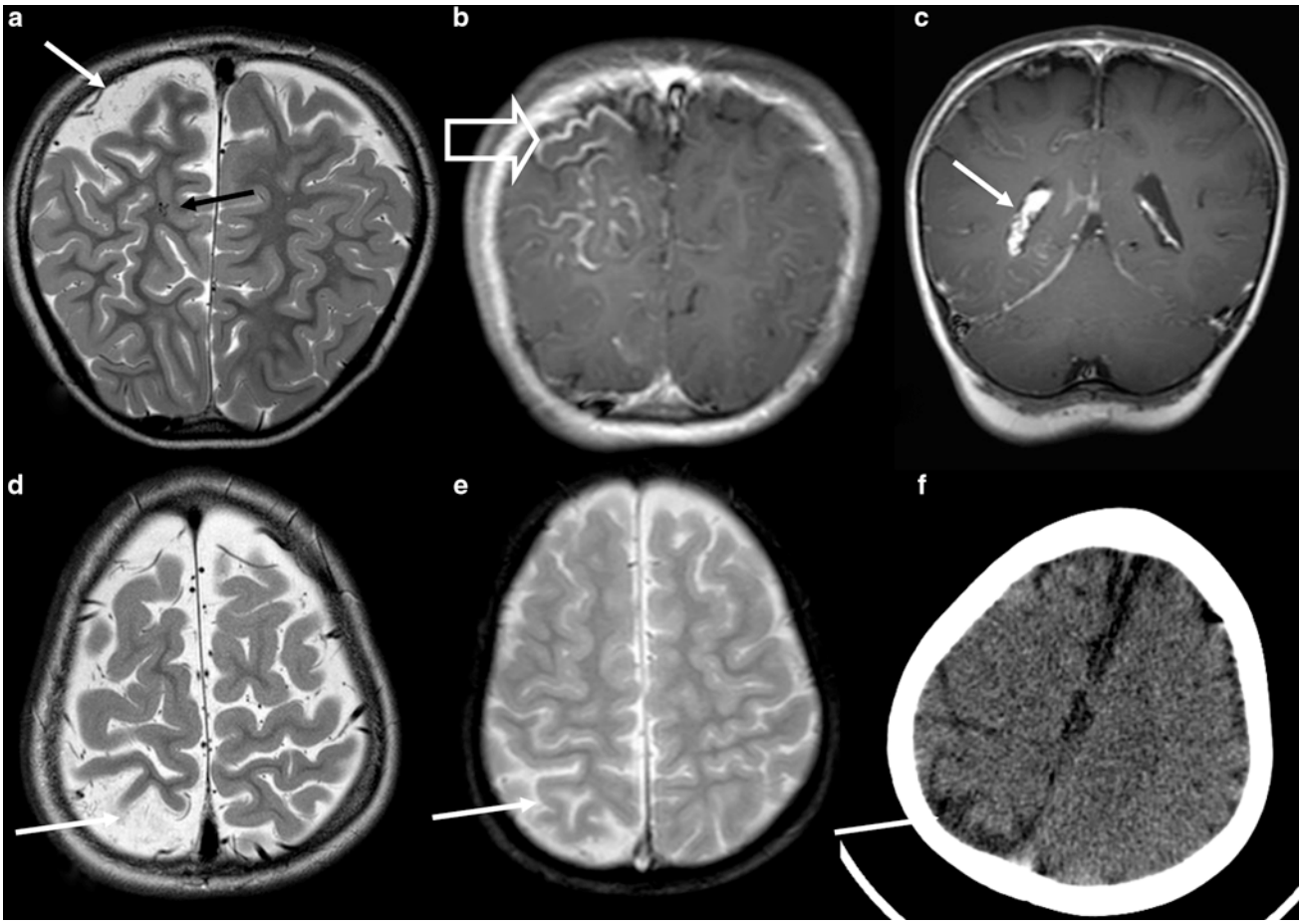

Fig. 2 Sturge–Weber syndrome in a 2.5-year-old boy with port-wine nevus in the right NV1 and V2 territories and complex focal motor seizures. MRI shows right-sided hemiatrophy with parietal accentuation (**a**, **d–f**: *arrow*) and pial angiomatosis covering the parietal, occipital, and temporal lobes (**b**: *hollow arrow*). T2-weighted images are rather unremarkable besides tiny flow void structures (**a**: *black arrow*). Choroid plexus "angioma" is another key feature of Sturge–Weber syndrome (**c**: *arrow*). In the first years of life, tram-track calcifications may be absent (**e**, **f**)

4 Neurofibromatosis Type 1

Synonym: von Recklinghausen disease

Epidemiology: Neurofibromatosis was initially described by the German pathologist Friedrich von Recklinghauen in 1882. It is an autosomal-dominant disorder with a prevalence of 1:3,000. However, 50 % of cases are new mutations. There are eight different neurofibromatosis subtypes, with NF1 accounting for 85 % of cases. The incidence of epilepsy in NF1 is around 5–10 %. All types of seizures, including infantile spasms, may occur.

Pathogenesis: The gene product of the *NF1* gene on chromosome 17q12 is neurofibromin, which acts as a tumor suppressor. Mutation of the *NF1* gene allows cell proliferation and tumor development.

Clinical presentation: NF1 may be diagnosed if two or more of the following features are present (NIH Consensus Conference 1988):

- Café au lait spots: These are well-delineated macules with a coffee-with-milk color. As an isolated finding, they are relatively common: 10–20 % of the general population has one or a few spots. Multiple café au lait spots are present in 90 % of NF1 patients. The presence of more than five spots having a diameter >5 mm in children and >15 mm in adults is suggestive for NF1. Note that café au lait spots may be the only clinical sign in children, who should be followed until early adulthood.
- Neurofibromas: Two neurofibromas or one plexiform neurofibroma: Neurofibromas are intracutaneous or subcutaneous tumors measuring from a few millimeters to several centimeters. They are sometimes found in children younger than 10 years of age and steadily increase in number with age. Plexiform neurofibromas are nonencapsulated cutaneous and subcutaneous tumors, which can be very large and continuous with intracranial or intraspinal tumors.

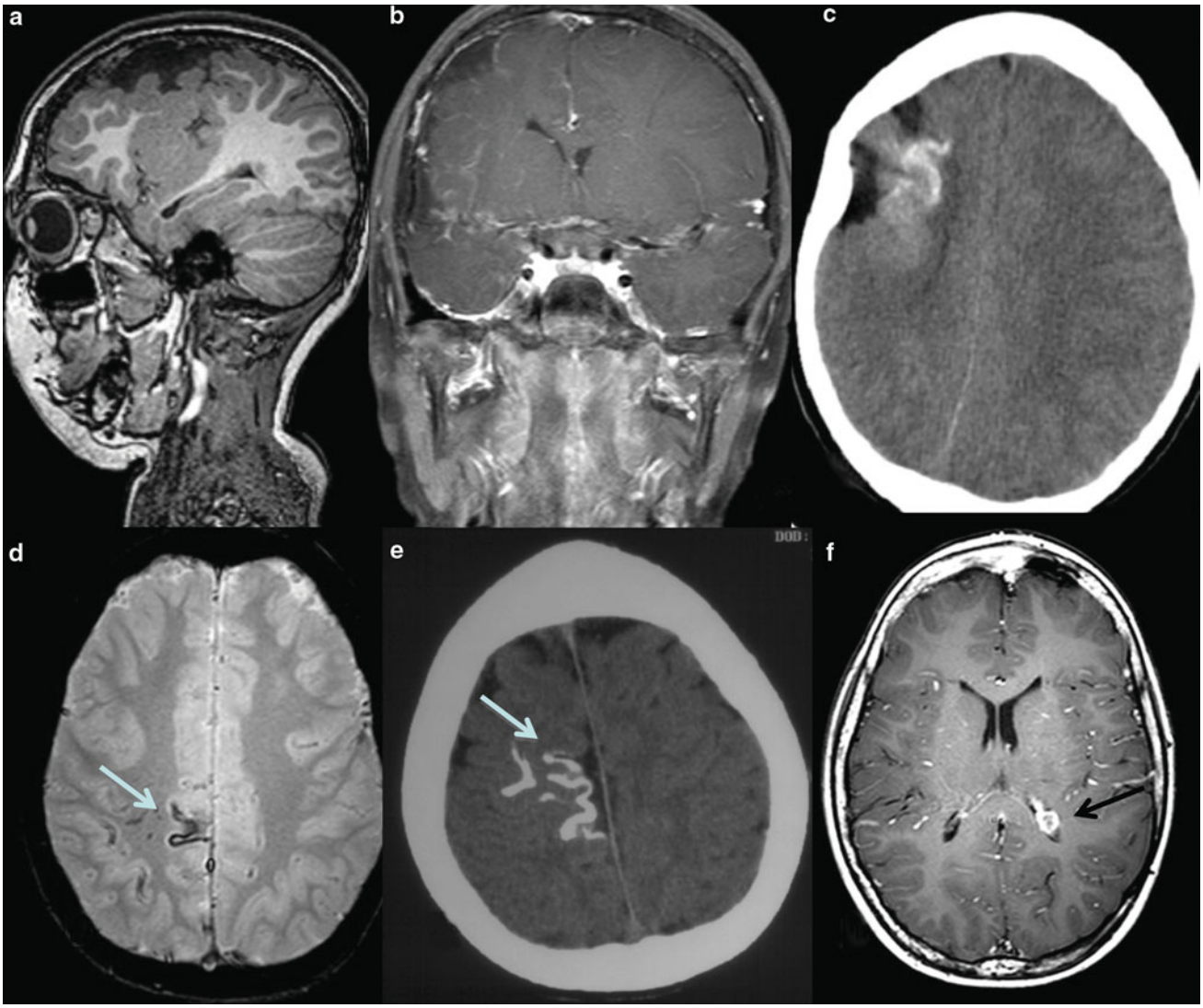

Fig. 3 (**a**–**c**) Atypical Sturge–Weber syndrome in a 16-year-old boy with focal frontal lobe atrophy associated with calcifications and large subcortical heterotopia. (**d**–**f**) Bilateral Sturge–Weber syndrome in a 12-year-old boy with bilateral port-wine nevi. MRI and CT in this case show vessel structures (**d**: *arrow*) and tram-track calcifications in the right hemisphere (**e**: *arrow*), but also an enlarged choroid plexus in the left trigone (**f**: *arrow*)

- Axillary and/or inguinal freckling: Smaller café au lait spots in the axillary and inguinal areas are seen in 20 % of NF1 patients.
- Optic glioma.
- Two or more Lisch nodules of the iris: Lisch nodules are pigmented iris hamartomas and found in 22–30 % of NF1 patients by 6 years of age and in nearly all patients after 12 years of age.
- Distinctive bony lesions (sphenoid bone dysplasia, others).
- First-degree relative with NF1.

Imaging: Optic nerve and hypothalamic gliomas are present in 15–20 % of NF1 patients. They are typically benign pilocytic astrocytomas differing from other optic gliomas by the presence of an arachnoid gliomatosis around the optic nerve. They are typically bilateral, may be limited to the optic nerves, or may involve the chiasm and the retrochiasmatic visual pathway. Half of the tumors remain stable; the other half increase in size and threaten vision. Progression beyond the age of 10 years is rare.

Intraaxial brain tumors, including astrocytomas and typical childhood tumors like medulloblastoma and ependymoma, are somewhat more frequent than in the general population.

In 60–70 % of children with NF1, focal, non-space-occupying, bilateral, somewhat asymmetrical, not-well-defined lesions in the globus pallidus, thalamus, brainstem, and cerebellar white matter are found ("spongious lesions"). Spongious lesions may measure up to 3 cm and are T2- and FLAIR-hyperintense, and T1-hypointense, -isointense, or slightly hyperintense. Histologically, foci of

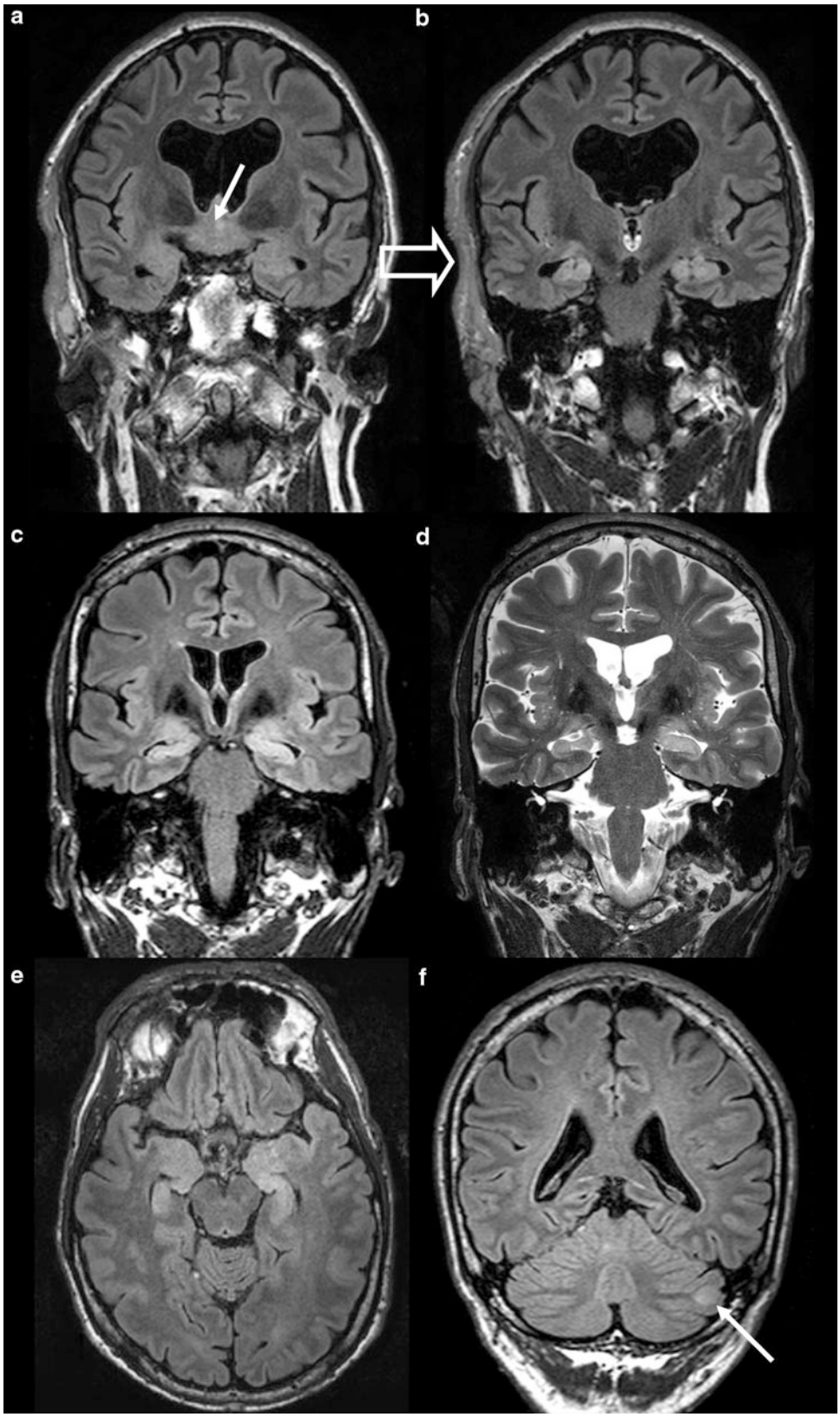

Fig. 4 Two neurofibromatosis type 1 patients with chiasm glioma (**a**: *arrow*), plexiform neurofibromas (**b**: *open arrow*), and spongious or hamartomatous lesion (**f**: *arrow*). Note bilateral hippocampal signal changes suggesting bilateral hippocampal sclerosis. Histopathological evaluation of the right hippocampus failed to show hippocampal sclerosis in one case (**a**, **b**), while it was proven in the other case (**c**–**f**)

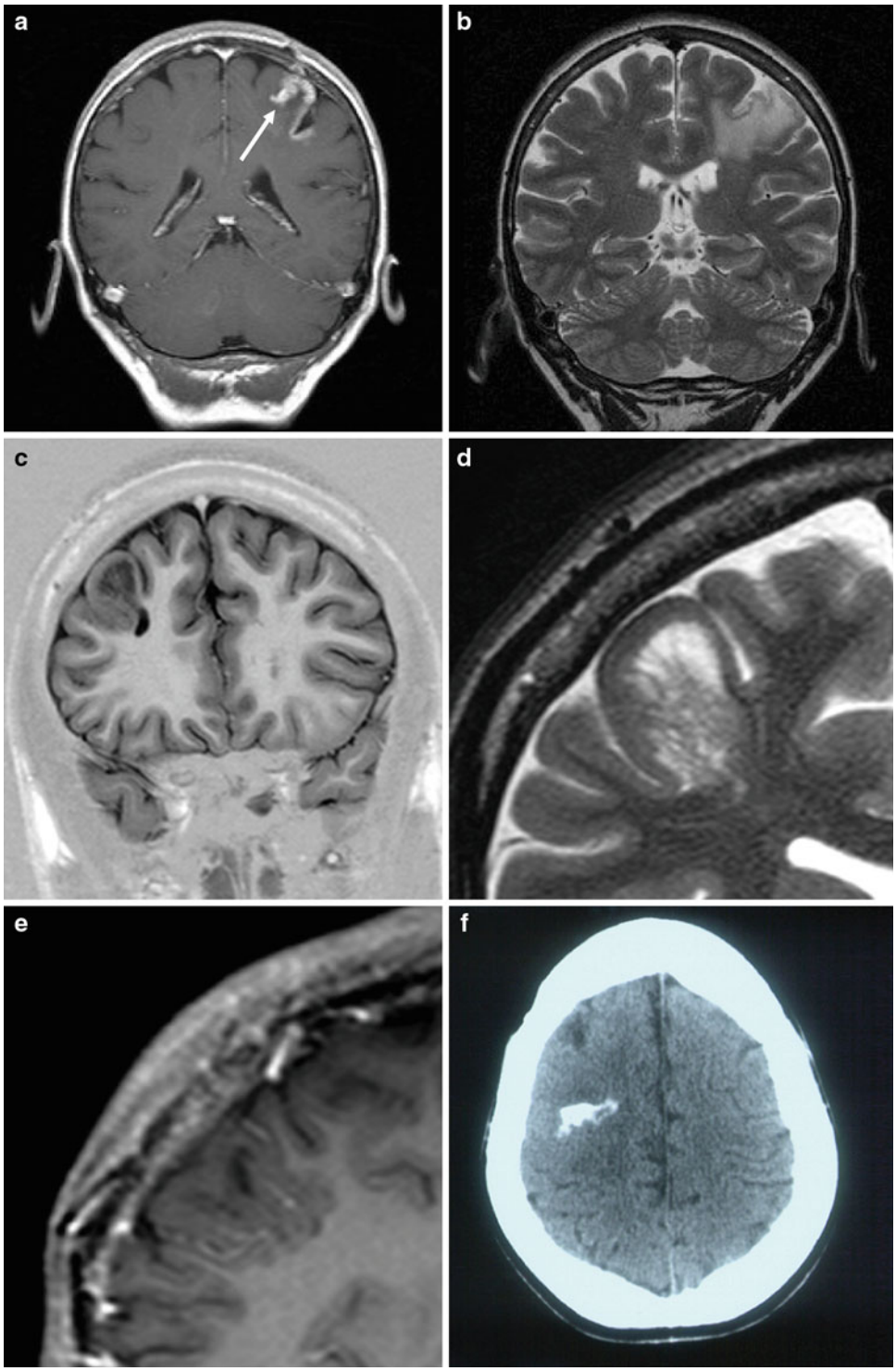

Fig. 5 Two examples of meningioangiomatosis: The hallmark of MRI is a leptomeningeal-cortical contrast enhancement (**a**: *arrow*) and a T2-weighted subcortical hyperintensity (**b**). With high resolution (**c**; **d**: 3T, voxel 0.47 × 0.64 × 2 mm), a radial orientation is visible: Meningeal cells proliferate along perivascular (Virchow–Robin) spaces. Contrast enhancement can be subtle or absent (**e**). CT is helpful to prove calcification (**f**)

myelin vacuolization are found, but no demyelination or inflammation is found. Spongious lesions increase in number and size in the first decade, regress afterwards, and are rarely found in the third decade of life.

Dural ectasia can produce bilateral enlargement of the internal auditory canals and should not be mismatched with NF2.

Vascular lesions caused by intimal proliferation are more common in the extracranial circulation; however, aneurysms, a Moya pattern, and others have been described.

In 80 % of NF1 children, coronal FLAIR and T2-weighted fast spin echo images show both hippocampi of higher signal intensity compared to healthy controls. There may be some asymmetry and the involvement of the amygdala and

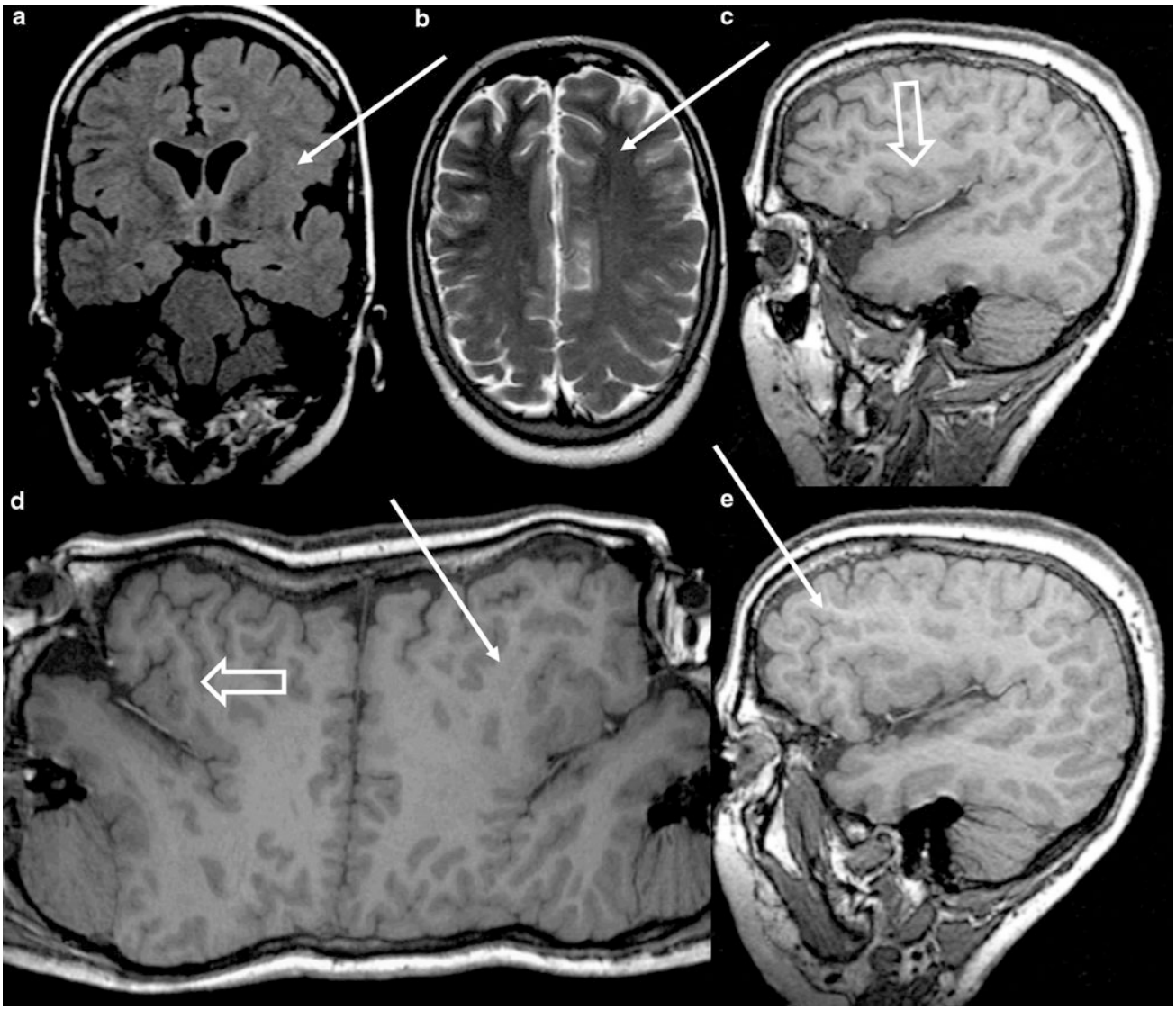

Fig. 6 Hypomelanosis of Ito in a 24-year-old severely disabled woman. The left hemisphere is hemimegalencephalic, showing a distorted anatomy of the frontal lobe and the perisylvian region (**a**, **b**, **d**, **e**: *arrow*). Note, however, also irregular insula and Sylvian fissure configuration on the right side (**c**, **d**: *hollow arrow*)

parahippocampal gyrus (Gill 2006). The consequence with respect to postsurgical seizure freedom is not clear yet: In the Bonn University epilepsy surgery program, one of five patients with NF1 and bilateral hippocampal changes underwent amygdalohippocampectomy. He became seizure-free, and histology revealed hippocampal sclerosis (Fig. 4).

5 Meningioangiomatosis

Epidemiology: Rare, hamartomatous, cortical/leptomeningeal dysplasia in childen; m > f.

Pathogenesis: Not known: A hamartoma, a meningioma with brain invasion, and a vascular malformation are discussed.

Clinical presentation: Usually children with drug-resistant seizures. Half of them have neurofibromatosis (frequently NF2), so that sometimes meningioangiomatosis lesions are detected while imaging for other NF manifestations (Jallo et al. 2005).

Pathology: Cortical meningovascular dysplasia with calcification and the proliferation of meningoendothelial cells along perivascular spaces. No malignant degeneration.

Imaging: Circumscribed lesion with (80 %) or without calcifications (20 %) and cortical and subcortical T2-weighted hyperintensity.

Contrast enhancement on the brain surface with radial extention in the depth. Contrast enhancement is sometimes subtle and may be absent.

With high resolution, radial T2-weighted hyperintense stripes representing the enlarged perivascular spaces can be visible (Fig. 5).

6 Hypomelanosis of Ito

Synonym: Incontinentia pigmenti achromians

Epidemiology: Rare neurocutaneous disease, which was initially described by Ito in (1952). Prevalence: 1:8,000–10,000.

Pathogenesis: Not known; several chromosomal mosaicisms have been found. A gene mutation affecting neuronal progenitor-derived cells and chromosomal stability is supposed to generate cytogenetic anomalies of neurons and melanocytes.

Clinical presentation: Cutaneous manifestations: Hypopigmented patches and swirls along the lines of Blaschko, which are present at birth or develop early in childhood.

Extracutaneous manifestations: mental retardation (65 %); epileptic seizures (53 %); autism (12 %); psychiatric symptoms; macrocephaly; teeth, ocular, skeletal, and cardiac abnormalities.

Imaging: Nonuniform pattern including hemimegalencephaly, pachygyria, cortical dysplasias, gray matter heterotopias, white matter anomalies, and others (Fig. 6).

7 Epidermal Nevus Syndromes

Epidemiology: Several very rare neurocutaneous syndromes are characterized by large skin nevi, ipsilateral brain malformations, and often ocular, skeletal, and other anomalies. Head and body asymmetries with overgrowth on the side of the skin changes are other characteristic features (Sugarman 2007; Happle 2010).

These syndromes may be summarized under the umbrella term "epidermal nevus" or "organoid nevus syndromes". Some of these syndromes can be distinguished by the type of epidermal nevus and by the criterion of the presence or absence of heritability. More common subtypes are the linear sebaceous nevus or nevus sebaceous of Jadassohn syndrome and the Proteus syndrome. However, several names are sometimes used for the same syndrome, and syndromes clinically show overlaps (Turner et al. 2004). From an MRI perspective, it is important to know that hemimegalencephaly is a common brain malformation (Pavone et al. 1991), but other malformations (agenesis of the corpus callosum, Dandy–Walker syndrome, myelomeningocele, Arnold–Chiari malformation, vascular malformations, brain tumors) may also occur.

Linear sebaceous nevus or nevus sebaceous of Jadassohn syndrome:

The syndrome (also known as Schimmelpfennig–Feuerstein–Mims syndrome) is characterized by linear sebaceous nevi, often on the face, that typically follow the lines of Blaschko (Hornstein and Knickenberg 1974; Bouwes Bavinck and van de Kamp 1985). All cases are sporadic. The syndrome is considered to be caused by an autosomal-dominant lethal mutation that survives by somatic mosaicism (Gorlin et al. 2001).

Proteus syndrome: Proteus was a Greek sea god who could change his shape. The name "Proteus syndrome" was proposed by the German pediatrician Hans-Rudolf Wiedemann in 1983; the disorder was initially described by Cohen and Hayden in 1979 (Wiedemann et al. 1983). Proteus syndrome is a very rare congenital disorder (up to 20 % have *PTEN* mutations) with a progressive course of asymmetric and disproportionate overgrowth of body parts, connective tissue and epidermal nevi, vascular malformations, skull and brain anomalies, and tumors often over the half of the body (Dietrich et al. 1998). A newly defined syndrome that was formerly misclassified as Proteus syndrome is associated with lipomatous overgrowth and has been designated as CLOVE syndrome (Sapp et al. 2007; McCall et al. 1992).

Clinical presentation: Craniofacial epidermal nevus, ipsilateral cerebral abnormalities, ocular and skeletal abnormalities, mental retardation, and often drug-resistant seizures.

Imaging: Consider epidermal nevus syndrome and variants in patients with skin changes and ipsilateral cerebral abnormalities, vascular anomalies, tumors, and tumorlike conditions. Among the relatively common vascular anomalies, aortic coarctation and aneurysm, renal artery stenosis, and carotid artery stenosis have been reported (Greene et al. 2007).

8 Incontinentia Pigmenti (Bloch–Sulzberger Syndrome)

Epidemiology: Rare X-linked multisystem disorder with pathognomonic skin manifestations initially described by the dermatologists Bloch in 1926 and Sulzberger in 1928, respectively. Neurological manifestations occur in 30 % of patients, typically in the neonatal period (Meuwissen and Mancini 2012).

Pathogenesis: Mutations of the *NEMO* gene on chromosome Xq28 encoding for a transcription factor that regulates apoptosis, reactions on various cytokines, and cell adhesion.

Clinical presentation: Skin changes comprise hypopigmentation, linear and swirled vesicular lesions (Hubert and Callen 2002). Ocular findings comprise a range of retinal vascular changes and optic atrophy, but also developmental defects like microphthalmia and cataract (Meuwissen and

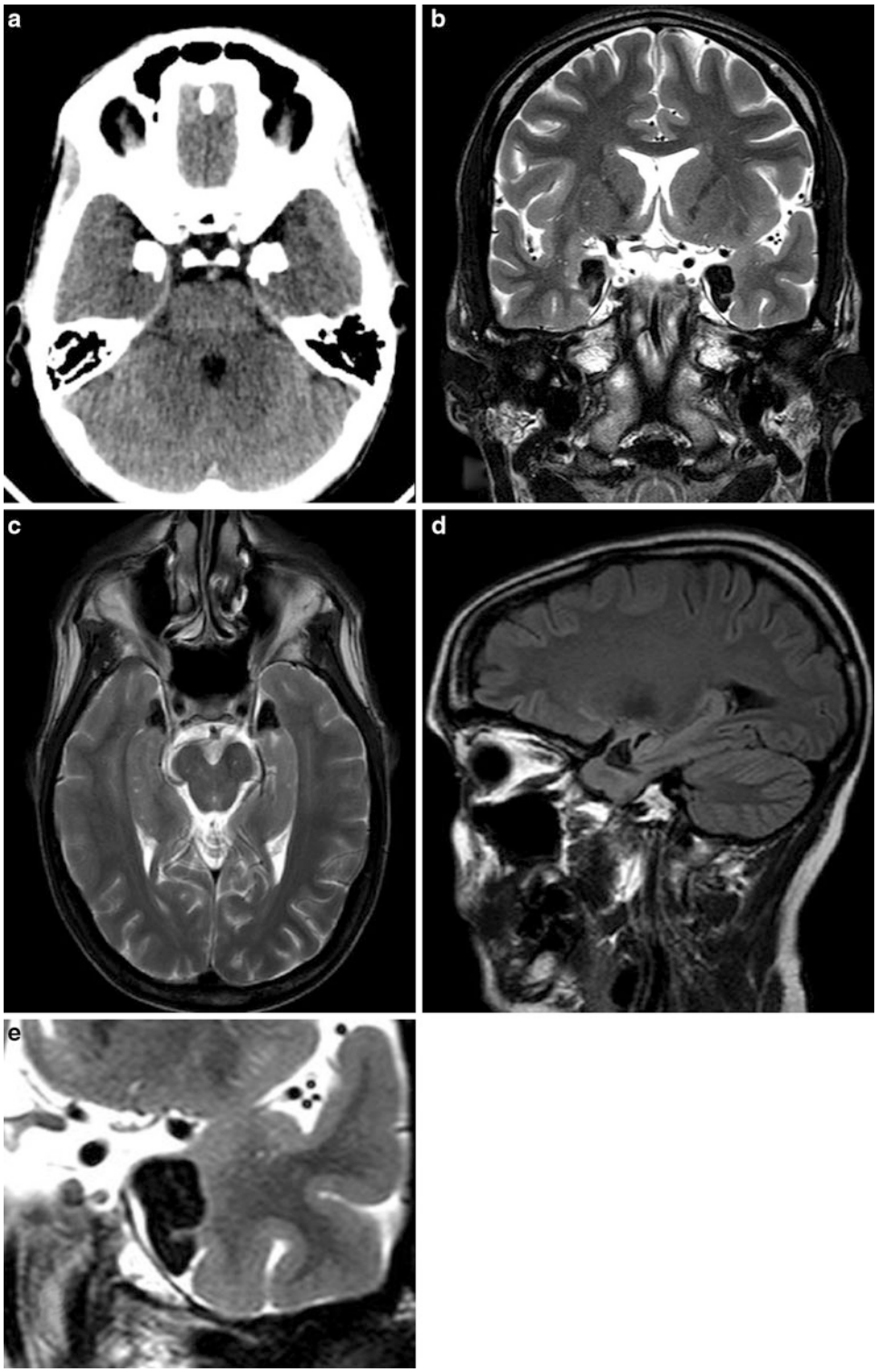

Fig. 7 CT (**a**) and MRI (**b**–**e**) in a 36-year-old woman with Urbach–Wiethe syndrome. Characteristic are the nearly complete amygdala calcifications with a taillike extension into the parahippocampal gyrus

Mancini 2012). Neurological manifestations comprise epileptic encephalopathy, seizures of different types, acute disseminated encephalomyelitis, and ischemic stroke. Seizures of different types seem to correlate with the degree of cerebrovascular damage.

Imaging: MRI findings likely reflect changes following microvascular brain injury and include periventricular and subcortical white matter disease, including diffusion-restricted lesions and atrophy, hemorrhagic changes, and corpus callosum hypoplasia (Pascual-Castroviejo et al.

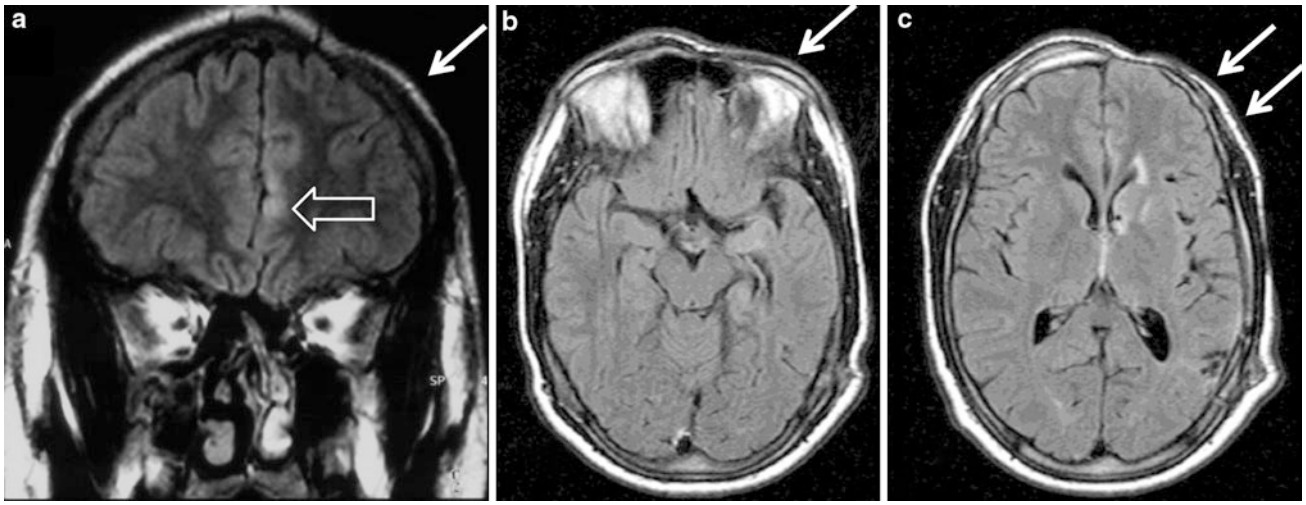

Fig. 8 Parry–Romberg syndrome and Rasmussen encephalitis in a 16-year-old boy. Initially, atrophic skin, subcutaneous and bone tissue (**a**: *arrow*) as well as cortical swelling suggestive of the acute stage of Rasmussen encephalitis (**a**: *open arrow*) were observed. Atrophic skin changes slowly progressed (**b**, **c**: *arrows*), and histologically proven Rasmussen encephalitis evolved into a chronic stage with tissue atrophy

1994; Hennel et al. 2003; Wolf et al. 2005; Hsieh and Chang 2011; Meuwissen and Mancini 2012).

9 Lipoid Proteinosis (Urbach–Wiethe Syndrome)

Epidemiology: Described for the first time by Urbach and Wiethe in 1929. Autosomal-recessive inherited disorder with deposits of amorphous hyaline material in skin and mucosal membranes and of calcifications in amygdala and basal ganglia. Around 300 cases have been described.

Pathogenesis: Mutation of the *ECM1* gene on chromosome 1q21 encodimg for the glycoprotein ECM1, which is expressed in skin, endothelial cells, and developing bone.

Clinical presentation: Skin changes with thickening, scarring, and xanthelasma-like nodules of the eyelids. Hoarseness since childhood; thin and fragile hair. Epileptic seizures may occur; cognitive deficits and lack of emotional "involvement" are predominant clinical symptoms (Claeys et al. 2007).

Imaging: Symmetric, half-moon-shaped calcifications of the amygdalae are pathognomonic. Calcifications may also occur in the hippocampus, parahippocampal gyrus, and striate (Gonçalves et al. 2010) (Fig. 7).

10 Linear Scleroderma (en coup de sabre syndrome) and Parry–Romberg Syndrome

Epidemiology: Linear scleroderma is an indented, vertical, colorless line of skin on the forehead, also called en coup de sabre, meaning "sword stroke" syndrome. It is typically associated with a focal linear atrophy of the skin and subcutaneous tissue. Parry–Romberg syndrome (progressive facial hemiatrophy) is a rare disease of unknown origin clinically sometimes associated with focal seizures and even epilepsia partialis continua. Several case reports indicate a close relationship between both entities (Carreño et al. 2007; Chiang et al. 2009; Longo et al. 2011; Seifert et al. 2011).

Pathogenesis: The exact pathogenesis is unclear. Some cases of Parry–Romberg syndrome are associated with Rasmussen encephalitis.

Clinical presentation: Parry–Romberg syndrome is characterized by a slowly progressive, unilateral atrophy of facial tissue, including muscles, bones, and skin. Atrophy typically starts in the first or second decade of life, slowly progresses over several years, and eventually becomes stable. Neurological involvement includes focal seizures (Epilepsia partialis continua), migraine, and facial pain.

Imaging: Unilateral progressive atrophy of skin, subcutaneous tissue, and bones of the face. Progressive hemiatrophy of the ipsilateral hemisphere and sometimes signal changes like those in Rasmussen encephalitis (initial swelling and hyperintense signal of the cortex with periinsular accentuation; later on progressive atrophy of the hyperintense tissue) (Fig. 8).

References

Bouwes Bavinck JN, van de Kamp JJP (1985) Organoid naevus phakomatosis: Schimmelpenning–Feuerstein–Mims syndrome. Br J Derm 113:491–492

Carreño M, Donaire A, Barceló MI et al (2007) Parry–Romberg syndrome and linear scleroderma in coup de sabre mimicking Rasmussen encephalitis. Neurology 68(16):1308–1310

Chiang KL, Chang KP, Wong TT, Hsu TR (2009) Linear scleroderma "en coup de sabre": initial presentation as intractable partial seizures in a child. Pediatr Neonatol 50(6):294–298

Claeys KG, Claes LR, Van Goethem JW et al (2007) Epilepsy and migraine in a patient with Urbach–Wiethe disease. Seizure 16:465–468

Cohen MM Jr, Hayden PW (1979) A newly recognized hamartomatous syndrome. Birth Defects Orig Artic Ser 15:291–296

Dietrich RB, Glidden DE, Roth GM et al (1998) The Proteus syndrome: CNS manifestations. Am J Neuroradiol 19(5):987–990

Enjoltas O, Riche MC, Merland JJ (1985) Facial port-wine stains and Sturge–Weber syndrome. Pediatrics 76:48–51

Gill DS (2006) Age-related findings on MRI in neurofibromatosis type 1. Pediatr Radiol 36:1048–1056

Gonçalves FG, de Melo MB, de L Matos V et al (2010) Amygdalae and striatum calcification in lipoid proteinosis. Am J Neuroradiol 31(1):88–90

Gorlin RJ, Cohen MM, Hennekam RCM (2001) Syndromes of the Head and Neck, 4th edn. Oxford University Press, New York, pp 484–488

Greene AK, Rogers GF, Mulliken JB (2007) Schimmelpenning syndrome: an association with vascular anomalies. Cleft Palate Craniofac J 44:208–215

Happle R (2010) The group of epidermal nevus syndromes. Part I. Well defined phenotypes. J Am Acad Dermatol 63(1):1–22

Hennel SJ, Ekert PG, Volpe JJ, Inder TE (2003) Insights into the pathogenesis of cerebral lesions in incontinentia pigmenti. Pediatr Neurol 29(2):148–150

Hornstein OP, Knickenberg M (1974) Zur Kenntnis des Schimmelpenning-Feuerstein-Mims-Syndroms (Organoide Naevus-Phakomatose) [in German]. Arch Derm Forsch 250:33–50

Hsieh DT, Chang T (2011) Incontinentia pigmenti: skin and magnetic resonance imaging findings. Arch Neurol 68(8):1080

Hubert JN, Callen JP (2002) Incontinentia pigmenti presenting as seizures. Pediatr Dermatol 19(6):550–552

Ito M (1952) Studies of melanin: XI. Incontinentia pigmenti achromiens. Tohoku J Exp Med 55(suppl):55–57

Jallo GI, Kothbauer K, Mehta V et al (2005) Meningioangiomatosis without neurofibromatosis: a clinical analysis. J Neurosurg 103(4 Suppl):319–324

Krueger DA, Care MM, Holland K et al (2010) Everolimus for subependymal giant-cell astrocytomas in tuberous sclerosis. N Engl J Med 363(19):1801–1811

Longo D, Paonessa A, Specchio N et al (2011) Parry–Romberg syndrome and Rasmussen encephalitis: possible association. Clinical and neuroimaging features. J Neuroimaging 21(2):188–193

McCall S, Ramzy MI, Cure JK, Pai GS (1992) Encephalocraniocutaneous lipomatosis and the Proteus syndrome: distinct entities with overlapping manifestations. Am J Med Genet 43:662–668

Meuwissen ME, Mancini GM (2012) Neurological findings in incontinentia pigmenti; a review. Eur J Med Genet 55(5):323–331

NIH Consensus Development Conference (1988) Neurofibromatosis: conference statement. Arch Neurol 45:575–578

Osborne JP, Fryer A, Webb D (1991) Epidemiology of tuberous sclerosis. Ann NY Acad Sci 615:125–127

Pascual-Castroviejo I, Roche MC, Martinez Fernández V et al (1994) Incontinentia pigmenti: MR demonstration of brain changes. Am J Neuroradiol 15(8):1521–1527

Pavone L, Curatolo P, Rizzo R et al (1991) Epidermal nevus syndrome: a neurologic variant with hemimegalencephaly, gyral malformation, mental retardation, seizures, and facial hemihypertrophy. Neurology 41:266–271

Roach ES, Gomez MR, Northrup H (1998) Tuberous Sclerosis Complex Consensus Conference: revised clinical diagnostic criteria. J Child Neurol 13:624–628

Sapp JC, Turner JT, van de Kamp JM et al (2007) Newly delineated syndrome of congenital lipomatous overgrowth, vascular malformations, and epidermal nevi (CLOVE syndrome) in seven patients. Am J Med Genet 143A:2944–2958

Seifert F, Bien CG, Schellinger PD et al (2011) Parry–Romberg syndrome with chronic focal encephalitis: two cases. Clin Neurol Neurosurg 113(2):170–172

Sugarman JL (2007) Epidermal nevus syndromes. Semin Cutan Med Surg 26(4):221–230

Turner JT, Cohen MM, Biesecker LG (2004) Reassessment of the Proteus syndrome literature: application of diagnostic criteria to published cases. Am J Med Genet 130A:111–122

Urbach E, Wiethe C (1929) Lipoidosis cutis et mucosae. Virch Arch Pathol Anat 273:285–319

Wiedemann HR, Burgio GR, Aldenhoff P et al (1983) The Proteus syndrome. Partial gigantism of the hands and/or feet, nevi, hemihypertrophy, subcutaneous tumors, macrocephaly or other skull anomalies and possible accelerated growth and visceral affections. Eur J Pediatr 140(1):5–12

Wolf NI, Krämer N, Harting I et al (2005) Diffuse cortical necrosis in a neonate with incontinentia pigmenti and an encephalitis-like presentation. Am J Neuroradiol 26:1580–1582

Trauma

Horst Urbach

Contents

Abstract

Trauma is a major risk factor for epilepsy. However, one should have in mind that posttraumatic MRI changes can be the cause or the consequence of epilepsy.

1 Epidemiology

Trauma is the cause of epilepsy in around 4 % of cases (Serles et al. 2003).

Trauma incidence is highest between the ages of 15–24 years and males are more often affected than females (Langendorf and Pedley 1997; Boswell et al. 2002).

Seizures occur in 10–15 % of adults and 30–35 % of children after severe head trauma (Glasgow Coma Score <9) (Caveness et al. 1979; Hahn et al. 1988).

2 Pathogenesis

Primary brain parenchymal injuries comprise cortical contusions and diffuse axonal injuries (DAI). Cortical contusions result from impact injuries compressing the brain against a bony structure or dural fold ("coup" lesions) or stretching the partly fixed brain on the opposite impact side ("contrecoup" lesions). Other mechanisms are penetrating brain injuries with intracranial hematomas and retained metallic fragments.

DAI typically result from high-velocity motor vehicle accidents, typically deceleration injuries although impact is not necessarily needed. DAI are shearing injuries with axonal stretching when the cortex moves at a different speed as compared to the underlying white matter. Eighty percent of DAI lesions are microscopic nonhemorrhagic lesions and MRI visible lesions rather represent the "tip of the iceberg."

H. Urbach (✉)
Department of Neuroradiology,
University Hospital Freiburg,
Germany
e-mail: horst.urbach@uniklinik-freiburg.de

H. Urbach (ed.), *MRI in Epilepsy*, Medical Radiology. Diagnostic Imaging,
DOI: 10.1007/174_2012_748, © Springer-Verlag Berlin Heidelberg 2013

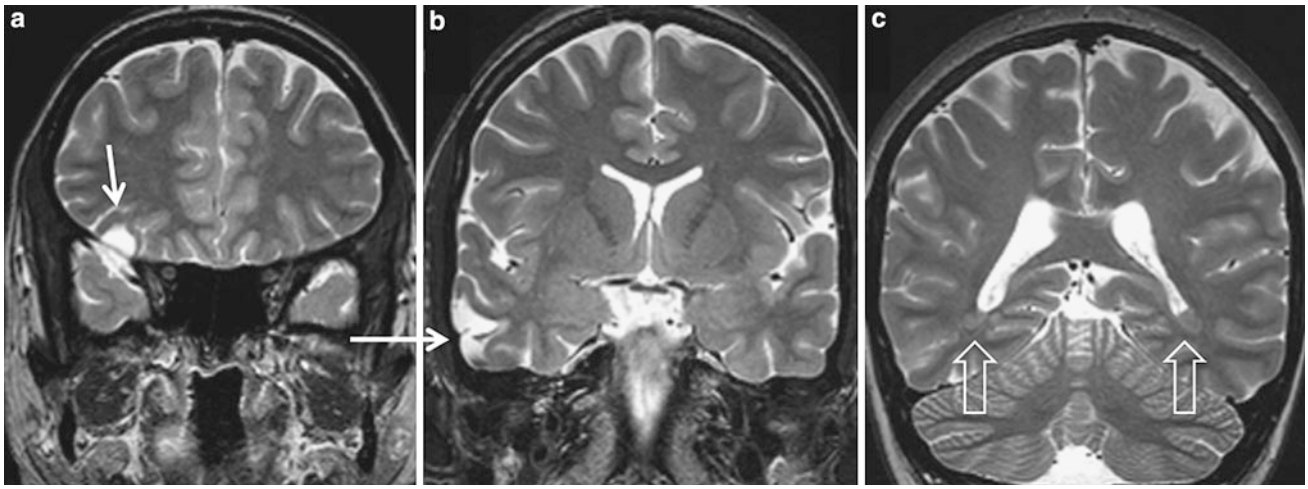

Fig. 1 31-year-old woman with at least two cortical contusions (**a**, **b** *arrow*) resulting from a prior trauma. Epileptic seizures were already present before trauma and are most likely due to bilateral periventricular nodular heterotopias (BPNH) (**c** *hollow arrows*)

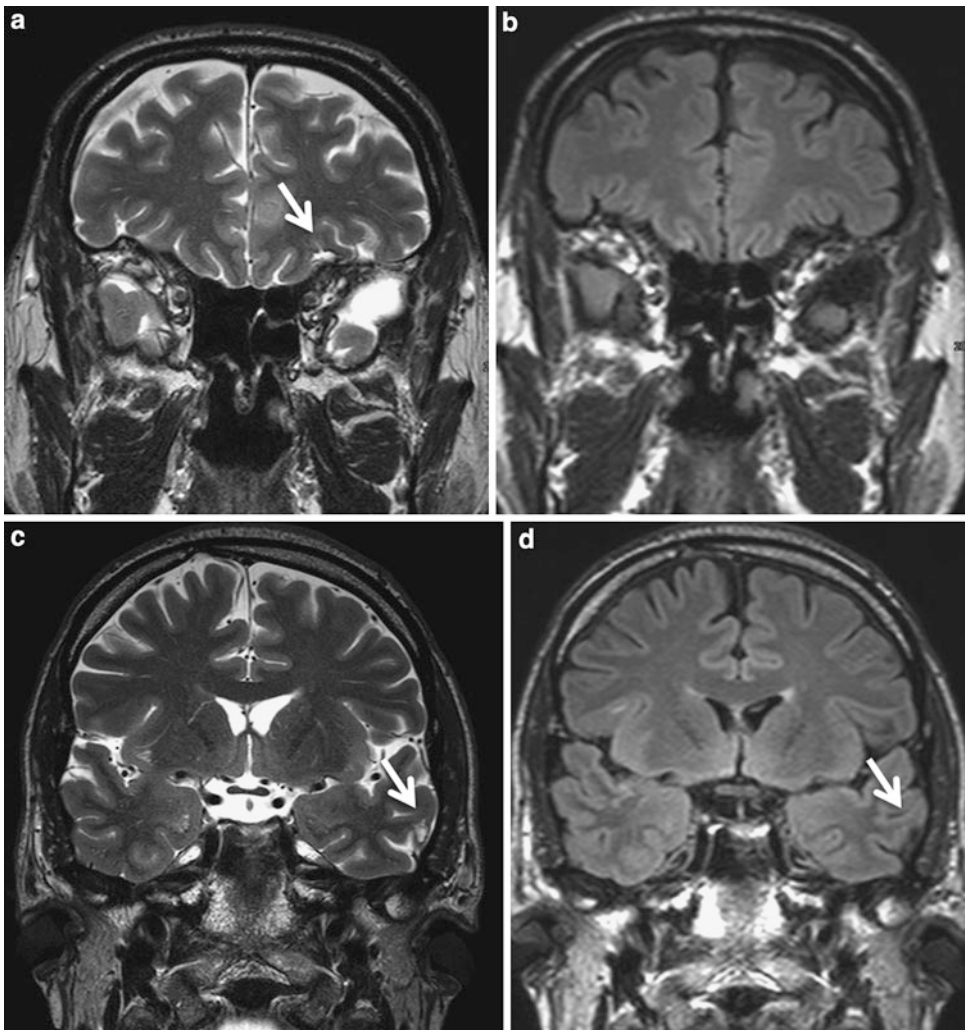

Fig. 2 Small cortical contusions in a 51-year-old man with tonic-clonic seizures following a head trauma at the age of 20. (**a**, **c**, **d** *arrows*). The cortical lesions with hemosiderin deposits are best visible on high-resolution T2-weighted images. They are missed on FLAIR images due to a lower anatomical resolution (**b**) and on T2-weighted gradient echo images (not shown) due to susceptibility artifacts from the frontal sinuses

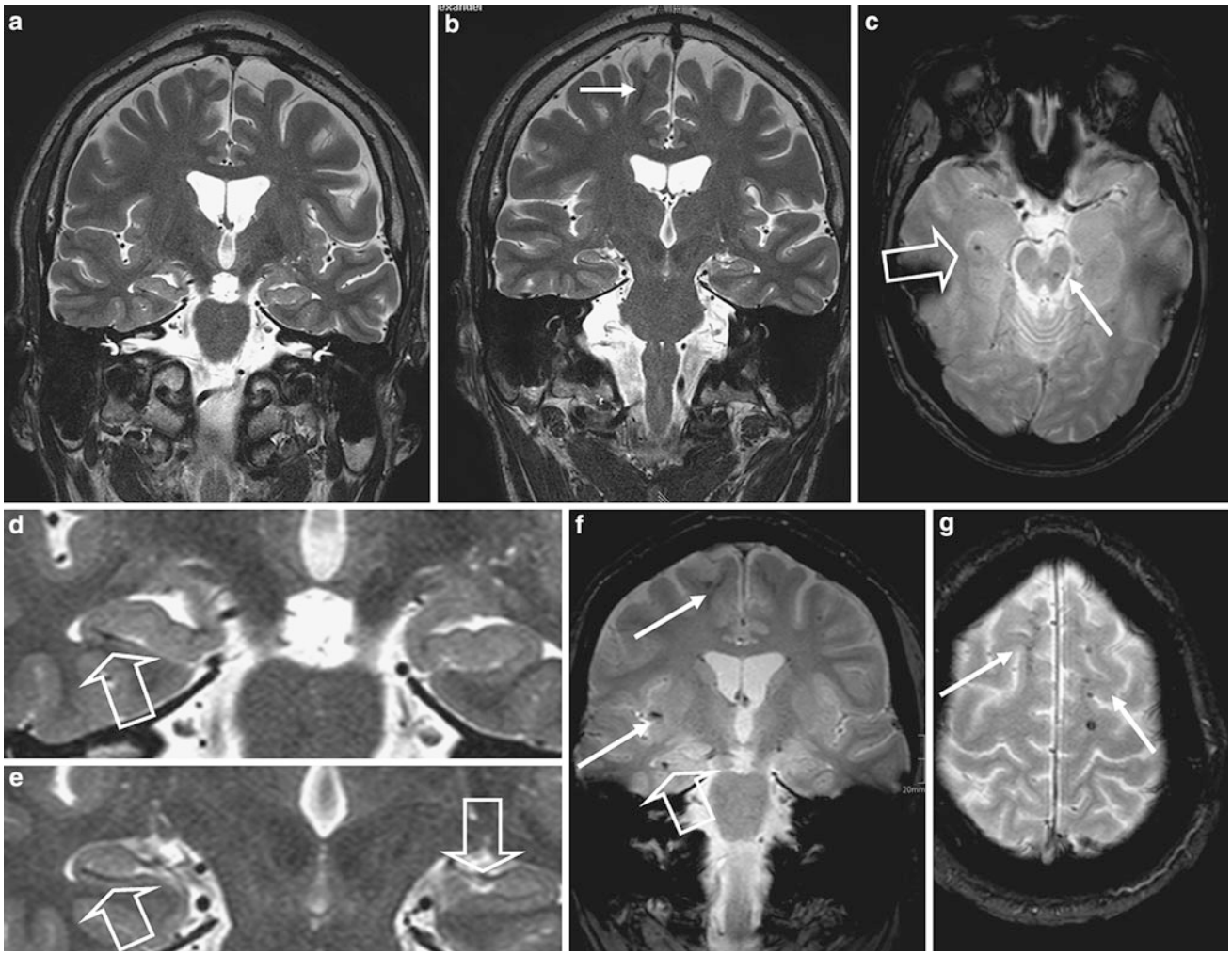

Fig. 3 Coronal high-resolution T2-weighted images (**a**, **b**) with magnified views of the hippocampi show multiple hemosiderin deposits as sequelae of diffuse axonal brain injury. These shearing injuries are typically located in subcortical white matter bordering the cortex (**b**, **f**, **g**: *arrows*, the corpus callosum, and the brainstem, typically in dosolateral mesencephalon (**c** *arrow*). In this case of a 28 year old man hemosiderin deposits are also found in the CA1 sector of both hippocampi (**c**–**f** *hollow arrow*)

3 Clinical Presentation

Seizures occurring within 1 week following the trauma are considered as early posttraumatic seizures. Seizures occurring later than 1 week following the trauma are late posttraumatic seizures. Posttraumatic injuries may occur decades following the trauma. The risk is particularly high with penetrating brain injuries and retained metallic fragments (Raymont et al. 2010; Agrawal et al. 2006).

Seizures can be the result of or induce a trauma (Fig. 1). Careful evaluation, as to whether the semiology of seizures has changed after the trauma is needed.

4 Imaging

Cortical contusions occur in locations where the brain is adjacent to bony protuberances or dural folds: basal frontal lobe, temporal pole and inferior surface, parasagittal ("gliding" contusions). Initial CT often shows only subtle, ill-defined, discretely hyperdense, superficial lesions, which, however, "blow up" after 24–48 h. In the chronic stage, there is cortical and subcortical volume loss and hemosiderin deposition. Lesions may be subtle and it is important to inspect the cortical surface in classical locations (Fig. 2).

Diffuse axonal injury is characterized by multiple punctate hypointense lesions on T2-weighted gradient echo sequences (Fig. 3). CT scans are often unremarkable and do not fit the clinical state of the patients. However, with more severe DAI circumscribed and transient hyperdensity in the interpeduncular cistern or in the dorsolateral upper brainstem may indicate DAI. Specific locations for the multiple punctate hemorrhages are the gray–white matter interfaces, the corpus callosum, and the dorsolateral upper brainstem (Adams et al. 1982). The gray–white matter interface is especially susceptible for shearing injuries as the density of the tissue abruptly changes. The corpus callosum is the second most common DAI location with the splenium most commonly affected (Gentry et al. 1988). Small blood-CSF levels in the posterior horns of the lateral ventricles may indicate corpus callosum DAI. Brainstem DAIs typically involve the dorsolateral quadrant of the mesencephalon adjacent to the superior cerebellar peduncle. They are only observed with severe trauma and multiple deep white matter and corpus callosum hemorrhages (Zuccarello et al. 1983). Differential diagnosis includes Duret's hemorrhage, a dorsolateral upper brainstem hemorrhage that is considered a secondary lesion resulting from downward trantentorial herniation due to a rapidly developing supratentorial mass.

If an epilepsy patient has a clinical trauma history, carefully study the basal frontal and the temporal lobes (Fig. 1). Coronal T2-weighted images should cover the entire frontal lobes. T2-weighted gradient echo images are needed to display DAI lesions, however, cortical contusions may be masked by susceptibility artifacts at brain–bone interfaces.

References

Adams JH, Graham DI, Murray LS, Scott G (1982) Diffuse axonal injury due to nonmissile head injury in humans: an analysis of 45 cases. Ann Neurol 12:557–563

Agrawal A, Timothy J, Pandit L, Manju M (2006) Post-traumatic epilepsy: an overview. Clin Neurol Neurosurg 108(5):433–439

Boswell JE, McErlean M, Verdile VP (2002) Prevalence of traumatic brain injury in an ED population. Am J Emerg Med 20:177–180

Caveness WF, Meirowsky AM, Rish BL, Mohr JP, Kistler JP, Dillon JD, Weiss GH (1979) The nature of posttraumatic epilepsy. J Neurosurg 50(5):545–553

Gentry LR, Thompson B, Godersky JC (1988) Trauma to the corpus callosum: MR features. Am J Neuroradiol 9:1129–1138

Hahn YS, Fuchs S, Flannery AM, Barthel MJ, McLone DG (1988) Factors influencing posttraumatic seizures in children. Neurosurgery 22(5):864–867

Langendorf F, Pedley TA (1997) Post-traumatic seizures. In: Engel J Jr, Pedley TA (eds) Epilepsy: a comprehensive textbook. Lippincott-Raven Publishers, Philadelphia, pp 2469–2474

Raymont V, Salazar AM, Lipsky R, Goldman D, Tasick G, Grafman J (2010) Correlates of posttraumatic epilepsy 35 years following combat brain injury. Neurology 75(3):224–229

Serles W, Baumgartner C, Feichtinger M, Felber S, Feucht M Podreka I, Prayer D, Trinka E (2003) Richtlinien für ein standardisiertes MRT-Protokoll für Patienten mit epileptischen Anfällen in Österreich. Mitteilungen der Österreichischen Sektion der Internationalen Liga gegen Epilepsie 3:2–13

Zucarello M, Fiore DL, Trincia G, De Caro R, Pardatscher K, Andrioli GC (1983) Traumatic primary brain stem haemorrhage. A clinical and experimental study. Acta Neurochir 67:103–113

Vascular Malformations

Horst Urbach and Timo Krings

Contents

H. Urbach (✉)
Department of Neuroradiology,
University Hospital Freiburg, Germany
e-mail: horst.urbach@uniklinik-freiburg.de

T. Krings
Department of Neuroradiology,
University of Toronto, Toronto, ON, Canada

Abstract

Vascular malformations are described in this chapter in the following order: cavernomas, arteriovenous malformations, dural arteriovenous fistulae, developmental venous anomalies, and capillary telangiectasias. The order is derived from their propensity to cause epileptic seizures. In cavernomas, epileptic seizures are the most common symptom, followed by the incidental MRI detection of nonspecific symptoms such as headaches and dizziness. In arteriovenous malformations, seizures occur in around 30 % of patients. Incidental detection or presentation with hemorrhage is either more common or has a higher therapeutic relevance owing to the distinctly higher hemorrhage-related morbidity and mortality and rebleeding risk. Dural arteriovenous fistulae are typically acquired vascular lesions causing epileptic seizures among other symptoms if cortical venous reflux is present. Developmental venous anomalies are of therapeutic relevance only if they are associated with cavernomas and—in very rare cases—if the draining collector vein becomes thrombosed. Capillary telangiectasias are of no therapeutic relevance.

1 Cavernomas

1.1 Synonym(s)

A synonym is "cavernous malformation." Use of the term "cavernous hemangioma" should be avoided since a cavernous hemangioma is a true vasoproliferative neoplasm.

1.2 Epidemiology

Cavernomas are relatively frequent vascular malformations with a prevalence of approximately 0.5 %. Cavernomas are solitary in around 75 % of cases and multiple in around

H. Urbach (ed.), *MRI in Epilepsy*, Medical Radiology. Diagnostic Imaging,
DOI: 10.1007/174_2012_753, © Springer-Verlag Berlin Heidelberg 2013

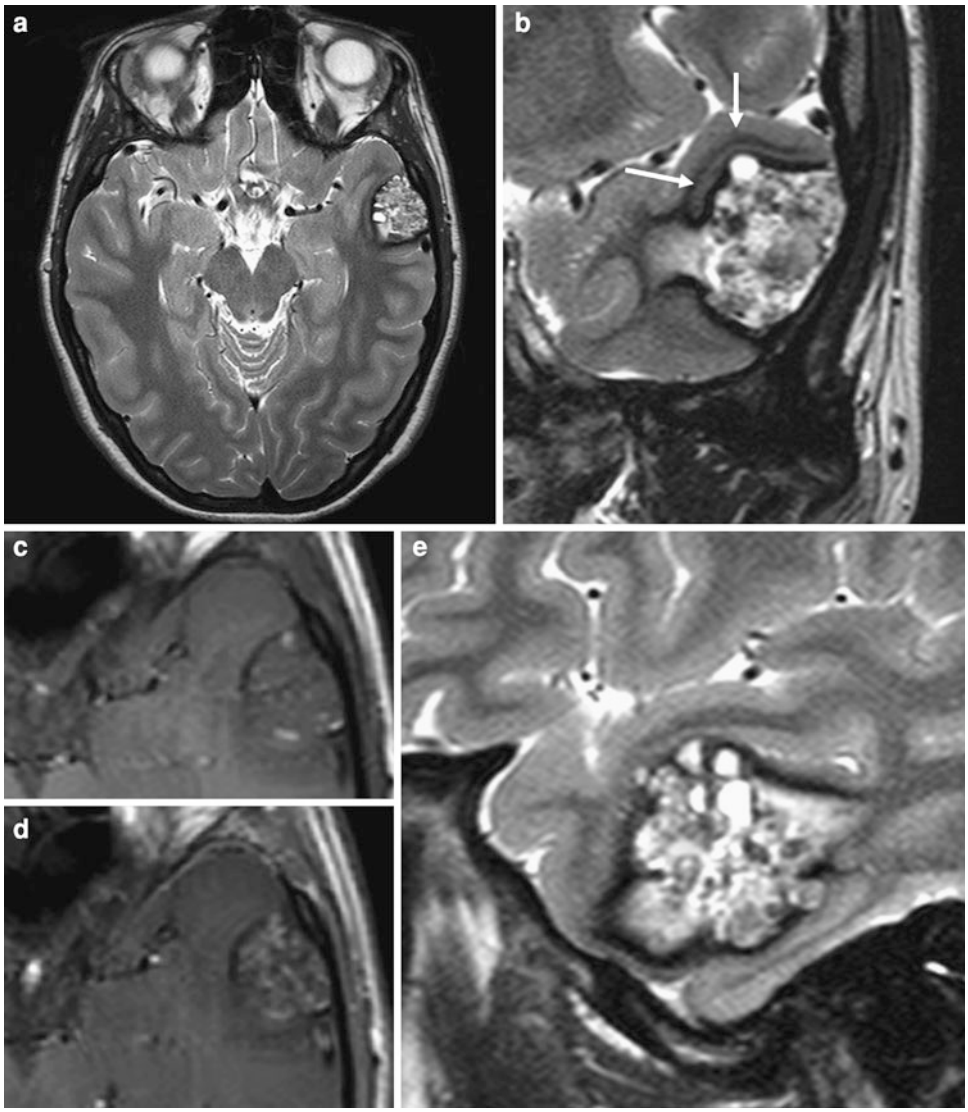

Fig. 1 A 17-year-old woman presented with daily auras with fearful feelings and déjà vu phenomena and monthly complex focal seizures. MRI revealed a 2-cm Zabramski type 2 cavernoma in the left middle temporal gyrus. The cavernoma itself has a popcorn-ball appearance with hyperintense and hypointense signal on T2-weighted sequences (**a**, **b**, **e**). It is surrounded by a hypointense rim reflecting the impregnation of the adjacent brain parenchyma with hemosiderin (**b**, *arrows*). The T1-weighted unenhanced sequence shows some hyperintense intralesional signal (**c**), and the T1-weighted contrast-enhanced sequence shows intralesional enhancement (**d**)

25 % of cases. Around 10 % of cavernomas are familial cases with autosomal dominant inheritance, variable penetrance, and three identified genes (CCM1, CCM2, and CCM3). Up to 20 % of cavernomas are accompanied by developmental venous anomalies (DVAs), and there is some evidence that an anomalous venous drainage triggers cavernoma evolution (Wurm et al. 2005) (Fig. 4).

1.3 Pathogenesis

Cavernomas are immature lesions with endothelial proliferation and upregulated angiogenesis. Histopathologically, they consist of dilated, endothelium-lined blood vessels without arterial features. Sinusoidal blood cavities typically lie back-to-back and there is no substantial brain tissue interposed between the vessels. Thrombosis, organization, and inflammatory changes and occasional calcifications may be seen in larger cavernomas (Raabe et al. 2012). Evidence of prior hemorrhage is a nearly constant feature of cavernomas, and the lesions are considered to grow and produce symptoms by recurrent episodes of hemorrhage or intralesional thrombosis. Hemorrhage is characteristically confined within the lesion, and produces neurological deficits secondary to a local mass effect rather than direct parenchymal injury. Smaller nonsymptomatic hemorrhages are thought to contribute to the development of seizures. These smaller hemorrhages result in the progressive deposition of hemosiderin in the brain parenchyma surrounding the cavernoma, and iron as content of hemosiderin is a well-known epileptogenic material that is used to induce seizures in laboratory models of epilepsy (Figs. 1, 2). Another mechanism, however, is the development of seizures following larger intralesional hemorrhage (Figs. 3, 4).

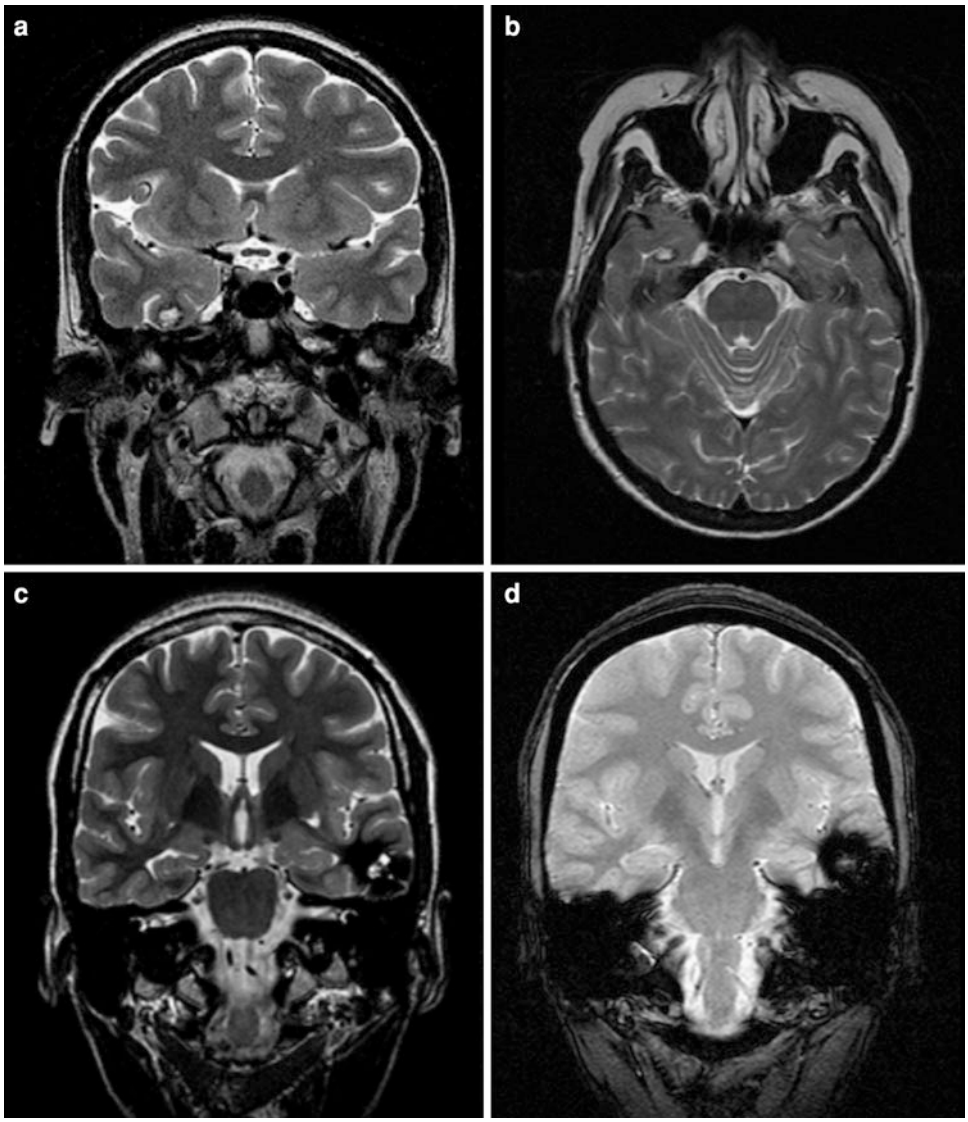

Fig. 2 Two different cavernomas of the inferior temporal gyrus. The right-sided small cavernoma could have been easily overlooked if only axial slices had been acquired. On T2-weighted images, cavernomas associated with long-term epilepsy usually have a hyperintense matrix surrounded by a less prominent (**a**, **b**) or more prominent (**c**, **d**) hemosiderin rim

1.4 Clinical Presentation

Up to 40 % of patients with cavernomas present with epileptic seizures (Awad and Jabbour 2006; Baumann et al. 2007; Del Curling et al. 1991; Gross et al. 2011; Moran et al. 1999; Moriality et al. 1999). Seizures are most prevalent in supratentorial cavernomas and progress to epilepsy in 40 % of these cases (Englot et al. 2011). Epileptic seizures are more common than symptomatic hemorrhages, which occur in around 0.5 % of lesions per year.

Around 75 % of patients become seizure-free following microsurgical resection (Englot et al. 2011). Prognostic factors with respect to postsurgical seizure freeness are mesiotemporal location, gross anatomical resection including the hemosiderin rim, small size (diameter less than 1.5 cm), surgery within 1 year after seizure onset, and absence of secondarily generalized seizures (Baumann et al. 2006, 2007; Chang et al. 2009; Englot et al. 2011).

1.5 Imaging

Magnetic resonance (MR) images typically show a popcorn-like pattern with mixed high and low signal intensities in the core and a dark rim of hemosiderin (Fig. 1). Hyperintense portions on T1-weighted images in the core represent subacute (intralesional) hemorrhage or thrombosis within the "berries" of the cavernoma. The cavernoma itself is surrounded by a hypointense rim on T2-weighted images which blooms on T2-weighted gradient echo images. The hypointense rim represents hemosiderin-stained brain. A cavernoma may profoundly bleed into the surrounding brain parenchyma (extralesional hemorrhage), but with respect to epileptic seizures, the hemosiderin staining of the surrounding brain parenchyma due to smaller nonsymptomatic intralesional hemorrhage/thrombosis and ongoing blood degradation is more relevant. In addition to T2-weighted fast spin echo sequences, which show the anatomical details best,

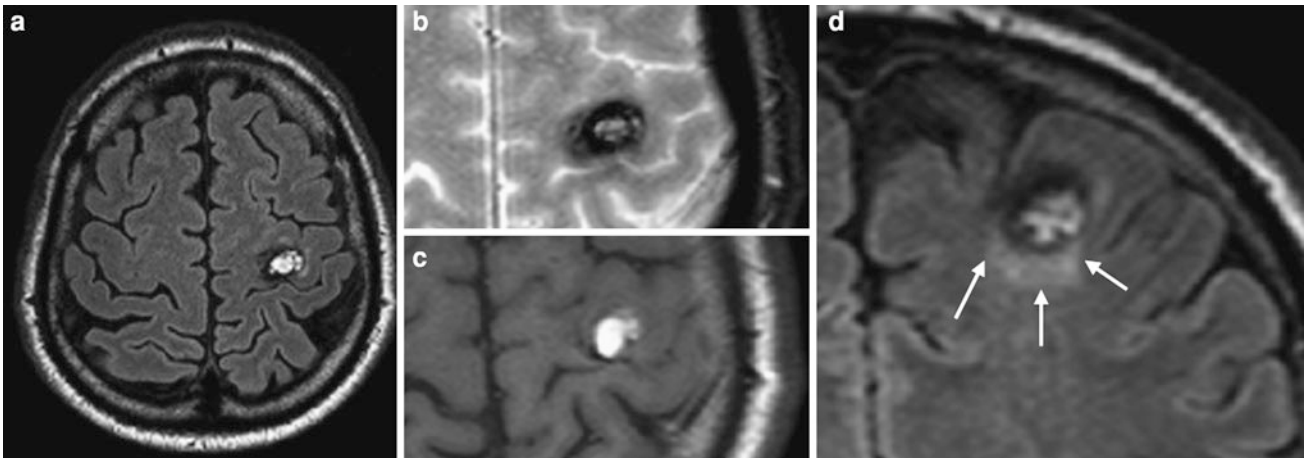

Fig. 3 A 53-year-old man presented with epilepsia partialis continua of the right neck muscles for 4 weeks. One year before he had observed this phenomenon for 1 day. Axial fluid-attenuated inversion recovery (FLAIR) (**a**), T2-weighted gradient echo (**b**), T1-weighted spin echo (**c**), and coronal FLAIR (**d**) images show a Zabramski type 1 cavernoma. Intralesional hemorrhage and adjacent edema (**d**, *arrows*) are likely the reason why the patient presented with epilepsia partialis continua

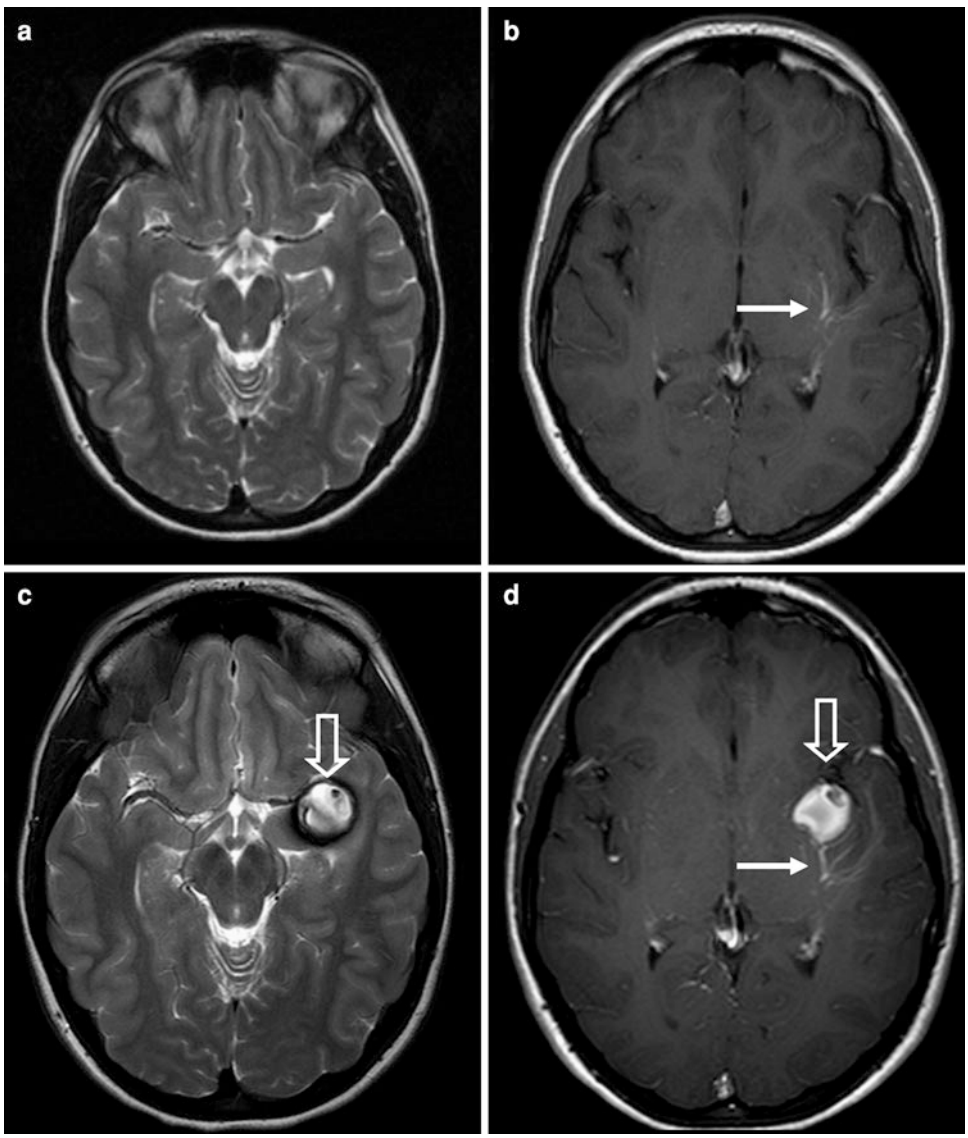

Fig. 4 MRI in a 14-year-old girl initially presenting with a transient difficulty to use her right arm was uneventful except for a small left insular developmental venous anomaly (**a**, **b**). Four years later, the patient presented with two complex focal seizures. MRI now showed a pathologically proven insular Zabramski type 1 cavernoma with intralesional subacute hemorrhage (**c**, **d**, *hollow arrows*). The adjacent developmental venous anomaly is characterized by caput meduase (**b**, **d**, *arrows*) and a draining subependymal vein (not shown)

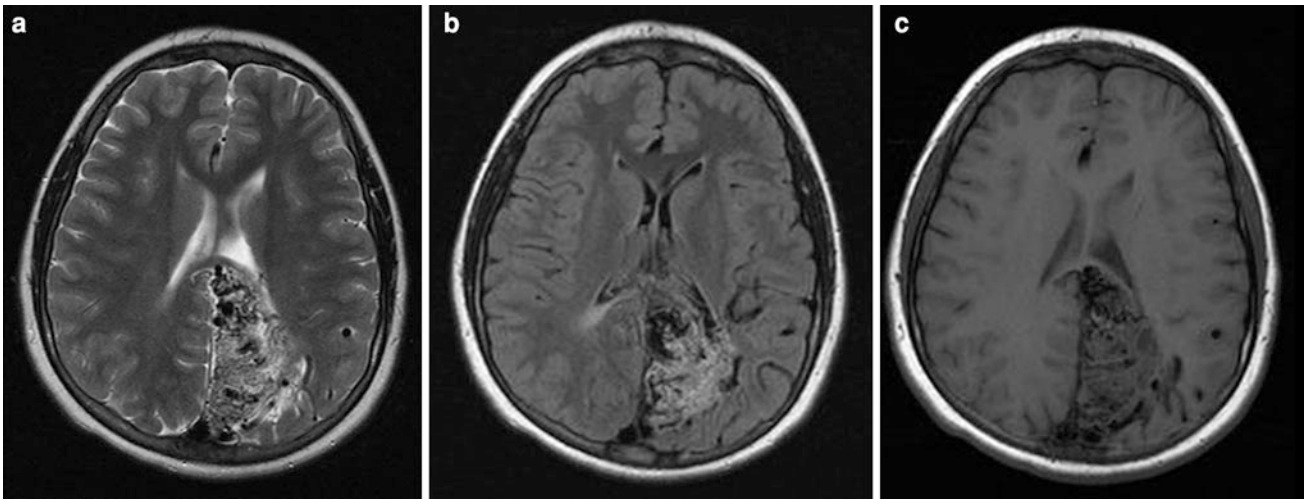

Fig. 5 Axial T2-weighted (**a**), FLAIR (**b**), and T1-weighted (**c**) images demonstrating an intraparenchymal nidus of flow voids indicative of an arteriovenous malformation (AVM). T2-weighted and FLAIR hyperintensity represents perifocal gliosis, which was thought to be the cause of the patient's seizures

T2-weighted gradient echo or susceptibility-weighted sequences are mandatory to discover additional so-called Zabramski type 4 cavernomas (Zabramski et al. 1994). However, because of susceptibility artefacts at bone–brain interfaces, small cortical/subcortical cavernomas can be easily missed on T2-weighted gradient echo sequences (Fig. 2). Since up to 20 % of cavernomas are associated with DVAs, which represent an anatomic variant of otherwise normal venous drainage and are characterized by dilated medullary white matter veins (caput medusae) converging on a collector vein draining into a dural sinus or ependymal vein, T1-weighted contrast-enhanced images should be additionally obtained (Fig. 4). If a mixed cavernoma/DVA is found, venous drainage of the DVA must be preserved if the cavernoma is surgically removed.

2 Arteriovenous Malformations

2.1 Epidemiology

Arteriovenous malformation (AVM) is the most common symptomatic vascular malformation, with a detection rate of 1.2/100,000 person-years (Stapf et al. 2001). The most common presentation is AVM-related hemorrhage, with an annual hemorrhage rate that ranges between 2.8 % (Stapf et al. 2006) and 4.6 % (daCosta et al. 2009).

2.2 Pathogenesis and Pathology

AVMs are abnormal collections of blood vessels wherein arterial blood flows into draining veins without the normal interposed capillary bed. AVMs are typically solitary lesions. In multiple lesions, hereditary hemorrhagic telangiectasia (Rendu–Osler–Weber syndrome) type 1 with mutations of the endoglin gene on bands 33 and 34 of the long arm of chromosome 9, Wyburn–Mason syndrome, and cerebrofacial arteriovenous metameric syndromes (types 1–3) should be considered (Bharatha et al. 2012; Krings et al. 2007).

2.3 Clinical Presentation

After hemorrhage (which in contrast to cavernomas is associated with 10 % mortality and 30–50 % morbidity from each bleed), seizures are the most common presentation. Seizures occur in around 30 % of patients (Garcin et al. 2012). The younger the patient at the time of diagnosis, the higher is the risk of developing seizures (Stapf et al. 2003). Seizure risk is higher for AVMs presenting with intracranial hemorrhage or focal neurologic deficit than for incidental AVMs (Josephson et al. 2011). Male sex, increasing AVM size, arterial borderzone location, frontal lobe location, superficial venous drainage, and venous ectasia have been identified as relative risk factors (Garcin et al. 2012). Venous congestion, perinidal hypoxemia, long pial vein, and a space-occupying effect are angiographic features associated with epileptic seizures (Shankar et al. 2012). Impaired perinidal cerebrovascular reserve capacity due to venous congestion is considered as an underlying pathophysiological mechanism which may trigger epileptic seizures (Fiestra et al. 2011). However, no difference in the 5-year risk of seizures has been observed with conservative or invasive treatment, irrespective of whether the patient presented with hemorrhage or with epileptic seizures (Josephson et al. 2012).

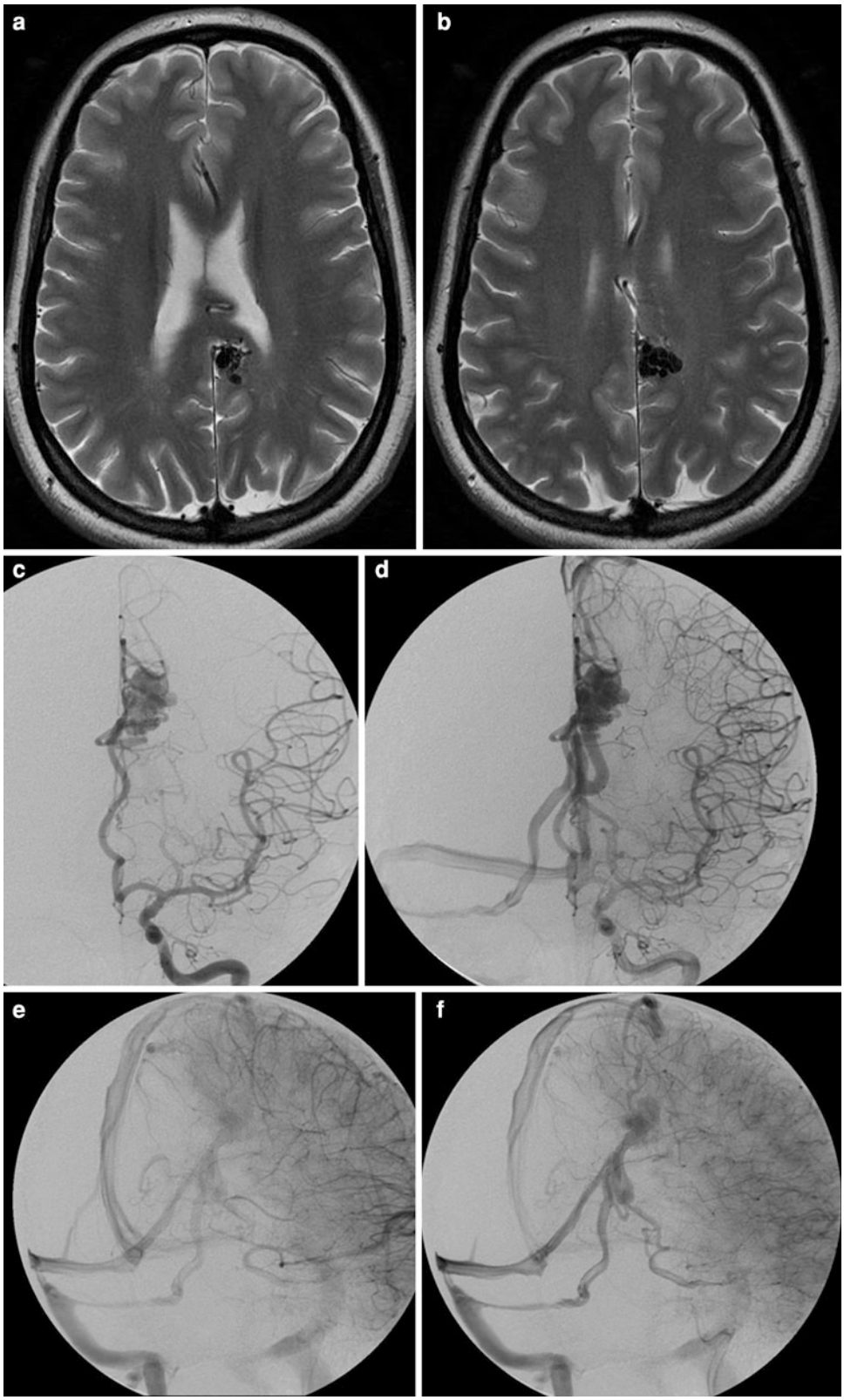

Fig. 6 A 33-year-old woman presented with classic left temporal lobe seizures despite a cingulate location of her AVM (**a**–**d**). However, the venous phases of the digital subtraction angiography demonstrate venous rerouting via the lateral perimesencephalic vein into the basal vein of Rosenthal on the left (**d**–**f**). As this vein also drains the hippocampus, it was felt that her seizures were related to venous congestion of her left hippocampus due to arterial overload of its venous drainage

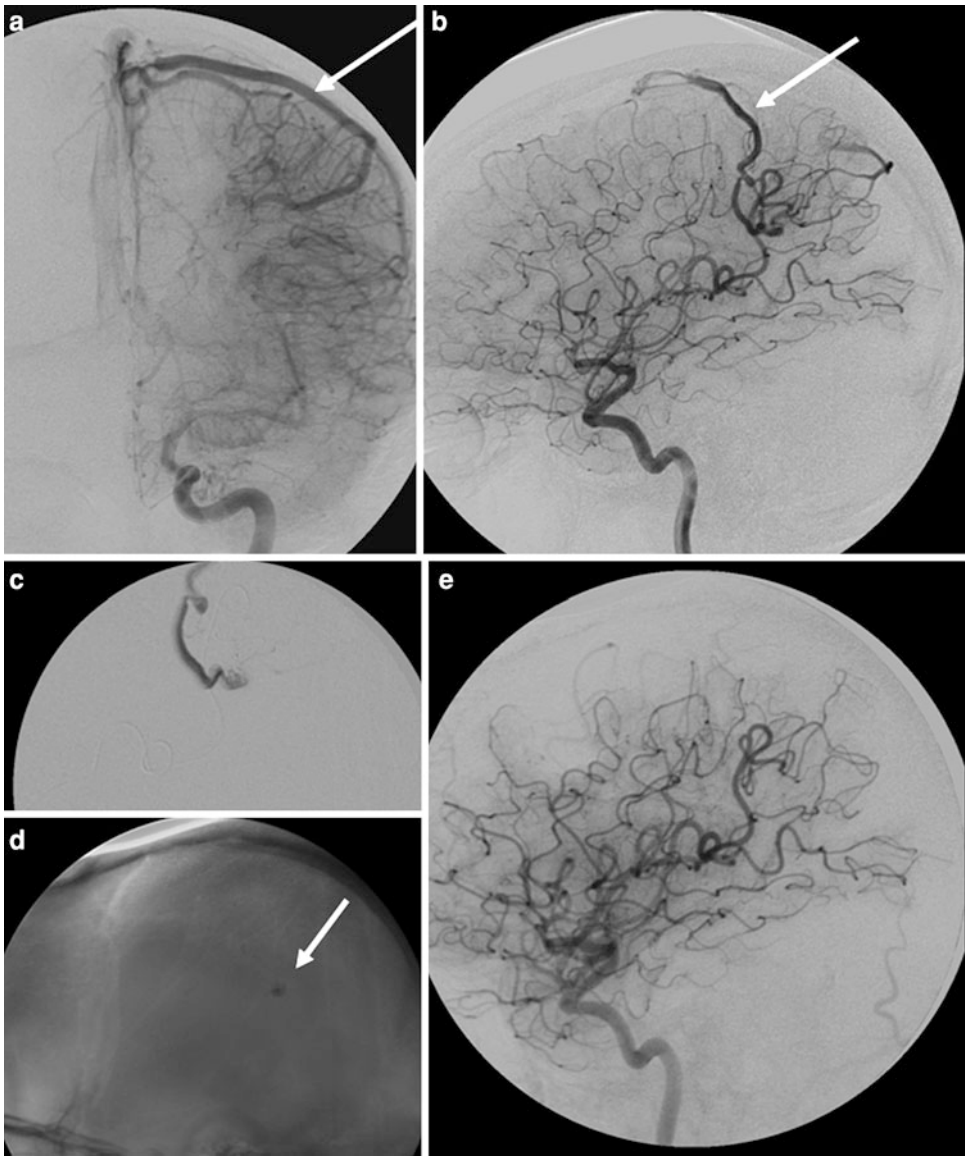

Fig. 7 Seizures in this patient are presumably related to the long pial course of the draining vein (**a**, **b**, *arrow*) leading to a widespread venous congestion over the left hemisphere. Following distal microcatheterization (**c**) and *n*-butyl cyanoacrylate injection (**d**, *arrow*), the AVM could be obliterated (**e**) and the seizures stopped

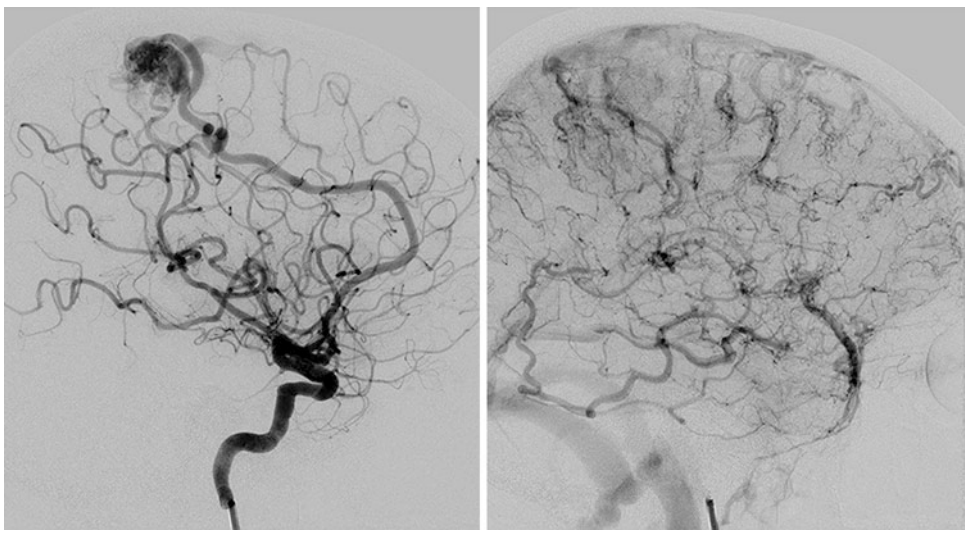

Fig. 8 The venous phase in this 34-year-old patient with seizures demonstrates the so-called pseudophlebitic aspect of the veins (dilated parenchymal veins) that is indicative of longstanding venous hypertension that is associated with seizure occurrence due to venous congestion

2.4 Imaging

On MRI (Figs. 5, 6, 7, 8), AVMs appear as a "bag of black worms" (flow void structures) with minimal or no mass effect. Draining veins have a larger caliber than the feeding arteries and can often be followed on their way to the sinuses or deep vein system. It is important to look for intranidal or flow-related aneurysms of the feeding arteries, which may bleed "instead" of the AVM. If there is significant edema around the lesion, it may be not an AVM but a tumor that has bled. The imaging features of AVMs are best visualized on (high-resolution) T2-weighted fast spin echo images. Three-dimensional time-of-flight MR angiography is helpful for gross depiction of flow; time-resolved contrast-enhanced MR angiography may additionally depict detailed angioarchitecture (Hadizadeh et al. 2012).

Owing to the significant consequences of AVM bleeding, AVM "removal" by surgery, embolization, or radiation treatment is generally intended. However, the risk of treatment must be weighed against the estimated risk of bleeding. A measure to describe the surgical treatment risk is the Spetzler–Martin classification (Spetzler and Martin 1986), in which the nidus size (smaller than 3 cm corresponds to 1 point, 3–6 cm corresponds to 2 points, larger than 6 cm corresponds to 3 points), the eloquence of adjacent brain parenchyma (eloquence corresponds to 1 point), and the pattern of venous drainage (deep venous drainage corresponds to 1 point) are considered. In addition, AVM location is of importance. For example, in temporomesial AVMs the anterior choroidal artery is difficult to separate from enlarged feeding AVM arteries, and surgery and embolization are associated with a higher hemiparesis risk.

3 Dural Arteriovenous Fistulae

3.1 Epidemiology

Dural arteriovenous fistulae are arteriovenous shunts that are located in the wall of a venous sinus and are typically fed by meningeal arteries. In adults, so-called dural arteriovenous fistulae are acquired and may develop following, e.g., a minor trauma and/or sinus thrombosis. In children, dural arteriovenous fistulae are often congenital.

3.2 Pathogenesis

Dural arteriovenous fistulae are communications between dural branches of the internal carotid artery, the external carotid artery, the vertebral artery, and intracerebral veins and/or sinuses.

3.3 Clinical Presentation

The clinical symptoms depend on the size, the location, and the venous drainage pattern. Risk of intracerebral hemorrhage is high in anterior skull base arteriovenous fistulae and risk of intracerebral hemorrhage and epileptic seizures is high in fistulae with retrograde filling of cortical veins (Fig. 9). The Cognard classification focuses on the venous drainage pattern: Grade 1 fistulae are arteriovenous shunts in the wall of a venous sinus, with normal antegrade flow. Grade 2A fistulae show retrograde flow in the sinus, but no reflux in cortical veins. Grade 2B fistulae show retrograde drainage from the sinus into cortical veins. Grade 3 fistulae have direct cortical venous drainage without venous ectasia, and grade 4 fistulae have direct cortical venous drainage with venous ectasia (Cognard et al. 1995). The risk of intracerebral hemorrhage and of epileptic seizures is low in grade 1 and grade 2A fistulae and high in grade 2B, grade 3, and grade 4 fistulae.

3.4 Imaging

Vasogenic edema, hemorrhage, and tubular/tortuous flow void (T2-weighted) and contrast-enhanced (T1-weighted contrast-enhanced sequences) structures are suggestive of a dural arteriovenous fistula. Coronal three-dimensional phase contrast angiography is needed to show venous sinus anatomy and may reveal a thrombosed or partially open venous sinus. Although time-resolved contrast-enhanced MR or CT angiography may discover dural arteriovenous fistulae, digital subtraction angiography with bilateral internal carotid artery, external carotid artery, and vertebral artery injections is needed if a dural arteriovenous fistula is suspected and in order to develop an endovascular treatment strategy.

4 Developmental Venous Anomalies

4.1 Synonym

A synonym is "venous angioma."

4.2 Epidemiology

DVAs are the most common vascular malformation, with a prevalence of 2.5–9 % on contrast-enhanced T1-weighted MR images (Osborn 2010).

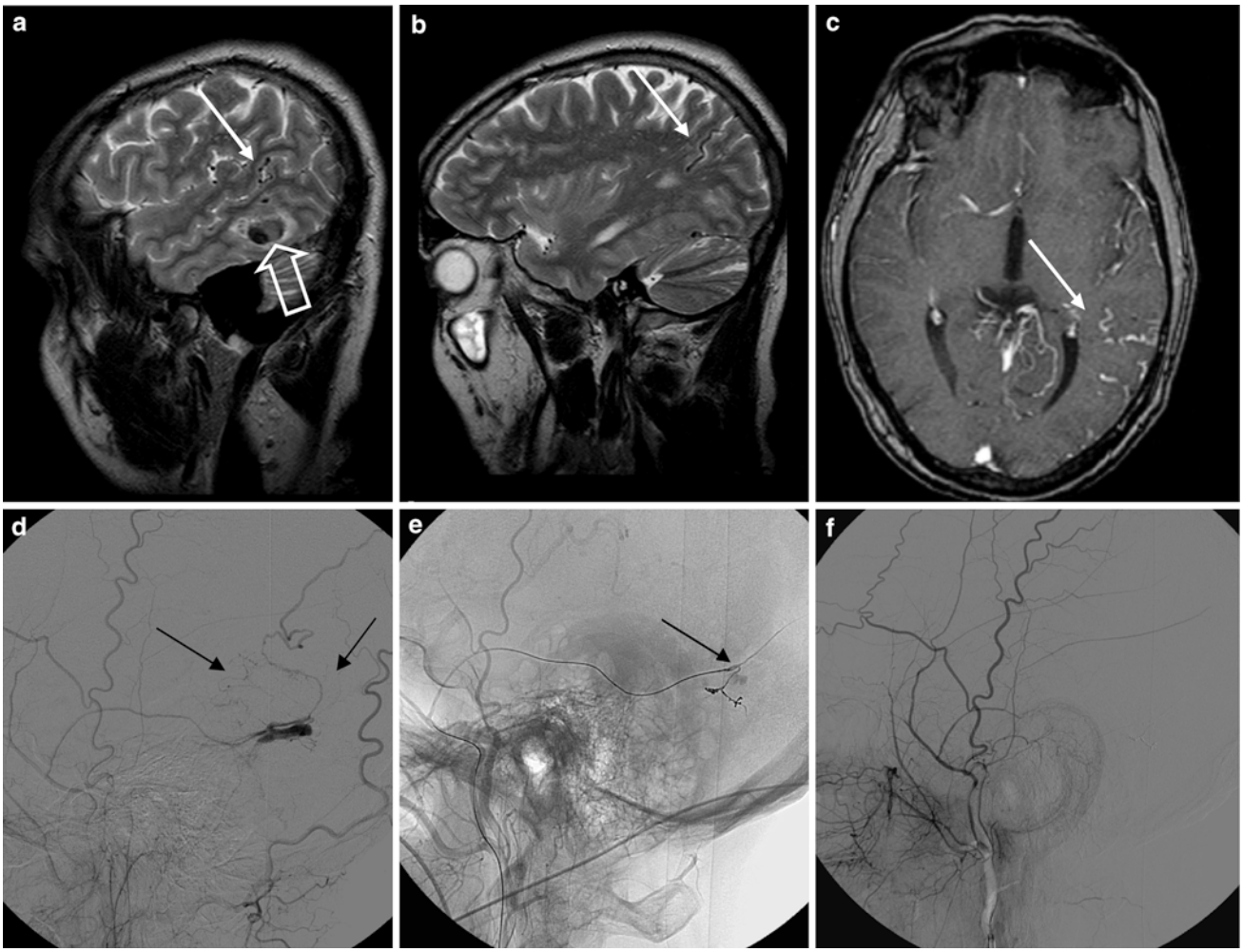

Fig. 9 A 54-year-old man presented with left-sided headache and complex focal seizures. Sagittal T2-weighted (**a**, **b**) and axial T1-weighted (**c**) gradient echo sequences showed a temporo-occipital hemorrhage (**a**, *hollow arrow*) and adjacent enlarged vessels (**a**–**c**, *arrows*). Catheter angiography revealed a small tentorial dural arteriovenous fistula with retrograde filling of cerebral veins (**d**, *arrows*). The fistula was occluded with Onyx injection (ev3 Neurovascular, Irvine, CA, USA) via the petrosqamous middle meningeal artery branch (**e**, *arrow*, **f**)

4.3 Pathogenesis and Pathology

DVAs are considered variants of otherwise normal venous drainage. Up to 20 % of cavernomas are associated with DVAs. There is some evidence that an anomalous venous drainage triggers cavernoma evolution (Fig. 4).

4.4 Clinical Presentation

DVAs are typically incidental findings. If they cause symptoms, they are likely due to associated cavernomas. In a systematic meta-analysis and prospective study, 4 % of patients presented with epileptic seizures (Hon et al. 2009). However, whether there was a causal relationship with the DVA remained unclear. In very rare cases, epileptic seizures can be elicited by thrombosis of the DVA collector vein, which may cause hemorrhage or venous congestive edema (Flacke et al. 2006; Pereira et al. 2008) (Fig. 10).

4.5 Imaging

DVAs are characterized by dilated medullary white matter veins (caput medusae) converging on a collector vein which drains into a dural sinus or ependymal vein. Around 5 % of DVAs are atypical, with some shunting between the arterial and venous system.

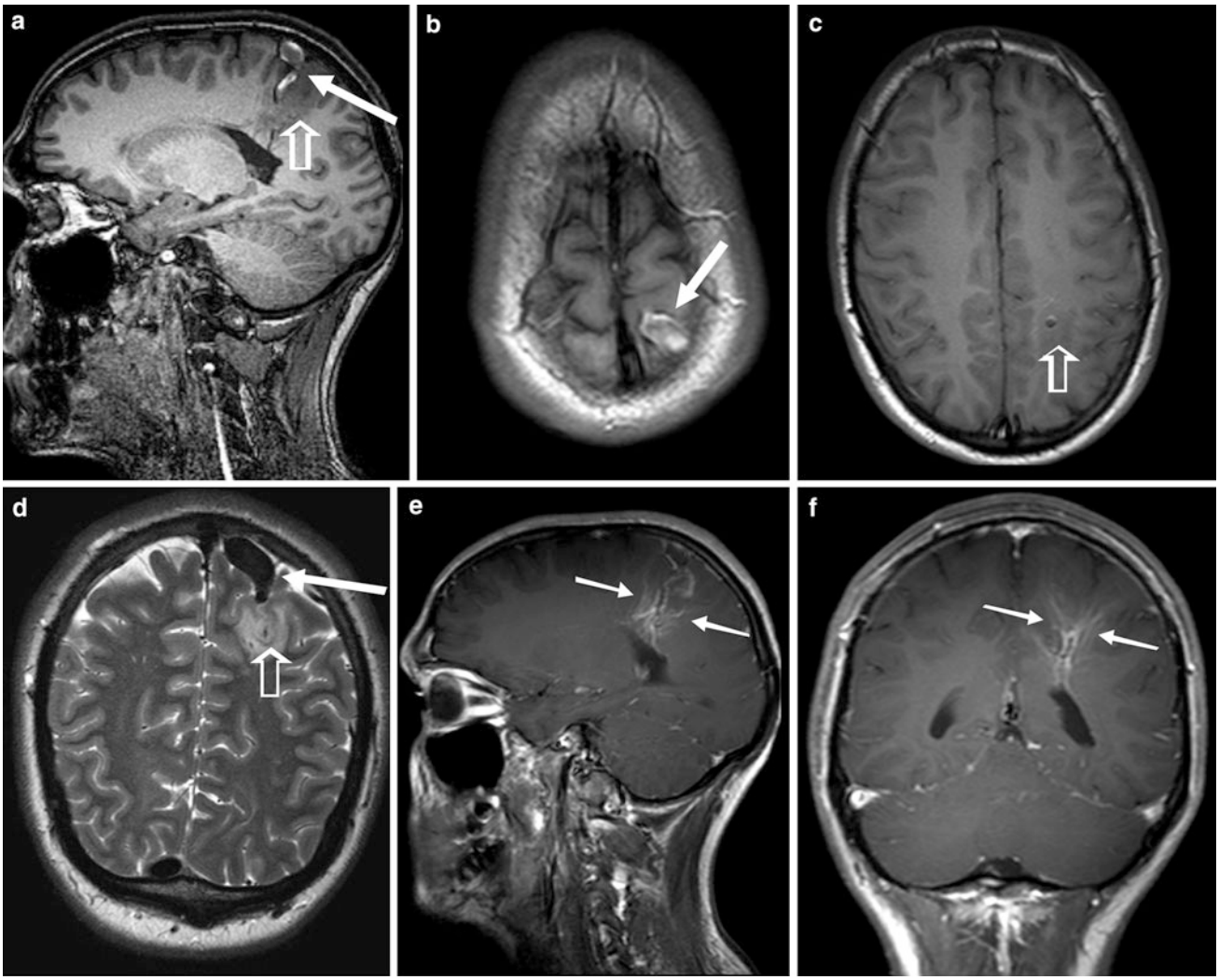

Fig. 10 A 21-year-old man presented with two focal motor seizures. MRI showed an enlarged and thrombosed cortical left parietal vein (**a**, **b**, **d**, *arrow*) surrounded by vasogenic edema (**a**, **c**, **d**, *hollow arrow*). The cortical vein collects the blood from tiny veins with a caput-medusae-like appearance (**e**, **f**, *arrows*)

5 Capillary Telangiectasias

5.1 Epidemiology

The true incidence of capillary telangiectasias is unknown since they are usually small and easily missed on MRI and autopsy.

5.2 Pathogenesis and Pathology

Capillary telangiectasias are clusters of dilated capillaries interspersed with normal brain parenchyma. They may be mixed with DVAs.

5.3 Clinical Presentation

Capillary telangiectasias are usually an incidental finding unrelated to epileptic seizures. However, larger capillary telangiectasias can elicit epileptic seizures that have been explained with a slow flow and hypoperfusion and hypoxic injury in these lesions (Samaya et al. 2010). Hereditary hemorrhagic telangiectasia (Rendu–Osler–Weber syndrome), ataxia telangiectasia, and past radiation therapy in children in lesions outside the brainstem should be considered.

5.4 Imaging

Capillary telangiectasias are typically small (less than 1 cm), non-space-occupying lesions with spatial preponderance for

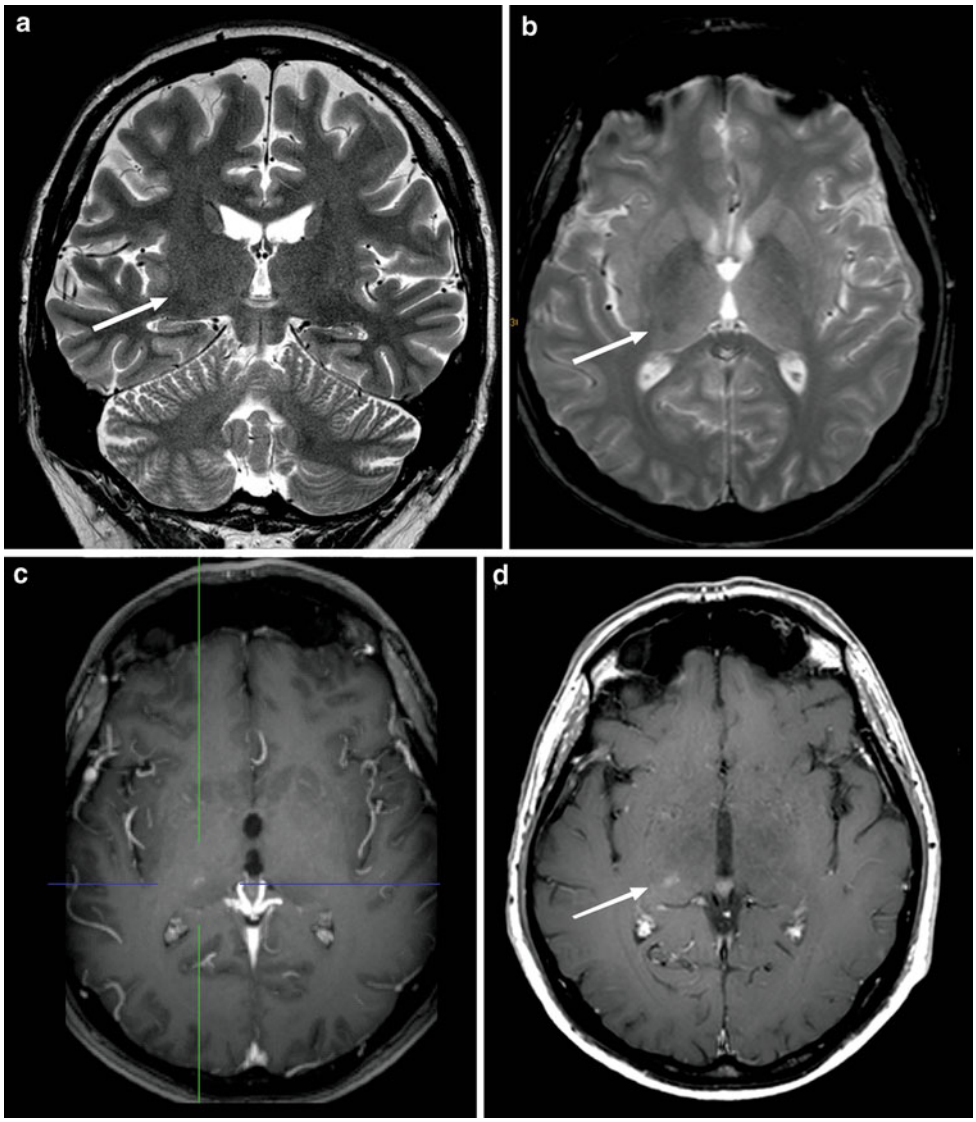

Fig. 11 Capillary teleangiectasia as an incidental finding in a 36-year-old man with temporal lobe seizures. The small, non-space-occupying lesion adjacent to the right thalamus is invisible on the T2-weighted fast spin echo image (**a**) and is moderately hypointense on the T2-weighted gradient echo image (**b**, *arrow*). It shows a faint contrast enhancement on T1-weighted gradient echo (**c**) and spin echo (**d**) images

the pons (Fig. 11) (Castillo et al. 2001). Lesions with a size greater than 1 cm are found in around 7 % of cases (Sayama et al. 2010).

Capillary telangiectasias are best visualized on T1-weighted contrast-enhanced images, on which a faint radial enhancement and the interspersed normal brain parenchyma are visible. T2-weighted gradient echo sequences are specific when they display a moderate hypointensity. Lesions can be missed on fluid-attenuated inversion recovery and T2-weighted fast spin echo sequences or show punctate hyperintense foci within the lesion.

References

Awad I, Jabbour P (2006) Cerebral cavernous malformations and epilepsy. Neurosurg Focus 21:e7

Bharatha A, Faughnan ME, Kim H, Pourmohamad T, Krings T, Bayrak-Toydemir P, Pawlikowska L, McCulloch CE, Lawton MT, Dowd CF, Young WL, Terbrugge KG (2012) Brain arteriovenous malformation multiplicity predicts the diagnosis of hereditary hemorrhagic telangiectasia: quantitative assessment. Stroke 43(1):72–78

Baumann CR, Schuknecht B, Lo Russo G, Cossu M, Citterio A, Andermann F, Siegel AM (2006) Seizure outcome after resection of cavernous malformations is better when surrounding hemosiderin-stained brain also is removed. Epilepsia 47:563–566

Baumann CR, Acciarri N, Bertalanffy H, Devinsky O, Elger CE, Lo Russo G, Cossu M, Sure U, Singh A, Stefan H, Hammen T, Georgiadis D, Baumgartner RW, Andermann F, Siegel AM (2007) Seizure outcome after resection of supratentorial cavernous malformations: a study of 168 patients. Epilepsia 48:559–563

Castillo M, Morrison T, Shaw JA, Bouldin TW (2001) MR imaging and histologic features of capillary telangiectasia of the basal ganglia. Am J Neuroradiol 22(8):1553–1555

Chang EF, Gabriel RA, Potts MB, Garcia PA, Barbaro NM, Lawton MT (2009) Seizure characteristics and control after microsurgical resection of supratentorial cerebral cavernous malformations. Neurosurgery 65(1):31–37

Cognard C, Gobin YP, Pierot L, Bailly AL, Houdart E, Casasco A, Chiras J, Merland JJ (1995) Cerebral dural arteriovenous fistulas: clinical and angiographic correlation with a revised classification of venous drainage. Radiology 194:671–680

da Costa L, Thines L, Dehdashti AR, Wallace MC, Willinsky RA, Tymianski M, Schwartz ML, ter Brugge KG (2009) Management and clinical outcome of posterior fossa arteriovenous malformations: report on a single-centre 15-year experience. J Neurol Neurosurg Psychiatry 80(4):376–379

Del Curling O Jr, Kelly DL Jr, Elster AD, Craven TE (1991) An analysis of the natural history of cavernous angiomas. J Neurosurg 75:702–708

Englot DJ, Han SJ, Lawton MT, Chang EF (2011) Predictors of seizure freedom in the surgical treatment of supratentorial cavernous malformations. J Neurosurg 115(6):1169–1174

Fierstra J, Conklin J, Krings T, Slessarev M, Han JS, Fisher JA, Terbrugge K, Wallace MC, Tymianski M, Mikulis DJ (2011) Impaired peri-nidal cerebrovascular reserve in seizure patients with brain arteriovenous malformations. Brain 134(Pt 1):100–109

Flacke S, Stuer C, Stoffel M, Urbach H (2006) Symptomatic developmental venous anomaly after spontaneous thrombosis of the collector vein. Clin Neuroradiol 16:131–133

Garcin B, Houdart E, Porcher R, Manchon E, Saint-Maurice JP, Bresson D, Stapf C (2012) Epileptic seizures at initial presentation in patients with brain arteriovenous malformation. Neurology 78(9): 626–631

Gross BA, Lin N, Du R, Day AL (2011) The natural history of intracranial cavernous malformations. Neurosurg Focus 30(6):E24

Hadizadeh DR, Kukuk GM, Steck DT, Gieseke J, Urbach H, Tschampa HJ, Greschus S, Kovàcs A, Möhlenbruch M, Bostroem A, Schild HH, Willinek WA (2012) Noninvasive evaluation of cerebral arteriovenous malformations by 4D-MRA for preoperative planning and postoperative follow-up in 56 patients: comparison with DSA and intraoperative findings. AJNR Am J Neuroradiol 33(6):1095–1101

Hon JM, Bhattacharya JJ, Counsell CE, Papanastassiou V, Ritchie V, Roberts RC, Sellar RJ, Warlow CP, Al-Shahi Salman R (2009) SIVMS Collaborators. The presentation and clinical course of intracranial developmental venous anomalies in adults: a systematic review and prospective, population-based study. Stroke 40(6):1980–1985

Josephson CB, Leach JP, Duncan R, Roberts RC, Counsell CE, Al-Shahi Salman R (2011) Scottish Audit of Intracranial Vascular Malformations (SAIVMs) Steering committee and collaborators. Seizure risk from cavernous or arteriovenous malformations: prospective population-based study. Neurology 76(18):1548–1554

Josephson CB, Bhattacharya JJ, Counsell CE, Papanastassiou V, Ritchie V, Roberts R, Sellar R, Warlow CP, Al-Shahi Salman R (2012) On behalf of the Scottish Audit of Intracranial Vascular Malformations (SAIVMs) steering committee and collaborators. Seizure risk with AVM treatment or conservative management: prospective, population-based study. Neurology 79(6):500–507

Krings T, Geibprasert S, Luo CB, Bhattacharya JJ, Alvarez H, Lasjaunias P (2007) Segmental neurovascular syndromes in children. Neuroimaging Clin N Am 17(2):245–258

Moran NF, Fish DR, Kitchen N, Shorvon S, Kendall BE, Stevens JM (1999) Supratentorial cavernous haemangiomas and epilepsy: a review of the literature and case series. J Neurol Neurosurg Psychiatry 66:561–568

Moriarity JL, Clatterbuck RE, Rigamonti D (1999) The natural history of cavernous malformations. Neurosurg Clin N Am 10:411–417

Osborn AG, Salzman KL, Barkovich AJ (eds) (2010) Diagnostic imaging. Brain Amirsys Inc, Salt Lake City

Pereira VM, Geibprasert S, Krings T, Aurboonyawat T, Ozanne A, Toulgoat F, Pongpech S, Lasjaunias PL (2008) Pathomechanisms of symptomatic developmental venous anomalies. Stroke 39(12):3201–3215

Raabe A, Pernhorst K, Schmitz AK, Grote A, Urbach H, Friedman A, Albert J. Becker AJ, Elger CE, Niehusmann P (2012) Clinico-neuropathological correlations in vascular lesions suggest astroglial albumin storage as common epileptogenic factor. Epilepsia 53: 539–548

Sayama CM, Osborn AG, Chin SS, Couldwell WT (2010) Capillary telangiectasias: clinical, radiographic, and histopathological features. Clinical article. J Neurosurg 113(4):709–714

Shankar JJS, Menezes R, Pohlman-Eden B, Wallace C, Terbrugge K, Krings T (2012) Angio-architecture of brain AVM determines seizures presentation- proposed scoring system. AJNR Am J Neuroradiol [Epub ahead of print]

Spetzler RF, Martin NA (1986) A proposed grading system for arteriovenous malformations. J Neurosurg 65:476–483

Stapf C, Mohr JP, Pile-Spellman J, Solomon RA, Sacco RL, Connolly ES Jr (2001) Epidemiology and natural history of arteriovenous malformations. Neurosurg Focus 11(5):e1

Stapf C, Khaw AV, Sciacca RR, Hofmeister C, Schumacher HC, Pile-Spellman J, Mast H, Mohr JP, Hartmann A (2003) Effect of age on clinical and morphological characteristics in patients with brain arteriovenous malformation. Stroke 34(11):2664–2669

Stapf C, Mast H, Sciacca RR, Choi JH, Khaw AV, Connolly ES, Pile-Spellman J, Mohr JP (2006) Predictors of hemorrhage in patients with untreated brain arteriovenous malformation. Neurology 66(9):1350–1355

Wurm G, Schnizer M, Fellner FA (2005) Cerebral cavernous malformations associated with venous anomalies: surgical considerations. Neurosurgery 57(Suppl 1):42–58

Zabramski JM, Wascher TM, Spetzler RF, Johnson B, Golfinos J, Drayer BP, Brown B, Rigamonti D, Brown G (1994) The natural history of familial cavernous malformations: results of an ongoing study. J Neurosurg 80:422–432

Ischemia

Horst Urbach

Contents

Abstract

A vascular etiology of epileptic seizures is common in the fetal and perinatal period and again in adults. In adults, more than 50 % of newly diagnosed epilepsy cases are related to cerebrovascular diseases, but the exact underlying mechanism is often difficult to prove. This chapter summarizes different vascular lesions with characteristic MRI patterns.

1 Hypoxic-Ischemic Encephalopathies in Utero and in Infancy

Background:

The gestational age and the severity of the hypoxic-ischemic insult determine how the brain reacts to it.

Between the 20th and 28th weeks of gestation, the immature brain cannot react with gliosis; typical lesions are hydranencephaly (Fig. 1) or (agenetic) porencephaly.

Between the 28th and 32nd weeks, periventricular-intraventricular hemorrhages (PIVH) predominate. They originate in the subependymal germinal matrix, which is a highly cellular area that gives rise to neurons and glia during gestation and involutes before term. Most of these hemorrhages occur in the first week of life and are related to perinatal stress, including low blood pressure, hypoxia, hypercarbia, etc.

Between the 32nd and 36th weeks, periventricular leukomalacia (PVL) is the typical lesion pattern, which, however, may also occur in immature term newborns, for instance, in combination with cardiac defects. It also has an overlap with (PIVH), since periventricular leukomalacia is found in 75 % of patients who died with PIVH, and 25 % of PVL cases are hemorrhagic.

As the brain further matures, the vascular border zones shift toward the periphery. Accordingly, white matter lesions "move" from the periventricular to the subcortical

H. Urbach (✉)
Department of Neuroradiology, University Hospital Freiburg, Germany
e-mail: horst.urbach@uniklinik-freiburg.de

H. Urbach (ed.), *MRI in Epilepsy*, Medical Radiology. Diagnostic Imaging,
DOI: 10.1007/174_2012_781,

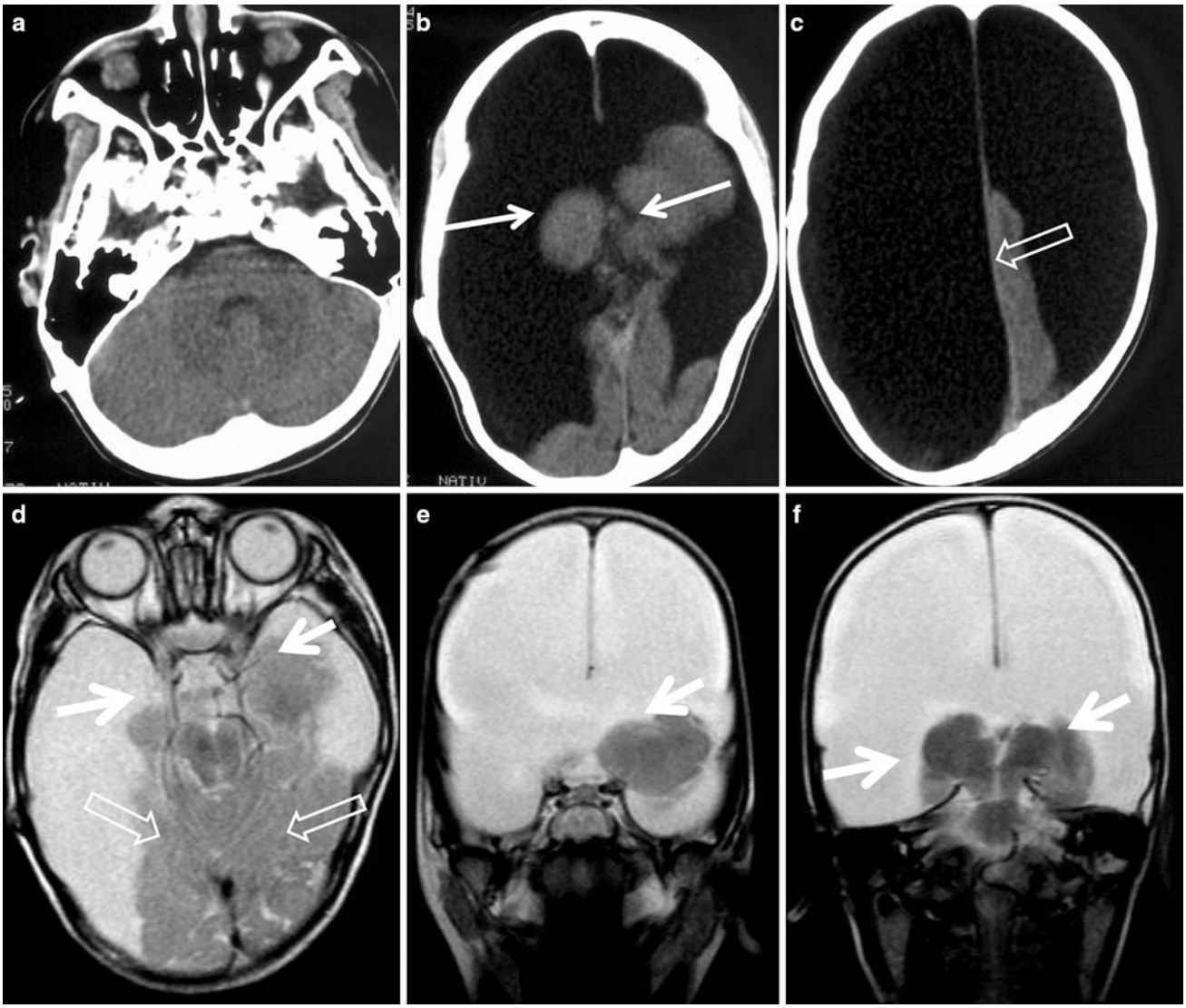

Fig. 1 Hydranencephaly in a 4-year-old boy. The cerebral hemispheres are nearly completely replaced by CSF-filled sacs. Brain tissue, which normally is supplied via the posterior cerebral arteries like the thalami (**b** *arrows*), the medial aspects of the temporal lobes (**d–f** *thick arrows*), and the occipital lobes (**d**: *hollow arrows*), is preserved. The brainstem and cerebellum are normal (**a**). The intact falx cerebri (**c**: *hollow arrows*) helps to distinguish between hydranencephaly and alobar holoprosencephaly

zone. Periventricular and subcortical leukomalacias are not considered separate entities but rather represent a continuous disease spectrum.

In the term infant, the lesion pattern again depends on the degree of asphyxia:

Acute profound episodes of asphyxia may cause a widespread replacement of cerebral cortex and white matter by one or more CSF-filled cavities of variable sizes (multicystic encephalomalacia) or more or less pronounced injury in the thalami, basal ganglia, hippocampi, dorsal mesencephalic structures, and perirolandic cortex with relative sparing of the rest of the cortex (Figs. 5 and 6). Infants with mild to moderate hypoxia (prolonged partial hypoxia–ischemia, primarily hypotensive episodes) show cortical and subcortical injury in a watershed parasagittal distribution. The injury comprises cortical necrosis involving the immediately subjacent white matter, encompassing the parasagittal, superomedial areas of the convexities bilaterally, with the parietooccipital region more involved than frontal regions (Fig. 7). At a chronic phase, the cortex of the affected gyri shrinks and the term "ulegyria" ($o\upsilon\lambda\eta$ = scar) is used to define the type of cortical abnormality characterized by atrophy at the depth of the sulci and relative sparing of the crown of the gyri (Fig. 9) (Table 1).

Table 1 Classification of hypoxic-ischemic encephalopathies in utero and infancy

Disease	Timepoint of hypoxic event and description	MRI
Hydranencephaly Porencephaly	<20–28th gestational week: The immature brain cannot "react" with gliosis	Liquified tissue defect with enlargement of the benachbarte CSF spaces. No or nearly no hyperintensity on FLAIR sequences
Periventricular intraventricular (germinal matrix-) hemorrhage	28–32nd gestational week: The germinal matrix has involuted by 34 weeks of gestation	Grade I: subependymal bleeding only (typically between the caudate nucleus and thalamus) Grade II: <50 % of ventricles filled with blood, no ventricle dilatation Grade III: >50 % of ventricles filled with blood, ventricle dilatation Grade IV: parenchymal blood
Periventricular leukomalacia	32–36th gestational week: Pre-or perinatal insult in preterm newborns bilateral coagulation necrosis with white matter loss, gliosis, and cavitated lesions adjacent to the external angles of the lateral ventricles or diffuse white matter injury and hypomyelination due to injury of preoligodendrocytes (Counsell et al. 2003)	Type "focal cystic periventricular" Grade I: along posterior horns of the lateral ventricles Grade II: along anterior and posterior horns of lateral ventricles Grade III: along entire length of lateral ventricles Grade IV: with cavitating lesions of subcortical white matter Type of "diffuse white matter injury and hypomyelination"
Subcortical leukomalacia	Pre- or perinatal insult in "older" preterm newborns	Subcortical white matter lesions with white matter loss
Hypoxic-ischemic encephalopathy of the term newborn	Profound asphyxia: multicystic encephalomalacia Less profound asphyxia: deep gray matter and perirolandic cortical lesions (high O_2 demand)	Multicystic destructive lesions Symmetric lesions of basal ganglia (dorsal putamen, ventrolateral thalamus), hippocampi, dorsal brain stem, pre- and postcentral gyri
Ulegyria	Pre- or perinatal insult in term newborns	Gyral scarring and CSF widening in the depth of the (parieto-occipital) sulci in a parasagittal distribution = "mushroom gyri"

1.1 Hydranencephaly

Epidemiology. 1:5,000–10,000 live births; approximately ten times more common in teenage mothers.

Pathology and Pathogenesis. Insult to the developing brain between the 20th and 27th weeks of gestation (Myers 1989). At this time the brain cannot react to an insult with gliosis yet; instead, liquefication necrosis develops. Hydrancephaly is considered to develop secondarily to the occlusion of internal carotid arteries above the supraclinoid level. A hint for hydranencephaly as a destructive disorder and against a congenital disorder is the fact that some hemispheric brain tissue is usually preserved (Fig. 1). Common identified causes of hydranencephalies are feto-fetal transfusion syndromes, congenital infections (toxoplasmosis, CMV), and toxins. Rare causes are autosomal-recessive diseases such as Fowler syndrome or microhydranencephaly (Williams et al. 2010; Kavaslar et al. 2000; Behunova et al. 2010).

Clinical Presentation. Newborns may have a small, a normal-sized, or even a large head due to CSF production of the intact choroid plexus and the presence of hydrocephalus. Hyperexcitability and epileptic seizures are common. Only brainstem functions are intact. Death usually occurs during infancy.

In rare cases with unilateral hydranencephaly, a nearly normal living may be possible. Patients' disabilities are confined to deficits in fine motor control (pincer's grip). In left hemispheric hydranencephaly, language functions are transferred to the right hemisphere (Ulmer et al. 2005).

Imaging. The territory normally supplied by the internal carotid arteries is replaced by CSF-filled cavities. Brain parenchyma supplied by the posterior cerebral arteries is usually preserved. In contrast to the differential diagnosis of alobar holoprosencephaly, the falx cerebri is intact (Fig. 1).

1.2 Porencephaly, Encephalomalacia, and Perinatal Stroke

Epidemiology. Since a wide range of conditions may cause porencephaly, encephalomalacia, and perinatal stroke, encephalomalacia and perinatal stroke are not fully disjunct diagnoses, and the exact numbers are difficult to obtain. However, perinatal stroke is common, with a prevalence of 1 in 2,300–5,000 live births (Raju et al. 2007).

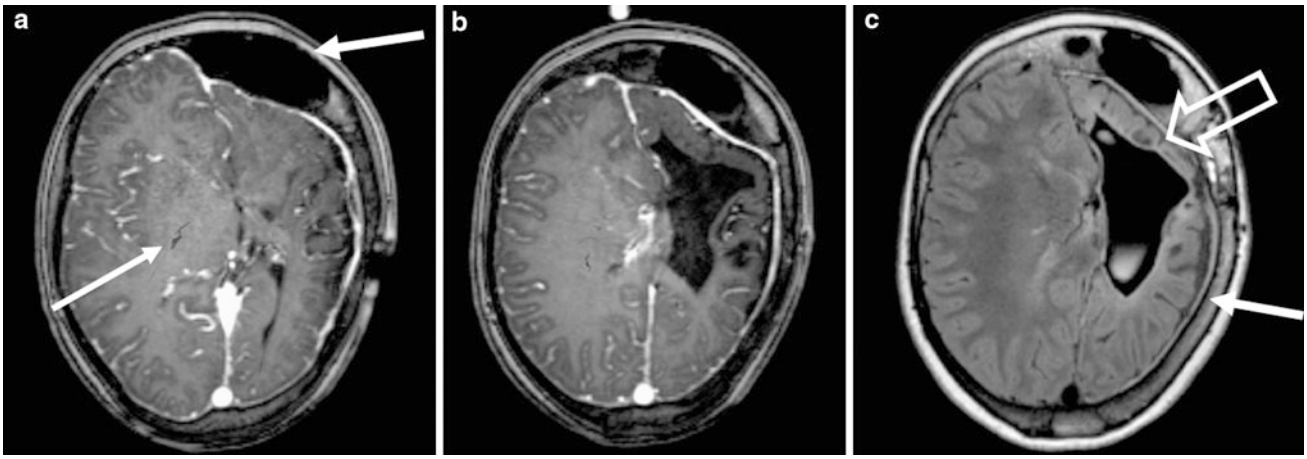

Fig. 2 MRI in a 15-year-old girl with congenital right-sided hemiparesis and drug-resistant seizures shows porencephalic extension of the left lateral ventricle (**b**, **c**) associated with gliotic gyri around the left frontal horn (**c** *arrow*). Next to the left-sided hemiatrophy, frontal sinus hypertrophy and thickened calvaria (**c** *hollow arrow*) have developed (Dyke–Davidoff–Masson syndrome). A pyramidal tract is displayed with diffusion tensor tractography and co-registered to the 3D T1-weighted data set only on the right side (**a** *arrow*). This condition, with rather prominent gliotic changes, could also be designated as encephaloclastic porencephaly

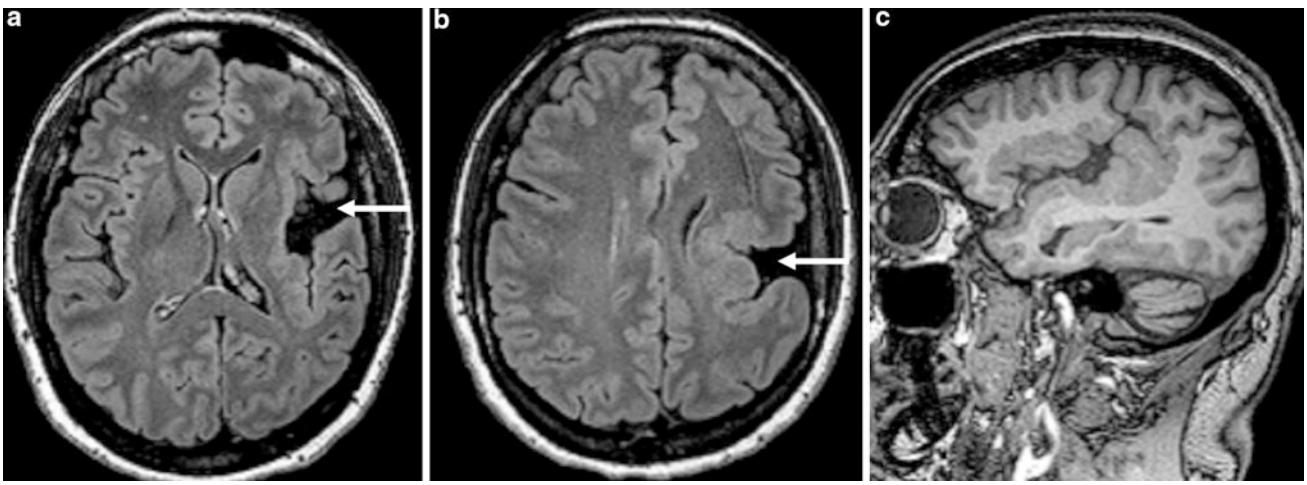

Fig. 3 Schizencephaly/polymicrogyria complex in a 35-year-old woman with a mild right-sided hemiparesis who has suffered from simple focal and complex focal seizures since the age of 8. A widened Sylvian fissure (**a**, **b** *arrow*) is surrounded by polymicrogyriform cortex without any gliotic changes (**b**, **c** *black arrows*). Schizencephaly/polymicrogyria complex is most often the result of a vascular insult in the late second or third trimester and could also be designated as agenetic porencephaly

Pathology and Pathogenesis. Porencephalies are unilateral or bilateral cavitary lesions due to hemispheric necrosis that occurs in utero before the cerebral hemispheres are formed (Friede 1989). These cavities develop prior to approximately the 20th gestational week, the adjacent cortex is often dysplastic, and gliotic reaction is absent or minimal (agenetic porencephaly). If the insult to the developing brain takes place in the late second or third trimester, glial reaction lining the cavities is more prominent and the adjacent cortex is atrophic, but not dysplastic. These lesions are better designated as encephaloclastic porencephaly or (macro-)cystic encephalomalacia. If cavitary lesions are confined to the territory of a major intracerebral artery, the term "ischemic perinatal stroke" is appropriate. Ischemic perinatal stroke is defined as a group of heterogeneous conditions in which there is a focal disruption of blood flow secondary to arterial or venous thrombosis or embolization between 20 weeks of fetal life through the 28th postnatal day (Raju et al. 2007).

The mechanism of porencephaly, encephalomalacia, and perinatal stroke is usually vascular (ischemia or resolution of an intracerebral hemorrhage). The risk is higher in (monochorionic, diamniotic) twins (Friede 1989), and an autosomal-dominant form with *COL4A1* mutations on chromosome 13 and porencephaly due to fetal infections (mostly CMV infections) has been described (Aguglia et al.

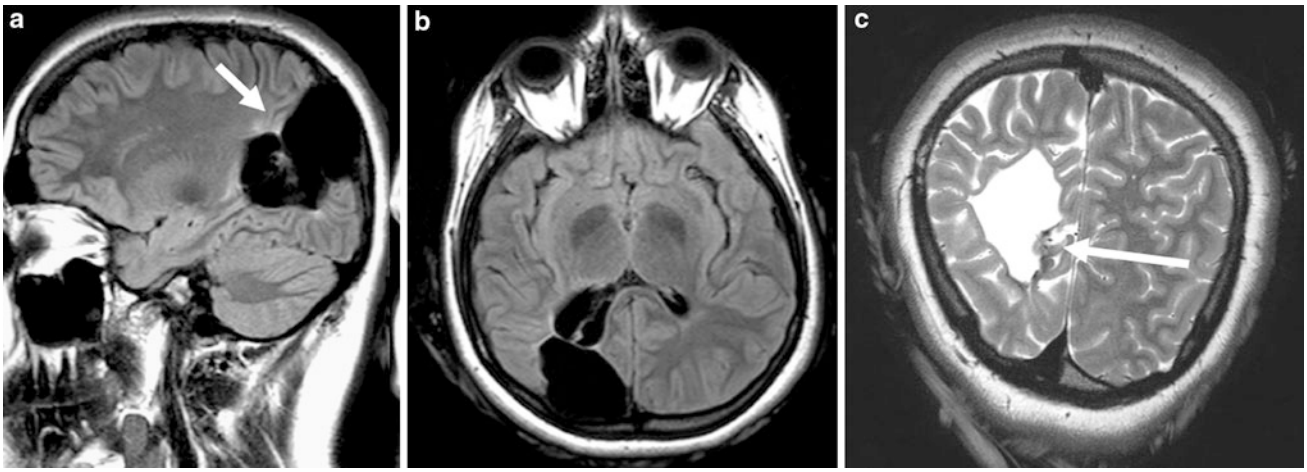

Fig. 4 Parietooccipital porencephalic cyst in a 15-year-old girl with drug-resistant secondarily generalized tonic–clonic seizures, left-sided hemiparesis, and left lower quadrant anopia (**a**–**c**). The cystic lesion has a CSF-like signal, communicates with the lateral ventricle and the superficial subarachnoid space, and is lined by glitoic tissue (**a** *arrow*). A coronal T2-weighted fast spin echo sequence shows a hypointense structure (**c** *arrow*), suggesting that the porencephalic cyst is secondary to the resorption of an intracerebral hemorrhage

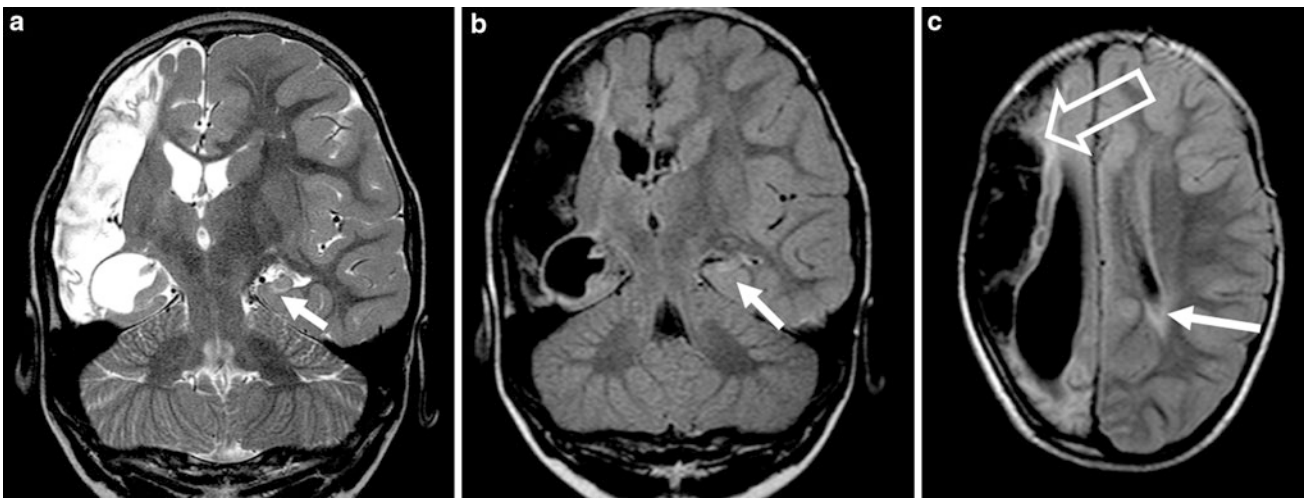

Fig. 5 Postnatal ischemic stroke in a 3-year-old boy who suddenly developed a left-sided hemiparesis at the age of 2 months. Simple and complex focal seizures started at the age of 4. The porencephalic cavity is confined to the right MCA territory and communicates with the superficial subarachnoid space. Distinct right-sided hemiatrophy and gliotic changes (**c** *hollow arrow*) are suggestive of a fetal, perinatal, or early postnatal origin. Increased peritrigonal signal intensity (**c** *arrow*) and hippocampal atrophy and signal increase of the CA1 sector (**a**, **b** *arrow*) indicate hypoxic-ischemic encephalopathy

2004; Gould et al. 2005; Breedveld et al. 2006; van der Knaap et al. 2006; Alamowitch et al. 2009). In bilateral lesions with glial reactions, the term "multicystic encephalomalacia" is often used, and next to bilateral thromboembolic infarcts, profound hypotension and neonatal hypoglycemia must be considered.

Clinical Presentation. The correlation between porencephalic lesion location and seizure semiology is weak, and many patients have temporal lobe seizures, which may be explained with coexisting hippocampal damage (dual pathology) (Ho et al. 1998). Perinatal stroke patients typically present with congenital or early acquired hemiparesis or hemiplegia.

Imaging. Porencephalic lesions are CSF-filled cystic lesions with minimal surrounding gliosis that communicate with the lateral ventricle, the subarachnoid space, or both. The adjacent cortex is atrophic and may be dysplastic (Figs. 2–4).

Encephalomalacia can be macrocystic or microcystic. Macrocystic encephalomalacia is characterized by cavitary lesions with CSF-like signal and increased FLAIR signal intensity lining the CSF-filled cavities. Microcystic

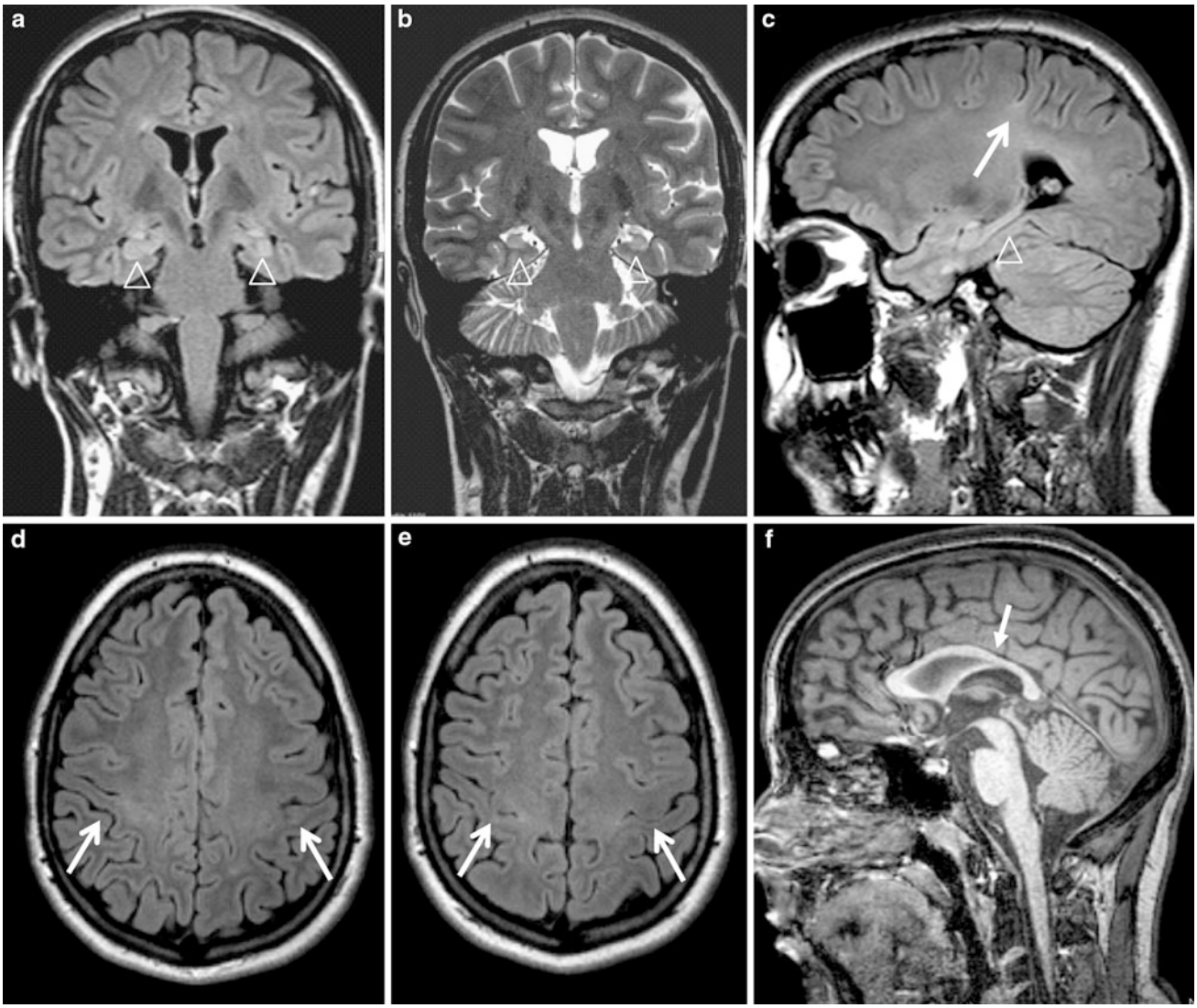

Fig. 6 Less profound hypoxic-ischemic encephalopathy of a term newborn. A 20-year-old woman presented with drug-resistant temporal lobe seizures since the age of 8. Past medical history revealed successful resuscitation at the age of 2 weeks. MRI showed gliotic changes and tissue volume loss of both hippocampi (R > L) (**a**–**c** *triangles*) and of the pre- and postcentral gyri, respectively (**c**–**e** *arrows*). Note that the cortex in the depth of the sulci is more heavily affected (**c** *arrow*). Gliotic changes and tissue volume loss are due to selective neuronal loss and the sequelae of the high O_2 and metabolic demand due to the fact that the pre- and postcentral gyri are myelinating around birth. Midsagittal T1-weighted shows a rather thin callosal body resulting from the degeneration of transcallosal axons (**f** *arrow*)

encephalomalacia designates damaged, gliotic brain with increased water content but without overt cavitary necrosis. It is characterized by increased signal intensity on FLAIR sequences. Perinatal ischemic stroke caused by thromboembolic infarction shows cavitary lesions confined to the territory of one or more intracerebral arteries. The affected hemisphere is severely atrophic and the corticospinal tract extremely thin (Fig. 5). Microcystic, gliotic cortical and subcortical signal changes in a watershed parasagittal distribution are in favor of moderate neonatal hypoxia/hypotension (Fig. 8) and those with prominent parietal and occipital lobe changes in favor of neonatal hypoglycemia (Barkovich et al. 1998).

1.3 Periventricular Leukomalacia, Subcortical Leukomalacia, and Ulegyria

Clinical presentation. Patients with milder grades of periventricular leukomalacia typically present with spastic diparesis and visual impairment. More severe grades have leg-dominant spastic quadriparesis and may show severe cognitive

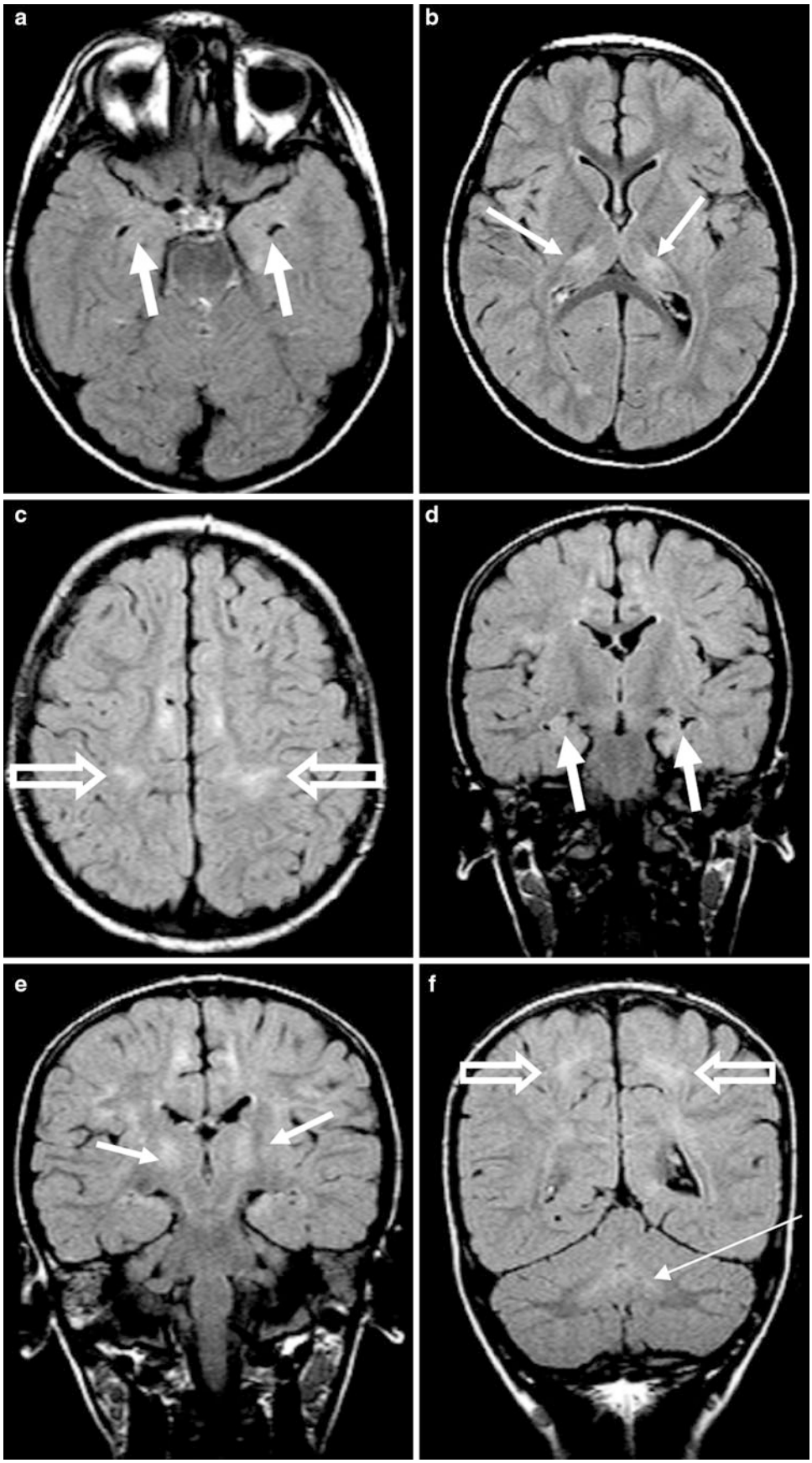

Fig. 7 Hypoxic-ischemic encephalopathy of a term newborn. MRI of a 5-year-old child with complex focal seizures and suspected hypoxia during birth. Hippocampi (**a**, **d** *thick arrows*), ventrolateral thalami (**b**, **e** *arrows*), Purkinje cells and dentate nuclei (**f** *long arrow*), and actively myelinating brain regions around term birth (pre- and postcentral gyri) (**c**, **f** *hollow arrows*) show gliosis interpreted as selective neuronal necrosis of brain structures with high O_2 demand

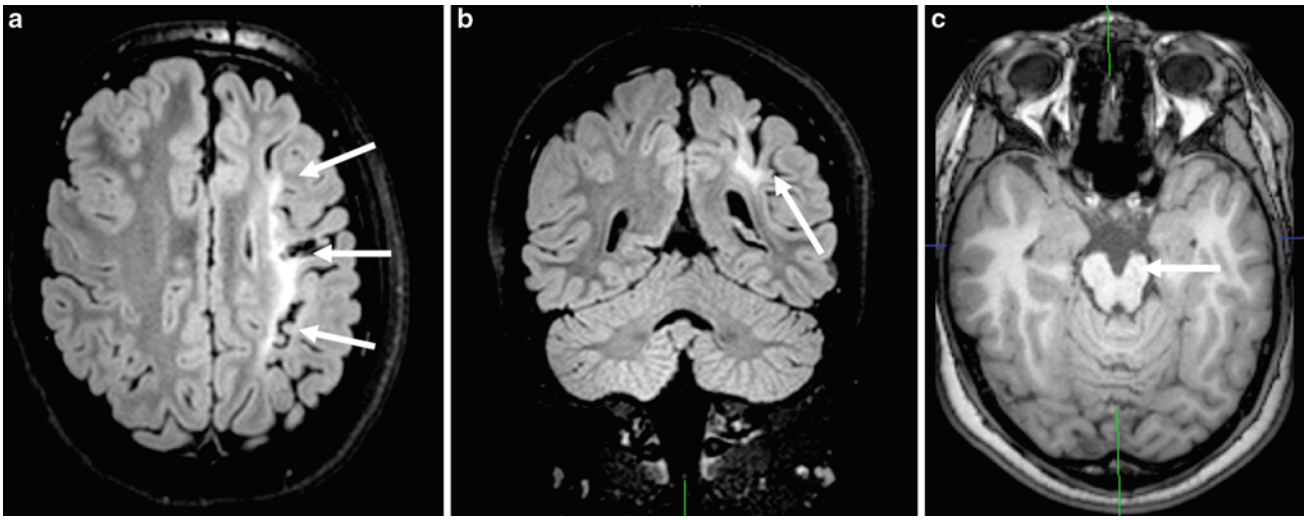

Fig. 8 A 12-year-old boy suffered from meconium aspiration during birth. He developed a right-sided spastic hemiparesis and started to have clonic seizures of the right arm at the age of 2. MRI shows left-sided hemiatrophy and gliotic changes in the "watershed areas," suggesting mild to moderate hypoxia during birth (**a**, **b** *arrows*). Note atrophy of the left cerebral peduncle (**c** *arrow*)

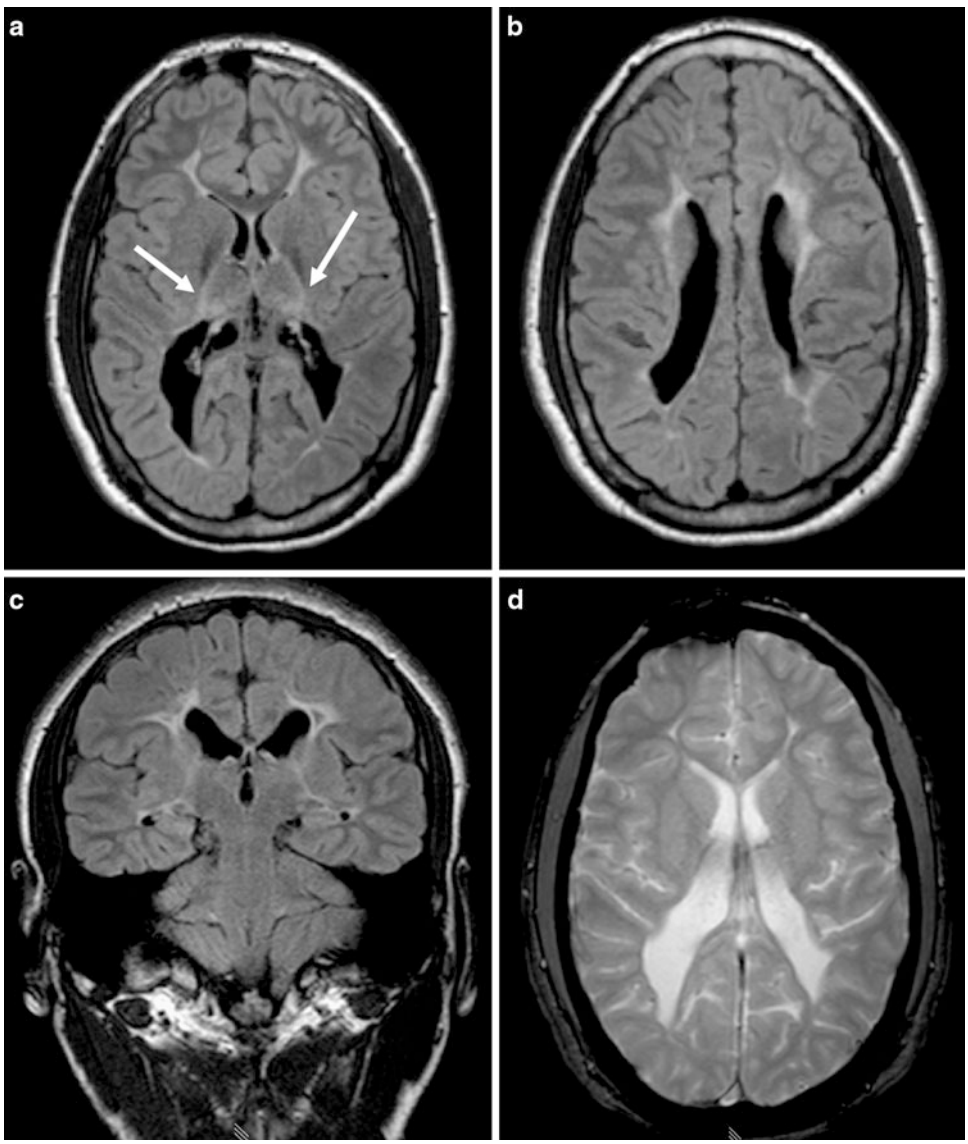

Fig. 9 Periventricular leukomalacia with periventricular white matter signal intensities (**b**, **c**), irregular ventricle dilatation, profound white matter volume loss, and thin corpus callosum. See also symmetrical basal ganglia hyperintensities centered in the thalami (**a** arrows). Axial T2-weighted gradient echo image (**d**) fails to show hemosiderin deposits. This 8-year-old boy was born at the 37th gestational week and underwent MRI after two complex focal seizures

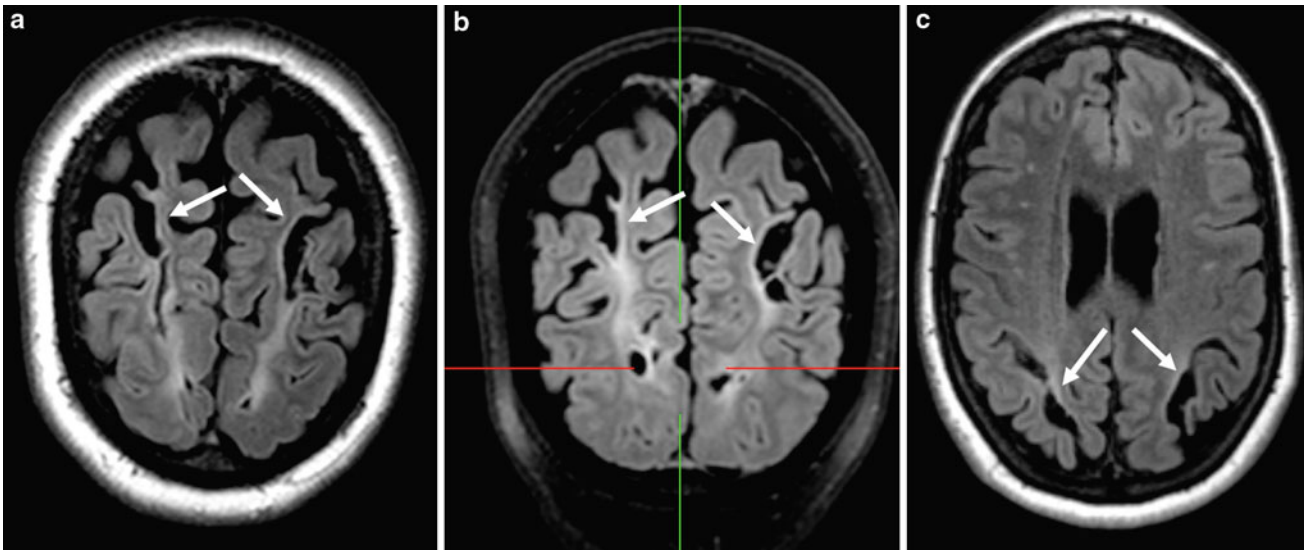

Fig. 10 Ulegyria in a 47-year-old woman with "complicated birth" and complex focal seizures since the age of 18. Coronal (**a**, **b**) and axial FLAIR (**c**) images show widened sulci around atrophic and hyperintense cortex (*arrows*). A biparietal location is typical, and the cortex in the depth of the intraparietal sulci is often more heavily affected than on the crown of the gyri

impairment. Twenty-five to 50 % of patients with periventricular leukomalacia have epilepsy with multiple, often multifocal seizure types. Among those, complex focal and seizures are most common (Gurses et al. 1999; Humphreys et al. 2007). There is a correlation between the grade of periventricular leukomalacia on MRI, the presence of other radiologic abnormalities, the risk of epilepsy, and the type of epilepsy syndrome. For example, periventricular leukomalacia is found in 5 % of patients with a West syndrome.

Patients with ulegyria typically have some degree of spastic teteraparesis, have intellectual impairment, and may have seizures.

Imaging. Periventricular leukomalacia is characterized by white matter atrophy with deeply indented sulci, enlarged and irregularly configured trigones of the lateral ventricles, and periventricular, typically peritrigonal, white matter lesions. The body and splenium of the corpus callosum are thin (Fig. 9).

In subcortical leukomalacia, white matter lesions are located predominantly in the subcortical white matter.

Ulegyria is characterized by gyral scarring affecting the gyri in the depth of the sulci more heavily than on their crowns. Scars are typically bilateral and symmetric and have a predilection for the parietal and occipital regions. FLAIR sequences are best suited to show gyral atrophy and increased signal intensity as well as sulcus widening (Figs. 6, 7, 8, 9, 10).

2 Adult Stroke

Epidemiology. In the adult population (older than 35 years), stroke is the most common cause of epilepsy. More than 50 % of newly diagnosed epilepsy cases in elderly persons are related to cerebrovascular diseases (Hauser et al. 1993; Loiseau et al. 1990). Around 11 % of stroke patients will have subsequent seizures within 5 years, and about one third of this group will develop recurrent seizures (Burn et al. 1997; Bladin et al. 2000).

Pathogenesis. The exact mechanisms are poorly understood. An increase in intracellular Na^+ and Ca^{2+} with a resultant lower level for depolarization, glutamate exicotoxicity, hypoxia, metabolic dysfunction, global hypoperfusion (Fig. 11), and hyperperfusion injury have been discussed as putative mechanisms (Myint et al. 2006).

Clinical presentation. Early-onset (within 2 weeks) and late-onset seizures are distinguished. Early-onset seizures typically occur during the first days as simple focal seizures without secondary generalization. Late-onset seizures (three times more often than early-onset seizures) have a peak incidence between 6 months and 2 years after a stroke and are more frequently complex focal seizures with or without secondary generalization (Shinton et al. 1988; Bladin et al. 2000; Arboix et al. 2003).

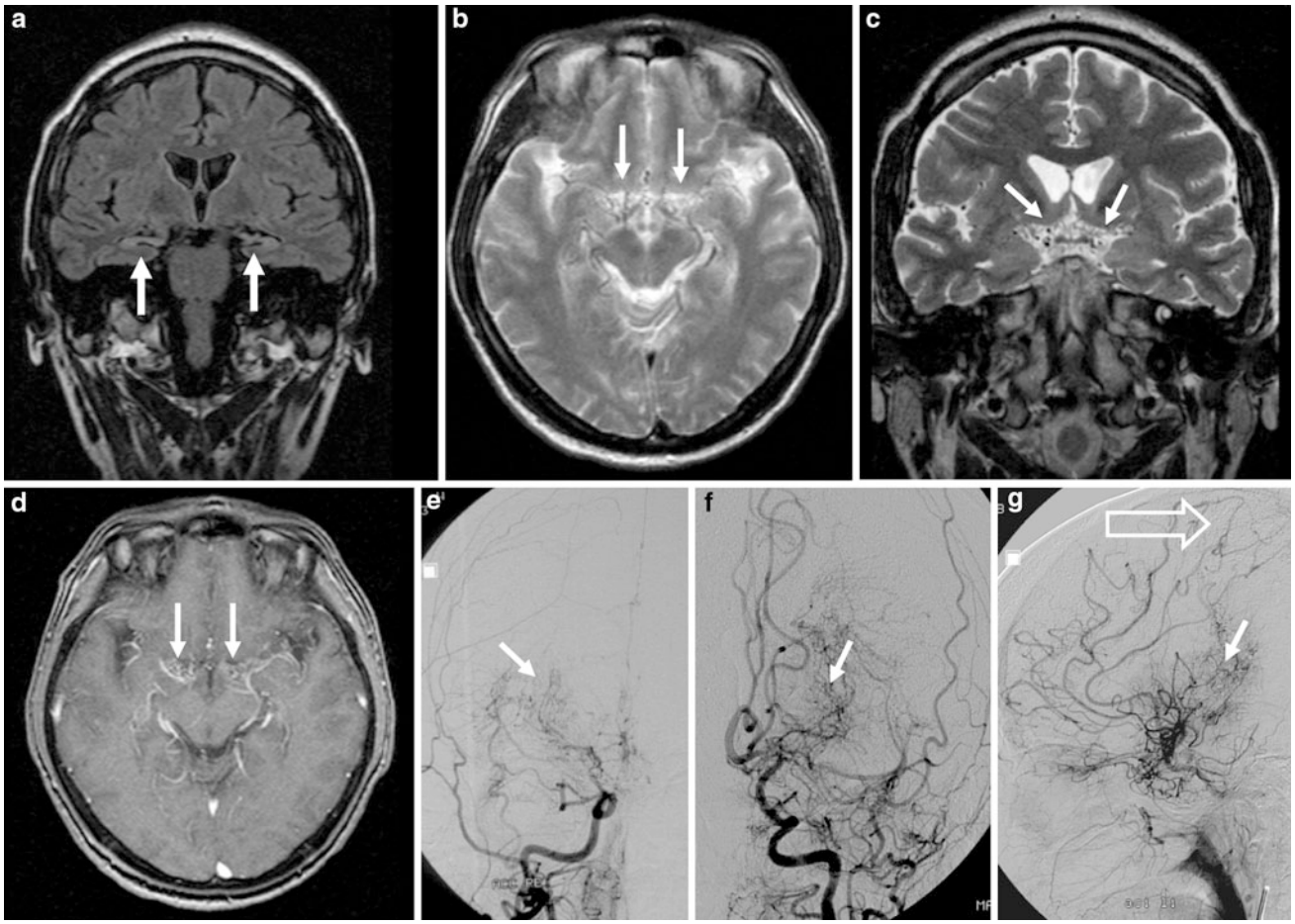

Fig. 11 Moyamoya disease in a 28-year-old man who presented with simple focal, complex focal, and secondarily generalized seizures, most likely of temporal origin. Coronal FLAIR sequence shows bilateral hippocampal sclerosis (**a** *arrows*). Axial (**b**) and coronal (**c**) T2-weighted fast spin echo and axial T1-weighted gradient echo sequences (**d**) showed tiny vessels in the basal cisterns (*arrows*). Catheter angiography showed bilateral supraclinoid ICA stenosis, an extensive moyamoya net in the basal cisterns (**e–g** *arrow*), and leptomeningeal collaterals between anterior cerebral artery branches (**g** *hollow arrow*)

Who will develop seizures is difficult to predict. Intracerebral hemorrhage (estimated incidence 10–15 %) and subarachnoid hemorrhage (8.5 %) carry a higher risk than ischemic stroke (6.5–8.5 %). Known risk factors associated with a higher risk of epileptic seizures in ischemic macroangiopathic stroke are thromboembolic stroke with cortical damage, infarct location in posterior insular and hippocampal regions, the involvement of multiple sites or a larger lesion, the severity of the initial neurological deficit, and the severity of persistent disability after stroke (Bladin et al. 2000).

Even microangiopathy is a risk factor for epileptic seizures: Nearly one fourth of patients with CT- or MR-proven cerebral microangiopathy suffer from epileptic seizures; the exact meachanism is unclear (Okroglic et al. 2013).

In subarachnoid hemorrhage (SAH), middle cerebral artery aneurysms and intraparenchymal hematomas are known risk factors (Myint et al. 2006). The incidence of poststroke epilepsy is likely highest in hemorrhagic stroke due to venous occlusion.

Following endovascular therapy, seizures within 24 h of stroke onset are rather predictive of a poor prognostic outcome (Jung et al. 2012).

Imaging. In patients with cerebral microangiopathy, white matter lesions in the frontal and parietooccipital regions rather than in the temporal lobe and basal ganglia lesions are correlated with epileptic seizures (Okroglic et al. 2013).

3 Moyamoya

Epidemiology. Moyamoya is a progressive vasculopathy characterized by stenoses or occlusions of the proximal portions of the major intracerebral arteries, which was initially described in Japan in 1962 (Subirana and Subirana

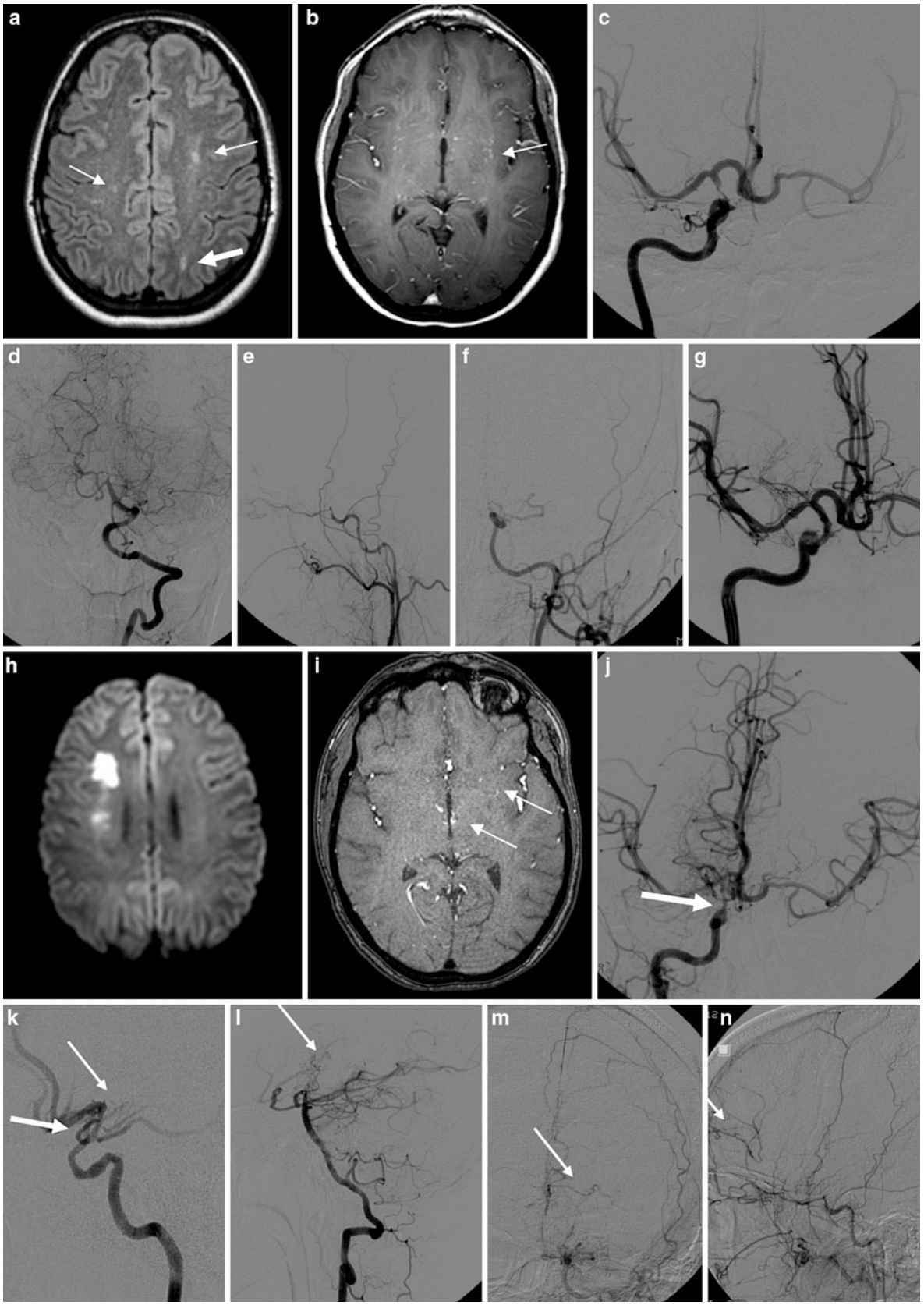
a
b
c
d
e
f
g
h
i
j
k
l
m
n

◀**Fig. 12** Moyamoya syndrome in a 31-year-old woman, who presented with bilateral complex focal seizures, which were likely due to cerebral hypoperfusion. Axial FLAIR image (**a**) showed small hemodynamic infarcts in both hemispheres (*arrows*), the parietal one (*thick arrow*) with reduced diffusion. Hypertrophied lenticulostiate arteries on the left side were identified in retrospect only (**b**). DSA showed right-sided supraclinoid ICA stenosis (**c**), left-sided supraclinoid ICA occlusion (**e**, **f**), and basilar artery tip stenosis (**d**). After angioplasty of the right-sided supraclinoid ICA stenosis with a balloon-mounted stent (Pharos 3 × 13 mm, Codman Neurovascular, Miami, FL), seizures stopped and the patient fully recovered (**g**). However, 1 year later, she presented with a transient left-sided hemiparesis and a right-sided infarct (**h**). Right-sided supraclinoid ICA showed stenosis again (**j**, **k** *thick arrows*). Perforating arteries were more prominent (**i**, **k**, **l** *arrows*), and transdural supply to left-sided frontal anterior cerebral artery branches had developed (**m**, **n** *arrows*). EC-IC-bypass was scheduled

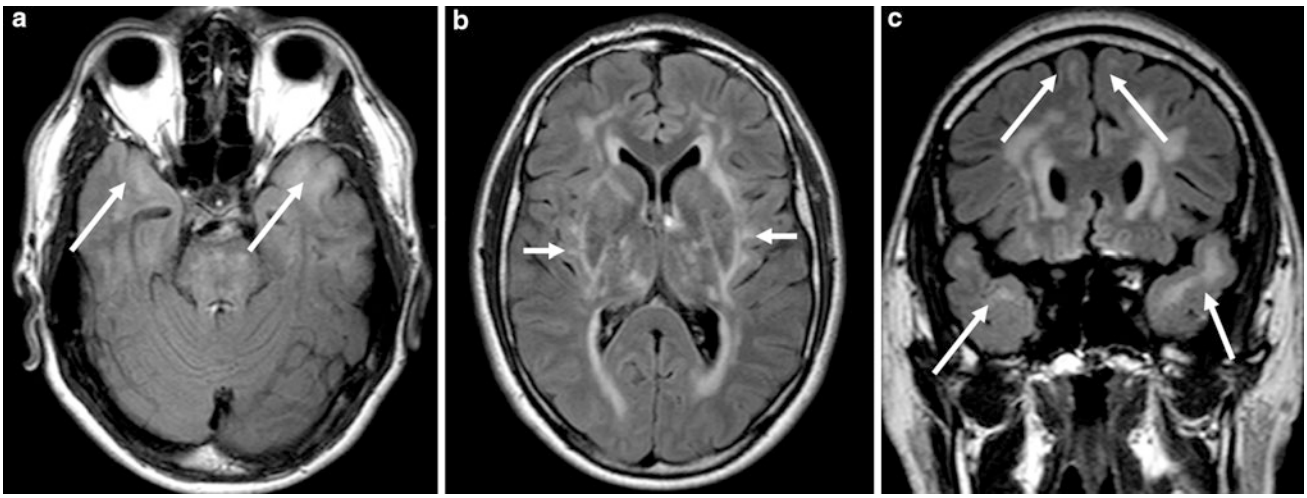

Fig. 13 CADASIL in a 41-year old man with recurrent transitory ischemic attacks presenting with a left-sided hemiparesis due to acute lacunar infarct in the right centrum semiovale (not shown). MRI shows extensive microangiopathy involving the basal ganglia (**b**) and pons (**a**). Confluent hyperintense lesions involving the U-fibers in the temporal poles and to a lesser extent in the frontal lobes (**a**, **c** *arrows*) and hyperintensity of the external capsules (**b** *arrows*) are characteristic for CADASIL

1962). Classic locations of stenoses and occlusions are the carotid T and the basilar bifurcation. Lenticulostriate and thalamoperforating arteries and—later on—external carotid and vertebral artery branches supplying the dura try to compensate for the progressive stenoses. This hypertrophied collateral network was originally described by the Japanese term "moyamoya," which translates to "a hazy cloud like a puff of cigarettes" (Kudo 1968; Suzuki and Takaku 1969).

Pathogenesis. The current concept is to distinguish an idiopathic form with regional differences in incidence (moyamoya disease) and an acquired form (moyamoya syndrome) (Kleinloog et al. 2012). Conditions such as radiation therapy, genetic factors, infections (Epstein–Barr virus, human immunodeficiency syndrome, tuberculous meningitis), and several heterogeneous diseases (sickle cell anemia, neurofibromatosis type 1, Down's syndrome, congenital heart defects, antiphospholipid syndrome, renal artery stenosis, thyroiditis, and others) have been found to be associated with moyamoya syndrome (Lutterman et al. 1998).

Clinical presentation. Seventy percent of patients (m:f = 1:1.8) present before the age of 20, typically before the age of 10, mostly with transitory ischemic attacks (TIAs), progressive neurological deficits, recurrent headaches, and/or complex focal or secondarily generalized seizures (15 % of cases).

Thirty percent of patients present in the fourth decade of life, often with subarachnoid or intraparenchymal hemorrhages.

Imaging. FLAIR sequences best visualize chronic infarcts, which typically have a hemodynamic (watershed) pattern and localized or diffuse atrophy. Diffusion-weighted sequences are needed to detect acute infarcts. T2-weighted sequences or contrast-enhanced T1-weighted sequences depict prominent flow void structures in the basal cisterns or within the brain parenchyma, representing hypertrophied collateral vessels or dilated capillaries. TOF-MRA, especially at 3 T, may be sufficient to show stenoses and occlusions and may show collateral vessels at the base of the brain (Fig. 12). However, in order to fully depict the collateral

vessels, catheter angiography is needed. Perfusion MRI or HMPAO-SPECT without and with acetacloamide challenge are used to discover hemodymamic compromise.

4 CADASIL

CADASIL is an acronym for cerebral autosomal dominant arteriopathy with subcortical infarcts and leukoencephalopathy.

Epidemiology. CADASIL is a rare, autosomal-dominant disease, initially described by Tournier-Lasserve et al. in 1993 (Tournier-Lasserve et al. 1993). If middle-aged family members suffer from migraine episodes, recurrent transient ischemic attacks, strokes, and show slowly progressive cognitive decline, CADASIL should be considered.

Pathogenesis. Nonamyloid, nonatherosclerotic angiopathy with osmophilic granular depositions within the tunica media of small (100–400 μm) arteries.

Autosomal-dominant inherited mutations of the *NOTCH3* gene on chromosome 19q12 (Tournier-Lasserve et al. 1993). Penetrance of 100 %, but intrafamiliar phenotypic variability (Dichgans et al. 1998).

Clinical presentation. Initial symptoms are typically migraine epidoses with aura starting around the age of 30 (40 % of cases). At this time, 20–30 % of patients show some psychiatric symptoms (mostly mood disturbances). In the fifth and sixth decades, recurrent transient ischemic attacks and ischemic strokes take place, and a slowly progressive subcortical dementia with additional stepwise deterioration develops. Many of the demented patients also suffer from gait disturbances, urinary incontinence, and pseuodbulbar palsy (Dichgans et al. 1998). Around 10 % of patients develop epileptic seizures, most often generalized tonic–clonic seizures, which typically occur following TIAs or ischemic infarcts. Rarely, seizures may precede ischemic events and cognitive impairment (Velioza et al. 2011).

Imaging. Lacunar infarcts in basal ganglia, thalamus, brain stem, and periventricular white matter. Confluent, non-space-occupying FLAIR and T2-hyperintense lesions of the subcortical white matter of the temporal poles and frontal lobes including the subcortical U-fibers are more characteristic than hyperintensities along the external capsules (Dichgans et al. 1998; Chabriat et al. 1998, 2009; Yousry et al. 1999) (Fig. 13). DTI shows a distinct increase in mean water diffusivity and a parallel loss of diffusion anisotropy in T2-hyperintense lesions (Chabriat et al. 1999).

References

Aguglia U, Gambardella A, Breedveld GJ et al (2004) Suggestive evidence for linkage to chromosome 13qter for autosomal dominant type 1 porencephaly. Neurology 62(9):1613–1615

Alamowitch S, Plaisier E, Favrole P et al (2009) Cerebrovascular disease related to *COL4A1* mutations in HANAC syndrome. Neurology 73(22):1873–1882

Arboix A, Comes E, Garcia-Eroles L et al (2003) Prognostic value of very early seizures for in-hospital mortality in atherothrombotic infarction. Eur Neurol 50:78–84

Barkovich AJ, Ali FA, Rowley HA, Bass N (1998) Imaging patterns of neonatal hypoglycemia. AJNR Am J Neuroradiol 19:523–528

Behunova J, Zavadilikova E, Bozoglu TM et al (2010) Familial microhydranencephaly, a family that does not map to 16p13.13-p12.2: relationship with hereditary fetal brain degeneration and fetal brain disruption sequence. Clin Dysmorphol 19(3):107–118

Bladin CF, Alexandrov AV, Bellavance A et al (2000) Seizures after stroke: a prospective multicenter study. Arch Neurol 57:1617–1622

Breedveld G, de Coo IF, Lequin MH et al (2006) Novel mutations in three families confirm a major role of COL4A1 in hereditary porencephaly. J Med Genet 43(6):490–495

Burn J, Dennis M, Bamford J et al (1997) Epileptic seizures after a first stroke: the Oxfordshire community stroke project. BMJ 315:1582–1587

Chabriat H, Levy C, Taillia H et al (1998) Patterns of MRI lesions in CADASIL. Neurology 51(2):452–457

Chabriat H, Pappata S, Poupon C et al (1999) Clinical severity in CADASIL related to ultrastructural damage in white matter: in vivo study with diffusion tensor MRI. Stroke 30(12):2637–2643

Chabriat H, Joutel A, Dichgans M et al (2009) Cadasil. Lancet Neurol 8(7):643–653 (Review)

Counsell SJ, Allsop JM, Harrison MC et al (2003) Diffusion-weighted imaging of the brain in preterm infants with focal and diffuse white matter abnormality. Pediatrics 112:1–7

Dichgans M, Mayer M, Uttner I et al (1998) The phenotypic spectrum of CADASIL: clinical findings in 102 cases. Ann Neurol 44:731–739

Friede R (1989) Developmental neuropathology. Springer-Verlag, Berlin

Gould DB, Phalan FC, Breedveld GJ et al (2005) Mutations in *Col4a1* cause perinatal cerebral hemorrhage and porencephaly. Science 308(5725):1167–1171

Gurses C, Gross DW, Andermann F et al (1999) Periventricular leukomalacia and epilepsy: incidence and seizure pattern. Neurology 52:341–345

Hauser WA, Annegers JF, Kurland LT (1993) Incidence of epilepsy and un-provoked seizures in Rochester, Minnesota: 1935–1984. Epilepsia 34:453–468

Ho SH, Kuzniecky RI, Gilliam F et al (1998) Congenital porencephaly: MR features and relationship to hippocampal sclerosis. AJNR Am J Neuroradiol 19:135–141

Humphreys P, Deonandan R, Whiting S et al (2007) Factors associated with epilepsy in children with periventricular leukomalacia. J Child Neurol 22:598–605

Jung S, Schindler K, Findling O et al (2012) Adverse effect of early epileptic seizures in patients receiving endovascular therapy for acute stroke. Stroke 43:1584–1590

Kavaslar GN, Onengüt S, Derman O et al (2000) The novel genetic disorder microhydranencephaly maps to chromosome 16p13.3-12.1. Am J Hum Genet 66(5):1705–1709

Kleinloog R, Regli L, Rinkel GJ, Klijn CJ (2012) Regional differences in incidence and patient characteristics of moyamoya disease: a systematic review. J Neurol Neurosurg Psychiatry 83(5):531–536

Kudo T (1968) Spontaneous occlusion of the circle of Willis. A disease apparently confined to Japanese. Neurology 18(5):485–496

Loiseau J, Loiseau P, Duche B et al (1990) A survey of epileptic disorders in southwest France: seizures in elderly patients. Ann Neurol 27:232–237

Lutterman J, Scott M, Nass R, Geva T (1998) Moyamoya syndrome associated with congenital heart disease. Pediatrics 101:57–60

Myers RE (1989) Cerebral ischemia in the developing primate fetus. Biomed Biochim Acta 48:S137–S142

Myint PK, Staufenberg EF, Sabanathan K (2006) Post-stroke seizure and post-stroke epilepsy. Postgrad Med J 82(971):568–572

Okroglic S, Widmann CN, Urbach H, Scheltens P, Heneka M (2013) Clinical symptoms, risk factors and cardiovascular medication in patients diagnosed with cerebral microangiopathy. PLoS ONE 8(2): e53455

Raju TN, Nelson KB, Ferriero D (2007) NICHD-NINDS perinatal stroke workshop participants. Ischemic perinatal stroke: summary of a workshop sponsored by the national institute of child health and human development and the national institute of neurological disorders and stroke. Pediatrics 120(3):609–616

Shinton RA, Gill JS, Melnick SC et al (1988) The frequency, characteristics and prognosis of epileptic seizures at the onset of stroke. J Neurol Neurosurg Psychiatry 51:273–276

Subirana A, Subirana M (1962) Malformations vasculaires du type de l'angiome arterial racemeux [in French]. Rev Neurol 107:545–550

Suzuki J, Takaku A (1969) Cerebrovascular "moyamoya" disease: disease showing abnormal net-like vessels in base of brain. Arch Neurol 20:288–299

Tournier-Lasserve F, Loutel A, Melki J et al (1993) Cerebral autosomal dominant arteriopathy with subcortical infarcts and leukoencephalopathy maps to chromosome 19q12. Nat Genet 3:256–259

Ulmer S, Moeller F, Brockmann MA et al (2005) Living a normal life with the nondominant hemisphere: magnetic resonance imaging findings and clinical outcome for a patient with left-hemispheric hydranencephaly. Pediatrics 116(1):242–245

van der Knaap MS, Smit LM, Barkhof F et al (2006) Neonatal porencephaly and adult stroke related to mutations in collagen IV A1. Ann Neurol 59(3):504–511

Velioza R, Mourand I, Serafini A et al (2011) Focal epilepsy as first symptom in CADASIL. Seizure 20:502–504

Williams D, Patel C, Fallet-Bianco C et al (2010) Fowler syndrome—a clinical, radiological, and pathological study of 14 cases. Am J Med Genet A 152A(1):153–160

Yousry TA, Seelos K, Mayer M et al (1999) Characteristic MR lesion pattern and correlation of T1 and T2 lesion volume with neurologic and neuropsychological findings in cerebral autosomal dominant arteriopathy with subcortical infarcts and leukoencephalopathy (CADASIL). AJNR Am J Neuroradiol 20:91–100

Infection and Inflammation

Horst Urbach

Contents

H. Urbach (✉)
Department of Neuroradiology,
University Hospital Freiburg, Germany
e-mail: horst.urbach@uniklinik-freiburg.de

Abstract

This chapter summarizes common CNS infections and inflammations associated with epilepsy.

Central nervous system (CNS) infections are common; patients may present with a broad clinical spectrum ranging from mild symptoms to severe neurological deficits. Around 25 % of patients with CNS infections have acute symptomatic seizures (Kim et al. 2008). The occurrence of seizures during the acute course of meningitis, encephalitis, and brain abscess is the main risk factor for the development of postinfectious epilepsy (Sellner and Trinka 2012).

CNS infections can be classified into congenital/neonatal and acquired infections. Congenital infections are the result of transplacental transmission; the consequences depend on the pathogenicity of the infectious agent and of the timing of the infection. Congenital brain infections are typically grouped together and called TORCH (toxoplasmosis, rubella, cytomegalovirus, herpes) or TORCHS infections if congenital syphilis is included. Another important congenital infection is congenital human immunodeficiency virus (HIV) infection (Osborn et al. 2010).

"Acquired" infections can be classified by etiology, for instance, bacterial, viral, granulomatous, parasitic, or fungal disease. The disease course can be very different: acute and fulminant as in herpes encephalitis or rather subacute or chronic, depending on whether or not the patient is immunocompromised or which therapy he or she receives.

H. Urbach (ed.), *MRI in Epilepsy*, Medical Radiology. Diagnostic Imaging,
DOI: 10.1007/174_2012_756, © Springer-Verlag Berlin Heidelberg 2013

Table 1 Common CNS infections associated with epilepsy

Congenital/neonatal infections
TORCH(S): Toxoplasma, Rubella, Cytomegalovirus, HSV2, (syphilis)
Human Immunodeficiency Virus (HIV) infection
"Acquired" infections
Viral infections:
Herpes simplex virus 1 encephalitis
Human herpesvirus 6 (HHV6) infection
Bacterial infections causing brain abscesses
Streptococcus, *Staphylococcus*, *Pseudomonas*, Enterobacteriaceae, *Bacteroides*, etc.
Specific conditions:
from otogenic infections: *Proteus*, *Enterobacter*, *Pseudomonas*, *Pneumococcus*, *Hemophilus* (Penido et al. 2005)
postsurgical or posttraumatic: *Staphylococcus*
immunocompromised patients: *Tuberculosis* and other mycobacteriaceae, *Klebsiella*, *Listeria*, *Nocardia*
newborns: *Citrobacter*, *Proteus*, *Pseudomonas*, *Serratia*
Parasitic infections
Toxoplasmosis (*Toxoplasma gondii*)
Neurocysticercosis (*Taenia solium*)
Echinococcosis (*Echinococcus granulosus*, *Echinococcus multilocularis/alveolaris*)

This chapter addresses common CNS infections typically associated with epilepsy (Table 1). In addition, neurosarcoidosis as an important noninfectious inflammation is described.

1 TORCH(S)

TORCH(*S*) is an acronym for toxoplasmosis, rubella, cytomegalovirus, herpes simplex virus type 2, (syphilis) infection.

1.1 Epidemiology

Toxoplasmosis is a relatively common congenital infection with an estimated incidence between 1:3000 and 1:5000 live births. Due to immunisation programs, rubella virus infection has become very rare in Western countries. CMV infection is the most common congenital viral infection and occurs in about 1 per 100 births (Neto et al. 2004). Congenital herpes simplex encephalitis has an incidence of 1:3000–20,000 live births (Pickering 2006).

1.2 Pathogenesis

Toxoplasmosis is a transplacentar infection. The infection risk is especially high (20–50 %) when the mother-to-be acquires *Toxoplasma* infection (mostly from contaminated meat) during pregnancy.

Rubella virus infection is a very rare transplacentar infection.

Cytomegalovirus (CMV) is also transmitted via the placenta; the earlier the transmission occurs, the poorer the outcome (Trincado and Rawlinson 2001). The vast majority of infected neonates are asymptomatic, but about 10 % present with low birthweight, hepatitis, pneumonitis, and/or neurologic and hematologic abnormalities.

Congenital herpes simplex virus encephalitis is usually caused by HSV-2. In true congenital infections, the virus has crossed the placenta and is found in amniotic fluid (5–10 % of cases). In 90–95 % of cases, HSV-2 encephalitis is a neonatal infection resulting from contact with infected lesions or secretions during or shortly after birth (Baskin and Hedlund 2007).

1.3 Clinical Presentation

Most children are severely disabled with frequent seizures of many types.

1.4 Imaging

The imaging hallmarks of TORCH infections are periventricular calcifications. Other findings are microcephaly, ventriculomegaly, delayed myelination, hippocampal malrotation, and cortical dysplasias, among others (Fig. 1).

2 Herpes Simplex Encephalitis

2.1 Epidemiology

Herpes simplex virus type 1 (HSV-1) encephalitis is the most common identified cause of sporadic viral encephalitis.

2.2 Pathogenesis

HSV-1 is a ubiquitous virus that rarely causes neurologic complications. Children usually become infected with the virus early in life from direct contact with the secretions or lesions of infected individuals. The primary infection is often asymptomatic or mild and self-limiting (e.g., gingivostomatitis). After primary infection, the virus persists in a latent form within the trigeminal sensory ganglion. HSV-1 encephalitis is caused by reactivation of the virus, which may occur spontaneously or by local trauma, immunosuppression, etc.

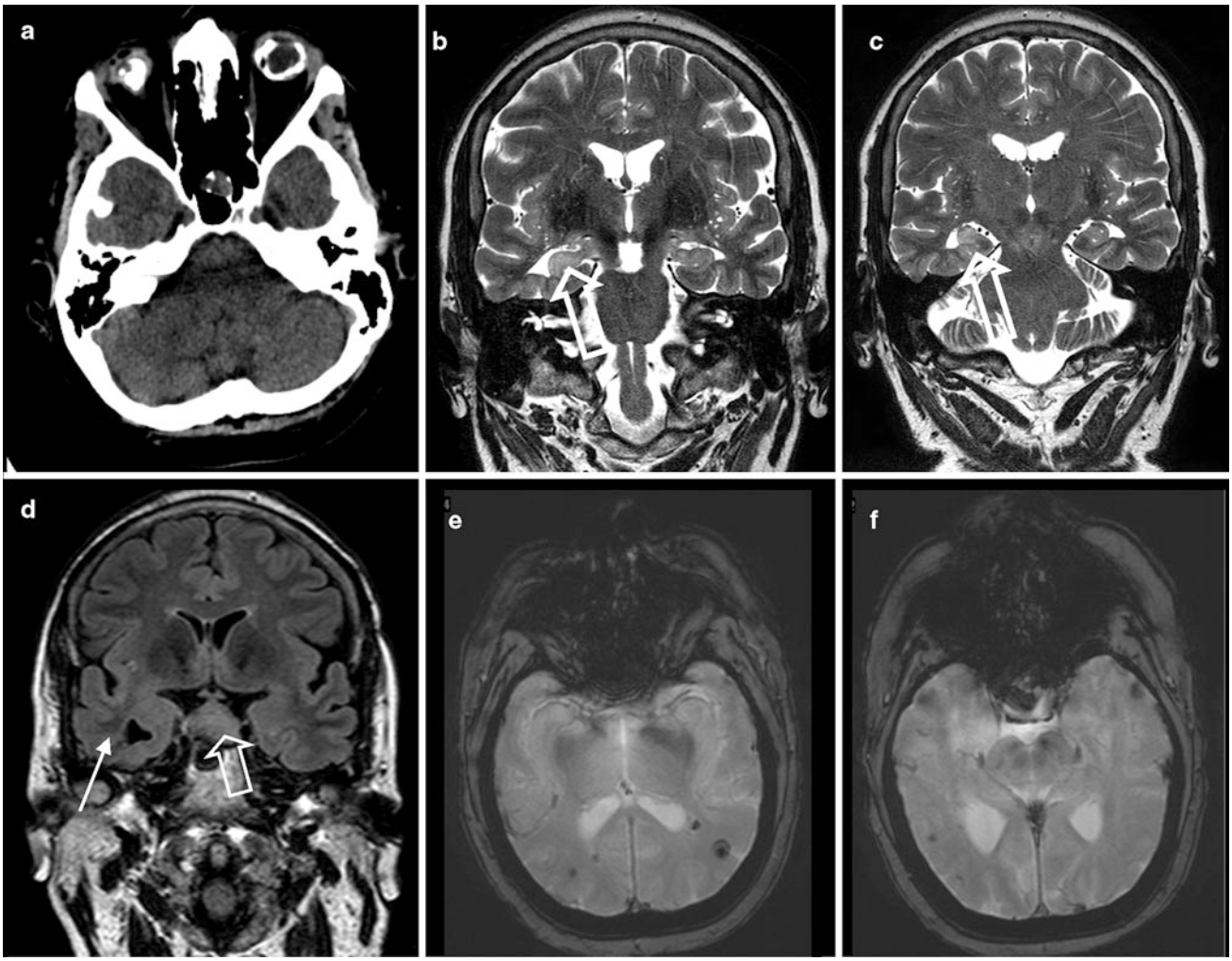

Fig. 1 MRI of a 54-year-old woman who has suffered from drug-resistant temporal lobe epilepsy since early childhood shows *right*-sided hippocampal sclerosis (**b**, **c**: *hollow arrow*) and a rather hypoplastic temporal pole (**d**: *arrow*). Multiple parenchymal calcifications on axial T2-weighted gradient echo images represent calcified abscesses from connatal toxoplasma infection (**e**, **f**). Note distinct ocular globe calcifications (**a**) and hypophyseal macroadenoma (**d**: *hollow arrow*) as additional findings

2.3 Clinical Presentation

HSV-1 patients present with acute monophasic illness with seizures, fever, and progressive neurologic deficits.

Mortality and morbidity are as high as 50–70 % without treatment. The importance of early diagnosis and the initiation of treatment with the antiviral drug acyclovir before establishing the diagnosis are stressed.

Diagnosis is based on HSV detection in CSF by polymerase chain reaction (PCR) (Rowley et al. 1990). However, since a negative PCR can occur in the first 48–72 h and after 10 days of illness, an abnormal MRI is an important clue to the diagnosis.

2.4 Imaging

MRI shows abnormalities in a typical limbic system distribution in more than 90 % of patients. Edema with restricted diffusion on DWI, hemorrhages, and gyriform contrast enhancement occur bilaterally, but somewhat asymmetrically in the mesial temporal lobes, the basal frontal lobes, and the insular cortices. The involvement of the cingulate gyri is a rather late finding and may be associated with the involvement of the efferent connections of the hippocampus (Tien et al. 1993) (Figs. 2–4).

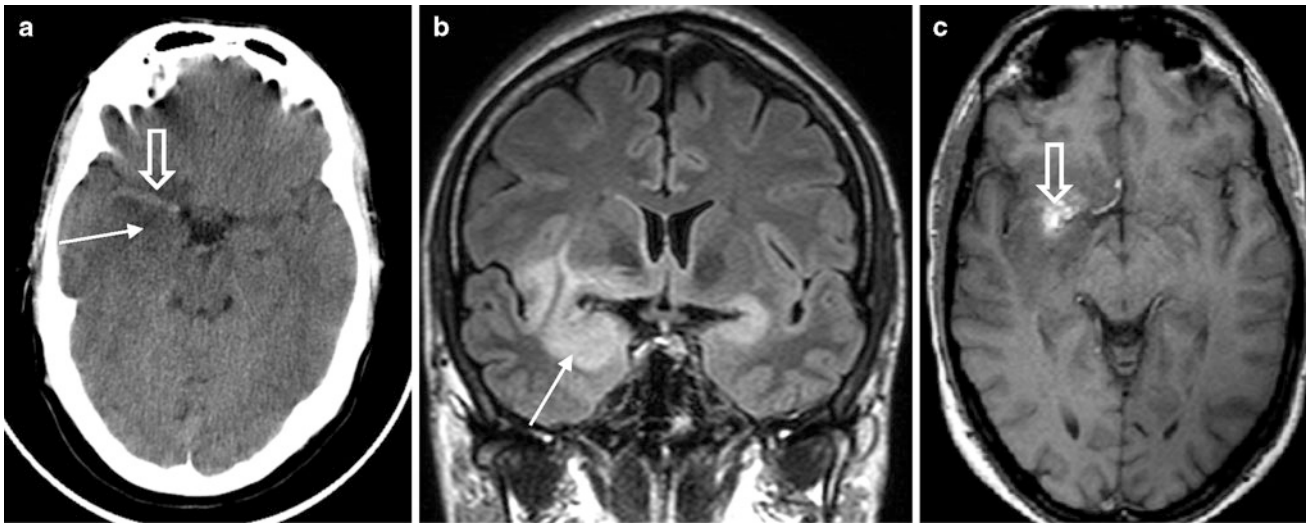

Fig. 2 Herpes simplex 1 encephalitis in a 40-year-old man who initially complained of olfactory hallucinations and déjà vu phenomena involving memories of the odor of a youth hostel where he had stayed decades ago. Within 12 h he became fully amnesic and psychotic. CT (**a**) and MRI (**b**, **c**) show a swollen *right*-sided uncus (**a**, **b**: *arrow*), insula, basal frontal lobe and opposite hemisphere involvement, and a hemorrhagic component (**a**, **c**: *hollow arrow*)

3 Human Herpes Virus 6 Encephalitis

3.1 Epidemiology and Pathogenesis

HHV-6 types A and B are ubiqitous viruses; almost all children are infected before the age of 2 years. The virus enters the body through the salivary glands, where it replicates and sheds further particles via infectious saliva. It usually remains latent throughout the body, including the salivary glands, white blood cells, and the brain. Acute HHV-6B infection is associated with febrile seizures in infants. More commonly, however, HHV-6 encephalitis is due to reactivation of the HHV-6 virus in immunosuppressed patients (Baskin and Heglund 2007).

3.2 Clinical Presentation

Acute HHV-6 infection causes a febrile exanthema known as roseola infantum in 10 % of children. Thirteen percent of children have seizures (Hall et al. 1994), and almost 30 % of first-time febrile seizures in infants are due to acute HHV-6 infection (Baskin and Heglund 2007).

Reactivation of HHV-6 in immunocompromized patients is seen, for instance, in 50 % of bone marrow transplant patients, usually 2–4 weeks after transplantation (Singh and Paterson 2000). However, the CNS is affected in a minority of patients only. Patients with reactivation of HHV-6 encephalitis present with mental status changes, fever, seizures, and headache, and diagnosis is confirmed by the proof of HHV-6-DNA in the CSF by PCR (Singh and Paterson 2000; Baskin and Heglund 2007).

3.3 Imaging

Imaging studies reveal bilateral > unilateral increased signal intensity and swelling of the amaygdala, hippocampus, and parahippocampal gyrus, reflecting limbic encephalitis (Wainwright et al. 2001). In young children, necrotizing encephalitis with bilateral striatal necrosis has been described (Murakami et al. 2005).

4 Tuberculosis

4.1 Epidemiology

Tuberculosis is a CNS infection with a high morbidity and a significant mortality. The incidence and prevalence are low in the Western but high in developing countries (an estimated annual incidence in developing countries of 139/100,000 persons and an estimated prevalence of 206/100,000 persons, respectively) (WHO Report 2009). About 10 % of tuberculosis patients develop CNS disease, particularly immunocompromised patients, including those with HIV infections (Dye et al. 1999; Bishburg et al. 1986).

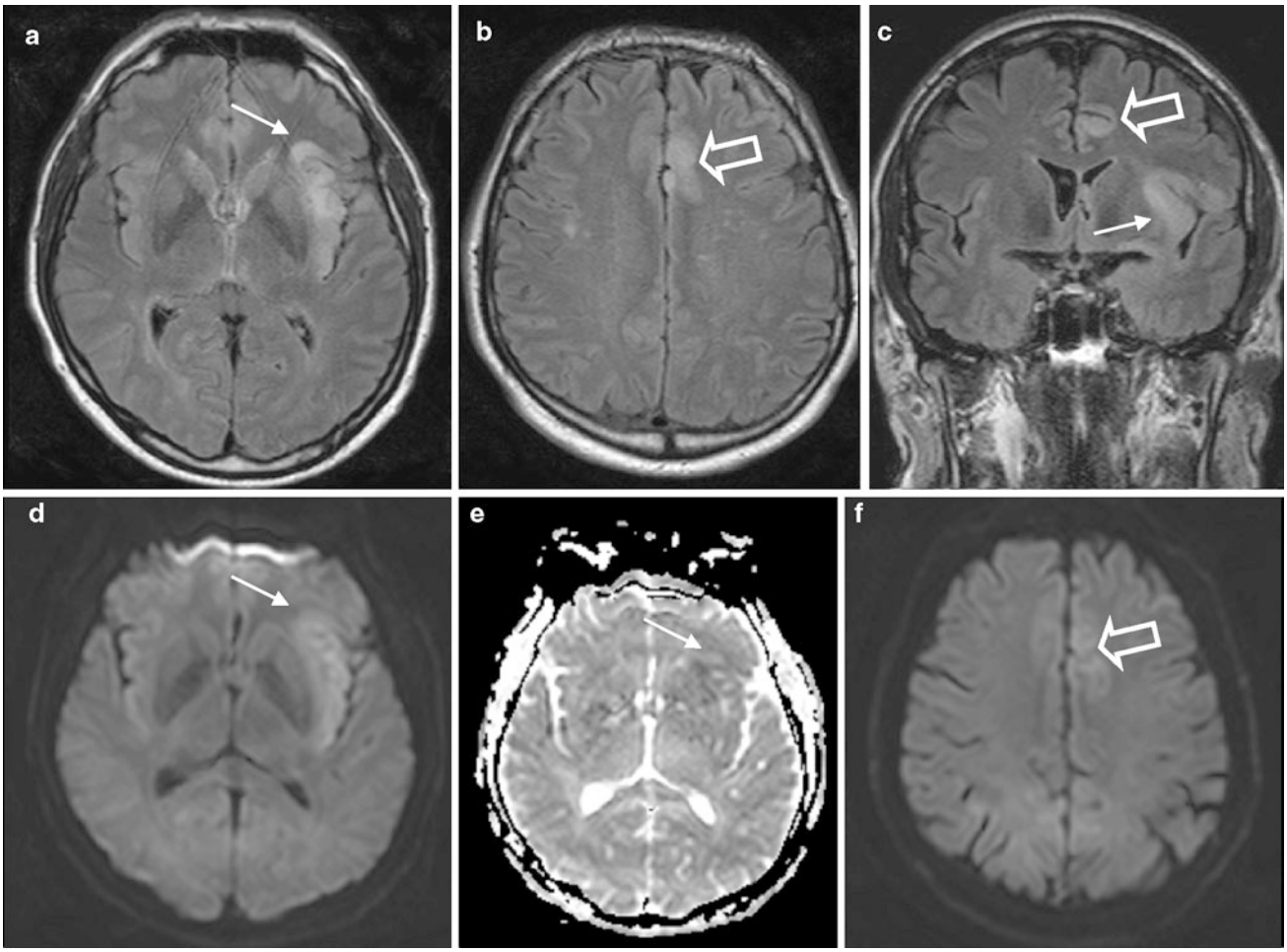

Fig. 3 Herpes simplex 1 encephalitis in a 59-year-old man who presented with aphasia, confusion, and fever. MRI shows edematous swelling with restricted diffusion of the *left* insula (**a**, **c**, **d**, **e**: *arrow*) and the *left* cingulate gyrus (**b**, **c**, **f**: *hollow arrow*). Limbic system involvement with edematous swelling and hemorrhagic foci in an asymmetric, typically bilateral distribution are the clue to the diagnosis of herpes simplex encephalitis

4.2 Pathogenesis

The CNS is typically infected via the hematogenous spread of bacteria belonging to the mycobacterium tuberculosis complex, mostly from pulmonary tuberculosis. The tubercles usually rupture into the subarachnoid space, and miliary tubercles forming around the outer sheaths of the blood vessel cause a granuolomatous meningitis. Either the basal exsudate or concomitant arteriitis of perforating arteries may cause arterial infarcts, which are most often located in the basal ganglia (Dastur et al. 1995). When the basal exsudate becomes caseous and dries and a thick capsule forms around it, a tuberculoma has developed (AlSemari et al. 2012).

4.3 Clinical Presentation

Seizures occur in about 50 % of children and in 5 % of adults; recurrent seizures are common (Udani et al. 1971; Narayanan and Murthy 2007a, b). Rarely, convulsive and nonconvulsive status epilepticus occurs (Murthy et al. 2007; Narayanan and Murthy 2007a, b; Arman et al. 2011).

4.4 Imaging

Tuberculous meningitis: Basal meningitis with hyperintense CSF on FLAIR and contrast enhancement on T1-weighted contrast enhanced images.

Tuberculomas: Round or oval contrast-enhancing lesions with a central necrosis, which may appear as target sign. Multiple lesions are more common than solitary lesions. Tuberculomas developing from tuberculous meningitis are typically contiguous with the subarachnoid space. Tuberculomas developing from a hematogenous spread are located at the gray/white matter junction and have a supratentorial (parietal) preference location. A dural tuberculoma location is not unusual.

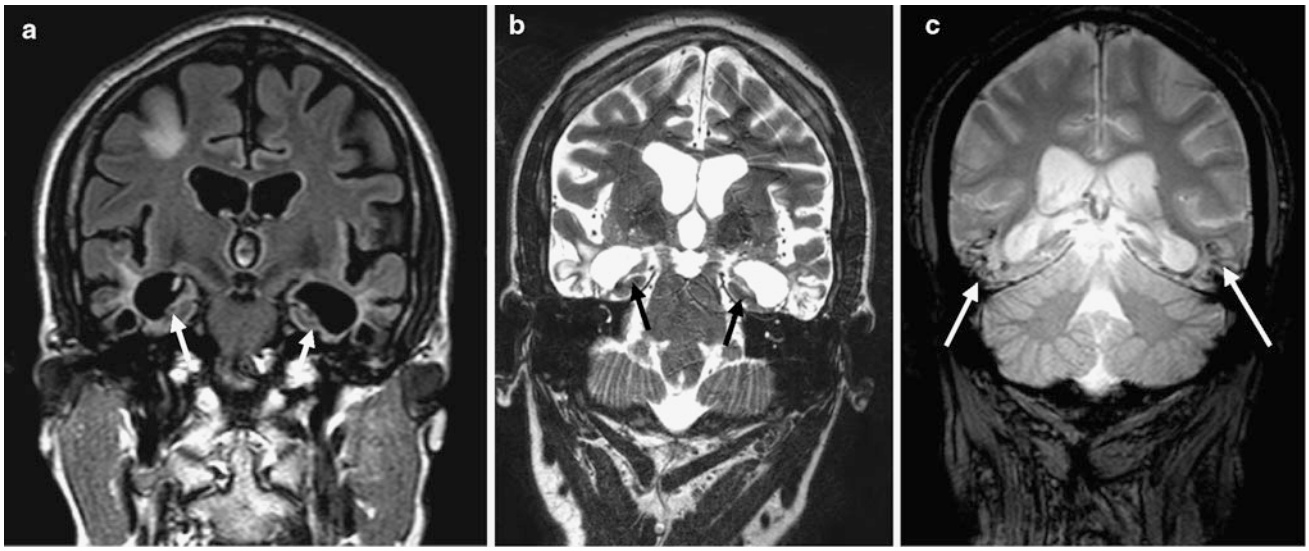

Fig. 4 A 31-year-old man presented with daily complex focal temporal lobe seizures. He became ill with herpes simplex encephalitis 5 years earlier, leaving him in an amnesic and dependent state. MRI shows extensive bilateral tissue destruction mainly of the basal and mesial temporal lobes (**a**, **b**: *arrows*). Hemosiderin deposits on T2-weighted images indicate that a hemorrhagic, necrotizing encephalitis had occurred (**c**: *arrows*)

Hydrocephalus and arterial infarcts are complications due to meningitis and arteriitis.

A clue to the diagnosis is the proof of extracerebral, most often reactivated pulmonary tuberculosis (Fig. 5).

5 Toxoplasmosis

5.1 Epidemiology

Toxoplasmosis is the most common human parasite worldwide and is the most common opportunistic CNS infection in AIDS patients. Infection via the placenta is possible; a first infection during pregnancy has a 50 % infection risk for the child [see Sect. 1: TORCH(S)].

5.2 Pathogenesis

Oocytes are ingested with infected meat, raw milk, or cat feces; they evolve over various stages in the host intenstine and enter different organs (brain, heart, peripheral muscles) after hematogenous spreading.

5.3 Clinical Presentation

Patients present with subacute headaches, fever, (focal) seizures, and focal neurological signs.

5.4 Imaging

Imaging studies typically reveal 1–3-cm-large lesions with a T2-hypointense wall and a T2-hyperintense center with increased ADC values. Multifocality is seen in 70 % of cases (Chang et al. 1995). Lesions are surrounded by perifocal edema and lesions, and edema may be confined to a vascular territory.

The lesion wall typically strongly enhances, and enhancement may also occur in the necrotic center, which is designated as a target sign. A target sign consisting of an innermost enhancing core, which is more often eccentric than central, an intermediate hypointense zone, and a peripheral enhancing rim is considered highly suggestive of toxoplasmosis but may also occur in other CNS infections, such as tuberculosis (Chang et al. 1995; Bargalló et al. 1996) (Fig. 6).

6 Cysticercosis

6.1 Epidemiology

Cysticercosis is the most common parasitic CNS infection, a leading cause of acquired epilepsy worldwide, and the main reason for a higher prevalence of epilepsy in developing countries (Del Brutto 2012).

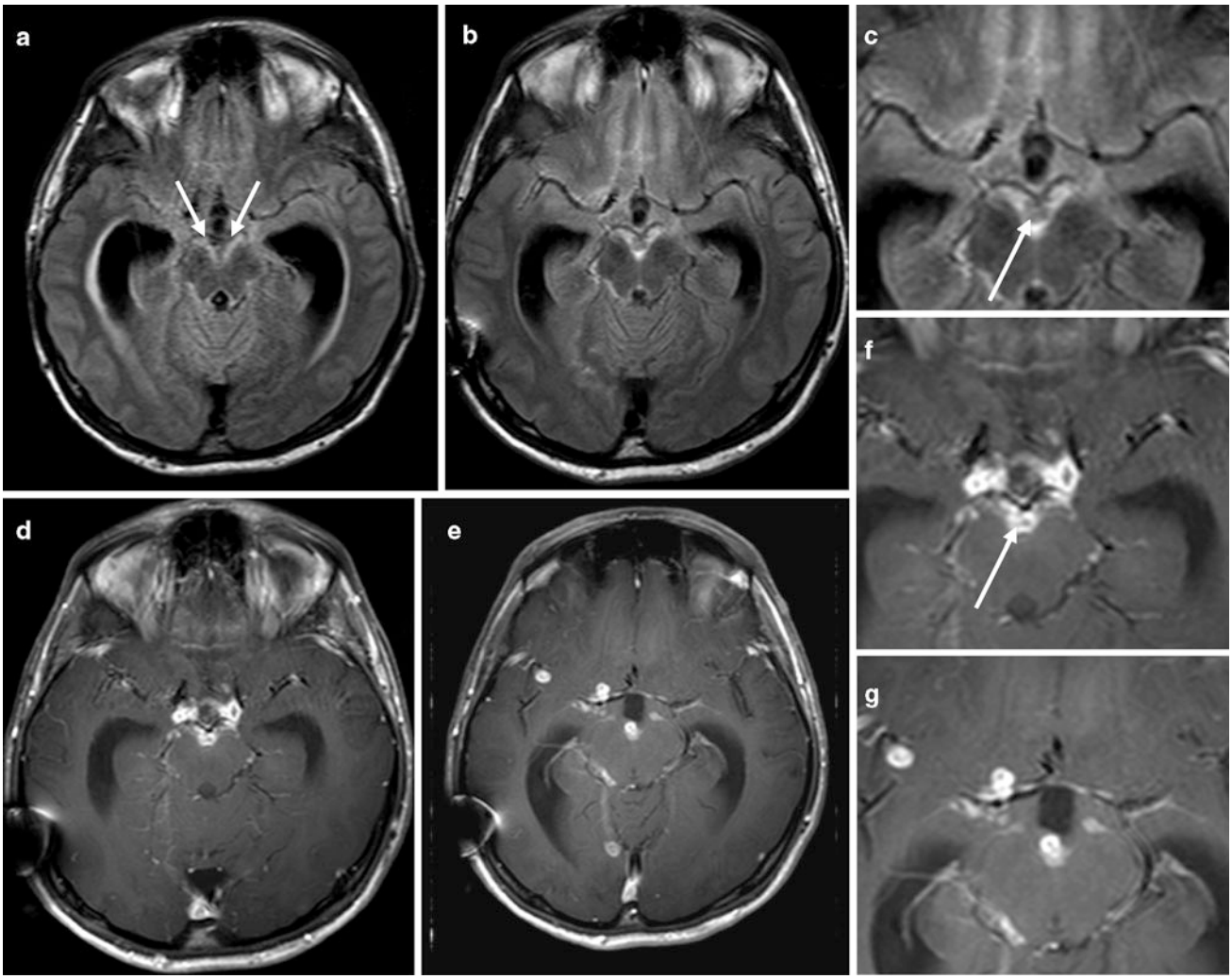

Fig. 5 Tuberculosis in a 21-year-old man who presented with fever, headache, and meningism. The initial MRI showed a basal meningitis with FLAIR-hyperintense CSF (**a**: *arrows*) and hydrocephalus. The 6-month follow-up MRI showed multiple tuberculomas that had developed in the basal cisterns despite anti-tuberculotic therapy (**b**–**g**). One predilection site is the interpeduncular cistern (**c**, **f**: *arrows*)

6.2 Pathogenesis

Neurocysticercosis occurs when humans become intermediate hosts of *Taenia solium* by ingesting its eggs from contaminated food or, most often, directly from a *Taenia* tapeworm carrier via the fecal-to-oral route. Infective embryos (hatched from the ingested eggs) reach systemic circulation after actively crossing the intestinal mucosa and lodge in capillaries (mostly in muscle and brain tissue), where they develop into "adult" cysticerci consisting of two main parts, the vesicular wall and the scolex (the knob-like cephalic end of the tapeworm). The first cysticercus stage is the vesicular stage, in which the parasites are protected from the host's immune response by the blood–brain barrier. As a result of the host's immunological attack or of drug treatment, cysticerci enter in a process of degeneration that ends with their transformation into calcifications. The first stage of involution is the colloidal stage, in which the vesicular fluid becomes turbid, and the scolex shows signs of hyaline degeneration. Thereafter, the wall of the cyst thickens and the scolex is transformed into mineralized granules; this stage, in which the cysticercus is no longer viable, is called the granular stage. Finally, the parasite remnants appear as a mineralized nodule (calcified stage) (Del Brutto 2012).

6.3 Clinical Presentation

The clinical picture ranges from asymptomatic infection to severe life-threatening disease. The most common presentation (70 % of cases), however, is focal seizures (with or

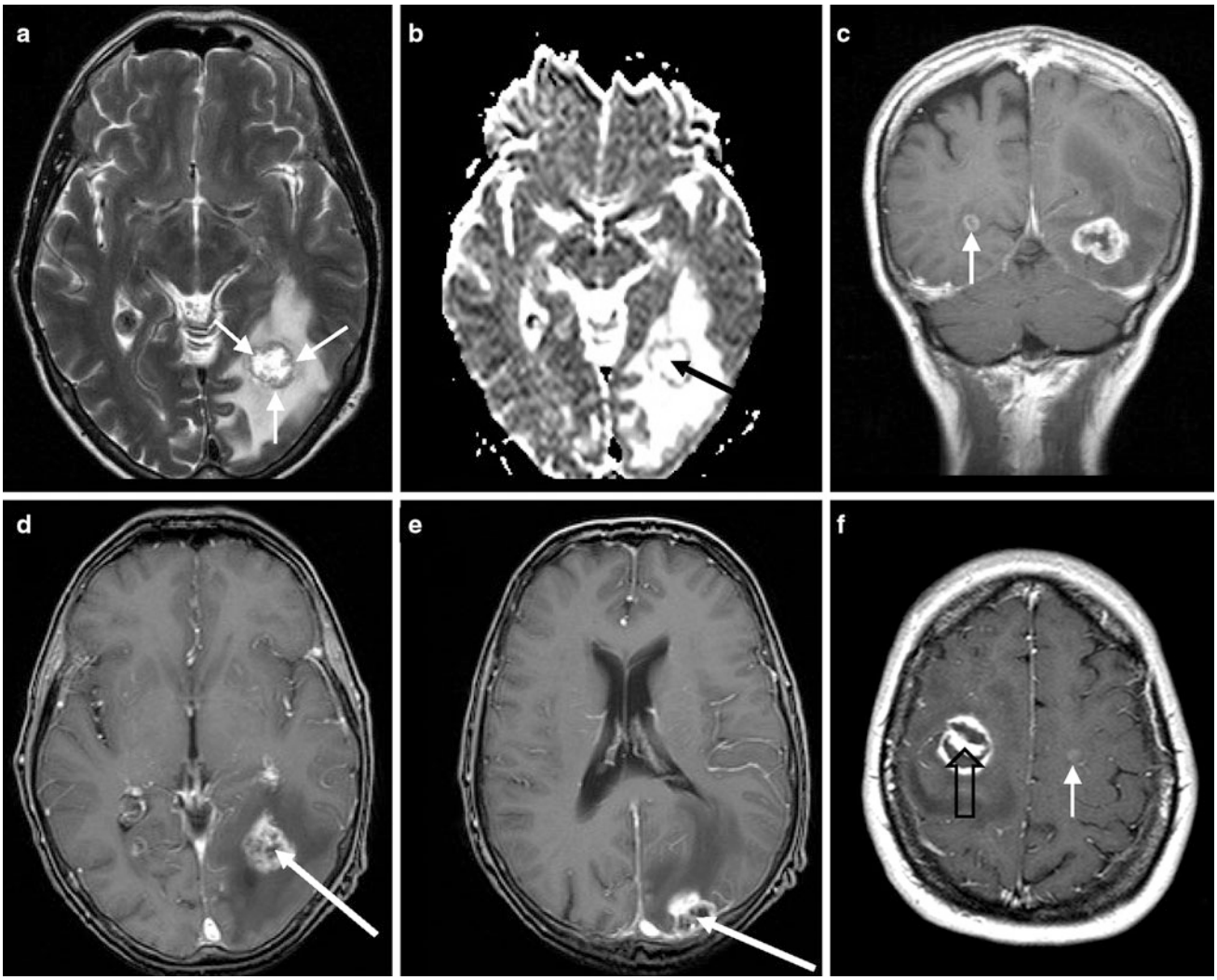

Fig. 6 A 54-year-old patient with AIDS presented with a homonymous hemianopia to the *right* side of 8 h'duration. T2-weighted MRI (**a**) shows a 15-mm lesion in the *left* occipital lobe with a hyperintense center, a hypointense wall (**a**: *arrows*), and perifocal edema. DWI (**b**: ADC *map*) shows increased diffusivity within the necrotic center (**b**: *arrow*). T1-weighted contrast-enhanced images (**c**–**e**) show multifocal lesions. Smaller lesions show ring (**c**: *arrow*) or homogeneous (**f**: *arrow*) enhancement; larger lesions show enhancement within the necrotic center also (**d**, **e**: *arrow*). Another example shows a toxoplasma abscess in an AIDS patient with a so-called target sign defined as a central enhancement surrounded by a ring of enhancement (**f**: *hollow arrow*)

without secondary generalisation) (Del Brutto et al. 1992). Other presentations include headache, raised intracranial pressure, stroke, and neuropsychiatric disturbances.

6.4 Imaging

Imaging findings depend on several factors, including the stage of the cysticerci at presentation, the number and location, and associated complications such as vascular involvement, inflammatory response, and, in ventricular forms, degree of obstruction.

With respect to the stage, vesicular cysticerci elicit little inflammatory reaction in the surrounding tissue. In contrast, colloidal cysticerci are often surrounded by a collagen capsule and by a mononuclear inflammatory reaction with astrocytic gliosis and edema in the surrounding brain parenchyma. When the cysticerci enter into the granular and calcified stages, the edema subsides, but the astrocytic changes in the vicinity of the lesions may become more intense (Del Brutto 2012).

With respect to location, neurocysticercosis has traditionally been classified into subarachnoid-cisternal, parenchymal, intraventricular, and spinal forms. The subarachnoid-cisternal location is the most common. "Parenchymal" cysticerci are located at the gray/white matter junction; it has been argued that the parenchymal location represents subarachnoid cysticercosis located in deep sulci or in perforating branches of perivascular spaces (Villagran-Uribe and Olvera-Rabiela 1988).

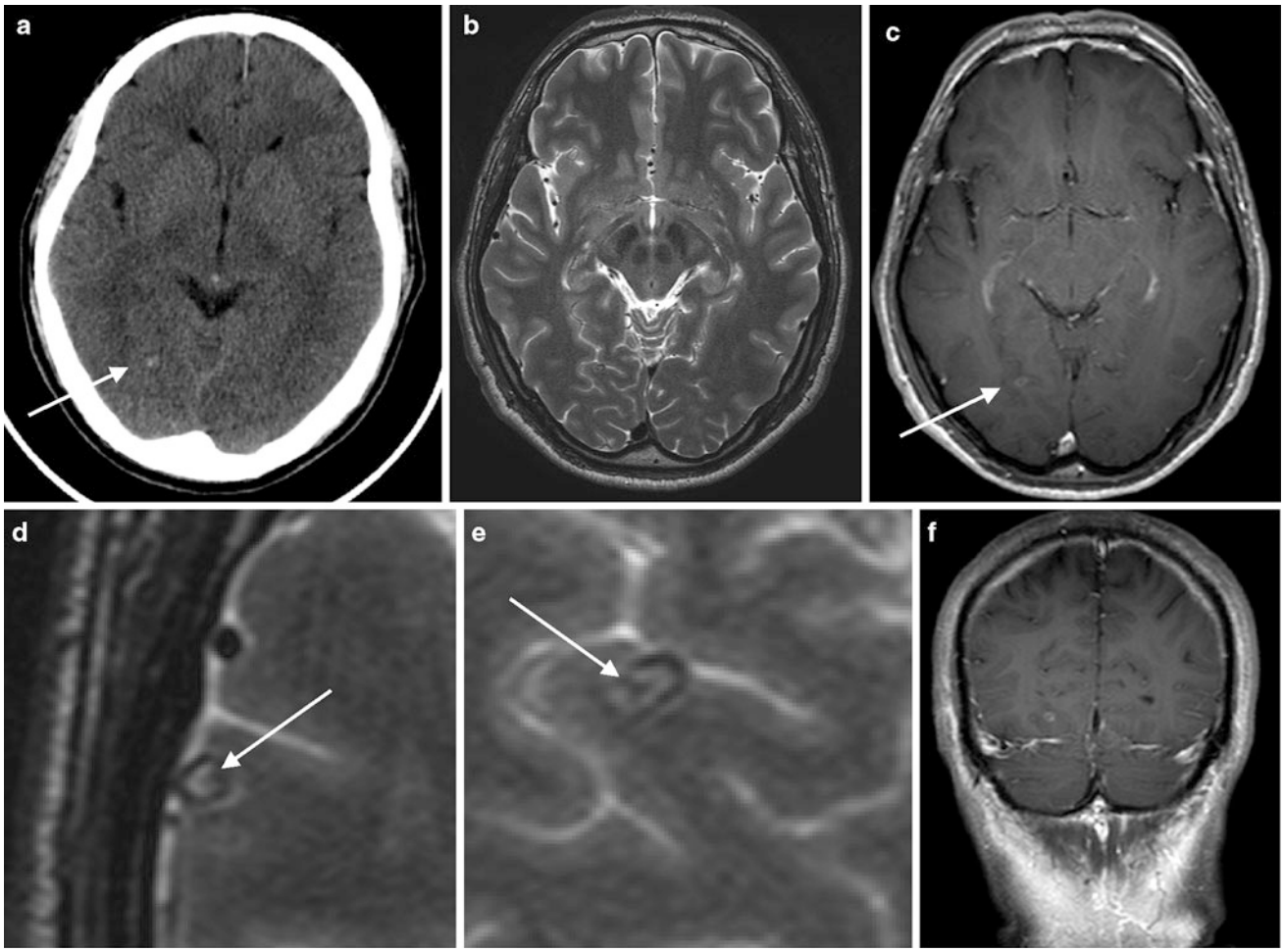

Fig. 7 Neurocysticercosis in a 54-year-old man suffering for many years from complex focal and secondarily generalized seizures. CT (**a**) and MRI (**b**–**f**) show multiple tiny lesions. Lesions are calcified (**a**: *arrow*), are contiguous with the subarachnoid space, are ring-enhancing (**c**: *arrow*), and have a T2-hypointense rim and an excentric structure within the cystic cavity, suggesting a scolex (**d**, **e**: *arrow*)

An important clue to diagnosis is the detection of an eccentric nodule within the cystic cavity. It represents the scolex and is best visible on FLAIR sequences, where the scolex is hyperintense and the cystic cavity has no signal (see Fig. 7).

7 Echinococcosis (Hydatid Disease)

7.1 Epidemiology

Echinococcosis is an endemic disease in many parts of the world, particularly in the Middle East, Australia, New Zealand, South America, and Central and South Europe. In humans, two main types exist: *Echinococcos granulosus*, with dog as the main host, and *Echinococcus multilocularis/alveolaris*, with fox as the main host (Bükte et al. 2004).

7.2 Pathogenesis

Adult tapeworms live in the intestine of their hosts and release their eggs through feces. After oral ingestion, larvae form in the human intestine, penetrate the mucosa, and enter different organs (liver 50–70 %, lung 15–30 %, brain 2–6 %, spleen, kidneys) via the venous and/or lymphatic system.

7.3 Clinical Presentation

The majority of patients are children and young adults presenting with headache, vomiting, papilloedema, focal seizures (33 %), and focal neurological deficits (Bükte et al. 2004).

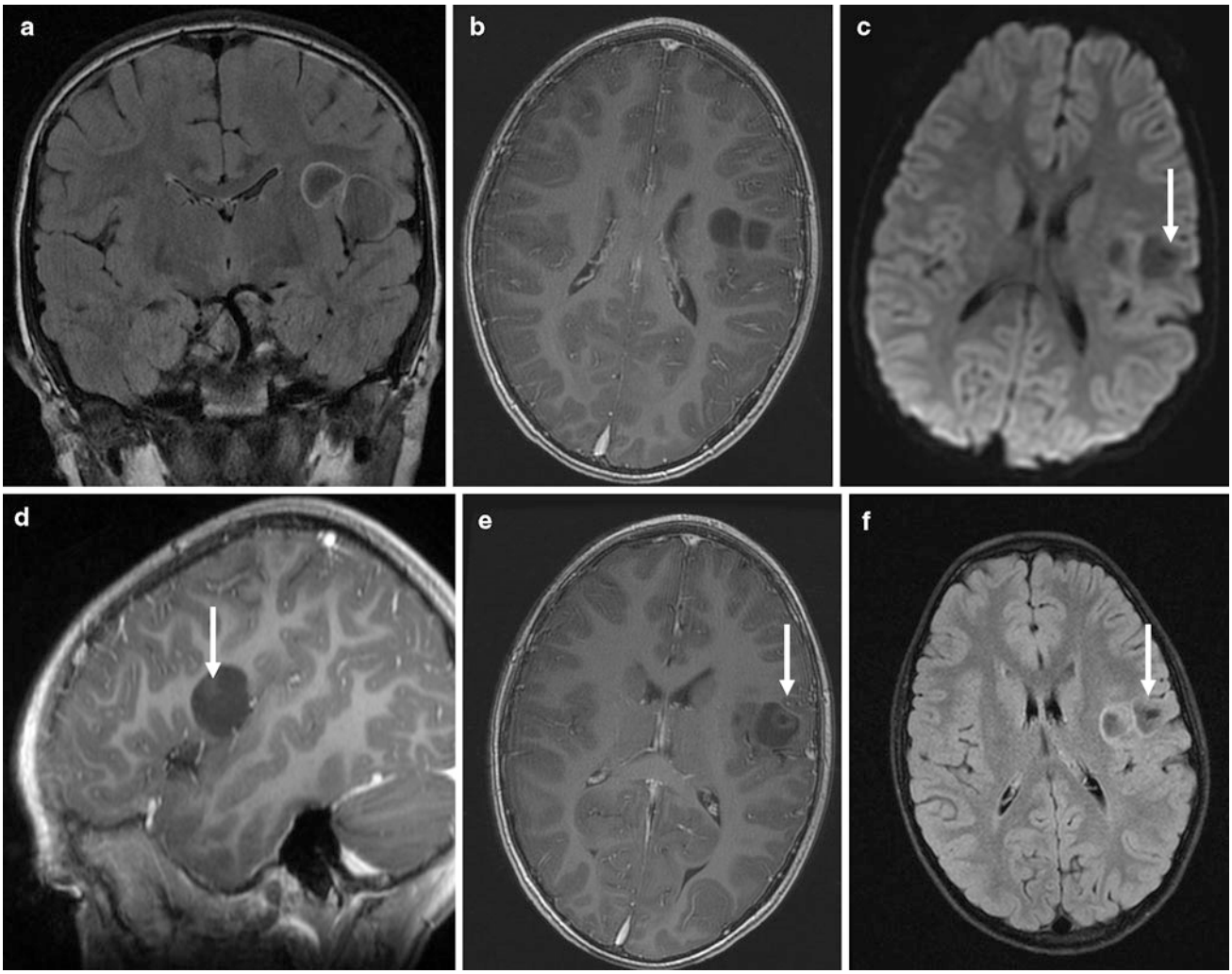

Fig. 8 Echinococcosis in an 11-year-old boy who presented with focal seizures of the *right* face. Coronal (**a**) and axial (**f**) FLAIR, axial (**b**, **e**) and sagittal (D) T1-weighted contrast-enhanced gradient echo, and axial diffusion-weighted (**c**) images show a bilobular cystic lesion at the base of the *left* precentral gyrus. Since the signal is not completely identical to CSF, the cyst likely contains a fluid with a higher protein content than CSF. A structure within the larger bubble could respresent daughter scolices (**c**–**f**: *arrow*). (Courtesy of J. Linn, Department of Neuroradiology, University of Munich, Germany.)

7.4 Imaging

E. granulosus forms large, uni-, bi-, or multilocular (hemispheric) cysts that are nearly isointense to CSF and have a thin, well-defined wall, which is hypointense on T2-weighted sequences and usually enhance the contrast medium. Sometimes an inner structure within the cystic cavity becomes visible, which may represent daughter scolices, hydatid sand (aggregation of scolices), or a germinal layer detached from the outer two layers of the wall (see Fig. 8).

E. multilocularis/alveolaris forms multiple, small cysts with a nodular or ring enhancement. Edema is more common than in *E. granulosus* infection.

8 Sarcoidosis

8.1 Epidemiology

Sarcoidosis is a multisystem inflammatory granulomatous disease of unknown etiology although current opinion favors an immune response to an as-yet-unknown antigen (Lannuzzi et al. 2007). The incidence in North America is estimated at 3–10 per 100,000 among Caucasians and 35–80 per 100,000 among African Americans (Rybicki and Iannuzzi 2007).

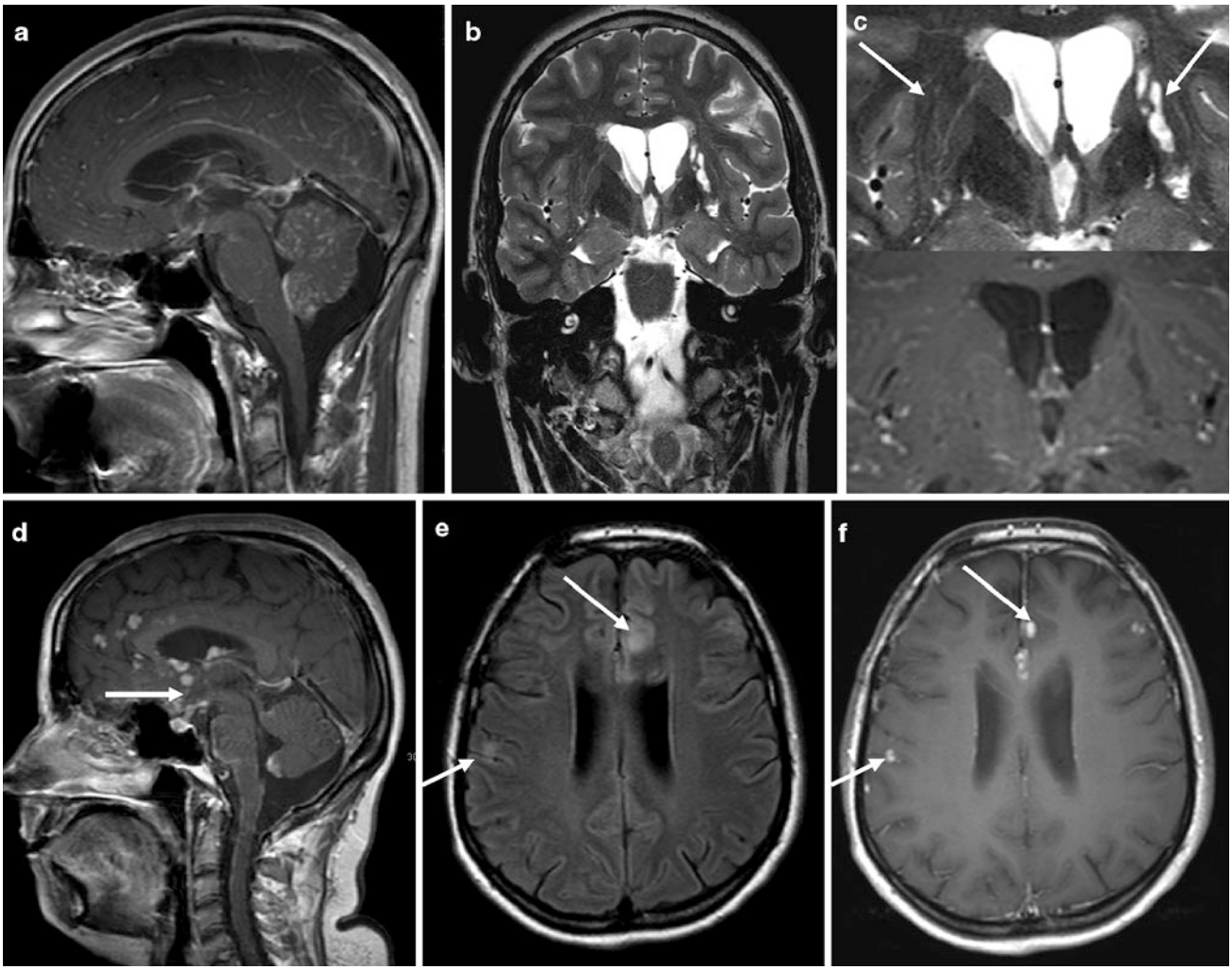

Fig. 9 Neurosarcoidosis in a 29-year-old man (**a–c**) and a 44-year-old woman (**d–f**) who presented with headaches and complex focal seizures. Sarcoidosis is most often a granulomatous meningitis with a predilection for the basal cisterns, particularly the area around the anterior third ventricle (**d**: *arrow*). Parenchymal infiltration via dilated Virchow–Robin spaces is illustrated on T2-weighted (**c**: *arrows*) and contrast-enhanced T1-weighted images (**b–d**). E and F show granulomas in the subarachnoid sulci, which cause parenchymal edema (**e–f**: *arrows*)

8.2 Pathogenesis

Sarcoidosis causes inflammation with noncaseating granulomas, which can occur in any organ system. Lungs and draining mediastinal lymph nodes are the most common sites of involvement. Neurosarcoidosis, that is, sarcoidosis involving the nervous system, is thought to occur in fewer than 5 % of patients, with systemic sarcoidosis and isolated neuroscarcoidosis in 17 % of neurosarcoidosis cases (Pawate et al. 2009; Chapelon et al. 1990).

8.3 Clinical Presentation

Seizures are the initial manifestation in 17 % of neurosarcoidosis cases (Pawate et al. 2009). All types of seizures can be seen, but generalized tonic–clonic seizures are common (Krumholz et al. 1991).

8.4 Imaging

The most common imaging finding is T2-hyperintense lesions, which enhance in approximately 25 % of patients (Pawate et al. 2009; Smith et al. 2004). Enhancement is typically homogeneous, lacking a central necrosis (Fig. 9). Lesions may be indistinguishable from MS lesions (Smith et al. 1989), and optic nerve enhancement and neuritis may occur in both diseases, too.

Meningeal enhancement is seen in only 20 % of cases (Pawate et al. 2009).

Sarcoidosis may also present as extraaxial or intraaxial mass lesions (Urbach et al. 1997). If located within the parenchyma, a spread from the subarachnoid space via Virchow–Robin spaces should be carefully searched for (Mirfakhraee et al. 1986) (Fig. 8). As in tuberculosis, a clue to the diagnosis is the proof of systemic, most often pulmonary involvement.

References

AlSemari A, Baz S, Alrabiah F, Al-Khairallah T, Qadi N, Kareem A, Alrajhi AA (2012) Natural course of epilepsy concomitant with CNS tuberculomas. Epilepsy Res 99(1–2):107–111

Arman F, Kaya D, Akgün Y, Kocagöz S (2011) Tuberculous meningitis presenting with nonconvulsive status epilepticus. Epilepsy Behav 20(1):111–115

Bargalló J, Berenguer J, García-Barrionuevo J et al (1996) The "target sign": is it a specific sign of CNS tuberculoma? Neuroradiology 38(6):547–550

Baskin HJ, Hedlund G (2007) Neuroimaging of herpesvirus infections in children. Pediatr Radiol 37(10):949–963

Bishburg E, Sunderam G, Reichman LB, Kapila R (1986) Central nervous system tuberculosis with the acquired immunodeficiency syndrome and its related complex. Ann Intern Med 105:210–213

Bükte Y, Kemaloglu S, Nazaroglu H et al (2004) Cerebral hydatid disease: CT and MR imaging findings. Swiss Med Wkly 134(31–32):459–467 (Review)

Chang L, Cornford ME, Chiang FL et al (1995) Radiologic-pathologic correlation. Cerebral toxoplasmosis and lymphoma in AIDS. AJNR Am J Neuroradiol 16(8):1653–1663

Chapelon C, Ziza JM, Piette JC et al (1990) Neurosarcoidosis: signs, course and treatment in 35 confirmed cases. Medicine 69:261–276

Dastur DK, Manghani DK, Udani PM (1995) Pathology and pathogenetic mechanisms in neurotuberculosis. Radiol Clin N Am 33:733–752

Del Brutto OH (2012) Neurocysticercosis: a review. Scientific World J. 2012:159821

Del Brutto OH, Santibanez R, Noboa CA et al (1992) Epilepsy due to neurocysticercosis: analysis of 203 patients. Neurology 42:389–392

Dye C, Scheele S, Dolin P, Pathania V, Raviglione MC (1999) Consensus statement. Global burden of tuberculosis: estimated incidence, prevalence, and mortality by country. WHO Global Surveillance and Monitoring Project. JAMA 282:677–686

Hall CB, Long CE, Schnabel KC et al (1994) Human herpesvirus-6 infection in children. A prospective study of complications and reactivation. N Engl J Med 331:432–438

Kim MA, Park KM, Kim SE, Oh MK (2008) Acute symptomatic seizures in CNS infection. Eur J Neurol 15(1):38–41

Krumholz A, Stern BJ, Stern EG (1991) Clinical implications of seizures in neurosarcoidosis. Arch Neurol 48:842–844

Lannuzzi M, Rybicki B, Tierstein A (2007) Sarcoidosis. New Engl J Med 357:2153–2165

Mirfakhraee M, Crofford MJ, Guinto FC Jr et al (1986) Virchow–Robin space: a path of spread in neurosarcoidosis. Radiology 158(3):715–720

Murakami A, Morimoto M, Adachi S et al (2005) Infantile bilateral striatal necrosis associated with human herpes virus-6 (HHV-6) infection. Brain Dev 27:527–530

Murthy JM, Jayalaxmi SS, Kanikannan MA (2007) Convulsive status epilepticus: clinical profile in a developing country. Epilepsia 48:2217–2223

Narayanan JT, Murthy JM (2007a) Nonconvulsive status epilepticus in a neurological intensive care unit: profile in a developing country. Epilepsia 48:900–906

Narayanan JT, Murthy JM (2007b) New onset acute symptomatic seizures in neurological intensive care unit. Neurol India 55:136–140

Neto EC, Rubin R, Schulte J, Giugliani R (2004) Newborn screening for congenital infectious diseases. Emerg Infect Dis 10:1068–1073

Osborn AG, Salzman KL, Barkovich AJ (eds) (2010) Diagnostic imaging. Brain Amirsys Inc, Salt Lake City

Pawate S, Moses H, Sriram S (2009) Presentations and outcomes of neurosarcoidosis: a study of 54 cases. QJM 102(7):449–460

Penido Nde O, Borin A, Iha LC, et al (2005) Intracranial complications of otitis media: 15 years of experience in 33 patients. Otolaryngol Head Neck Surg 132(1):37–42 (Review)

Pickering LK (ed) (2006) Red book: report of the Committee on infectious diseases. American Academy of Pediatrics, Elk Grove Village, pp 361–371

WHO Report (2009) Global tuberculosis control: epidemiology, strategy, financing (publication No. WHO/HMT/TB/2009.411). World Health Organization, Geneva

Rowley AH, Whitley RJ, Lakeman FD et al (1990) Rapid detection of herpes-simplex-virus DNA in cerebrospinal fluid of patients with herpes simplex encephalitis. Lancet 335:440–441

Rybicki BA, Iannuzzi MC (2007) Epidemiology of sarcoidosis: recent advances and future prospects. Semin Respir Crit Care Med 28:22–35

Sellner J, Trinka E (2012) Clinical characteristics, risk factors and presurgical evaluation of post-infectious epilepsy. Eur J Neurol. doi: 10.1111/j.1468-1331.2012.03842.x [Epub ahead of print]

Singh N, Paterson DL (2000) Encephalitis caused by human erpesvirus-6 in transplant recipients: relevance of a novel neurotropic virus. Transplantation 69:2474–2479

Smith JK, Matheus MG (2004) Castillo M imaging manifestations of neurosarcoidosis. AJR Am J Roentgenol 182:289–295

Smith AS, Meisler DM, Weinstein MA, et al (1989) High-signal periventricular lesions in patients with sarcoidosis: neurosarcoidosis or multiple sclerosis? AJR Am J Roentgenol 153(1):147–152

Tien RD, Felsberg GJ, Osumi AK (1993) Herpesvirus infections of the CNS: MR findings. AJR Am J Roentgenol 161:167–176

Trincado DE, Rawlinson WD (2001) Congenital and perinatal infections with cytomegalovirus. J Paediatr Child Health 37:187–192

Udani PM, Parekh UC, Dastur DK (1971) Neurological and related syndromes in CNS tuberculous meningitis: clinical features and pathogenesis. J Neurol Sci 14:341–357

Urbach H, Kristof R, Zentner J et al (1997) Sarcoidosis presenting as an intra- or extra-axial cranial mass: report of two cases. Neuroradiology 39(7):516–519

Villagran-Uribe J, Olvera-Rabiela JE (1988) Cisticercosis humana: e studio clinico y patologico de 481 casos de autopsia. Pathologia 26:149–156 [in Spanish]

Wainwright MS, Martin PL, Morse RP et al (2001) Human herpesvirus 6 limbic encephalitis after stem cell transplantation. Ann Neurol 50:612–619

Rasmussen Encephalitis

Horst Urbach and Christian G. Bien

Contents

Abstract

Rasmussen encephalitis is typically a chronic inflammatory disease of a one brain hemisphere in children. A MRI course of initial swelling and progressive brain atrophy and tissue destruction later on reflects the inflammatory changes; however, many patients show some brain atrophy already at their initial MRI examination.

1 Epidemiology

Rasmussen encephalitis is a rare, sporadic, chronic inflammatory disease of unknown origin, which usually affects one brain hemisphere. It was initially described by Theorore Rasmussen in 1958. Rasmussen encephalitis typically affects children (mean age 6 years); however, adolescent and adult cases may occur (Hart et al. 1997). Both genders are equally affected. The incidence is 2.4 patients per ten million people of age 18 years or younger (Bien et al. unpublished data).

2 Pathogenesis

Histopathological evaluation of Rasmussen encephalitis brain specimens reveals a cytotoxic T-cell reaction against neurons (Bien et al. 2002a, b, c) and astrocytes (Bauer et al. 2007) leading to apoptotic death of these cell types. Brain regions with swollen tissue and increased T2 and fluid-attenuated inversion recovery (FLAIR) signal intensity show an increased density of cytotoxic T cells and glial fibrillary acidic protein (GFAP)-positive astrocytes (acute phase). In the chronic phase, tissue destruction and low inflammatory activity with a decreasing number of T cells and reactive astrocytes predominate (Bien et al. 2002a, b, c). These findings support the hypothesis of an early active inflammation that "burns out" later (Robitaille 1991).

H. Urbach (✉)
Department of Neuroradiology,
University Hospital Freiburg, Germany
e-mail: horst.urbach@uniklinik-freiburg.de

C. G. Bien
Epilepsy Centre Bethel, Bielefeld, Germany

H. Urbach (ed.), *MRI in Epilepsy*, Medical Radiology. Diagnostic Imaging,
DOI: 10.1007/174_2012_573,

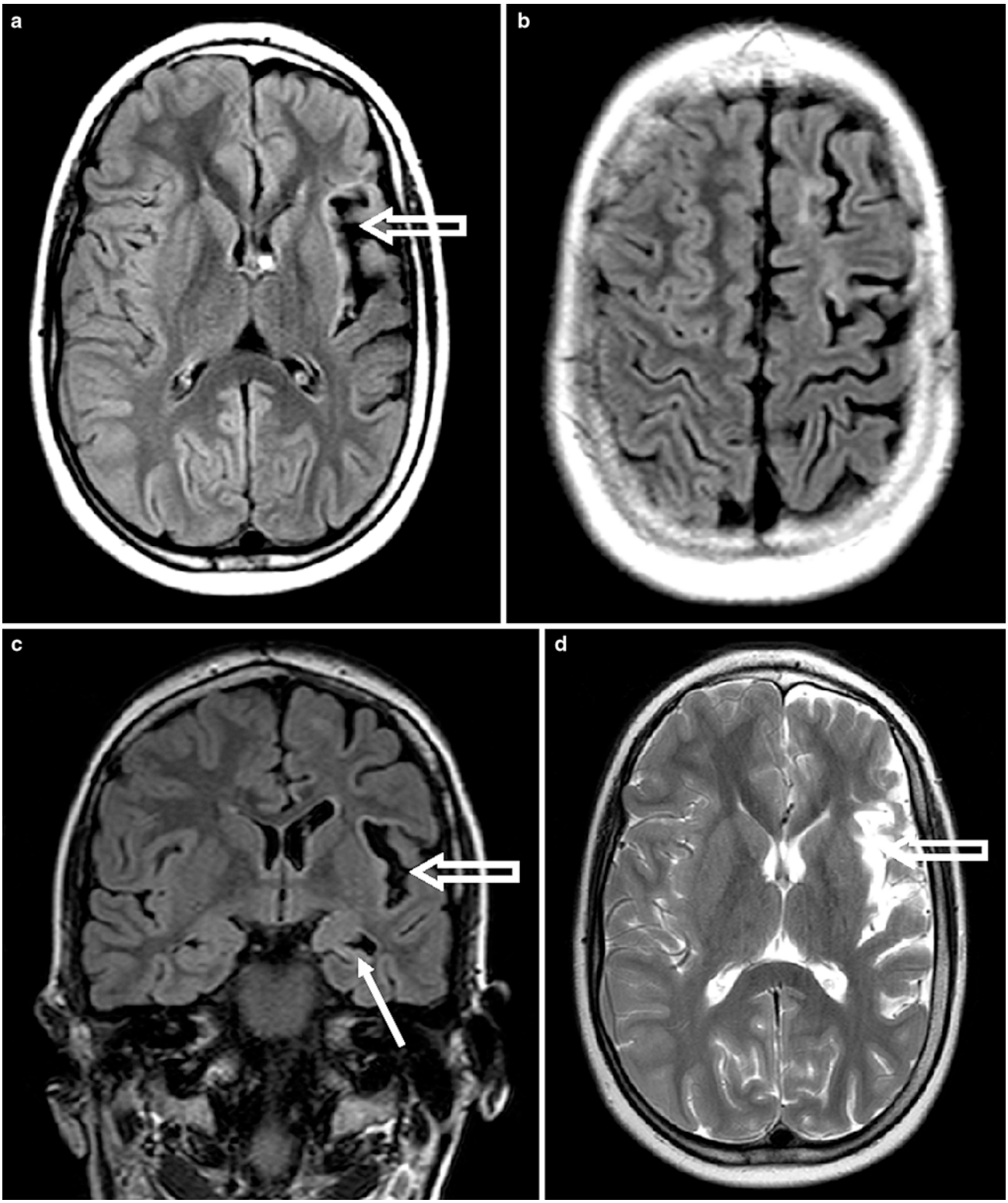

Fig. 1 Rasmussen encephalitis of the left hemisphere associated with accentuated perinsular atrophy and hyperintense cortex signal (**a**, **c**, **d**, *hollow arrow*). In this case, the hippocampus is sclerotic (**c**, *arrow*) but the ipsilateral head of the caudate nucleus is not

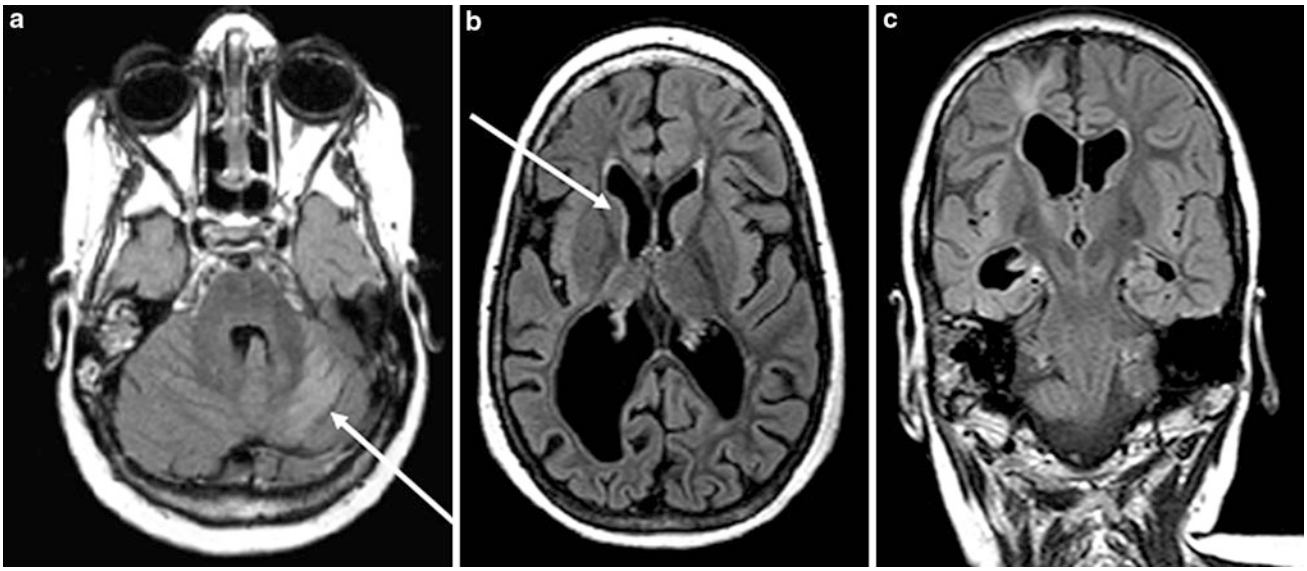

Fig. 2 Marked brain atrophy in a chronic stage of Rasmussen encephalitis in a 9-year-old girl with onset of epilepsia partialis continua of the left arm and leg 3 years before. Note contralateral cerebellar atrophy ("cerebellar diaschisis") (**a**, *arrow*), right-sided caudate head atrophy (**b**, *arrow*), and pronounced right-sided, but also left-sided brain atrophy (**b**, **c**)

3 Clinical Presentation

Rasmussen encephalitis is characterized by intractable focal onset seizures, namely, epilepsia partialis continua (EPC) (56–92% of all patients), and deterioration of functions associated with the affected hemisphere (Oguni et al. 1991). It has three stages (Bien et al. 2005). There may be a prodromal phase with a median duration of 7 months (0 months to 8.1 years) characterized by a relatively low seizure frequency and rarely a mild hemiparesis. The prodromal phase is followed by an acute phase with a high seizure frequency or EPC. Within weeks to months, progressive tissue destruction and associated loss of neurological functions, including hemiparesis, hemianopia, and aphasia (if the dominant hemisphere is affected), occur. Cognitive function deteriorates. After around 1 year, a residual or chronic phase is reached. At this point in time, brain volume loss remains stable, and seizure frequency slows down.

In the acute phase of the disease, immunomodulation including tacrolimus may be able to reduce the degree of hemiparesis, although seizure frequency is not affected (Bien et al. 2004). In long-term treatment, immunomodulation may slow progressive tissue and function loss and prevent the development of intractable epilepsy (Bien et al. unpublished data). The most effective treatment with regard to seizure freedom is functional hemispherectomy. This procedure, however, is usually performed only at later stages of the disease when a patient has developed a fixed hemiparesis with loss of fine finger movements (Honavar et al. 1992).

4 Imaging

Serial MRI may reveal a spread of the inflammatory lesion over the affected hemisphere. In a given brain region, a characteristic course from increased volume and T2/FLAIR signal to a final stage of atrophy without signal abnormalities may be observed.

Most patients, however, show some degree of unilateral enlargement of the inner and outer CSF spaces on their initial MRI examination. Atrophy is pronounced in the perisylvian region and may be accompanied by increased cortical and subcortical signal on T2-weighted/FLAIR images. Rarely, patients show a swollen hemisphere with slightly increased cortex and white matter signal or a normal MRI findings, respectively. There is no contrast enhancement.

Atrophy of the ipsilateral head of the caudate nucleus is considered a typical finding (Chiapparini et al. 2003; Granata et al. 2003); however, it does not occur or is not prominent in some patients (Fig. 1). Temporomesial structures, including the hippocampus, are atrophic in around 50% of cases. The cerebellum may show increased cortical signal and atrophy on the contralateral side (crossed cerebellar diaschisis), the ipsilateral side, or both sides (Fig. 2).

Follow-up MRI shows a progressive tissue loss of the ipsilateral hemisphere, and less pronounced loss of the contralateral hemisphere (Larionov et al. 2005). Most of the tissue loss occurs within the first 12 months after onset of the acute phase; however, it may progress for several years (Fig. 3). To assess the temporal evolution of

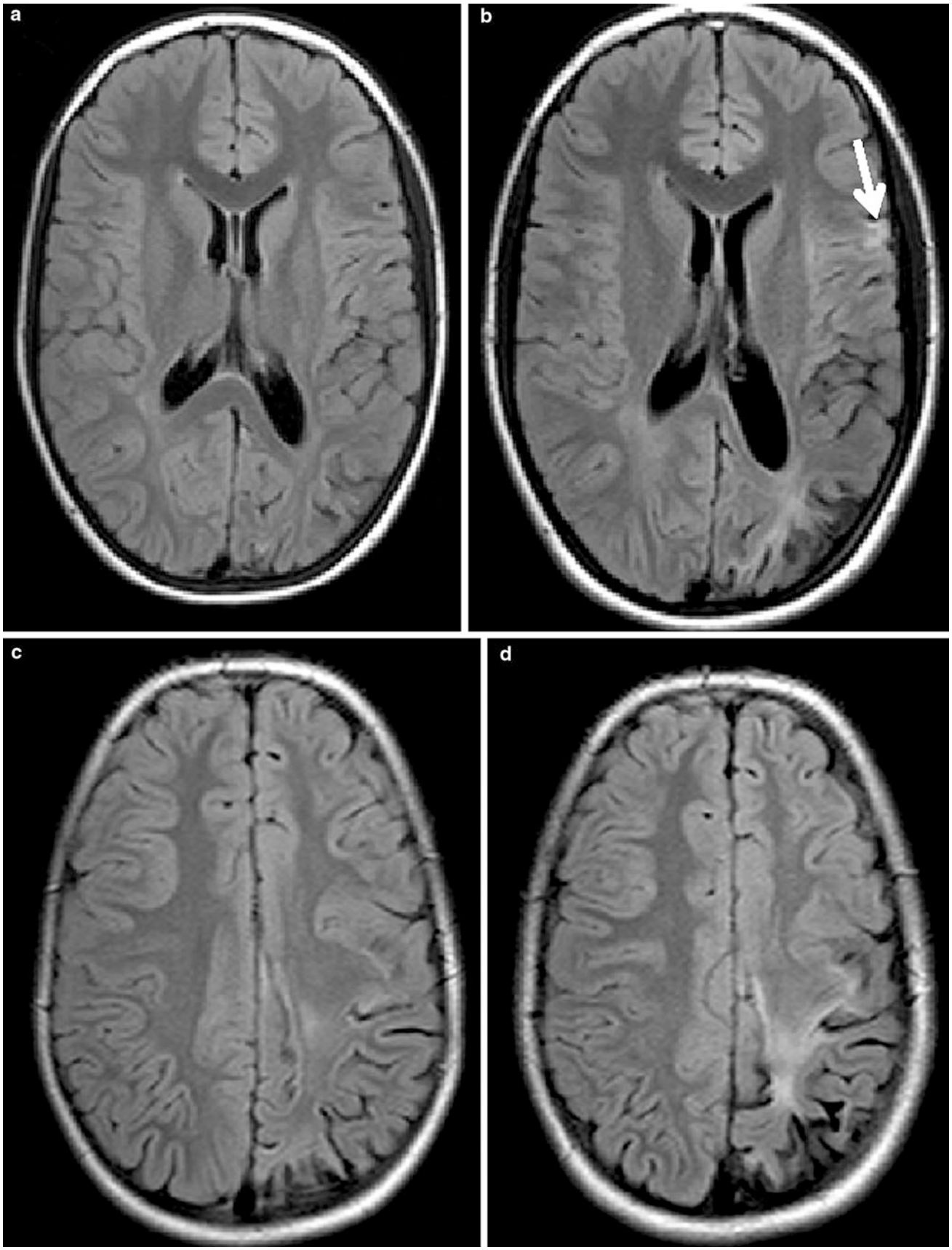

Fig. 3 Progressive atrophy in a 12-year-old girl with Rasmussen encephalitis. Note progressive tissue loss and gliotic changes in the left parietal lobe and new signal intensity in the frontal operculum on follow-up MRI (**b**, *arrow*) 5 years after onset of symptoms and 4 years after the first scan (**a**, **c**)

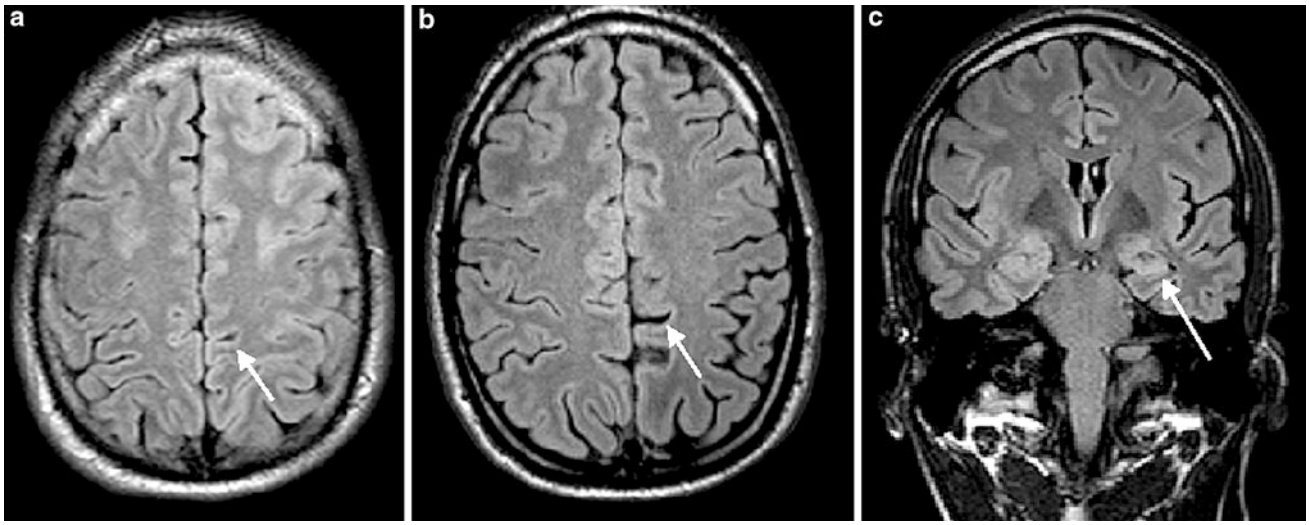

Fig. 4 Following three generalized tonic–clonic seizures, a 28-year-old man with diabetes mellitus type 1 showed aphasia and right-sided hemiparesis for hours. Initial MRI after 3 days (**a**) was unrevealing but follow-up MRI after 6 months (**b**) showed left-sided hemiatrophy. For comparison, see the *arrow* pointing to the pars marginalis cinguli in **a** and **b**. Also note the atrophy and slight signal increase of the left hippocampus (**c**, *arrow*)

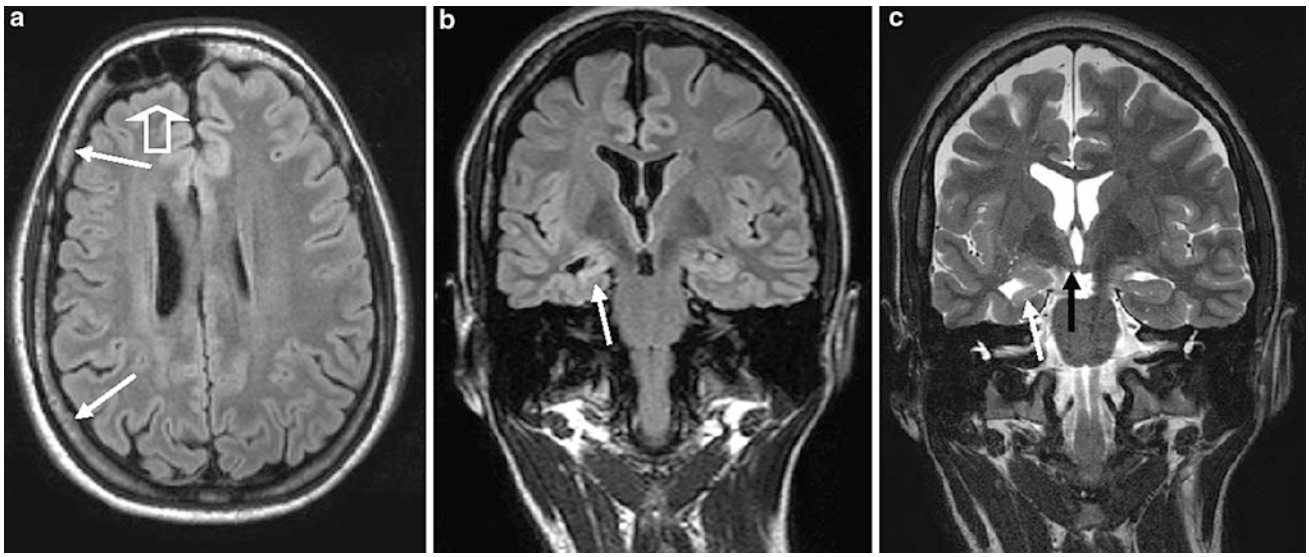

Fig. 5 Dyke–Davidoff–Masson syndrome in a 30-year-old woman with perinatal hypoxia. MRI shows a hypertrophied right frontal sinus (**a**, *hollow arrow*), calvarial thickening (**a**, *arrows*), and right-sided hemiatrophy and hippocampal sclerosis (**b**, **c**, *arrow*) associated with mammillary body atrophy (**c**, *black arrow*). Enlargement of the frontal sinus and calvarial thickening are compensatory mechanism and fit with a congenital or early postnatal cause

hemiatrophy, Bien et al. (2002a, b, c) introduced a planimetric measure called the hemispheric ratio. It allows one to compare images from different time points that were even acquired with different sequences and orientations. Axial images displaying the third ventricle at its largest extent and coronal images at the level of the optic chiasm are scanned, brains are manually segmented and thresholded, and the

Table 1 MRI stages of Rasmussen encephalitis (Bien et al. 2002a, b, c)

Stage 1	Swelling and increased T2/FLAIR signal
Stage 2	Normal volume, increased T2/FLAIR signal
Stage 3	Atrophy, increased T2/FLAIR signal
Stage 4	Atrophy, normal signal

FLAIR fluid-attenuated inversion recovery

Table 2 Causes of epilepsia partialis continua (adapted from Bien and Elger 2008)

Disease	Frequency (%)
Vascular (stroke, intracranial bleeding, venous thrombosis, vasculitis)	20
Infectious (Rasmussen encephalitis, autoimmune encephalitis, Creutzfeldt–Jakob disease)	20
Tumor (glioma, meningioma, lymphoma)	10
Metabolic (nonketotic hyperglycemia, mitochondrial disorders, Alpers syndrome, MERRF, intoxications)	10
Other diseases (MS, genetic epilepsies, SREAT, SLE)	20
Undetermined	20

MERRF myoclonus epilepsy with ragged red fibers, *MS* multiple sclerosis, *SREAT* steroid-responsive encephalopathy associated with autoimmune thyroiditis, *SLE* systemic lupus erythematosus

Table 3 Other diseases associated with hemiatrophy

Disease	MRI clues
Sturge–Weber angiomatosis	Angiomatosis with contrast enhancement, cortical calcifications, ipsilateral choroid plexus enlargement
Fetal/perinatal hemispheric infarct (Dyke–Davidoff–Masson syndrome) (Dyke et al. 1933)	Calvarial skull thickening, enlargement of ipsilateral air sinuses, elevation of petrous ridge and frontal skull base (see Fig. 5)
Hemispheric atrophy following status epilepticus or frequent seizures	Initial swollen or normal hemisphere. Follow-up MRI shows widened sulci, thin cortex with rather hyperintense signal, and diminished white matter volume (see Fig. 4)
Porencephaly	More circumscribed lesion
Hemiconvulsion–hemiplegia–epilepsy syndrome	Vascular distribution or entire hemispheric destruction
Contralateral hemimegalencephaly	Distorted perisylvian anatomy with steeper course of the sylvian fissure
MELAS	Bilateral and basal ganglia lesions

MELAS mitochondrial encephalomyopathy, lactic acidosis, and stroke-like symptoms

volumes of the hemispheres (in number of brain pixels in the scanned picture) are calculated and divided through each other. A ratio of 1 indicates that both hemispheres on the assessed slice are of equal size. Values less than 1 indicate atrophy of the affected hemisphere. Apart from the progressive tissue loss, new areas of increased cortical/subcortical signal increase may appear in brain regions which did not show signal changes before. Novel ways of volumetric quantification of the disease process rely on voxel-based measures (Wagner et al. 2012) (Table 1).

EPC is the clinical hallmark of Rasmussen encephalitis. EPC is defined as spontaneous regular or irregular clonic muscular twitching affecting a limited part of the body, sometimes aggravated by action or sensory stimuli, occurring for a minimum of 1 h and recurring at intervals of no more than 10 s. Apart from Rasmussen encephalitis, the diseases given in Table 2 have to be taken into consideration.

If MRI shows hemiatrophy, the differential diagnoses given in Table 3 should be considered.

References

Bauer J, Elger CE, Hans VH, Schramm J, Urbach H, Lassmann H et al (2007) Astrocytes are a specific immunological target in Rasmussen's encephalitis. Ann Neurol 62:67–80

Bien CG, Widman G, Urbach H et al (2002a) The natural history of Rasmussen's encephalitis. Brain 125:1751–1759

Bien CG, Bauer J, Deckwerth TL, Wiendl H, Deckert M, Wiestler OD et al (2002b) Destruction of neurons by cytotoxic T cells: a new pathogenic mechanism in Rasmussen's encephalitis. Ann Neurol 51:311–318

Bien CG, Urbach H, Deckert M, Schramm J, Wiestler OD, Lassmann H et al (2002c) Diagnosis and staging of Rasmussen's encephalitis by serial MRI and histopathology. Neurology 58:250–257

Bien CG, Elger CE (2008) Epilepsia partialis continua: semiology and differential diagnosis. Epileptic Disord 10:3–7

Bien CG, Gleissner U, Sassen R, Widman G, Urbach H, Elger CE (2004) An open study of tacrolimus therapy in Rasmussen's encephalitis. Neurology 62:2106–2109

Bien CG, Granata T, Antozzi C et al (2005) Pathogenesis, diagnosis, and treatment of Rasmussen encephalitis. A European consenus statement. Brain 128:454–471

Bien CG, Tietmeier H, Sassen R, Kuczaty S, Urbach H, von Lehe M, Becker A, Bast T, Brückmann D, Diers A, Herkenrath P, Jansma C, Karenfort A, Kieslich M, Kruse B, Kurlemann G, Rona S, Schubet S, Vieker S, Wilken B, Elger CE Rasmussen encephalitis: a first randomized clinical trial for an orphan disease (submitted)

Chiapparini L, Granata T, Farina L, Ciceri E, Erbetta A, Ragona F et al (2003) Diagnostic imaging in 13 cases of Rasmussen's encephalitis: can early MRI suggest the diagnosis? Neuroradiology 45:171–183

Dyke CG, Davidoff LM, Masson CB (1933) Cerebral hemiatrophy with homolateral hypertrophy of the skull and sinuses. Surg Gynecol Obstet 57:588–600

Granata T, Gobbi G, Spreafico R, Vigevano F, Capovilla G, Ragona F et al (2003) Rasmussen's encephalitis: early characteristics allow diagnosis. Neurology 60:422–425

Hart YM, Andermann F, Fish DR, Dubeau F, Robitaille Y, Rasmussen T et al (1997) Chronic encephalitis and epilepsy in adults and adolescents: a variant of Rasmussen's syndrome? Neurology 48:418–424

Honavar M, Janota I, Polkey CE (1992) Rasmussen's encephalitis in surgery for epilepsy. Dev Med Child Neurol 34:3–14

Larionov S, Koenig R, Urbach H, Sassen R, Elger CE, Bien CG (2005) MRI brain volumetry in Rasmussen encephalitis: the fate of affected and "unaffected" hemispheres. Neurology 64:885–887

Oguni H, Andermann F, Rasmussen TB (1991) The natural history of the syndrome of chronic encephalitis and epilepsy: a study of the MNI series of fortyeight cases. In: Andermann F (ed) Chronic encephalitis and epilepsy. Rasmussen's syndrome. Butterworth-Heinemann, Boston, pp 7–35

Rasmussen T, Olszewski J, Lloyd-Smith D (1958) Focal seizures due to chronic localized encephalitis. Neurology 8:435–445

Robitaille Y (1991) Neuropathologic aspects of chronic encephalitis. In: Andermann F (ed) Chronic encephalitis and epilepsy. Rasmussen's syndrome. Butterworth-Heinemann, Boston, pp 79–110

Rogers SW, Andrews PI, Gahring LC, Whisenand T, Cauley K, Crain B et al (1994) Autoantibodies to glutamate receptor GluR3 in Rasmussen's encephalitis. Science 265:648–651

Wagner J, Schöne-Barke C, Bien CG, Urbach H, Elger CE, Weber B (2012) Automated 3D MRI volumetry reveals regional atrophy differences in Rasmussen's encephalitis. Epilepsia 2012 Apr 53(4): 613−621. doi: 10.1111/j.1528-1167.2011.03396.x

Metabolic Disorders

Horst Urbach and Jens Reimann

Contents

H. Urbach (✉)
Department of Neuroradiology, University Hospital Freiburg, Germany
e-mail: horst.urbach@uniklinik-freiburg.de

J. Reimann
Department of Neurology, University of Bonn, Bonn, Germany

Abstract

Epileptic seizures are a frequent symptom in metabolic disorders. However, it is neither seizure semiology nor EEG or MRI findings that guide the physician to the correct diagnosis. It is more important to consider the clinical syndrome, the age at presentation, and appropriate laboratory investigations.

It is beyond the scope of this textbook to give a complete overview of the more than 200 metabolic disorders that together are a rather rare cause of epilepsy. However, epilepsy is a frequent symptom in metabolic disorders; sometimes, epileptic seizures or even epileptic encephalopathy are predominating clinical symptoms (Saudubray et al. 2006; Sedel et al. 2007; Stöckler-Ipsiroglu and Plecko 2009; Thomas et al. 2010).

Metabolic disorders can be classified in many different ways (metabolic defect, age at presentation, clinical symptoms, type of seizures). Relevant metabolic disorders associated with epilepsy and more or less specific MRI findings are grouped in Table 1 according to the typical age at presentation.

1 Mitochondrial Disorders

With frequent seizures: Leigh syndrome; MELAS (mitochondrial myopathy, encephalopathy with lactic acidosis and stroke-like episodes); MERRF (myoclonic epilepsy and ragged red fibers); Alpers–Huttenlocher syndrome; ataxia-neuropathy spectrum, including mitochondrial recessive ataxia (MIRAS) and sensory ataxia with neuropathy, dysarthria, and ophthalmoparesis (SANDO) syndromes, myoclonic epilepsy, myopathy, and sensory ataxia (MEMSA) syndrome, also known as spino-cerebellar ataxia with epilepsy (SCAE) syndrome.

H. Urbach (ed.), *MRI in Epilepsy*, Medical Radiology. Diagnostic Imaging,
DOI: 10.1007/174_2012_757,

Table 1 Metabolic disorders associated with epilepsy and MRI findings

Age at presentation	Disorder	Clinical presentation—diagnosis	MRI
Neonatal	Disorders of vitamin B6 metabolism Pyridoxine-dependent seizures (PDS) Folinic acid–responsive seizures Pyridoxal phosphate–dependent seizures (PLP)	Early myoclonic encephalopathy EEG: No specific pattern (Gospe 2010) PDS: Pipecolic acid elevation in plasma and CSF. Seizures stop after 50–100 mg of IV pyridoxine (Stöckler-Ipsiroglu and Plecko 2009) PLP: Vanillatic acid in urine Improvement of seizures upon oral pyridoxalphosphate (Stöckler-Ipsiroglu and Plecko 2009)	Wide range from normal, disturbed white matter myelination to cortical dysplasia (Mills et al. 2010)
	Nonketotic hyperglycinemia (aminoacidopathy)	Early myoclonic encephalopathy Myoclonic and generalized seizures EEG: Burst suppression and hypsarrhythmia Increased glycine in plasma, urine and CSF	Callosal hypogenesis, delayed myelination, myelin vacuolation with diffusion restriction in the pyramidal tracts, middle cerebral peduncles, and dentate nuclei ^{H1}Spectroscopy: Elevated glycine levels (short and long TE) (Press et al. 1989, Sener 2003, Huisman et al. 2002)
	Methylmalonic aciduria (aminoaciduria: error in the metabolism of isoleucine, valine, threonine, and the odd-chain fatty acids)	Various clinical phenoptyes with acute metabolic crises	Acute metabolic crisis with brain swelling and T2/FLAIR hyperintensity of globi pallidi. Gliosis and volume loss in chronic stage (Brismar and Ozand 1994)
	Glutaric aciduria type 1 (organic aciduria: error in the metabolism of the aminoc acids L-lysine, hydroxyl-L-lysine, L-trypthophan)	Macrocephaly, cephalgia, cognitive deficits, pyramidal signs, epilepsy, tremor	Bilateral signal abnormalities of the putamina, subdural effusions/ haematomas, large head with prominent Sylvian fissures (Brismar and Ozand 1995) (see Fig. 1)
	L2 hydroxyglutaric aciduria (organic aciduria)	Mental retardation, epilepsy, parkinsonism, pyramidal signs, ataxia	T2/FLAIR hyperintensity of subcortical white matter with U-fibers, anterior limbs of internal capsule, external and extreme capsule, dentate nuclei (Seijo-Martínez et al. 2005)
	Maple syrup urine disease	Neonatal seizures, vomiting, ketoacidosis, hypoglycemia. Odor of maple syrup	White matter edema with diffusion restriction of corticospinal tracts, optic radiation, brain stem white matter tracts, cerebellar white matter ^{H1}Spectroscopy: Characteristic broad peak at 0.9 ppm (branched chain ketoacids) (Jan et al. 2003)
	Serine deficiency (aminoacidopathy)	West syndrome. Psychomotor retardation, spastic tetraparesis. EEG: hypsarrhythmia Two types: 3-Phosphoglycerate dehydrogenase deficiency, 3-phosphoserine phosphatase (3-PSP) deficiency (de Koning and Klomp 2004)	Congenital microcephaly, white matter hypomyelination (de Koning et al. 2000, de Koning and Klomp 2004)
	GABA transaminase deficiency (aminoacidopathy)	Early epileptic encephalopathy High levels of GABA in CSF and serum	No specific finding (Pearl and Gibson 2004)
	Methylene tetrahydrofolate reductase (MTHFR) deficiency	Early epileptic encephalopathy	White matter atrophy, delayed myelination, demyelination (Engelbrecht et al. 1997; Prasad et al. 2011a, b)
	Congenital glutamine deficiency (urea cycle disorder)	Early myoclonic encephalopathy	Reduced white matter volume and increased signal intensity on T2-weighted images, atrophic basal ganglia (Haeberle et al. 2012)

(continued)

Table 1 (continued)

Age at presentation	Disorder	Clinical presentation—diagnosis	MRI
	Zellweger syndrome (peroxisomal disorder)	Craniofacial dysmorphism, profound hypotonia, neonatal seizures Hepatomegaly, cardiac and ocular abnormalities	Delayed myelination, bilateral perisylvian polymicrogyria, periventricular germinolytic cysts, gray matter heterotopia (Barkovich and Peck 1997; Weller et al. 2008)
	Molybdenum cofactor deficiency	Classical: early epileptic encephalopathy Atypical: global developmental impairment Sulfite test in urine positive	Gray matter swelling with diffusion restriction. Cerebral hemispheric infarctions (Appignani et al. 1996; Vijayakumar et al. 2011)
Infancy	Glucose transporter protein type 1 (*GLUT1*) deficiency	Different forms of epilepsy, including myoclonic and atypical absence seizures EEG: generalized spike-wave and polyspike-wave discharges Low CSF, but normal blood glucose, *GLUT1* gene mutations on chromosome 1p35-31.3 (Klepper and Leiendecker 2007) Ketogenic diet	Acquired microcephaly MRI otherwise uninformative (Klepper and Leiendecker 2007)
	Phenylketonuria (aminoacidopathy)	Clinical symptoms depend on phenylalaline levels and whether phenylalaline-restricted diet is implemented at birth: Early myoclonic encephalopathy in infancy—spastic paresis, dementia, and/or optic atrophy in adults	MRI abnormalities depend on phenylalaline levels: High T2-/FLAIR signal intensity and impaired diffusion of the peritrigonal white matter (Kono et al. 2005)
	Menkes kinky hair disease (trichopoliodystrophy)	Partial clonic status epilepticus—infantile spasms—multifocal seizures EEG: hypsarrhythmia Low copper and ceruloplasmin after 2 weeks of life	MRI normal at birth. Rapidly developing cerebral and cerebellar atrophy. T1 hyperintensity of basal ganglia. Chronic bilateral subdural hematomas. Tortous intracranial arteries (Prasad et al. 2011a, b)
	Biotinidase (multiple carboxylase) deficiency	Epileptic seizures, West syndrome starting at 3 or 4 months of age, muscular hypotonia, alopecia, and skin rash (Wolf et al. 1983, 1985)	MRI: Increased T2/FLAIR white matter signal, suggestive of interstitial edema, with frontal predominance and U-fiber involvement (Desai et al. 2008)
	Creatine deficiency	Epileptic seizures and psychomotor retardation Arginine-glycine amindinotransferase (AGAT)-, guanidinoacetate methyltransferae (GAMT)- or creatine transporter (CRTR) deficiency	Normal, ^{H1}spectroscopy: decreased creatine peak guanidinoacetate methyltransferae (GAMT)-deficiency: increased T2/FLAIR signal of globi pallidi (Stöckler et al. 1994; Barkovich 2007)
	Gangliosidosis (GM2): infantile forms Type B Tay–Sachs, Type O Sandhoff, Type AB (lysosomal disorder)	Accumulation of GM2 gangliosides within neuronal lysosomes Macrocrania, blindness (cherry-red spot macula), seizures	Bilateral, symmetric thalamic > globus pallidus, putamen and caudate nucleus T1-hyperintensity and T2-hypointensity, diffuse T2-hyperintensity of white matter with sparing of the corpus callosum (Van der Knaap and Valk 2005)
	Neuronal ceroid lipofuscinosis (infantile type, Santavuori, CLN1) (lysosomal disorder)	Normal psychomotor development until the age of 8–18 months, rapid decline with epileptic seizures. Cardinal symptom is visual failure; most patients are blind before the age of 2 (Santavuori et al. 1993).	Cerebral atrophy, thalamic hypointensity to white matter and basal ganglia, and thin periventricular high-signal rims from 13 months onward on T2-weighted images (Vanhanen et al. 1995)

(continued)

Table 1 (continued)

Age at presentation	Disorder	Clinical presentation—diagnosis	MRI
Toddlers	Succinic semialdehyde dehydrogenase deficiency (SSADH) 4-hydroxybutyric aciduria, disorder of GABA metabolism	Disorder of GABA metabolism. Tonic–clonic and absence-like seizures, delayed development, hypotonia, abnormal behavior, ocular abnormalities Mean age at onset 2 years, although diagnoses in the 3rd or 4th decade have been made (Pearl et al. 2011) High concentration of 4-hydroxybutyric acid in CSF, urine, plasma (Pearl et al. 2003a, b)	Increased signal intensity of globi pallidi on T2-weighted images, cerebral and cerebellar atrophy, T2-weighted subcortical hyperintensities in subcortical white matter, dentate nuclei and brainstem, delayed myelination (Pearl et al. 2003a, b; Gordon 2004)
	Neuronal ceroid lipofuscinosis (late infantile type, Janksy–Bielschowsky, CLN2) (lysosomal disorder)	Normal psychomotor development until the age of 2–4 years. Rapid decline with epileptic seizures (myoclonic, tonic–clonic, atonic, atypical absence). Cardinal symptom is visual failure; most patients are blind around the age of 6.	Diffuse cerebral and cerebellar atrophy. T2 hypointensity of thalami and basal ganglia
	Mitochondrial disorders	See Table 2.	See Table 2.
School-age children	Neuronal ceroid lipofuscinosis (juvenile, Spielmeyer–Vogt or Batten, CLN3) (lysosomal disorder)	Rapid decline of vision and progressive dementia. Myoclonic and tonic–clonic seizures	Diffuse cerebral and cerebellar atrophy. T2 hypointensity of thalami and basal ganglia
	Mitochondrial disorders	See Table 2.	See Table 2.
	Progressive myoclonic epilepsies	See Table 4.	See Table 4.
Adolescents and adults	Neuronal ceroid lipofuscinosis (adult, Kufs, CLN4) (lysosomal disorder)	Generalized seizures, extrapyramidal symptoms, no blindness	Diffuse cerebral and cerebellar atrophy. T2 hypointensity of thalami and basal ganglia
No specific age relation	Mitochondrial disorders	See Table 2.	See Table 2.
	Niemann–Pick disease type C	Autosomal recessive disorder with mutations of the *NPC1* or *NPC2* genes Clinical signs: hepatomegaly, splenomegaly, lymphadenopathy, cerebellar ataxia (76 %), vertical supranuclear ophthalmoplegia (75 %), dysarthria, (63 %), cognitive deficits (61 %), movement disorders (58 %), splenomegaly (54 %), psychiatric disorders (45 %), dysphagia (37 %), epilepsy (18 %), and cataplexy (Sévin et al. 2007) Clinical spectrum ranges from a neonatal rapidly fatal disorder to an adult-onset neurodegenerative disease (Sévin et al. 2007).	Gray matter disease with moderate cortical, brainstem, cerebellar, and corpus callosum atrophy without signal abnormalities. Atrophy location correlates to clinical symptoms (Sévin et al. 2007).

With occasional seizures: infantile-onset spino-cerebellar ataxia (IOSCA); Leber hereditary optic neuropathy (LHON); chronic progressive external ophthalmoplegia (CPEO) and Kearns–Sayre syndrome (KSS); leucoencephalopathy with brain stem and spinal cord involvement and lactacidosis (LBSL) syndrome; neuropathy, ataxia, and retinitis pigmentosa (NARP) syndrome

Without seizures: mitochondrial neurogastrointestinal encephalomyopathy (MNGIE) syndrome (Finsterer and Zarrouk Mahjoub 2012).

1.1 Introduction

Mitochondria are double-membrane organelles producing the energy necessary for different cell functions. A cell contains hundreds of mitochondria and depends on them for the production of ATP. Cells in metabolically active tissues, such as the central nervous system (including the eye and the optic nerve), cardiac conduction system, skeletal muscle, endocrine pancreas, kidneys, and liver, have a high number of mitochondria (Haas and Dietrich 2004).

The main role of mitochondria is ATP synthesis by so-called oxidative phosphorylation. Other mitochondrial processes include the detoxification of reactive oxygen species, the regulation of cellular apoptosis, and aspects of iron metabolism, fatty acid oxidation, and amino acid biosynthesis. Oxidative phosphorylation is accomplished by the mitochondrial respiratory chain, a five-complex chain of polypeptides embedded in the inner mitochondrial membrane. The first four complexes (complexes I–IV) oxidize NADH and $FADH_2$, while complex V harnesses the resultant electrochemical gradient to phosphorylate ADP to ATP. Cofactors, including ubiquinone (also called CoQ_{10}) and cytochrome c, act as electron shuttles between respiratory complexes. Pyruvate and fatty acids are the most important substrates of energy metabolism. Pyruvate is carried across the mitochondrial membrane by monocarboylate translocase and decarboylated by the pyruvate dehydrogenase complex (Haas and Dietrich 2004).

Mitochondria have their own genome consisting of 37 genes (mtDNA), which encode for 13 structural proteins (all of which are subunits of the five mitochondrial respiratory complexes), two ribosomal RNAs (rRNAs), and 22 transfer RNAs (tRNAs). The majority of the protein subunits of the five mitochondrial respiratory complexes, however, are encoded by nuclear DNA and are imported into the mitochondria from the cytosol.

mtDNA is nearly exclusively transferred from the mother to the child: Although approximately 100 paternal mitochondria enter the ovum at fertilization, these organelles are tagged with ubiquitin for prompt proteolytic destruction by the zygote, and virtually all the zygote's mitochondria come from its mother (maternal inheritance).

Each mitochondrion contains several copies of mtDNA. Usually, all copies are identical (homoplasmy). After a mutation has arisen in one copy of mtDNA, however, wild-type and mutant mtDNA coexist within the same mitochondrion (heteroplasmy). Heteroplasmy becomes important during division of the host cell, as mitochondria (and the mtDNA they contain) are partly distributed randomly between the two daughter cells (replicative segregation). Heteroplasmy and replicative segregation contribute strongly to the heterogeneity of disease phenotypes, even among individuals of the same pedigree.

It is therefore conceivable that mitochondrial disorders are extremely heterogeneous, with a variable age of onset, progression, and severity. Well-known clinical phenotypes with epileptic seizures are Leigh syndrome, MELAS, MERRF, and Alpers–Huttenlocher syndrome. Well-known clinical phenotypes with occasional seizures are chronic progressive external ophthalmoplegia (CPEO) and Kearns–Sayre syndrome (KSS), and Leber hereditary optic neuropathy (LHON). Other clinical phenotypes comprising the ataxia-neuropathy spectrum, myoclonic epilepsy, myopathy and sensory ataxia (MEMSA)—also known as spino-cerebellar ataxia with epilepsy (SCAE) syndrome—mitochondrial neurogastrointestinal encephalomyopathy (MNGIE), and neuropathy, ataxia, and retinitis pigmentosa (NARP) syndromes, are less well known (Hakonen et al. 2005; Tzoulis et al. 2006; Finsterer and Zarrouk Mahjoub 2012) (see Table 2). Moreover, a significant proportion of cases with mitochondrial dysfunction have uncategorized non-specific encephalopathy syndromes.

Most mitochondrial disorders occur in childhood and produce a wide range of epileptic seizures, including generalized (myoclonic, tonic, tonic–clonic, atonic), simple focal, complex focal, and secondarily generalized seizures. Moreover, specific electro-clinical syndromes (Otahara syndrome, West syndrome, Lennox–Gastaut syndrome, Landau–Kleffner syndrome) can be caused by mitochondrial disorders (Lee et al. 2008).

From an imaging point of view, one should consider mitochondrial disorders in symmetric basal ganglia, brainstem, and cerebellum lesions (Barkovich et al. 1993, Saneto et al. 2008). The basal ganglia are selectively vulnerable to failure of energy metabolism; however, this pattern is not specific and may also occur in carbon monoxide poisoning, bilirubin toxicity, disorders of fat metabolism, organic acidurias, and others. Moreover, even a leukodystrophy pattern may reflect mitochondrial disease (Santorelli et al. 1993, Lebre et al. 2011). When oxidative phosphorylation is impaired, energy metabolism follows the alternative route of anaerobic glycolysis and produces lactic acid. Since lactate has a chemical shift of 1.3 ppm and presents as a doublet peak, H_1-MR spectroscopy is particularly helpful to diagnose mitochondrial disease.

1.2 Leigh Disease

Subacute necrotizing encephalomyelopathy.

1.2.1 Epidemiology

First described by Dennis Leigh in 1951 as a disease with recurrent acute episodes of neurodegeneration affecting brainstem, cerebellar, or basal ganglia function.

1.2.2 Pathogenesis

Autosomal recessive, X-linked recessive, or maternal inheritance with a variety of biochemical and molecular defects: 39 % complex I deficiency, 25 % pyruvate dehydrogenase deficiency, 25 % COX deficiency, 15 % ATPase mtDNA mutations.

1.2.3 Clinical Presentation

Severe and progressive infant and childhood encephalopathy with global developmental delay, feeding and

Table 2 Overview of common mitochondrial disorders

Mitochondrial disorder	Age of onset (years)	Major clinical signs	Classic pattern of inheritance	Genetic defect	MR imaging
Leigh	Majority <2	Progressive encephalopathy with brain stem dyfunctions.	Autosomal recessive, maternal, X-linked	Heterogeneous	Bilateral T2-/FLAIR hyperintensities of putamina, periaqueductal gray matter
MELAS	Mean 10 < 40	Stroke-like episodes, migraine-like episodes, hearing loss, myopathy, occasional seizure.	Maternal	$tRNA^{Leu}$: 3243A > G (>80 % of cases) *POLG1*	Cortical/subcortical lesions not related to a vascular territory with mixed DWI signal intensities
MERRF	Late adolescence/ early adulthood	Progressive myoclonus, focal and generalized epilepsy, cerebellar ataxia, deafness, myopathy, retinopathy.	Maternal	Maternal: $tRNA^{Lys}$: 8344A > G (80 % of cases) 3243A > G *POLG1*	Variable: cerebellar and cerebral atrophy, symmetric brainstem, basal ganglia lesions
Alpers-Huttenlocher	Very variable, typically <2	Visual phenomena, refractory seizures, liver failure acute after exposure to valproic acid.	Autosomal recessive	*POLG1*	Thalamus > occipital hyperintensities
LHON	Early adulthood	Visual loss, early optic disc microangiopathy/edema, later atrophy. Remission in some. Male carrier predominatly symptomatic.	Maternal	11778G > A 14484T > C 3460G > A	Normal or optic nerve/chiasm edema and enhancement (acute stage) or optic nerve/ chiasm atrophy (chronic stage)
CPEO/KSS	>10/<20	Ptosis, ophthalmoparesis/plus retinitis pigemtosa. Cerebellar ataxia, cardiac conduction defect, dementia, endocrine symptoms.	Mostly sporadic (50 %), autosomal dominant, autosomal recessive, maternal	Single/ multiple mtDNA deletions	Symmetric brainstem, basal ganglia, peripheral white matter hyperintenisities
MNGIE	<20	Progressive external ophthalmoplegia and ptosis, severe gastrointestinal dysmotility, cachexia, peripheral neuropathy. Epilepsy is not a feature.	Autosomal recessive	*Thymidine phosphorylase* gene mutations, rarely *POLG1*	Leukoencephalopathy sparing the corpus callosum
NARP	<20	Pigmentary retinopathy, peripheral axonal neuropathy, ataxia.	Maternal	8993T > G/C, with high heteroplasmic mutation load	Variable: pontocerebellar atrophy, leukoencephalopathy, ADEM-like, PVL-like, MELAS-like

swallowing difficulties, central respiratory hypoventilation, dystonia, optic atrophy, ataxia, nystagmus, seizures, hearing loss, lactic acidosis, and early death. Occurs rarely in adults.

1.2.4 Imaging

Rather symmetric T2-weighted hyperintense and partly contrast-enhancing lesions of the basal ganglia (putamen, globus pallidus, and caudate), thalami, midbrain (red nucleus, substantia nigra, and periaqueductal region), brainstem and dentate nuclei. Lesions reflect necrotic degeneration, capillary proliferation, and gliosis with an appearance similar to Wernicke's encephalopathy. Putaminal lesions are considered characteristic. Mamillary bodies may be involved, but some authors consider mamillary body involvement a hint for the presence of Wernicke's encephalopathy. In the acute stage, affected structures are swollen; in later stages, there is pronounced atrophy (Fig. 2).

1.3 MELAS

Mitochondrial myopathy, encephalopathy with lactic acidosis and stroke-like episodes.

1.3.1 Epidemiology

First described as a distinctive syndrome by Pavlakis in 1984 as a disease with high phenotypic variability.

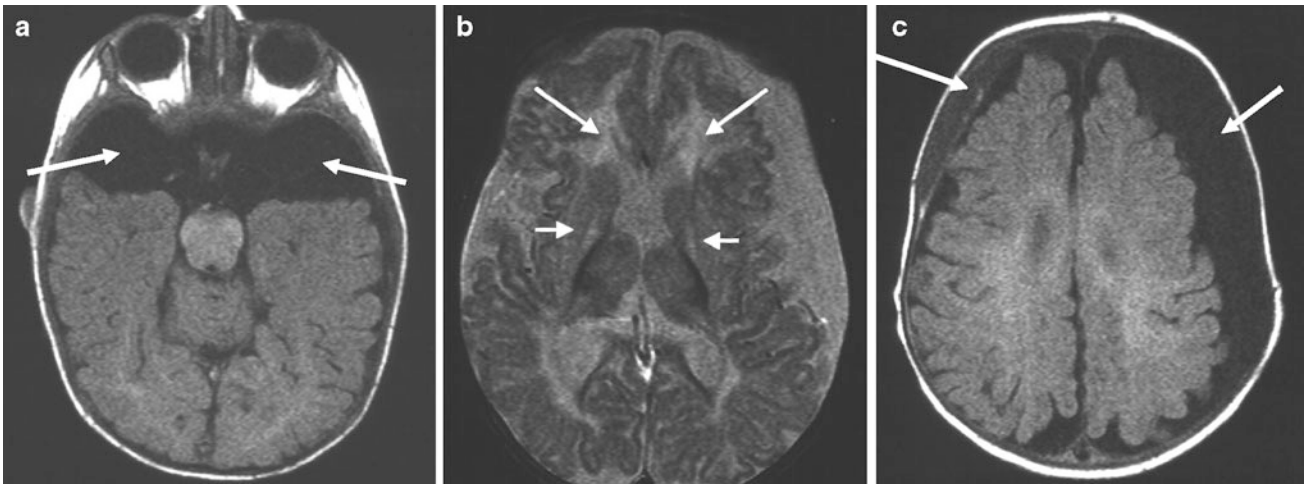

Fig. 1 Glutaric aciduria type 1 in a 7-month-old girl. MRI shows widened subarachnoid space and subdural hygromas/hematomas in the temporal poles and over the convexities (**a**, **c**: *arrows*). Due to ongoing myelination, the brain parenchyma is more difficult to assess. However, symmteric bilteral striatal (**b**: *short arrows*) and white matter abnormalities (**b**: *long arrows*) are notable

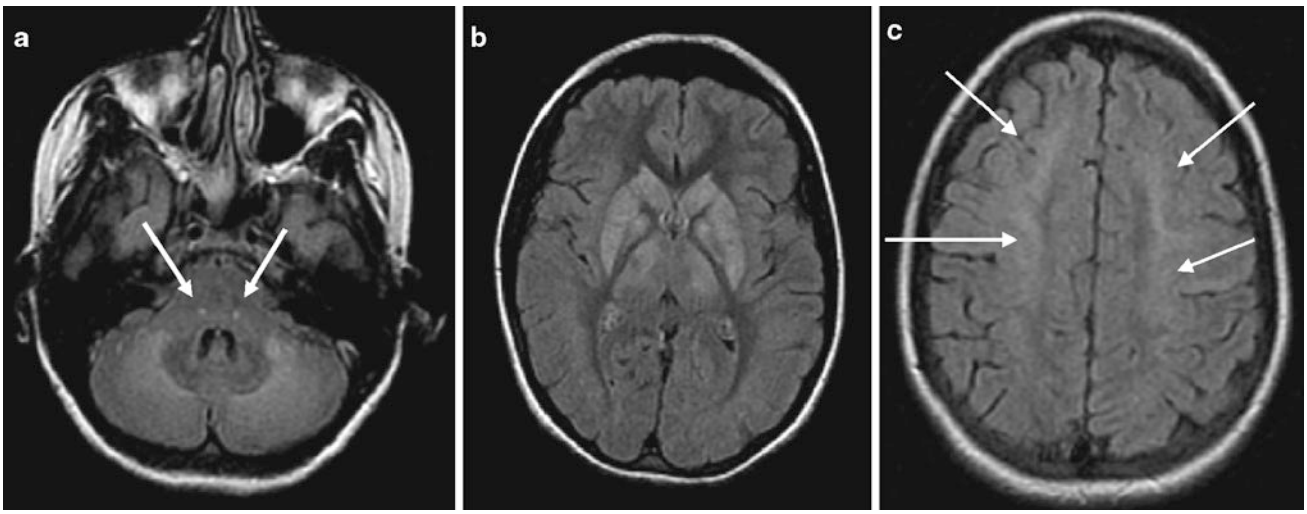

Fig. 2 A 20-year-old woman suffered from migraine with aura attacks and stroke-like epsiodes for several years. MRI showed symmetric globus pallidus, striatal, thalamic (**b**), and brainstem lesions (**a**: *arrows* pointing to the central tegmental tract) and diffuse cerebellar and cerebral white matter signal increase (**c**: *arrows*). This pattern is suggestive of Leigh disease, which is typically an acute disease in infancy. Muscular biopsy revealed mitochondrial cytopathy with complex IV > I deficiency

1.3.2 Pathogenesis

Several point mutations of mtDNA: Most common is the 3243A > G point mutation of the *MTTL1* gene encoding for mitochondrial $tRNA^{Leu}$ (>80 % of cases).

1.3.3 Clinical Presentation

Clinical triad of (1) stroke-like episodes before 40 years of age, typically <15 years of age, (2) encephalopathy characterized by seizures (85–90 %), dementia (50–90 %), or both, and (3) lactic acidosis, ragged red fibers on muscle biopsy, or both. Other frequent abnormalities include muscle weakness and early fatigability, sensorineural hearing loss (25–90 %), mostly axonal sensory peripheral neuropathy, diabetes mellitus, short stature (80 %), cardiomyopathy, cardiac conduction defects, and renal and gastrointestinal dysfunction. Seizures are commonly simple partial seizures, rarely epilepsia partialis continua (Ribacoba et al. 2006).

Stroke-like episodes are seen in virtually all MELAS patients and often have a stuttering onset, accompanied by a migraine-like prodrome with headache and vomiting lasting hours. The episodes have a predilection for the occipital and parietal lobes and result in homonymous hemianopia in up to 80 % of patients. Loss of consciousness is common, and other focal neurological deficits may also occur, including aphasia, alexia without agraphia, and hemiplegia.

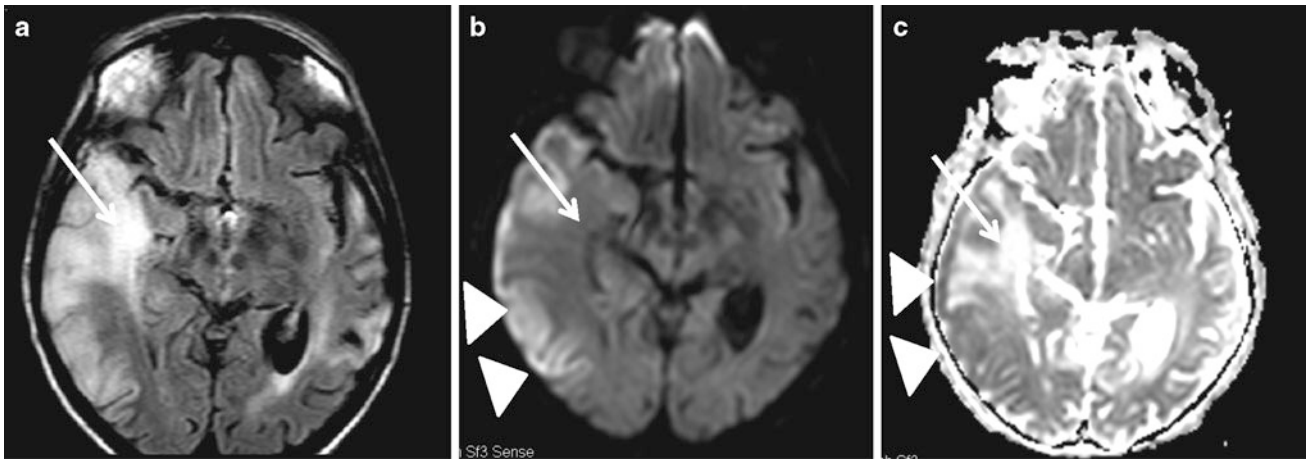

Fig. 3 MELAS in a 53-year-old woman who presented with complex focal seizures. Further medical history revealed long-known sensory hearing loss. MRI showed a space-occupying right temporal lesion and a left temporal defect. In MELAS, multifocal lesions are typically not confined to a vascular territory. Acute lesions often show reduced diffusion of the cortical (**b**, **c**: *arrowheads*) and increased diffusion of the white matter part of the lesion (**a**, **b**: *arrows*)

1.3.4 Imaging

Consider MELAS in patients with stroke-like episodes and lesions that are not confined to a vascular territory and do not show cytotoxic edema on DWI. A closer look, however, may reveal ribbon-like cytotoxic edema within the cortex. The posterior parts of the hemispheres are predominantly affected, and stroke-like lesions typically evolve into cortical–subcortical defects.

A significant portion of patients with 3243A > G point mutations have a non-MELAS phenotype without stroke-like episodes and either prominent deep gray matter calcifications (basal ganglia, dentate nuclei) or subtle globus pallidus lesions on T2-weighted gradient echo images (Fig. 3).

1.4 MERRF

Myoclonic epilepsy and ragged red fibers.

1.4.1 Epidemiology

First described by Berkovic in 1989 as a disease starting in adulthood with myoclonic seizures, muscular weakness, and ragged red fibers on muscle biopsy (Berkovic et al. 1989).

1.4.2 Pathogenesis

Maternal inheritance with mtDNA point mutations encoding $tRNA^{Lys}$. The 8344G > A mutation accounts for 80–90 % of cases.

1.4.3 Clinical Presentation

Broad spectrum, ranging from oligosymptomatic proximal myopathy to severe impairment with deafness, ataxia, spasticity, myoclonus, pigmentary retinopathy, optic atrophy, and dementia.

1.4.4 Imaging

No specific pattern. Cerebellar, brainstem and cortical atrophy. Symmetric T2-hyperintense brainstem (inferior olivary nuclei, superior cerebral peduncles, periaqueductal gray matter), basal ganglia lesions (striatal hyperintensities, globus pallidus calcifications), subcortical white matter, and cortical lesions may occur (Ito et al. 2008). Lesion pattern is not specifically different from other mitochondrial disorders such as, for instance, CPEO/KSS (Fig. 4).

1.5 Alpers–Huttenlocher Syndrome

Hepatocerebral degeneration

1.5.1 Epidemiology

Severe hepatocerebral disease with mtDNA depletion that presents at various ages depending on the type of mutation within the *POLG1* gene.

1.5.2 Pathogenesis

A gamut of *POLG1* mutations and changes of respiratory chain complexes, mtDNA, and *POLG1* activity far beyond the scope of this chapter have been reported. Online databases can provide a quick cross-reference of a case in question.

1.5.3 Clinical Presentation

Age at seizure onset is typically before the second year of life, but very variable and may occur as late as the sixth

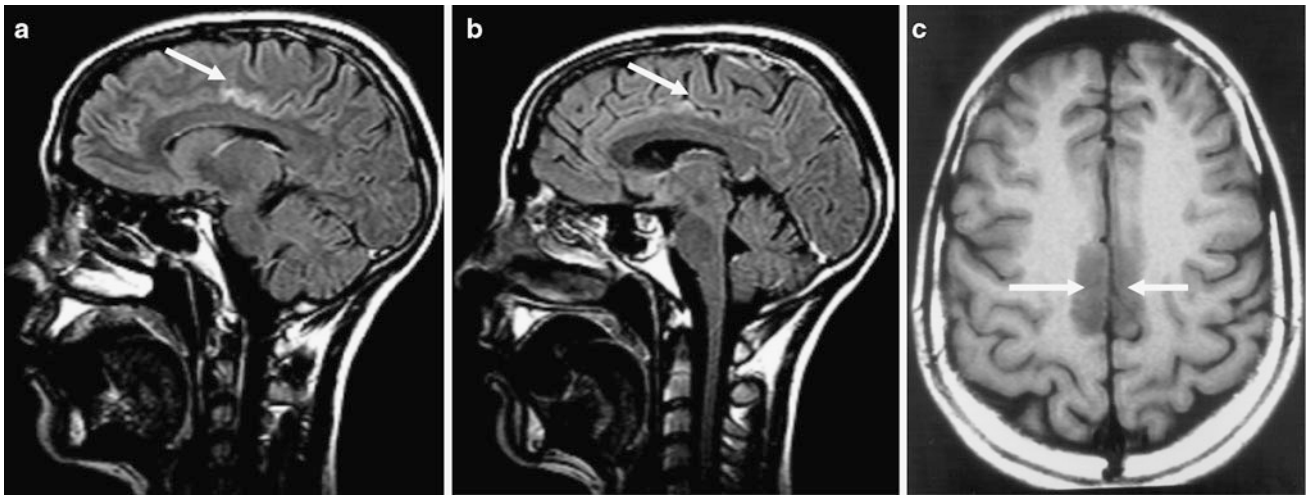

Fig. 4 A 29-year-old woman (**a**, **b**) and her 14-year-old brother (**c**) suffered from progressive myoclonic and generalized tonic–clonic seizures. Sagittal FLAIR (**a**, **b**) and axial T1-weighted MRI (**c**) showed bilateral cingulate gyrus lesions (*arrows*). MERRF with a 8344G > A mutation was diagnosed

decade. Initial features of occipital lobe dysfunction with flickering colored light, ictal visual loss, nystagmus, oculoclonus, and dysmorphopsia. Simple and complex focal seizures, clonic and/or myoclonic seizures with epilepsia partialis continua, frequent convulsive status epilepticus. Encephalopathic episodes are sometimes precipitated by fever. Liver dysfunction and liver failure elicited by valproic acid treatment (Engelsen et al. 2008).

1.5.4 Imaging

Initial MRI may be normal. With disease onset—commonly with seizures or epilepsia partialis continua—focal T2-/FLAIR high-signal-intensity changes in the thalami, occipital cortex, deep cerebellar structures, extraoccipital cortex, and inferior olivary nuclei of the medulla oblongata may occur. Brain and cerebellar atrophy develop (Fig. 5).

1.6 Chronic Progressive External Ophthalmoplegia and Kearns–Sayre Syndrome

1.6.1 Epidemiology

Chronic progressive external ophtalmoplegia (CPEO) is a frequent manifestation of mitochondrial disorders characterized by painless bilateral progressive ptosis and ophthalmoparesis. Kearns–Sayre syndrome is a more severe CPEO subtype, first described in 1958, with the features of retinitis pigmentosa, external opthalmoplegia, and complete heart block.

1.6.2 Pathogenesis

Sporadic > autosomal dominant, autosomal recessive, or maternally inherited disease with single (large) deletion (80% KSS) or mtDNA point mutations.

1.6.3 Clinical Presentation

Cardinal symptoms of CPEO are painless progressive bilateral ptosis and ophthalmoparesis, with ptosis typically preceding ophthalmoparesis by months to years. All extraocular muscles are symmetrically involved. Skeletal muscle weakness is present in most patients and may involve the neck, proximal limb, or bulbar musculature, with bifacial weakness the rule. CPEO frequently starts in childhood or early adulthood (90 %) but may occur at any age. It may be isolated or occur with other "mitochondrial" symptoms (pigmentary retinopathy, cataract, optic neuropathy, sensorineural hearing loss, ataxia, spasticity, peripheral neuropathy, encephalopathy, gastrointestinal dysmotility, cardiac conduction defects, respiratory insufficiency, hormonal and electrolyte imbalances, short stature, skin and skeletal abnormalities).

Kearns–Sayre syndrome (KSS) is a rather severe subtype of CPEO, defined by the following criteria: (1) onset before the age of 20; (2) CPEO; (3) one or more of the following: cardiac conduction abnormality, CSF protein >100 mg/dl, cerebellar dysfunction.

1.6.4 Imaging

Most common MRI findings are cortical, brainstem, and cerebellar atrophy with symmetrical (T1- and) T2-/FLAIR

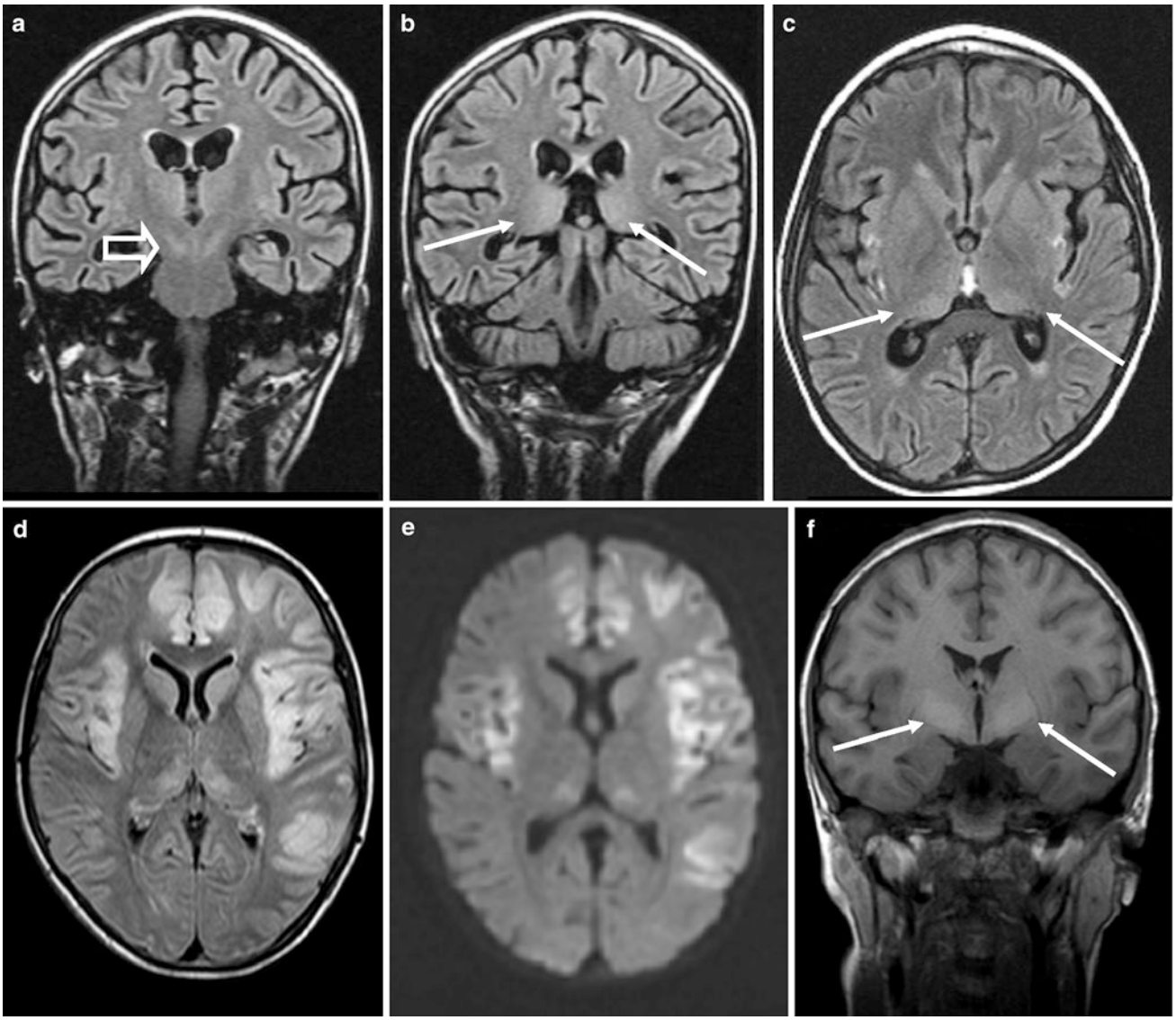

Fig. 5 Coronal and axial FLAIR images of a 7-year-old boy (**a**–**c**) and axial FLAIR (**d**), axial DWI (**e**), and coronal T1-weighted spin echo images (**f**) of a 12-year-old girl with *POLG1* mutations. Note the characteristic symmetrical, slightly increased signal intensity of the pulvinar thalami (**b**, **c**: *arrows*) and, to a lesser extent, of the substantia nigra (**a**: *open arrows*). A more severe MRI pattern is found in the 12-year-old girl, which shows widespread cortical with impaired diffusion next to the thalamic lesions. Symmetrical globus pallidus T1-hyperintensity (**f**: *arrows*) is likely due to liver failure

hyperintense lesions in the brainstem, basal ganglia, thalami, and subcortical white matter. The involvement of the subcortical U-fibers with sparing of the periventricular white matter helps to differentiate CPEO/KSS from most lysosomal and peroxisomal disorders (Fig. 6). Basal ganglia lesions may be calcified on CT. External ocular muscles are either normal or atrophic, which helps to differentiate CPEO/KSS from Graves' disease.

MR spectroscopy shows elevated lactate in lesional and nonlesional brain tissue.

1.7 Leber Hereditary Optic Neuropathy

1.7.1 Epidemiology

First defined as a clinical entity by the German ophthalmologist Theodore Leber in 1871.

1.7.2 Pathogenesis

Maternal inheritance with three common point mutations (11778G > A, 14484T > C, 3460G > A) affecting complex I of the mitochondrial respiratory chain in 96 % of patients.

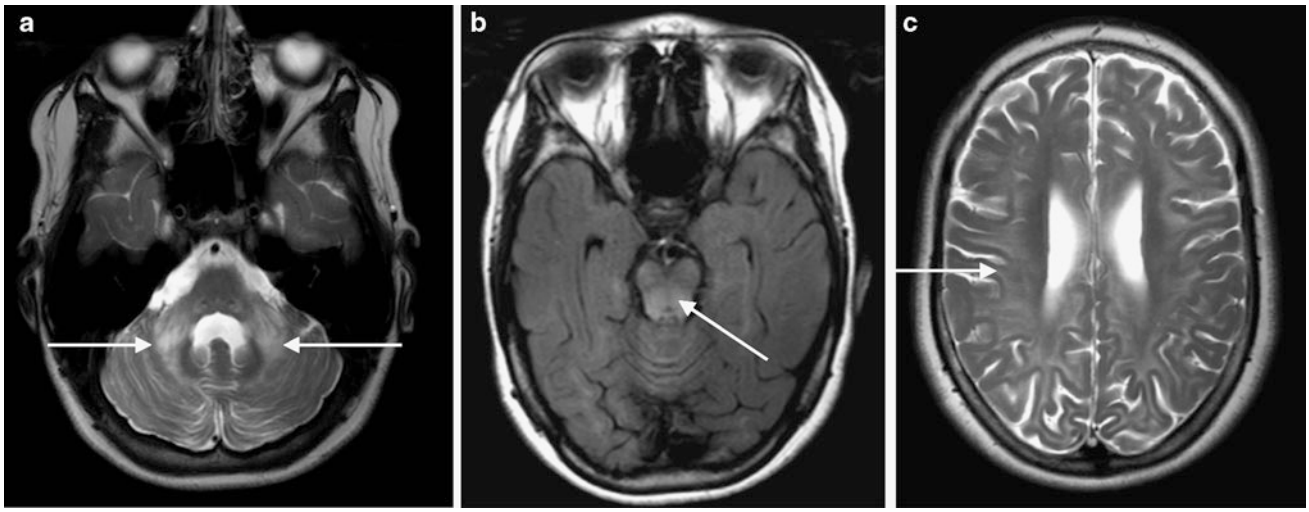

Fig. 6 Axial T2-weighted (**a**, **c**) and FLAIR images of a 15-year-old boy with ataxia, retinitis pigmentosa, and myopathy due to a Kearns–Sayre syndrome. MRI shows brainstem, cerebellar, and cerebral atrophy with symmetrical hyperintense lesions in the middle (**a**: *arrows*) and superior cerebral peduncles, in the dorsal brainstem, in and around the periaqueductal *gray* matter (**b**: *arrow*), and in white matter sparing the periventricular regions (**c**: *arrow*)

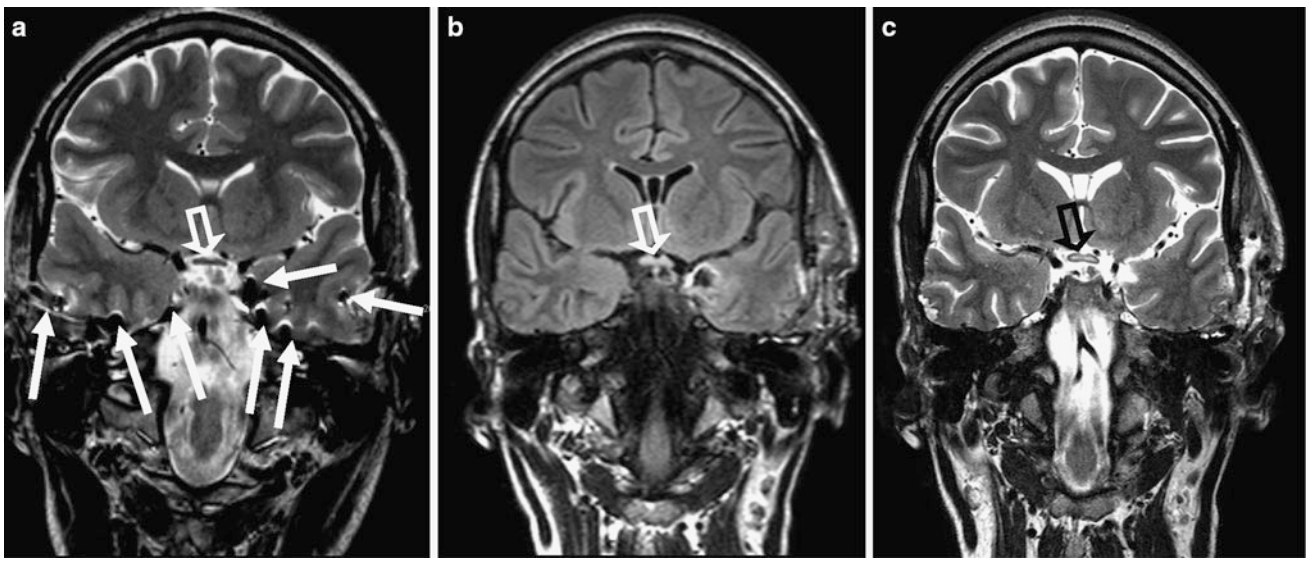

Fig. 7 Leber hereditary optic neuropathy (LHON) in a 27-year-old woman with temporal lobe epilepsy. Two to three weeks following the implantation of intrahippocampal depth and subdural strip electrodes (**a**: *arrows*), the patient developed progredient loss of vision. While the optic chiasm was initially normal (**a**: *hollow arrow*), MRI now showed optic chiasm edema with swelling and increased signal intensity (**b**, **c**: *hollow arrow*). Optic chiasm edema developing during presurgical evaluation is likely due to the use of barbiturates for general anesthesia, which are known to inhibit complex I of the mitochondrial respiratory chain

1.7.3 Clinical Presentation

Most common phenotype: rapid, painless loss of central vision in one eye, followed by similar loss of vision in the fellow eye within days to months. The onset of symptoms typically occurs between the ages of 15 and 35 years. ♂:♀ = 8:1. Sometimes the attack is precipitated by ethambutol. The individual tendency to recover depends on the respective mutation. Epilepsy is a rare feature.

1.7.4 Imaging

Most patients have a normal MRI. However, optic nerve and chiasm edema and contrast enhancement may be observed in the acute stage, and optic nerve and chiasm atrophy in the chronic stage, respectively (Inglese et al. 2001; Lamirel et al. 2010; Niehusmann et al. 2011). Rarely, extensive white matter demyelination has been described (Kovacs et al. 2005) (Fig. 7).

1.8 Pyruvate Dehyrogenase Complex Deficiency

1.8.1 Epidemiology

Well-defined mitochondrial disorder with a broad clinical spectrum: Many patients have either severe, often fatal, neonatal or infantile lactic acidosis and a phenotype resembling Leigh's disease or a more chronic neurodegenerative disease with episodes of lactic acidosis and recurrent ataxia. Even patients with relatively normal mental ability and with episodic dystonia, developing during childhood, have been described (Head et al. 2005; Barnerias et al. 2010).

1.8.2 Pathogenesis

PDH is a mitochondrial enzyme complex that catalyzes the conversion of pyruvate to acetyl coenzyme A. The complex contains multiple copies of three enzymes: E1 (PDH), E2 (dihydrolipoamide acetyltransferase), and E3 (dihydrolipoamide dehydrogenase).

1.8.3 Clinical Presentation

Consider two types:

1. Abnormal prenatal brain development resulting in severe nonprogressive encephalopathy with callosal agenesis, gyration anomalies, microcephaly with intrauterine growth retardation, or dysmorphia in both males and females.
2. Acute energy failure in infants producing basal ganglia lesions with paroxysmal dystonia, neuropathic ataxia due to axonal transport dysfunction, or epilepsy typically in males.

1.8.4 Imaging

Variable MRIs ranging from minor degrees of cerebral atrophy (often in patients with severe neonatal lactic acidosis) to gross cerebral atrophy with corpus callosum dysgenesis, widespread increased diffusion in the white matter, and bilateral subependymal cysts. Between these two groups are patients with a Leigh-like pattern consisting of symmetric basal ganglia, but not brainstem lesions (Head et al. 2005; Soares-Fernandes et al. 2008; Lebre et al. 2011).

2 Neuronal Ceroid Lipofuscinosis

2.1 Definition

Neuronal Ceroid Lipofuscinosis (CLN) is an autosomal recessive neurodegenerative disease with the accumulation of ceroid lipofuscin material in lysosymes of neurons and other cell types. The triad of blindness due to retinopathy, dementia, and epilepsy is considered characteristic for the childhood-onset forms, while adult and some juvenile varieties occur without visual loss. These diseases are progressive and lethal.

A previous classification based on disease onset, that is, infantile (Santavuori), late infantile (Janksy–Bielschowsky), juvenile (Spielmeyer–Vogt, Batten), and adult (Kufs), has been replaced by a gene-based classification. This has led to the discovery of "atypical" presentations, that is, adult cases of diseases formerly thought as childhood-onset disorders, widening the phenotypic spectrum.

Diagnosis is suspected on clinical grounds, with initial normal development and disease onset at a specific age with visual failure that may progress to blindness, myoclonic or tonic–clonic seizures, and progressive psychomotoric decline, including dementia and ataxia. Diagnosis can be confirmed by blood spot enzyme analysis or detection of characteristic lymphocyte vacuoles in some varieties; however, electron microscopic detection of characteristic granular osmiophilic deposits, curvilinear, fingerprint, and rectilinear profiles in lymphocytes or other tissues is needed for others.

2.2 Clinical Presentation

Table 3 lists the types of CLN according to typical age at onset.

2.3 Imaging

CLN will only be diagnosed with appropriate clinical information. The following imaging features support the clinical diagnosis:

Pronounced hypointensity of basal ganglia, thalami, substantia nigra/red nucleus on T2-weighted fast spin < gradient echo sequences (Autti et al. 2007)

Distinct atrophy of the supratentorial brain more than of the cerebellar hemispheres

Slightly increased (periventricular) T2 signal intensity

3 Progressive Myoclonic Epilepsies

3.1 Definition

Progressive myoclonic epilepsies are a group of disorders characterized by myoclonic seizures, tonic–clonic seizures, and progressive neurologic decline, in particular dementia and ataxia. Myoclonic seizures may be bilateral synchronous or multifocal asynchronous and affect limbs, facial, and bulbar muscles (see Table 4).

Table 3 Neuronal ceroid lipofuscinosis types according to typical age at onset

Disease type	Age at onset	Major clinical signs	Laboratory and genetic features
CLN 1 (infantile form, Santavuori)	1–2	Normal psychomotor development until the age of 6 months, rapid decline with epileptic seizures. Cardinal symptom is visual loss; most patients are blind before the age of 2	Reduced enzyme activity in blood spot test. Granular osmiophilic deposits in lymphocytes or other tissues at electron microscopy Autosomal recessive: *PPT1*
CLN 2 (late infantile form, Janksy–Bielschowsky)	2–4	Normal psychomotor development until the age of 2–4 years. Rapid decline with epileptic seizures (myoclonic, tonic–clonic, atonic, atypical absence) and retinal atrophy. Cardinal symptom is visual failure; most patients are blind around the age of 6	Reduced enzyme activity in blood spot test. Curvilinear membrane-bound lysosomal aggregates in electron microscopy Autosomal recessive: *TPP1*
CLN 5 (Finnish variant), 6, 7	Infancy	Progressive epilepsy with mental retardation. Tonic–clonic seizures, complex focal seizures with decreasing frequency after puberty, cognitive decline starting 2–5 years after onset of seizures	Granular osmiophilic deposits, curvilinear, fingerprint, and rectilinear profiles in electron microscopy Autosomal recessive: *CLN5, CLN6, MSFD8*
CNL8/Northern epilepsy	juvenile	Visual loss, developmental regression, seizures, ataxia, speech and language difficulties, myoclonus. No blindness, no myoclonus, slower progression in Northern Epilepsy	Mixed combinations of granular, curvilinear, and fingerprint profiles in EM Autosomal recessive *CLN8*
CLN 3 (juvenile form, Spielmeyer–Vogt, Batten)	5–10	Rapid decline of vision and progressive dementia. Myoclonic and tonic–clonic seizures. Death around 20–40 years	Typical vacuolated lymphocytes in blood smear (light microscope). Fingerprint profiles in electron microscopy Autosomal recessive: *CNL3*
CLN 4 (Kufs)	3rd–4th decade	Generalized seizures, myoclonus, dementia, ataxia, behavioral changes, depression, hallucinations, no blindness	"Fingerprint" deposits in lymphocytes or other tissues at electron microscopy Autosomal recessive 4A: *CLN6* or autosomal dominant 4B: *DNAJC5*

There are some very rare causes of progressive myoclonic epilepsies: Action Myoclonus–Renal Failure syndrome (AMRF) is an autosomal-recessive disorder characterized by proteinuria and glomerusclerosis occurring as early as 9 years of age, followed by severe progressive action myoclonus, dysarthria, and ataxia symptoms between 17 and 25 years of age (Ramachandran et al. 2009). In Gaucher disease type 3 (subacute neuronopathic form), abnormal glucocerebrosidase accumulates in the liver, spleen, and bone marrow. Predominant clinical symptoms are hepatosplenomegaly, hematological changes, and skeletal complications (Ramachandran et al. 2009; Kraoua et al. 2011; Shahwan et al. 2005). Familial encephalopathy with neuroserpin inclusion bodies is an autosomal-dominant disease causing progressive dementia and in some cases a familial form of progressive myoclonic epilepsy (Davis et al. 1999). A juvenile form of Huntington's disease may also cause progressive myoclonic epilepsy (Gambardella et al. 2001).

4 Epilepsy with Occipital Calcifications and Celiac Disease

4.1 Epidemiology

A rare syndrome with celiac disease, epilepsy, and cerebral calcifications (CEC syndrome) initially described by Sammaritano et al. (1985). Occipital calfications are radiologically similar to those of Sturge–Weber syndrome. For unknown reasons, CEC syndrome is more frequent in Italy, Spain, and Argentina (Gobbi 2005). Patients with celiac disease and epilepsy without calcifications and with celiac disease and calcifications without epilepsy are considered to suffer from atypical forms. In patients with epilepsy and calcifications without celiac disease, silent celiac disease is assumed.

4.2 Pathogenesis

Celiac disease is an autoimmune disease with chronic inflammation of the small intestine due to a permanent intolerance to gluten protein; a gluten-free diet leads to clinical improvement.

The coincidence of celiac disease and epilepsy with cerebral calcifications may be random, genetically determined, or epilepsy with cerebral calcifications the consequence of untreated celiac disease. Histopathological specimens showed small cortical veins overlying the parieto-occipital cortex with calcified walls and intima fibrosis nearly occluding the lumen. Cerebral calcifications are similar to those of Sturge–Weber syndrome; however, the cortical architecture is likely less preserved and patients do not have portwine nevi (Taly et al. 1987).

Table 4 Progressive myoclonic epilepsies: Major clinical features, diagnostics, and MRI

Progressive myoclonic epilepsies	Age at onset, major clinical signs	Laboratory features and genetics	MRI
Unverricht–Lundborg disease	6–13, Progresses in gradual stages to severe myoclonus, mild mental deterioration and ataxia	Autosomal recessive: *CSTB*	Normal or brain stem, cerebellar, and less often cerebral atrophy (Mascalchi et al. 2002)
Lafora body disease	8–18, Relatively rapid progression from insidious onset to severe myoclonus, occipital seizures, visual hallucinations, psychosis, dementia. Survival approximately 10 years	Lafora (polyglucosan inclusion) bodies in various tissues, including skin, autosomal recessive: *EPM2A, NHLRC1 (EPM2B)*,	No signal changes (Villanueva et al. 2006)
Myoclonic epilepsy and ragged red fibers (MERRF)	Late adolescence/early adulthood. Deafness, optic atrophy, myoclonus, myopathy, cardiac conduction defects	Maternal: $tRNA^{Lys}$, (80 % 8344G > A) ragged red fibers (SDH positive, COX negative) on muscle biopsy (but may be normal)	Variable: cerebellar and cerebral atrophy, symmetric brain stem, basal ganglia lesions
Sialidosis type 1 (neuraminidase deficiency)	8–20, Severe myoclonus, tonic–clonic seizures, visual failure, ataxia, nystagmus, muscle weakness and atrophy, dysarthria	Macula: cherry red spot. Urine: elevated sialyloligosaccharides. Leukocytes and cultured skin fibroblasts: neuraminidase deficiency autosomal recessive: *NEU1*	No signal changes
Sialidosis type 2 (neuraminidase deficiency)	Congenital—20, severe myoclonus, ataxia, visual failure, hearing loss, dysmorphic features, hepato-splenomegaly	Macula: cherry red spot. Urine: elevated sialyloligosaccharides. Leukocytes and cultured skin fibroblasts: neuraminidase deficiency, vacuolated lymphocytes, bone marrow foam cells autosomal recessive: *NEU1*	No signal changes
Neuronal ceroid lipofuscinosis	Congenital to adult forms	Electron microscopy: granular osmiophilic, curvilinear, or fingerprint profiles	Variable: cerebellar and cerebral atrophy, T2 hypointensity of globi pallidi and thalami
Dentatorubral-pallidolysian atrophy (DRPLA)	Higher frequency in Japan (0.2–0.7/100,000), very rare in Europe and North America. Myoclonic epilepsy and cognitive decline starting before the age of 20 (Whaley et al. 2011). Myoclonic epilepsy, dementia, ataxia, and choreoathetosis	CAG repeat expansion of DRPLA (*ATN1*) gene, autosomal dominant; clinical features and age of onset are correlated with the size of CAG repeats (1st–7th decade), genetic anticipation	Cerebellar and brainstem atrophy, high periventricular white matter T2 signal (Whaley et al. 2011; Muñoz et al. 2004)

4.3 Clinical Presentation

Celiac disease typically manifests in the first 2 years of life with chronic diarrhea, weight loss, dystrophic appearance, and anorexia. Atypical or silent forms are more frequent in children over 2 years and adults and characterized by nonbowel involvement and extraintestinal symptoms such as dermatitis herpetiformis and dental enamel defects.

Focal seizures occur in up to 5 % of patients with celiac disease and originate in at least 90 % of cases in the occipital cortex. Half of these seizures persist despite a gluten-free diet, and 25 % of patients develop an encephalopathic syndrome.

Accordingly, all patients with epilepsy and cerebral calcifications should be investigated for celiac disease following the ESPGAN criteria, which may include jejunal mucosa biopsy before and—if positive—1 year after adoption of gluten-free diet (Walker-Smith et al. 1990).

4.4 Imaging

Characteristic features are bilateral, symmetrical, or somewhat asymmetrical occipital calcifications, without contrast enhancement and brain atrophy. Calcifications can be punctate or amorphous measuring several centimeters. Additional calcifications can be in extraoccipital location. Calcifications may increase in size and new calfications may appear in midterm follow-up. In contrast to Sturge–Weber syndrome, circumscript atrophy, contrast enhancement, and ipsilateral choroid plexus enlargement are lacking (Fig. 8).

5 Nonketotic Hyperglycemia

5.1 Epidemiology

Nonketotic hyperglycemia is a relatively common complication of diabetes mellitus type 2, especially in patients

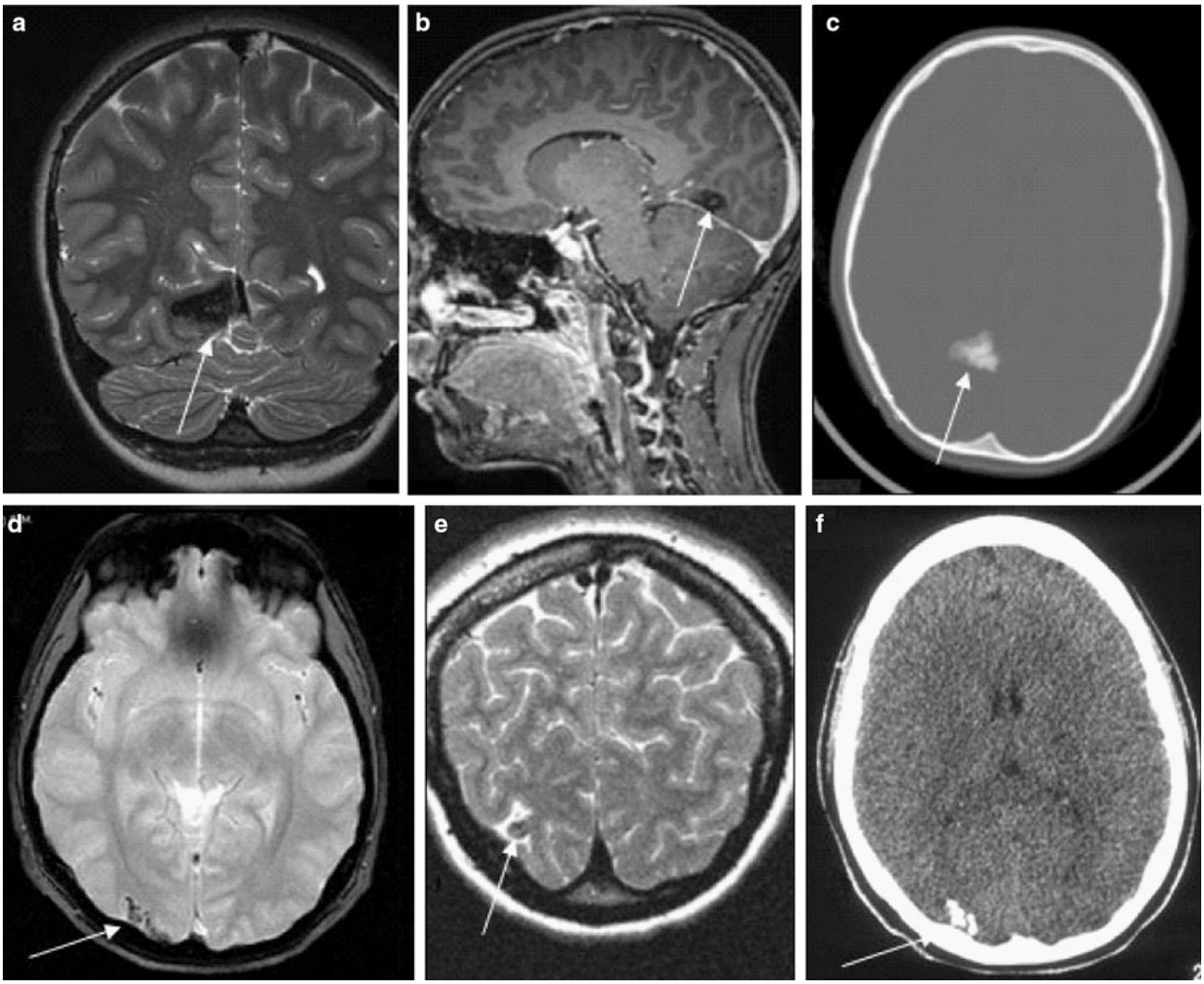

Fig. 8 Epilepsy with occipital calcifications and celiac disease in a 12-year-old girl (**a–c**) and in a 19-year-old woman (**d–f**). Occipital calcifications may be bilateral and resemble Sturge–Weber angiomatosis, which was also the histopathological diagnosis in the 19-year-old woman

above 50 years of age. However, several cases in children have been described. The severity can vary widely, ranging from asymptomatic (for months, even years) to severely symptomatic (hyperosmolar coma and sometimes even death). Approximately 15–40 % of patients with nonketotic hyperglycemia develop seizures.

5.2 Clinical Presentation

Focal motor seizures, which may generalize secondarily, are observed in most cases, sometimes with epilepsia partialis continua. Seizures may be tonic, clonic, tonic–clonic; may affect limbs, the face, or one half of the body; and may be followed by a postictal motor deficit. Seizures are sometimes elicited or set off by movement, even passive or active elevation of a limb (arm or leg). EEG between seizures is normal.

Rapid recognition of nonketotic hyperglycemia is vital because treatment with insulin and rehydration can prevent negative outcomes. Diagnosis is also essential for management of the seizures because they are usually refractory to antiepileptic drugs, and some treatments (phenytoin) may even aggravate them. These seizures nonetheless stop spontaneously after hyperglycemia is corrected.

5.3 Imaging

Often normal. Rarely and in close temporal relationship to seizures restricted diffusion reflecting cytotoxic edema on DWI and/or transient subcortical T2-weighted and FLAIR

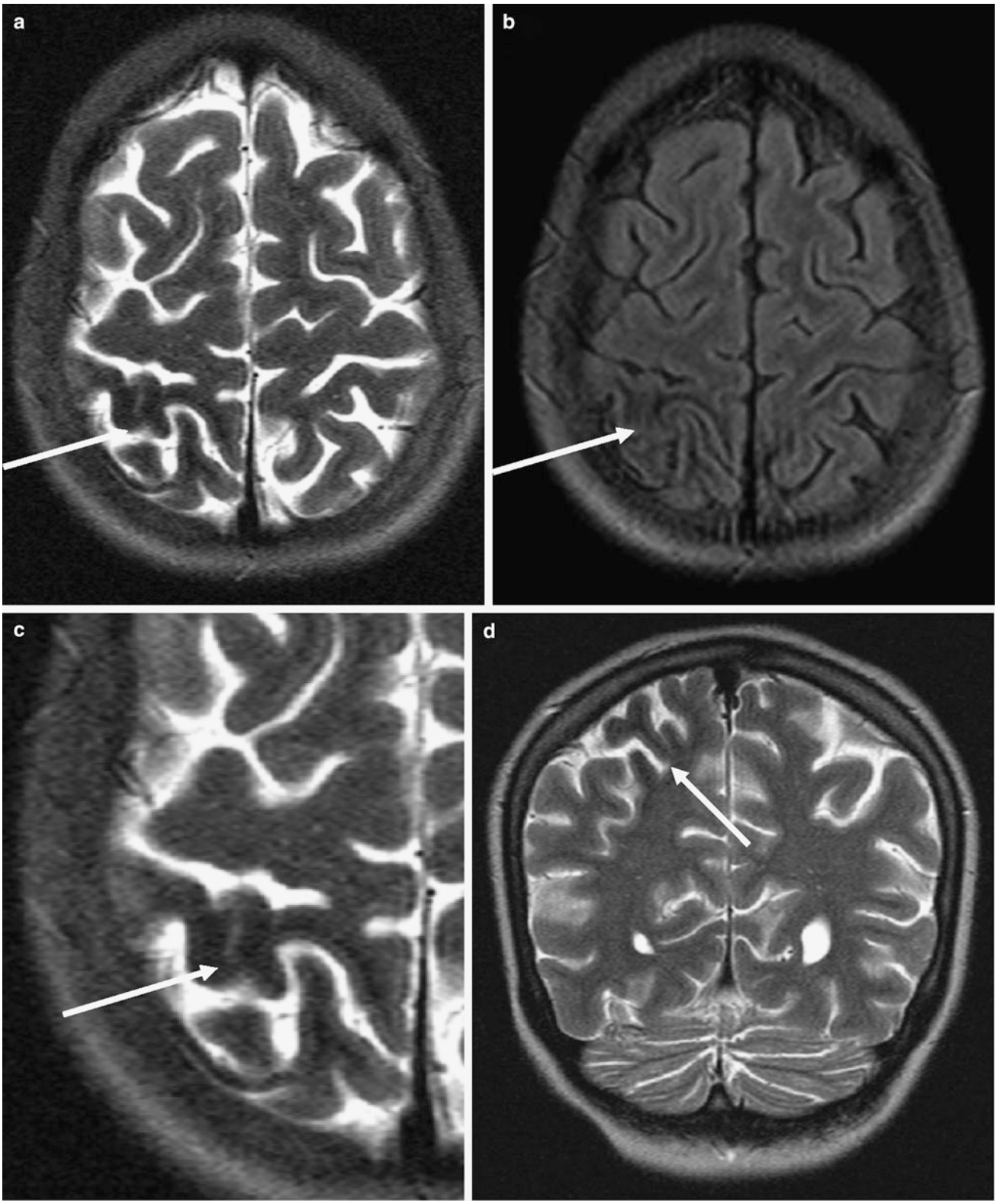

Fig. 9 A 16-year-old girl with known type 1 diabetes mellitus developed epilepsia partialis continua of the left hand. MRI displayed a subcortical T2-hypointensity of the postcentral gyrus on T2-weighted (**a**, **c**, **d**: *arrows*) and FLAIR images (**b**) associated with nonketotic hyperglycemia

hypointensity predominantly in the posterior brain regions (Wang et al. 2005; Raghavendra et al. 2007). Unilateral striatal hyperintensity is another hint for nonketotic hyperglycemia (Chu et al. 2002) (Fig. 9).

References

Appignani BA, Kaye EM, Wolpert SM (1996) CT and MR appearance of the brain in two children with molybdenum cofactor deficiency. AJNR Am J Neuroradiol 17(2):317–320

Autti T, Joensuu R, Aberg L (2007) Decreased T2 signal in the thalami may be a sign of lysosomal storage disease. Neuroradiology 49(7):571–578

Barkovich AJ, Good WV, Koch TK, Berg BO (1993) Mitochondrial disorders: analysis of their clinical and imaging characteristic. AJNR Am J Neuroradiol 14:1119–1137

Barkovich AJ, Peck WW (1997) MR of Zellweger syndrome. AJNR Am J Neuroradiol 18(6):1163–1170

Barkovich AJ (2007) An approach to MRI of metabolic disorders in children. J Neurorad 34:75–78

Barnerias C, Saudubray JM, Touati G et al (2010) Pyruvate dehydrogenase complex deficiency: four neurological phenotypes with differing pathogenesis. Dev Med Child Neurol 52:e1–e9

Berkovic SF, Carpenter S, Evans A et al (1989) Myoclonus epilepsy and ragged-red fibres (MERRF). 1. A clinical, pathological, biochemical, magnetic resonance spectrographic and positron emission tomographic study. Brain 112:1231–1260

Brismar J, Ozand PT (1994) CT and MR of the brain in disorders of the propionate and methylmalonate metabolism. AJNR Am J Neuroradiol 15(8):1459–1473 Review

Brismar J, Ozand PT (1995) CT and MR of the brain in glutaric acidemia type I: a review of 59 published cases and a report of 5 new patients. AJNR Am J Neuroradiol 16(4):675–683

Chu K, Kang DW, Kim DE et al (2002) Diffusion-weighted and gradient echo magnetic resonance findings of hemichorea-hemiballismus associated with diabetic hyperglycemia: a hyperviscosity syndrome? Arch Neurol 59:448–452

Davis RL, Holohan PD, Shrimpton AE et al (1999) Familial encephalopathy with neuroserpin inclusion bodies. Am J Pathol 155:1901–1913

de Koning TJ, Jaeken J, Pineda M et al (2000) Hypomyelination and reversible white matter attenuation in 3-phosphoglycerate dehydrogenase deficiency. Neuropediatrics 31(6):287–292

de Koning TJ, Klomp LW (2004) Serine-deficiency syndromes. Curr Opin Neurol 17(2):197–204

Desai S, Ganesan K, Hegde A (2008) Biotinidase deficiency: a reversible metabolic encephalopathy—neuroimaging and MR spectroscopic findings in a series of four patients. Pediatr Radiol 38:848–856

Engelsen BA, Tzoulis C, Karlsen B et al (2008) POLG1 mutations cause a syndromic epilepsy with occipital lobe predilection. Brain 131:818–828

Engelbrecht V, Rassek M, Huismann J, Wendel U (1997) MR and proton MR spectroscopy of the brain in hyperhomocysteinemia caused by methylenetetrahydrofolate reductase deficiency. AJNR Am J Neuroradiol 18(3):536–539

Finsterer J, Zarrouk Mahjoub S (2012) Epilepsy in mitochondrial disorders. Seizure 21:316–321

Gambardella A, Muglia M, Labate A et al (2001) Juvenile Huntington's disease presenting as progressive myoclonic epilepsy. Neurology 57(4):708–711

Gobbi G (2005) Coeliac disease, epilepsy and cerebral calcifications. Brain Dev 27:189–200

Gordon N (2004) Succinic semialdehyde dehydrogenase deficiency (SSADH) (4-hydroxybutyric aciduria, gamma-hydroxybutyric aciduria). Eur J Paediatr Neurol 8(5):261–265

Gospe SM Jr (2010) Pyridoxine-dependent epilepsy and pyridoxine phosphate oxidase deficiency: unique clinical symptoms and nonspecific EEG characteristics. Dev Med Child Neurol 52(7):602–603

Haas R, Dietrich R (2004) Neuroimaging of mitochondrial disorders. Mitochondrion 4:471–490

Haeberle J, Shahbeck N, Ibrahim K et al (2012) Glutamine supplementation in a child with inherited GS deficiency improves the clinical status and partially corrects the peripheral and central amino acid imbalance. Orphanet J Rare Dis 7(1):48

Hakonen AH, Heiskanen S, Juvonen V et al (2005) Mitochondrial DNA polymerase W748S mutation: a common cause of autosomal recessive ataxia with ancient European origin. Am J Hum Genet 77(3):430–441 (Epub 2005 Jul 27)

Head RA, Brown RM, Zolkipli Z et al (2005) Clinical and genetic spectrum of pyruvate dehydrogenase deficiency: dihydrolipoamide acetyltransferase (E2) deficiency. Ann Neurol 58:234–241

Huisman TA, Thiel T, Steinmann B, Zeilinger G, Martin E (2002) Proton magnetic resonance spectroscopy of the brain of a neonate with nonketotic hyperglycinemia: in vivo-in vitro (ex vivo) correlation. Eur Radiol 12(4):858–861

Inglese M, Rovaris M, Bianchi S et al (2001) Magnetic resonance imaging, magnetisation transfer imaging, and diffusion weighted imaging correlates of optic nerve, brain, and cervical cord damage in Leber's hereditary optic neuropathy. J Neurol Neurosurg Psychiatry 70(4):444–449

Ito S, Shirai W, Asahina M, Hattori T (2008) Clinical and brain MR imaging features focusing on the brain stem and cerebellum in patients with myoclonic epilepsy with ragged-red fibers due to mitochondrial A8344G mutation. Am J Neuroradiol AJNR 29(2):392–395

Jan W, Zimmerman RA, Wang ZJ et al (2003) MR diffusion imaging and MR spectroscopy of maple syrup urine disease during acute metabolic decompensation. Neuroradiology 45(6):393–399

Klepper J, Leiendecker B (2007) GLUT1 deficiency syndrome—2007 update. Dev Med Child Neurol 49(9):707–716

Kono K, Okano Y, Nakayama K et al (2005) Diffusion-weighted MR imaging in patients with phenylketonuria: relationship between serum phenylalanine levels and ADC values in cerebral white matter. Radiology 236(2):630–636

Kovacs GG, Höftberger R, Najtenyl K et al (2005) Neuropathology of white matter disease in Lebers hereditary optic neuropathy. Brain 128:35–41

Kraoua I, Sedel F, Caillaud C et al (2011) A French experience of type 3 Gaucher disease: phenotypic diversity and neurological outcome of 10 patients. Brain Dev 33(2):131–139

Lamirel C, Cassereau J, Cochereau I et al (2010) Papilloedema and MRI enhancement of the prechiasmal optic nerve at the acute stage of Leber hereditary optic neuropathy. J Neurol Neurosurg Psychiatry 81(5):578–580

Lebre AS, Rio M, Faivre d'Arcier L et al (2011) A common pattern of brain MRI imaging in mitochondrial diseases with complex I deficiency. J Med Genet 48(1):16–23

Lee YM, Kang HC, Lee JS et al (2008) Mitochondrial respiratory chain defects: underlying etiology in various epileptic conditions. Epilepsia 49:685–690

Mascalchi M, Michelucci R, Cosottini M et al (2002) Brainstem involvement in Unverricht–Lundborg disease (EPM1): An MRI and (1)H MRS study. Neurology 58(11):1686–1689

Mills PB, Footitt EJ, Mills KA et al (2010) Genotypic and phenotypic spectrum of pyridoxine-dependent epilepsy (ALDH7A1 deficiency). Brain 133(Pt 7):2148–2159

Muñoz E, Campdelacreu J, Ferrer I et al (2004) Severe cerebral white matter involvement in a case of dentatorubropallidoluysian atrophy studied at autopsy. Arch Neurol 61(6):946–949

Niehusmann P, Surges R, von Wrede RD, Elger CE, Wellmer J, Reimann J, Urbach H, Vielhaber S, Bien CG, Kunz WS (2011) Mitochondrial dysfunction due to Leber's hereditary optic neuropathy as a cause of visual loss during assessment for epilepsy surgery. Epilepsy Behav 20(1):38−43

Pearl PL, Gibson KM (2004) Clinical aspects of the disorders of GABA metabolism in children. Curr Opin Neurol 17(2):107–113

Pearl PL, Gibson KM, Acosta MT (2003a) Clinical spectrum of succine semialdehyde dehyfrogenase deficiency. Neurology 60:1413–1417

Pearl PL, Novotny EJ, Acosta MT et al (2003b) Succinic semialdehyde dehydrogenase deficiency in children and adults. Ann Neurol 54(Suppl 6):S73–S80

Pearl PL, Shukla L, Theodore WH et al (2011) Epilepsy in succinic semialdehyde dehydrogenase deficiency, a disorder of GABA metabolism. Brain Dev 33:769–805

Prasad AN, Levin S, Rupar CA, Prasad C (2011a) Menkes disease and infantile epilepsy. Brain Dev 33:866–876

Prasad AN, Rupar CA, Prasard C (2011b) Methylene tetrahydrofolate reductase (MTHFR) deficiency and infantile epilepsy. Brain Dev 33:758–789

Press GA, Barshop BA, Haas RH et al (1989) Abnormalities of the brain in nonketotic hyperglycinemia: MR manifestations. AJNR Am J Neuroradiol 10(2):315–321

Raghavendra S, Ashalatha R, Sanjee V et al (2007) Focal neuronal loss, reversible subcortical focal T2 hypointensity in seizures with a nonketotic hyperglycemic hyperosmolar state. Neuroradiology 49:299–305

Ramachandran N, Girard JM, Turnbull J, Minassian BA (2009) The autosomal recessively inherited progressive myoclonus epilepsies and their genes. Epilepsia 50(Suppl 5):29–36

Ribacoba R, Salas-Puig J, Gonzalez C, Astudillo A (2006) Characteristics of status epilepticus in MELAS. Analysis of four cases. Neurologia 21:1–11

Sammaritano M, Andermann F, Helanson D et al (1985) The syndrome of epilepsy and bilateral occipital cortical calcifications. Epilepsia 26:530

Saneto RP, Friedman SD, Shaw DWW (2008) Neuroimaging of mitochondrial disease. Mitochondrion 8:296–413

Santavuori P, Vanhanen SL, Sainio K et al (1993) Infantile neuronal ceroid-lipofuscinosis (INCL): diagnostic criteria. J Inherit Metab Dis 16(2):227–229 (Review)

Santorelli FM, Shanske S, Macaya A et al (1993) The mutation at nt 8993 of mitochondrial DNA is a common cause of Leigh's syndrome. Ann Neurol 34:827–834

Saudubray JM, Sedel F, Walter JH (2006) Clinical approach to treatable inborn metabolic diseases: an introduction. J Inherit Metab Dis 29(2–3):261–274

Sedel F, Gourfinkel-An I, Lyon-Caen O et al (2007) Epilepsy and inborn errors of metabolism in adults: a diagnostic approach. J Inherit Metab Dis 30(6):846–854

Seijo-Martínez M, Navarro C, Castro del Río M et al (2005) L-2-hydroxyglutaric aciduria: clinical, neuroimaging, and neuropathological findings. Arch Neurol 62(4):666–670

Sener RN (2003) Nonketotic hyperglycinemia: diffusion magnetic resonance imaging findings. J Comput Assist Tomogr 27(4):538–540

Sévin M, Lesca G, Baumann N et al (2007) The adult form of Niemann–Pick disease type C. Brain 130(Pt 1):120–133

Shahwan A, Farrell M, Delanty N (2005) Progressive myoclonic epilepsies: a review of genetic and therapeutic aspects. Lancet Neurol 4(4):239–248

Soares-Fernandes JP, Teixeira-Gomes R, Cruz R et al (2008) Neonatal pyruvate dehydrogenase deficiency due to a R302H mutation in the *PDHA1* gene: MRI findings. Pediatr Radiol 38:559–562

Stöckler S, Holzbach U, Hanefeld F et al (1994) Creatine deficiency in the brain: a new, treatable inborn error of metabolism. Pediatr Res 36(3):409–413

Stöckler-Ipsiroglu S, Plecko B (2009) Metabolic epilepsies: approaches to a diagnostic challenge. Can J Neurol Sci 36(Suppl 2):S67–S72

Taly AB, Nagaraja D, Das S et al (1987) Sturge–Weber–Dimitri disease without facial nevus. Neurology 37:1063–1064

Thomas B, Al Dossary N, Widjaja E (2010) MRI of childhood epilepsy due to inborn errors of metabolism. AJR Am J Roentgenol 194(5):W367–W374

Tzoulis C, Engelsen BA, Telstad W et al (2006) The spectrum of clinical disease caused by the *A467T* and *W748S* POLG mutations: a study of 26 cases. Brain 129(Pt 7):1685–1692

Van der Knaap M, Valk J (2005) GM2 gangliosidosis. In: Magnetic resonance of myelin and myelination disorders, 3rd edn. Springer, Berlin, Heidelberg, New York, pp 103–111

Vanhanen SL, Raininko R, Autti T, Santavuori P (1995) MRI evaluation of the brain in infantile neuronal ceroid-lipofuscinosis. Part 2: MRI findings in 21 patients. J Child Neurol 10(6):444–450

Vijayakumar K, Gunny R, Grunewald S et al (2011) Clinical neuroimaging features and outcome in molybdenum cofactor deficiency. Pediatr Neurol 45(4):246–252

Villanueva V, Alvarez-Linera J, Gómez-Garre P et al (2006) MRI volumetry and proton MR spectroscopy of the brain in Lafora disease. Epilepsia 47(4):788–792

Walker-Smith JA, Guendalini S, Schmitz J et al (1990) Revised criteria for diagnosis of coeliac disease. Arch Dis Child 65:909–911

Wang CP, Hsieh PF, Chen CC et al (2005) Hyperglycemia with occipital seizures: images and visual evoked potentials. Epilepsia 46:1140–1144

Weller S, Rosewich H, Gärtner J (2008) Cerebral MRI as a valuable diagnostic tool in Zellweger spectrum patients. J Inherit Metabol Dis 31:270–280

Whaley NR, Fukoja S, Wszolek ZK (2011) Autosomal dominant cerebellar ataxia type I: a review of the phenotypic and genotypic characteristics. Orphanet J Rare Dis 6:33

Wolf B, Grier RE, Allen RJ et al (1983) Biotinidase deficiency: the enzyme defect in late-onset multiple carboxylase deficiency. Clin Chem Acta 131:273–281

Wolf B, Heard GS, Weissbecker KA et al (1985) Biotinidase deficiency: initial clinical features and rapid diagnosis. Ann Neurol 18(5):614–617

Other Epilepsy-Associated Diseases and Differential Diagnoses

Horst Urbach

Contents

H. Urbach (✉)
Department of Neuroradiology,
University Hospital Freiburg, Germany
e-mail: horst.urbach@uniklinik-freiburg.de

Abstract

This chapter summarizes (1) rare diseases with epilepsy as the core feature and a specific MRI pattern, (2) common diseases with specific clinical features but without epilepsy as the core feature, and (3) MRI changes associated with antiepileptic drug therapy.

1 Hemiconvulsion–Hemiplegia–Epilepsy Syndrome

1.1 Epidemiology

The clinical syndrome was initially described by Schaffer (1927) and coined as hemiconvulsion–hemiplegia–epilepsy syndrome by Gastaut et al. (1960). It is one of the sequelae of convulsive status epilepticus. Its incidence has dramatically decreased since the 1970s due to successful medical therapy of convulsive status epilepticus.

1.2 Pathogenesis

A high metabolic demand of a hemisphere due to convulsive status epilepticus likely leads to laminar necrosis and edema in cortical layers 3 and 5 extending through the hemisphere and including the hippocampal, especially in its CA1 sector. In the acute phase, there is hemispheric hyperperfusion which is followed by hypoperfusion starting at around day 3. Within weeks to months, profound hemiatrophia cranii et cerebri develops.

1.3 Clinical Presentation

Hemiconvulsion–hemiplegia–epilepsy syndrome is characterized by prolonged clonic seizures which in most cases develop in the course of a febrile illness with consecutive

H. Urbach (ed.), *MRI in Epilepsy*, Medical Radiology. Diagnostic Imaging,
DOI: 10.1007/174_2012_750, © Springer-Verlag Berlin Heidelberg 2013

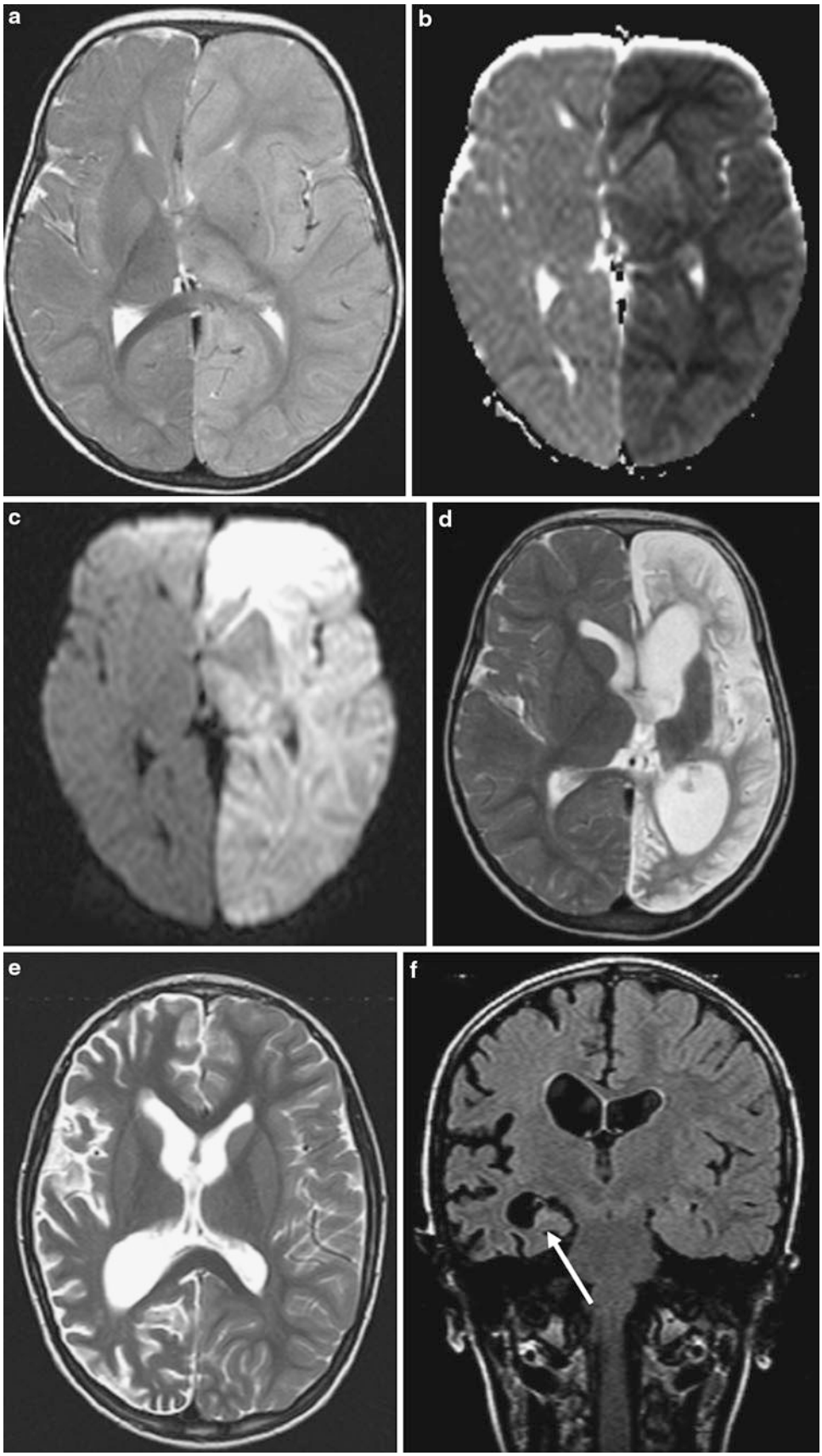

Fig. 1 MRI of a 13 months old girl with cytotoxic edema of the left hemisphere (**a**–**c**) including the thalamus and occipital lobe (**a**–**c**). No vessel occlusion on TOF-MRA (not shown). Follow-up MRI after 1 year shows profound left-sided hemiatrophia cerebri et cranii (**d**). **e**–**f** A 5 year old boy presented with a prolonged complex febril seizure with persisting left-sided hemiparesis. MRI after 2 months showed right-sided hemiatrophy und hippocampal sclerosis (**f**: *arrow*)

Table 1 Differential diagnosis TGA versus TEA

	TGA	TEA
Duration of attacks	2–8 (−24) h	<1 h
Recurrence of attacks	Rare	Frequent
EEG	−	Interictal temporal or fronto-temporal abnormalities
Other ictal symptoms	−	+
Response to antiepileptic drugs	−	+
MRI	Punctate DWI lesions in CA1 field after 24–48 h	Subtle hippocampal volume loss

development of hemiplegia. It occurs most frequently in children younger than 2 years of age, however, cases in children up to 11 years have been described. Seizures are unilateral or predominantly unilateral, but may cross over to the other side or be initially generalized. Seizures are usually clonic in type, often in the form of status epilepticus lasting over several hours. They are generally associated with coma and immediately followed by hemiplegia. When the convulsions start on one side and cross to the other, the side involved last predicts the hemiplegic site. Hemiplegia is initially flaccid and eventually becomes spastic. However, it may disappear in 20 % of patients with only some degree of spasticity, increased deep tendon reflexes and pyramidal tract signs remaining.

Hemiconvulsion–hemiplegia–epilepsy syndrome will evolve to the secondary appearance of focal seizures in around 60 % of cases, usually within 3 years after disease onset.

1.4 Imaging

In the acute phase, there is DWI-proven cytotoxic edema of a hemisphere that is not confined to a vascular territory (Freemann et al. 2002). Within weeks to months hemiatrophia cranii et cerebri with cerebral peduncle atrophy (Wallerian degeneration of the pyramidal tract) and possible contralateral cerebellar atrophy develop (Fig. 1).

2 Transient Global Amnesia and Transient Epileptic Amnesia

2.1 Epidemiology

Transient global amnesia (TGA) is a rare condition with isolated anterograde and retrograde amnesia lasting for several hours, which was initially described by Fischer and Adams (1964). In contrast, transient epileptic amnesia (TEA) is likely an epilepsy syndrome, in which amnesia is not an isolated syndrome but accompanied by other epileptic phenomena (Kapur 1993).

2.2 Pathogenesis

Transient global amnesia is characterized by delayed neuronal loss in the cornu ammonis CA1 field of the hippocampus, which is highly vulnerable to metabolic stress (Bartsch and Deuschl 2010). TEA is considered as an epilepsy syndrome with amnesia as a postictal phenomenon or symptom during nonconvulsive status epilepticus (Bilo et al. 2009).

2.3 Clinical Presentation

Transient global amnesia is characterized by a sudden onset of anterograde and retrograde amnesia lasting for usually 2–8, and rarely up to 24 h. The neurological state is otherwise normal. During the attack, patients are anxious, ask the same question again and again, and rapidly forget the answer. With resolution of the attack, there is a stepwise return of anterograde memory; however, because patients had not been able to lay down new memories during the attack, they will never be able to recall the episode itself. TGA often occurs with or after emotional or physical "stress" and has no gender predilection (Bartsch 2006).

In TEA, "long" attacks with pure amnesia lasting for less than 1 h and "short" attacks with amnesia preceded by typical epileptic ictal phenomena such as clouding of consciousness and/or motor automatisms, have been described. Both show a tendency to recur and accordingly, the diagnosis of TEA requires the presence of: (1) history of recurrent witnessed episodes of transient amnesia; (2) cognitive functions other than memory judged to be intact

during typical episodes; (3) evidence for a diagnosis of epilepsy based on one or more of the following: epileptiform EEG abnormalities, concurrent onset of other features of epilepsy, and clear-cut response to antiepileptic treatment (Kapur 1993; Zeman et al. 1998). TEA typically begins in late-middle to old age, TEA attacks often occur on awakening, retrograde amnesia is often more severe than anterograde amnesia, and many patients have a partial memory of the amnesic episode, reporting that they "were not able to remember." TEA is responsive to relatively low doses of antiepileptic drugs (AEDs), but many patients report persistent interictal memory disturbances, consisting of accelerated long-term forgetting and autobiographic amnesia (Zeman et al. 1998; Butler et al. 2007). See Table 1.

2.4 Imaging

Transient global amnesia patients typically show punctate DWI lesions in the upper and lateral segment of the hippocampus (CA1 field) which may be faintly visible within 4–6 h following the TGA attack (Fig. 2). However, DWI signal intensity increases and is most prominent between 36 and 48 h (Sedlaczek et al. 2004; Bartsch et al. 2006). Single lesions are found in 75 % of cases, the left hippocampus is involved three times more often than the right hippocampus, and two or more punctate or bilateral lesions are found in 25 % of cases. Lesions can be seen as hyperintense on high-resolution T2-weighted images and clearly separated from the vestigial sulcus hippocampi, and follow-up MRI shows complete disappearance of T2-lesions (Nakada et al. 2005; Bartsch et al. 2006).

In TEA patients, hippocampal volumetry reveals a subtle volume loss (about 8 %), which is pronounced in the hippocampal body (Butler et al. 2009). MRI may show focal temporal lobe lesions but is in most cases normal (Della Marca et al. 2010).

3 Epilepsy and Multiple Sclerosis

3.1 Epidemiology

Multiple sclerosis patients have a 3 % risk of developing epileptic seizures, which is around three to six times higher than epileptic seizures in the general population (Olafsson et al. 1999; Nyquist et al. 2001, 2002; Nicoletti et al. 2003; Lebrun 2006; Viveiros and Alvarenga 2010).

3.2 Pathogenesis

Although MS predominantly affects the deep and periventricular white matter, demyelinating lesions are also found in the juxtacortical location (17 %) and in the cerebral cortex (5 % in pathological specimens, respectively) (Brownell and Hughes 1962). Apart from cortical lesions, there is likely a risk for temporal lobe seizures in patients with demyelinating lesions along the surface of the temporal horns. This may be explained with disconnection of the cortex (the so-called chronic isolated cortex) (Echlin and Battista 1963).

3.3 Clinical Presentation

Patients typically suffer from simple and complex focal seizures, with or without secondary generalization, whereas primarily generalized epilepsy is rare (Kelley and Rodriguez 2009). Seizure might be the first MS manifestation (Fig. 3), however, they mostly occur in the acute and chronic phases and are not related to the severity or duration of MS (Fig. 4).

3.4 Imaging

Although many cortical lesions are not seen on MRI (Geurts et al. 2005), MS patients with epilepsy have a fivefold increase in the number of cortical lesions and a sixfold larger volume of cortical lesions than MS patients without epilepsy (Calabrese et al. 2008) (Fig. 3). Apart from cortical lesions, there is likely a risk for temporal lobe seizures in patients with demyelinating lesions along the surface of the temporal horns (Figs. 4, 5).

4 Chorea-Acanthocytosis

4.1 Epidemiology

A group of very rare genetically defined diseases characterized by the association of red blood cell acanthocytosis and progressive degeneration of the basal ganglia (Jung et al. 2011).

4.2 Pathogenesis

Autosomal-recessive mutations in the *VPS13A* gene on chromosome 9q21, encoding for chorein (Velayos-Baeza

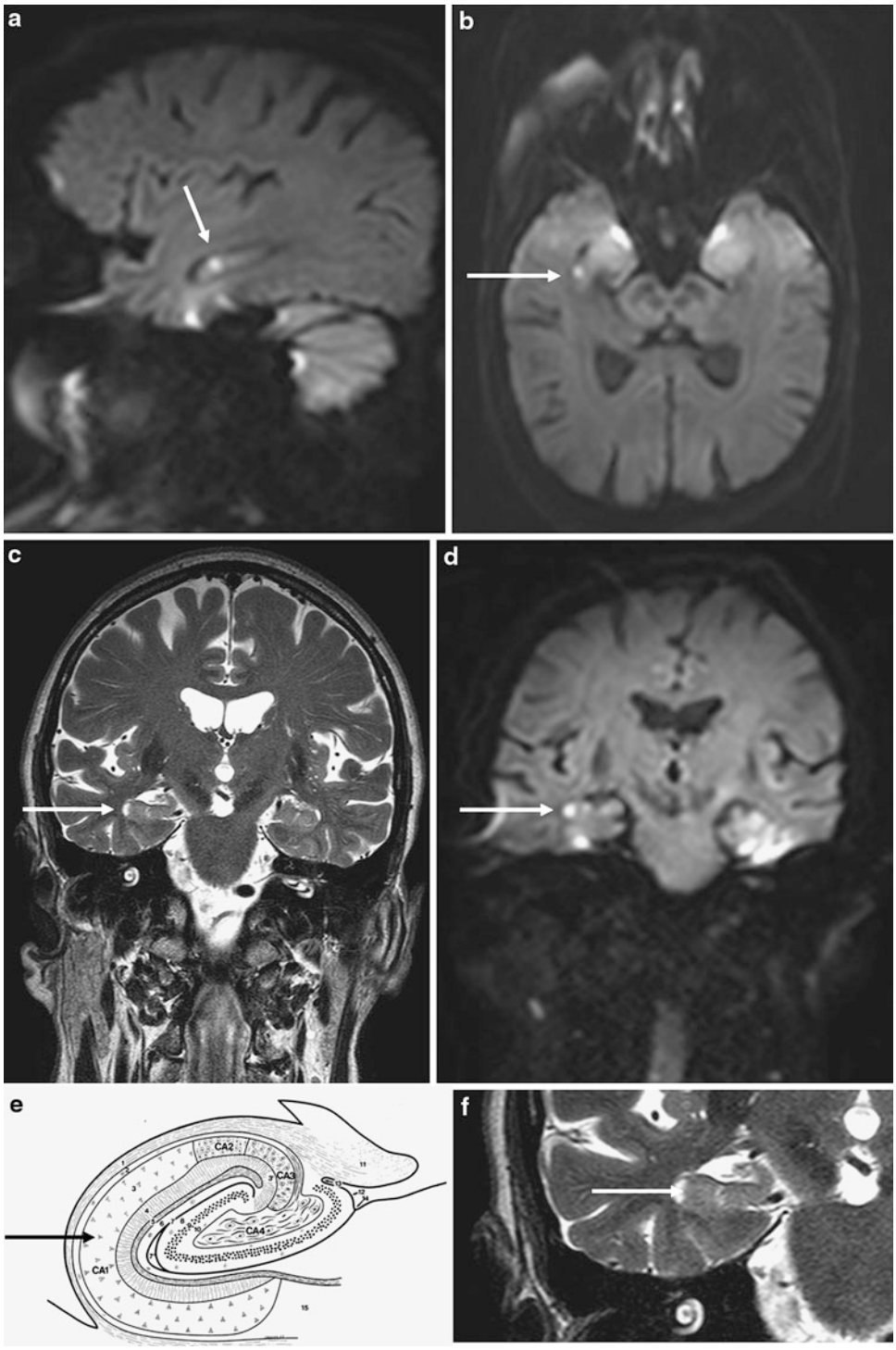

Fig. 2 Transient global amnesia (TGA): Punctate hyperintense DWI (**a**, **b**, **d**: *arrow*) and T2 (**c**, **f**) lesion in the lateral and upper part of the right hippocampal head representing the cornu ammonis (CA) 1 field (**e**: schematic drawing, adapted from Duvernoy HM. The human hippocampus Springer 1998, with permission). The CA 1 field is highly vulnerable to metabolic stress. Typically, MRI immediately after the attack is normal, while MRI after 24–48 h reveals one or more, uni- or bilateral DWI lesions

et al. 2004; Dobson-Stone et al. 2004). Altered molecular hippocampal architecture, defects of the erythrocyte membrane, and remote effects of the basal ganglia as the predilection site of neurodegeneration in chorea–acanthocytosis are discussed (Scheid et al. 2009; Bader et al. 2011).

4.3 Clinical Presentation

Psychiatric symptoms and cognitive decline may start in the twenties. Later, most patients develop a characteristic phenotype including chorea, orofacial dyskinesias, involuntary

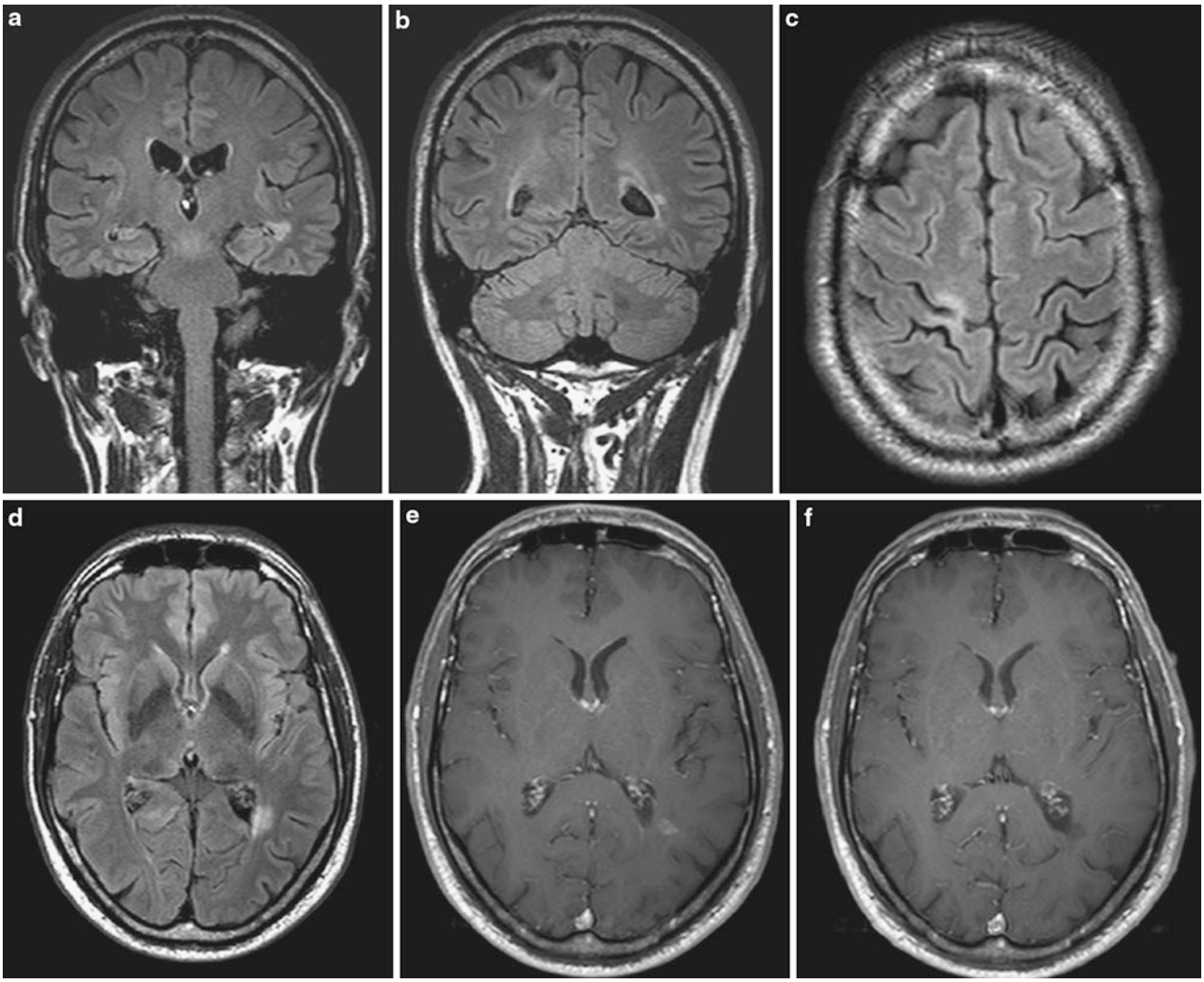

Fig. 3 MRI in a 51 year old man, who presented with myoclonic seizures of the left leg. MRI showed a right-sided cortical pre and postcentral lesion (**b**, **c**: *arrow*) and periventricular lesions (**a**, **d**: *arrow*). Contrast enhancement of a periventricular lesion at the right trigone disappeared on follow-up MRI after 6 months

vocalizations, dysarthria, and involuntary tongue- and lip-biting (Jung et al. 2011). In at least one-third of patients, seizures are the first manifestation of disease (Jung et al. 2011). Seizures are of different types and temporal lobe seizures are common (Al-Asmi et al. 2005; Scheid et al. 2009; Bader et al. 2011). Most patients have elevated levels of creatine phosphokinase (Jung et al. 2011).

4.4 Imaging

Consider chorea–acanthocytosis if there is caudate head and to a lesser degree putaminal atrophy. Caudate head and putaminal atrophy are related to disease duration, easily missed on visual inspection, and highlighted with volumetric analyses (Huppertz et al. 2008) (Fig. 6).

Developing hippocampal sclerosis related to the disease or as a consequence of frequent seizures has been described (Scheid et al. 2009).

5 "Reversible" Splenium Lesions

5.1 Epidemiology

Rare, but pathognomonic imaging finding likely caused by rapid reduction of antiepileptic drugs (AEDs). A common situation is AED withdrawal during presurgical work-up in

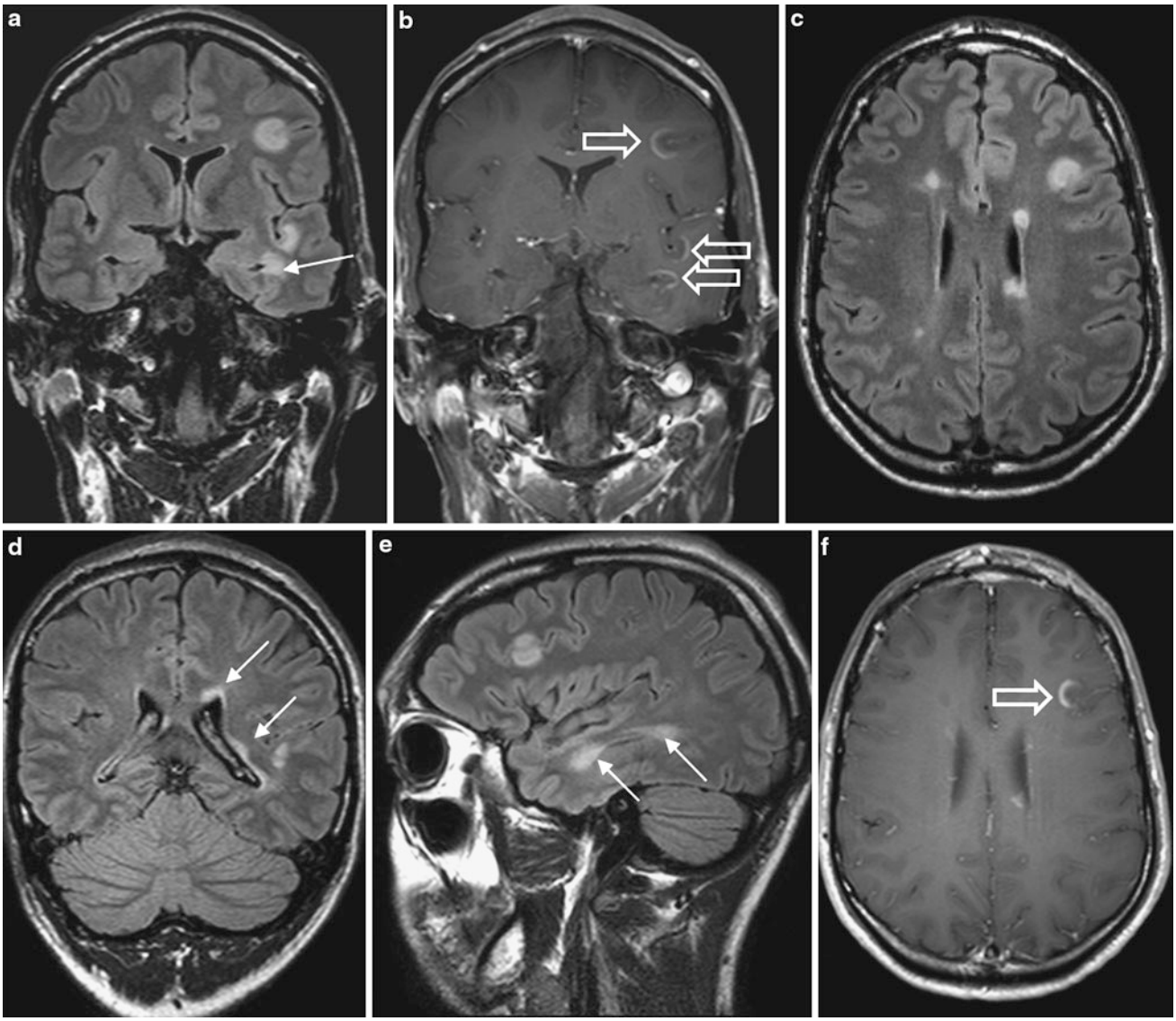

Fig. 4 MRI in a 31 year old patient with a generalized tonic–clonic seizure as first manifestation of multiple sclerosis. MRI shows multiple periventricular and juxtacortical demyelinating lesions (**a**–**e**). Many lesions are contrast-enhancing with some of the larger lesions displaying a so-called open-ring sign (**b**, **f**: *hollow arrows*). If MS patients present with epileptic seizures, a pattern with (confluent) lesions lining the temporal horns is often found (**a**, **d**, **e**: *arrows*)

order to provoke seizures. However, reversible splenium lesions are also rarely found in patients with infections, chemotherapy, or other diseases affecting fluid balance systems.

5.2 Pathogenesis

Abrupt disorder of fluid balance systems due to central sodium channel blockade or disturbance of the arginine–vasopressin system. A typical withdrawn AED carbamazepine, for example, enhances the antidiuretic effect of the arginine–vasopressin system.

5.3 Clinical Presentation

None.

5.4 Imaging

Non space-occupying symmetric lesion in the center of the splenium with reduced diffusion. There is no contrast enhancement. Complete or near-complete regression on follow-up MRI within 1–2 weeks (Nelles et al. 2006) (Fig. 7).

Some authors consider high-altitude cerebral edema (HACE) a reversible splenium lesion, although MRI in HACE typically show a splenium lesion with increased

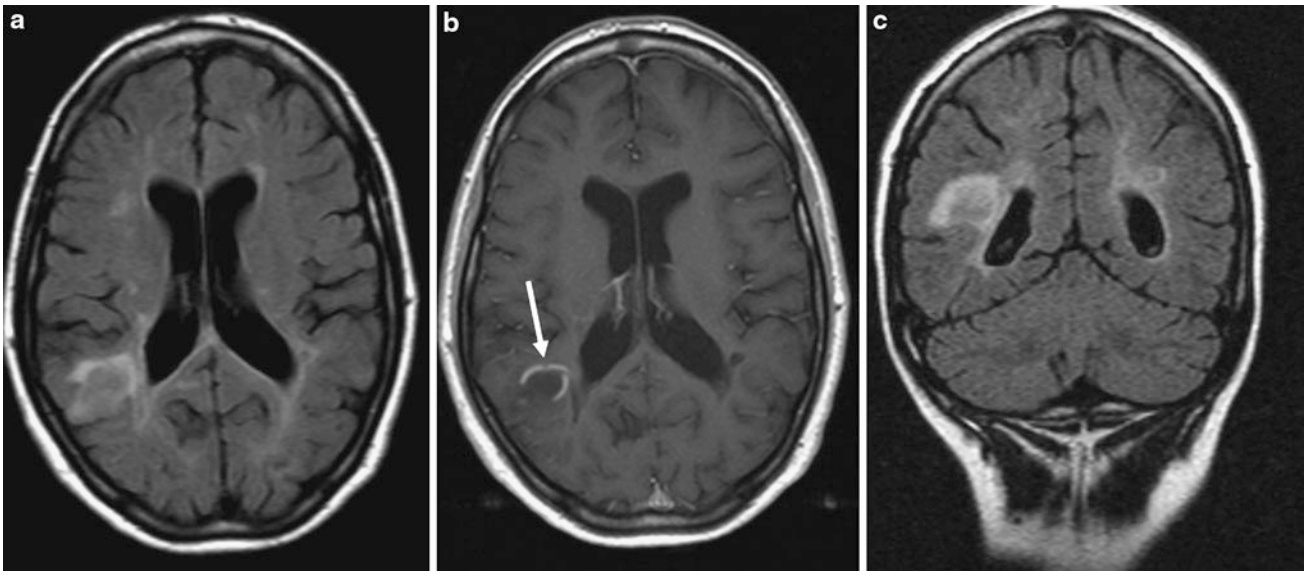

Fig. 5 MRI in a 49 year old woman with relapsing–remitting multiple sclerosis and a generalized tonic–clonic seizure. MRI shows multiple periventricular demyelinating lesions (**a**, **c**) and a large temporo-occipital contrast-enhancing lesion with open-ring sign, which extends from the periventricular region to the U-fibers (**b**: *arrow*)

diffusion and additional corpus callosum and white matter microbleeds (Kallenberg et al. 2008).

6 MRI Changes in Antiepileptic Drug Therapy

Numerous AEDs are prescribed either as mono- or as combined drug therapy (Nicholas et al. 2012; Hamer et al. 2012). Of those, AED that may elicit MRI changes are briefly mentioned here.

6.1 Carbamazepine

Carbamazepine is the most often prescribed drug in the treatment of focal epilepsies. The exact mechanism of action is unknown; general suppression of EEG activity is likely (Jokeit et al. 2001). Typical side effects are nystagmus, dizziness, and ataxia, which are dose-dependent and related to the degree of pre-existing cerebellar atrophy (Specht et al. 1997). Most common MRI changes are so-called reversible splenium lesions which are likely due to rapid carbamazepine withdrawal (Fig. 7).

6.2 Phenytoin

Phenytoin is widely used for the treatment of focal and generalized seizures and convulsive status epilepticus. Prescription frequency, however, is decreasing (Nicholas et al. 2012; Hamer et al. 2012). Side effects of long-lasting phenyoin therapy are cerebellar atrophy, causing ataxia, tremor, nystagmus, diplopia, reversible splenium lesions, cranial vault thickening, and gingival overgrowth (Fig. 8). Cerebellar atrophy is likely caused by direct toxic effects (Laxer et al. 1980; Luef et al. 1994). Cases with reversible splenium lesions or with leucoencephalopathy likely due to deficiency of the enzyme methylenetetrahydrofolate reductase (MTHFR) have been described (Kim et al. 1999; Arai and Osaka 2011).

6.3 Valproate

Valproate is a broad-spectrum AED and primarily used in idiopathic generalized epilepsies. The mechanism of action is not fully clear; effects include GABAergic inhibition and attenuation of glutamergic excitation. Significant side effects are liver toxicity and teratogenicity. Neurological

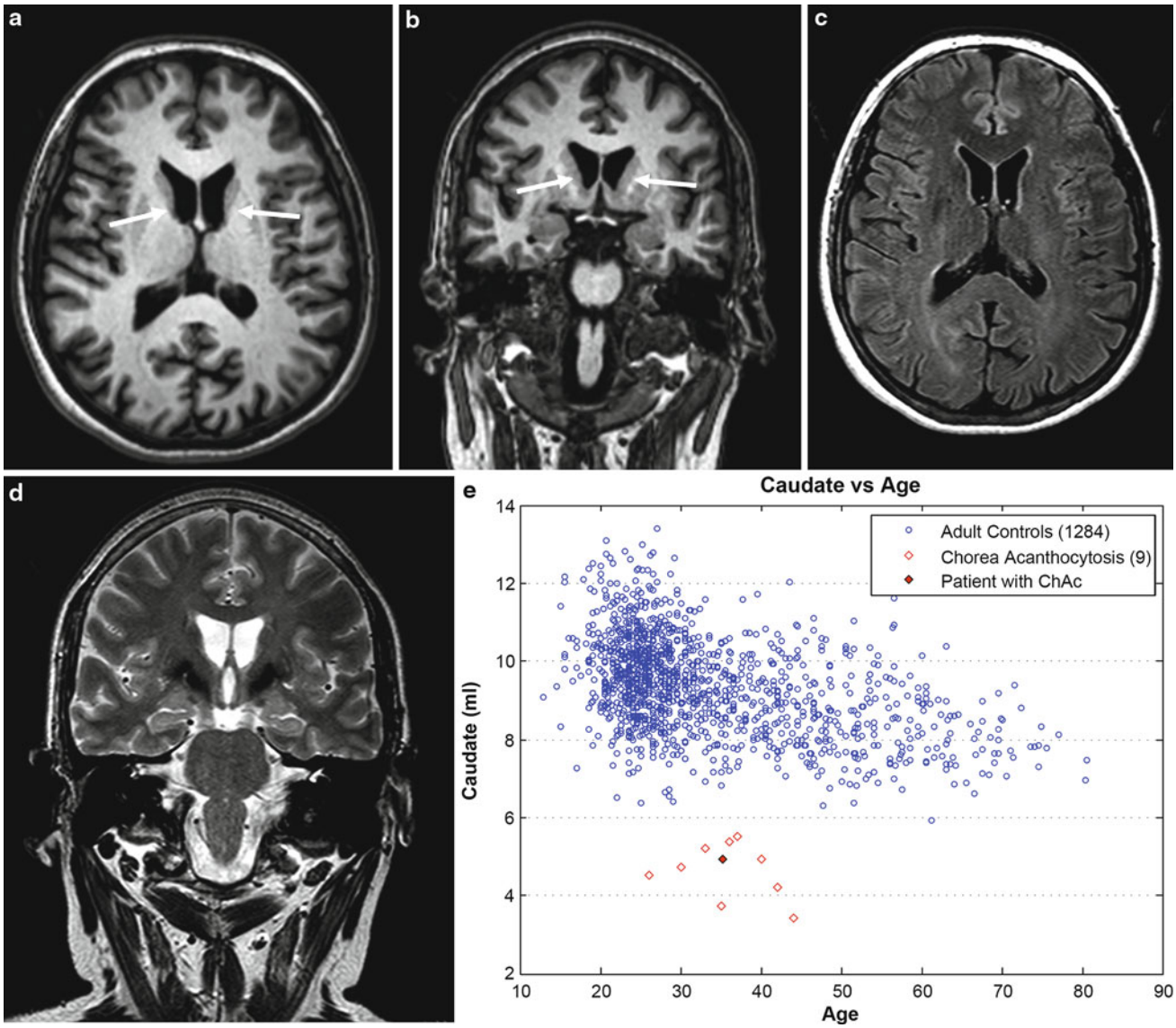

Fig. 6 Axial (**a**) and coronal (**b**) reformatted T1-weighted gradient echo, axial FLAIR (**c**), and coronal T2-weighted images (**d**) in a 35 year old woman with chorea–acathocytosis. First manifestation of the disease were epileptic seizures. Later on, the patient also developed chorea and facial dyskinesias. MR images show moderate caudate head atrophy (**a**, **b**: *arrows*) with some enlargement but without ballooning of the anterior horns. Caudate head and putaminal atrophy can be easily missed on visual inspection but are highlighted by volumetric MRI analysis (**d**, **e**) (Huppertz et al. 2008). Courtesy of Huppertz HJ, Swiss Epilepsy Centre, Zurich, Switzerland

side effects are tremor, parkinsonism, drowsiness, lethargy, and confusion.

On MRI, T1-hyperintense basal ganglia and cortical lesions reflecting hyperammonemic encephalopathy (Grubben et al. 2004) and widened CSF spaces, which disappear after valproate withdrawal (pseudoatrophy) (Evans et al. 2011) may be observed.

6.4 Vigabatrin

Vigabatrin is an AED that acts by irreversibly inhibiting γ-aminobutyric acid transaminase (GABA transaminase). It is used in infantile spasms, particularly in patients with tuberous sclerosis and drug-resistant complex focal seizures (Pearl et al. 2009). Usually, it is well tolerated. MRI

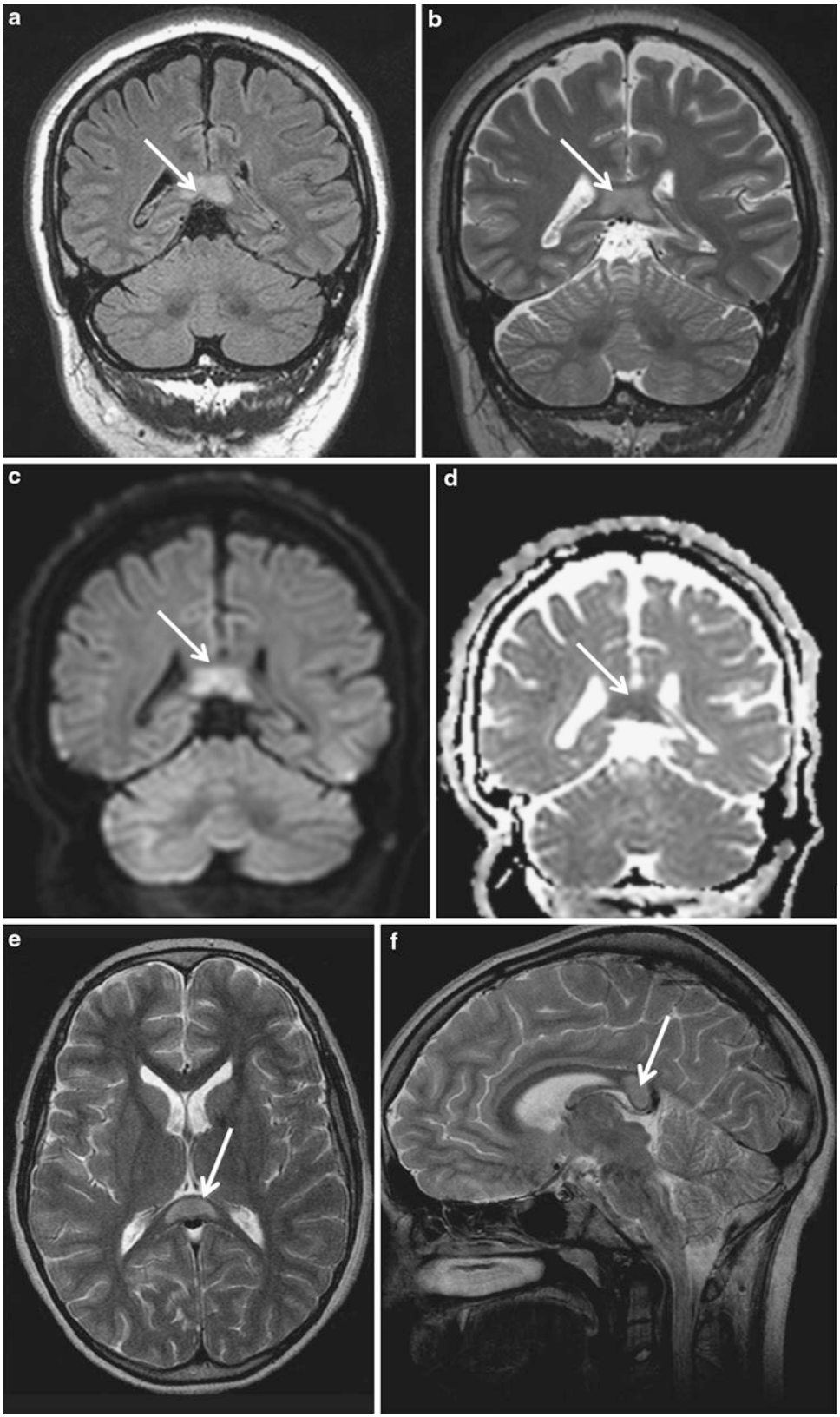

Fig. 7 "Reversible" splenium lesions: non space-occupying cytotoxic edema within the center of the splenium after antiepileptic drug withdrawl for presurgical evaluation (**a**–**d**: *arrow*) and due to lymphocytic encephalitis (**e**, **f**: *arrow*), respectively

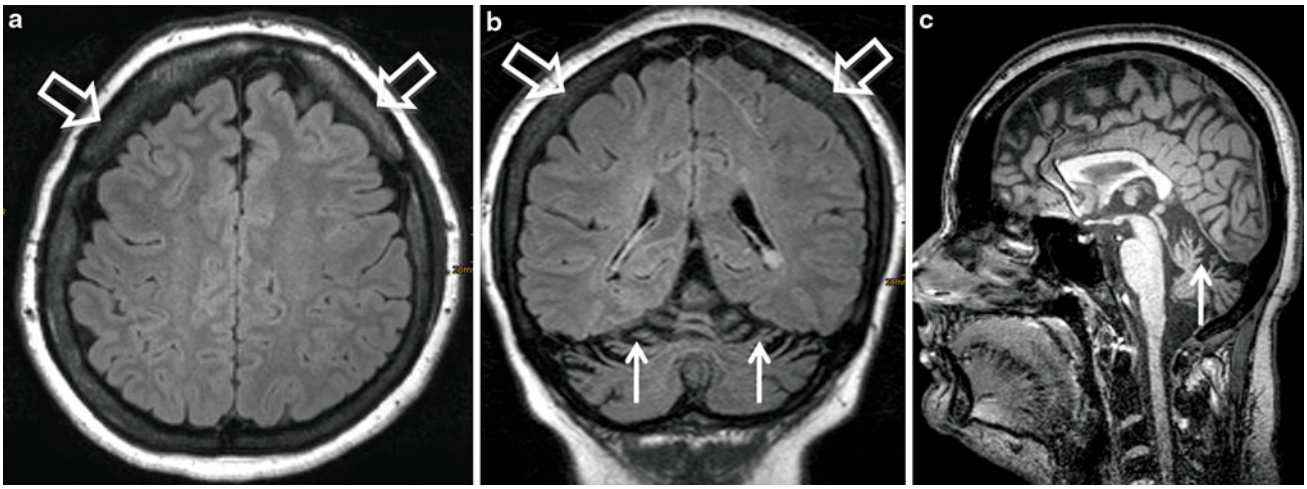

Fig. 8 Sequelae of long-lasting phenytoin therapy in a 38 year old woman who presented with epileptic seizures 22 years ago and was taking phenytoin since this time. Marked cerebellar atrophy (**b**, **c**: *arrows*) and distinct cranial vault thickening (**a**, **b**: *hollow arrows*) are distinct imaging features

changes have occasionally been described and consist of bilateral symmetric lesions with usually reversible cytotoxic edema in the thalami, tegementum of the midbrain, globi pallidi, and dentate nuclei. Despite these changes, patients are usually asymptomatic (Iyer et al. 2011; Simao et al. 2011; Pearl et al. 2009).

No specific MRI changes have been described for the newer AED including Levetiracetam, Lamotrigine, Topiramate, and Gabapentin.

References

Al-Asmi A, Jansen AC, Badhwar A et al (2005) Familial temporal lobe epilepsy as a presenting feature of choreoacanthocytosis. Epilepsia 46:1256–1263

Arai M, Osaka H (2011) Acute leukoencephalopathy possibly induced by phenytoin intoxication in an adult patient with methylenetetrahydrofolate reductase deficiency. Epilepsia 52:e58–e61

Bader B, Vollmar C, Ackl N, Ebert A, la Fougere C, Noachtar S, Danek A (2011) Bilateral temporal lobe epilepsy confirmed with intracranial EEG electrodes in chorea–acanthocytosis. Seizure 20:340–342

Bartsch T, Deuschl G (2010) Transient global amnesia: functional anatomy and clinical implications. Lancet Neurol 9(2):205–214

Bartsch T, Alfke K, Stingele R, Rohr A, Freitag-Wolf S, Jansen O, Deuschl G (2006) Selective affection of hippocampal CA-1 neurons in patients with transient global amnesia without long-term sequelae. Brain 129(Pt 11):2874–2884

Bilo L, Meo R, Ruosi P, de Leva MF, Striano S (2009) Transient epileptic amnesia: an emerging late-onset epileptic syndrome. Epilepsia 50(Suppl 5):58–61

Brownell B, Hughes JT (1962) The distribution of plaques in the cerebrum in multiple sclerosis. J Neurol Neurosurg Psychiatry 25:315–320

Butler CR, Graham KS, Hodges JR, Kapur N, Wardlaw JM, Zeman AZ (2007) The syndrome of transient epileptic amnesia. Ann Neurol 61:587–598

Butler CR, Bhaduri A, Acosta-Cabronero J, Nestor PJ, Kapur N, Graham KS, Hodges JR, Zeman AZ (2009) Transient epileptic amnesia: regional brain atrophy and its relationship to memory deficits. Brain 132(Pt 2):357–368

Calabrese M, De Stefano N, Atzori M et al (2008) Extensive cortical inflammation is associated with epilepsy in multiple sclerosis. J Neurol 255(4):581–586

Della Marca G, Dittoni S, Pilato F, Profice P, Losurdo A, Testani E. Colicchio S, Gnoni V, Colosimo C, Di Lazzaro V (2010) Teaching neuroimages: transient epileptic amnesia. Neurology 75(10):e47–e48

Dobson-Stone C, Velayos-Baeza A, Filippone LA et al (2004) Chorein detection for the diagnosis of chorea–acanthocytosis. Ann Neurol 56:299–302

Echlin F, Battista J (1963) Epileptiform seizures from chronic isolated cortex. Arch Neurol 9:154–170

Evans MD, Shinar R, Yaari R (2011) Reversible dementia and gait disturbance after prolonged use of valproic acid. Seizure 20(6):509–511

Fisher CM, Adams RD (1964) Transient global amnesia. Acta Neurol Scand 40:1–83

Freemann JL, Coleman LT, Smith LJ, Shield LK (2002) Hemiconvulsion–hemiplegia–epilepsy syndrome: characteristic early magnetic resonance imaging findings. J Child Neurol 17:10–16

Gastaut H, Poirier F, Payan H, Salamon G, Toga M, Vigoroux M (1960) H.H.E. syndrome; hemiconvulsions, hemiplegia, epilepsy. Epilepsia 1:418

Geurts JJ, Bo L, Pouwels PJ et al (2005) Cortical lesions in multiple sclerosis: combined postmortem MR imaging and histopathology. AJNR 26:572–577

Grubben B, De Jonghe P, Cras P, Demey HE, Parizel PM (2004) Valproate-induced hyperammonemic encephalopathy: imaging findings on diffusion-weighted MRI. Eur Neurol 52(3):178–181

Hamer HM, Dodel R, Strzelczyk A, Balzer-Geldsetzer M, Reese JP, Schöffski O, Graf W, Schwab S, Knake S, Oertel WH, Rosenow F, Kostev K (2012) Prevalence, utilization, and costs of antiepileptic drugs for epilepsy in Germany—a nationwide population-based study in children and adults. J Neurol 2012 Apr 28 [Epub ahead of print]

Huppertz HJ, Kröll-Seger J, Danek A, Weber B, Dorn T, Kassubek J (2008) Automatic striatal volumetry allows for identification of patients with chorea–acanthocytosis at single subject level. J Neural Transm 115:1393–1400

Iyer RS, Chaturvedi A, Pruthi S, Khanna PC, Ishak GE (2011) Medication neurotoxicity in children. Pediatr Radiol 41:1455–1464

Jokeit H, Okujava M, Woermann FG (2001) Carbamazepine reduces memory induced activation of mesial temporal lobe structures: a pharmacological fMRI-study. BMC Neurol 18:1–6

Jung HH, Danek A, Walker RH (2011) Neuroacanthocytosis syndromes. Orphanet J Rare Dis 6:68

Kallenberg K, Dehnert C, Dörfler A, Schellinger PD, Bailey DM, Knauth M, Bärtsch PD (2008) Microhemorrhages in nonfatal high-altitude cerebral edema. J Cereb Blood Flow Metab 28:1635–1642

Kapur N (1993) Transient epileptic amnesia—a clinical update and a reformulation. J Neurol Neurosurg Psychiat 56:1184–1190

Kelley BJ, Rodriguez M (2009) Seizures in patients with multiple sclerosis: epidemiology, pathophysiology and management. CNS Drugs 23:805–815

Kim SS, Chang KH, Kim ST et al (1999) Focal lesion in the splenium of the corpus callosum in epileptic patients: antiepileptic drug toxicity? AJNR Am J Neuroradiol 20:125–129

Laxer KD, Robertson LT, Julien RM, Dow RS (1980) Phenytoin: relationship between cerebellar function and epileptic discharges. Adv Neurol 27:415–427

Lebrun C (2006) Epilepsy and multiple sclerosis. Epileptic Disord 8:555–558

Luef G, Chemelli A, Birbamer G, Aichner F, Bauer G (1994) Phenytoin overdosage and cerebellar atrophy in epileptic patients: clinical and MRI findings. Eur Neurol 34(Suppl 1):79–81

Nakada T, Kwee IL, Fujii Y, Knight RT (2005) High-field, T2-reversed MRI of the hippocampus in transient global amnesia. Neurology 64:1170

Nelles M, Bien CG, Kurthen M, von Falkenhausen M, Urbach H (2006) Transient splenium lesions in presurgical epilepsy patients: incidence and pathogenesis. Neuroradiology 48:443–448

Nicholas JM, Ridsdale L, Richardson MP, Ashworth M, Gulliford MC (2012) Trends in antiepileptic drug utilisation in UK primary care 1993–2008: Cohort study using the General Practice Research Database. Seizure 21(6):466–470

Nicoletti A, Sofia V, Biondi R et al (2003) Epilepsy and multiple sclerosis in Sicily: a population-based study. Epilepsia 44: 1445–1448

Nyquist PA, Cascino GD, Rodrigue M (2001) Seizures in patients with multiple sclerosis seen at Mayo Clinic, Rochster, Minn, 1990–1998. Mayo Clin Proc 76:983–986

Nyquist PA, Cascino GD, McClelland RL et al (2002) Incidence of seizures in patients with multiple sclerosis: a population-based study. Mayo Clin Proc 77:910–912

Olafsson E, Benedikz J, Hauser WA (1999) Risk of epilepsy in patients with multiple sclerosis: a population-based study in Iceland. Epilepsia 40:745–747

Pearl PL, Vezina LG, Saneto RP et al (2009) Cerebral MRI abnormalities associated with vigabatrin therapy. Epilepsia 50:184–194

Schaffer AJ (1927) The etiology of infantile acquired hemiplegia. Arch Neurol Psychiatry 18:323

Scheid R, Bader B, Ott DV, Merkenschlager A, Danek A (2009) Development of mesial temporal lobe epilepsy in chorea–acanthocytosis. Neurology 73:1419–1422

Sedlaczek O, Hirsch JG, Grips E, Peters CNA, Gass A, Wöhrle J, Hennerici M (2004) Detection of delayed focal MR changes in the lateral hippocampus in transient global amnesia. Neurology 62:2165

Simao GN, Zarei Mahmoodabadi S, Snead OC, Go C, Widjaja E (2011) Abnormal axial diffusivity in the deep gray nuclei and dorsal brain stem in infantile spasm treated with vigabatrin. AJNR Am J Neuroradiol 32:199–203

Specht U, May TW, Rohde M, Wagner V, Schmidt RC, Schütz M, Wolf P (1997) Cerebellar atrophy decreases the threshold of carbamazepine toxicity in patients with chronic focal epilepsy. Arch Neurol 54(4):427–431

Velayos-Baeza A, Vettori A, Copley RR, Dobson-Stone C, Monaco AP (2004) Analysis of the human VPS13 gene family. Genomics 84:536–549

Viveiros CD, Alvarenga RM (2010) Prevalence of epilepsy in a case series of multiple sclerosis patients. Arq Neuropsiquiatr 68:731–736

Zeman AZ, Boniface SJ, Hodges JR (1998) Transient epileptic amnesia: a description of the clinical and neuropsychological features in 10 cases and a review of the literature. J Neurol Neurosurg Psychiatry 64:435–443

Postsurgical MRI

Marec von Lehe and Horst Urbach

Contents

Abstract

The goal of the surgical procedure is to resect or disconnect the epileptogenic area, defined as the cortex area indispensable for the generation of seizures. The epileptogenic area is—among others and, depending on the pathological substrate of the lesion—often larger than the epileptogenic lesion itself, so that extended lesionectomy (e.g., with a 5–10-mm rim of perilesional tissue) is performed. Several standardized neurosurgical procedures have been developed and refined to date.

1 Extended Lesionectomy

1.1 Indications

Focal epilepsy caused by a cortical lesion is a heterogeneous group of disorders that arises from a variety of pathologies and from different anatomical areas. The presurgical workup determines the focal origin (a critical prerequisite) and the resection strategy. In addition to the evaluation of clinical parameters, different imaging modalities are applied; in some cases, an invasive workup with implanted electrodes is necessary. In each case, the spatial relationship of the lesion to eloquent cortex areas is the most important parameter influencing the surgical strategy (Schramm and Clusmann 2008).

The decision making is—as always in epilepsy surgery—a multidisciplinary process and at the end results in the best possible counseling of the patient about the benefits (chance of freedom from seizures) and risks (neurological and neuropsychological deficits).

1.2 Surgical Techniques

The aim of epilepsy surgery is to resect as much tissue as deemed necessary to provide complete seizure relief without causing unacceptable permanent neurological damage.

M. von Lehe
Department of Neurosurgery, University of Bonn, Bonn, Germany

H. Urbach (✉)
Department of Neuroradiology, University Hospital Freiburg, Germany
e-mail: horst.urbach@uniklinik-freiburg.de

H. Urbach (ed.), *MRI in Epilepsy*, Medical Radiology. Diagnostic Imaging,
DOI: 10.1007/174_2012_775,

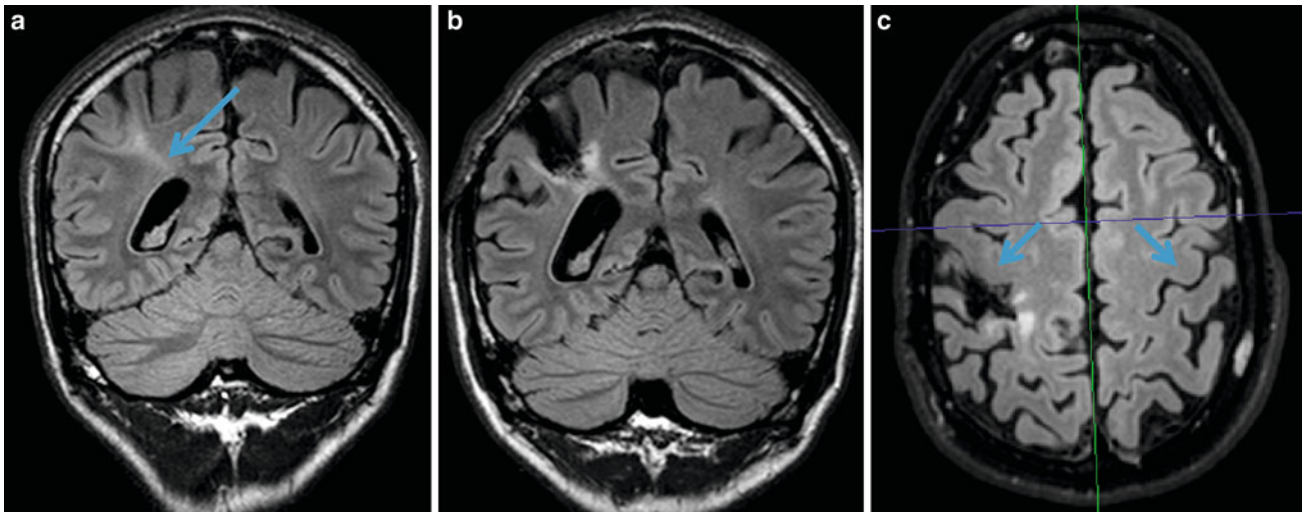

Fig. 1 Lesionectomy of an FCD IIB of the right postcentral gyrus. **a** shows a bottom of sulcus dysplasia with the funnel-shaped hyperintensity tapering to the lateral ventricle (**a** *arrow*), **b** and **c** the resection cavity. *Arrows* in **c** point to the hand knobs of the precentral gyri

The typical extended lesionectomy includes a 5–10-mm rim of "unaffected tissue." In some cases of well-circumscribed lesions (e.g., focal cortical dysplasia type IIB), just a pure lesionectomy without extension (but possibly combined with MST; see below) is feasible due to the close relationship with eloquent cortex areas.

Principles of the resection are independent of the pathology or location and can be done even in highly eloquent areas with adequate safety (von Lehe et al. 2009). After identification of the area to be removed (neuronavigation, electrocorticography, and results of invasive EEG are determinants), the subpial removal of the gray matter is performed. The sulci with the passing vascular structures are carefully preserved as well as the surrounding cortical areas, as such injury may cause neurological deficits or seizures itself. The removal of underlying white matter will not improve seizure control and may cause deficits due to injury to passing fibers.

In neocortical temporal lesionectomies, an extension may include the resection of the mesial structures (hippocampus, amygdala), depending on the presurgical workup.

1.3 Imaging

The extent of resection should be ideally controlled with postsurgical MRI. The goal is to prove the complete resection of the lesion, to exclude surgical complications, and to serve as the base for follow-up MRI imaging in case neoplastic lesions occur. If there are no clinical reasons for immediate postsurgical MRI, it is ideally performed about 3 months after surgery, when acute surgery-related changes have regressed (See Fig. 1).

2 Amygdalohippocampectomy and Anterior Temporal Lobectomy

2.1 Indications

Mesial temporal lobe epilepsy is the most frequent form of refractory focal epilepsy, and hippocampal sclerosis is the typical underlying histopathological substrate. In addition to extended lesionectomies in the temporal lobe, there are so-called standard resections, such as the anterior temporal lobectomy and the selective amygdalohippocampectomy. With improved imaging techniques and more experience in presurgical workup, limited surgical strategies have evolved over the last decades (Clusmann et al. 2002, 2006). Nevertheless, standard temporal lobectomy is still used in many centers to resect the epileptogenic focus.

2.2 Surgical Techniques

The classic temporal lobectomy ("two-third anterior lobectomy") usually combines neocortical resection with removal of the mesial structures (Nayel et al. 1991). The typical length of the resection from the temporal pole is 5.5 cm in the nondominant hemisphere and 4.5 cm in the dominant hemisphere. Usually, the surgical technique comprises two steps: First, the neocortical block and the underlying white matter are removed, with subsequent opening of the temporal horn of the lateral ventricle. After that, mesial structures (uncus, amygdala, hippocampus, and parahippocampal gyrus) are removed by subpial dissection (Fig. 2).

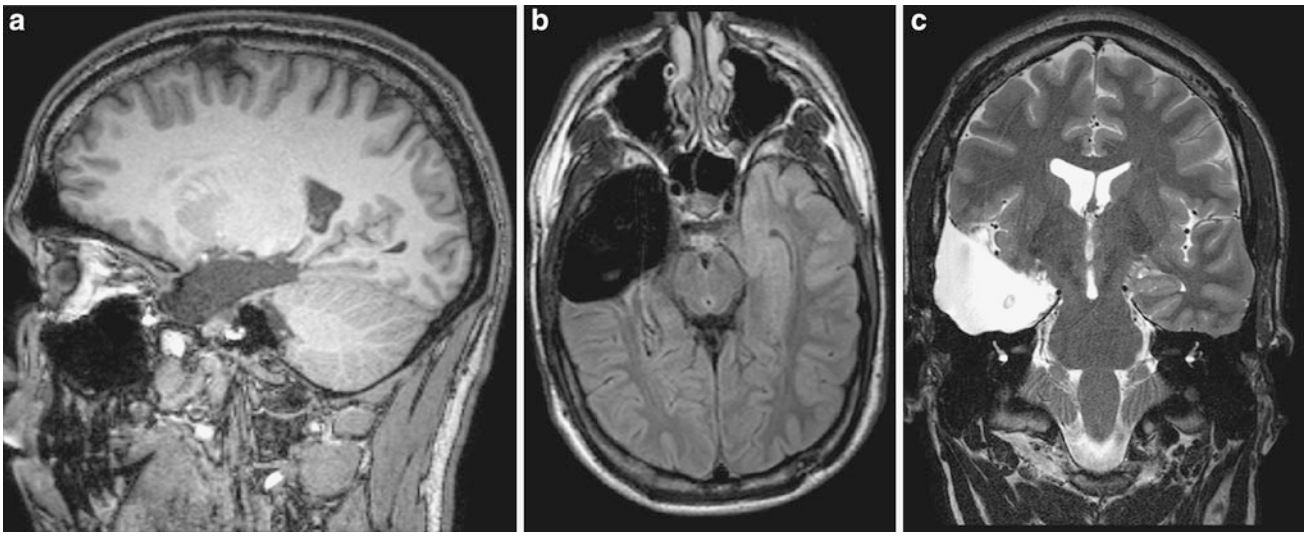

Fig. 2 Anterior temporal lobectomy in a 19 year old patient MRI-negative patient. (**A**: sagittal 1 mm thick T1-weighted gradient echo, **B**: axial 2 mm thick FLAIR, **C**: coronal 2 mm thick T2-weighted image). The patient was operated following intrahippocampal depth and subdural electrode implantation. Histology was unrevealing, but the patient is seizure free 2 years after surgery. MRI at this time showed a 5.5 cm measuring resection cavity on the right side including amygdala and hippocampal resection

Many variations of the surgical steps have been described. A well-known variant is the "Spencer technique," with limited anterior neocortical resection for access to the mesial structures ("one-third anterior lobectomy") (Spencer et al. 1984).

With clear-cut temporomesial seizure onset, a limited mesial resection without the removal of neocortical structures is appropriate. Strictly speaking, the selective amygdalohippocampectomy comprises removal of the head and body of the hippocampus, amygdala, uncus, and parahippocampal gyrus.

Yasargil et al. introduced the widely applied transsylvian approach (Yasargil et al. 1985). It comprises the followings steps: pterional craniotomy approximately 5 cm in diameter; microsurgical dissection of the Sylvian fissure (2.5–3 cm); entering the inferior circular sulcus to approach the temporal horn of the lateral ventricle through the temporal stem with the choroid plexus as landmark for orientation; resection of the mesial structures (see above); the area of the maximum brain stem diameter is the intended dorsal resection border (Figs. 3, 4).

Olivier introduced the transcortical approach, in which the route to the temporal horn is different: A 3-cm craniotomy is centered on the projection of the middle temporal gyrus. After a 2-cm corticotomy, the temporal horn is approached through the white matter with the aid of neuronavigation (Olivier 2000).

Another approach is the subtemporal approach, in which the route to the temporal horn is from the base of the temporal lobe (Hori et al. 1993; Thudium et al. 2010) (Fig. 5).

The rationale behind selective approaches as compared to (anterior) temporal lobectomies is to achieve similar seizure freedom rates while minimizing neuropsychological deficits. It has been shown that seizure freedom rates are comparable between selective amygdalohippocampectomies and anterior temporal lobectomies, and sparing non-lesional tissue is beneficial for the neuropsychological outcome. Verbal memory deficits are common after left-sided surgery and visual memory deficits after right-sided surgery (2008, 2011a, von Rhein et al. 2012). Interestingly, the resection length of the hippocampus (2.5 cm compared to 3.5 cm) is not relevant for the seizure outcome, but longer resections are associated with a poorer memory outcome (Hemstaedter et al. 2011b).

Another concern after all types of temporal resection is postoperative visual field deficits caused by intraoperative damage or ischemia of parts of the optic radiation. The anterior part of the optic radiation ("Meyer's loop") runs around the temporal horn, shows some interindividual variation, and is likely damaged when approaching the temporal horn before resecting the amygdala, hippocampus, and parahippocampal gyrus (Yeni et al. 2008; Renowden et al. 1995; Ebeling and Reulen 1988; Sincoff et al. 2004; Thudium et al. 2010). Even in seizure-free patients, visual field defects may prevent driving and thus diminish quality of life. Despite the more selective nature of selective amygdalohippocampectomy, significant visual field defects such as incomplete or even complete quadrantanopia have been described in up to 37 % (Yeni et al. 2008) and even 53 % (Renowden et al. 1995) of cases. With the subtemporal approach and a more basal entry into the temporal horn, more optical track fibers are likely spared, leading to a reduced rate of significant visual field defects (Thudium et al. 2010).

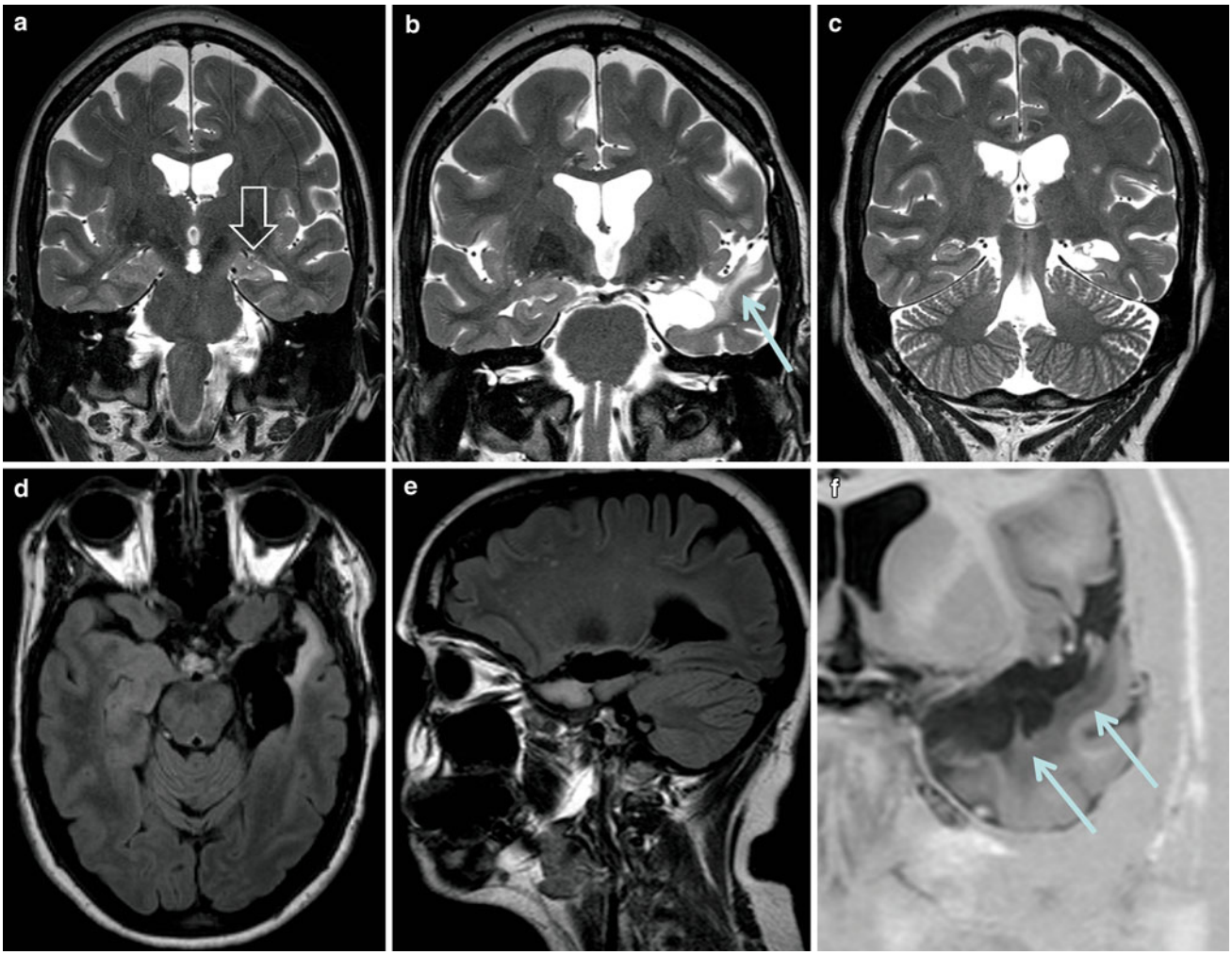

Fig. 3 Selective amygdalohippocampectomy (sAH) via a transsylvian approach. **a** shows a left-sided hippocampal sclerosis (*open arrow*), **b–f** the resection cavity 1 year following surgery. Amygdala, hippocampus, and parahippocampalis have been removed; some "collateral damage" with gliosis along the superior temporal gyrus is best visible on coronal slices (**b**, **f** *arrows*)

2.3 Imaging

MRI is performed to prove the extent of resection (removal of the amygdala, removal of the hippocampus with the maximum brain stem diameter as the intended dorsal resection border, removal of the parahippocampal gyrus).

Sometimes small infarcts of perforating arteries arising from the posterolateral or anterior choroidal or from thalamogeniculate arteries, branches of the P2 segment of the posterior cerebral artery, are found (Fig. 6). Usually, these small infarcts cause (sometimes transient) neurological deficits.

MRI signal intensity changes adjacent to the approach are labeled "collateral changes" (Figs. 3, 4). It has been shown that these changes are correlated with memory decline, particularly verbal learning and recognition deficits (Helmstaedter et al. 2003).

3 Functional Hemispherectomy or Hemispherotomy

3.1 Indications

A functional hemispherectomy, or hemispherotomy, is indicated when congenital or early acquired unilateral lesions of the entire or major parts of a hemisphere are associated with severe, medically intractable seizures.

Typical lesions are congenital or early acquired hemispheric infarcts (mostly MCA) with large porencephalic lesions, Rasmussen encephalitis, hemimegalencephaly, large hemispheric dysplasias, and Sturge–Weber disease.

The chance of seizure freedom following hemispheric surgery depends on the etiology and can be as high as 95 % in patients with porencephalic lesions (Schramm et al. 2012).

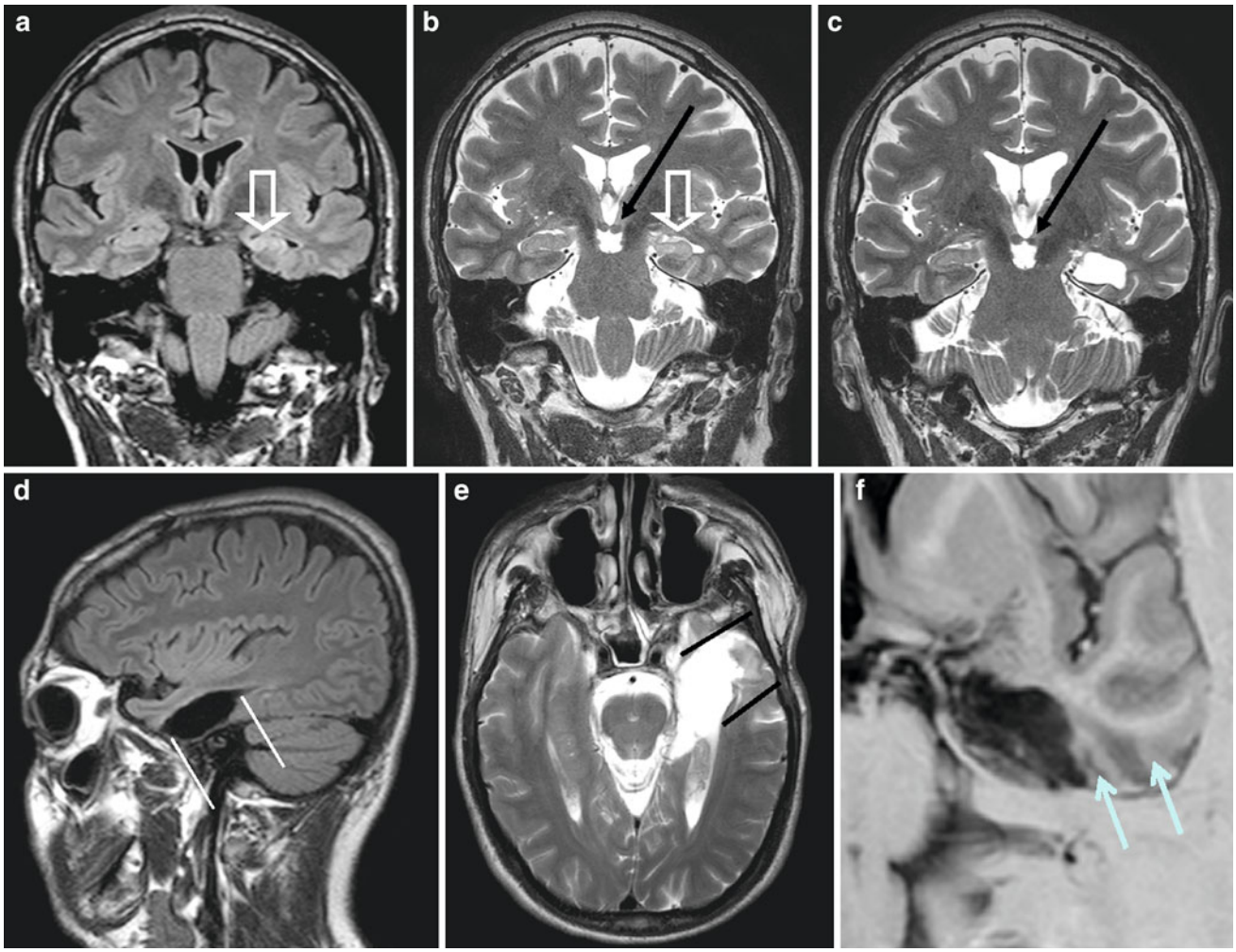

Fig. 4 Selective amygdalohippocampectomy (sAH) via a subtemporal approach. **a** and **b** show a left sided hippocampal sclerosis (*open arrow*), **c**-**f** the resection cavity one year following surgery. Amygdala, hippocampus and parahippocampal gyrus have been removed, the subtemporal „window" is marked with lines (**d**, **e**). Some „collateral damage" with gliosis is visible at the base of the temporal lobe (**f**: *arrows*) Note secondary atrophy of the left mamillary body when comparing its size pre and post surgery (**b**, **c**: *arrow*)

Whether a preexisting hemiparesis will deteriorate postoperatively mainly depends on the timing of the insult and the preoperative motor capacity. If the lesion is acquired very early (fetal, perinatal), it is assumed that ipsilateral corticospinal fibers compensate for the loss of motor function. If the patient is able to perform fine finger movements (e.g., pincer movement), pure ipsilateral innervation is unlikely and hemiparesis—mainly hand function—is likely to deteriorate. If not preexisting, patients always acquire homonymous hemianopia.

Presurgical workup proves the unilateral seizure onset and in patients with advanced language development contralateral speech representation. After early left hemispheric damage, language areas will be transferred to the healthy hemisphere; in case of later disease onset (e.g., Rasmussen encephalitis), fMRI or a Wada test is required.

3.2 Surgical Techniques

Anatomical hemispherectomy was first performed by Dandy in 1928 for the treatment of gliomas and by McKenzie in 1938 for the treatment of epilepsy. Due to severe short- and long-term mortality, the hemispheric surgery became less and less resective and more and more disconnective (Rasmussen 1983). Apart from intraoperative blood loss, the major concerns were early and late hydrocephalic complications. Modern hemispherotomy techniques almost exclusively disconnect the affected hemisphere without leaving large resection cavities behind (Villemure and Daniel 2006; Delalande et al. 2007; Schramm et al. 2012).

Rasmussen developed a technique called "functional hemispherectomy" with resection of the central cortex and

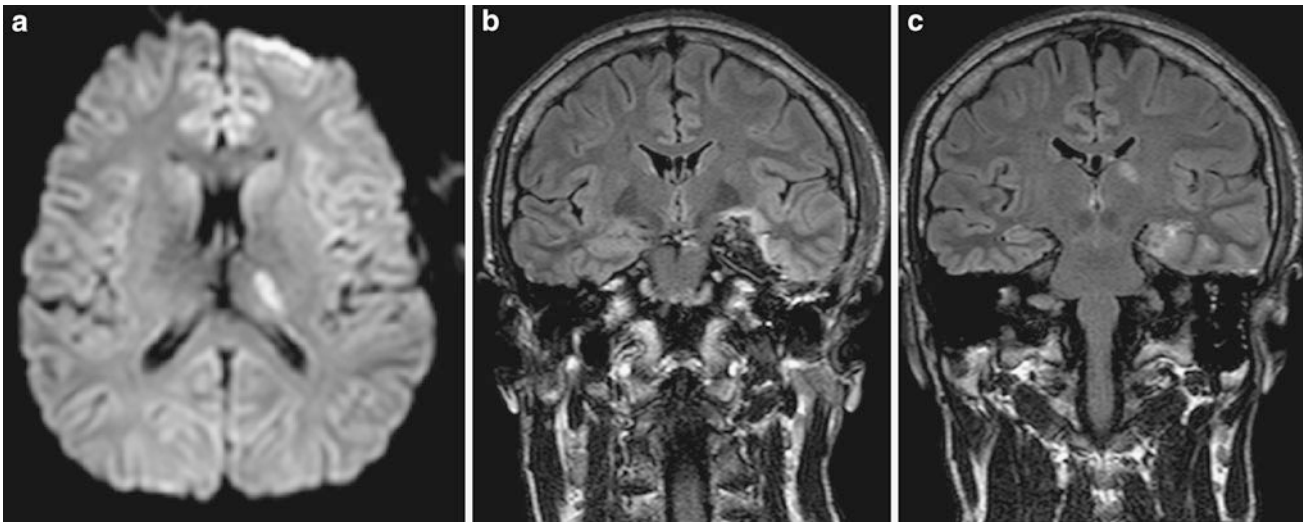

Fig. 5 A 29 year old man complained of right-sided „pain“ of the body and face following left-sided subtemporal amygdalohippocamectomy. MRI (**a**: axial 5 mm DWI slice, **b**-**c**: coronal 3 mm FLAIR slices) shows an acute thalamus infact likely due to injury of the thalamogeniculate arteries arising from the P2-sgement of the posterior cerebral artery

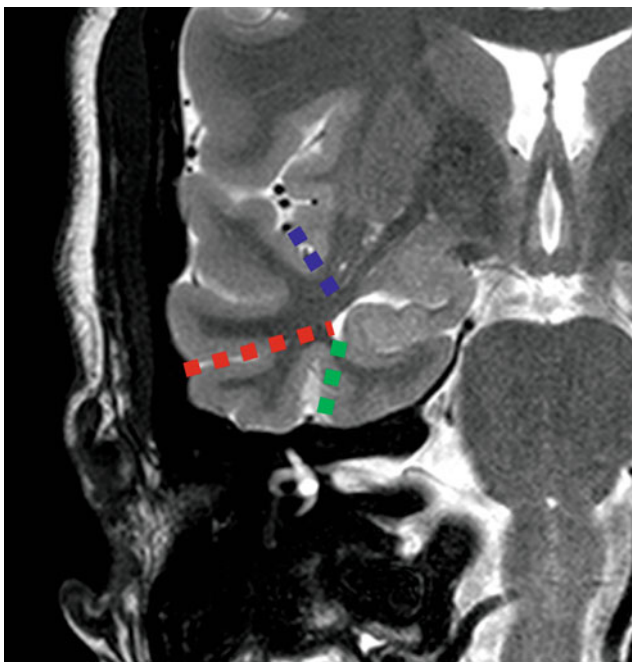

Fig. 6 Schematic approaches for selective amgydalahippocamepctomy: transsylvian apporach (*blue*), trancortical approach with corticotomy of the medial temporal gyrus (*red*), and subtemporal approach (*green*)

temporal lobectomy combined with callosotomy and disconnection of the frontal and parieto-occipital brain (Rasmussen 1983). Villemure described a perisylvian technique with resection of the frontal and temporal opercula and underlying white matter, disconnection of the frontobasal white matter, mesial disconnection through the corpus callosum, and temporomesial disconnection with resection of the amygdala and anterior hippocampus (Villemure and Mascott 1995). Delalande introduced a vertical parasagittal approach with opening of the roof of the lateral ventricle, callosotomy, anterior disconnection through the frontobasal white matter, and disconnection of the insular cortex and hemispheric white matter by dissection from the lateral ventricle through the lateral parts of the basal ganglia block to the mesial aspect of the temporal lobe (Delalande et al. 1992). Schramm introduced a transsylvian transventricular approach consisting of the following steps: transsylvian exposure of the insular cortex; resection of amygdala and hippocampus; opening of the lateral ventricle through the circular sulcus of the insula from the tip of the temporal horn to the tip of the frontal horn; frontobasal disconnection along the anterior cerebral

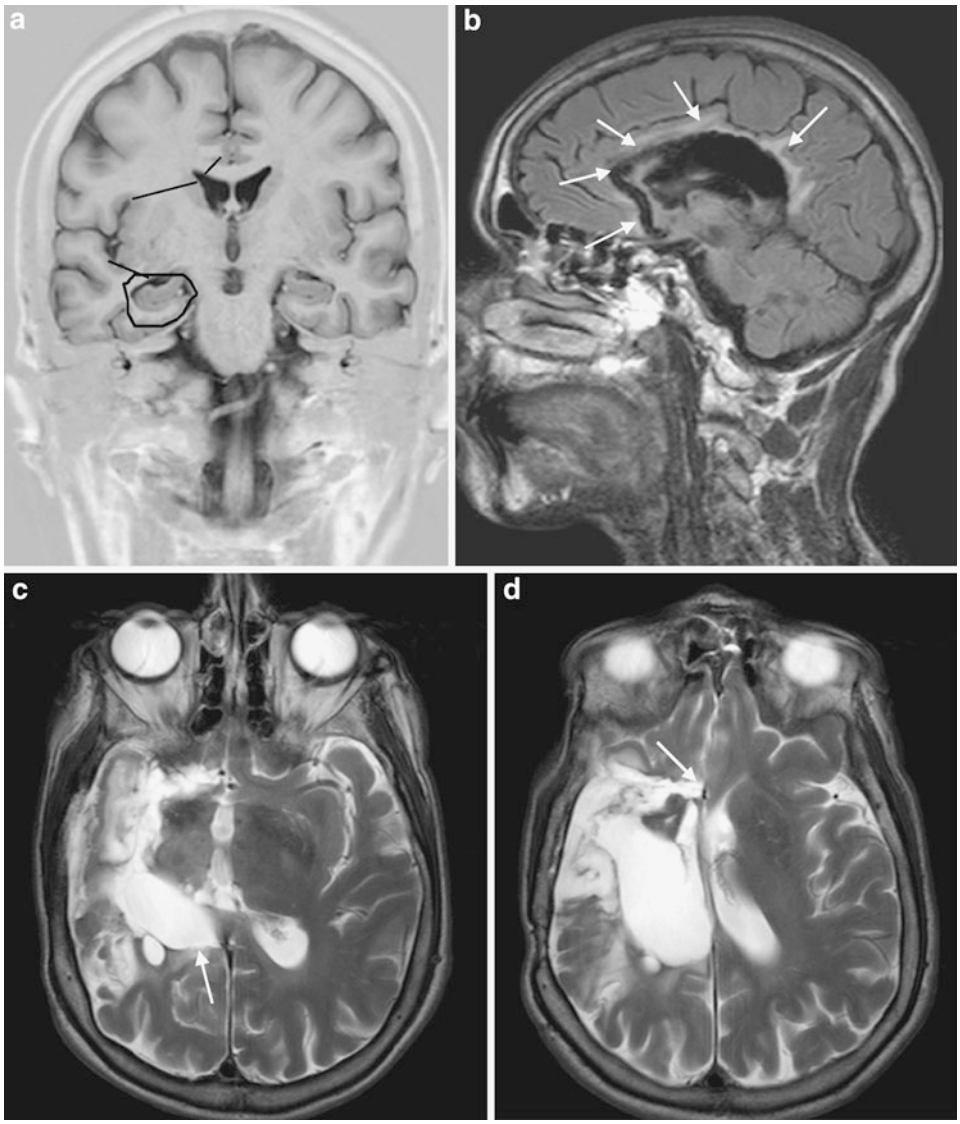

Fig. 7 Schematic drawing (**a**) and an example (**b**-**d**) of a transsylvian, transventricular functional hemispherotomy according to Schramm. A 50 year old woman with secondarily generalized seizures since early childhood showed a right hemispheric porencephalic defect (pre-operative MRI not shown). Functional hemispherotomy comprised the following steps: Transsylvian approach. Resection of the temporo-mesial structures including amygdala and hippocampus (**a**: circle). Transcortical access to the ventricular system along the circular sulcus of the insula from the tip of the temporal horn to the tip of the frontal horn (**a**: long stripes), preserving the branches of the middle cerebral artery. Fronto-basal disconnection along the anterior cerebral artery (**a**: short stripe, **d**: *arrow*). Transventricular callosotomy following the pericallosal artery (**b**: *arrows*). Completion of the disconnection from the trigone following the outline of the falco-tentorial border to the temporo-mesial resection cavity (**c**: *arrow*). Resection of the insular cortex

artery; transventricular callosotomy; resection of the insular cortex (Schramm et al. 1995).

3.3 Imaging

Postoperative MRI is performed in order to prove the completeness of the disconnection of the whole hemisphere along the intended route (Fig. 7). The seizure outcome might be worse if cortical areas are still connected (e.g., critical areas like the frontobasal or insular cortex). The above-mentioned modern disconnective techniques avoid larger resections so that the postoperative MRI shows intact cortical and subcortical structures. Larger disconnected ischemic areas may lead to brain swelling with a midline shift but remain without any effect on the seizure outcome postoperatively. Sometimes early hydrocephalic complications may occur due to the large opening of the ventricular system.

Depending on the surgical technique, the rate of late postoperative hydrocephalus is up to 20 %. Resective procedures have a significant higher rate of hydrocephalic complications and shunt rates. Some patients may show traction of midline structures into the disconnected and atrophic hemisphere in midterm follow-up and may be a reason for headaches.

4 Corpus Callosotomy

4.1 Indications

Corpus callosotomy is a palliative procedure for patients with intractable focal epilepsy who are not suitable for resective surgery. The rationale for the disconnecting procedure is to prevent the fast spread of epileptic activity from one hemisphere to the other. Uncontrolled generalized epilepsy with

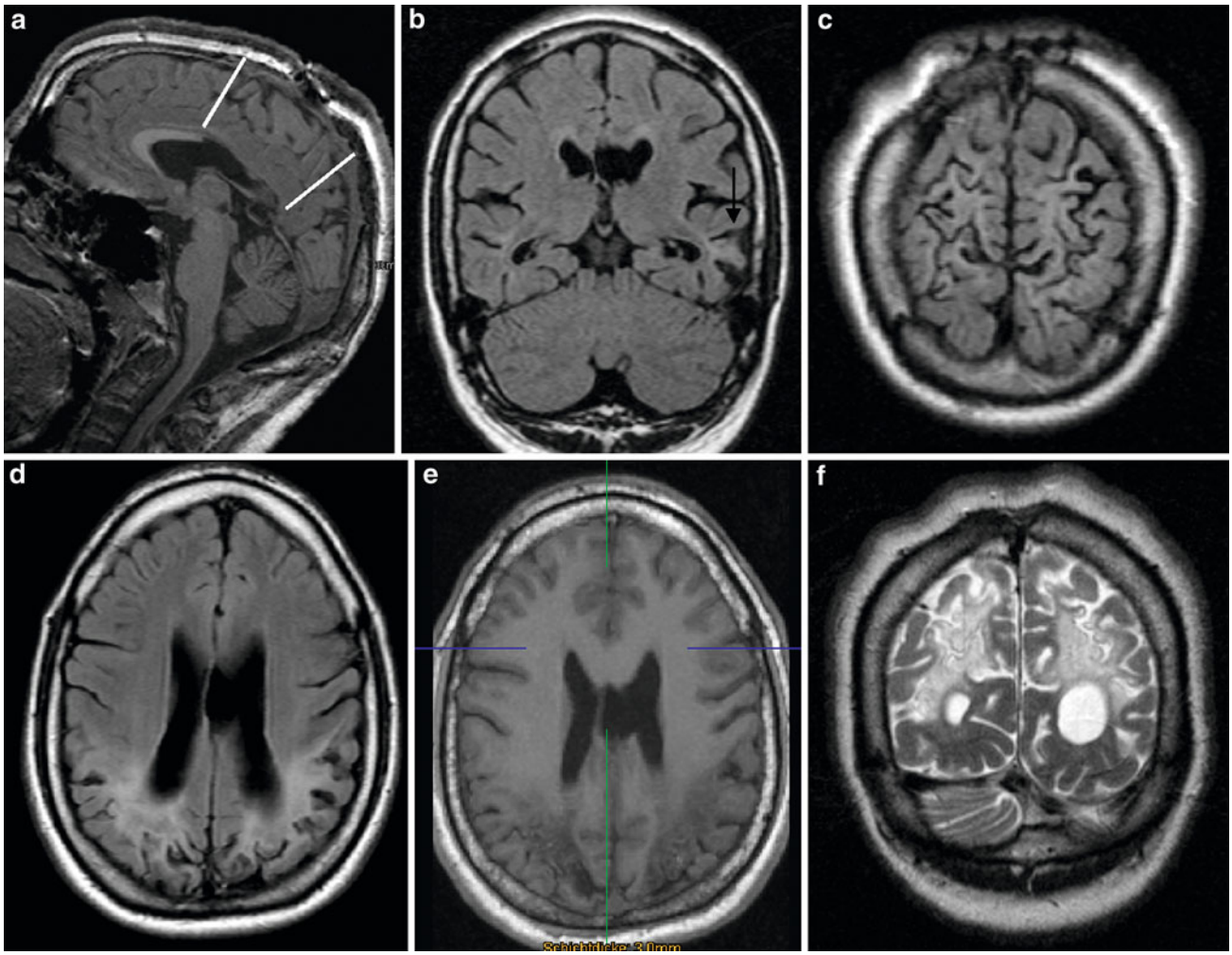

Fig. 8 Posterior callosotomy in a 15 year old boy with bilateral posterior parasagittal ulegyria, a hypoxic ischemic encephalopathy often due to neonatal hypoglycemia. The goal of callosotomy was to prevent atonic seizures induced by rapid epileptic discharges propagating from hemisphere to the other. The extent of callosal removal is assessed on sagittal T1-weighted images (**a**: lines). Posterior parasagittal ulegyria shows shrunken and gliotic gyri, enlarged sulci, white matter gliosis and volume loss (**b**-**f**)

atonic or tonic seizures originating in one hemisphere ("drop-attacks") with a high risk of injury often responds well in terms of reduced generalized seizure frequency. Most patients are categorized as having Lennox-Gastaux syndrome. Only a few patients become completely seizure-free after surgery (Cukiert et al. 2006), and sometimes severe side effects, such as a disconnection syndrome, occur. Due to modern antiepileptic drug medication and the use of vagal nerve stimulators, callosotomy is only rarely performed to date but still has its place in desolate seizure situations.

4.2 Surgical Technique

After dissection of the interhemispheric cleft with preservation of the interhemispheric arteries and bridging veins, the complete callosum should be exposed for anatomic orientation. The white matter of the callosum is the visual guide of the disconnective step of the procedure until the ependym is visible. Neuronavigation is a very helpful adjunct to define the posterior border of the callosotomy. Here, the vein of Galen will be visualized after transecting the splenium.

In some centers a staged approach was developed with an anterior callosotomy (two-thirds) performed as first step. If this fails to improve seizure control, complete disconnection is performed (Spencer and Spencer 1989). Different radiosurgical approaches have been published in the last decade (Pendl et al. 1999).

4.3 Imaging

Postoperative MRI is performed in order to prove the extent of the disconnection (two-thirds or complete) (Fig. 8). Hydrocephalus may be present as a complication due to

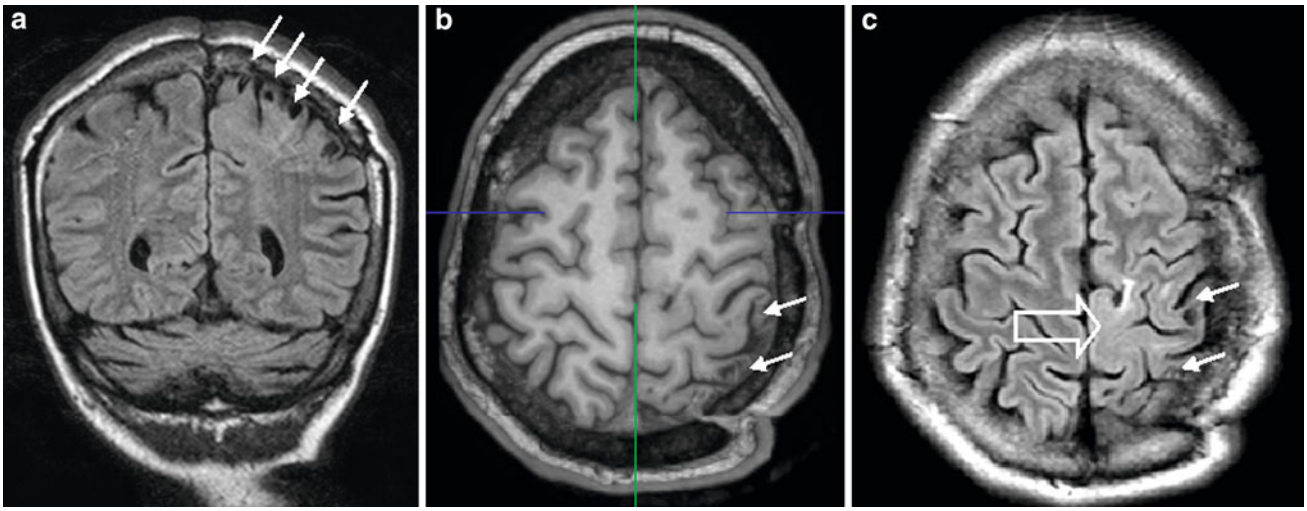

Fig. 9 Multiple subpial transsections in a 26 year old woman with a subtotally resected FCD IIB of the left parietal lobe extending into the prescentral gyrus (**c**: *open arrow*). The subpial transsections are visualized as thin stripes in the postcentral gyrus which are isointense to CSF and oriented perpendicular to the cortical surface (**a**-**c**: **arrows**)

intraventricular blood; deep vein thrombosis has been reported as a rare complication.

5 Multiple Subpial Transsections

5.1 Indications

Multiple subpial transsections (MST) are a disconnective procedure, introduced by Morrell and co-workers, to treat focal epilepsy in "unresectable" eloquent cortex (Morrell et al. 1989). The procedure is based upon experimental evidence indicating that epileptogenic discharge requires substantial side-to-side or horizontal interaction of cortical neurons and that the major functional properties of cortical tissue depend upon the vertical fiber connections of the columnar units. MST are mostly combined with resective surgery near eloquent cortex (Spencer et al. 2002). The effect on seizure outcome as a standalone procedure is measurable and may be considered as palliative surgery (Schramm et al. 2002).

Some authors propose MST in children with Landau-Kleffner syndrome, but the results are variable (Cross and Neville 2009).

5.2 Surgical Technique

The cortical area for MST is defined anatomically (neuronavigation is essential) and/or electrophysiologically with intraoperative eletrocorticography. The subpial transsections are performed with specially designed knives (Morrell et al. 1989). After a small pial opening, intragriseal incisions spaced at 5-mm intervals are placed over the crown of the cortical gyri, perpendicular to the long axis of the respective gyrus. MST (and cortical resection) are guided by repeated eletrocorticography. Morrell et al. used awake craniotomy for functional mapping in some patients.

5.3 Imaging

On MRI, subpial transsections are displayed as thin strips isointense to CSF that are oriented perpendicularly to the cortical surface (Fig. 9).

References

Clusmann H, Kral T, Schramm J (2006) Present practice and perspective of evaluation and surgery for temporal lobe epilepsy. Zentralbl Neurochir 67(4):165–182

Clusmann H, Schramm J, Kral T et al (2002) Prognostic factors and outcome after different types of resection for temporal lobe epilepsy. J Neurosurg 97(5):1131–1141

Cross JH, Neville BG (2009) The surgical treatment of Landau–Kleffner syndrome. Epilepsia 50(Suppl 7):63–67

Cukiert A, Burattini JA, Mariani PP et al (2006) Extended, one-stage callosal section for treatment of refractory secondarily generalized epilepsy in patients with Lennox–Gastaut and Lennox-like syndromes. Epilepsia 47(2):371–374

Delalande O, Bulteau C, Dellatolas G et al (2007) Vertical parasagittal hemispherotomy: surgical procedures and clinical long-term outcomes in a population of 83 children. Neurosurgery 60(2 Suppl 1):ONS19–ONS32

Delalande O, Pinard JM, Basdevant C et al (1992) Hemispherotomy: a new procedure fro central disconnection. Epilepsia 33(Suppl3): 99–100

Ebeling U, Reulen HJ (1988) Neurosurgical topography of the optic radiation in the temporal lobe. Acta Neurochir (Wien) 92:29–36

Egan RA, Shults WT, So N et al (2000) Visual field deficits in conventional anterior temporal lobectomy versus amygdalohippocampectomy. Neurology 55:1818–1822

Helmstaedter C, Petzold I, Bien CG (2011a) The cognitive consequence of resecting nonlesional tissues in epilepsy surgery—results from MRI- and histopathology-negative patients with temporal lobe epilepsy. Epilepsia 52(8):1402–1408

Helmstaedter C, Van Roost D, Clusmann H et al (2004) Collateral brain damage, a potential source of cognitive impairment after selective surgery for control of mesial temporal lobe epilepsy. J Neurol Neurosurg Psychiatry 75:323–326

Helmstaedter C, Richter S, Röske S et al (2008) Differential effects of temporal pole resection with amygdalohippocampectomy versus selective amygdalohippocampectomy on material-specific memory in patients with mesial temporal lobe epilepsy. Epilepsia 49(1):88–97

Helmstaedter C, Roeske S, Kaaden S et al (2011b) Hippocampal resection length and memory outcome in selective epilepsy surgery. J Neurol Neurosurg Psychiatry 82(12):1375–1381

Helmstaedter C, Van Roost D, Clusmann H et al (2004) Collateral brain damage, a potential source of cognitive impairment after selective surgery for control of mesial temporal lobe epilepsy. J Neurol Neurosurg Psychiatry 75:323–326

Hori T, Tabuchi S, Kurosaki M, et al (1993) Subtemporal amygdalohippocampectomy for treating medically intractable temporal lobe epilepsy. Neurosurgery 33:50–56 (discussion 56–57)

Morrell F, Whisler WW, Bleck TP (1989) Multiple subpial transection: a new approach to the surgical treatment of focal epilepsy. J Neurosurg 70(2):231–239

Nayel MH, Awad IA, Luders H (1991) Extent of mesiobasal resection determines outcome after temporal lobectomy for intractable complex partial seizures. Neurosurgery 29(1):55–60

Olivier A (2000) Transcortical selective amygdalohippocampectomy in temporal lobe epilepsy. Can J Neurol Sci 27(Suppl 1):S68–S76 (discussion S92–S66)

Pendl G, Eder HG, Schroettner O, Leber KA (1999) Corpus callosotomy with radiosurgery. Neurosurgery 45(2):303–307

Rasmussen T (1983) Hemispherectomy for seizures revisited. Can J Neurol Sci 10(2):71–78

Renowden SA, Matkovic Z, Adams CB et al (1995) Selective amygdalohippocampectomy for hippocampal sclerosis: postoperative MR appearance. AJNR Am J Neuroradiol 16:1855–1861

Schramm J (2002) Hemispherectomy techniques. Neurosurg Clin North Am 37:113–134

Schramm J, Aliashkevich AF, Grunwald T (2002) Multiple subpial transections: outcome and complications in 20 patients who did not undergo resection. J Neurosurg 97(1):39–47

Schramm J, Behrens E, Entzian W (1995) Hemispherical deafferentiation: an alternative to functional hemipherectomy. Neurosurgery 36:509–516

Schramm J, Kral T, Clusmann H (2001) Transsylvian keyhole functional hemispherotomy. Neurosurgery 49:891–901

Schramm J, Clusmann H (2008) The surgery of epilepsy. Neurosurgery 62(Suppl 2):463–481

Schramm J, Kuczaty S, Sassen R et al (2012) Pediatric functional hemispherectomy: outcome in 92 patients. Acta Neurochir (Wien) 154(11):2017–2028

Sincoff EH, Tan Y, Abdulrauf SI (2004) White matter fiber dissection of the optic radiations of the temporal lobe and implications for surgical approaches to the temporal horn. J Neurosurg 101:739–746

Spencer DD, Spencer SS (1989) Corpus callosotomy in the treatment of medically intractable secondarily generalized seizures of children. Cleve Clin J Med 56(Suppl Pt 1):S69–S78

Spencer SS, Schramm J, Wyler A et al (2002) Multiple subpial transection for intractable partial epilepsy: an international meta-analysis. Epilepsia 43(2):141–145

Spencer DD, Spencer SS, Mattson RH et al (1984) Access to the posterior medial temporal lobe structures in the surgical treatment of temporal lobe epilepsy. Neurosurgery 15(5):667–671

Thudium MO, Campos AR, Urbach H, Clusmann H (2010) The basal temporal approach for mesial temporal surgery: sparing the Meyer loop with navigated diffusion tensor tractography. Neurosurgery 67:(2 Suppl Operative):385–390

van der Knaap LJ, van der Ham IJ (2011) How does the corpus callosum mediate interhemispheric transfer? A review. Behav Brain Res 223(1):211–221

Villemure JG, Daniel RT (2006) Peri-insular hemispherotomy in paediatric epilepsy. Childs Nerv Syst 22(8):967–981

Villemure JG, Mascott CR (1995) Peri-insular hemispherectomy: surgical principles and anatomy. Neurosurgery 36:509–516

von Lehe M, Wellmer J, Urbach H et al (2009) Insular lesionectomy for refractory epilepsy: management and outcome. Brain 132(Pt 4): 1048–1056

von Rhein B, Nelles M, Urbach H et al (2012) Neuropsychological outcome after selective amygdalohippocampectomy: subtemporal vs. transsylvian approach. J Neurol Neurosurg Psychiatry 83(9): 887–893

Yaşargil MG, Teddy PJ, Roth P (1985) Selective amygdalo-hippocampectomy. Operative anatomy and surgical technique. Adv Tech Stand Neurosurg 12:93–123

Yeni SN, Tanriover N, Uyanik O et al (2008) Visual field defects in selective amygdalohippocampectomy for hippocampal sclerosis: the fate of Meyer's loop during the transsylvian approach to the temporal horn. Neurosurgery 63:507–513

Index

H. Urbach (ed.), *MRI in Epilepsy*, Medical Radiology. Diagnostic Imaging,
DOI: 10.1007/978-3-642-17860-3, © Springer-Verlag Berlin Heidelberg 2013